

Combining Heat-Pipes Heat-Exchanger and Solar Energy for Comfort Cooling

by Zulkarnaini bin Abdullah

Thesis submitted in fulfilment of the requirements for
the degree of

Doctor of Philosophy

under the supervision of Dr Ba Phuoc Huynh

University of Technology Sydney
Faculty of Engineering and Information Technology

September 2021

Certificate of Original Authorship Template

Graduate research students are required to make a declaration of original authorship when they submit the thesis for examination and in the final bound copies. Please note, the Research Training Program (RTP) statement is for all students. The Certificate of Original Authorship must be placed within the thesis, immediately after the thesis title page.

Required wording for the certificate of original authorship

CERTIFICATE OF ORIGINAL AUTHORSHIP

I, *Zulkarnaini Abdullah* declare that this thesis, is submitted in fulfilment of the requirements for the award of *Doctor of Philosophy*, in the *Mechanical and Mechatronic Engineering, Faculty of Engineering and Information Technology* at the University of Technology Sydney.

This thesis is wholly my own work unless otherwise referenced or acknowledged. In addition, I certify that all information sources and literature used are indicated in the thesis.

This document has not been submitted for qualifications at any other academic institution.

**If applicable, the above statement must be replaced with the collaborative doctoral degree statement (see below).*

**If applicable, the Indigenous Cultural and Intellectual Property (ICIP) statement must be added (see below).*

This research is supported by the Australian Government Research Training Program.

Production Note:

Signature: Signature removed prior to publication.

Date: 15/09/2021

Collaborative doctoral research degree statement

I certify that the work in this thesis has not previously been submitted for a degree nor has it been submitted as part of the requirements for a degree at any other academic institution except as fully acknowledged within the text. This thesis is the result of a Collaborative Doctoral Research Degree program with *[insert collaborative partner institution]*.

Indigenous Cultural and Intellectual Property (ICIP) statement

This thesis includes Indigenous Cultural and Intellectual Property (ICIP) belonging to *[insert relevant language, tribal or nation group(s) or communities]*, custodians or traditional owners. Where I have used ICIP, I have followed the relevant protocols and consulted with appropriate Indigenous people/communities about its inclusion in my thesis. ICIP rights are Indigenous heritage and will always remain with these groups. To use, adapt or reference the ICIP contained in this work, you will need to consult with the relevant Indigenous groups and follow cultural protocols.

DECLARATION

Certificate of Authorship/Originality

I certify that the work in this thesis has not been previously submitted for a degree nor has it been submitted as a part of the requirements for other degrees except as fully acknowledged within the text.

I also certify that the thesis has been written by me. Any help that I have received in my research and in the preparation of the thesis itself has been fully acknowledged. Also, I certify that all information sources and literature used are quoted in the thesis.

Production Note:
Signature removed
prior to publication.

ABSTRACT

COMBINING HEAT-PIPES HEAT EXCHANGER AND SOLAR ENERGY FOR COMFORT COOLING

By

Zulkarnaini Abdullah

There are concerns over energy difficulties, resource exhaustion and environmental impacts. Among the substantial reasons for these concerns is the increase in the energy demand, to maintain the comfort levels and the time spent in buildings which contribute to the rise in energy consumption. The energy consumed for heating, ventilation and air conditioning is so significant that energy-saving and efficiency have become the main objective in every energy policy. As a result of the growing demand, there is always a great need for energy reduction in the heating and cooling processes. Thus, this research aimed to evaluate the potential of solar energy in energy-saving applications. The first task involved modelling a room using an acrylic test-box with different opening configurations for temperature distribution collection. The second task was designing a 'heat-pipes heat-exchanger' to be attached to the test box to lower the air intake to the box. The third task involved operating a refrigerator that runs on plate photovoltaic solar panels without the need for grid electricity. It is an understandable fact that solar energy is no match against the grid electrical energy; however, a room's cooling system could benefit from the abilities of the heat pipes in transferring heat, thus resulting in a reduction of energy consumption. A refrigerator that runs on solar energy reduces energy consumption by cutting the dependency on non-renewable energy resources.

The methods used were both experimental and computational. Regarding the experiments, the capabilities of the heat-pipes heat-exchanger in reducing temperature were tested with the test-box in five opening configurations. Three of the configurations were tested in Sydney's medium ambient temperature while the other two configurations and the solar energy refrigerator were

tested in Kuala Lumpur's high ambient temperature. The aim was to verify the solar energy's capability in operating a cooling system with optimal converted solar energy. Regarding computation, the commercial software CFD-ACE and ANSYS-Fluent were used. Various room air intake openings, locations, side edges and boundaries were replicated rigorously and verified. Additionally, the natural and forced ventilation that influences the airflow to the room has been considered. SOLARGIS software was applied to verify the annual energy consumption of the solar panels.

The Computational Fluid Dynamics satisfactorily converge all the properties and the conditions using the RANS method to solve the velocity components, pressure and $k-\epsilon$ (epsilon) scheme. Numerical and graphical presentations with different plots, streamline data and curves were compared to predict the best room-airflow configurations. Based on the governing equations of fluid dynamics, namely the conservation of mass, momentum, and energy, the computational fluid dynamic solved the mathematical modelling. By the simulation, the heat-pipes heat-exchanger of R134a as a refrigeration medium recorded a 5 K of differences from the inlet evaporator end to the outlet condenser end, while with the experimental studies the difference is between 5 to 9 K.

The main achievement obtained from the experiments is that the heat-pipes heat-exchanger was found capable of pre-cooling a room by up to 9 K. The best opening configuration showed that the cooling energy saving was in the range of 93 W/m^3 to 140 W/m^3 or about 25% to 33% of the room's required energy. The experiment using the solar energy refrigerator found that the application could achieve the desired temperature of 5°C with 31% savings of annual power consumption. An additional experiment was also performed for a refrigerator driven by solar and wind energy. The objective was to verify the energy-saving capability of wind turbines combined with solar energy. It was thus demonstrated that the installed wind turbine was capable of operating the refrigerator for 7 hours.

The significance of the research is that the heat-pipes heat-exchanger reduces room temperature while solar energy reduces the dependence on grid electricity. Thus, the combined solar energy and passive cooling have a huge potential in reducing energy while maintaining comfort cooling.

Thesis directed by Dr Ba Phuoc Huynh

School of Mechanical and Mechatronic Engineering

ACKNOWLEDGMENTS

I would like to express my sincerest gratitude to my supervisor, Dr Phuoc Huynh and my co-supervisor, Dr Thanh Nguyen for their guidance and assistance throughout every stage of the experimental work and the writing of the thesis. Their guidance did not only cover the scope of my research work but also helped to develop the necessary skills in my academic and professional life.

I would also like to thank the technical staff of the Faculty of Engineering and IT, particularly Mr Vahik who assisted in the construction of the heat pipes and the acrylic test-box model. I would like to thank the staff of the School of Mechanical Engineering, especially Mrs Tamsin, Mr David Brennan, and Mrs Razia for their contributions to the documentation work.

I am indebted to my friends and colleagues, especially Awang Idris, Amir Rezza, Kashif, Peter Abdou and Miraz for their comments and suggestions towards the making of this thesis.

Finally, I am highly indebted to my mother, my wife, my sons and my friends for their encouragement and support throughout this research endeavour. Without their moral and financial support, this work may not have been realised.

This research would not have been possible without the financial support of the Faculty of Engineering and IT, University of Technology Sydney, Majlis Amanah Rakyat (MARA, Malaysia) and Universiti Kuala Lumpur, Malaysia.

Zulkarnaini Abdullah
Sydney, Australia, 2021.

CONTRIBUTION BY THE AUTHOR

Articles Peer-reviewed and Presented in Conferences

Author

A total of ten conferences and journal papers have been produced throughout the study. Five of the papers are Scopus-Elsevier Excellence in Research for Australia (ERA) Ranked-A category, including one international conference of the Scopus h - index. Two papers related to passive cooling options.

1. Abdullah Z., Huynh B.P., Idris A. (2014). Numerical Study of Heat-pipes heat-exchanger to a 3-Dimensional Room with Natural Driven Ventilation. *ASME IMECE2014 Montreal, Canada.*
ERA ID: 42383, American Society of Mechanical Engineering Rank-A, FoR1: 0913, FoR1Name: Mechanical Engineering, FoR2: 0905, FoR2 Name: Civil Engineering.
2. Abdullah Z., Huynh B.P., Idris A. (2014). Numerical Study of Heat-pipes Effects to a 3-Dimensional Room with Driven Ventilation. *19th AFMC Melbourne, Australia.*
ERA ID: 42494, Australasian Fluid Mechanics Conference Rank-A, FoR1: 0913, FoR1Name: Mechanical Engineering.
3. Z. Abdullah, B.P. Huynh, and A. Idris. (2016). CFD-Simulation of the Effect of Heat-pipes Attached to an Evaporator and Condenser of an Air-Cooled-Air-Conditioner. *20th Australasian Fluid Mechanics Conference, Perth, Australia.*
ERA ID: 42494, Australasian Fluid Mechanics Conference Rank-A, FoR1: 0913, FoR1Name: Mechanical Engineering.
4. Abdullah Z., Huynh B.P., Idris A. (2015). Numerical Simulation of the Flow and Heat Behaviour for a Heat-pipes heat-exchanger in an Outdoor Power Supply Cabinet. *ASME IMECE2015 Houston, Texas, USA.*
ERA ID: 42383, American Society of Mechanical Engineering Rank-A, FoR1: 0913, FoR1Name: Mechanical Engineering, FoR2: 0905, FoR2 Name: Civil Engineering.
5. Abdullah Z., Huynh B.P., Idris A. (2016). CFD-Simulation of a Heat-pipes -Heat-Exchanger Effect on a Tubular Air-Cooled Condenser. *ASME IMECE2016 Phoenix, Arizona, USA.*

ERA ID: 42383, American Society of Mechanical Engineering Rank-A, FoR1: 0913, FoR1Name: Mechanical Engineering, FoR2: 0905, FoR2 Name: Civil Engineering, Scopus h-index.

6. Abdullah Z., Huynh B.P. (2018). Experimental Study on Cooling Energy Reduction Using Passive Cooling Heat-pipes heat-exchanger. *21st AFMC Adelaide, Australia.*
ERA ID: 42494, Australasian Fluid Mechanics Conference Rank-A, FoR1: 0913, FoR1Name: Mechanical Engineering.
7. Z. Abdullah, M. S. Shaadan, Z. Jusoh, Z. Engsa. (2019). Study of Wind-Assisted Energy for Cooling System in Bangi, Malaysia. *Journal of Advanced Manufacturing Technology, International Conference on Advanced Processes and System in Manufacturing (APSIM 2019), Malaysia.*

Co-author

8. Z. Jusoh, N. Ibrahim, Z. Abdullah and Z. Engsa. (2019). Simulation Study of Cooling a Small Domestic Refrigeration System Using Solar-Assisted Energy in Bangi, Malaysia. *Journal of Advanced Manufacturing Technology, International Conference on Advanced Processes and System in Manufacturing (APSIM 2019), Malaysia.*
9. Possibility of Using Silica Gel-Water Adsorption Chiller in the Cold Chain. M. A. Ahamat, M. J. Tierney, Zulkarnaini Abdullah, Zakaria Jusoh, *2nd IIR International Conference on Sustainability and Cold Chain, Paris.*
10. Theoretical and Experimental Analysis of Desiccant Wheel Performance of Solar Hybrid Desiccant Air-Conditioning System. Zuraini Hashim, Tri Suyono, Arifidian Rachman, Zulkarnaini, Sohif Mat. *Solar Energy Research Institute, National University of Malaysia.*

LIST OF TABLES

Chapter I INTRODUCTION

Tables 1.1	A 20-year comparison of the required fresh air intake, between ASHRAE 1981 and ASHRAE 2001.....	3
Table 1.2.	The average temperature recorded in NSW in 2017.....	4

Chapter II LITERATURE REVIEW

Table 2.1:	The average temperature in Sydney, New South Wales from January to December 2018.....	16
Table 2.2:	The global irradiance and diffuse fraction, depending on the cloud condition....	18
Table 2.3:	The comparisons between absorption using water-lithium bromide (H ₂ O-LiBr) and ammonia-water (NH ₃ -H ₂ O).....	29
Table 2.4:	COP comparison between an absorption system to other systems.....	31
Table 2.5:	Working fluids for heat-pipes.....	43
Table 2.6:	The latest experimental works and results from several researchers.....	45
Table 2.7:	Refrigerant data comparison between R134a and other potential refrigerants.	53
Table 2.8:	Summary of experimental studies on applications of heat-pipes in HVAC.....	53

Chapter IV RESEARCH METHODOLOGY

Table 4.1:	The specification of the heat-pipes heat-exchanger used.....	78
Table 4.2:	Air velocity requirement for comfort cooling.....	88
Table 4.3:	Table of working parameters for desired temperature ranges and the airflow....	100
Table 4.4:	Temperature monitoring locations of the acrylic box with the heat-pipes attached.....	109

Table 4.5:	The specification of models for all domains.....	111
Table 4.6:	The specification of models and boundaries of computational fluid dynamic domains.....	112
Table 4.7:	The properties of the heat-pipes, cooling medium and the temperature of the outlet achieved when running with ANSYS Fluent computational fluid dynamics simulations.....	116
Table 4.8:	Cases and configurations for the study of the effects of the heat-pipes heat-exchanger to a room with natural ventilation.....	121
Table 4.9:	Total cells and nodes used for modelling from CFD ACE-GEOM and GUI. The grids used are structured grids and the number of cells and nodes are different for all cases as there are only slight differences in air flow rate result at about 1 % when using bigger cells and nodes range.....	121

Chapter V RESULT AND DISCUSSION

Table 5.1:	The nodes and elements of the fluid-solid meshes when running with ANSYS Fluent.....	131
Table 5.2:	Temperature, relative humidity and the enthalpy when the air circulated in the outdoor cabinet.....	133
Table 5.3:	The specification of models for all domains.....	136
Table 5.4:	The specification of nodes and elements for all domains.....	137
Table 5.5:	Comparison of the temperature difference between cases. Case 3 shows the highest temperature difference compared to other cases.....	139
Table 5.6:	Comparison of the refrigeration cycle parameters when the condensing temperature changed from 319 K (46°C) to 305 K (32°C).	140
Table 5.7:	Problem description in all cases.	143
Table 5.8:	The specification of nodes and elements for the condenser.	143

Table 5.9:	Comparison of the temperature difference K at the condenser coil for all the cases. Case 3 shows the best result.....	145
Table 5.10:	Comparison of temperature difference K at the evaporator coils for all the cases. Case 3 shows the best result.....	146
Table 5.11:	Comparison of the normal refrigeration cycle compared to coils with a heat pipe.....	146
Table 5.12:	Models specifications where fresh air intake locations that best suit the domain.....	148
Table 5.13:	The specifications of the heat-pipes heat-exchanger used.....	152
Table 5.14:	Comparison of temperature difference K in Case 1.....	162
Table 5.15:	Rate of energy-saving for Case 1.....	162
Table 5.16:	Comparison of the temperature difference, K in Case 2. The supplied air is from the top of the box.....	170
Table 5.17:	Rate of energy-saving for Case 2.....	170
Table 5.18:	The table shows the comparison of temperature difference K in Case 3. The supplied air is from the top of the box and the exit opening is on the sidewall of the box.....	178
Table 5.19:	Rate of energy-saving for Case 3.....	179
Table 5.20:	Comparison of the temperature difference across the heat-pipes inlet and outlet for supplied air of between 303 K and 318 K. The higher temperature of the supplied air shows a bigger differential temperature of the heat-pipes concerning its capability to transfer heat from the evaporator section to the condenser section.....	179
Table 5.21:	The thermal resistance calculations.....	185
Table 5.22:	Point of measurements where the thermocouples were located.....	186
Table 5.23:	The measured average temperature at every point in Case 1, in °C.....	187

Table 5.24:	The measured average temperature at every point in Case 1, in K.....	187
Table 5.25:	The measured average temperature at every point in Case 2, in °C.....	189
Table 5.26:	The measured average temperature at every point in Case 2, in K.....	189
Table 5.27:	The measured average temperature at every point in Case 3, in °C.....	190
Table 5.28:	The measured average temperature at every point in Case 3, in K.....	191
Table 5.29:	The parameters of R134a when simulated using ANSYS Fluent.....	193
Table 5.30:	The energy-saving with the application of heat-pipes heat-exchanger.....	198
Table 5.31:	The estimated sensible cooling load for all cases with the air supply temperature of 303 K and 318 K. The rate of the energy-saving capability of the heat-pipes heat-exchanger in the table is compared to standard air of 297 K.....	199
Table 5.32:	The result of the simulation for the heat-pipes heat-exchanger in assisting the pre-cooling of the intake air to a room with driven ventilation.....	205
Table 5.33:	The comparisons of the result between the simulation and the experimental work for the heat-pipes heat-exchanger in assisting the pre-cooling of intake air to an outdoor power cabinet. The high temperature of 328K in the cabinet is reduced to 14K different.....	206
Table 5.34:	The results of the simulation work for the heat-pipes heat-exchanger in assisting the pre-cooling of supplied air that passed through an air conditioning condenser.....	206
Table 5.35:	The results of the simulation work for the heat-pipes heat-exchanger in assisting the pre-cooling of supplied air that passed through an air conditioning evaporator.....	207
Table 5.36:	Comparison of the temperature difference across the heat-pipes inlet and outlet for supplied air of between 303 K and 318 K. The higher temperature of the supplied air shows a bigger differential temperature of the heat-pipes concerning its capability to transfer heat from the evaporator section to the condenser section..	207

Table 5.37:	The outlet air temperature and the average temperature of the acrylic box presented in a. K and b. °C for all cases. The temperature of 273K is taken as equal to 0°C.	208
Table 5.38:	The air temperature properties taken for plotting the psychrometric charts. The wet-bulb result will correspond to the dry-bulb result of the room air temperature at 297 (24°C).....	210
Table 5.39:	The air temperature properties taken for plotting the psychrometric charts. The wet-bulb result will correspond to the dry-bulb result of the room air temperature.	211
Table 5.40:	The air temperature difference recorded between the inlet and out air.....	212
Table 5.41:	The air temperature properties taken for plotting the psychrometric charts for a. 303 K and b. 318 K.....	216
Table 5.42:	Case 1.....	219
Table 5.43:	Case 2.....	219
Table 5.44:	Case 3.....	219
Table 5.45:	Energy-saving rate for all cases.....	220

LIST OF FIGURES

Chapter I INTRODUCTION

Figure 1.1:	Annual mean temperature anomalies for Australia (red) with a 10-year mean (light grey). Departures are from 1960–1990 average.....	2
Figure 1.2a, b:	The average temperature of New South Wales recorded in 2017 compared to the data from 1859. The temperature of Sydney had increased by about 4K during the 160 years (1859 to 2017)	4
Figure 1.3:	Global capacity in operation (GW_{el}), (GW_{th}) 2017 and annual energy yields (TWh_{el}), (TWh_{th}).....	5

Chapter II LITERATURE REVIEW

Figure 2.1:	ASHRAE comfort chart.....	13
Figure 2.2:	Acceptable range of operating temperature and airspeed.	14
Figure 2.3:	Psychrometric chart showing the thermal comfort zone. The levels of comfort are within the range of 20°C, 70%; 23 °C, 30%; to 26°C, 70%; 29°C, 30%. Feeling comfortable and un-comfort always refers to the difference between outdoor and indoor at the time of entrance.....	15
Figure 2.4:	The mean maximum temperature gradient for Sydney, New South Wales from January to December 2018.....	15
Figure 2.5:	Cooling strategies	17
Figure 2.6:	Method of passive cooling strategies.....	17
Figure 2.7:	Global solar thermal capacity in operation and annual energy yield 2000-2016. International Energy Agency (IEA).....	18
Figure 2.8:	Global solar thermal capacity in operation and annual energy yields for 2016.....	19
Figure 2.9:	Graph of global solar thermal energy usage and electricity generated from solar energy.....	19
Figure 2.10:	Australia market growth of new installed capacity (glazed and unglazed water collectors) 2014/2015 compared to other regions.....	20
Figure 2.11:	Typical single-stage vapour compression refrigeration cycle.....	21
Figure 2.12:	Pressure-enthalpy for a single-stage vapour compression refrigeration.....	21
Figure 2.13:	Overview of physical ways to convert solar radiation into cooling or air-conditioning system. Processes marked in dark grey are market available technologies that are used for solar-assisted air-conditioning. Processes marked in light blue are technologies that are of pilot project or system testing status.....	22

Figure 2.14:	Basic structure of a solar air-conditioning system.....	23
Figure 2.15:	The main parts of a solar-assisted air-conditioning system.....	24
Figure 2.16:	The solar-assisted air-conditioning system using low electrical energy.....	24
Figure 2.17:	The natural ventilation triangle for buoyancy-driven displacement flows that are assisted by the wind. The base and vertical sides of the triangle are set by the magnitudes of the wind and buoyancy produced velocities, U_w and U_b , respectively. The length of the hypotenuse determines the total fluid velocity, U produced by buoyancy forces reinforced by the wind.	26
Figure 2.18:	The process of refrigeration cycle.....	28
Figure 2.19:	Schematic drawing an absorption cycle.....	39
Figure 2.20:	Heat transfer configuration of an ideal absorption system. I. Adsorption process. II. Desorption process.....	30
Figure 2.21:	The heat-pipes heat-exchanger. The refrigerant liquid in the heat-pipes heat-exchanger at the bottom of the tube absorbs heat at the evaporator section and releases it at the condenser area in the upper section. The liquid evaporates into a vapour phase in the evaporator and moves towards the condenser section, which in turn changes the vapour back to the liquid phase by releasing the heat to the surrounding.....	33
Figure 2.22:	Schematic of conventional heat-pipes operation.....	35
Figure 2.23:	Axial variation of the liquid-vapour interface along the heat-pipes at a. Low b. Moderate and c. High vapour flow rates.....	36
Figure 2.24:	Thermal resistance model for heat-pipes.....	37
Figure 2.25:	Thermodynamic cycle of heat-pipes components.....	37
Figure 2.26:	Thermodynamic cycle of heat-pipes, temperature-entropy diagram.....	38
Figure 2.27:	Gravity-assisted wickless heat-pipes.....	39
Figure 2.28:	Conventional capillary-driven heat-pipes.....	39

Figure 2.29:	a. Conventional b. Concentric annular heat-pipes.....	40
Figure 2.30:	Operation of a gas-loaded variable conductance heat pipe. a. Condenser partially active. b. The condenser is fully active.....	41
Figure 2.31:	Loop heat-pipes.....	41
Figure 2.32:	Rotating heat-pipes.....	42
Figure 2.33:	Pulsating heat-pipes. a. Un-looped. b. Looped.....	42
Figure 2.34:	Logarithmic temperature scale for some of working fluids for heat-pipes	44
Figure 2.35:	Vapour pressure of different refrigerants versus temperature. The R134a works at a lower evaporating temperature.....	47
Figure 2.36:	Computational fluid dynamics work on the solar chimney and air to earth.....	48
Figure 2.37:	Computational fluid dynamics work on ventilation flow in a room.....	49
Figure 2.38:	Computational fluid dynamics works on solar chimney.....	49
Figure 2.39:	Coupled solar chimney and earth to air heat exchange.....	50
Figure 2.40:	Meshes used to simulate the heat-pipes heat-exchanger by ANSYS Fluent.....	50
Figure 2.41:	Simulation of a heat-pipes heat-exchanger by ANSYS Fluent using water as a cooling medium.....	50
Figure 2.42:	Vapour pressure of different refrigerants versus temperature. The R134a works at a lower evaporating temperature.....	54
 Chapter III MATHEMATICAL MODEL		
Figure 3.1:	Schematic drawing of solar air conditioning.....	58
Figure 3.2:	The schematic drawing of the research methodology flow chart for the air conditioning system with the assistance of solar energy and heat-pipes heat-exchanger as passive cooling.....	58

Figure 3.3:	Heat-pipes heat-exchanger application in a room to assist in lowering the air supply for comfort cooling.....	59
Figure 3.4:	Thermodynamic scheme of a heat-driven heat pump or chiller.....	60
Figure 3.5:	Schematic process of solar air conditioning.....	61
Figure 3.6:	Schematic diagrams of solar flat plate type collectors for thermal refrigeration...62	
Figure 3.7:	Schematic diagrams of solar evacuated tube type collectors for thermal refrigeration.....	62
Figure 3.8:	Log (p) -h diagrams of R134a.....	64
Figure 3.9:	Refrigerating effect.....	64
Figure 3.10:	Compressor work-done.....	65
Figure 3.11:	Condensing effect.....	65
Figure 3.12:	Heat transfer in a heat-pipes	67

Chapter IV RESEARCH METHODOLOGY

Figure 4.1:	Schematic drawing of a standard refrigeration cycle equipment for air conditioning application.....	73
Figure 4.2:	Pressure-enthalpy diagrams of the work done by each equipment.....	74
Figure 4.3:	A schematic drawing of a solar air conditioning system with heat-pipes heat-exchanger that assists in the pre-cooling of the evaporator and condenser airside.....	74
Figure 4.4:	Heat-pipes heat-exchanger application in a room to assist in lowering the air supply for comfort cooling.....	75
Figure 4.5:	Schematic drawing of the research methodology for air conditioning system with the assistance of solar energy and heat-pipes heat-exchanger as passive cooling...75	
Figure 4.6:	The workflow of the experimental project.	77

Figure 4.7:	The layout of the fresh air intake and the exhaust air outlet locations with the heat-pipes heat-exchanger installed on the wall side and at the top of the box.....	79
Figure 4.8:	The acrylic box is used to collect the temperature and air distributions.....	79
Figure 4.9:	The acrylic box and the test measuring components installed. The measurement shown is taken from the top opening.....	80
Figure 4.10:	The acrylic box and the test measuring components installed. The measurement shown is taken from the wall side opening.....	80
Figure 4.11:	Flow chart of heat-pipes simulations and interactions.....	83
Figure 4.12:	Solar air conditioning booster using heat-pipes as temperature reduction, based on Francis Meunier's proposal.....	86
Figure 4. 13:	Human is sensitive to the blowing of air and the temperature difference of the room. The location of the air vents must take into account the geometry of the room, the obstacles and the position of the occupants.....	88
Figure 4.14:	a. Diffusion of air by induction or mixed air, b. By displacement	89
Figure 4.15:	Return air placement.....	89
Figure 4.16:	Distributions of air at low velocity.....	89
Figure 4.17:	Distributions of air at high velocity.....	90
Figure 4.18:	The schematic drawing of the experimental setup.....	90
Figure 4.19:	Method 1 for Case 1 showing the arrangement of the heat-pipes, the acrylic box and the inlet and outlet of air. Thermocouple sensors are located at a proposed point in the box to find the average box temperature.....	92
Figure 4.20:	Method 2 for Case 2 showing the arrangement of the heat-pipes, the acrylic box and the inlet and outlet of air. Thermocouple sensors are located at a proposed point in the box to find the average box temperature.....	94

- Figure 4.21: Method 3 showing the arrangement of heat-pipes, acrylic box and the inlet and outlet of air. Thermocouple sensors are located at the proposed point in the box to find the average box temperature.....96
- Figure 4.22: The workflow of the experimental project. The pre-cooling of the air section is the main interest as the ambient hot air is lowered before entering the test-box.....97
- Figure 4.23: Case 4. The configuration of the opening for a. The incoming and leaving of the air in the test box. b. 10° horizontal inclination. c. The thermocouple position is seen from behind the test box.....98
- Figure 4.24: Case 5. The configuration of the opening for a. The incoming and leaving of the air in the test box. b. 90° angle positions. c. The thermocouple position is seen from behind the test box.....99
- Figure 4.25: An acrylic box showing the top opening for Method 2 and 3.....101
- Figure 4.26: An acrylic box and a heat-pipes heat-exchanger attached to the sidewall. The opening is created to let the air pass through the inlet and outlet.....102
- Figure 4.27: A heater blower and the location of installation. The blower is attached to the inlet of the opening to create a warm air supply to the heat-pipes heat-exchanger.103
- Figure 4.28: The basic method of data collection. The outside ambient air properties are compared to the processes data recorded in the acrylic box.....103
- Figure 4.29: The 10 terminal point data logger for data collections. The main purpose is to measure the outside ambient air temperature and compared to the processed data recorded in the acrylic box.....104
- Figure 4.30: A Sensirion SHT31 hygrometer record a digital temperature and humidity of the outside ambient air.....104
- Figure 4.31: A Lutron LM-8000A Type K anemometer collects the velocity and the temperature.....105
- Figure 4.32: A Testo Hot-wire Anemometer record the velocity and temperature.....106
- Figure 4.33: A Testo Thermal-Image 875 for digital imaging of temperature distribution....107

Figure 4.34:	A Monogram Omega data logger with a 10-point terminal to record the temperature.....	107
Figure 4.35:	A Type k thermocouple.....	108
Figure 4.36:	The basic concept of the data collections. The outside ambient air properties are compared to the processed data recorded in the acrylic box.....	108
Figure 4.37:	Models of the acrylic box specification where fresh air intake locations and openings that best suits the domain.....	110
Figure 4.38:	Heat-pipes heat-exchanger technology.....	113
Figure 4.39:	Straight heat-pipes model using R134a as a refrigerant medium. An optional ventilation fan is shown to discharge warm air from the condenser side to the outdoor.....	114
Figure 4.40:	Meshes used to run the simulation of the heat-pipes heat-exchanger by ANSYS Fluent.....	115
Figure 4.41:	Simulation of a heat-pipes heat-exchanger by ANSYS Fluent using water as a cooling medium. The temperature difference is about 2 K.....	115
Figure 4.42:	Simulation of a heat-pipes heat-exchanger by ANSYS Fluent using acetone as a cooling medium. The temperature difference is about 3 K.....	116
Figure 4.43:	Simulation of a heat-pipes heat-exchanger by ANSYS Fluent using R134a as a cooling medium. The temperature difference is about 5 K.....	116
Figure 4.44:	Simulation of ANSYS Fluent on a row of a heat-pipes heat-exchanger with airflow at a temperature of 293 K passing the evaporator section of the heat-pipes. The average leaving temperature is about 294 K.....	118
Figure 4.45:	Simulation of ANSYS Fluent on a row of a heat-pipes heat-exchanger with airflow at a temperature of 303 K passing the evaporator section of the heat-pipes. The average leaving temperature is about 301 K.....	118
Figure 4.46:	Simulation of ANSYS Fluent on a row of a heat-pipes heat-exchanger with airflow at a temperature of 318 K. The lowest leaving temperature is 310 K.....	119

Figure 4.47:	Case 1 which is single-sided ventilation with sharp edges at the inlet and outlet opening.....	120
Figure 4.48:	Case 2 which is single-sided ventilation with round edges at the inlet and outlet opening.....	120
Figure 4.49:	Case 3 with an outlet located on the sidewall of the building.....	120
Figure 4.50:	Case 1 showing the graphic distributions of a. Velocity magnitude, b. Temperature, and c. Flow path.....	122
Figure 4.51:	Case 2 showing the graphic distributions of a. Velocity magnitude, b. Temperature, and c. Flow path.....	123
Figure 4.52:	Case 3, show graphic distributions of a. Velocity magnitude, b. Temperature, and c. Flow path.....	124
Figure 4.53:	Case 1 a. Velocity and b. Magnitude.....	125
Figure 4.54:	Case 2 a. Velocity and b. Magnitude.....	125
Figure 4.55:	Case 3 a. Velocity and b. Magnitude.....	126

Chapter V RESULT AND DISCUSSION

Figure 5.1:	Schematic of an outdoor cabinet with the application of straight heat-pipes showing the inlet and outlet air paths. The source of heat is from the operation of the electro-mechanical equipment inside the cabinet and the solar heat.....	130
Figure 5.2:	The contour of a. Air temperature and b. The airflow which is simulated to a heat-pipes heat-exchanger by ANSYS Fluent.....	132
Figure 5.3:	Airflow traces inside the outdoor cabinet after passing through the heat-pipes heat-exchanger inlet based on the simulation model run on CFD-ACE. The air velocity shows that the warmer air moves to the upper side of the cabinet before exiting to the outlet. a. Temperature. b. Velocity.....	132

- Figure 5.4: a. Temperature b. Velocity distribution along the inside length of the outdoor cabinet133
- Figure 5.5: The condenser is a heat exchanger used to reject the heat of the refrigerant to another medium. The high-pressure refrigerant vapour flows in the tube of the condenser and rejects heat, condenses from vapour to liquid state in the process.136
- Figure 5.6: Schematic of a condenser with the application of straight horizontal heat-pipes showing the inlet and outlet of air paths. The source of heat is from the condenser refrigerant inlet with a temperature of 319 K and it then exits through the liquid line with a reduced temperature of 315 K..... 136
- Figure 5.7: The model and meshes used to run the simulations on air-cooled condenser by ANSYS Fluent..... 137
- Figure 5.8: Simulation of ANSYS Fluent on an air-cooled condenser. The lowest temperature recorded for a condenser is about 304 K to 307 K heat rejection to the ambient..... 138
- Figure 5.9: Case 2 with a heat-pipes heat-exchanger attached closely together. The lowest temperature recorded is about 303 K to 304 K..... 138
- Figure 5.10: Simulation of ANSYS Fluent on an air-cooled condenser with a heat-pipes heat-exchanger separately attached 100mm at the air inlet. The lowest temperature recorded is 302K.....138
- Figure 5.11: Graph from CFD-ACE for Case 3. The air flowing over the condenser coil was recorded at about 301 K.....139
- Figure 5.12: Solar air conditioning booster.....142
- Figure 5.13: The Refrigeration Cycle. The condenser coil is a heat exchanger used to reject the heat of the refrigerant to the surrounding. The evaporator coil absorbs room heat and lowers the room temperature.143

Figure 5.14:	Schematic of a refrigeration coil with the application of straight horizontal heat pipe showing the inlet and outlet of air paths. An evaporation temperature of 295K is used for the simulation of the heat pipe heat-exchanger	143
Figure 5.15:	Case 1a for the condenser and 1b for the evaporator.	144
Figure 5.16:	Case 2 and 3.	144
Figure 5.17:	The simulation for all cases.	145
Figure 5.18:	The layout of the fresh air intake locations with the heat-pipes heat-exchanger installed at the side and the top of the box.....	149
Figure 5.19:	The workflow of the experimental project.....	149
Figure 5.20:	Finned type cross-flow in-line heat-pipes heat-exchanger with R134a as the cooling medium.....	150
Figure 5.21:	Finned type cross-flow in-line heat-pipes heat-exchanger with R134a as the cooling medium. a. Temperature profile of the experimental test. b. Grooves structured tube of the heat-pipes heat-exchanger used for the experiment compared to, c. Smooth structured copper tube.....	150
Figure 5.22:	The temperature distributions recorded by Testo Imaging on the evaporator side of the heat-pipes heat-exchanger set up.....	151
Figure 5.23:	The temperature distributions recorded by Testo Imaging on the condenser side of the heat-pipes heat-exchanger set up.	151
Figure 5.24:	The temperature profile of the air-to-heat-pipes heat-exchanger	152
Figure 5.25:	The temperature distribution inside the box captured by Testo Imaging.....	153
Figure 5.26:	Case 1a and b: The path of air temperature blown from the supplied air (SA) to the heat-pipes evaporator side (1) moves to the inlet of the test-box (3), mixes with the box air temperature (5-9), is forced to the outlet (2) and the condenser side of the heat-pipes (10), and then exits to the ambient outlet (4). The average temperature difference is 8K to 10K.....	154

- Figure 5.27: Case 1. The average temperature inside the box with supplied air of 303 K (30°C) is about 293 K (20°C)155
- Figure 5.28: Case 1. The average temperature inside the box with supplied air of 318 K (45°C) is about 302 K (29°C)..... 155
- Figure 5.29: Case 1. The maximum temperature of the heat-pipes heat-exchanger at evaporator end 1, compared to the condenser end 2..... 156
- Figure 5.30: Case 1. The inlet air temperature at the box opening compared to the outlet air..... 156
- Figure 5.31: Case 1. The comparison of different temperatures between the heat-pipes inlet and the pipe outlet for both 303 K and 318 K..... 157
- Figure 5.32: Case 1. The average temperature inside the box compared to the heat-pipes heat-exchanger, condenser section where the outlet airflows. The supply air is 303 K.157
- Figure 5.33: Case 1. The average temperature inside the box compared to the heat-pipes heat-exchangers condenser section where the outlet air flows. The supplied air is 318 K.....158
- Figure 5.34: The comparison of the supply air inlet and the return air outlet of the acrylic box.158
- Figure 5.35: The comparison of the temperature at the evaporator and the condenser side of the heat-pipes.159
- Figure 5.36: The graph shows the temperature recorded inside the acrylic test box, 5 & 6 where the thermocouple is placed in the middle-lower and upper level, 7 on the left, 8 on the right side, and 9 at the air return side near the exit of the box. Thermocouple 9 shows the lowest temperature (294K) before the air is being blown away to the exit opening.....159
- Figure 5.37: The graph shows the average temperature recorded inside the acrylic test box. The average box temperature is about 301K (28°C), agreed with the return air temperature.....160

- Figure 5.38: When the average temperature of 303K is supplied to the heat-pipes and the acrylic box, the average temperature is reduced to about 293K, a differential of 10 K. This is compared to the difference between the average temperature and the condenser section of the heat pipe at 295K which is 8 K. For the energy-saving calculation, the differential temperature of the average box temperature and the condenser section of the heat pipe (8 K) is used as the minimum value. The rate of energy-saving is calculated to be at 25% of the installation.....160
- Figure 5.39: The average temperature when the air temperature of 318K is supplied to the heat-pipes and the acrylic box. At 318K, the average temperature reduced is about 302K, a differential of 16 K. This is compared to the difference between the average temperature and the temperature of the condenser section of the heat pipe at 311K, which is 7 K. The rate of energy-saving is calculated to be at 14% of the installation.....161
- Figure 5.40: Case 1: The comparison of air temperature at supply and exit.....161
- Figure 5.41: Case 1: The comparison of air temperature at evaporator and condenser side....161
- Figure 5.42: Case 2a and b: The path of air temperature that is blown from the supplied air (SA) to the heat-pipes evaporator side (1) moves to the inlet of the test-box (3), mixes with the box air temperature (5-9), is forced to the outlet (2) and the condenser side of the heat-pipes (10), and then exits to the ambient outlet (4). The average temperature difference is 8K.....164
- Figure 5.43: Case 2. The average temperature inside the box with supplied air of 303 K (30°C) is about 294 K (21°C)..... 164
- Figure 5.44: Case 2. The average temperature inside the box with supplied air of 318 K (45°C) is about 301 K (28°C).....165
- Figure 5.45: Case 2. The temperature of the heat-pipes heat-exchanger at evaporator ends 1, compare to the condenser ends 2..... 165
- Figure 5.46: Case 2. The inlet air temperature at the box opening as compared to the outlet air.....166

- Figure 5.47: Case 2. The average temperature inside the box compared to the heat-pipes heat-exchangers condenser section where the outlet air flows. The supplied air is 303 K.....166
- Figure 5.48: Case 2. The average temperature inside the box compared to the heat-pipes heat-exchangers condenser section where the outlet air flows. The supplied air is 318 K.....166
- Figure 5.49: Comparison of the supplied air inlet and the return air outlet of the acrylic box. The high heat from the temperature of 303K to 333K (30°C to 60°C) is being cooled by the heat-pipes at the inlet supplied-air opening of the acrylic box. The cooled air travels within the box and is blown out to the outlet. The temperature difference between the inlet and the outlet is about 16 K. Any increase or additional heat to the heat-pipes will not increase the reduction capability of the installation.....167
- Figure 5.50: Comparison of the temperature at the evaporator and the condenser side of the heat-pipes. The high heat from the temperature of 303K to 333K (30°C to 60°C) is being transferred by the heat-pipes from the evaporator to the condenser. The air passing through the evaporator will be cooled down before entering the box and will travel within the box before being blown out to the outlet. The temperature difference from the evaporator to the condenser is about 20 K..... 167
- Figure 5.51: The comparison of the temperature at the acrylic box inlet 3, and the box outlet 4. The average inlet temperature is about 52°C compared to 28°C at the outlet. About 13 K heat had been reduced by the heat-pipes transfer process in lowering the box temperature. The hypothesis is that the bigger the heat-pipes is or the more refrigerant inside the heat-pipes is, the bigger the temperature difference could be achieved.....168
- Figure 5.52: The graph shows the temperature recorded inside the acrylic test box, 5 & 6 where the thermocouple is placed in the middle-lower and upper level, 7 at the left, 8 on the right side and 9 at the air return side near the exit of the box. Thermocouples 9

- shows the lowest temperature (294) before the air is blown away to the exit opening..... 168
- Figure 5.53: The graph shows the average temperature recorded inside the acrylic test box. The average box temperature is about 301K (28°C), agreed with the return air temperature.....169
- Figure 5.54: When the average temperature of 303K is supplied to the heat-pipes and the acrylic box, the average temperature is reduced to about 296K, a differential of 7 K. This is compared to the difference between the average temperature and the temperature of the condenser section of the heat pipes at 310K, which is 8 K. For the energy-saving calculation, the differential temperature of the average box temperature and the condenser section of the heat pipe (7 K) is used as the minimum value. The rate of energy-saving is calculated to be at 17% of the installation.....169
- Figure 5.55: The average temperature when the air temperature of 318K is supplied to the heat-pipes and the acrylic box. At 318K, the average temperature reduced is about 310K, a differential of 8 K. Compared to the difference between the average temperature and the condenser section of the heat pipe 310K which is 8 K. The rate of energy-saving is calculated to be 33% of the installation. Even though the energy-saving is higher than Case 1, the temperature 318K of the supply air at the time will be reduced and the savings return to 17%.....170
- Figure 5.56: Case 3. a and b: The path of air temperature blown from the top of the supplied air (SA) to the heat-pipes evaporator side (1) moves to the inlet of the test-box (3), mixes with the box air temperature (5-9), is forced to the outlet (2) and the condenser side of the heat-pipes (10), and exits to the ambient outlet (4). The average temperature difference is 7K.....172
- Figure 5.57: Case 3. The average temperature inside the box with supplied air of 303 K (30°C) is about 294 K (21°C).....172
- Figure 5.58: Case 3. The average temperature inside the box with supplied air of 318 K (45°C) is about 301 K (28°C)..... 173

- Figure 5.59: Case 3. The temperature of the heat-pipes heat-exchanger at the evaporator ends 1 compared to the condenser ends 2..... 173
- Figure 5.60: Case 3. The inlet air temperature at the box opening compared to the outlet air.....174
- Figure 5.61: Case 3. The average temperature inside the box compared to the heat-pipes heat-exchanger, condenser section where the outlet airflows. The supplied air is 303 K.....174
- Figure 5.62: Case 3. The average temperature inside the box compared to the heat-pipes -heat-exchanger, condenser section where the outlet airflows. The supplied air is 318 K.....174
- Figure 5.63: Comparison of the temperature of the supplied air inlet and the return air outlet of the acrylic box. The high heat from the temperature of 303K to 333K (30°C to 50°C) is being cooled by the heat-pipes at the inlet supplied-air opening of the acrylic box. The cooled air travels within the box and is blown out to the outlet. The temperature difference between the inlet and the outlet is about 20 K. Any increase or additional heat to the heat-pipes will not increase the temperature reduction capability of the installation..... 175
- Figure 5.64: Comparison of the temperature at the evaporator and the condenser section of the heat-pipes. The high heat from the temperature of 303K to 333K (30°C to 60°C) is being transferred by the heat-pipes from the evaporator to the condenser. The air passing through the evaporator will be cooled down before entering the box and will travel within the box before being blown out to the outlet. The temperature difference from the evaporator to the condenser is about 22 K.....175
- Figure 5.65: Comparison of the temperature at the acrylic box inlet and outlet. The average inlet temperature is about 321K compared to 300K (48°C to 27°C) at the outlet. About 21 K of heat is reduced by the heat-pipes transfer process in lowering the temperature of the box. The hypothesis is that the bigger the heat-pipes or the more refrigerant inside the heat-pipes, the bigger the temperature difference that could be achieved..... 176

- Figure 5.66: The graph shows the temperature recorded inside the acrylic test boxes 5 & 6 where the thermocouple is placed in the middle-lower and upper level, 7 on the left, 8 on the right side, and 9 at the air return side near the exit of the box. Thermocouple 9 shows the lowest temperature (294K) before the air is being blown away to the exit opening.....176
- Figure 5.67: The graph shows the average temperature recorded inside the acrylic test box compared to the inlet's supplied air temperature. The average box temperature is about 301K (28°C), agreeing with the return air temperature.....177
- Figure 5.68: When the average temperature of 303K is supplied to the heat-pipes and the acrylic box, the average temperature is reduced to about 294K, a differential of 9 K. For the energy-saving calculation, the differential temperature of the average box temperature and the condenser section of the heat pipe (9 K) is used as the minimum value. The rate of energy-saving is calculated to be 33% of the installation..... 177
- Figure 5.69: The average temperature when the air temperature of 318K is supplied to the heat-pipes and the acrylic box. At 318K, the average temperature reduced is about 302K, a differential of 16 K. Compared to the difference between the average temperature and the condenser section of the heat pipe 311K which is 7 K. The rate of energy-saving is calculated to be 14% of the installation..... 178
- Figure 5.70: Comparison of the temperature difference between supplied-air inlet temperature at 303K (30°C) and the average temperature of the box for all the cases.....180
- Figure 5.71: Comparison of the temperature difference between supplied-air inlet temperature at 318 K (45°C) and the average temperature of the box for all the cases.....180
- Figure 5.72: The maximum temperature recorded in Kuala Lumpur for the year 2018. The average maximum condition is about 305 K (32°C)183
- Figure 5.73: The relative humidity recorded in Kuala Lumpur for the year 2018. The average maximum condition is about 80%.....183
- Figure 5.74: Thermosiphon operation of a heat-pipe heat-exchanger and the associated thermal resistance network.....184

- Figure 5.75: The experimental unit of a. Aluminium fins. b. Staged type 3x3 heat-pipes heat-exchanger excluding the fins.....185
- Figure 5.76: Case 1: The air path and temperature points..... 186
- Figure 5.77: Case 1: The path of air temperature blown from the supplied air (SA) to the heat-pipes evaporator side (1) moves to the inlet of the test-box (3), is mixed with the box air temperature (5-9) and is forced to the outlet (2) and the condenser side of the heat-pipes (10), and then exits to the ambient outlet (4). The average temperature difference is between 8K to 10K..... 188
- Figure 5.78: Case 2: The air path and temperature points..... 188
- Figure 5.79: Case 2: The path of air temperature blown from the supplied air (SA) to the heat-pipes evaporator side (1) moves to the inlet of the test-box (3), is mixed with the box air temperature (5-9), forced to the outlet (2) and the condenser side of the heat-pipes (10), and then exits to the ambient outlet (4). The average differential temperature is 8K.....189
- Figure 5.80: Case 3: The air path and temperature points..... 190
- Figure 5.81: Case 3: The path of air temperature blown from the top of the supplied air (SA) to the heat-pipes evaporator side (1) moves to the inlet of the test-box (3), is mixed with the box air temperature (5-9), forced to the outlet (2) and the condenser side of the heat-pipes (10), and then exits to the ambient outlet (4). The average differential temperature is 7K..... 191
- Figure 5.82: The heat-pipes with R134a as refrigerant show that the lowest temperature is 296.5 K. The inlet and outlet difference is 3.5K.....192
- Figure 5.83: The heat transfers from the R134a heat-pipes heat-exchanger could achieve a temperature difference of 7 K (300K – 307K) as shown by ANSYS Fluent simulation.....192
- Figure 5.84: The temperature recorded by the thermocouple inside the test box has a difference of about 3K.....193

- Figure 5.85: The heat-pipes heat-exchanger is capable of transferring heat of about 2.3K to 3.3K from the evaporator end towards the condenser end.....194
- Figure 5.86: In Case 4, the polynomial curve predicts that the outlet temperature stays at about 300.7 K (27.7°C)194
- Figure 5.87: The temperature recorded by the thermocouple inside the test box has a difference of about 2K.....195
- Figure 5.88: The heat-pipes heat-exchanger is capable of transferring heat of about 1.3K to 1.6K from the evaporator end towards the condenser end.....195
- Figure 5.89: In Case 5 the polynomial curve predicts that the outlet temperature stays at about 301.5 K (28.5°C). With added heat to the heat-pipes, the heat-pipes will not be capable of converting any more heat and the temperature will be linear for both the inlet and outlet.....196
- Figure 5.90: The energy-saving recorded in the experiment compared to the temperature difference of the heat-pipes heat-exchanger Q_o and Q_o' . The graph shows that the heat-pipes heat-exchanger could save an average of 20% of the installation....197
- Figure 5.91: The graph shows the energy-saving using a heat-pipes heat-exchanger for Case 1 (303 K)200
- Figure 5.92: The graph shows the sensible cooling load of Case 1 with a supplied inlet temperature of 303 K.....200
- Figure 5.93: The graph shows the energy-saving using a heat-pipes heat-exchanger for Case 1 (318)200
- Figure 5.94: The graph shows the sensible cooling load of Case 1 with a supplied inlet temperature of 318 K.....201
- Figure 5.95: The graph shows the energy-saving using a heat-pipes heat-exchanger for Case 2 (303K)201
- Figure 5.96: The graph shows the sensible cooling load of Case 2 with the supply inlet temperature of 303 K.....201

Figure 5.97: The graph shows the energy-saving using a heat-pipes heat-exchanger for Case 2 (318).....	202
Figure 5.98: The graph shows the sensible cooling load of Case 2 with the supply inlet temperature of 318 K.....	202
Figure 5.99: The graph shows the energy-saving using a heat-pipes heat-exchanger for Case 3 (303).....	202
Figure 5.100: The graph shows the sensible cooling load of Case 3 with the supply inlet temperature of 303 K.....	203
Figure 5.101: The graph shows the energy-saving using a heat-pipes heat-exchanger for Case 3 (318).....	203
Figure 5.102: The graph shows the sensible cooling load of Case 3 with the supply inlet temperature of 318K.....	203
Figure 5.103: Comparison of the energy-saving using a heat-pipes heat-exchanger for all cases.....	204
Figure 5.104: The outlet air temperature and the average temperature of the acrylic box in all cases.....	204
Figure 5.105: Schematic drawing of a building that uses a solar air conditioning system. A heat-pipes heat-exchanger is used as passive equipment to reduce the supplied air that enters the building.....	209
Figure 5.106: The proposed schematic process of air distribution from the ambient to the room. The heat-pipes feed the cooling coil with a lower temperature of supplied air from the outdoor ambient temperature.....	209
Figure 5.107: Normal solar air conditioning operating condition for a supplied-air temperature of 303 K (30°C).	210
Figure 5.108: Normal air conditioning operating condition for a supplied-air temperature of 318K (45°C).	211
Figure 5.109: The schematic process of air distribution.....	212

Figure 5.110: The air states comparison between 303K and new supplied temperature of 296.6K (23.6°C) for Case 1.....	213
Figure 5.111: The air states comparison between 303K and new supplied temperature of 300.08K (27.08°C) for Case 2.....	213
Figure 5.112: The air states comparison between 303K and new supplied temperature of 299.15K (26.15°C) for Case 3.....	214
Figure 5.113: The air states comparison between 318K and new supplied temperature of 302.56K (29.56°C) for Case 1.....	214
Figure 5.114: The air states comparison between 318K and new supplied temperature of 303.88K (30.88°C) for Case 2.....	215
Figure 5.115: The air states comparison between 318K and new supplied temperature of 298.77K (25.77°C) for Case 3.....	215
Figure 5.116: Comparison of the sensible heat between 303 K and 318 K for all cases.....	216
Figure 5.117: The different air supply inlet and outlet for all cases. The parameter shows the location of thermos-couple for temperature reading.....	217
Figure 5.118: The different temperature comparison of cases, between supplied-air inlet at 303K (30°C) and the box average temperature.....	218
Figure 5.119: Comparison of temperature difference for all the cases between the supplied air inlet at 318 K (45°C) and the box average temperature.....	218
Figure 5.120: Air distributions for all cases. The simulations were run by ANSYS Fluent software	221

Chapter VI CONCLUSION

Figure 6.1: A proposed schematic drawing to upgrade the HVAC system embedded with a hybrid system for Building 11 the University of Technology Sydney.....	228
--	-----

Figure 6.2:	The plant room with the Organic Rankine Cycle (ORC) in Building 11 University of Technology Sydney.....	228
Figure 6.3:	The fluid thermal expansion system in Building 11 University of Technology Sydney.....	228
Figure 6.4:	The PV panels and the wind turbine on the rooftop of Building 11, University of Technology Sydney.....	230

LIST OF SYMBOLS

%	Relative humidity percentage
ε	Dissipation rate, m^2/s^3
η	Efficiency
g	Gravity acceleration, m/s^2
$^{\circ}\text{C}$	Temperature Celsius
C_{μ}	Empirical constant, 0.09
T_i	Turbulence intensity
U_{ave}	The average flow velocity, m/s
$U_j (j = 1 - 3)$	A component of the average velocity vector, m/s
μ_t	Turbulent viscosity, $\text{Pa}\cdot\text{s}$
A_s	Solar panel surface area
COP	Coefficient of performance
GW_{el}	Giga Watts of electrical
GW_{th}	Giga Watts of thermal
I_p	Solar irradiation
K	Temperature Different
K	Temperature Kelvin
K	Turbulent kinetic energy, m^2/s^2
κ	Von Karman's constant, 0.41

l/s	litre per second
L	Length scale, m
Q_c	Condenser work done kJ/kg
Q_e	Evaporator work done kJ/kg
Q_e	Cooling power
Q_s	Solar power
T_c	Condensing temperature °C
T_e	Evaporating temperature °C
TW_{el}	Total Watts of electrical
TW_{th}	Total Watts of thermal
W, kW, kWh	Watts, kilowatts, kilowatt hour,
W/m^2	Watts per square meter
W/m^3	Watts per cubic meter
W	Compressor work done kJ/kg
x	Flash gas %

ABBREVIATIONS

ABM	Australian Bureau of Meteorology, Climate Statistics.
ACORN-SAT	Australian Climate Observations Reference Network – Surface Air Temperature.
AEC	U.S. Atomic Energy Commission
AEL	United Kingdom Atomic Energy Laboratory

AER	Australia Energy Resource.
AFMC	Australasian Fluid Mechanics Conference
ASHRAE	American Society of Heating, Refrigeration and Air Conditioning Engineers.
ASME	American Society of Mechanical Engineers
CFC/HCFC	Chlorofluorocarbon/ Hydro-chlorofluorocarbon.
CFD	Computational Fluid Dynamics.
CLTD	Cooling Load Temperature Different.
CPU	Central Processing Unit
DOS	Daily Observation of Sydney.
ESDU	Engineering Sciences Data Unit, United Kingdom
GWP	Global Warming Potential.
H ₂ O-LiBr	Water- Lithium Bromide
HPHE	Heat-pipes Heat-exchanger
HVAC	Heating, Ventilating, and Air-Conditioning.
IEA	International Energy Agency.
IIF/IIR	International Institute of Refrigeration
IMECE	International Mechanical Engineering Congress and Exposition
LHP	Loop Heat-pipes
NH ₃ -H ₂ O	Ammonia-Water
<i>NTU</i>	Number of Transfer Units
ODP	Ozone Depletion Potential.
PV	Photovoltaic Panel

RANS Reynolds-Averaged Navier–Stokes Equations

UTS University of Technology Sydney.

CONTENTS

Declaration: Certificate of Authorship/Originality	ii
Abstract	iv
Acknowledgment	vi
Contribution by the Author	vii
List of Tables	ix
List of Figures	xiii
List of Symbols	xxxv
Abbreviations	xxxvi

CHAPTER I: INTRODUCTION

1.1	Introduction.....	1
1.2	Research Objectives	5
1.3	Aims and Research Scope	7
1.4	Research Benefits.....	8
1.5	Problem Formulation.....	9
1.6	Thesis Structure.	10
1.7	Summary.	11

CHAPTER II: LITERATURE REVIEW

2.1	Introduction.	12
2.2	Thermal Comfort Conditions.....	13
2.3	Passive Cooling Technology for Thermal Comfort Conditions.....	16
2.3.1	Solar Cooling Technology.....	17
2.3.2	Solar Heat and Thermal Market.....	18
2.3.3	Solar Air Conditioning: Cooling and Heating.....	20
2.3.4	The Main Parts of Solar Cooling System.....	23
2.3.5	Thermal Mass.....	25
2.3.6	Natural Ventilation.	26
2.3.7	Building Shades.....	27
2.3.8	Active Cooling Technology.....	27
2.3.8.1	Vapour Compression System.	27
2.3.8.2	Absorption System.	29
2.3.8.3	Adsorption System.	30
2.4	Heat-pipes Heat-exchanger for Cooling Technology.....	31
2.4.1	Heat-Pipes Heat-Exchanger for Passive Cooling Equipment.....	31
2.4.2	Heat-pipes Heat-exchanger Operations.....	32
2.4.3	Experimental Study on Heat-pipes.	34
2.4.4	Historical Development of Heat-pipes	34
2.4.5	Principles, Operation of Heat-pipes.	35
2.4.6	Types of Heat-pipes	38

2.4.7	Gravity-Assisted Wickless Heat-pipes.....	38
2.4.8	Capillary-Driven Heat-pipes.....	39
2.4.9	Annular Heat-pipes.	40
2.4.10	Gas-Loaded Heat-pipes	40
2.4.11	Loop Heat-pipes	41
2.4.12	Other Design of Heat-pipes.	42
2.4.13	Working Fluids and Temperature Ranges of Heat-pipes Application.....	43
2.5	Simulation of Heat-Pipes Heat-Exchanger Using Computational Fluid Dynamics.....	46
2.5.1	Background.....	48
2.5.2	Simulation Works on the Passive Cooling Using Computational Fluid Dynamics.	48
2.6	Knowledge Gap: Combining Solar Air-Conditioning and Heat-Pipes Heat-Exchanger. .	51

CHAPTER III: MATHEMATICAL MODEL

3.1	Introduction.	56
3.2	Solar Cooling.....	59
3.3	Formula for Solar Thermal Refrigeration and Heat Exchangers.....	60
3.3.1	Solar Based Cooling and Refrigeration Systems.....	60
3.3.2	Solar Thermal Refrigeration.....	61
3.3.3	Electrical Refrigeration System.....	63
3.3.3.1	Refrigerating Effect (W_e).....	64
3.3.3.2	Compressor Work-done (A_w).	64
3.3.3.3	Condensing Effect (W_c).....	65
3.3.3.4	Coefficient of Performance (COP).	66

3.3.3.5	Compression Ratio.	66
3.3.3.6	Suction Gas Density.....	66
3.3.4	Heat-exchanger	66
3.3.5	Heat-pipes Heat-exchanger.....	67
3.3.6	Blower.	69
3.3.7	Procedure for Energy-saving.....	69
3.4	Formula for the Computational Fluid Dynamics	69

CHAPTER IV: RESEARCH METHODOLOGY

4.1	Introduction.	72
4.2	Project Arrangement for Experimental Cases.....	85
4.2.1	Solar Air-Conditioning.....	86
4.2.2	Air-conditioning System.....	87
4.2.3	Blower and Heater.....	87
4.2.4	Air Inlet and Outlet Opening.....	87
4.2.5	Heat-pipes Heat-exchanger	90
4.2.6	Design of the System: Case 1.....	91
4.2.7	Design of the System: Case 2.....	93
4.2.8	Design of the System: Case 3.....	95
4.2.9	Design of the System: Case 4.....	97
4.2.10	Design of the System: Case 5.....	99
4.2.11	Table of Working Parameters.....	99

4.3	Tools and Measuring Equipment.....	101
4.3.1	Heat-pipes Heat-exchanger and the Acrylic Box.....	101
4.3.2	Heater and Blower.....	102
4.3.3	Digital Equipment.....	103
4.3.4	Hygrometer.....	104
4.3.5	Anemometer.....	105
4.3.6	Hot-wire Anemometer.....	105
4.3.7	Thermal Imaging Equipment.....	106
4.3.8	Data Logger.....	107
4.3.9	Thermocouple.....	108
4.4	Data Collection.....	108
4.4.1	Monitoring Parameter.....	108
4.5	Simulation Using Computational Fluid Dynamics.....	110
4.5.1	Simulation Study on Heat-pipes Heat-exchanger.....	112
4.5.2	Mesh, Solver and Post Processing of Heat-pipes heat-exchanger.....	114
4.5.3	Simulation of a Heat-pipes Heat-exchanger as Passive Cooling Equipment for Pre-Cooling of Air Intake.....	117
4.5.4	Simulation of a Heat-pipes Heat-exchanger with Driven Ventilation.....	119

CHAPTER V: RESULTS AND DISCUSSIONS

5.1	Introduction.....	128
5.2	Flow Field and The Temperature Distribution in The Room Simulation Using Computational Fluid Dynamics.....	129

5.2.1	Simulation of a Heat-pipes Heat-exchanger with High Ambient Outdoor Temperature Condition.....	130
5.2.2	Simulation of a Heat-pipes Heat-exchanger Effect on an Air-Cooled Condenser.	134
5.3	Solar Radiation.	140
5.3.1	Experimental Study on Solar Energy Air Conditioning Booster.....	141
5.4	Heat Transfer of Heat-pipes Heat-exchanger	147
5.4.1	Case 1.....	153
5.4.2	Case 2.....	163
5.4.3	Case 3.....	171
5.4.4	Case 4.....	181
5.4.4.1	Experimental Study of a Heat-Pipes Heat-Exchanger as Passive Cooling Equipment for A Tropical Climate Condition.....	181
5.4.4.2	Problem Description: Thermal Modelling.....	183
5.4.4.3	Summary of the Temperature Pathway Graph by Points of Measurement....	186
5.4.4.4	Estimated Energy-Saving by the Heat-Pipes Heat-Exchanger.....	196
5.4.4.5	Conclusion.....	197
5.5	Estimated Energy-saving by the Heat-pipes Heat-exchanger by Energy Calculation Method.....	198
5.6	The Temperature Comparisons Between the Simulation and Experimental Works.....	204
5.7	Estimated Energy savings of the Solar Air-Conditioning with Heat-pipes Heat-exchanger in using Psychrometric Chart Calculations.	208
5.7.1	303K vs New Supply Air Temperature.....	212

5.7.2	318K vs New Supply Air Temperature.....	214
5.7.3	Summarise on the Comparison of New Supply Air Temperature.....	215
5.8	Summarizes on the Temperature Profile and Estimated Energy Savings All Cases.....	217

CHAPTER VI: CONCLUSION

6.1	Achievement of this research.....	222
6.2	Suggestions.....	226
6.2.1	Drawback.	227
6.2.2	Application to UTS HVAC System.....	228

REFERENCES.....	231
------------------------	------------

APPENDIXES

Appendix 1: Psychrometric Chart.....	242
Appendix 2: Heat-pipes Heat-exchanger Calculation.....	243
Appendix 3: Solar Energy Output Calculation.....	244
Appendix 4: Simulations of Heat-pipes Heat-exchanger with different configuration	252
Appendix 5: Study of Wind-Assisted Energy for Cooling System in Bangi, Malaysia.....	246
Appendix 6: Simulation Study On Cooling a Small Domestic Refrigeration System Using Solar-Assisted Energy in Bangi, Malaysia	255

LIST OF REVIEWED PAPER ATTACHED.....	253
---	------------

CHAPTER I

INTRODUCTION

CHAPTER OVERVIEW

This chapter discusses the research objectives and the background of the work. It explains the necessary factors that lead to comfort cooling maintenance while reducing energy consumption. The importance of solar energy applications in comparison with conventional electric grid applications is also discussed. The research aimed to examine the use of solar thermal energy and ‘heat-pipes heat-exchanger’ as passive cooling equipment. The thesis structure and contents are explained in six chapters which discussed the work that was carried out and the motivations related to the subject.

1.1 INTRODUCTION

The study of comfort cooling is inspired by two components in cooling technologies: the interest in passive cooling and the search for low energy building applications using solar energy. Comfort cooling is an essential factor for healthy and productive lives for people living in interior building spaces. Temperature, humidity, and fresh airflow within a room are important elements that keep a room ‘*comfortable*’ for quality human life. As suggested by the American Society of Heating, Refrigeration and Air Conditioning Engineers (ASHRAE 1989), there is a link between internal air and fresh air supply. Seppanen (2002) said that a prolonged sufficient amount of fresh air is required to make the environment safe and the internal air healthier. Temperature control plays an important role in various situations as it affects humidity as well. Comfort cooling in the ‘90s was managed by a heating, ventilation and air conditioning (HVAC) system and was intended to isolate the internal and outdoor climate conditions. Such HVAC systems suffered from high space heating costs (Voss 2005). Nowadays, a good indoor climate for comfort cooling refers to healthy approaches to technical services. Although there is a certain level of discomfort, dissatisfaction, and complaints regarding ‘*sickroom syndrome*’, an HVAC maintains the objective

of thermal comfort. There are options of comfort control by introducing natural ventilation and passive-cooling equipment to the system to suit the purpose. Zimmermann (2003) mentioned that a combination of integrated measures to achieve passive-cooling is a pre-requisite if summer comfort is to be ensured without actively cooling or dehumidifying the inlet air. Westphalen (2001) stated that buildings are designed to operate with combined cooling and heating equipment to provide efficient cooling with a minimum rate of external air. Unfortunately, this design lacks sufficient continuous fresh air intake as recommended by ASHRAE guides. This study, therefore, examined the options of comfort, control, and the need for fresh intake air in building spaces. A survey of commercial buildings in Washington, DC by Douglas (2006) found that humidity and internal temperature are unstable with the conventional cooling system.

The Australian Climate Observations Reference Network – Surface Air Temperature (ACORN-SAT) has monitored climate variability and change in Australia for the past 100 years. The data are robust and comparable through time, enabling climate researchers to better understand long-term changes in monthly and seasonal climate as well as changes in day-to-day weather, such as the frequency of heat and cold extremes. The 100 years' worth of data shows that there is a permanent increase in annual temperature for Australia and it is still increasing.

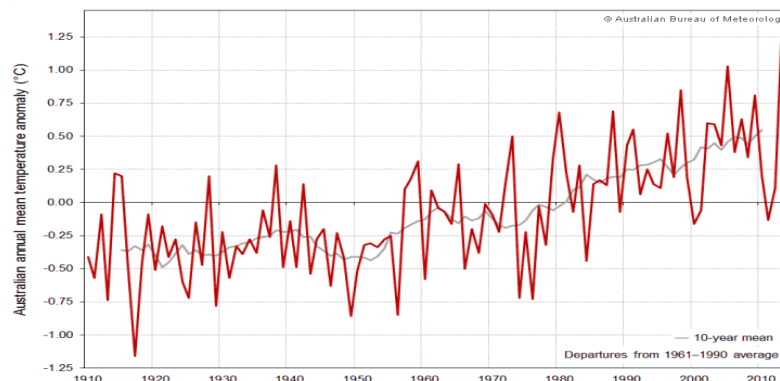


Figure 1.1. Annual mean temperature anomalies for Australia (red) with a 10-year mean (light grey). Departures are from the 1960–1990 average. *Australian Climate Observations Reference Network – Surface Air Temperature (ACORN-SAT)*.

To maintain the fresh air quality in an internal space, ASHRAE 2001 suggested a new guide to replace ASHRAE 1981. The required air intake changes over 20 years are shown in Table 1.1.

Table 1.1: A 20-year comparison of the required fresh air intake between ASHRAE 1981 and ASHRAE 2001. *The American Society of Heating, Refrigerating and Air-Conditioning Engineers.*

Building type	ASHRAE 62 (1981)	ASHRAE 62 (2001)	Increment
	L/s per person	L/s per person	%
Hotel	7.3	15	205
Auditorium	3.3	8	242
Meeting Room	3.4	10	294
Office	2.5	10	400

These changes are due to transformations in living standards and comfort levels as thermal comfort has become a necessity. Looking at the temperature graphs of New South Wales, Australia for 2017 in Figures 1.2a and b, the required temperature for thermal comfort to operate is within the low temperature of 8.1 °C for heating and 29.6 °C for cooling. The Daily Observations of Sydney’s recorded average temperatures from January to December 2017 are shown in Table 1.2.

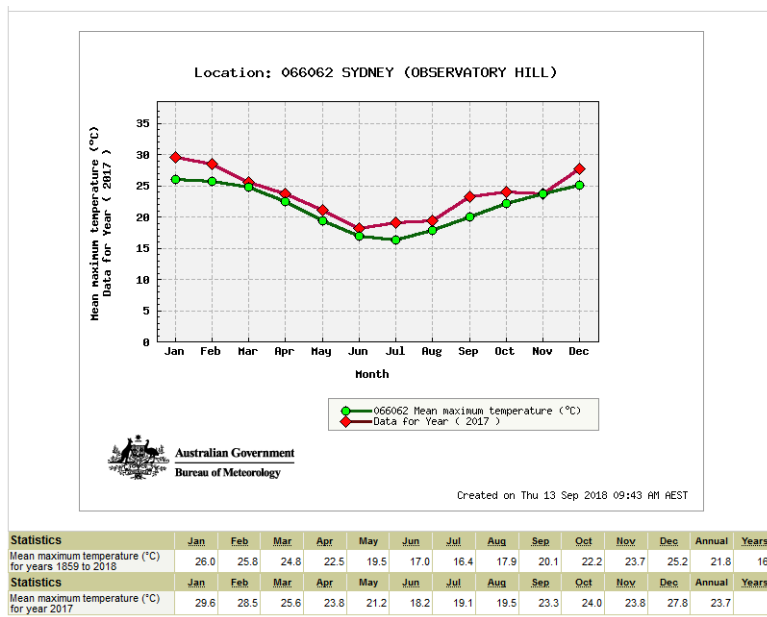


Figure 1.2 a

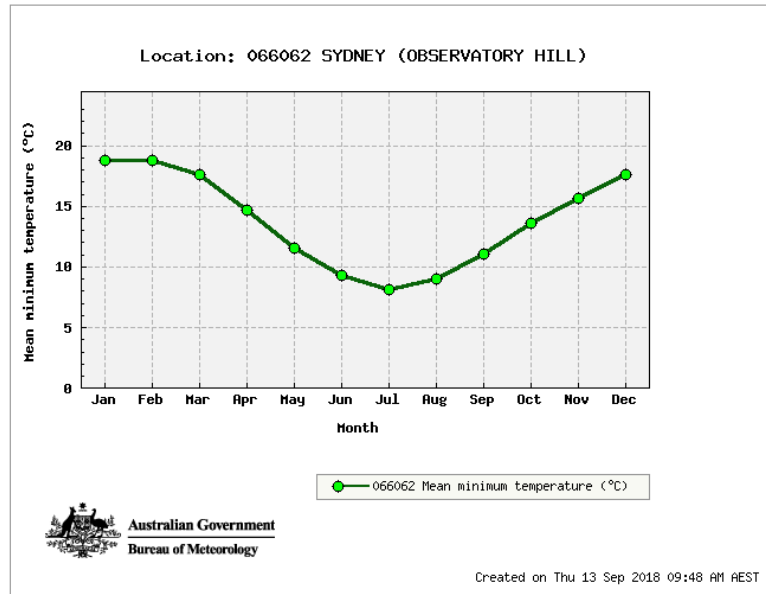


Figure 1.2 b

Figure 1.2a and b: The average temperature of New South Wales recorded in 2017 compared to the data from 1859. The temperature of Sydney had increased by about 4K during the 160 years (1859 to 2017). *The Daily Observation of Sydney*.

Table 1.2: The average temperature recorded in NSW in 2017. *The Daily Observation of Sydney*.

	Low-Temperature °C	High-Temperature °C
Minimum	8.1	18.8
Maximum	16.4	26

Temperatures ranging from 5.5°C to 36.5°C require large amounts of energy for cooling and heating. Solar energy applications have been used as an alternative power supply for the air conditioning system. Hoefker (2001) mentioned that the peak of electricity demand for cooling is normally during the peak sunrise. The heat from the sun will heat the building surfaces and the room requires more energy with the air conditioner running at full load. Inversely with solar energy, the more heat achieved from the sun, the less electrical energy will be used. Solar heat and thermal industries have been around since the beginning of the '90s. Solar panel collectors have been installed in over 49 countries involving 4 billion people. By 2007, a total of 209.2 million m² of solar panels had been installed. This corresponds to about 146.8 GW_{th} thermal capacity. By the end of 2017, the cumulated solar thermal capacity reached 472 GW_{th}, with wind power at 540 GW_{th}, and a total of 402 GW_{th} from photovoltaic installed capacity.

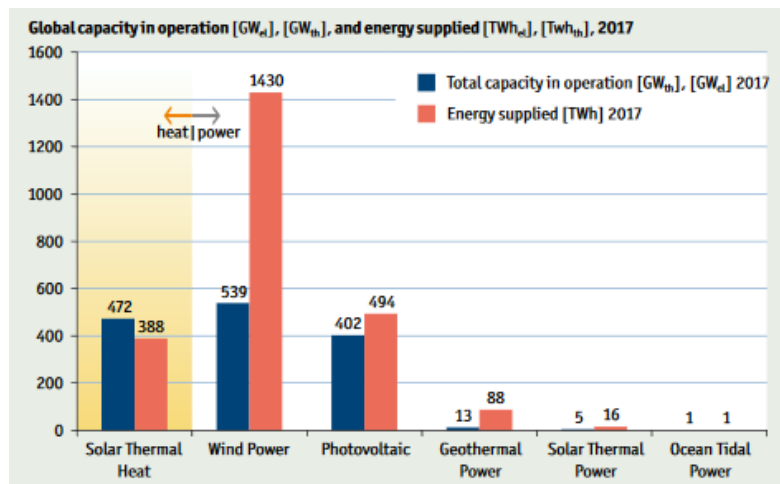


Figure 1.3: Global capacity in operation (GW_{el}), (GW_{th}) 2017 and annual energy yields (TWh_{el}), (TWh_{th}). Sources: AEE INTEC, Global Wind Energy Council (GWEC), Solar Power Europe, REN21-Global Status Report 2018.

This research examined the use of solar energy applications to run a cooling system, in which the passive-cooling equipment helped by decreasing the temperature of the intake air. The combination of these elements reduced the energy required by the room's cooling load. Additionally, the thermodynamic limits of comfort cooling in the solar energy and heat-pipes heat-exchanger application combination are also described. As the solar energy application in this study had no direct influence on cooling effects, data from findings of previous studies were used as a guide and reference.

In this study, passive technology using a heat-pipes heat-exchanger was examined and its development was discussed. The application of heat-pipes in comfort cooling was investigated using computational fluid dynamics software for flow patterns and temperature gradients in a room. While comparisons using solar thermal energy for comfort cooling were performed, the heat-pipes heat-exchanger was the main focus in the context of energy-saving for comfort cooling.

1.2 RESEARCH OBJECTIVES

Vapour-compression compressors are widely used in refrigeration and air-conditioning applications to obtain the desired cooling or heating temperature. By manipulating pressure in the refrigeration cycle, the thermodynamic state of the refrigeration medium allows for the absorbing and desorbing of heat. One has to remove heat from the required space to a place where it is not needed to feel colder; inversely, one has to add heat to their environment to feel warmer. The drawback is that the 'refrigeration cycle' process consumes energy. Linden (1999) stated that 50%

of the total energy used for typical buildings in terms of cooling and heating applications comes from indoor air-conditioning. About 30% of US total energy consumption are in non-domestic buildings, and 30% of that fraction is for the use of cooling and heating.

Cooling and heating using solar energy have been widely used in domestic and commercial air conditioning and refrigeration applications to reduce energy consumption. In Australia, where solar energy is in-grid, users can benefit by selling back the excess energy to the local electrical grid; however, in some countries, solar excess energy is a waste. Solar panels absorb the heat, converting it into electricity and using it as a driver to turn on the compressor. Even though it is widely used, solar refrigeration and cooling are not competitive with conventional systems. Lowering the first cost of the systems is still the main target to pursue to allow this technology to enter the market. Atkins (2007) conducted a study in Sydney that showed a reduction of 25% to 33% of occupant comfort satisfaction with naturally ventilated mixed-mode buildings. As suggested by Jamaluddin (2014), Nicol (2002), Su (2009), and Wong (2002), compared to heating, ventilating and air conditioning (HVAC) systems, natural ventilation is the best approach in providing comfort. However, not much attention has been paid to the room or space where cooling is required. The heat-pipes heat-exchanger is the answer for space cooling as it is passive cooling and heating equipment that is capable of transferring heat without a power source.

This research aimed to study the heat transfer coefficient of a solar energy compression cycle with an embedded heat-pipes heat-exchanger at the evaporator and condenser. Heat-pipes using R134a as working fluid was tested for performance as well as efficiency. The test results for the room temperature were recorded and compared to normal electric compression and domestic air-conditioner. The components of the study included a variable speed blower fan to create airflow, a variable temperature heater element to heat a room/test-box and a finned type cross-flow in-line straight heat-pipes heat-exchanger filled with refrigerant R134a. The location of the heat-pipes was on the sidewall of a room for Case 1 and the top side of a room for Case 2 and Case 3. A transparent acrylic box sized 1000 mm x 820 mm x 620 mm was used to replicate a room.

There has been no research on straight heat-pipes heat-exchanger with this mode before; however, some related research work on outdoor cabinets include that of Priyadumkol (2014) who studied energy conservation in data centres, Yuping (2008) who studied the cooling system of outdoor cabinets by simulation and experimentally using underground heat-pipes, and Marongiu

(1998) who proposed the design and development of passive cooling for an outdoor cabinet. The research was all on a closed-loop thermo-siphon heat pipe.

This research covered a computational fluid dynamics simulation study and a practical project which offers an energy strategy to be benefited from passive cooling. The practical project offers data and a novel method on how comfort cooling can be achieved using a heat-pipe exchanger. Data were compared to a conventional system and solar energy assisted air conditioning system. The performance of both systems was validated using mathematical and software calculations.

Computational Fluid Dynamics (CFD) software such as CFD-ACE and ANSYS Workbench/Fluent were used to run the heat-pipes heat-exchanger simulation project. The findings and data from each simulation were recorded and related conference papers have been presented and published. Air conditioning software such as cooling load temperature differentials (CLTD), psychrometric table, chart, and pressure-enthalpy ($p-h$) programmes were used to assist in the validation of the proposed system model. The variables from the data and the finding can be used to formulate an energy-saving system for comfort cooling.

1.3 AIMS AND RESEARCH SCOPE

The primary compositions of the research are listed below:

- To design solar-energy, air conditioning system for comfort cooling combining a heat-pipes heat-exchanger as air pre-cooling equipment. As the heat-pipes heat-exchanger is passive cooling equipment that consumes zero energy, the refrigeration system would only require minimal energy from the solar energy source. The system should be applied to buildings where the ambient condition is warmer for an optimum rate of energy-saving.
- To analyse heat-pipes heat-exchanger criteria in a building using simulation and a practical test unit. This would be used to predict the air conditioning system coefficient of performance. Comparisons to other systems would be made to evaluate the prediction.
- To make energy-efficient calculations of the cooling system with the assistance of solar energy as the source.

- To analyse the installation perspective of the combined solar energy system and the heat-pipes system and propose a new thermal comfort cooling using solar energy and heat-pipes based on the test results.

1.4 RESEARCH BENEFITS

The energy demand has been increasing while the output sources have been declining each year. This has resulted in the increase of electrical energy tariffs and prices worldwide. This research, therefore, offers energy-saving solutions by using the combined solar-energy and passive-cooling system as compared to the direct connected electrical cooling system. The use of solar energy and heat-pipes technology will result in the following contributions:

- The heat-pipes heat-exchanger technology with assisted solar energy is particularly beneficial in a hot climate country as it would result in savings of electrical energy. In Australia, where the temperature is at an intermediate level almost all year round, the use of the system will reduce power consumption. Environmental quality will be better with the respective reduction of carbon dioxide emissions.
- Reducing the dependence on the electrical grid connections, especially in cooling mode. The air-conditioner is well known as the major contributor to energy consumption. Solar assisted energy combined with heat pipes could be beneficial to maintain comfort cooling.
- With the use of heat-pipes heat-exchanger as passive cooling without the need of moving equipment to work, the risk of CFC/HCFC substance gas leaking into the environment can be minimised.
- The advantage of using heat-pipes heat-exchanger is that the amount of the refrigerant in the pipes is only one-third of the pipe total volume. The internal structure of the tube needs liquid, void and vapour sections to cause the heat to flow into operational. Compared to the vapour compression system, the amount of refrigerant in the heat-pipes heat-exchanger is at its minimum. Environmentally, global warming and the ozone depletion potential could be minimised.
- There are advantages of using heat pipes with the air conditioning systems in retrofits and new applications. For retrofit applications, the operating costs are reduced because of the reduction in energy (kWh) and peak demand (kW) consumptions. For

new installations, the heating and cooling equipment can be downsized, resulting in lower equipment and operating costs. To create natural ventilation in the stale ambient air, heat-pipes are fitted to a roof of a building to naturally induce stale air to the outside using solar heat and to supply fresh air into the building.

- The vaporisation process in the heat-pipes pushes the refrigerant to the other end of the pipe and releases the heat to the ambient. The air density differential between the indoor and outdoor moves the air to a lesser density and creates natural ventilation. This operation with heat-pipes requires a small amount of heat between the evaporator end and the condensation end, and without any energy sources.
- The motivation for the work is influenced by the design of the heat-pipes heat exchanger, the range of temperature application and the ability to transport high rates of heat at ambient temperature levels.
- The disadvantages of the system are due to the dimension of the heat-pipes heat exchanger and the solar radiation that depends on the orientation of the installation. The heat-pipes heat exchanger requires more refrigerants and larger tube dimensions to transfer heat in a large scale building. The solar energy collection and harvest volume are different from a country to another country depending on the time of exposure to the sun.

1.5 PROBLEM FORMULATION

The University of Technology Sydney, especially the Faculty of Engineering and IT, has been applying energy-based research in its academic environment. This helps researchers understand the importance of preserving natural energy compared to the limited and expensive hydro or fossil energy. The university has installed a thermal storage, the cooling system in Building 11 tower to show their commitment and to reduce energy consumption. A few types of studies have been developed in investigating natural airflow and solar energy; however, only a few have considered combining heat reduction equipment in the research.

The focus of this research is on heat cycle innovations to reduce electrical energy consumption by introducing a solar energy refrigeration cycle with the assistance of a heat-pipes heat-exchanger application. It is hoped that eventually, the new combined system will be used widely, especially in warm and hot environments where solar radiation is plentiful. As the

application of heat-pipes is maintenance-free, the cost of the heat reduction process will be reduced.

1.6 THESIS STRUCTURE

The thesis involves theoretical calculation, simulations, and practical experiments. It is organised in chapters as described below:

- Chapter I. Introduction. The chapter discusses the research objectives and the background of the study. It explains the necessary factors that lead to the research.
- Chapter II. Literature Review. The chapter explains the research work related to the cooling system. The solar energy, air conditioner and heat-pipes heat-exchanger applications are discussed. Additionally, past research work regarding active and passive cooling is reviewed in this chapter.
- Chapter III. Mathematical Model. A detailed mathematical model for each component, including a discussion on the theoretical background, equation, and formula used in the processes in this study are presented in this chapter. The energy-saving potential is also discussed.
- Chapter IV. Research Methodology. The design and experimental testing of the components are discussed in this chapter. The locations of the heat-pipes are explained in the test and measurement section of this chapter. Additionally, several air intake locations with the application of the heat-pipes heat-exchanger are also discussed.
- Chapter V. Result and Discussion. In this chapter, the mathematical models of the components are analysed and the experimental results are discussed. The simulation results of the CFD-ACE and ANSYS-Fluent are presented. New developments and progress related to previous efforts in energy-saving and comfort cooling are also examined. Relevant published papers that relate to this study are also attached.
- Chapter VI. Conclusion. This chapter summarises the research results of the experimental work conducted. It also highlights the proposed suggestions regarding the designed system. Finally, guidelines for using heat-pipes for future work are established.

1.7 SUMMARY

The understanding of how the solar energy system and the heat-pipes heat-exchanger component work would provide an important resource in developing an economic and friendly system. This would create an opportunity for the system to be used commercially, especially in tropical climates. Hence, it is the objective of the research to test the performance of the system through simulations and experimental studies.

CHAPTER II

LITERATURE REVIEW

CHAPTER OVERVIEW

This chapter discusses comfort cooling requirements and its technologies. The ASHRAE Standards 55 was taken as the threshold of comfort cooling, which requires 295.5 K to 298 K (22.5°C to 25°C) and 40% to 60% relative humidity as a human comfort zone. Solar energy technologies and active and passive cooling strategies are also discussed. The classic and latest method of removing heat applications is presented. The heat-pipes heat-exchanger technology as passive cooling equipment is discussed. The knowledge gap between the previous methodology and findings is reviewed.

2.1 INTRODUCTION

The comfortable temperature that we feel from an air conditioner is the result of the process of a cycle that reduces heat in our room. There are various types and processes of air conditioning, from domestic to commercial. Domestic air conditioning normally tends to have a temperature range of 293 K to 300 K (20°C to 27°C), irrespective of the types of requirements of the installation. In contrast, commercial air conditioning temperatures depend on the requirements. For example, a shopping complex has a different temperature requirement than a hospital while a computer data centre temperature requirement is different from that of an office room even when both are in the same building.

Ambient temperature changes all day; thus, cooling and heating is needed all year round. All of these types of systems require a power '*electricity*' source to perform the heat transfer processes. The medium of heat transfer in a refrigeration cycle is a refrigerant, which is high in either ozone depletion potential (ODP) or global warming potential (GWP). Conventional air

conditioning systems, therefore, need to be upgraded and enhanced to be environmentally friendly and cost-saving.

2.2 THERMAL COMFORT CONDITIONS

Comfort cooling plays a significant role in people's health and work productivity. To comply with the comfort zone, the built environment should be in the range of 295.5 K to 298 K (22.5 °C to 25 °C) and between 40% to 60% humidity (ASHRAE Standard 55). ASHRAE's (2003) psychrometric chart shows that the need for comfort cooling is different from one person to another. Some active people require more cooling while a static person in a building requires less cooling than a moving person.

Figure 2.1 shows the guide for comfort cooling by ASHRAE Standard 55. Building a comfort zone depends much on the ambient temperature and the surrounding air movement. Figure 2.2 shows the air movement needed to feel comfortable. All of these cooling and heating operations require energy to operate the refrigeration cycle. There are two types of cooling, namely passive and active.

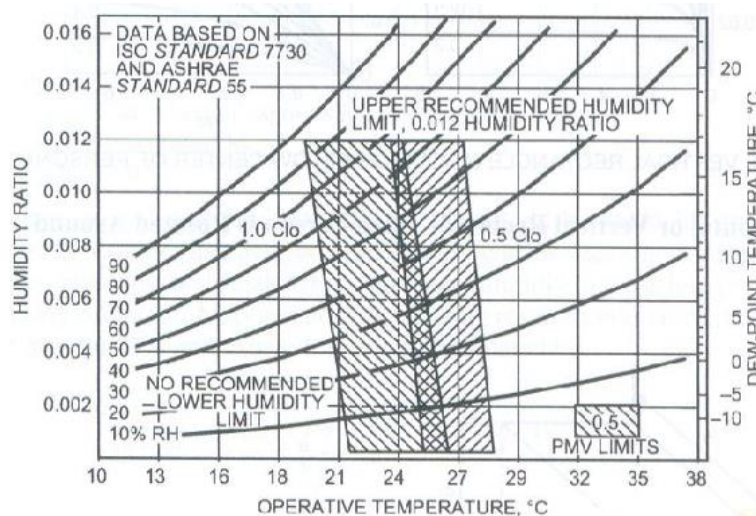


Figure 2.1: ASHRAE comfort chart. The comfort zone is between 295.5 K to 298 K (22.5 °C to 25 °C) and between 40% to 60% humidity. *The American Society of Heating, Refrigerating and Air-Conditioning Engineers Standard 55.*

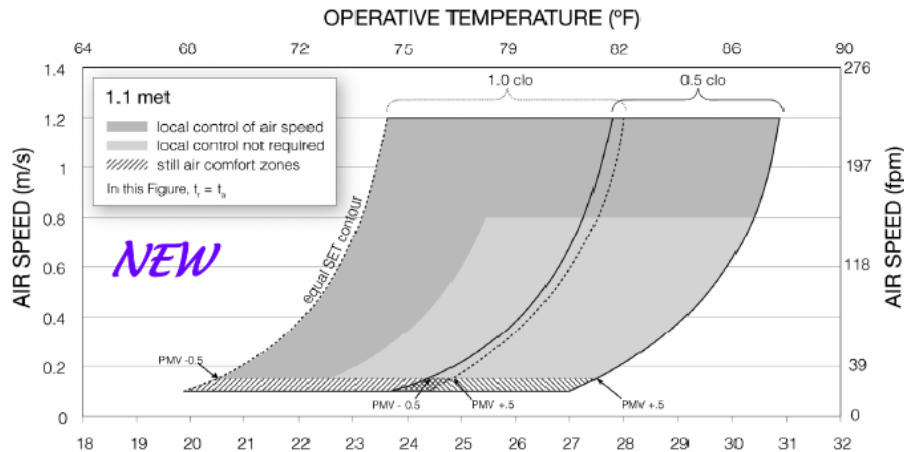


Figure 2.2: Acceptable range of operating temperature and airspeed. *The American Society of Heating, Refrigerating and Air-Conditioning Engineers.*

Buildings of the early 1990s were commonly designed with total isolation between the internal conditions and the outdoor climate conditions. Comfort cooling was managed by the building's heating, ventilating, and air-conditioning (HVAC) with high investment in controlling the condition which was accepted at the time. The stake was the high cost of energy consumption and for buildings, the main energy consumption was from HVAC (Weber, 2002). Space heating dominates the high consumption because of the proportion of glazing and air exchange rate (≥ 2 ACH), especially in the mid and northern European climates. Nowadays, comfort cooling is a healthy approach and technical services offer a good indoor climate. Although there is a level of discomfort, dissatisfaction and complaint regarding 'sick room syndrome', HVAC systems meet the objective for thermal comfort. Individuals can control their indoor climates with many options of natural ventilation and passive-cooling to suit the purpose. A combination of integrated measures to achieve passive-cooling is a pre-requisite if summer comfort is to be ensured without actively cooling or dehumidifying the inlet air (Zimmerman, 2003). For a lean building, the expectation for the comfort class and temperature is more of (class C: $\pm 4.2\text{K}$) and (class A: $\pm 2.5\text{K}$) comfort range.

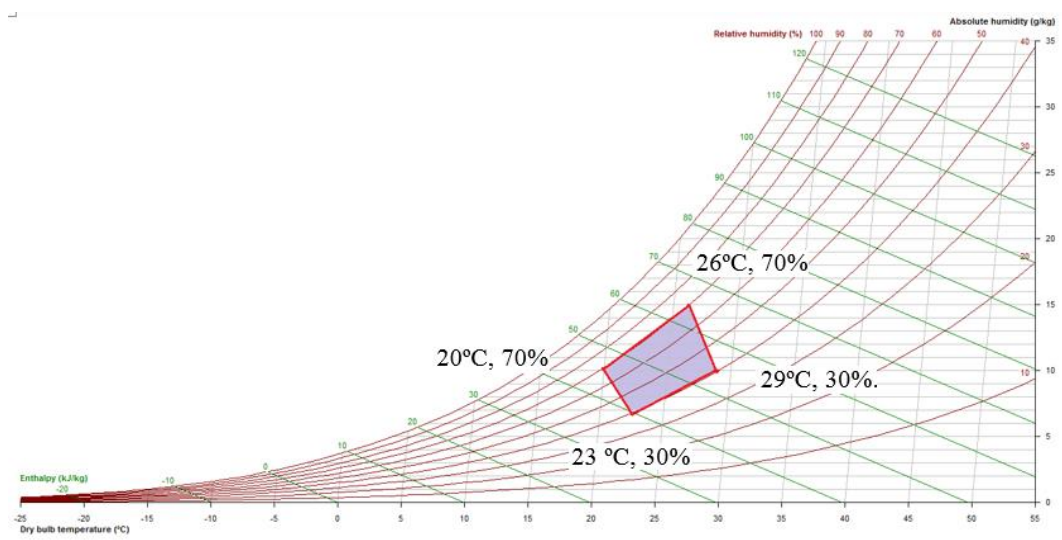


Figure 2.3: Psychrometric chart showing the thermal comfort zone. The levels of comfort are within the range of 20°C, 70% to 29°C, 30%. Feeling comfortable and un-comfort always refers to the difference between outdoor and indoor at the time of entrance. *Daikin Psychometrics Charts*.

Looking at the temperature graphs of New South Wales, Australia in 2018 as shown in Figure 2.4, the required temperature for thermal comfort was 280.7 K (7.7°C) for heating and 299 K (26°C) for cooling. Meanwhile, Table 2.1 presents the average temperatures in Sydney, New South Wales from January to December 2018 as recorded by the Bureau of Meteorology, Climate Statistics for Australia.

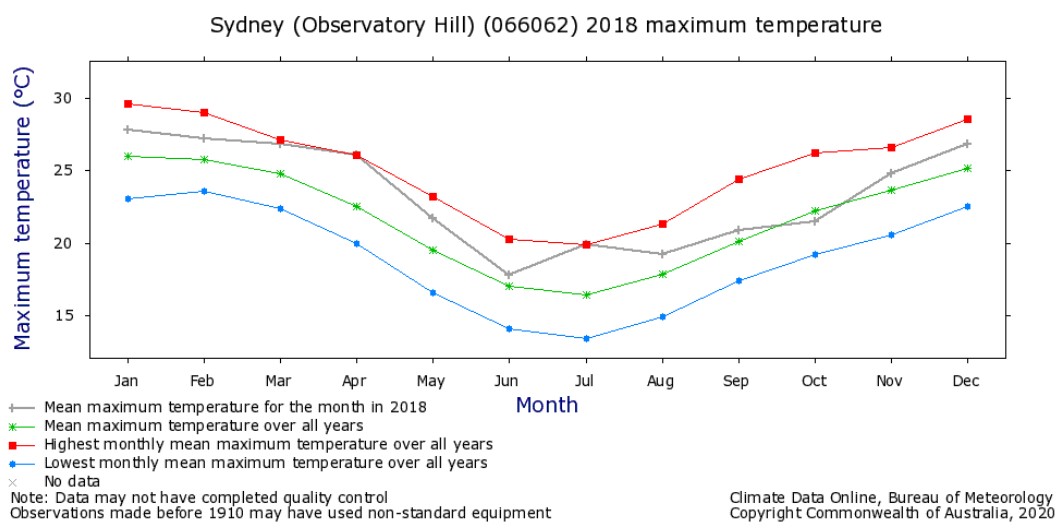


Figure 2.4: The mean maximum temperature gradient for Sydney, New South Wales from January to December 2018. *Bureau of Meteorology, Climate Statistics for Australia*.

Table 2.1: The average temperature in Sydney, New South Wales from January to December 2018. *Bureau of Meteorology, Climate Statistics for Australia.*

Statistic	Jan	Feb	Mar	Apr	May	Jun	Jul	Aug	Sep	Oct	Nov	Dec
Mean	26.0	25.8	24.8	22.5	19.5	17.0	16.4	17.9	20.1	22.2	23.7	25.2
Highest monthly mean	29.6	29.0	27.1	26.1	23.2	20.3	19.9	21.3	24.4	26.2	26.6	28.6
Lowest monthly mean	23.1	23.6	22.4	20.0	16.6	14.1	13.4	14.9	17.4	19.2	20.6	22.5
Highest Daily	45.8	42.1	39.8	35.4	30.0	26.9	26.5	31.3	34.6	38.2	41.8	42.2
Lowest Daily	17.2	15.6	16.2	13.8	11.3	9.7	7.7	9.1	9.5	12.1	12.6	15.2

2.3 PASSIVE COOLING TECHNOLOGY FOR THERMAL COMFORT CONDITIONS

Passive cooling technology has been used directly and indirectly over the centuries. It depends on the natural transfer of heat from the building structure to the surrounding. The ambience could be the conditioned air, the open air, and the soil condition. Passive cooling does not require electrical energy sources to produce cooling or heating. Ever since electricity was invented in the mid-1700s, it has played an important role in every aspect of human life. The work performed using electrical appliances moved people and technology faster. Nevertheless, demand has accompanied cost increases as well as environmental issues. The necessity of cooling has become essential in designing a domestic or commercial building. Conventional refrigeration and air-conditioning equipment using a vapour compression cycle consume electrical power in creating pressure and temperature differences, to operate its cycle. The International Institute of Refrigeration noted that of all the electrical energy produced, 15% is consumed by the process of refrigeration and air conditioning where 45% is used up for air conditioning of domestic and commercial buildings (Wimolsiri, 2005). Linden (1999) noted that 30% of the United States' total energy consumption is used by non-domestic buildings and 30% of that fraction is for heating and cooling. The technology applied in passive cooling is cost-effective and most importantly, it does not affect the environment. Methods such as natural air, infiltration, correct shadow, and added renewable energy, reduce the electrical consumption of a building. However, the drawback of using passive cooling on its own is that it will not fulfil the maximum need for a building's cooling or heating requirement. Figure 2.5 shows Z. Engsa (2016) cooling strategies. Figure 2.6 shows the Zold (2004) method of passive cooling.

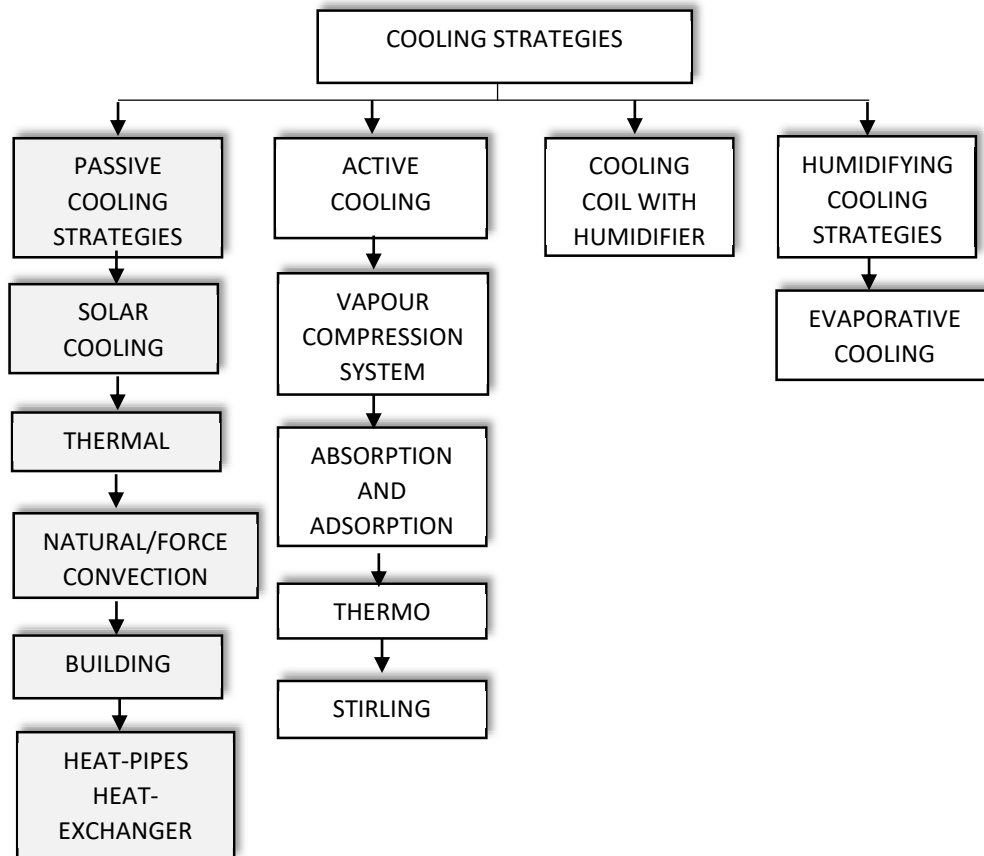


Figure 2.5: Cooling strategies. Z. Engsa (2016).

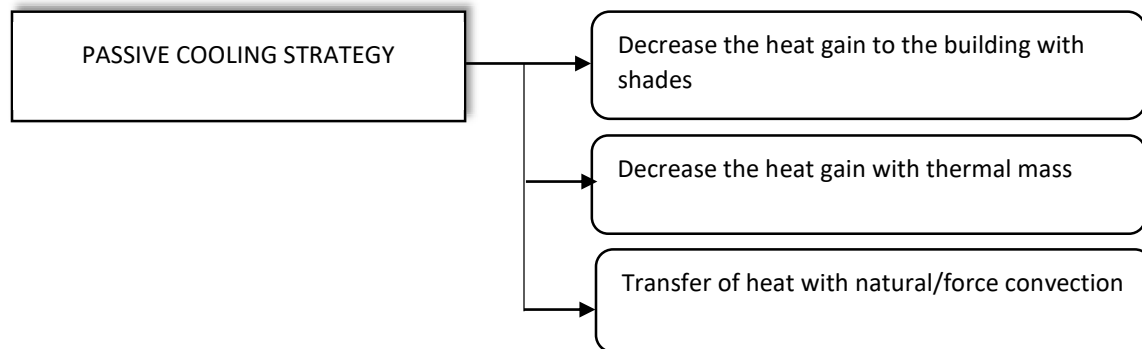


Figure 2.6: Method of passive cooling strategies. Zold (2004)

2.3.1 Solar Cooling Technology

The radiation intensity of the 6000°C solar surface corresponds to 70 000 kW/m² to 80 000 kW/m²; however, the earth receives only a very small portion of this energy. Despite this, the incoming solar radiation energy in a year is some 200 000 000 billion kWh; this is more than 10 000 times the yearly energy needs of the entire world. The solar radiation intensity outside the

atmosphere is an average of 1360 W/m^2 (solar constant). When solar radiation penetrates through the atmosphere, some are lost; thus, on a clear sky on a sunny day in summer, between 600 to 1000 W/m^2 (global radiation) can be obtained on the ground as presented in Table 2.2.

Table 2.2: The global irradiance and diffuse fraction, depending on the cloud condition. *AEE-Institute for Sustainable Technologies*

Sky Conditions	Clear, Blue Sky	Scattered Clouds	Overcast Sky
Solar irradiance (W/m^2)	600-1000	200-400	50-150
Diffuse fraction (%)	10-20	20-80	80-100

2.3.2 Solar Heat and Thermal Market

The International Energy Agency under the Solar Heating & Cooling Programme reported that the worldwide development of the solar thermal industry in 2015 was at €18 billion (US19.4 billion). Data which was plotted from 2000 to 2016 in Figure 2.7 show that the growth of global solar thermal capacity for glazed and unglazed water collectors was from $62 \text{ GW}_{\text{th}}$ (89 m^2) to $456 \text{ GW}_{\text{th}}$ (652 m^2), respectively. This corresponded to annual solar thermal energy yields that amounted to 51 TWh in 2000 and 375 TWh in 2016. Solar thermal energy contributed about $456 \text{ GW}_{\text{th}}$ in 2016, second after wind energy as can be observed in Figure 2.8. Figures 2.9 and 2.10 show the global solar thermal energy usage, and Australia's market growth capacity compared to other regions.

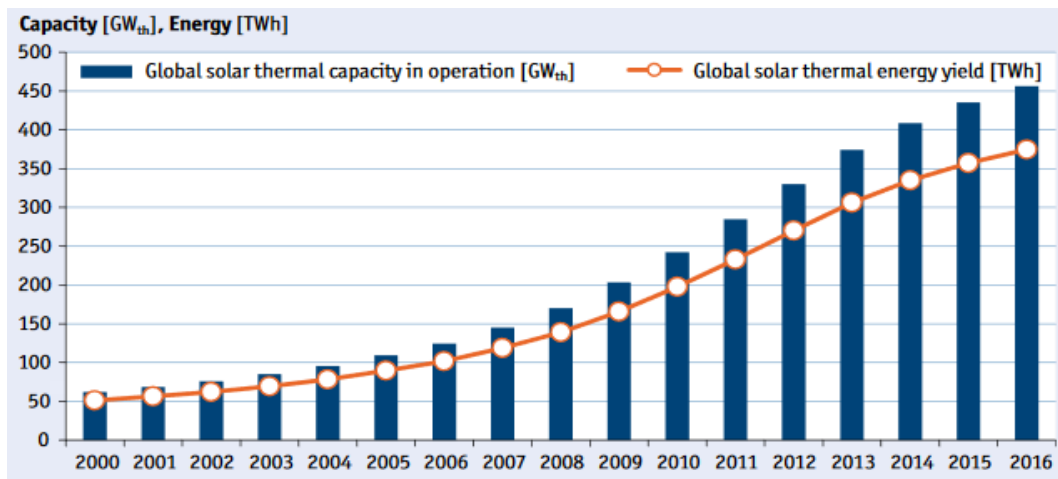


Figure 2.7: Global solar thermal capacity in operation and annual energy yield 2000-2016. *International Energy Agency (IEA)*.

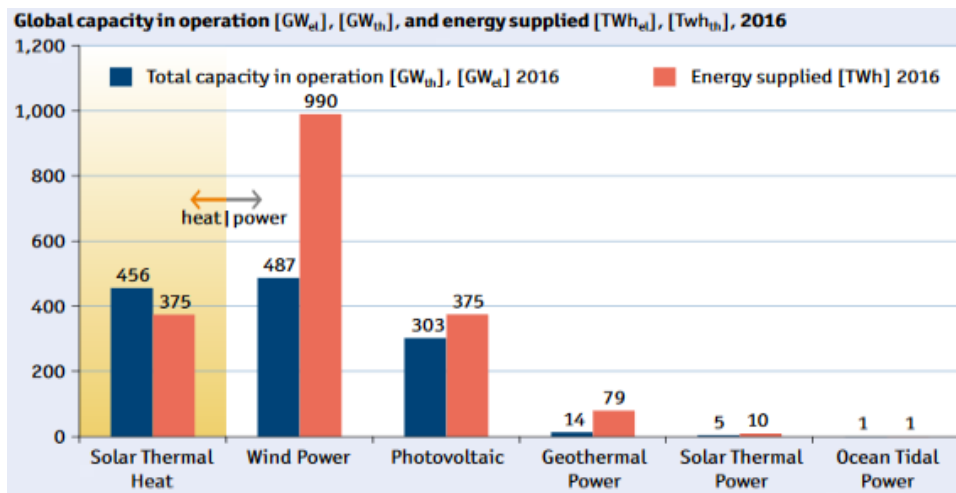


Figure 2.8: Global solar thermal capacity in operation and annual energy yields for 2016. *International Energy Agency (IEA).*

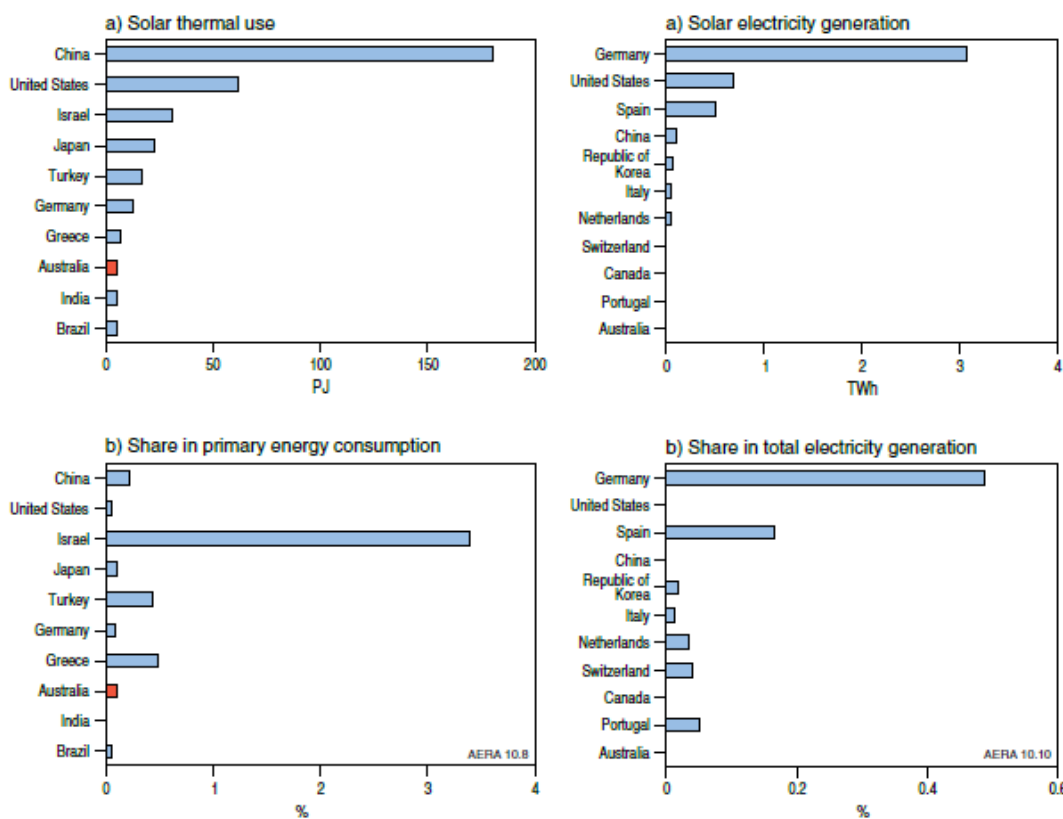


Figure 2.9: Graph of global solar thermal energy usage and electricity generated from solar energy. *Australia Energy Resource.*

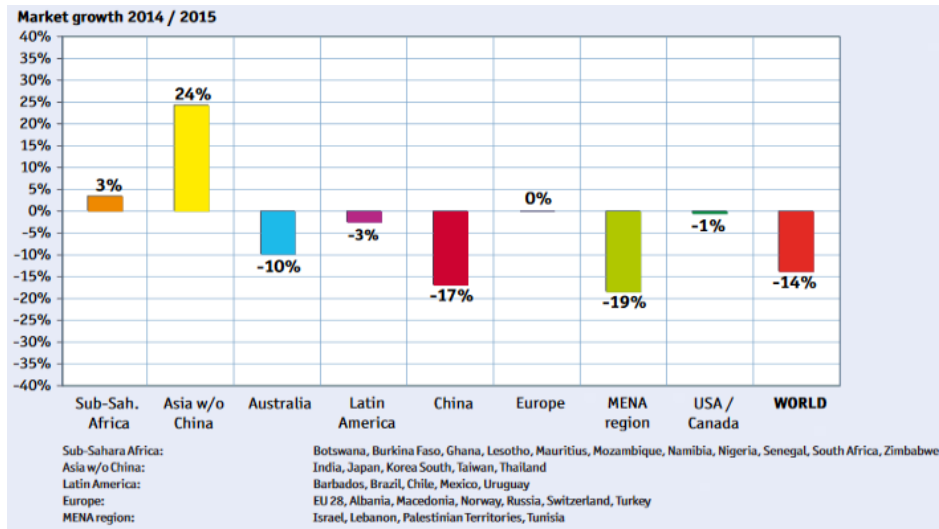


Figure 2.10: Australia's market growth of new installed capacity (glazed and unglazed water collectors) for 2014/2015 compared to other regions. *Australia Energy Resource.*

2.3.3 Solar Air Conditioning: Cooling and Heating

For decades, the modern vapour compression refrigeration cycle has been using a compressor as a prime mover and a refrigerant as a heat transfer medium for cooling and heating processes. Refrigeration may be defined as a process of cooling and maintaining the temperature of a product or some space to the required temperature below that of the surroundings. One of the most important applications of refrigeration has been the preservation of perishable food products by storing them at low temperatures. Refrigeration systems are also used extensively for providing thermal comfort to human beings through air conditioning. Air conditioning refers to the treatment of air to simultaneously control its temperature, moisture content, cleanliness, odour, and circulation, as required by occupants, a process, or products in the space. The main components of the 'refrigeration cycle' are the compressor as the prime mover and for building up the pressure; the condenser to remove heat away; the metering device to lower the pressure; the evaporator to gain heat from the surrounding. By manipulating pressure in the refrigeration cycle, the thermodynamic state of the refrigerant medium creates absorbing and desorbing of heat. To be able to feel colder, one has to remove heat to a place where it is not needed; in contrast, to feel warm, one has to add heat to the space. Heat gain and loss from the refrigeration cycle has been applied to many applications in domestic, commercial and industrial systems. The drawback is that compressors consume energy. Figures 2.11 and 2.12 show a single-stage vapour compression

cycle and its pressure-enthalpy relations. Best and Ortega (1998) remarked that solar refrigeration is no match to conventional systems. Lowering the first cost of the systems is still the main target to pursue to allow this technology to enter the market. Atkins (2007) who conducted a study in Sydney found a reduction of 25% to 33% in occupant comfort and satisfaction score in naturally ventilated mixed-mode buildings.

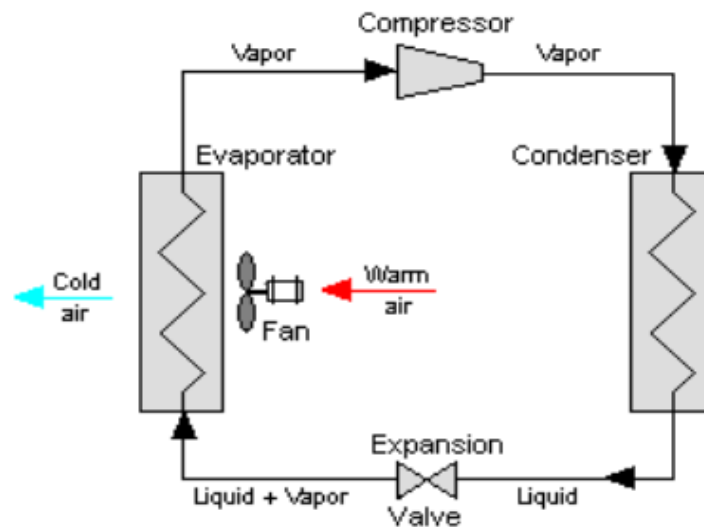


Figure 2.11: Typical single-stage vapour-compression refrigeration cycle. *Stoecker and Jones (1982).*

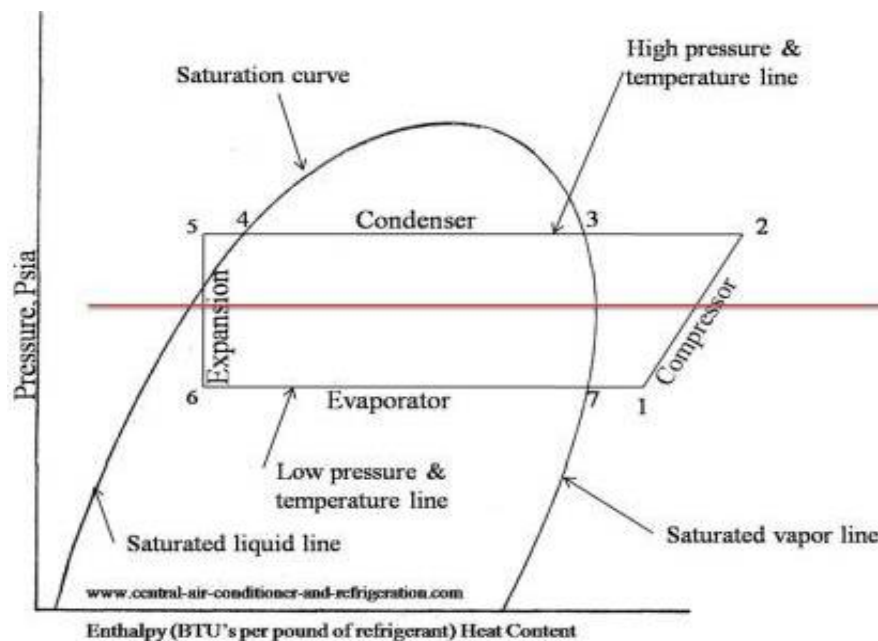


Figure 2.12: Pressure-enthalpy for a single-stage vapour compression refrigeration. *Stoecker and Jones (1982).*

From a thermodynamic point of view, there are many processes conceivable for the transformation of the solar cooling system. Figure 2.13 shows the physical ways to convert solar radiation into cooling processes. Compared to thermal driven technologies, which may use a solar thermal collector to provide heat to drive a cooling process, technologies based on heat transformation are the best to be developed. A basic figure to describe the quality of the conversion of heat into cold is the thermal coefficient of performance or COP. It is defined as Q_{cold} , over the driven heat, Q_{heat} .

$$COP = \frac{Q_{cold}}{Q_{heat}}$$

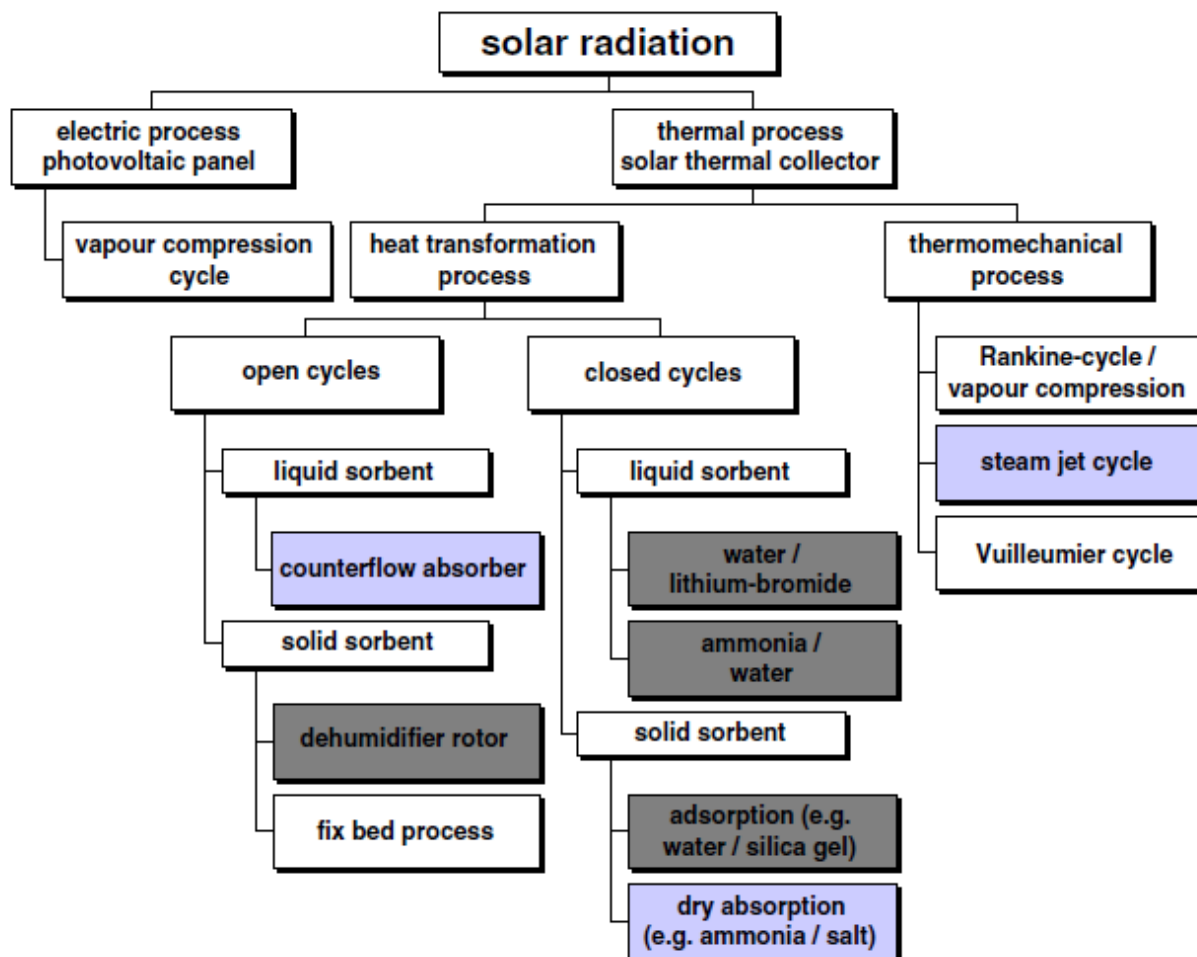


Figure 2.13: Overview of physical ways to convert solar radiation into cooling or air-conditioning system. Processes marked in dark grey are market available technologies that are used for solar-assisted air-conditioning. Processes marked in light blue are technologies that are of pilot projects or system testing status. *Hans-Martin Henning (2007).*

2.3.4 The Main Parts of a Solar Cooling System

The basic structure of a solar assisted air conditioning system consists of radiation absorbed from the sun and the process of thermally converting and conditioning the space. The main goal is to minimise power consumption. Figure 2.14 shows the basic structure of a solar air-conditioning system.

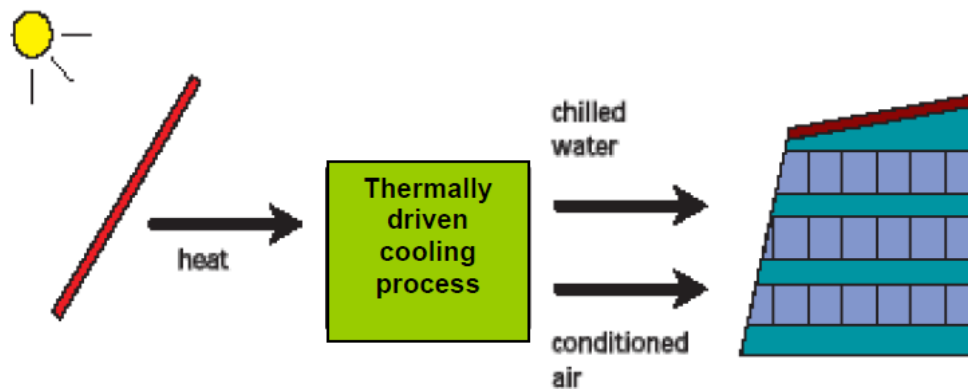


Figure 2.14: Basic structure of a solar air-conditioning system. *AEE-Institute for Sustainable Technologies.*

Figure 2.15 shows the main parts of a solar-assisted air-conditioning system. Four main parts normally act as an integrated unit in solar assisted cooling systems (Sayegh, 2007):

- Solar energy available – cooling needed. The heat from the solar collector is supplied directly to the cooling cycle.
- Solar energy available – cooling not needed. The gained heat from the solar collectors will be added to the storage equipment.
- Solar energy available - cooling not needed. If the storage is full, the heat from the solar collector will be discarded.
- Solar energy not available – cooling needed. An auxiliary source of energy will be used.

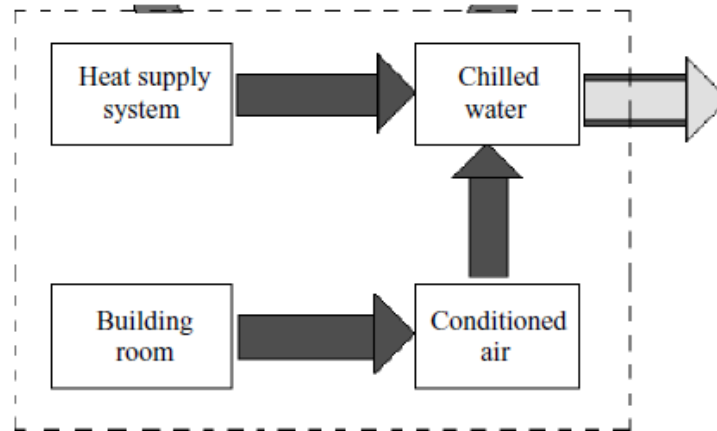


Figure 2.15: The main parts of a solar-assisted air-conditioning system. *Sayegh, (2007)*

Solar electric compression uses solar heat to produce a refrigerating effect, as a solar panel creates low electrical energy to work with the refrigeration cycle. Figure 2.16 shows the processes.

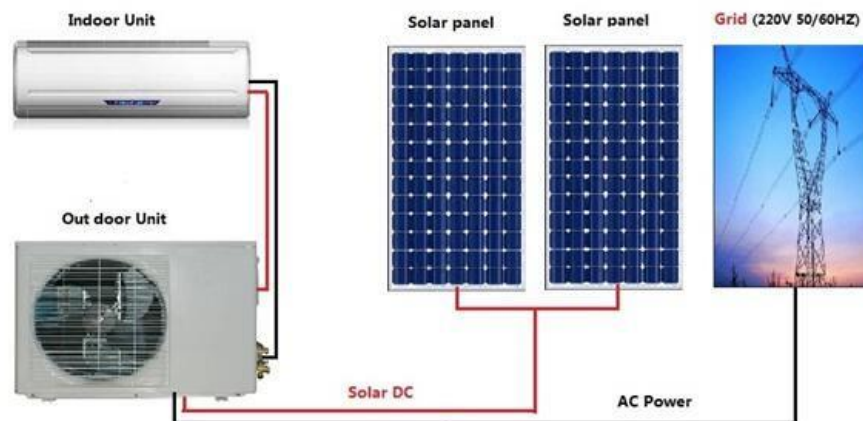


Figure 2.16: The solar-assisted air-conditioning system using low electrical energy. *Sealey Refrigeration International Limited.*

The interaction between solar radiation and the ground surface creates a series of natural conversion processes. A major part of the heat that originates from converted solar radiation can be found in the environment. Air, ground, and surface waters are heated by solar radiation and are considered renewable energy sources. Solar radiation that is converted through biochemical processes such as biomass becomes fossil fuel or stored energy. A small part of the solar radiation spurs wind, rain, and waves which can be converted into mechanical or electrical energy. Solar air conditioning uses solar power for the cooling process. Solar radiation can be converted into electricity through thermal energy, passive solar and photovoltaic conversion.

Due to social-economic and lifestyle requirements, the demand for air conditioning is high in populated places such as big cities compared to rural areas where natural ventilation and thermal comfort are naturally available. Solar sorption cooling systems are suitable for this application because of the low cost of installation with high cooling capacity. In the 1960s, solar-powered absorption systems were introduced in the air conditioning field (Kapur, 1960; Farber, 1966). The 1970s saw the United States with the greatest number of solar-powered air conditioning systems in which around 500 absorption systems using LiBr were installed (Wimolsiri, 2005).

Yeung (1992) designed and constructed a solar-powered LiBr absorption system to study the feasibility of utilising solar power for comfort cooling in Hong Kong. A flat plate solar collector with a hot water storage tank was used in the LiBr absorption air conditioning system. Syeda (2005) studied solar cooling in Spain and found that a maximum COP of 0.6 can be achieved using a single-effect absorption system. Assilzadeh (2005) studied the LiBr system in Malaysia's tropical climate using an evacuated tube solar collector with the TRNSYS programme. Argiriou (2005) develop a low-capacity H₂O-LiBr absorption system for residential and small building applications. Ming Qu (2010) studied a solar absorption system for buildings at Carnegie Mellon University. The solar cooling and heating system incorporates 52 m² of linear parabolic through solar collectors, a 16 kW double effect water-lithium bromide (H₂O-LiBr) absorption chiller, and a heat recovery heat-exchanger with circulation pumps and control valves. The system generates chilled and heated water, depending on the season, for space cooling and heating. A TRNSYS simulation programme was used to investigate the system's performance. It was found that the thermal system could potentially supply 39% of the cooling and 20% of the heating.

2.3.5 Thermal Mass

Passive cooling works by using cold night air temperature for ventilation, thereby reducing the thermal mass temperature of the living space. During the day when the temperature is high, the same thermal mass remains cool in the surrounding area. This passive cooling works in a moderate climate zone where the daily temperature range between day and night is high to improve the passive cooling performance of the building (Shaw et al., 1994; Roucoult et al., 1999). Passive cooling works best when located in a building's core where the ability to regulate the indoor temperature is greatest. One example is a thick stone wall constructed within a non-exposed area of the house.

2.3.6 Natural Ventilation

Differences in air density between the inside and outside of a building create natural ventilation. To achieve low-energy building and a clean environment, change of air is needed to be acceptable for human thermal comfort. According to ASHRAE Standard 55, a heat balance model of the human body is exclusively influenced by environmental factors such as temperature, thermal radiation, humidity, airspeed, human activity and clothing (De Dear, 2002). Great attention is being paid to the design of natural ventilation to replace indoor air with fresh outdoor air without any energy consumption as this may also help to overcome health problems related to insufficient maintenance of HVAC systems (Evola, 2006). Introduced by Hunt (1999), the ‘*natural ventilation triangle*’ depicted in Figure 2.17 shows buoyancy-driven displacement flows that are assisted by the wind. Hunt indicated that there is a non-linear relationship between the natural forces of wind and buoyancy.

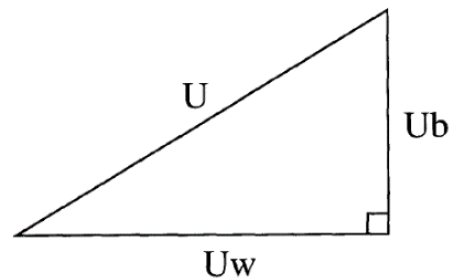


Figure 2.17: The natural ventilation triangle for buoyancy-driven displacement flows that are assisted by the wind. The base and vertical sides of the triangle are set by the magnitudes of the wind and buoyancy produced velocities, U_w and U_b , respectively. The length of the hypotenuse determines the total fluid velocity, U produced by buoyancy forces reinforced by the wind. *Hunt (1999)*.

As natural ventilation uses the natural energy of wind and air flotation to deliver fresh air into buildings, the principle of pressure difference that causes the wind to flow and the thermosiphon process is best utilised. Fresh air is needed in buildings to reduce odours and impurities, provide oxygen for breathing and improve human comfort. However, natural ventilation has its limit in warm and humid climates as it does not effectively reduce the inlet air humidity. In any case, the amount of ventilation will be critically dependent on the size and location of the openings on the building. It is useful to describe a natural ventilation system as a circuit, with the same consideration given to the inlet and outlet air. Room openings such as windows, grills, or open ducts are used to complement the airflow circuit through the building.

2.3.7 Building Shades

Shades play a big role in reducing heat gain in a building and indirectly reducing the cooling load. Outside shading via building umbrellas is much better than the inside shades such as blinds and black curtains as the radiation will heat them, and some will contribute to the building's heat gain. As the roof is the main heat source of a building, shading with flowering trees and other plants will reduce the heat. Trees absorb some of the solar radiation on the surface of the open roof. The surrounding air is evaporated from the plants, reducing the ambient temperature. Akbari and Taha (1992) and Akbari et al. (1992) stated that planting trees as a building shade results in a big reduction of temperature and could save up to 30% of energy consumption in a building.

2.3.8 Active Cooling Technology

The passive cooling method cannot lower the room temperature to the maximum comfort required, especially when the ambient air is highly humid. The active method of cooling can fulfil the task; however, it requires the consumption of energy as in heat or electricity.

2.3.8.1 Vapour Compression System

A conventional vapour compression system is a closed system of refrigerant running inside a room with a pipe. Along the piping circuit, the refrigerant absorbs and desorbs heat from the needed space to the unwanted ambient spaces. The temperature will decrease without heat and increase with heat in the surroundings. The four main components of a vapour compression system comprise the compressor, condenser, expansion valve and evaporator (Stoecker, 1982). In this cooling method, the evaporator is placed inside a room where cooling is needed. The refrigerant is a fluorocarbon liquid with a very low boiling point temperature. It interacts with the ambient temperature, allowing it to absorb heat when the surroundings are warmer and releasing it in the low - temperature surroundings.

A compressor is an electrical mechanism that increases the pressure and temperature of the refrigerant vapour and pushes it along with condenser pipes. As heat tends to flow from a higher to a lower temperature, the high heat condenser releases its heat to the lower ambient and condenses the refrigerant to a liquid phase. The high-pressure liquid refrigerant then moves along with the expansion valve in which the inlet opening is set to be smaller to drop the pressure from high to low. The low-pressure and low-temperature refrigerant liquid flow to the evaporator where

the surrounding heat is absorbed, evaporating the liquid to the vapour phase. The low-pressure vapour then flows to the compressor and restarts the cycle. Figure 2.18 shows the basic process of a refrigeration cycle.

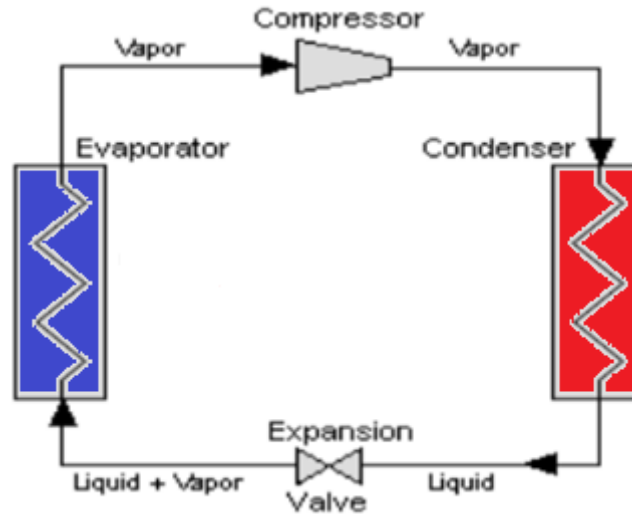


Figure 2.18: The process of a refrigeration cycle. *Stoecker and Jones (1982).*

The efficiency of converting the compression cycle to cooling capacity is the coefficient of performance, where Q_c is the cooling capacity and W is the work performed by the compressor. The relation is written as follows:

$$COP = \frac{Q_c}{W}$$

As the COP is the function of the temperature difference between the condenser and the evaporator, the bigger the difference is the smaller the COP. COP 2.5 is considered a suitable value for a hot climate (Jurinak & Mitchell, 1984). Apart from some drawbacks of the system, the vapour compression technology has been used for centuries as the best cooling technology in domestic and commercial settings. However, the disadvantage of using this system is that it uses electrical energy to run the compressor and other components. In addition, the refrigerant cooling medium is normally a chlorofluorocarbon (CFC) or hydrofluorocarbon (HCFC) which is associated with the potential destruction of the ozone layer (ODP) and global warming (GWP). According to the International Institute of Refrigeration in Paris (IIF/IIR), approximately 15% of all the electricity produced in the world are employed in refrigeration processes of various kinds. With the rising demand for global energy, the cost of electricity has seen a constant increase over the years.

2.3.8.2 Absorption System

The absorption cycle is the mixture of gas in a liquid where the fluids present a strong affinity to form a solution. The usual pair of absorption systems is water-lithium bromide ($\text{H}_2\text{O}-\text{LiBr}$) and ammonia-water ($\text{NH}_3-\text{H}_2\text{O}$).

Table 2.3: The comparisons between absorption using water-lithium bromide ($\text{H}_2\text{O}-\text{LiBr}$) and ammonia-water ($\text{NH}_3-\text{H}_2\text{O}$). *Dossat, (2001)*.

Working pair	Advantages	Disadvantages
$\text{NH}_3 - \text{H}_2\text{O}$	Evaporative at the temperature of 0°C	Toxic and dangerous for health (ammonia) In need of a column of rectifier Operation at high pressure
$\text{H}_2\text{O} - \text{LiBr}$	High COP Low operating pressure Environmentally friendly and innocuously Large latent heat of vaporisation	The risk of congelation, therefore an anti-crystallization device is necessary Relatively expensive (LiBr)

The process of absorption refrigeration is reversible. The explanation of how the ammonia-water ($\text{NH}_3-\text{H}_2\text{O}$) works and the schematic drawing of an absorption cycle are provided below:

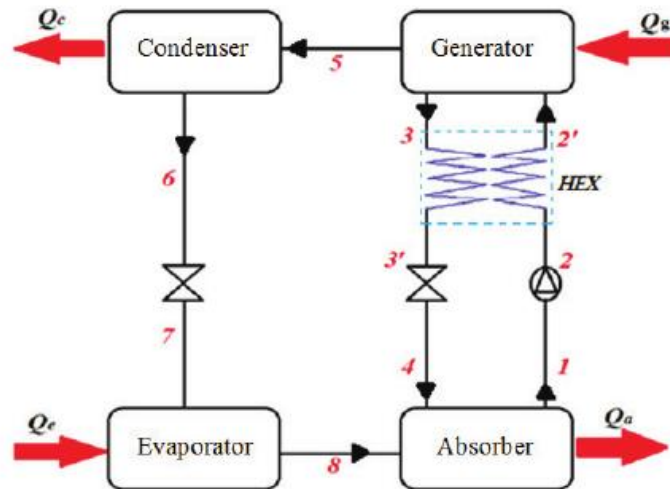


Figure 2.19: Schematic drawing of an absorption cycle. *Omar Ketfi (2015)*.

Generator: In a generator, a heat source produces ammonia vapour from a spray of strong ammonia solution and becomes high pressured. Ammonia is dehydrated through a rectifier and enters the condenser.

Condenser: The high-pressure ammonia is condensed by the cooling water and goes through the expansion valve where the pressure and temperature are reduced. The value must be lower than at the evaporator.

Evaporator: The cooled ammonia absorbs the heat from the surroundings and turns into saturated ammonia vapour. The vapour then flows to the absorber.

Absorber: The weak ammonia vapour is exposed to a spray of weak ammonia-water solution and becomes a strong solution. A pump directs the solution to the generator and the whole process starts again.

2.3.8.3 Adsorption System

A physical or a chemical reaction and an interaction between a solid (adsorbent) and a gas (refrigerant) result in the adsorption process. A developmental review of an adsorption system by Demira (2007) shows that the adsorption is separated into two cycles. In the first cycle, a low-level temperature source is evaporated by working fluid Q_L and releases the heat to an intermediate source Q_a while in the second cycle, a heat engine receives heat from high-temperature Q_Z and releases the heat to a second intermediate source Q_C .

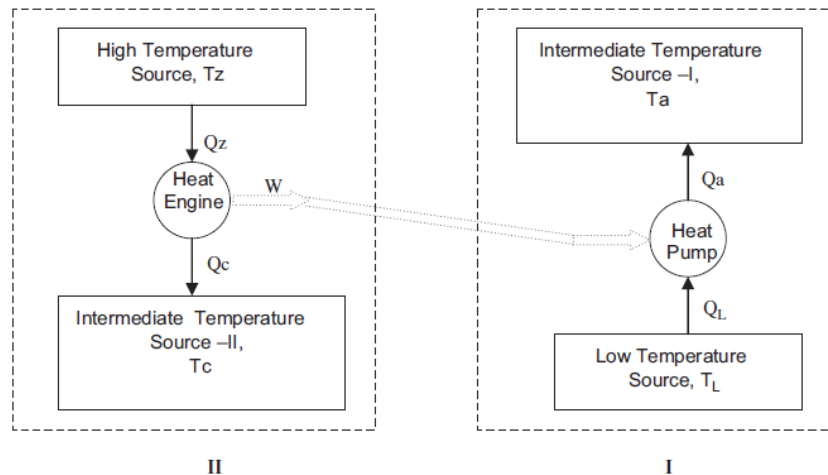


Figure 2.20: Heat transfer configuration of an ideal absorption system. I. Adsorption process. II. Desorption process. Demira (2007).

For cooling, the formula is

$$COP_{ref} = \frac{Q_L}{Q_Z} = \frac{1 - \left(\frac{T_c}{T_Z}\right)}{\left(\frac{T_c}{T_L}\right) - 1}$$

while for heating, the formula is represented by

$$COP_h = \frac{Q_c}{Q_z} = 1 + \frac{1 - \left(\frac{T_c}{T_z}\right)}{\left(\frac{T_c}{T_L}\right) - 1}$$

A Van der Waals connection consists of a generator, condenser, pressure relief valve, and evaporator. The generator is a solar plate containing an adsorbent that is heated by solar radiation. The working pair for adsorption includes activated carbon-methane or ammonia (Pons, 1986; Wang, 1997; Critoph, 2002) and silica gel (Grenier, 1988; Hildbrand, 2004). A solar-to-cooling COP between 0.1 to 0.5 using adsorption technology can produce ice of about 4 to 7 kg/m² (Wang, 2005; Chi, 1976).

Table 2.4: COP comparison between an absorption system and other systems. *Chi (1976), Wang (2005).*

Heat pump	Working pairs	Coefficient of performance COP _{ref}
Adsorption	Carbon-methanol	0.12-1.06
	Zeolite-water	0.28-14
	Silica gel-water	0.25-0.65
Absorption	Methanol-water	0.7-1-1
Vapour compression		3-4

2.4 HEAT-PIPES HEAT-EXCHANGER FOR COOLING TECHNOLOGY

2.4.1 Heat-Pipes Heat-Exchanger for Passive Cooling Equipment

Heat-pipes are becoming popular as a heat-exchanger to decrease or increase room temperature. As it is a passive, cost-effective and non-maintenance needed device with simple construction, heat-pipes offer energy-saving qualities because no external power is required in the process. A heat pipe consists of individual closed-end tubes that are charged with a suitable working fluid. Commonly used tubes are copper, and the fluid is normally a refrigerant fluid as it offers a lower boiling temperature point than the ambient air.

Due to its simple configuration and efficiency for heat transfer, heat-pipes applications cover a wide range of usages such as space heating, waste heat recovery, HVAC application, drying process, waste-steam reclamation, brick kilns, reverberates furnace, and many others. For

example, heat-pipes using a '*self-rewetting*' fluid (alcohol aqueous solution) under low gravity have been investigated for space applications (Savino, 2007). Results from the study showed improved capability for traditional heat pipes filled with water.

Many experimental works with different working fluids have been carried out. Among the refrigerant researched are R11, R12, R22 (Lee, 1972; Sumanthy, 1999; Sauciuc 1995; Wadowski 1992), and ethanol (Shiraisi, 1981; Abou-Ziyan, 2001).

2.4.2 Heat-pipes Heat-exchanger Operations

As heat is absorbed in the evaporator section, the working fluid is vaporised and becomes vapour. With the lower density of the vapour and higher energy, it travels through the middle section (adiabatic section) to the top section of the tube condenser section. In the condenser section, the working fluid becomes superheated vapour and heat is released to the ambient. Due to the temperature difference, the vapour fluid condenses and changes to the liquid state. As the density is higher, under gravitational force the liquid returns via the internal surface of the tube to the evaporator. The whole process is a cycle where the subcooled liquid in saturated liquid changes to a mixture of vapour and liquid to saturated vapour and superheated vapour.

Among the significant factors that affect the heat transfer performance of heat-pipes are the thermo-physical properties of the working fluid, geometry, orientation of the thermo-siphons, gravity field and the operating temperature. Compared to the conventional liquid form, heat transfer is higher because of phase transportation as a large amount of latent heat and superheated vapour are carried from the evaporator to the condenser.

Heat-pipes can be used with air conditioning systems in retrofits and new applications. For retrofit applications, the operating costs are reduced because of the reduction in energy (kWh) and peak demand (kW) consumptions. For new installations, the heating and cooling equipment can be downsized, resulting in lower equipment and operating costs. To create natural ventilation in the stale ambient air, heat-pipes are fitted to a roof of a building to naturally induce stale air to the outside using solar heat and to supply fresh air into the building.

The heat produced by the solar photovoltaic connected to a heat-pipe creates a heat source that evaporates the working refrigerant medium. The vaporisation process in the heat-pipes pushes the refrigerant to the other end of the pipe and releases the heat to the ambient. The air density

differential between the indoor and outdoor moves the air to a lesser density and creates natural ventilation.

A heat-pipes heat-exchanger was proposed in this experiment to assist in the cooling of hot ambient air intake to a room. A heat-pipes heat-exchanger is a passive, simple and cost-effective heat-exchanger that is used to transfer heat from one end to the other. With its capability to transfer a high amount of heat with only a small temperature difference, heat-pipes have been used in a wide range of applications. Its simplicity of design and manufacturing, small temperature drops, wide temperature application range and the ability to control and transport high rates of heat at various temperature levels are the unique characteristics of heat pipes (Ong, 2003). Brooke (2007) tested the heat transfer ability of heat-pipes heat-exchanger and found that heat-pipes were capable of converting a differential change of heat of about 1 to 10K. Figure 2.21 shows the phase change concept applied to a heat-pipes with the liquid cooling medium inside.

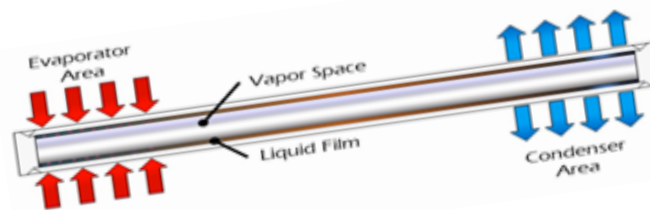


Figure 2.21: The heat-pipes heat-exchanger. The refrigerant liquid in the heat-pipes heat-exchanger at the bottom of the tube absorbs heat at the evaporator section and releases it at the condenser area in the upper section. The liquid evaporates into a vapour phase in the evaporator and moves towards the condenser section, which in turn changes the vapour back to the liquid phase by releasing the heat to the surrounding. *Ong (2003); Brooke (2007).*

In a low-energy and clean building environment, air change needs to be acceptable for thermal comfort. ASHRAE standard 55 stated that a heat balance model of a human body is exclusively influenced by environmental factors such as temperature, thermal radiation, humidity, airspeed, human activity, and clothing (Yau, 2010; Jones, 2001; Priyadumkol, 2014). The Commission of the European Communities conducted measurements on the air change in dwellings. The average air change for a sealed dwelling where the air escapes through valves, doors, windows, and closed ventilation system was found to be at 0.68 times per hour, and it was 3 to 4 times higher for an occupied dwelling. It was found from the measurement that some 20% (0.2 times per hour) of the occupied dwellings had an extremely low rate of air change. The calculations performed on natural ventilation systems show that air-escape valves with apertures

of 30 cm² per room are not adequate to create the requisite air change for sealed dwellings (Yau, 2010). It is important to improve the control of total air changes as this would satisfy both energy savings and a better indoor climate for the home.

2.4.3 Experimental Study On Heat-Pipes

The first patent of the heat-pipes concept put forth by Gaugler (1944) refers to heat absorption by evaporating the refrigerant liquid without expanding upon the liquid any additional work to lift the liquid to an elevation above the point at which condensation takes place. The returning of liquid from the condenser to the evaporator can be carried out using a capillary structure. Since then, several factors have contributed to the transformation of heat-pipes' science and technology. The development of loop heat-pipes, as well as micro and miniature heat-pipes that are related to the fields of electronic cooling and energy, have contributed to the cooling of laptops and the cooling of CPU's data centre. Indirectly, the numerical modelling and experimental simulation of heat-pipes have significantly progressed as a result of the understanding of the physical phenomena in heat-pipes.

2.4.4 Historical Development of Heat-pipes

Heat-pipes have an advantage over the conventional methods, measured by the large quantities of heat that can be transported through a small cross-sectional area over a considerable distance with no additional power input to the system. Wickless gravity-assisted Perkins tube, a predecessor of heat-pipes, works on the latent heat of evaporation which transfers heat by a phase change of water. Gaugler proposed a closed tube with a liquid that evaporates and absorbs heat at one location and then travels down the length of the tube, condensing the vapour while releasing its latent heat. His employer The General Motor, however, did not apply or convert the idea into reality.

Trefethen (1962) proposed the idea of using heat-pipes for the space programme and Grover et al. (1964) and Grover (1966) built prototypes that used water and sodium as the working fluid that worked at 1100 K. In his experimental studies and application of heat-pipes with the U.S. Atomic Energy Commission, where he used stainless steel heat-pipes with sodium, silver, and lithium as working fluid, Grover (Dec 2, 1963, Claims 165-105) acknowledged that "with certain limitations on the manner of use, a heat-pipes may be regarded as a synergistic engineering

structure which is equivalent to a material having a thermal conductivity greatly exceeding that of any known metal.”

Cotter's (1965) publication sparked worldwide research in the United Kingdom, Italy and other countries such as Germany, France, and the USSR researches in the area. In the beginning, due to the capillary action of heat-pipes, most work efforts were towards space applications; however, with the increase of energy cost, the industrial community began to be actively involved in the research and development of the heat-pipes application for commercial purposes. Electronic cooling and energy system requirements have transformed the heat-pipes technology and application into an important heat transfer equipment in modern computers and a data processor heat sink.

2.4.5 Principles, Operation of Heat-pipes

Faghri's (1995) schematic drawing of a cylindrical geometry explains the operation of heat-pipes. A sealed container with or without a wick structure is filled with a working fluid such as water, acetone, methanol, ammonia, or sodium, depending on the operating temperature. The heat-pipes are divided into three parts; evaporator, adiabatic and condenser section. The adiabatic is where the fluid transports from and to, both sections of the tube. In the evaporator section, external heat is applied, vaporising the working fluid. The vapour then drives through the adiabatic section to the condenser and releases the latent heat of vaporisation to a heat sink. The condensed fluid then travels back to the evaporator section via the capillary pressure and the gravitational force of the liquid.

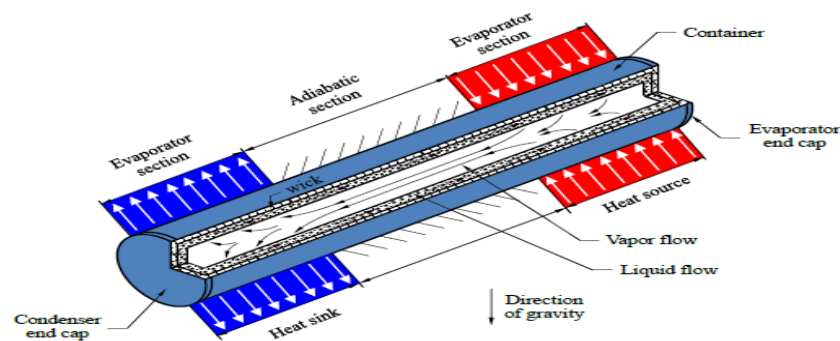


Figure 2.22: Schematic of conventional heat-pipes operation. *Faghri (1995).*

Due to friction, inertia, blowing and suction along the heat-pipes, the vapour pressure changes. A shape showing the axial variation of the liquid-vapour interface is shown in Figure 2.23a, b and c.

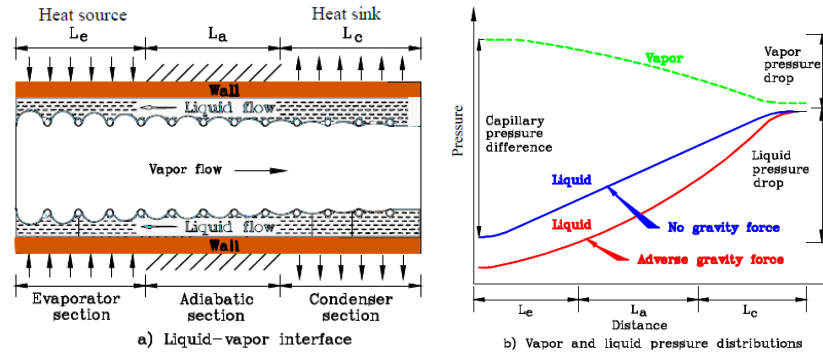


Figure 2.23 a.

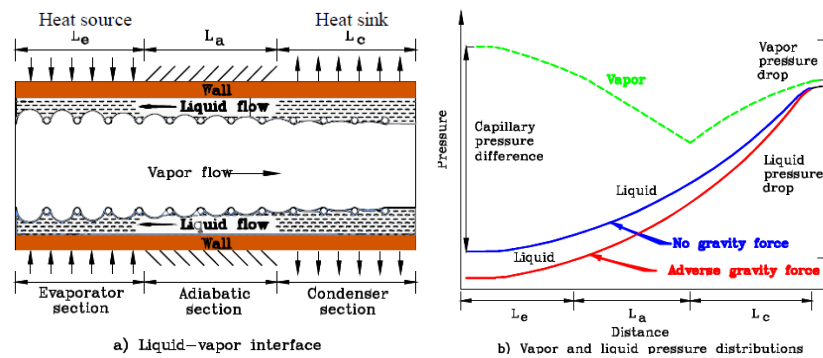


Figure 2.23 b.

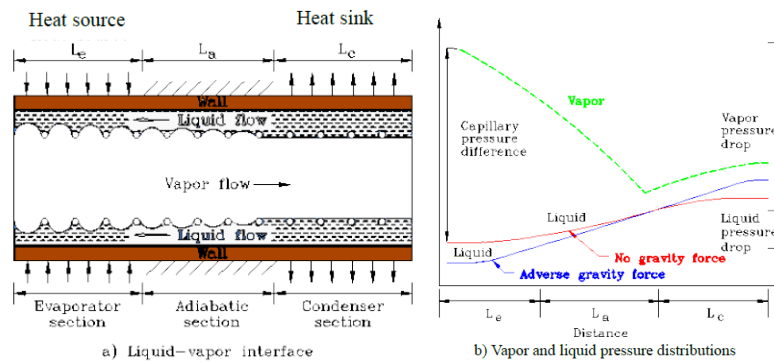


Figure 2.23 c.

Figure 2.23: Axial variation of the liquid-vapour interface along the heat-pipes at a. Low b. Moderate and c. High vapour flow rates. *Faghri (1995)*.

The theory of heat-pipes is related to the understanding of hydrodynamics and the heat transfer process. The fluid mechanics describes the pressure drop, pumping head, and vapour flow in the tube. Heat transfer theory models the heat into and out of the tube. The thermal resistances model and thermodynamic cycle for typical heat-pipes are shown in Figures 2.24 to 2.26.

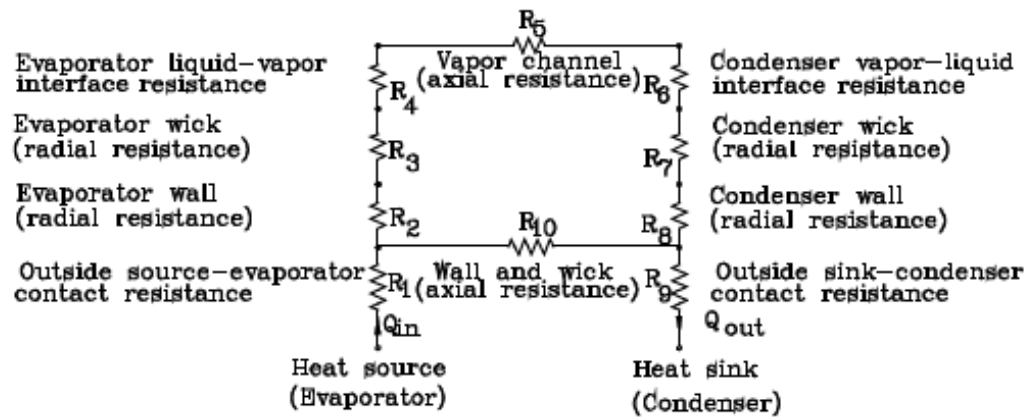


Figure 2.24: Thermal resistance model for heat-pipes. *Faghri (2014)*.

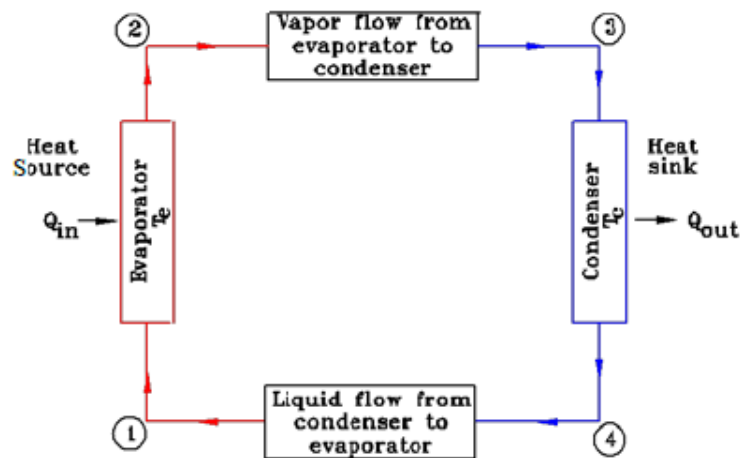


Figure 2.25: Thermodynamic cycle of heat-pipes components. *Faghri (2014)*.

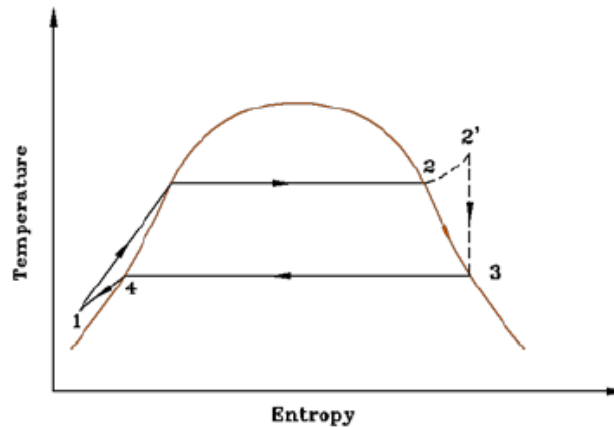


Figure 2.26: Thermodynamic cycle of heat-pipes, temperature-entropy diagram. *Khalkali (1999)*.

Khalkali (1999) has come up with a diagram to show the thermodynamic cycle of heat-pipes. He explained that fluid enters the evaporator at T_1 and leaves for T_2 , where T_2' is a saturated and superheated vapour. The vapour then flows from the evaporator to the condenser through the vapour channel. As a result of the differential pressure between the evaporator and the condenser, the vapour flows to T_3 as a saturated vapour mixture. The condensate enters the adiabatic section at T_4 and enters the evaporator again as a compressed liquid.

2.4.6 Types of Heat-Pipes

Whatever the size of heat-pipes, from micro heat-pipes to large heat-pipes, all heat-pipes will have an evaporator and a condenser section to evaporate and condense the working fluid. The working fluid is circulated by forces in the wick, namely gravitational, centrifugal, and electrostatic forces which return the fluid from the condenser to the evaporator. In this chapter, only circular tube related heat-pipes are discussed even though there are so many designs of heat-pipes that have been tested.

2.4.7 Gravity-assisted Wickless Heat-pipes

Faghri (1995) stated that the two-phase closed thermosiphon is a gravity-assisted wickless heat pipe. As the condenser section is located above the evaporator, the condensate will return by gravity. Figure 2.27 shows the gravity-assisted wickless heat-pipes.

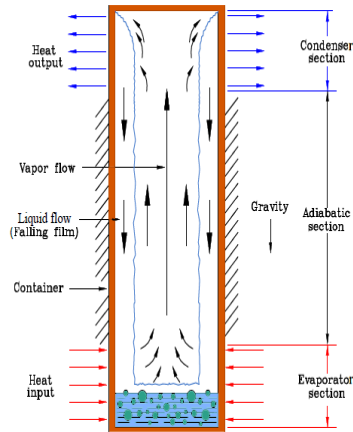


Figure 2.27: Gravity-assisted wickless heat-pipes. *Faghri et al. (1989)*.

2.4.8 Capillary-driven Heat-pipes

Conventional heat-pipes consist of a sealed container with a wick placed on the inner wall of a tube to provide a capillary-driven pump action in returning the condensate to the evaporator section. At the evaporator section, the heat input evaporates the liquid into vapour which then travels to the condenser section where the liquid condenses as the heat being removed releases the latent heat of vaporisation. The capillary forces generated at the liquid-vapour interface of the wick pump the condensate back to the evaporator. The heat-pipes are ideal for transferring heat over long distances with only a small drop in temperature. Conventional types are commonly used in laptops and computers as a heat sink to remove heat away and have been widely used for aerospace and commercial applications. Figure 2.28 shows the capillary-driven heat pipes.

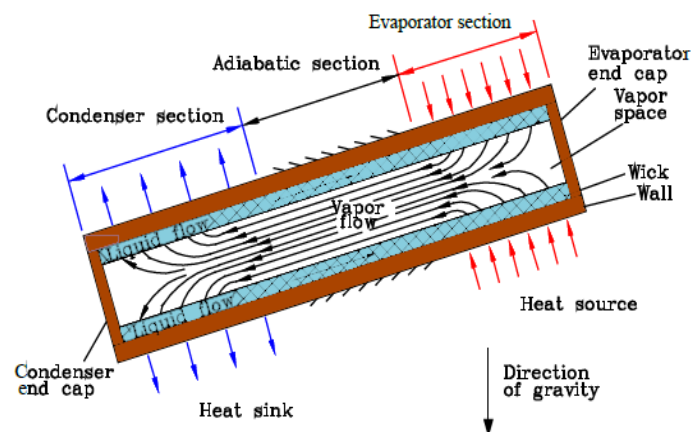


Figure 2.28: Conventional capillary-driven heat-pipes. *Faghri (2014)*

2.4.9 Annular Heat-pipes

The difference between annular and capillary heat-pipes is that the cross-section of the vapour space in an annular heat-pipe is annular in shape where else with the normal tube it is circular. The arrangement of the wick is such that it increases the surface area for heat transfer and increases the capillary limit compared to the conventional heat-pipes, without increasing the diameter of the pipe. Due to the fast response time to a cold charge and its capabilities in flattening the temperature, annular heat-pipes have been used with success as an isothermal furnace. Figure 2.29 compared the heat-pipes shape.

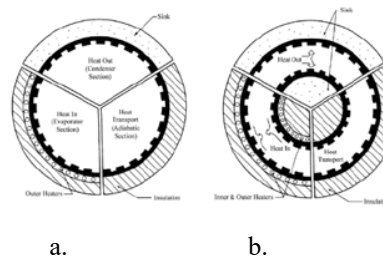
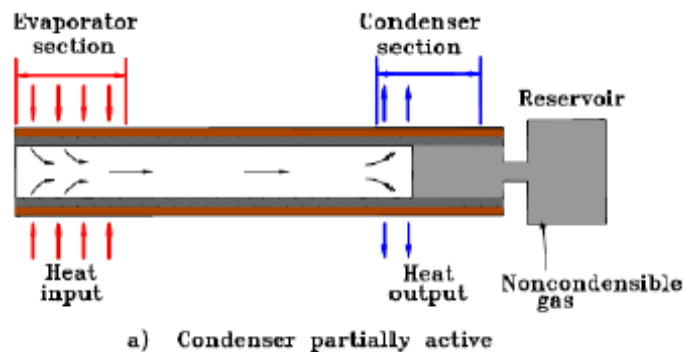


Figure 2.29: a. Conventional b. Concentric annular heat-pipes. *Faghri and Thomas (1989)*

2.4.10 Gas-loaded Heat-pipes

A non-condensing gas is introduced in the vapour space of gas-loaded heat-pipes. The purpose is to block a portion of condensation in the condenser from transferring heat to a heat sink as shown in Figure 2.30. As the evaporator heat input increases, the vapour and the gas temperature increase as well, which leads to the compression of the gas. In turn, this will increase the amount of condenser surface area to transfer heat.



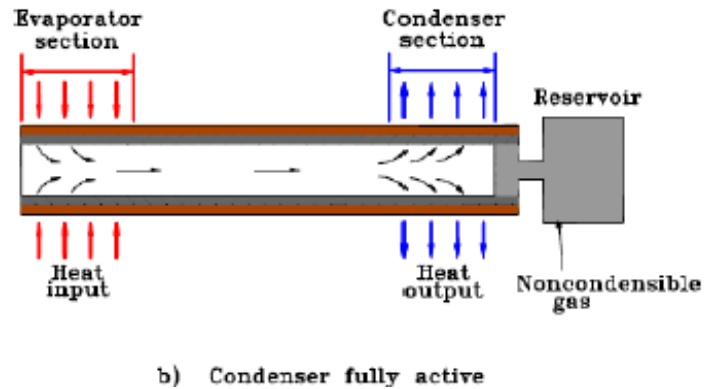


Figure 2.30: Operation of a gas-loaded variable conductance heat pipe. a. Condenser partially active. b. The condenser is fully active. *Faghri (2014)*.

2.4.11 Loop Heat-pipes

Invented by Gerasimov and Maydanik, a loop heat pipe (LHP) in Figure 2. 31, consists of a compensation chamber or reservoir in addition to the conventional heat-pipes (Maydanik et al., 1991). The chamber is an important component to accommodate the excess liquid during normal operation. Wicks made from fine pores such as nickel, titanium and copper powder create a high capillary force in the evaporator; these are placed in the evaporator and the compensation chamber.

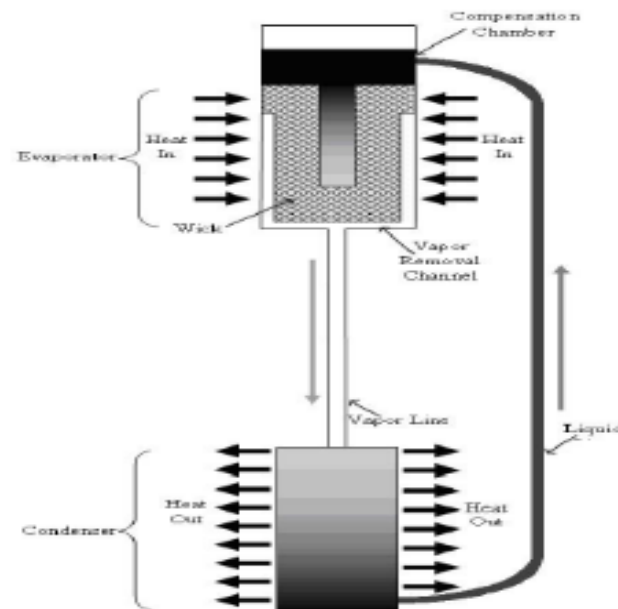


Figure 2.31: Loop heat-pipes. *Maydanik et al. (1991)*.

2.4.12 Other Designs of Heat-pipes

There are several other designs of heat-pipes that serve the purpose of transferring heat or a heat sink. Figures 2.32 and 2.33 below show a few diagrams of the heat-pipes and their operation.

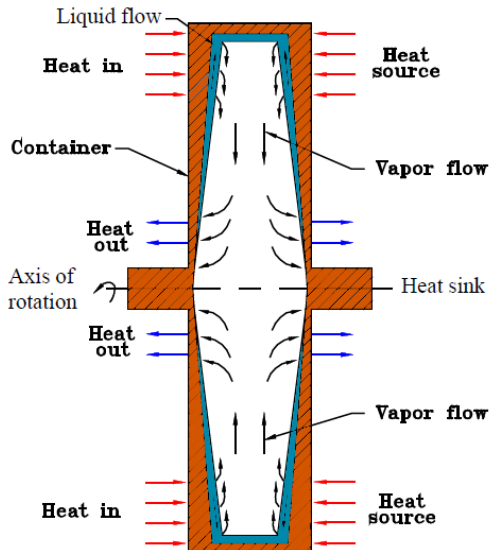


Figure 2.32: Rotating heat-pipes. Gray (1969)

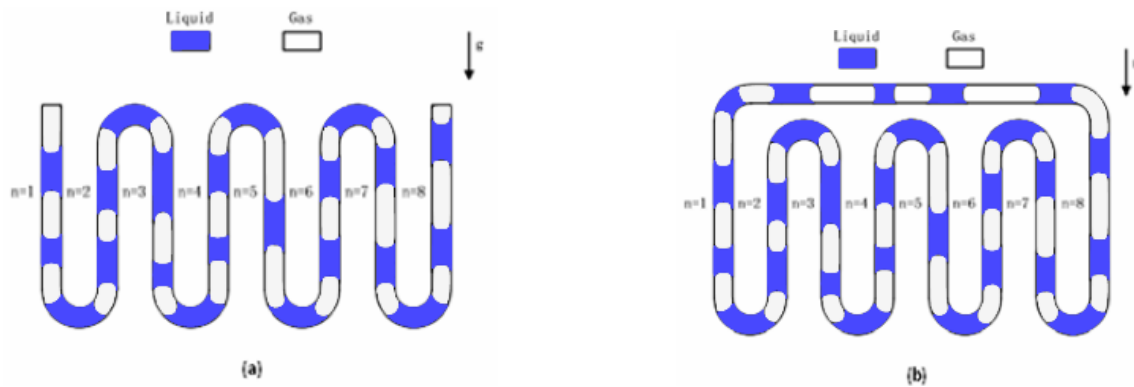


Figure 2.33: Pulsating heat-pipes. a. Un-looped. b. Looped. Faghri (2014)

2.4.13 Working Fluids and Temperature Ranges of Heat-Pipes Applications

A suitable working fluid for a particular temperature application should be considered when making a heat-pipe selection. The melting and the boiling points of the fluid at atmospheric pressure are normally taken as the measure. In Table 2.5 and Figure 2.34, Faghri (1995) lists some of the working fluids and their ranges for heat-pipes.

Table 2.5: Working fluids for heat-pipes. *Faghri (1995)*.

Working Fluid	Melting Point, K at 1 atm	Boiling Point, K at 1 atm	Useful Range, K
Hydrogen	13.8	20.38	14-31
Nitrogen	63.1	77.35	70-103
Oxygen	54.7	90.18	73-119
Methane	90.6	111.4	91-150
Ammonia	195.5	239.9	213-360
R22	113.1	232.2	193-297
R11	162.1	296.8	233-393
R113	236.5	320.8	263-373
Acetone	180.0	329.4	273-393
Water	273.1	373.1	303-550

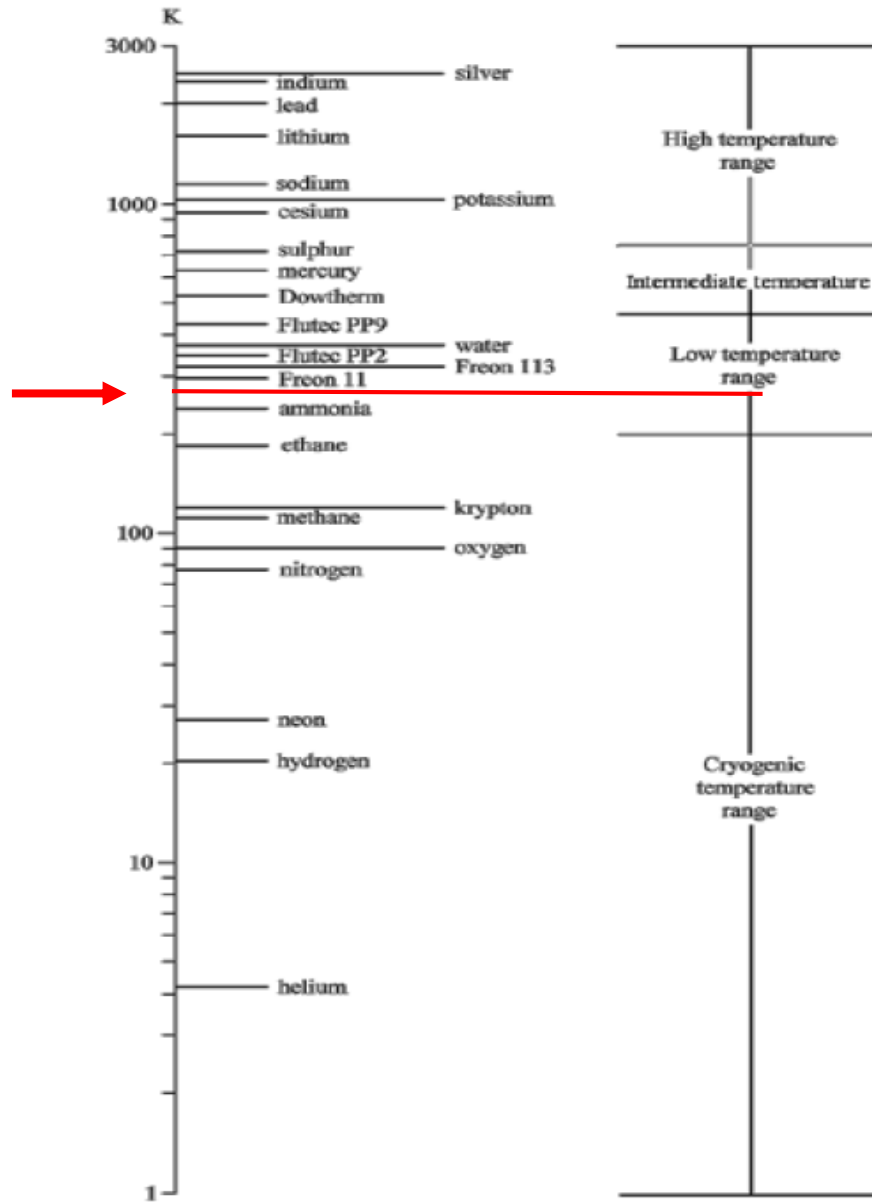


Figure 2.34: Logarithmic temperature scale for some of the working fluids for heat-pipes. *Faghri (1995)*. Refrigerant R134a has a boiling temperature of 246.8K. The arrow shows that the operating point is in the low-temperature range category.

Table 2.6: The latest experimental works and results from several researchers.

Reference	Fluid	Temp.	Material	Dimension	Axial Heat transport (W)	Heat transport Capability (W-m)	Heat Flux (W/cm ²)
Alario et al. (1982)	Ammonia	25°C	Aluminium	L _i = 5.5 m D _i = 6.32 mm	700	3200	7.26
Rosler et al. (1987)	Methane	-140°C	S Steel	L _i = 0.4 m D _i = 7 mm	12	3.93	1.82
Faghri and Thomas. (1989)	Water	50°C	Copper	D _o = 29.7 mm D _i = 25.4 mm	1300	940	Inner = 2.32 Outer = 1.47
Plesh et al. (1991)	Water	100°C	Copper	L _i = 0.120 m L _e = 20 mm L _c = 20 mm	70	8.4	35
El-Genk and Hung (1993)	Water	100°C	Copper	L _i = 610 m L _e = 393 mm L _c = 170 mm	570	187	2.4
Gao et al. (2000)	Water	100°C	Copper	L _i = 120 mm W= 7 mm H= 3 mm	50 Horizontal 70 vertical		25 Horizontal 35 Vertical
Tournier and El-Genk (2003)	Lithium	1227°C	Molybdenum	L _i = 1800 m L _e = 300 mm L _c = 1470 mm	4000	3660	22.2
Kempers et al. (2008)	Water	50, 70, 80°C	Cooper	L _i = 355.6 m D _i = 15.75 mm	20-180	4.6-41	0.33-2.96
Anderson and Tarau (2008)	NaK (with Argon as NCG)	700°C	304L S Steel	L _i = 600 mm L _e = 114 mm L _{c, 1} = 73 mm L _{c, 2} = 66 mm	250	57	3.65
Jouhara and Robinson (2009)	Therminol VP-1	300-400°C	316-S Steel	L _i = 209 mm L _e = 45 mm L _c = 100 mm	35-70	4.8-9.6	1.57-3.13
Vieira da Cunha and Mantelli (2009)	Mercury	630°C	316L S Steel	L _i = 1000 mm L _e = 200 mm L _c = 640 mm	1922	1115	12

2.5 SIMULATION OF HEAT-PIPES HEAT-EXCHANGER USING COMPUTATIONAL FLUID DYNAMICS

Computational Fluid Dynamics uses numerical methods and algorithms to solve the problem involving fluid flow and predicts the flow behaviour based on mathematical modelling. The model is based on fundamental governing equations of fluid dynamics, namely the conservation of mass, momentum, and energy. The fundamental basis of any CFD problem is the Navier-Stoke equations (conservation law). The four terms in the general differential equation are the unsteady term (transient), the convection term, the diffusion term, and the source term (Priyadumkol 2014). There is various research work on natural ventilation such as Bangalee (2013) who studied the flow structure of fluid-driven natural ventilation systems using Particle Image Velocimetry (PIV) measurement and Computational Fluid Dynamics (CFD), van Hooff (2013) who simulated natural ventilation of a large semi-enclosed stadium in an urban area using CO₂ concentration decay method with CFD, and Evola (2006) who studied wind-driven natural ventilation in buildings.

CFD is particularly dedicated to fluids that are in motion, and the effects of the fluid flow behaviours on different processes. The physical characteristics of the fluid motion can usually be described through fundamental mathematical equations, usually in partial differential form, which governs the process of interest and is often called governing equations. CFD is fundamentally based on the governing equations of fluid dynamics. They represent mathematical statements of the conservation laws of physics: mass conservation law, Newton's second law, and the first law of thermodynamics. A complete CFD analysis consists of a pre-processor, solver, and post-processor. It simply encompasses the procedures of appropriately setting up the flow problem, solving and monitoring the solution, and analysing the CFD results at the end of the simulation.

CFD has indeed become a powerful tool in both pure or applied research and industrial applications. The advantages of computer simulations and analyses are as follows:

- Presents the perfect opportunity to study specific terms in the governing equations in a more detailed fashion.
- Complements experimental and analytical approaches by providing an alternative cost-effective means of simulating real fluid flows. This substantially reduces lead

times and costs in designs and production compared to an experimental-based approach and offers the ability to solve a range of complicated flow problems.

- Able to simulate flow conditions that are not reproducible in experimental tests found in geophysical and biological fluid dynamics such as nuclear accident scenarios or scenarios that are too huge or too remote to be simulated experimentally.
- Provides rather detailed, visualised, and comprehensive information when compared to analytical and experimental fluid dynamics.

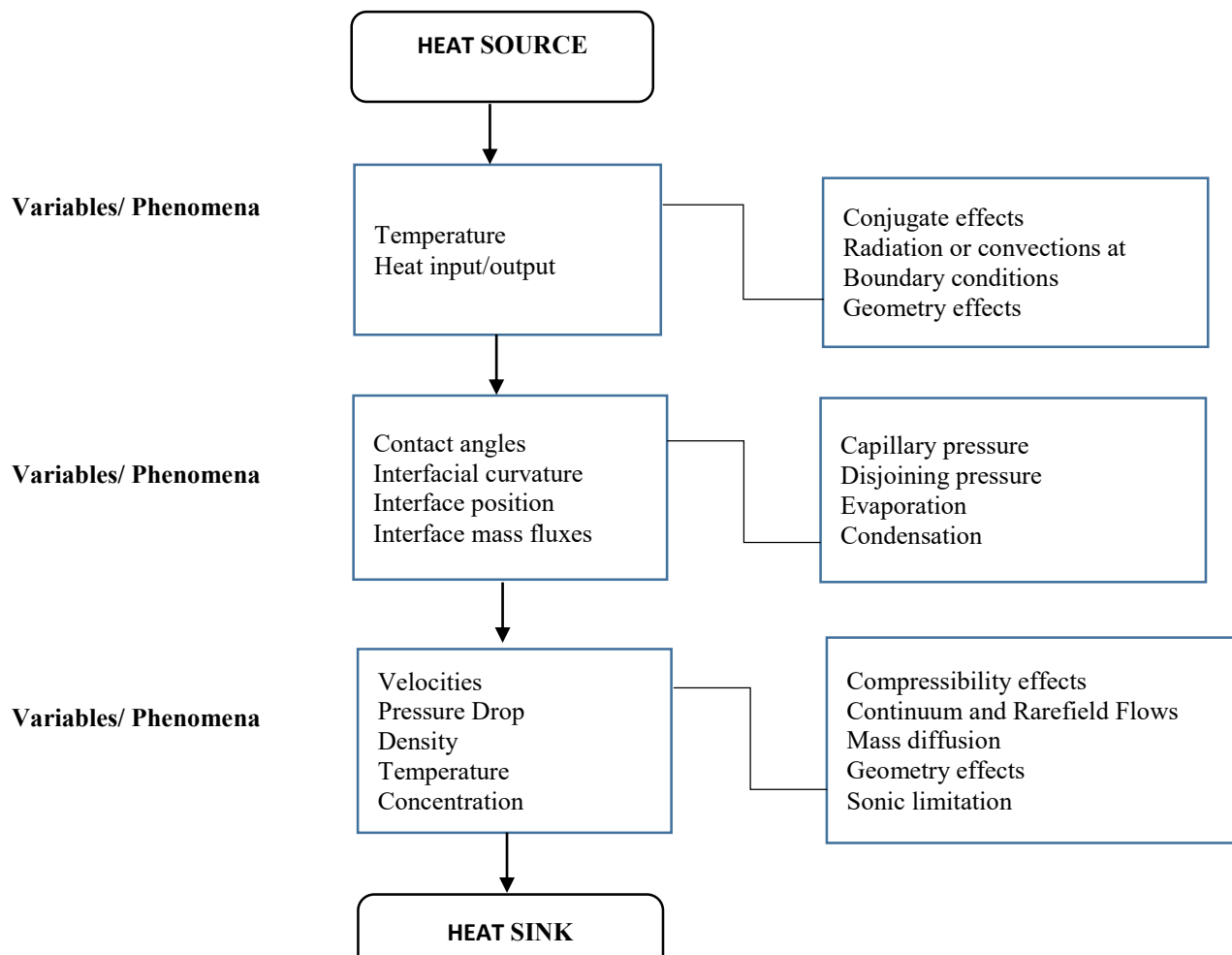


Figure 2.35: Flow chart of heat-pipes simulations and interactions. *ANSYS Fluent*.

2.5.1 Background

There has been significant progress in numerical and analytical simulations of heat-pipes applications. The objective of these simulations is to determine the heat capacity transmitted through the heat-pipes or to measure the performance characteristics. The heat conduction on the boundary, the vapour flow in the core region and the interaction between the liquid and the vapour flow are analysed with the help of computational fluid dynamics simulation programmes. Some flow interaction requires experimental information to be simulated. The flowchart in Figure 2.35 describes the heat-pipes interaction for the simulation.

2.5.2 Simulation Works on Passive Cooling Using Computational Fluid Dynamics

The use of computational fluid dynamics in the simulation works is motivated by the technology in passive cooling. Several methods of passive cooling had been simulated by researchers using computational fluid dynamics such as the work on a solar chimney by Bencheikh (2018), Serageldin (2018), Huynh (2012), ventilation flow by Kivva (2009) and natural ventilation by Idris (2013). Bencheikh (2018) uses the solar chimney and earth-to-air heat exchange in his work. The author uses the heat-pipes heat-exchanger simulations to show its capability in transferring heat.

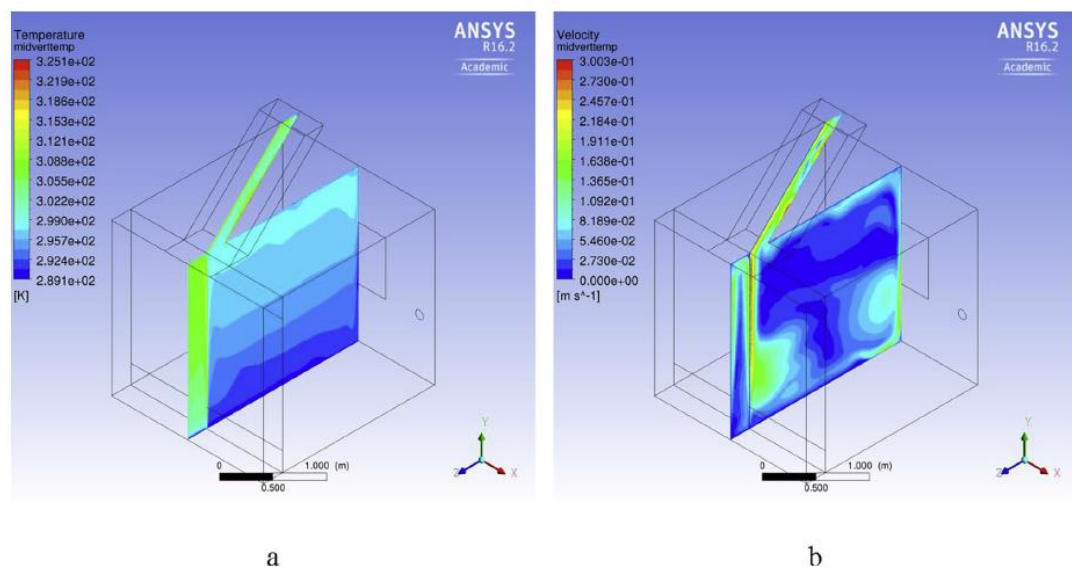


Fig. 13. Mid-vertical plane. (a) Temperature contours and (b) velocity contours at 10:00 AM.

Figure 2.36: Computational fluid dynamics work on solar chimney and air to the earth heat exchanger. *Serageldin (2018)*.

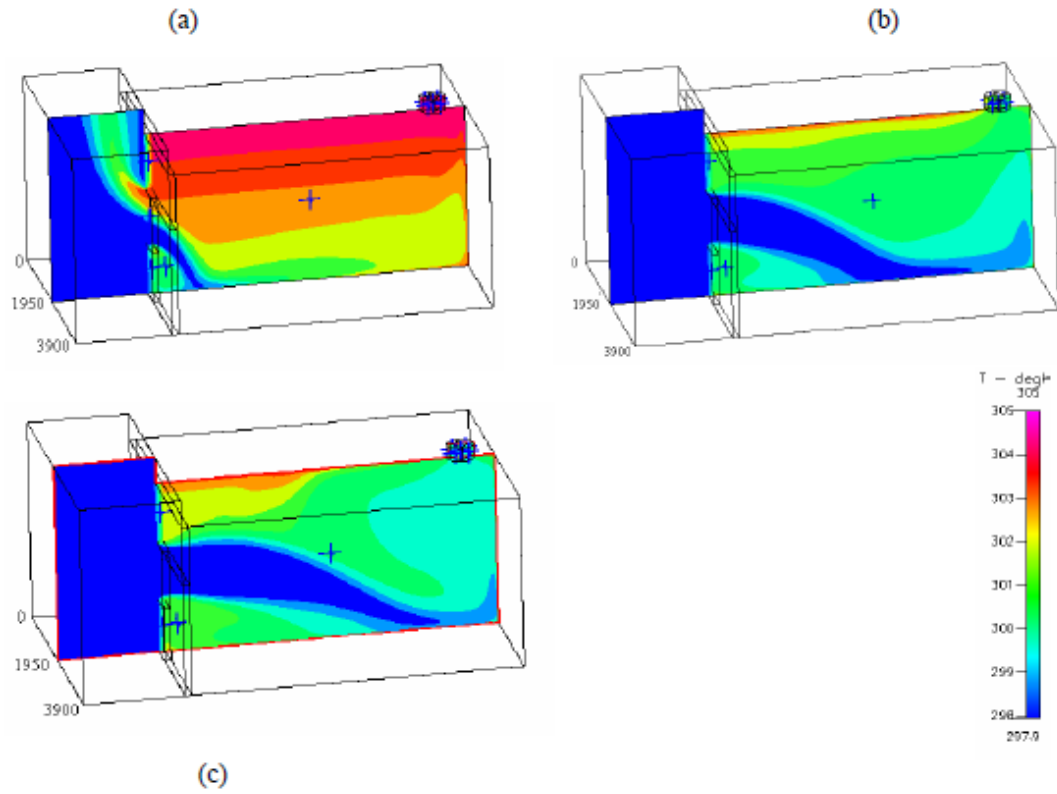


Figure 2.37: Computational fluid dynamics work on ventilation flow in a room. *Kivva (2009).*

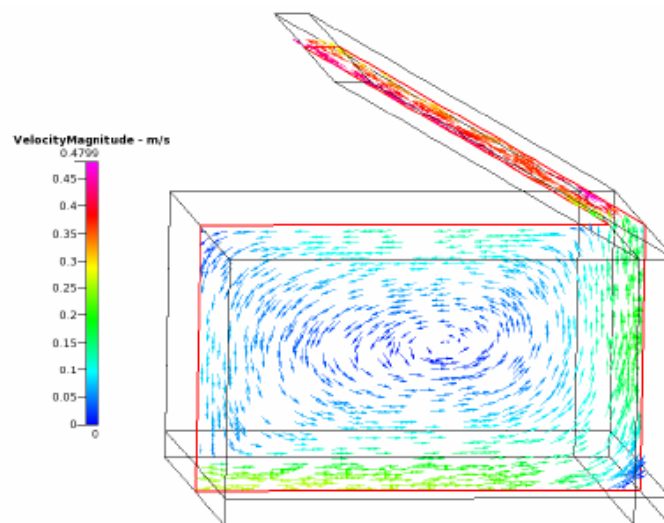


Figure 2.38: Computational fluid dynamics works on a solar chimney. *Huynh (2012).*

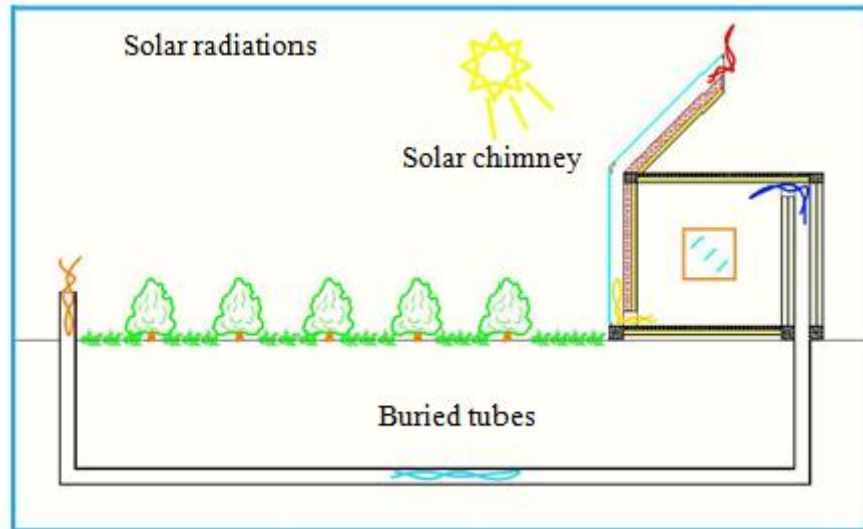


Figure 2.39: Coupled solar chimney and earth to air heat exchange. *Bencheikh (2018).*

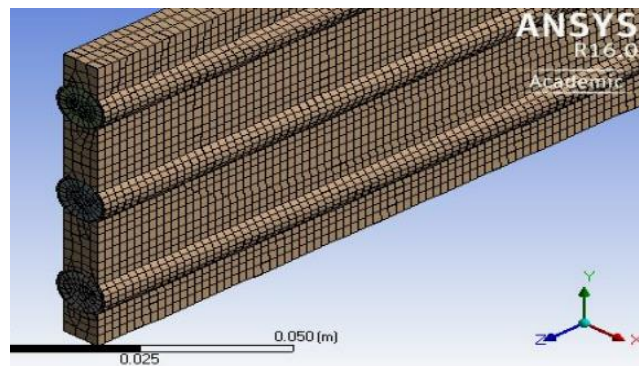


Figure 2.40: Meshes used to run the simulation of the heat-pipes heat-exchanger by ANSYS Fluent. *Abdullah (2018).*

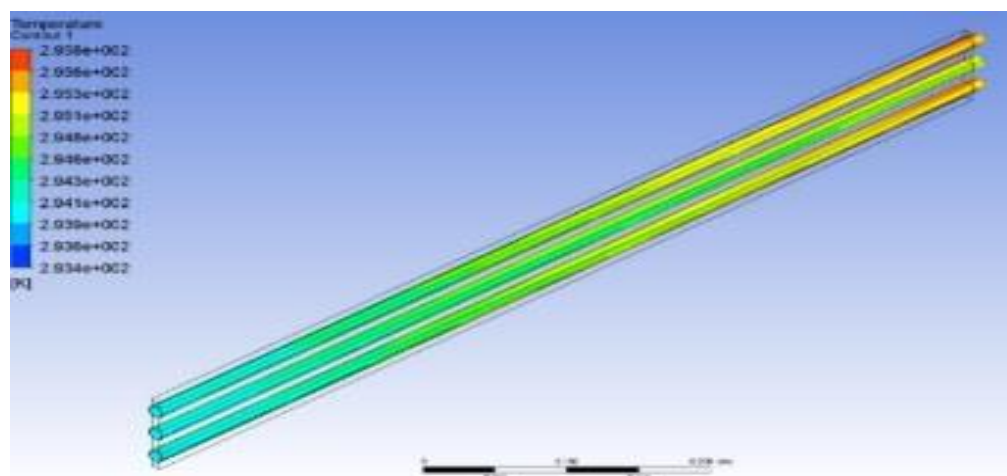


Figure 2.41: Simulation of a heat-pipes heat-exchanger by ANSYS Fluent using water as a cooling medium. *Abdullah (2018).*

2.6 KNOWLEDGE GAP: COMBINING SOLAR AIR-CONDITIONING AND HEAT-PIPES HEAT-EXCHANGER

The application method of cooling has been unchanged for hundreds of years. The method of reducing the space temperature is by transferring heat to the un-needed place. The vapour compression that generates the pressure difference and the heat transfer processes by the heat exchanger is run from the electrical motor fan and the compressor. However, there is still a lack of knowledge that is desirable regarding energy-saving with comfort cooling. The author, therefore, offers simulation and experimental studies to narrow the knowledge gap:

- i. The conventional method of refrigeration and air conditioning truly depends on the electrical grid as the energy source (Linden, 1999; Wimolsiri, 2005).
- ii. As demands grow, alternative energy is sought after to replace the un-renewable energy, where solar and wind energy is seen as alternative power sources.
- iii. With the abundance of solar radiation, refrigeration technology has to opt for solar-energy cooling. The survey carried out by the International Energy Agency under the Solar Heating & Cooling Programme showed that the demand for solar thermal energy is increasing; however, the countries that receive less radiation are the ones applying solar energy the most. The hottest ambient countries that receive higher amounts of solar radiation still do not use solar energy at its fullest. Germany, China, the United States, Israel, and other 'cold' countries are the leaders of solar thermal energy usage while countries like Australia, Brazil, India, and many parts of Asia are still left behind in its applications (IES, 2016).
- iv. Although the sun produces about 70 000 kW/m² of solar radiation, only about 1000 Watts at most (clear sky) can be used by the earth in solar-energy applications. This is no match to the electrical grid power source (Best and Ortega, 1998) unless other assisting accessories are introduced.
- v. The heat-pipes heat-exchanger as passive cooling equipment has been introduced in this work to assist the cooling process. Heat-pipes heat-exchanger is well known for its capability to transfer heat but with limited applications.
- vi. The author proposed the application of heat-pipes with pre-cooling of the air entering a room to assist the energy reduction of the cooling process. The energy reduction process

can be achieved as the heat-pipes heat-exchanger would not require any energy source to transfer heat.

- vii. The structure is simple, reliable and practical for installation in room condition. With its capability of transferring a high amount of heat with only a small temperature difference, heat-pipes have been used in a wide range of applications, from the cooling of computer components in our laptop to transferring of heat from an astronaut's outer space equipment. Its simplicity of design and manufacturing, small temperature drops, wide temperature application range and ability to control and transport high rates of heat at various temperature levels are the unique characteristics of heat-pipes. Heat-pipes are a cost-effective and non-maintenance needed device with simple construction. Heat-pipes offer energy-saving qualities because no external power is required in the process.
- viii. Previous heat-pipe configurations have been using either medium temperature refrigerant or low-temperature refrigerant; however, it comes with environmental impact characteristics. The CFC refrigerants used by previous researchers have now been found to affect the ozone layer or be linked to global warming impacts. Table 2.6 (Faghri, 1995) shows the work of previous researchers using other fluids.
- ix. Nethaji and Mohideen (2017) reviewed several experimental works on heat-pipes for the application of building. Most of the experiments proved that heat-pipes are applicable to be embedded with the air conditioning system to maintain the building air quality. Table 2.8 shows the summary of experimental studies on heat-pipes applications. Working fluids proposed by Faghri (1995) and the data of refrigerants are either toxic (ammonia), have a high boiling point (water, acetone), are highly flammable (propane, isobutene) or a mixture of fluids with high ODP and GWP (R22, R404A). The R134a's ozone depletion potential is 0 and the GWP is 1430 compared to R22 ODP 0.055, GWP 1810 and R404A, a mixture of R125 44%, R143a 52%, R134a 4%, with ODP 0, GWP 3922. The R134a works at a lower evaporating temperature, which is suitable for a heat-pipes heat-exchanger, heat transfer medium. Figure 2.43 shows the working vapour pressure for R134a compared to other available refrigerants.
- x. The author's work with R134a is as a refrigerant medium to transfer heat. The boiling point is at 247 K (-26°C) and the ozone depletion is 0. Its low evaporating temperature ensures its absorbing capability when exposed to the atmospheric condition while

maintaining the global warming potential (GWP). Table 2.7 and Figure 2.43 show the comparison of R134a to other refrigerants.

Table 2.7: Refrigerant data comparison between R134a and other potential refrigerants.

Refrigerant	R290	R134a	R404A	R22	R600a
Name	Propane	1,1,1,2-Tetra-flouro-ethane	Mixture R125 R143a R134a	Chloro-difluoro-methane	Isobutane
Formula	C ₃ H ₈	CF ₃ -CH ₂ F	44/ 52/4	CHF ₂ Cl	(CH ₃) ₃ CH
Critical temperature in °C	96.7	101	72.5	96.1	135
Molecular weight in kg/kmol	44.1	102	97.6	86.5	58.1
Normal boiling point in °C	-42.1	-26.5	-45.8	-40.8	-11.6
Pressure at -25 °C in bar (absolute)	2.03	1.07	2.50	2.01	0.58
Liquid density at -25 °C in kg/l	0.56	1.37	1.24	1.36	0.60
Vapour density at t _o -25/+32 °C in kg/m ³	3.6	4.4	10.0	7.0	1.3
Volumetric capacity at -25/55/32 °C in kJ/m ³	1164	658	1334	1244	373
Enthalpy of vaporisation at -25 °C in kJ/kg	406	216	186	223	376
Pressure at +20 °C in bar (absolute)	8.4	5.7	11.0	9.1	3.0

Table 2.8: Summary of experimental studies on applications of heat-pipes in HVAC systems. *Nethaji (2017)*.

Researchers	Type of heat pipe	Application area	Effects
Xiao Ping Wu <i>et al.</i> [1]	Wickless thermosyphon vertical HPHX,R22 working fluid	HVAC humidity control	Enhancement of cooling capacity by 20-32.7%, humidity reduced to 70-74% from 92-100%, increased air circulation pressure loss.
Khanh Dinh [2]	Serpentine heat pipe	HVAC dehumidification	Enhanced dehumidification
Mostafa A. Abd El Baky <i>et al.</i> [3]	Brass wickled, aluminium finned copper HPHX, R-11 working fluid,	HVAC coolness recovery	Enhancement of heat transfer effectiveness
Yau[4]	Inclined wick less HPHX	HVAC in tropical climate	Heat transfer effectiveness not affected due to HPHX configuration
Guiyin Fang <i>et al.</i> [5]	Separate helical heat pipe,R-22 working medium	HVAC ice storage air-conditioner	Cool thermal energy storage
Hussam Jouhara[6]	Finned wickless loop heat pipe,R-134a working fluid	Humidity control in HVAC	Energy savings due to pre cooling and reheating, enhanced dehumidification
Suprirattanaku <i>et al.</i> [7]	Closed loop oscillating heat pipe ,R 134a working medium	HVAC room air conditioning	Increased COP and EER
Ahmadzadehtalatapeh [8]	Vertical HPHX,aluminium finned, stainless steel meshed	HVAC system	Energy conservation
Yau <i>et al.</i> [9]	Wick less,R134a,R22,R410a, revolving copper heat pipes	HVAC heat recovery	Dehumidification, heat recovery and cooling of

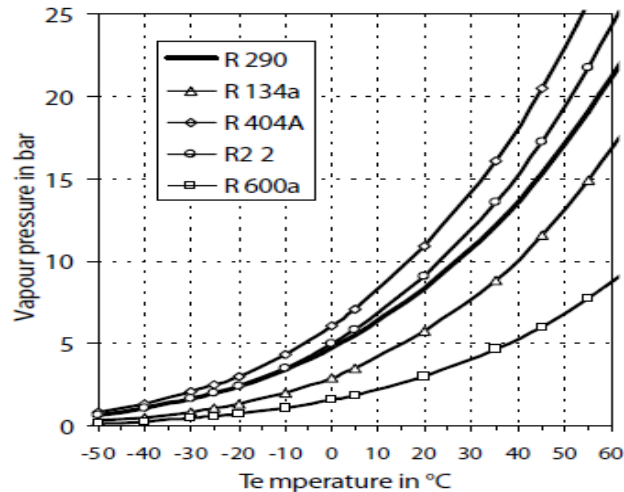


Figure 2.42: Vapour pressure of different refrigerants versus temperature. The R134a works at a lower evaporating temperature.

- xi. The combinations of solar-energy and the heat-pipes heat exchanger simulations and experimental works are presented in this thesis to show the energy-saving capability while maintaining comfort cooling. Yau (2004) in his thesis reported that 7.2 kW each, of pre-cooling and reheating, can be achieved when heat pipes are added to a recovery system.
- xii. Jouhara and Meskimmon (2010) proposed an energy-saving system using wraparound loop heat-pipes heat-exchanger in an air handling unit. Both researchers used the heat-pipes heat exchanger as additional equipment to cool the return air. The cooling components towards the AHU are run by a power source from the electrical grid such as the compressor, fan, and blower. The cooling energy-saving calculated was only from the wraparound loop heat-pipes heat-exchanger.
- xiii. The author proposed a stand-alone heat-pipes heat-exchanger installation in the room in assisting the solar-energy air conditioning system. The experimental test showed that about 31% of electrical energy could be saved by applying solar PV panels to the cooling cycle and on top of that, about 26% to 33% of sensible cooling energy can be saved by the heat-pipes heat-exchanger application.
- xiv. Simulation studies using CFD software were performed rigorously to find the best air intake position and location, and the heat-pipes ability in transferring heat. The solar and wind energy simulations predicted the energy-saving for the installations.

- xv. Extra experimental work on wind energy was carried out to relate the natural airflow and force ventilation to the conditioned space. The use of solar energy and heat-pipes heat-exchanger for comfort cooling is best for hot ambient and low airflow countries. Its practicality and simplicity, along with its ease of implementation, reliability and low cost have to be taken into consideration.

Combining heat-pipes and solar energy is a practical method for comfort cooling. Integrated applications with other renewable energy sources such as wind energy would help in reducing the dependence on the electric grid source.

CHAPTER III

MATHEMATICAL MODEL

CHAPTER OVERVIEW

This chapter discusses the mathematical method used to calculate the solar cooling processes. The heat-pipes heat-exchanger performance calculations are also presented. The calculations of the refrigeration system components, the properties of the evaporating effect W_e , the condenser effect W_c , the compressor work-done A_w , COP, the compression ratio, and the suction gas density are described by plotting data using the CoolPack software. The formulation of the computational fluid dynamics is presented. The method of calculation is based on the conservation of mass, energy equations, and turbulence models.

3.1 INTRODUCTION

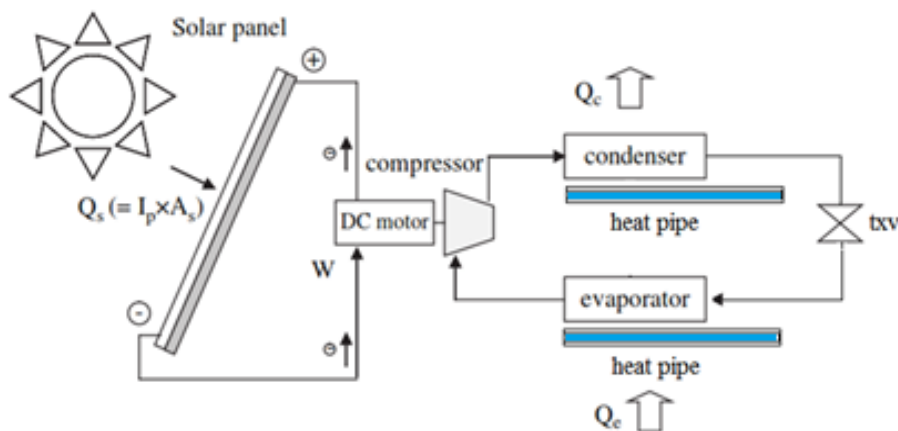
Nowadays, there is global attention placed on the development of active cooling and heating technology using solar energy. There are considerations of research into the combination of passive and vapour compression systems. A cooling system using solar energy to drive the power has several advantages as it is simple and requires only a small operational cost. Part of the air conditioning system is a combination of solar collectors, inverters, and conventional refrigeration systems. This research was conducted to study the heat transfer efficiency of a heat-pipes heat-exchanger as an additional component in the solar-assisted air-conditioning system for comfort cooling. The air temperature and the flow pattern in a room were tested and compared to those of a conventional system.

The energy consumption of a heat-pipes heat-exchanger running in a room is calculated based on the difference of temperature that has been reduced between the inlet and the outlet after the air has passed through the heat-pipes heat-exchanger. The best system to fulfil the user's comfort level of satisfaction and optimum power consumption is a combination of these system

components. The combination of refrigeration coils to heat-pipes and the right location of airflow will give an optimal result for comfort cooling.

Naturally, room heat comes from the environment, solar radiation, and the activities within the room to create an uncomfortable condition. With conventional cooling, the warm air from the room is recirculated into the room by passing through an evaporator coil. The exchange between the cold evaporator refrigerants in the coils with the circulating air will make it colder. As all air in the room passes through and exchanges heat with the coils, the room will eventually become colder.

A heat-pipes heat-exchanger can be purposely installed before the air enters the coils to assist the evaporator in further lowering the temperature. The heat from the airflow can be pre-cooled from 1 K to 5 K before making contact with the evaporator coil surface. This heat-pipes evaporator coil combination reduces the work of the compressor as it decreases the return air temperature to the coil, thus increasing the evaporating capacity. Since solar energy did not contribute directly to the air conditioning system, solar collector data were taken from the existing average temperature of solar panel conversion of thermal energy. The study of ventilation and the airflow requirement was carried out to suit the research project, and the heat-pipes heat-exchanger's temperature decreasing data were calculated to suit the applications. Theoretical discussion is presented on theories related to this research in terms of its main components, namely solar cooling, compression system, heat-exchanger, heat-pipes and blower. The schematic drawing and system applications of the work are presented below. The solar air conditioning system, the heat-pipes heat-exchanger and the room set-up are shown in Figures 3.1 to 3.3.



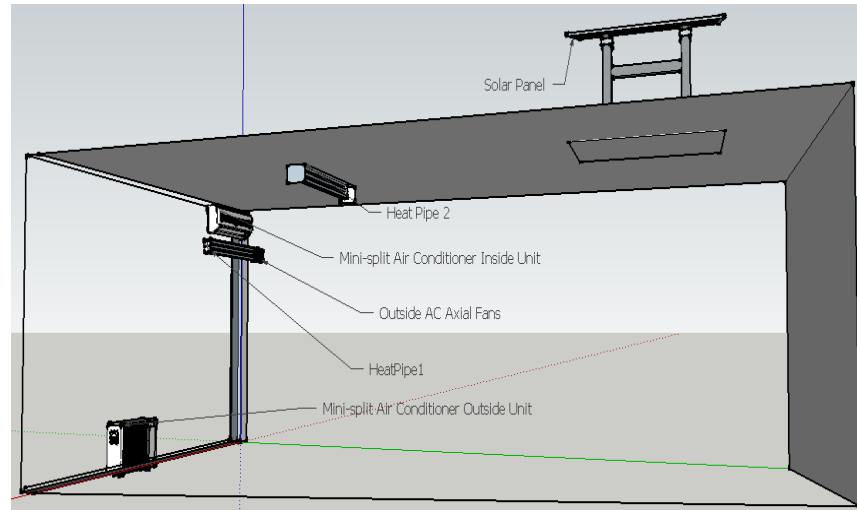


Figure 3.1: A schematic drawing of a solar air conditioning system with a heat-pipes heat-exchanger that assists in the pre-cooling of the evaporator and condenser airside. *Abdullah (2016)*.

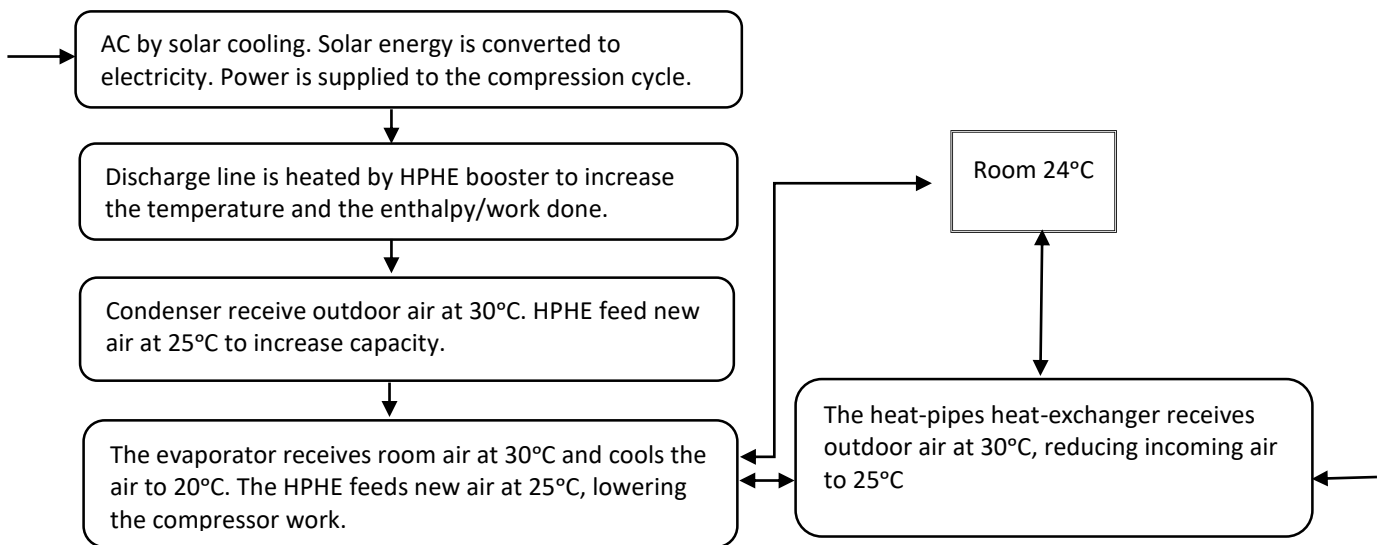


Figure 3.2: The schematic drawing of the research methodology flow chart for the air conditioning system with the assistance of solar energy and heat-pipes heat-exchanger as passive cooling. *Abdullah (2016)*.

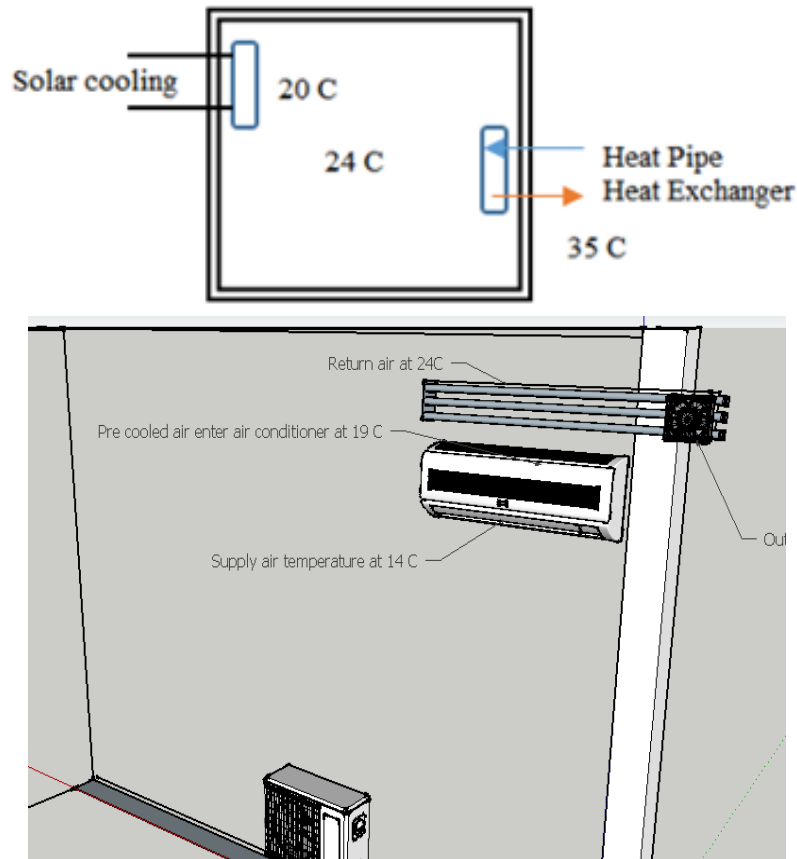


Figure 3.3: Heat-pipes heat-exchanger application in a room to assist in lowering the air supply for comfort cooling. *Abdullah (2016).*

3.2 SOLAR COOLING

Many cooling processes are feasible for the transformation of solar. Compared to the thermally driven technologies, which may use a solar thermal collector to provide heat to drive a cooling process, technologies based on heat transformation are the best to be developed. A basic figure to describe the quality of the conversion of heat into cold is the thermal performance, COP. Henning (2007) describes the thermal COP is defined as the useful cold Q_{cold} , per unit of invested driving heat, Q_{heat}

$$COP = \frac{Q_{cold}}{Q_{heat}} \quad (3.1)$$

where a basic process of the first and second law of thermodynamics is applied,

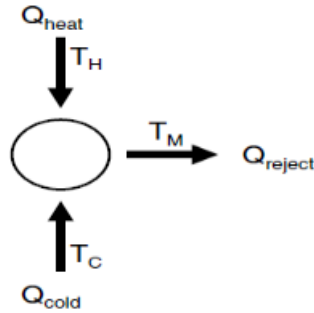


Figure 3.4: Thermodynamic scheme of a heat-driven heat pump or chiller. *Henning (2007)*.

$$COP_{ideal} = \frac{T_C}{T_H} \cdot \frac{T_H - T_M}{T_M - T_C} \quad (3.2)$$

where T_C is the cold source, T_H is the temperature of the driving heat source and T_M is the intermediate temperature level at which the heat is rejected to a heat sink (Henning 2007).

3.3 FORMULAS FOR SOLAR THERMAL REFRIGERATION AND HEAT EXCHANGERS

3.3.1 Solar Based Cooling and Refrigeration Systems

A solar electric refrigeration system consists of a photovoltaic panel (PV) and an electrical refrigeration compressor to create a high compressed vapour. The available PV for commercial use is silicon semiconductors. The efficiency can be defined by the ratio of power W (kW) to the surface area of the panel (A_s) and the direct irradiation of a solar beam I_p ,

$$\eta_{sol-pow} = \frac{W}{I_p \times A_s} = \frac{W}{Q_s} \quad (3.3)$$

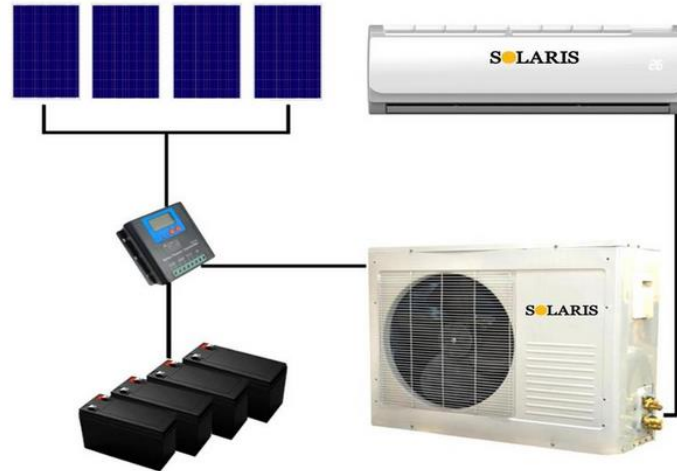


Figure 3.5: Schematic process of solar air conditioning. *BCI ENERGY*.

When applying to a refrigeration cycle, the product is a cooling power Q_e where;

$$\eta_{\text{pow-cool}} = \frac{Q_e}{W} \quad (3.4)$$

and,

$$\eta_{\text{sol-cool}} = \frac{Q_e}{Q_s} \quad (3.5)$$

Another common term used in solar air conditioning is the coefficient of performance (COP). For a standard cooling system that ranges from $T_e = 5^\circ\text{C}$ to 15°C and $T_c = 45^\circ\text{C}$ to 61°C , the COP of the vapour compression machines is 1.1 to 3.3. Figure 3.5 shows the schematic process of solar air conditioning.

3.3.2 Solar Thermal Refrigeration

The refrigeration effect is produced by solar thermal systems using solar heat rather than the electrical source. A solar collector is heated to become a heat engine or thermal compressor for the refrigeration machine. The efficiency of a solar collector is primarily determined by its working temperature. With a heat engine or thermal compressor, the higher temperatures make them work more efficiently. This trend has become a design consideration for a solar thermal system. Flat plate solar collectors are the most common type, which consists of a metallic absorber and an insulated casing topped with glass plates. The other type is evacuated type collectors, which perform better at high temperatures. They are made of glass tubes with metallic absorbers inserted into evacuated glass tubes to withstand the pressure difference between the vacuum and the atmosphere.

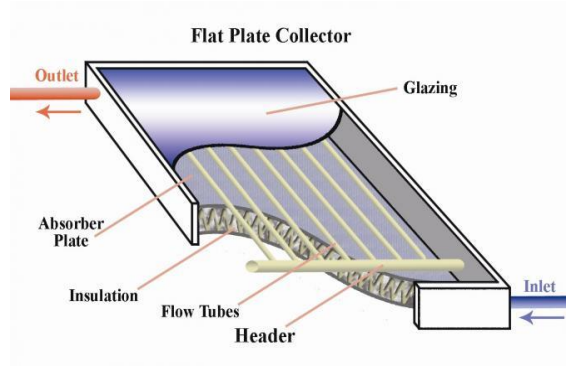


Figure 3.6: Schematic diagram of solar flat plate type collectors for thermal refrigeration. *Jiaying Passion New Technology Co. Ltd.*

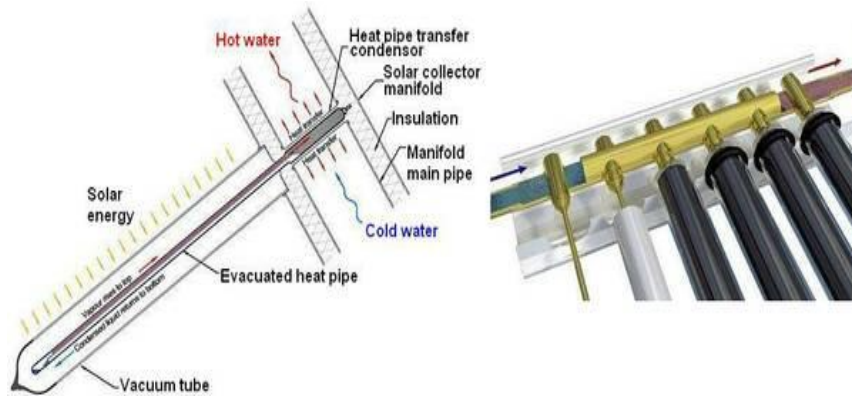


Figure 3.7: Schematic diagram of solar evacuated tube type collectors for thermal refrigeration. *Freefuelforever.*

In a solar thermomechanical refrigeration system, the solar heat is turned to mechanical work and drives the vapour compression compressor. A solar collector receives solar radiation Q_s ($A_s \times I_p$) and supplies Q_g to a heat engine at a temperature of T_H . This ratio between Q_g and Q_s is defined as the thermal efficiency of a solar collector, η_{sol_heat} ,

$$\eta_{sol_heat} = \frac{Q_g}{I_p \times A_s} = \frac{Q_g}{Q_s} \quad (3.6)$$

where η_{sol_heat} is less than 1 due to optical and thermal losses.

Mechanical work W is produced by a heat engine and rejects heat Q_a to ambient temperature T_M . The efficiency of the engine η_{heat_pow} is defined as the work produced per heat input Q_g ,

$$\eta_{heat_pow} = \frac{W}{Q_g} \quad (3.7)$$

The mechanical work W turns the compressor on the refrigeration system to remove heat Q_e from the cooling load of the room at temperature T_L . There is a condenser heat Q_c which is equal to the sum of Q_e and W that is rejected to ambient T_M . Then, the overall efficiency of a solar thermomechanical refrigeration system is given by

$$\eta_{sol_cool} = \eta_{sol_heat} \times \eta_{heat_pow} \times \eta_{pow_cool} = \frac{Q_e}{Q_s} \quad (3.8)$$

where the ideal efficiency of the Carnot power cycle is

$$\eta_{heat_pow}^{id} = \frac{T_H - T_M}{T_H} \quad (3.9)$$

$$\eta_{pow_cool}^{id} = \frac{T_L}{T_M - T_L} \quad (3.10)$$

$$\eta_{heat_pow}^{id} = \eta_{heat_pow}^{id} - \eta_{pow_cool}^{id} = \frac{T_L}{T_H} \left(\frac{T_H - T_M}{T_M - T_L} \right) \quad (3.11)$$

3.3.3 Electrical Refrigeration System

A refrigeration cycle produces cooling or heating when it can condense and evaporate refrigerant at atmospheric pressure. Ballaney (2005) mentioned that heat always flows from high temperature to lower temperature substances. This concept is applied to the refrigeration system, where a refrigerant absorbs heat in a liquid-to-vapour phase change and releases the heat at vapour-to-liquid phase change. In the phase change process, the temperature will remain constant, but the pressure will vary. The refrigeration cycle can be analysed using a pressure-enthalpy chart. The chart shows the refrigerant properties in terms of where the process point is and uses it to measure the capacity and the work performed by the components. Figure 3.4 shows the pressure-enthalpy chart of a refrigeration cycle for R134a. Figures 3.8 to 3.11 show the refrigeration capacity as measured by a pressure-enthalpy chart.

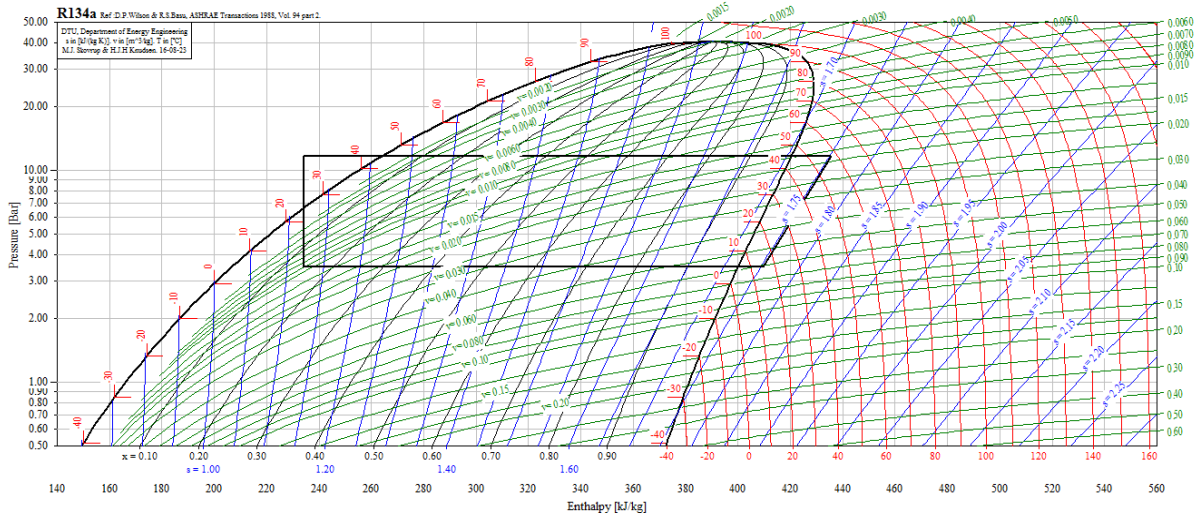


Figure 3.8: Log (p) -h diagrams of R134a. *CoolPack*.

3.3.3.1 Refrigerating Effect (W_e)

As the temperature of the cooling coils is lower than the room space, the heat flows from the room to the cooling coils. Refrigerating effect W_e are the heat that the evaporator absorbs in kJ/kg, inside the evaporator coils.

$$W_e(kJ/kg) = h1(kJ/kg) - h4(kJ/kg) \tag{3.12}$$

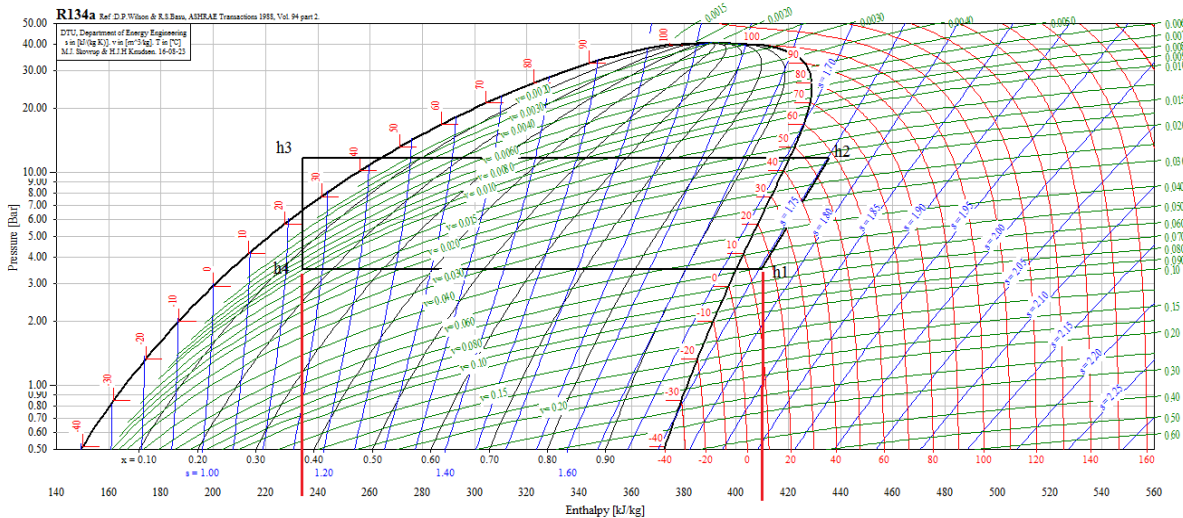


Figure 3.9: Refrigerating effect. *CoolPack*.

3.3.3.2 Compressor Work-done (A_w)

The compressor changes the refrigerant pressure to be higher than the ambient pressure so that the temperature will be higher than the ambient.

$$A_w(kJ/kg) = h_2(kJ/kg) - h_1(kJ/kg) \quad (3.13)$$

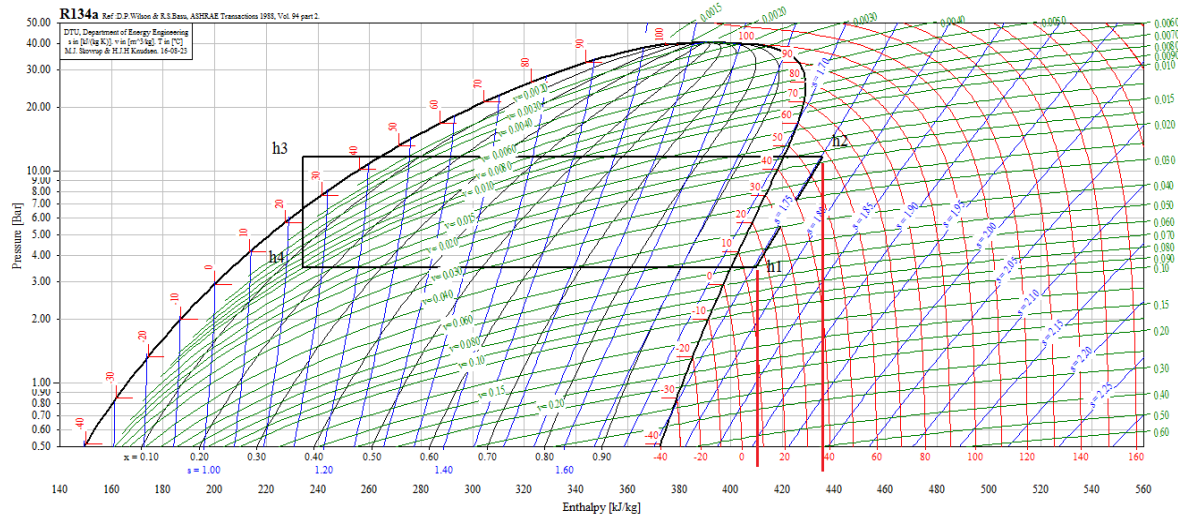


Figure 3.10: Compressor work done. *CoolPack*.

3.3.3.3 Condensing Effect (W_c)

The condenser releases the heat to the ambient through the heat transfer action between the refrigerant and the passing air. The work can be measured by

$$W_c(kJ/kg) = h_2(kJ/kg) - h_3(kJ/kg) \quad (3.14)$$

or

$$W_c(kJ/kg) = W_e(kJ/kg) + A_w(kJ/kg) \quad (3.15)$$

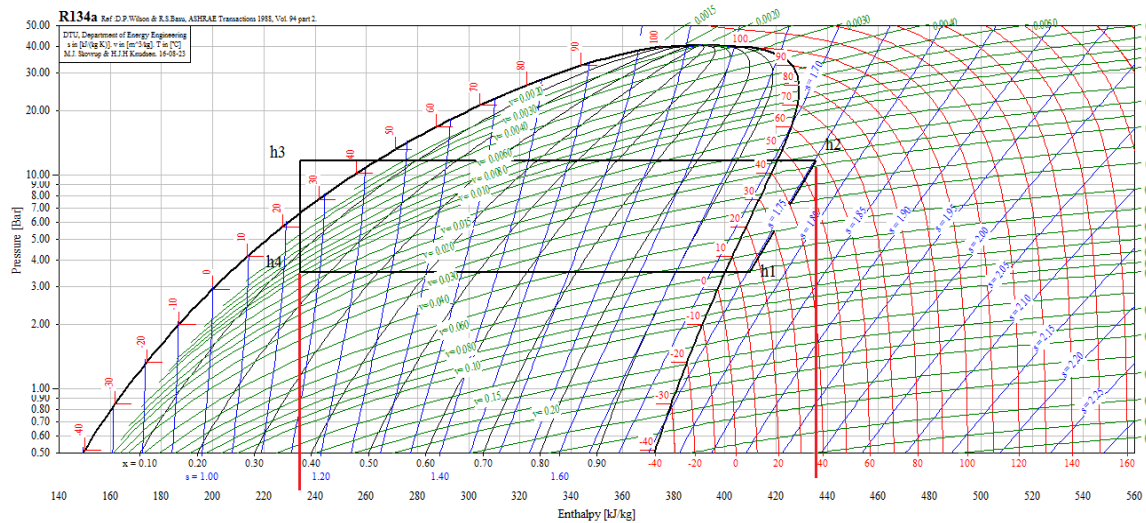


Figure 3.11: Condensing effect. *CoolPack*.

3.3.3.4 Coefficient of Performance (COP)

The electrical input of the compressor can be measured by a coefficient of performance. A bigger COP shows an efficient system operation

$$COP = \frac{W_e(kJ/kg)}{A_w(kJ/kg)} = \frac{h1(kJ/kg)-h4(kJ/kg)}{h2(kJ/kg)-h1(kJ/kg)} \quad (3.16)$$

3.3.3.5 Compression Ratio

Dossat (2001) suggested that the higher the compression ratio, the lower the capacity and the lesser the flow of refrigerant fluid in the cooling system. The ratio between the high pressure and the low pressure shows the flow of refrigerant fluid compressed by the compressor

$$Compression\ ratio = \frac{High\ pressure}{Low\ pressure} \quad (3.17)$$

3.3.3.6 Suction Gas Density

The bigger the suction gas density, the bigger the cooling system

$$Suction\ gas\ density\ (kg/m^3) = \frac{1}{v} (m^3/kg) \quad (3.18)$$

3.3.4 Heat-Exchanger

The heat-exchanger performance is determined by the inlet liquid temperature inside the exchanger tube, the temperature of the incoming air passing the fins and the desired air temperature. Cengel (1998) calculated the energy to the area of the heat-exchanger as

$$\dot{Q} = \dot{m}.C_p.(T_{in} - T_{out}) \quad (3.19)$$

$$A_i = n\pi D_i L \quad (3.20)$$

$$\dot{Q} = U_i.A_i.F\Delta T, \quad U_i = \frac{\dot{Q}}{A_i F \Delta T} \quad (3.21)$$

The efficiency of the heat-exchanger is calculated as

$$\varepsilon = \frac{\dot{Q}}{\dot{Q}_{max}} \quad (3.22)$$

where \dot{Q} is the actual heat transfer and \dot{Q}_{max} is the maximum heat transfer, and

$$\dot{Q} = C_a(T_{a,out} - T_{a,in}) = C_a(T_{w,in} - T_{w,out}) \quad (3.23)$$

$$\dot{Q}_{max} = C_{min}(T_{w,in} - T_{w,out}) \quad (3.24)$$

$$C_{min} = C_w$$

or

$$C_a = \dot{m}_a C_{p,a}$$

$$C_w = \dot{m}_w C_{p,w}$$

$$\varepsilon = \frac{\dot{Q}}{\dot{Q}_{max}} = \frac{C_c(T_{c,out} - T_{c,in})}{C_{min}(T_{h,in} - T_{c,in})} \rightarrow \frac{C_c(T_{c,out} - T_{c,in})}{C_{min}(T_{h,in} - T_{c,in})} = \varepsilon \frac{C_{min}}{C_c}$$

$$T_{c,out} = T_{c,in} + \frac{\dot{Q}}{\dot{C}_c} \quad (3.25)$$

The heat-exchanger area can be calculated as

$$NTU = \frac{UA_{HE}}{C_{min}}$$

$$A_{HE} = \left(\frac{C_{min}}{U} \right) NTU \quad (3.26)$$

3.3.5 Heat-Pipes Heat-Exchanger

The calculation for the heat-pipes heat-exchanger is based on ESDU (1979) performance design. The electrical Ohms law analogy is used to model the heat-pipes where the heat flow is proportional to the temperature difference of the evaporator and condenser, and proportionally inverse to the heat resistance of both regions. Figure 3.12 shows the heat transfer in a heat pipe.

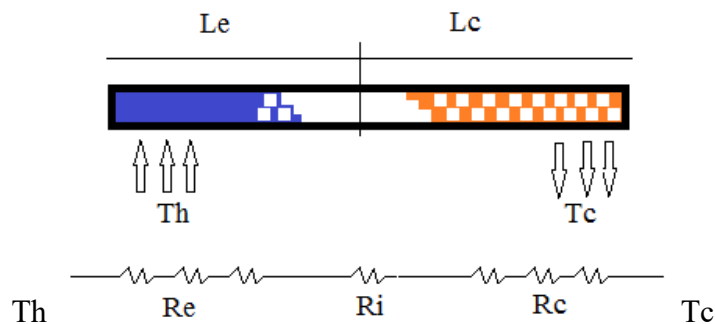


Figure 3.12: Heat transfer in a heat pipe. *ESDU (1979).*

$$Q = \frac{T_e - T_c}{R_{THR,eq}} \quad c.f. \quad I = \frac{\Delta V}{R_{eq}} \quad (3.27)$$

The heat resistance prevents heat flow. The resistance is

$$R = \frac{1}{\frac{1}{R_2 + R_3 + R_4 + R_6 + R_7} + \frac{1}{R_5}} \quad (3.28)$$

The resistance between the heat sink and the evaporator surface is

$$R_1 = \frac{1}{h_{co} A_{co}} \quad (3.29)$$

The resistance across the condenser wall is

$$R_2 = \frac{\ln(D_o/D_i)}{2\pi L c k_s} \quad (3.30)$$

The condenser fluid resistance is

$$R_3 = \frac{1}{h_{ci} A_{ci}} \quad (3.31)$$

The resistance of the flow from the evaporator to the condenser is

$$R_4 = \frac{\Delta T_{sat,e-c}}{Q} \quad (3.32)$$

The resistance of the heat-pipe length is

$$R_5 = \frac{(0.5L_e + L_a + 0.5L_c)}{A_{cs} K_s} \quad (3.33)$$

The resistance of the boiling fluid in the heat-pipes can be written as

$$R_6 = \frac{1}{h_{ei} A_{ei}} \quad (3.34)$$

The resistance across the evaporator wall is

$$R_7 = \frac{\ln(D_o/D_i)}{2\pi L c k_s} \quad (3.35)$$

The resistance between the heat source and the surface of the evaporator is

$$R_2 = \frac{1}{h_{eo} A_{eo}} \quad (3.36)$$

3.3.6 Blower

The airflow selected is $Q = V.A$ (3.37)

where Q = airflow rate, m³/s
 V = air velocity, m/s
 A = surface area, m²

3.3.7 Procedure for Energy-Saving

In this study, the energy-saving for a heat-pipes heat-exchanger for cooling system applications using solar energy has been compared to the conventional vapour compression system. Niu (2002) stated that the vapour compression system for space conditions is a system that uses air as the medium for cooling. ASHRAE (2001) mentioned that the air should be cooled to the dew point temperature, at a range from 282 K (4 °C) to 286 K (13 °C). Additionally, the cooling energy used by the heat-pipes application of the air conditioning system was compared to the conventional vapour compression system. Mezzei (2002) stated that the air should not be returned to the room and must be treated for a comfortable air range. The energy saved is equal to the energy used by the conventional vapour compression (+ the energy saved by the solar air-conditioning) minus the energy used by the heat-pipes application to the air conditioning as expressed by the equation:

$$\text{Energy}_{\text{saved}} = \text{Energy}_{\text{vp+sol}} + \text{Energy}_{\text{hphe}}$$

3.4 FORMULAS FOR THE COMPUTATIONAL FLUID DYNAMICS

The fundamental basis to solve computational fluids problems is the Navier-Stoke equations (conservation law). The three conservation principle methods of computational fluid dynamics calculations are mass, momentum and energy. The mass and momentum equations when combined with the conservation of energy equation, will form a set of non-linear partial differential equations. Priyadumkol (2014) stated that the four terms in the general differential equation are the unsteady term (transient), the convection term, the diffusion term and the source term.

The conservation of mass equation is

$$\frac{\partial \rho}{\partial t} + \nabla \cdot (\rho \vec{V}) = 0 \quad (3.38)$$

The conservation of momentum equation is

$$\rho \frac{\partial \vec{V}}{\partial t} + \rho(\vec{V} \cdot \nabla)\vec{V} = -\nabla p + \rho \vec{g} + \nabla \cdot \tau_{ij} \quad (3.39)$$

The different states of flows are identified as laminar and turbulent flow. As laminar flow occurs at low-to-moderate values of the Reynolds number, the turbulent flows occur in the opposite limit of high Reynolds numbers. The numerical modelling used the Reynolds Averaged Navier Stokes (RANS) equations which govern the mean velocity $\bar{u}(y)$ and pressure.

The Reynolds stress model is divided into two turbulence parameters, the kinetic energy k and the energy dissipation rate ε (epsilon). The k - ε turbulent energy parameters can be defined as

$$k \equiv \frac{1}{2}(\overline{u'^2} + \overline{v'^2} + \overline{w'^2}) \quad (3.40)$$

$$\varepsilon \equiv \nu \left[\left(\frac{\partial u'}{\partial x} \right)^2 + \left(\frac{\partial u'}{\partial y} \right)^2 + \left(\frac{\partial u'}{\partial z} \right)^2 + \left(\frac{\partial v'}{\partial x} \right)^2 + \left(\frac{\partial v'}{\partial y} \right)^2 + \left(\frac{\partial v'}{\partial z} \right)^2 + \left(\frac{\partial w'}{\partial x} \right)^2 + \left(\frac{\partial w'}{\partial y} \right)^2 + \left(\frac{\partial w'}{\partial z} \right)^2 \right] \quad (3.41)$$

When the fundamental laws of mechanics are applied to a fluid, the governing equations are

$$\frac{\partial U_j}{\partial x_j} = 0 \quad (3.42)$$

$$\frac{\partial U_i}{\partial t} + U_j \frac{\partial U_i}{\partial x_j} = -\frac{1}{\rho} \frac{\partial P}{\partial x_i} + \frac{\partial}{\partial x_j} \left[\nu \left(\frac{\partial U_i}{\partial x_j} + \frac{\partial U_j}{\partial x_i} \right) - \overline{u_i u_j} \right] - \beta(T - T_{ref})g_i \quad (3.43)$$

$$\overline{u_i u_j} = \nu_t \left(\frac{\partial U_i}{\partial x_j} + \frac{\partial U_j}{\partial x_i} \right) - \frac{2}{3} K \delta_{ij}$$

$$\rho c \left(\frac{\partial T}{\partial t} + U_j \frac{\partial T}{\partial x_j} \right) = k \frac{\partial^2 T}{\partial x_j \partial x_j} - \rho c \frac{\partial}{\partial x_j} (\overline{u_j T'}) + \Phi + \emptyset \quad (3.44)$$

$$\overline{u_j T'} = \frac{\nu_t}{\sigma_t} \left(\frac{\partial T}{\partial x_j} \right)$$

$$\Phi = \mu \left(\frac{\partial U_i}{\partial x_j} + \frac{\partial U_j}{\partial x_i} \right) \frac{\partial U_i}{\partial x_j}$$

$$\emptyset = \mu \left[\overline{\left(\frac{\partial u_i}{\partial x_j} \right) \left(\frac{\partial u_i}{\partial x_j} \right)} + \overline{\left(\frac{\partial u_i}{\partial x_j} \right) \left(\frac{\partial u_i}{\partial x_j} \right)} \right]$$

For k and ε turbulence model, where k is the turbulent kinetic energy and ε the dissipation rate of k , the equations written as

$$\frac{\partial K}{\partial t} + U_j \frac{\partial K}{\partial x_j} = \frac{\partial}{\partial x_j} \left[\left(\nu + \frac{\nu_t}{\sigma_K} \right) \frac{\partial K}{\partial x_j} \right] + \nu_t \left[\left(\frac{\partial U_i}{\partial x_j} + \frac{\partial U_j}{\partial x_i} \right) \frac{\partial U_i}{\partial x_j} + \frac{\beta}{\sigma_t} g_j \frac{\partial T}{\partial x_j} \right] - \varepsilon \quad (3.45)$$

$$k = \frac{1}{2} \overline{U_i U_j}$$

$$\varepsilon = \nu \overline{\left(\frac{\partial u_i}{\partial x_j} \right) \left(\frac{\partial u_i}{\partial x_j} \right)}$$

$$\frac{\partial \varepsilon}{\partial t} + U_j \frac{\partial \varepsilon}{\partial x_j} = \frac{\partial}{\partial x_j} \left[\left(\nu + \frac{\nu_t}{\sigma_\varepsilon} \right) \frac{\partial \varepsilon}{\partial x_j} \right] + C_1 \frac{\varepsilon}{K} \nu_t \left[\left(\frac{\partial U_i}{\partial x_j} + \frac{\partial U_j}{\partial x_i} \right) \frac{\partial U_i}{\partial x_j} + \frac{\beta}{\sigma_t} g_j \frac{\partial T}{\partial x_j} \right] - C_2 \frac{\varepsilon^2}{K} \quad (3.46)$$

where subscript t refers to turbulence

$$\mu_t = \rho C_\mu K^2 / \varepsilon; \nu_t = \mu_t / \rho;$$

$C_\mu=0.09$; $C_1=1.44$; $C_2 =1.92$; $\sigma_K =1.0$; $\sigma_\varepsilon=1.3$; reference temperature = 300K. For the simulation, the pressure is assumed to be constant and the K and ε value at the air inlet is set to

$$K = \frac{3}{2} (U_{ave} T_i)^2 \quad (3.47)$$

$$\varepsilon = \frac{C_\mu^{3/4} K^{3/2}}{\kappa L} \quad (3.48)$$

where U_{ave} is the inlet velocity, T_i is the turbulence and $\kappa = 0.41$ is the Von Karman constant.

CHAPTER IV

RESEARCH METHODOLOGY

CHAPTER OVERVIEW

This chapter discusses the research methodology of cooling a room with passive cooling equipment. The cooling method using solar air-conditioning and an air pre-cooling technique through the use of the heat-pipes heat-exchanger as a cooling tool are discussed in detail. The method used was both experimental and computational. The process started with a simulation using CFD, taking into consideration the ASHRAE Standards 55 for comfort cooling and later realised with the physical experiments. The simulations run on Laminar and Reynold Average Navier-Stokes equations, with the temperature, flow distributions and patterns recorded. The experimental test box which was equipped with thermocouples connected to a data logger collected all temperature information from the ambient air as the inlet, fan heater and the heat-pipes heat-exchanger. The air outlet from the test-box passing through the condenser side of the heat-pipes heat-exchanger was taken as the final data from the outlet air.

4.1 INTRODUCTION

This chapter presents the cooling system's method of using heat-pipes heat-exchanger as the passive cooling equipment in supplying pre-cooling air to the solar air-conditioning and the refrigeration cooling system. The heat-pipes are additional equipment fitted to the refrigeration system. The system will benefit from the solar energy conversion to electricity and pre-cooling of the air. This chapter also presents the overall overview of the heat-pipes' testing with different configurations.

The heat-pipes heat-exchangers were tested with a simulation using computational fluid dynamics to see the convergence of airflow, temperature, and traces. The software used for the simulations is the CFD-ACE and ANSYS-Fluent. The evaporator and the condenser coils of an air-conditioning are not presented in the test system as it is to be at standard temperature. The

average comfortable temperature according to ASHRAE Standards 55 is 295.5K to 298K (22.5 °C to 25 °C) for the indoor airside temperature and 303K (30 °C) for the outdoor air temperature.

The plate type photovoltaic (PV) solar collector calculation data is from an existing measurement. The standard cooling system consists of a compressor, condenser, expansion valve and evaporator to absorb and desorb heat from a room. The test is equipped with a data measurement system and sensing tools. An acrylic test box replicates a room with different configurations of opening. Figures 4.1 and 4.2 show the refrigeration equipment and its processes, while Figures 4.3 and 4.4 show the heat-pipes heat-exchanger locations as additional passive cooling equipment to lower the supply of air from the warm ambient temperature of the box. Figure 4.5 explained the research methodology flow chart.

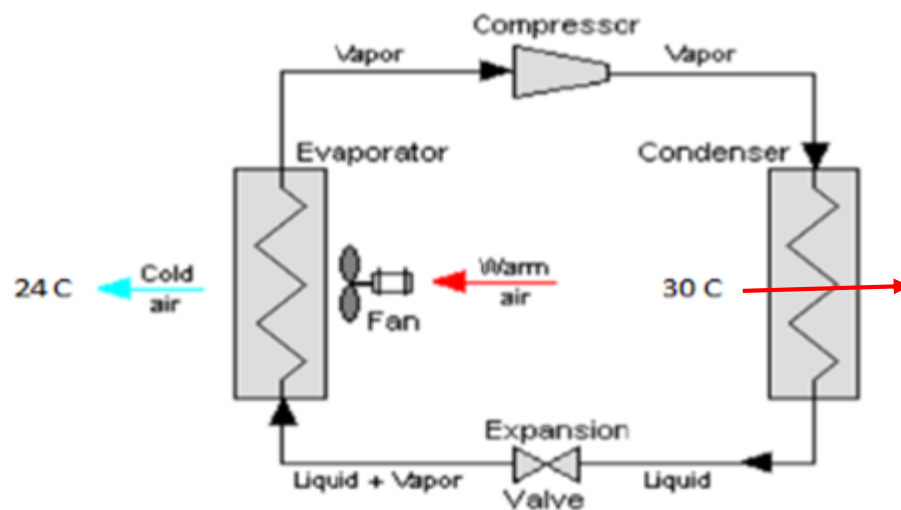


Figure 4.1: Schematic drawing of a standard refrigeration cycle equipment for air conditioning application. *Stoecker and Jones (1982).*

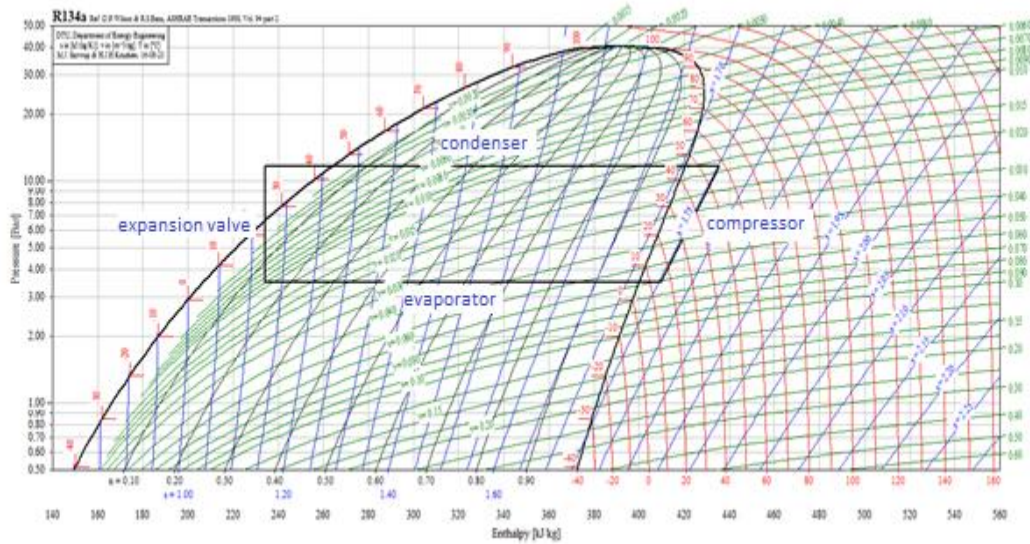


Figure 4.2: Pressure-enthalpy diagram of the work done by each equipment. The standard operating system for the refrigeration cycle. *CoolPack*.

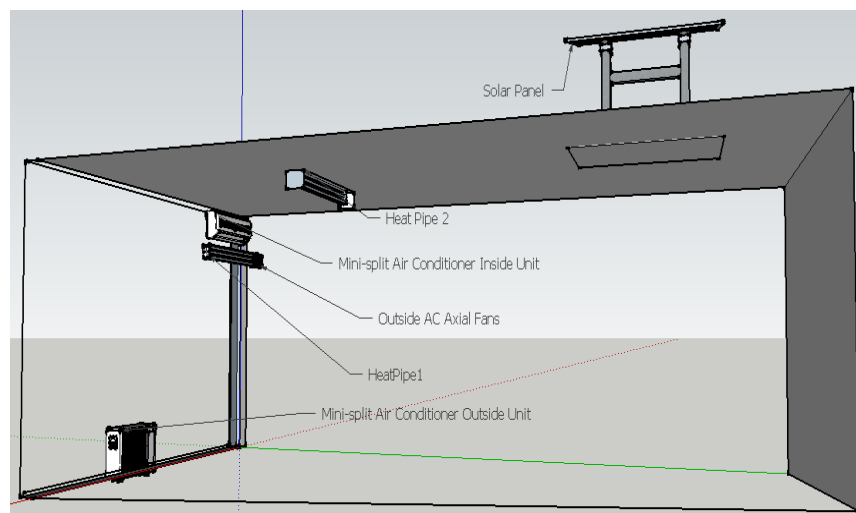
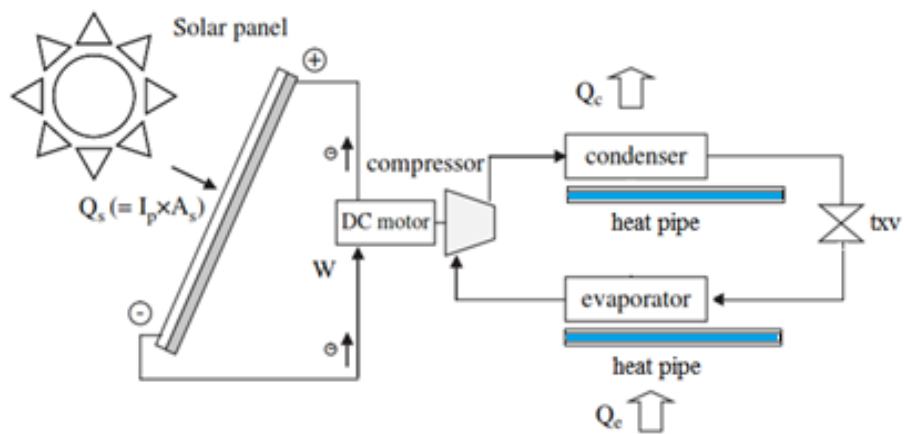


Figure 4.3: A schematic drawing of a solar air conditioning system with a heat-pipes heat-exchanger that assists in the pre-cooling of the evaporator and condenser airside. *Abdullah (2016)*.

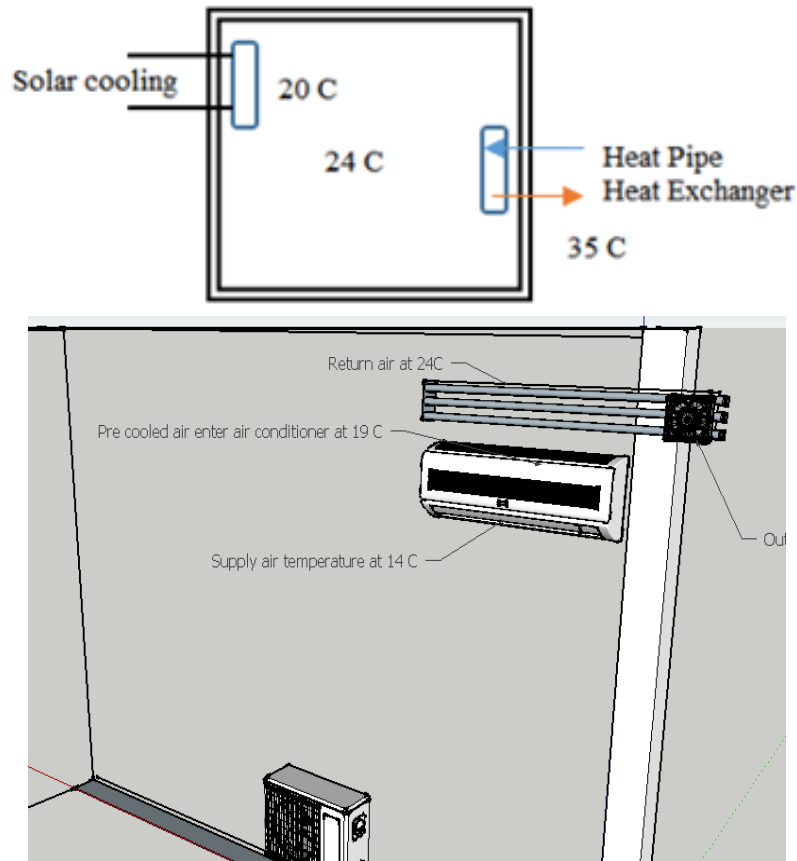


Figure 4.4: Heat-pipes heat-exchanger application in a room to assist in lowering the air supply for comfort cooling. *Abdullah (2016).*

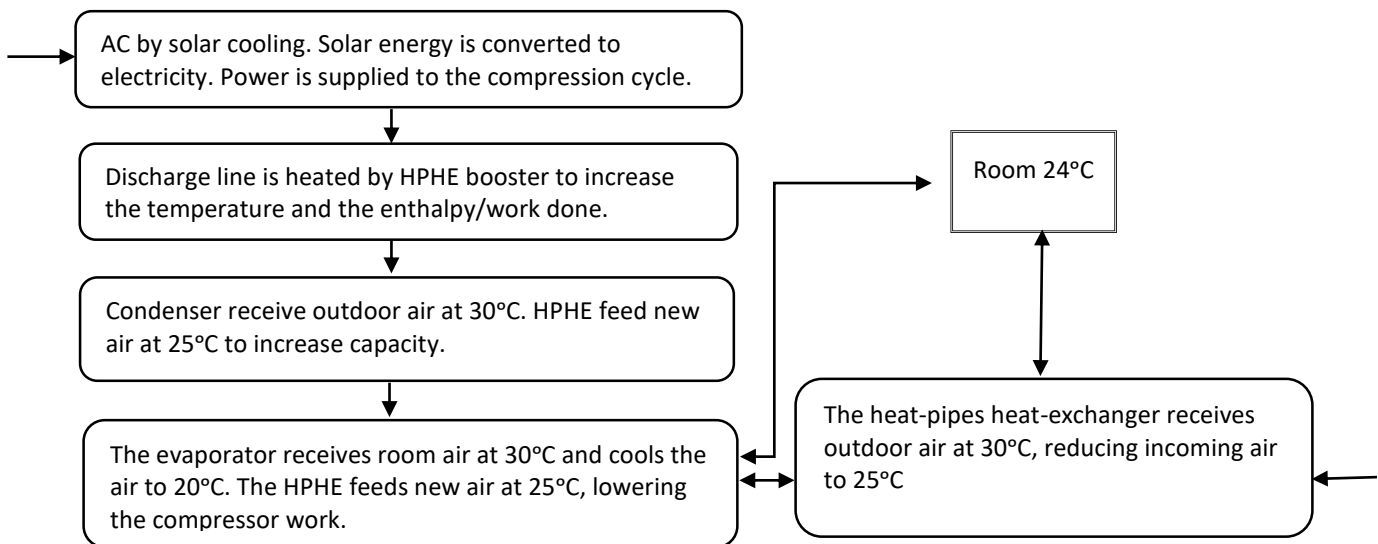


Figure 4.5: The schematic drawing of the research methodology flow chart for the air conditioning system with the assistance of solar energy and heat-pipes heat-exchanger as passive cooling. *Abdullah (2016).*

According to Ming Qu (2010), a solar thermal system could supply 39% of cooling and 20% of heating energy for his tested space. The system used an absorption refrigeration system and a heat recovery heat exchanger. In the '70s and '80s, significant research on solar thermal absorption cooling was conducted in the United States but did not become established in the global market due to high initial cost, lack of commercial hot water driven absorption chillers, scarcity of demonstrations and impartial assessments by reputable institutions (Kulkarni, 1994). Solar thermal energy has since been used in research, particularly in the high-temperature solar receiver with an absorption chiller (Duff et al. 2004; Hewett 1995).

Solar energy alone will not achieve the requirement for thermal and comfort cooling. Other factors such as air distribution, ventilation system, and pre-cooling should be considered in thermal comfort. Room air distributions through ventilation and flow direction are broad factors that contribute to thermal comfort. Kivva and Huynh (2009) used computational fluid dynamics to study the ventilation flow in a room by recording and tracing the entering and exhaust air patterns. Idris (2013) studied the edges of a room's window opening to select the best edge and location of the opening. Huynh (2012) studied natural ventilation in a room with a solar chimney using computational fluid dynamics and proposed that natural ventilation would significantly help to reduce heating, ventilating and air conditioning demand.

The practical project for the testing unit was designed and installed in Building 1, Level 2 of the Faculty of Engineering and IT workshop. Figure 4.8 below shows the photographic image of the test unit. The configurations of the acrylic box opening were designed to record the gradient of the temperature and velocity in the box that was affected by the heat-pipes heat-exchanger. The test unit was used to measure the temperature of the heat transfer process between the heat-pipes end and to record the inlet (supply) and the outlet (return) temperature of the room. The results were then compared to the standard cooling application. The test unit collected the measured pre-cooled air supplied to the evaporator and the condenser to minimise the system load and calculate the energy recovered. Figure 4.6 explained the process.

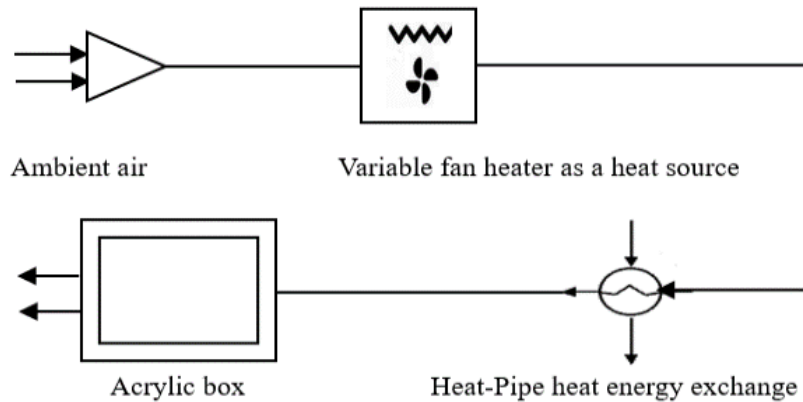


Figure 4.6: The workflow of the experimental project. Ambient airflow and temperature are regulated by a variable fan and heater before passing a finned type heat-pipes heat-exchanger. The acrylic box then collects the result of the inside temperature distributions. Thermocouples that are connected to a data logger are used at several locations for temperature data collection. *Abdullah (2018)*.

An adjustable fan with a heater was used for the test to create constant airflow to the internal space of the box. The fan is capable of supplying an airspeed up to 4m/s and the heater coil elements can be heated up to 338K (65°C). The reason for using an adjustable fan and heater is to mimic the ambient condition of tropical countries where the ambient temperature can sometimes reach 313K (40°C). A thermocouple sensor wire located between the outlet of the fan heater and the inlet of the heat-pipes heat-exchanger entering air was connected to a data logger.

The heat-pipes heat-exchanger was intended to reduce this high ambient temperature before entering the conditioned space. The low boiling point temperature of the refrigerant was used to manipulate the air density in the room by absorbing and desorbing heat. A heat-pipe heat-exchanger was used to create different air densities and air movement in the room. A cross-flow heat-exchanger with a row of in-line 3 by 3 straight copper tubes that had fins, filled with 11ml of liquid R134a was used for the test. The total length of the heat-pipes was 650mm in which 500mm of the tube's working length was finned. The liquid volume was one-third of the straight copper tube, allowing the optimum process of evaporation and condensation within the tube.

Table 4.1 shows the specification of the heat-pipes heat-exchanger for the experiment. The work started with the heat-pipes heat-exchanger evaporator section absorbing the heat of the incoming ambient air and transferring it to the condenser section. As the heat in the tube was warmer than the ambient temperature, the heat was released back to the surroundings. The transferring processes of heat were determined by the R134a refrigerant inside the tubes in contact

with the ambient surrounding air, and in the process, cooled the supplied air passing through the heat exchanger into the room.

The position of the heat-pipes heat-exchanger was lifted 10° from the horizontal axis, at the condenser section so that the slant position allowed the condensed liquid refrigerant to travel back to the evaporator section by gravitational action. Figure 4.7 shows the locations of the heat-pipes which were on the top and sides of the acrylic box.

Table 4.1: The specification of the heat-pipes heat-exchanger used. *Abdullah (2018)*.

Domains	Specifications
$C_{p_{air}}$, kJ/kg.K	1.213
Diameter, ID/OD mm	9/10
Length, mm finned	650/500
Heat transfer coefficient U_1 , kW/m ² .K	0.171
Energy balance \dot{Q} , kW	0.195
ΔT , °C/K	4.18/277.18

An acrylic panel was used as a constraint space for the temperature distribution collector box. As thermal imaging tools were used to capture the thermal distribution and traces in the box, the transparency of the material was valuable. Two openings for the evaporator and the condenser section on each side of the wall were cut to make way for the air entering and leaving. The two openings which were of the size 200 mm x 50 mm each was located on the sidewall and the top of the box while no opening was allowed in the adiabatic process. Only one heat-pipe heat-exchanger at the selected location was tested at a time, while the other opening was closed. Thermocouples were placed in several locations within the box and read by a data logger to show the distribution of air temperature. The average box temperature was then measured. Figures 4.9 and 4. 10 show the installations.

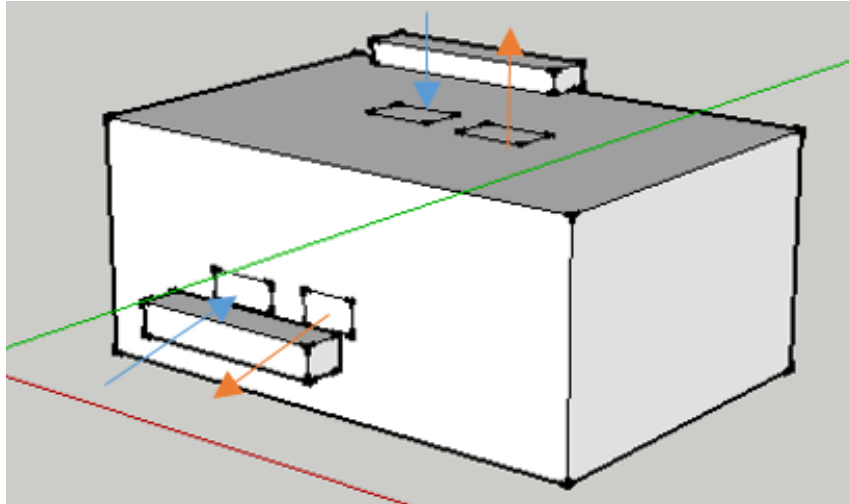


Figure 4.7: The layout of the fresh air intake and the exhaust air outlet locations with the heat-pipes heat-exchanger installed on the wall side and at the top of the box.

Top opening

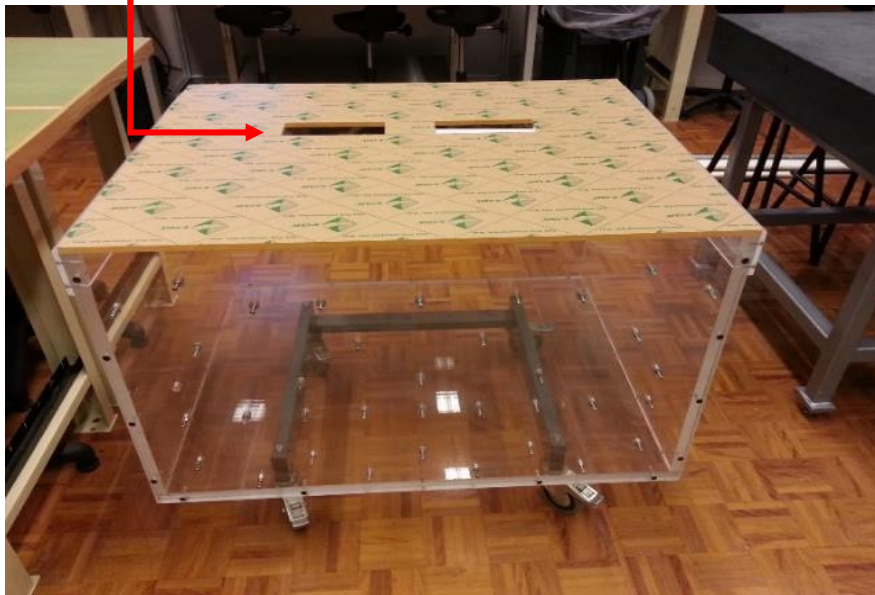
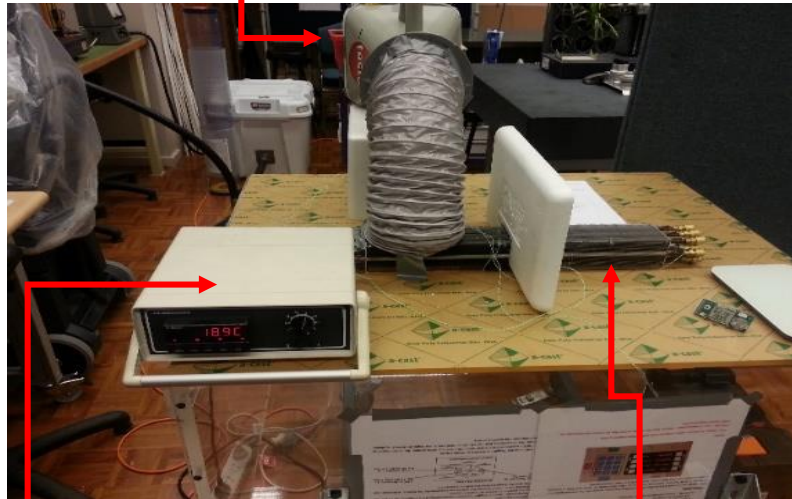


Figure 4.8: The acrylic box used to collect air temperature and flow distributions. The box size is 1000 mm L x 820 mm W x 620 mm H. The opening cut is 200 mm x 50 mm to incorporate the inlet and outlet of air.

Adjustable speed and temperature fan heater



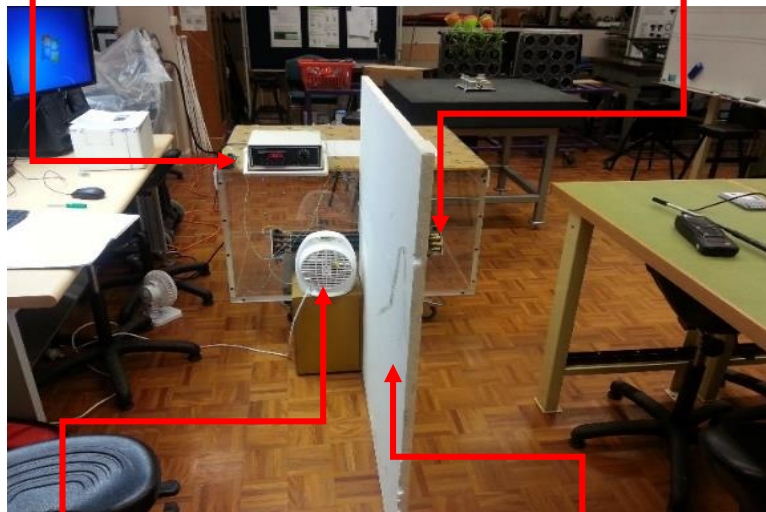
Data logger

Heat-pipes heat-exchanger

Figure 4.9: The acrylic box and the test measuring components installed. The measurement shown is taken from the top opening.

Data logger

Heat-pipes heat-exchanger



Adjustable speed and temperature fan heater

Divider for air entering and leaving

Figure 4.10: The acrylic box and the test measuring components installed. The measurement shown is taken from the wall side opening.

Conventional energy using solar energy systems could be reduced with this method. In this study, it has been shown that energy-saving is possible when the solar energy cooling system is supported by the heat-pipes heat-exchanger. The booster system, as a support system installed in the discharge line of the refrigeration system, increases capacity and lowers the compression work.

Pre-cooling to the inlet temperature of the heat-pipes heat-exchanger reduces the compression work as the temperature at the evaporator is reduced. Solar assisted cooling with the support of the heat-pipes heat-exchanger is emphasised in this study.

Computational Fluid Dynamics (CFD) with numerical methods and algorithms are used to solve problems that involve fluid flow and to predict flow behaviours. In fluid dynamics, the fundamental governing equations, namely the conservation of mass, momentum, and energy are used to build simulation modelling. The conservation of law equation is used as the basic fundamental in solving CFD problems. The four terms in the general differential equation are the unsteady term (transient), the convection term, the diffusion term, and the source term (Priyadumkol, 2014). Computational fluid dynamic programmes, namely CFD-ACE, ANSYS Workbench, and ANSYS-Fluent were used to simulate the experimental project before the practical installation was made. Various simulations and numerical studies were tested in suitable parts of the system to see its significance to the project. The R134a refrigerant filled heat-pipes heat-exchanger was found to have the capability to drop the temperature up to 5 K differential, from the evaporator section to the condenser section. Simulations were run on the effect of the heat-pipes which were attached to the evaporator and the condenser of the air-cooled air-conditioner.

Heat-pipes heat-exchanger simulations were run extensively to verify the influences of natural and driven ventilation to the room, where opening types and locations were critically taken into consideration. Reduction of the outdoor power supply cabinet temperature using CFD simulation was performed to show the heat sink process and the simulation of the refrigerated condenser to reduce coil temperature. All simulation work was related to the significance of the project and led to the application selections of the project.

The simulation of the refrigeration condenser side was traced to show the airflow pattern of the air entering and leaving. The ambient supplied air passed through the heat-pipes heat-exchanger before entering the condenser for the condensation process. Abdullah (2016) showed that a pre-cooling of supplied air at the refrigeration condenser could enhance the process of heat rejection. The heat-pipes heat-exchanger which was attached at 100 mm from the condenser's on-coil façade was simulated using ANSYS-Fluent. Many research studies on condenser efficiency and on-coil temperature of condensers have been conducted. It has been shown that the cooling air

temperature of an outdoor unit has a significant effect on an air-conditioner's performance. If the on-coil temperature of an outdoor unit is raised by 1°C, the coefficient of performance (COP) of the air-conditioner drops by around 3% (Chow, 2002).

The optimal placement of a condenser is an important factor that can lead to a lower on-coil temperature and consequently lower energy consumption (Avara, 2008; Chow et al., 1999). Chow et al. (2002) used EXACT3 CFD code to simulate the location and the arrangements of their condenser units. They analysed the effect of different condenser arrangements in the case of a building's re-entrant on the on-coil temperature and efficiency of the condensing unit. Xue et al. (2007) studied the effects of re-entrant dimensions, air velocity across the condenser and heat rejection of each condenser on the velocity and temperature distribution of the air at re-entrant. In this study, CFD modelling was used to determine the optimum distance of the installation of the heat-pipes heat-exchanger from the condenser to enhance the heat rejection process of the condenser.

The simulation of an air heat rejection profile of an outdoor power cabinet was studied and presented in this thesis to show the thermal siphon effectiveness of passive cooling from the heat-pipes heat-exchanger. In Abdullah's (2015) simulation, it was shown that the effectiveness of the heat-pipes heat-exchanger using R134a had an effect of 33%. Abdullah (2014) performed a CFD simulation study on the effects of a heat-pipes heat-exchanger on a 3-dimensional room with natural driven ventilation. In the numerical study, ANSYS-Fluent was used to simulate and solve the decreasing method of heat using heat-pipes heat-exchanger as heat sink equipment. Various openings in the room were studied to determine the best configuration for the project. Additionally, the temperature gradient in the room, the distribution of air and flow pattern were also shown. In this study, the evaluation of the system theoretically using computational fluid dynamics calculations was carried out to analyse the significant methods. The experimental project underwent processes and tests as required by the plan. Figure 4.11 shows the flow chart of heat-pipes simulations and interactions. The study involved the following:

- The operating system, on the whole, the method, and the parameter used on the test unit project.
- Analyse the variables and adjustable parameters that could affect the system's capacity.
- A study on the energy consumption that the system could offer.

- Validation of the result of the theoretical and the simulation method.

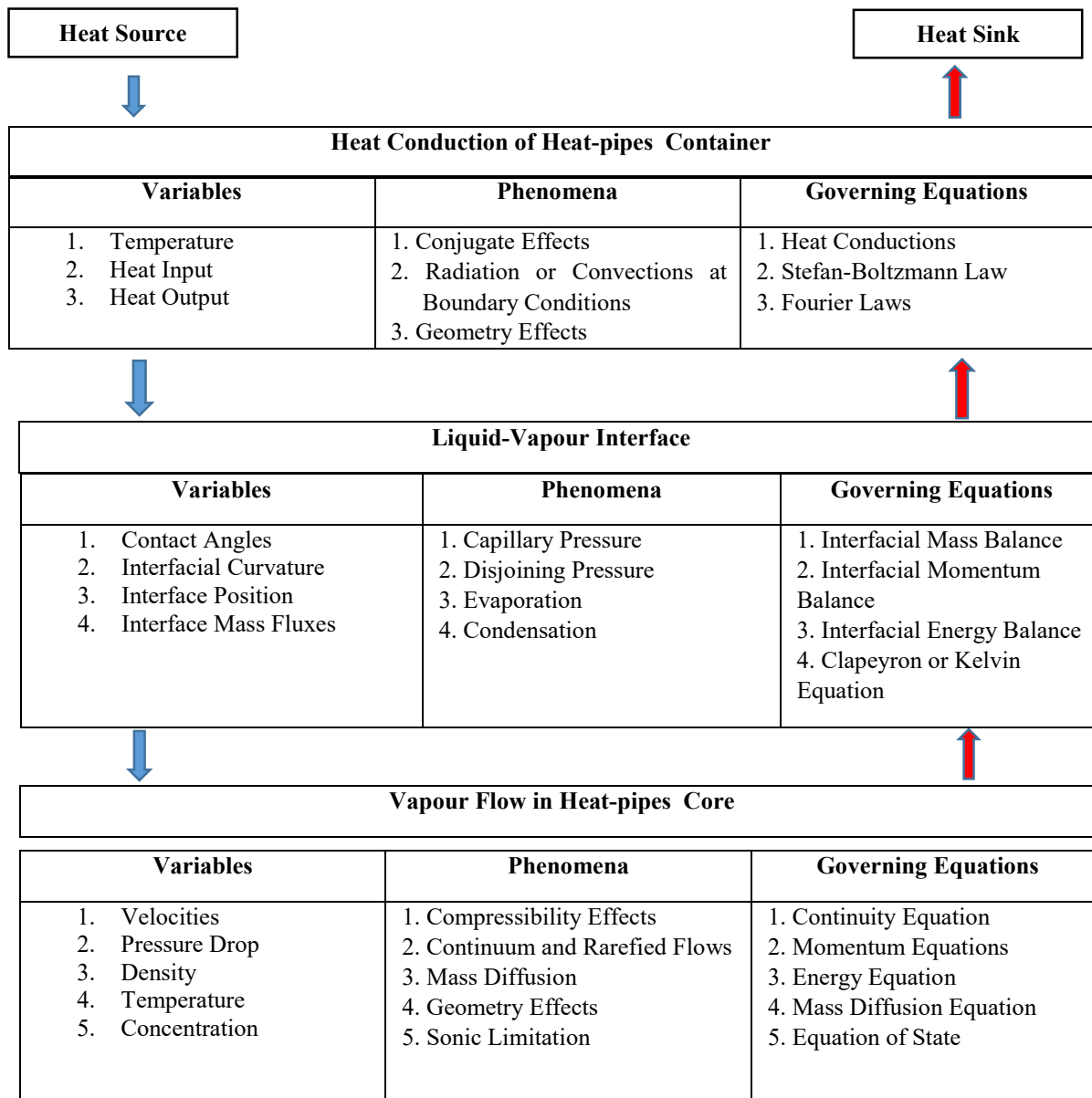


Figure 4.11: Flow chart of heat-pipes simulations and interactions. *ANSYS Fluent*.

The fundamental basis to solve computational fluids problems is the Navier-Stoke equations (conservation law). The three conservation principle methods of computational fluid dynamics calculations are mass, momentum and energy. The mass and momentum equations when combined with the conservation of energy equation, will form a set of non-linear partial differential equations. Priyadumkol (2014) stated that the four terms in the general differential equation are the unsteady term (transient), the convection term, the diffusion term and the source term.

The conservation of mass equation is

$$\frac{\partial \rho}{\partial t} + \nabla \cdot (\rho \vec{V}) = 0 \quad (4.1)$$

The conservation of momentum equation is

$$\rho \frac{\partial \vec{V}}{\partial t} + \rho (\vec{V} \cdot \nabla) \vec{V} = -\nabla \rho + \rho \vec{g} + \nabla \cdot \tau_{ij} \quad (4.2)$$

The different states of flows are identified as laminar and turbulent flow. As laminar flow occurs at a low-to-moderate value of the Reynolds number, the turbulent flows occur in the opposite limit of high Reynolds numbers. The numerical modelling used the Reynolds Averaged Navier Stokes (RANS) equations which govern the mean velocity $\bar{u}(y)$ and pressure.

The Reynolds stress model is divided into two turbulence parameters, the kinetic energy k and the energy dissipation rate ε (epsilon). The k - ε turbulent energy parameters can be defined as

$$k \equiv \frac{1}{2} (\overline{u'^2} + \overline{v'^2} + \overline{w'^2}) \quad (4.3)$$

$$\varepsilon \equiv v \left[\left(\frac{\partial u'}{\partial x} \right)^2 + \left(\frac{\partial u'}{\partial y} \right)^2 + \left(\frac{\partial u'}{\partial z} \right)^2 + \left(\frac{\partial v'}{\partial x} \right)^2 + \left(\frac{\partial v'}{\partial y} \right)^2 + \left(\frac{\partial v'}{\partial z} \right)^2 + \left(\frac{\partial w'}{\partial x} \right)^2 + \left(\frac{\partial w'}{\partial y} \right)^2 + \left(\frac{\partial w'}{\partial z} \right)^2 \right] \quad (4.4)$$

When the fundamental laws of mechanics are applied to a fluid, the governing equations are

$$\frac{\partial U_j}{\partial x_j} = 0 \quad (4.5)$$

$$\frac{\partial U_i}{\partial t} + U_j \frac{\partial U_i}{\partial x_j} = -\frac{1}{\rho} \frac{\partial P}{\partial x_i} + \frac{\partial}{\partial x_j} \left[v \left(\frac{\partial U_i}{\partial x_j} + \frac{\partial U_j}{\partial x_i} \right) - \overline{u_i u_j} \right] - \beta (T - T_{ref}) g_i \quad (4.6)$$

$$\overline{u_i u_j} = v_t \left(\frac{\partial U_i}{\partial x_j} + \frac{\partial U_j}{\partial x_i} \right) - \frac{2}{3} K \delta_{ij}$$

$$\rho c \left(\frac{\partial T}{\partial t} + U_j \frac{\partial T}{\partial x_j} \right) = k \frac{\partial^2 T}{\partial x_j \partial x_j} - \rho c \frac{\partial}{\partial x_j} (\overline{u_j T'}) + \Phi + \phi \quad (4.7)$$

$$\overline{u_j T'} = \frac{v_t}{\sigma_t} \left(\frac{\partial T}{\partial x_j} \right)$$

$$\Phi = \mu \left(\frac{\partial U_i}{\partial x_j} + \frac{\partial U_j}{\partial x_i} \right) \frac{\partial U_i}{\partial x_j}$$

$$\Phi = \mu \left[\left(\frac{\partial \bar{u}_i}{\partial x_j} \right) \left(\frac{\partial \bar{u}_i}{\partial x_j} \right) + \left(\frac{\partial \bar{u}_i}{\partial x_j} \right) \left(\frac{\partial \bar{u}_i}{\partial x_j} \right) \right]$$

For k and ε turbulence model, where k is the turbulent kinetic energy and ε the dissipation rate of k , the equations written as

$$\frac{\partial K}{\partial t} + U_j \frac{\partial K}{\partial x_j} = \frac{\partial}{\partial x_j} \left[\left(\nu + \frac{\nu_t}{\sigma_K} \right) \frac{\partial K}{\partial x_j} \right] + \nu_t \left[\left(\frac{\partial U_i}{\partial x_j} + \frac{\partial U_j}{\partial x_i} \right) \frac{\partial U_i}{\partial x_j} + \frac{\beta}{\sigma_t} g_j \frac{\partial T}{\partial x_j} \right] - \varepsilon \quad (4.8)$$

$$k = \frac{1}{2} \overline{U_i U_j}$$

$$\varepsilon = \nu \overline{\left(\frac{\partial u_i}{\partial x_j} \right) \left(\frac{\partial u_i}{\partial x_j} \right)}$$

$$\frac{\partial \varepsilon}{\partial t} + U_j \frac{\partial \varepsilon}{\partial x_j} = \frac{\partial}{\partial x_j} \left[\left(\nu + \frac{\nu_t}{\sigma_\varepsilon} \right) \frac{\partial \varepsilon}{\partial x_j} \right] + C_1 \frac{\varepsilon}{K} \nu_t \left[\left(\frac{\partial U_i}{\partial x_j} + \frac{\partial U_j}{\partial x_i} \right) \frac{\partial U_i}{\partial x_j} + \frac{\beta}{\sigma_t} g_j \frac{\partial T}{\partial x_j} \right] - C_2 \frac{\varepsilon^2}{K} \quad (4.9)$$

where subscript t refers to turbulence

$$\mu_t = \rho C_\mu K^2 / \varepsilon; \nu_t = \mu_t / \rho;$$

$C_\mu=0.09$; $C_1=1.44$; $C_2=1.92$; $\sigma_K=1.0$; $\sigma_\varepsilon=1.3$; reference temperature = 300K. For the simulation, the pressure is assumed to be constant and the K and ε value at the air inlet is set to

$$K = \frac{3}{2} (U_{ave} T_i)^2 \quad (4.10)$$

$$\varepsilon = \frac{C_\mu^{3/4} K^{3/2}}{\kappa L} \quad (4.11)$$

where U_{ave} is the inlet velocity, T_i is the turbulence and $\kappa = 0.41$ is the Von Karman constant.

4.2 PROJECT ARRANGEMENT FOR EXPERIMENTAL CASES

The heat-pipes heat-exchanger project for thermal cooling was built at Level 2 of the Faculty of Engineering and IT workshop at the University of Technology, Sydney. The test unit for the experimental work consisted of an acrylic box for collections of temperature in a room, heat-pipes heat-exchanger, an adjustable speed blower fan with adjustable temperature heater, data logger, a temperature sensor as well as instrumentation for the system to operate perfectly.

The system ran on three methods of measurement which took into consideration the supplied air incoming direction and the ambient temperature setting. Each method included two conditions, namely low and high ambient temperature tests. For solar energy air conditioning, the energy converted is the primary concern. Attention should be given to the type of air conditioning, room cooling load, air ventilation, and infiltration. This project, therefore, proposed a design cooling load where a heat-pipe assisted in the pre-cooling of the air on the room side while boosting the condenser on the refrigeration side. For every test method, a temperature of 302K (29°C) to 304K (31°C) was set for lower ambient temperature and 313K (40°C) to 325K (52°C) for high ambient temperature setting. This suited the ambient temperature of a tropical climate in some parts of Australia and other hot climates where air conditioning cooling is needed.

4.2.1 Solar Air-Conditioning

The system was divided into a solar collector system and an electrical supply system. The solar heating system continuously supplied the radiation heat from the sun and the electrical system converted it to electricity. In this thesis, the electrical power converted by the solar collector was taken from the existing data and the requirements produced by the manufacturers. The role of the electrical system was to run the compressor in the refrigeration system. Another application of solar energy to refrigeration was as a booster in assisting the refrigeration cycle. The solar panel was installed on the discharge pipe of the cycle before a condenser to superheat the refrigerant vapour. This would increase the discharge temperature and boost the heat transfer in the condenser. Figure 4.12 shows the application of the system.

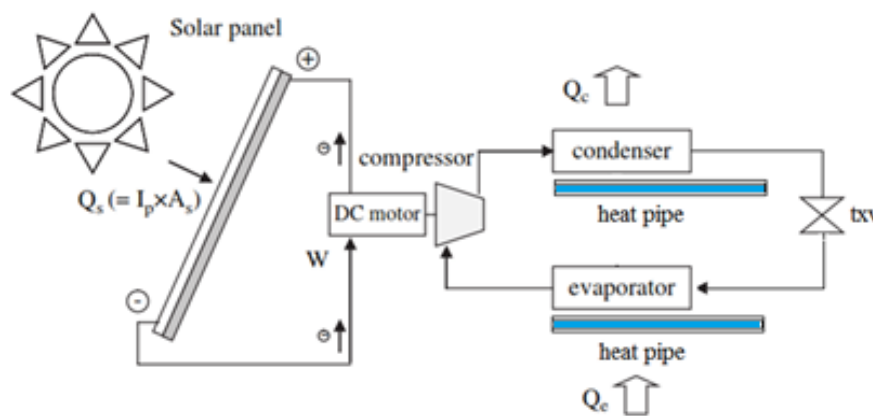


Figure 4.12: Solar air conditioning booster using heat-pipes as temperature reduction, based on Francis Meunier's proposal. *Meunir (2013)*.

4.2.2 Air-conditioning System

The moving component in the solar energy's air conditioning system is the compressor and fans. Although the system has an evaporator and condenser fan, the biggest energy consumption is from the rotational part of the compressor. The standard operating temperature of air conditioning for domestic application is 278K (5°C) on the evaporator side and 318K (45°C) on the condenser side. According to ASHRAE Standards 55, to maintain room comfort, the air temperature should be about 297K (24°C). The experiment, therefore, aimed to achieve the required temperature and increase the COP of the system with minimum energy consumption through the assistance of passive cooling.

4.2.3 Blower Fan and Heater

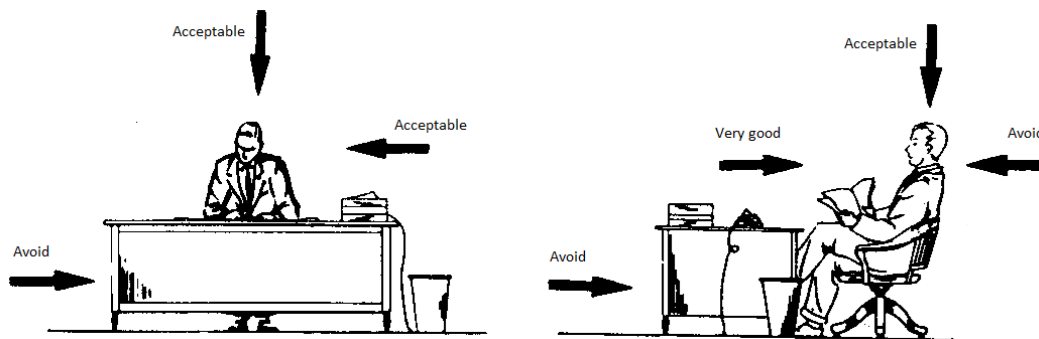
A test was conducted to run the system for natural ventilation; however, the capacity of the heat-pipes was small when manipulating the air density to create differential pressure inside the box. As different air densities will make the air flows, warm air will flow upward. This would not happen if the test is from the wall opening of the box. A fan and a coil heater were thus introduced to the test project. The fan was an adjustable speed fan at about 4 m/s and the heater could electrically heat the coil to 338 K (65 °C). The specification of the blower fan heater was enough to create an airflow in the box. The fan was located in front of the evaporator section of the heat-pipes heat-exchanger and connected to a flexible duct.

4.2.4 The Inlet and Outlet Air Opening

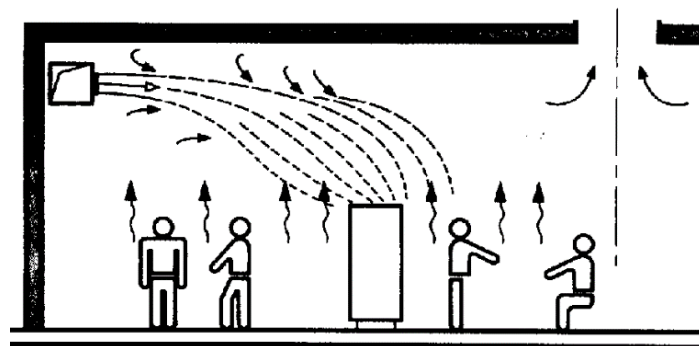
It is necessary to level the ambient air and the air blown into the occupied zone at a different temperature and hygrometer condition without the occupants experiencing discomfort. An area or a zone that covers the height of 1.8 m from the ground and stops at 0.60 m from the vertical walls require an air displacement speed or the residual speed of between 0.10 and 0.30 m/s. Table 4.2 shows the airspeed requirement. Figure 4.13 shows the sensitivities of air blowing for comfort cooling.

Table 4.2: Air velocity requirement for comfort cooling. *ASHRAE*.

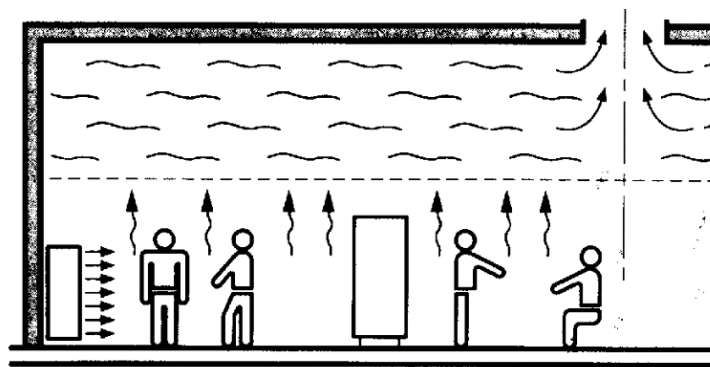
Air velocity, m / s	Reaction of occupants	Area of application
0 to 0.1	Unfavourable reaction: an impression of suffocation, stagnant air	None
0.1 to 0.2	Favourable reaction	Comfort air conditioning
0.2 to 0.3	Adverse reaction of seated persons, the favourable reaction of persons standing or moving slowly	Comfort air conditioning shops, banks, utilities.
> 0.3	Adverse reaction: the impression of over airflow	Industrial Air Conditioning

**Figure 4.13:** Humans are sensitive to the blowing of air and the temperature difference of the room. The location of the air vents must take into account the geometry of the room, the obstacles and the position of the occupants. *ASHRAE, Mémotech génie énergétique*.

The location of return vents is based on the air outlets, such that the entire air volume of the room is brewed and renewed. The blown air with a high initial velocity of higher than 2 m/s draws air from the room to which it is mixed. This method of supplying air to the room is shown in Figure 4.14.



a.



b.

Figure 4. 14: a. Diffusion of air by induction or mixed air, b. By displacement. *ASHRAE, Mémotech génie énergétique.*

In the condition of supplied air, the circulation of air is less disturbed, and an air return on a wall is favourable, provided that the opening is located in the lower part near the ceiling. Figures 4.15 and 4.16 show the distribution of air at high and low side openings. The experimental study selected openings at the top and the sidewall of the acrylic box.

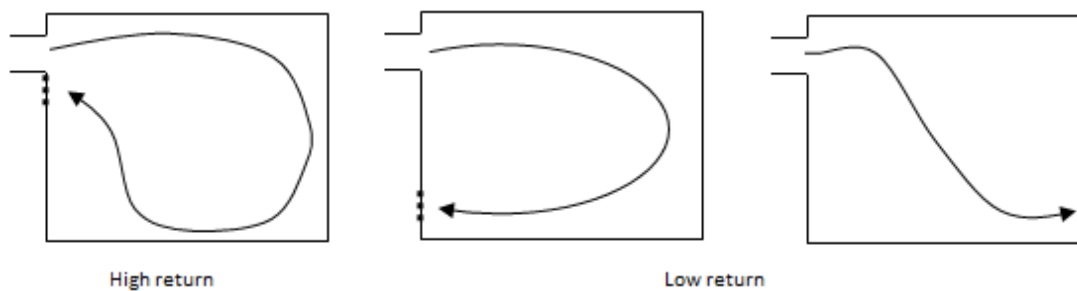


Figure 4. 15: Return air placement. *ASHRAE; Mémotech génie énergétique.*

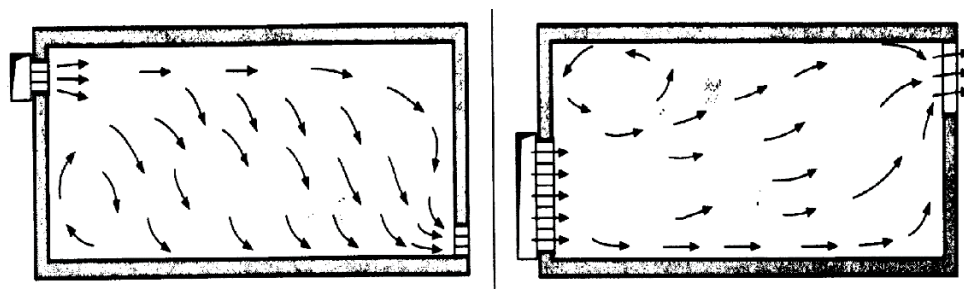


Figure 4. 16: Distributions of air at low velocity. *ASHRAE; Mémotech génie énergétique.*

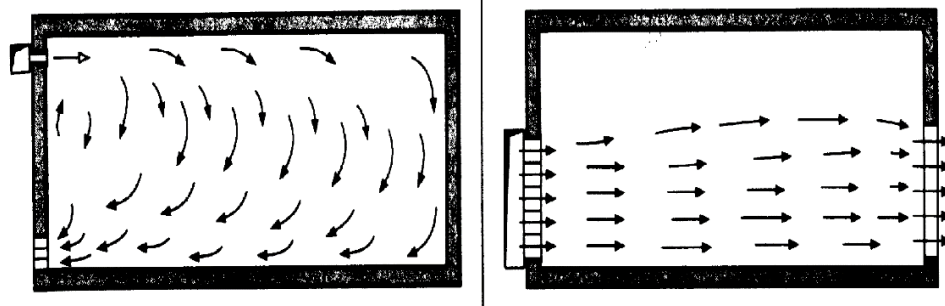


Figure 4.17: Distributions of air at high velocity. *ASHRAE; Mémotech génie énergétique.*

4.2.5 Heat-pipes heat-exchanger

In this study, the absorption and desorption of heat were performed by the heat-pipes. The evaporator section was horizontally attached to the inlet air opening of the box while the condenser section was on the air outlet opening. The heat-pipes heat-exchanger was lifted to 10° horizontally at the condenser section to allow the condensed liquid to flow via gravitational force.

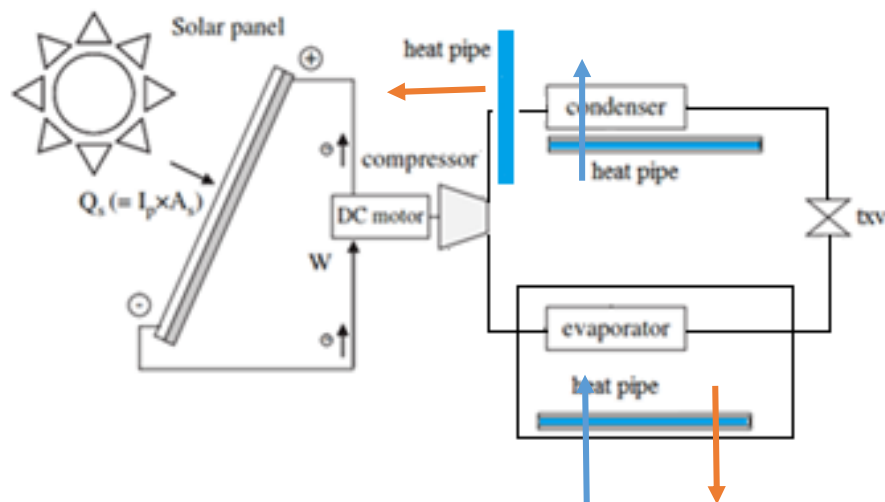


Figure 4.18: Proposal of the schematic drawing of the experimental setup using heat-pipes as temperature reduction, based on *Francis Meunir's (2013)* suggestion.

4.2.6 Design of the System: Case 1

The test method consisted of a fan with a heater, a heat-pipes heat-exchanger, an acrylic box, temperature sensors, and data logger instrumentation. The fan speed was at 1 m/s and the heater was set to be in the range of 302 K to 304 K (29°C to 31°C). The heater coil was adjusted to supply an electrical heat of the required ambient temperature for low tropical temperatures. Two openings were cut in the sidewall of the acrylic box where the heat-pipes were installed. One side of the opening had the evaporator section while the other opening faced the condenser section. The adiabatic side was separated between the openings.

The fan blew air to pass through the evaporator section of the heat-pipes heat-exchanger before entering into the acrylic box through the opening. Several points of k type thermocouple temperature sensors were placed in each corner of the box to capture the average temperature. The thermocouple was connected to a data logger which recorded the temperature at each point. By force ventilation of the fan, the air was distributed inside the box before leaving through the condenser opening. The air temperature was measured and the thermal images were then captured.

When the heated air was blown through the evaporator side of the heat pipe, the liquid refrigerant R134a evaporated inside the tube. As the boiling temperature of the refrigerant was lower than the air temperature, the air heat energy was absorbed by the refrigerant medium. In the process, the liquid changed to a vapour phase, which was less dense and moved towards the condenser side of the tube. The air that passed through the evaporator section became colder, moved into the acrylic box and mixed with the room air. As there was only one exit opening, the mixed air then escaped through the outlet where the condenser side of the heat-pipes was located. The mixed airflows then passed through the condenser section of the heat-pipes and in the process, it condensed the refrigerant vapour to a liquid phase. The heat-pipes heat-exchanger was positioned to a slightly 10° slant horizontally, and by gravitational action, the liquid then moved back to the evaporator side, restarting the process again.

In the experiment with high ambient temperature, the process was repeated with the coil heater temperature increased to the range of 313K to 325K (40°C to 52°C). There were only two-way flows of the air into the acrylic box that is through the inlet opening and the outlet opening. A flexible duct was used to direct the air at the evaporator section for force-driven ventilation. Figure 4.19 shows the arrangement of the experimental measurement.

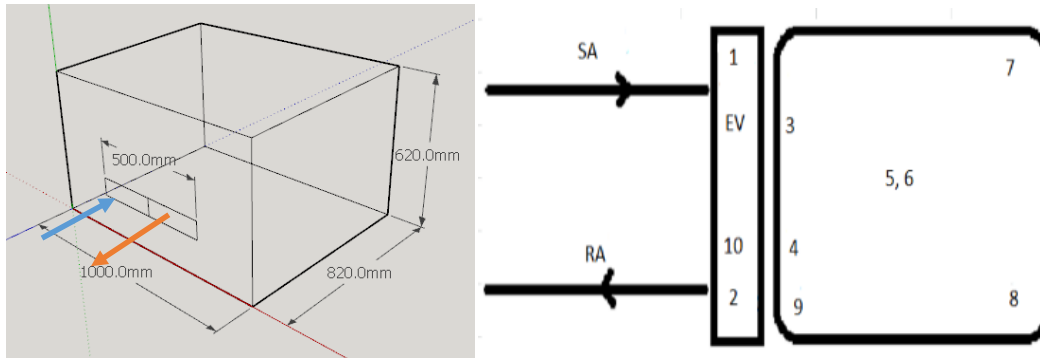


Figure 4.19 a

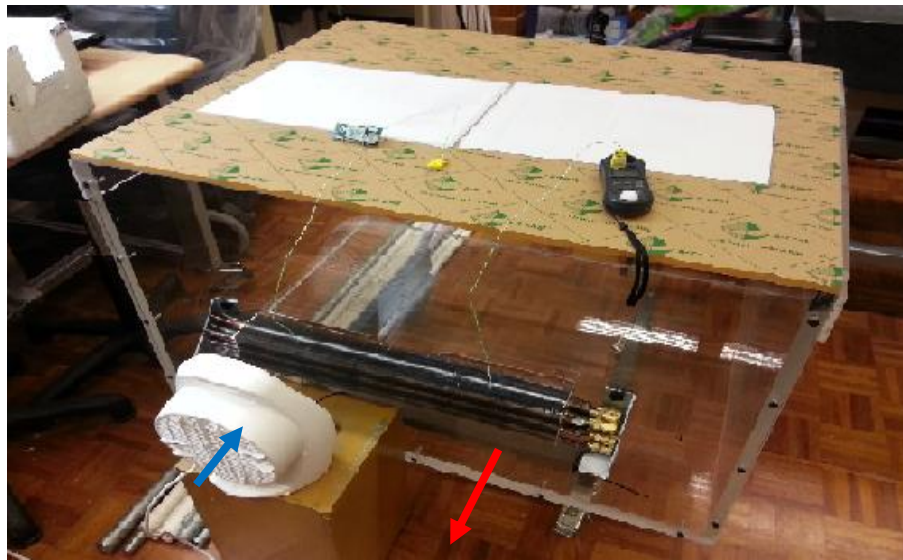


Figure 4.19 b

Figure 4.19 a and b: Method 1 for Case 1 showing the arrangement of the heat-pipes, the acrylic box and the inlet and outlet of air. Thermocouple sensors are located at a proposed point in the box to find the average box temperature.

4.2.7 Design of the System: Case 2

The second test method consisted of a fan with a heater, a heat-pipes heat-exchanger, an acrylic box, temperature sensors, and data logger instrumentation. The fan speed was at 1m/s and the heater was set to be in the range of 302 K (29°C) to 304 K (31°C). The heater coil was adjusted to supply an electrical heat of the required ambient temperature for low tropical temperatures. Two openings were cut on the top roof of the acrylic box where the heat-pipes were installed. One side of the opening had the evaporator section and the other opening faced the condenser section. The adiabatic side was separated between the openings. The fan blew air to pass through the evaporator section of the heat-pipes heat-exchanger before entering into the acrylic box through the opening. Several points of k type thermocouple temperature sensors were placed in each corner of the box so that the average temperature could be calculated. The thermocouple was connected to a data logger which recorded the temperature at each point. Through the forced ventilation of the fan, the air was distributed inside the box before leaving through the condenser opening. The air temperature was measured, and the thermal images were captured.

When the heated air was blown through the evaporator side of the heat pipe, the liquid refrigerant R134a evaporated inside the tube. As the boiling temperature of the refrigerant was lower than the air temperature, the air heat energy was absorbed by the refrigerant medium. In the process, the liquid changed to a vapour phase, which was less dense and moved towards the condenser side of the tube. The air that passed through the evaporator section became colder, moved into the acrylic box and then mixed with the room air. As there was only one exit opening, the mixed air then escaped through the outlet where the condenser side of the heat-pipes was located. The mixed airflows then passed through the condenser section of the heat-pipes and in the process, it condensed the refrigerant vapour to a liquid phase.

The heat-pipes heat-exchanger was positioned to a slightly 10° slant horizontally, and by gravitational action, the liquid then moved back to the evaporator side, restarting the process again. In the experiment with high ambient temperature, the process was repeated by increasing the coil heater temperature to the range of between 313 K (40°C) to 325 K (52°C). There were only two-way flows of the air into the acrylic box; these were through the inlet opening and the outlet opening.

A flexible duct was used to direct the air at the evaporator section for force-driven ventilation. Compared to Method 1, this method blew the air from the top into the box. The air then mixed with the box air before leaving the box through an opening at the top. Figure 4.20 shows the arrangement of the experimental measurement.

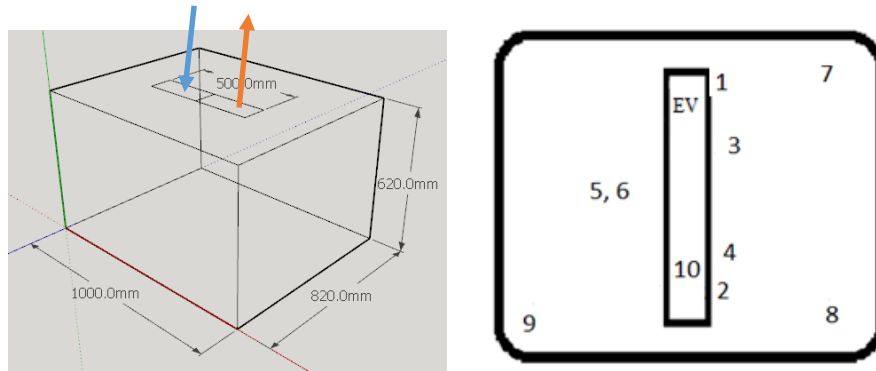


Figure 4.20 a

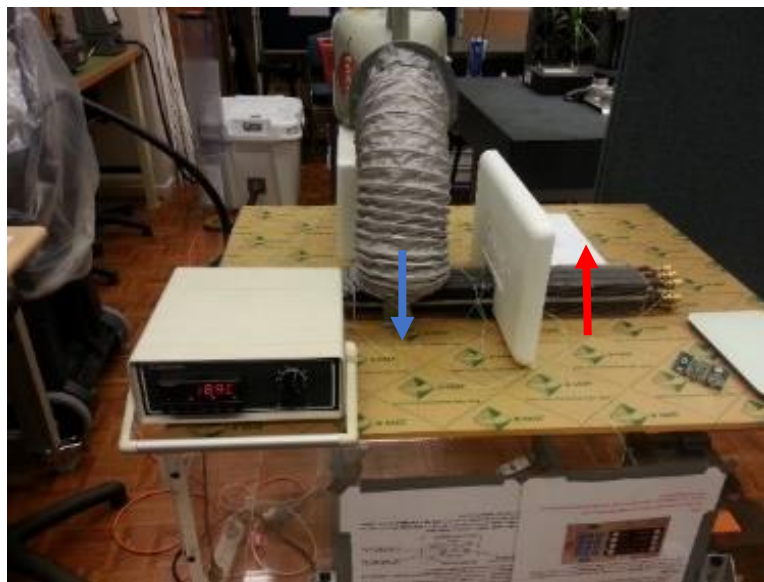


Figure 4.20 b

Figure 4.20a and b: Method 2 for Case 2 showing the arrangement of the heat-pipes, the acrylic box and the inlet and outlet of air. Thermocouple sensors are located at a proposed point in the box to find the average box temperature.

4.2.8 Design of the System: Case 3

The third test method consisted of a fan with a heater, a heat-pipes heat-exchanger, an acrylic box, temperature sensors, and data logger instrumentation. The fan speed was set at 1 m/s and the heater was set to be in the range of 302 K (29°C) to 304 K (31°C). The heater coil was adjusted to supply an electrical heat of the required ambient temperature for low tropical temperatures. Two openings were cut on the acrylic box where the heat-pipes were installed. One side of the opening had the evaporator section and the other opening faced the condenser section. The adiabatic side was separated between the openings. The fan blew air that passed through the evaporator section of the heat-pipes heat-exchanger before entering the acrylic box through the opening.

Several points of k type thermocouple temperature sensors were placed in each corner of the box so that the average temperature could be calculated. The thermocouple was connected to a data logger which recorded the temperature at each point. Via the forced ventilation of the fan, the air was distributed inside the box before leaving through the condenser opening. The air temperature was measured, and the thermal images were captured.

When the heated air was blown through the evaporator side of the heat pipe, the liquid refrigerant R134a evaporated inside the tube. As the boiling temperature of the refrigerant was lower than the air temperature, the air heat energy was absorbed by the refrigerant medium. In the process, the liquid changed to a vapour phase which was less dense and moved towards the condenser side of the tube. The air that passed through the evaporator section became colder, moved into the acrylic box and mixed with the room air. As there was only one exit opening, the mixed air then escaped through the outlet where the condenser side of the heat-pipes was located. The mixed airflows then passed through the condenser section of the heat-pipes, condensing the refrigerant vapour to a liquid phase.

The heat-pipes heat-exchanger was positioned to a slight slant of 10° horizontally, and by gravitational action, the liquid then moved back to the evaporator side, restarting the process again. In the experiment with high ambient temperature, the process was repeated by increasing the coil heater temperature to the range of between 313 K (40°C) to 325 K (52°C). There were only two-way flows of the air into the acrylic box, namely through the inlet opening and the outlet opening. A flexible duct was used to direct the air at the evaporator section for force-driven ventilation.

Unlike Methods 1 and 2, in this method, the required air was blown from the top into the box. The air then mixed with the box air before leaving the box through an opening at the sidewall. Figure 4.21 shows the arrangement of the experimental measurement.

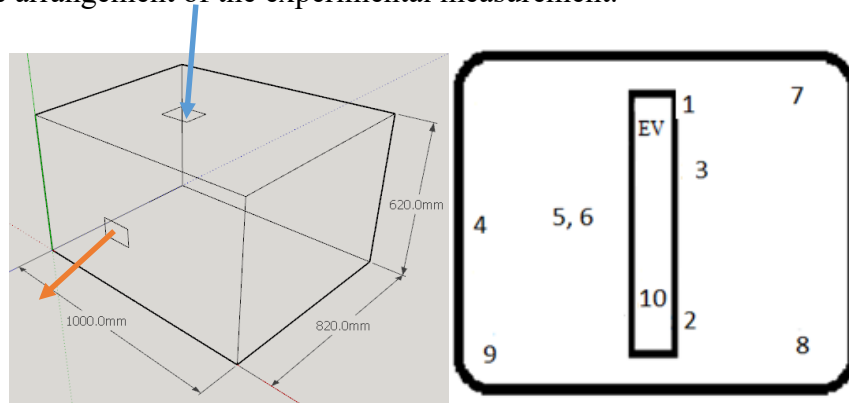


Figure 4.21 a

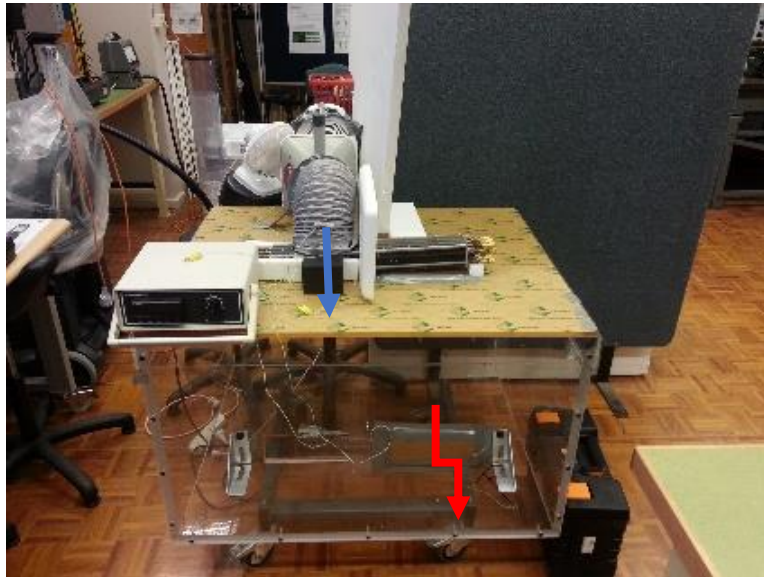


Figure 4.21 b

Figure 4.21 a and b: Method 3 showing the arrangement of the heat-pipes, the acrylic box and the inlet and outlet of air. Thermocouple sensors are located at a proposed point in the box to find the average box temperature.

4.2.9 Design of the System: Case 4

This experimental work examined the heat sink ability of heat-pipes to absorb heat from the surrounding air. The process started when the ambient air at 308 K (35°C) entered the inlet opening of the box, passing through the evaporator section of the heat-pipes heat-exchanger. The heat-pipes heat-exchanger evaporator section lowered the air temperature before the air entered the inlet of the box. An assumption of 10% by-pass contact between the air and the fins was taken into consideration. The cold air then mixed with the internal air in the box, cooling the box as near as possible to the evaporator temperature. The mixed air would then be exhausted out through the outlet. The process continued to maintain the temperature inside the box. Figure 4.22 shows the workflow.

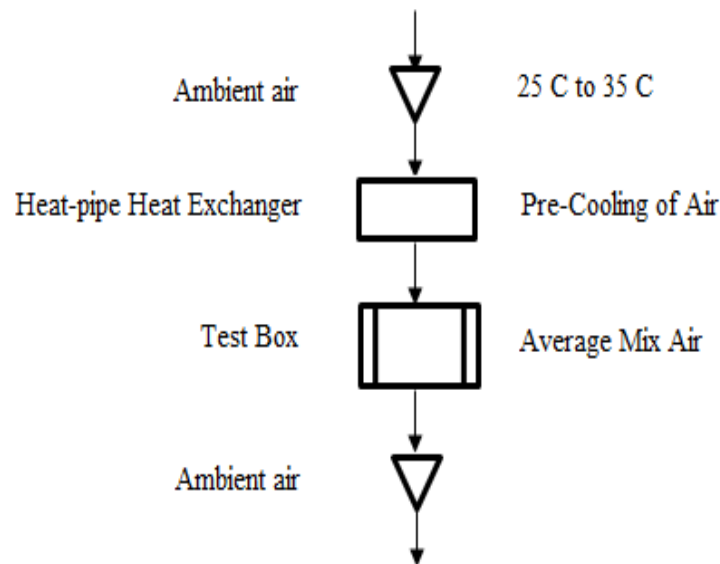


Figure 4.22: The workflow of the experimental project. The pre-cooling of the air section is the main interest as the ambient hot air is lowered before entering the test box.

By-pass contact between the air and the fins was taken as 10% and the temperature leaving the heat-pipes can be calculated using

$$\text{Bypass factor} = \frac{t_{ldb} - t_{tadp}}{t_{edb} - t_{tadp}}$$

t_{ldb} Temperature leaving the dry bulb,

t_{edb} Temperature entering dry bulb,

t_{tadp} Temperature apparatus dew point.

where from the calculation, t_{ldb} was found to be 297.65 K (24.65 °C).

The test box was constructed as described below. The previous attempt by Z. Abdullah (2016) on a heat-pipe heat-exchanger at various locations of an air-conditioner condenser, where the inlet temperature was 293 K (20°C), revealed that a 5 K difference can be achieved.

Based on the suggestion by Charoensawan and Terdtoon (2008), the author in this experiment used hot ambient temperature in the range of 303K (30°C) to 308K (35°C) for the inlet temperature. A heat-pipe heat-exchanger was installed on the façade of the box before the supplied air entered the test box. As suggested by Beckert (1996), the heat-pipes' inclination position should be at least 6° when placed horizontally. This experiment, therefore, had taken the position of 10° inclination for refrigerant gravity-return.

Models of the test boxes illustrated below show the configurations as to where the fresh air intake locations and openings that best suit the domain should be positioned. Figure 4.23 shows the configuration of Case 4. Incoming air at 308 K flowed on the surface of the heat-pipes heat-exchanger from the side and exited on the sidewall. The condenser side was equipped with an exhaust fan to induce air to flow out. The heat-pipes were placed in an inclining position of 10° horizontally.

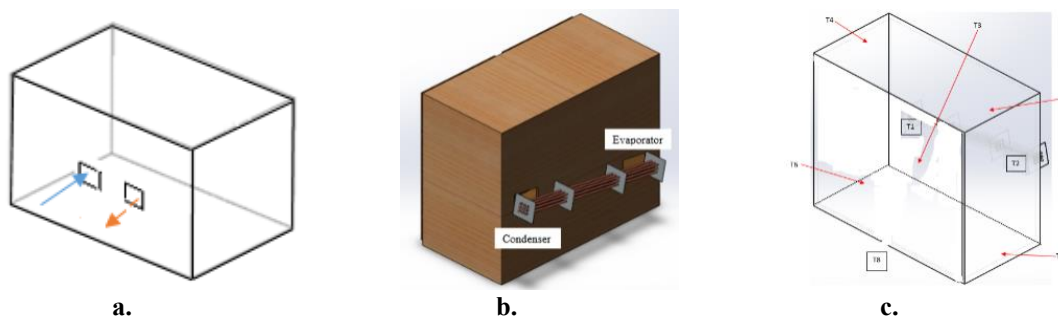


Figure 4.23: Case 4. The configuration of the opening for a. The incoming and leaving of the air in the test box. b. 10° horizontal inclination. c. The thermocouple position is seen from behind the test box.

4.2.10 Design of the System: Case 5

Figure 4.20 shows the configuration of Case 5. Incoming air at 308 K flowed on the surface of the heat-pipes heat-exchanger from the bottom and exited at the top of the heat-pipes. The condenser side was equipped with an exhaust fan to induce air to flow out. The heat-pipes were in a 90° vertical position.

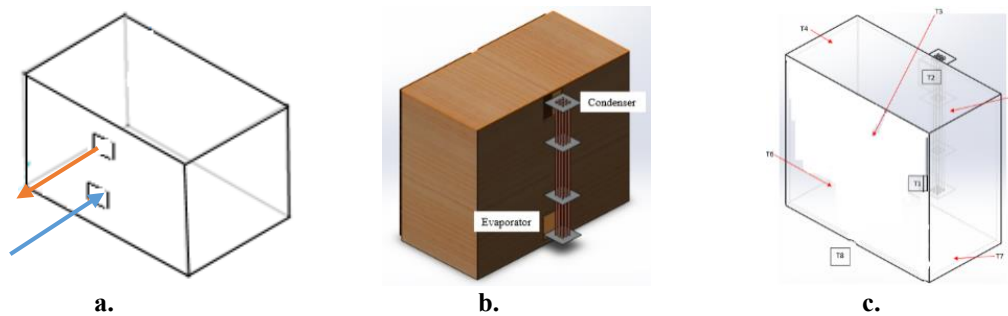


Figure 4.24: Case 5. The configuration of the opening for a. The incoming and leaving of the air in the test box. b. 90° angle positions. c. The thermocouple position is seen from behind the test box.

4.2.11 Table of Working Parameters

The experimental work, simulated and investigated the air temperature reduction ability of an R134a heat-pipe heat-exchanger. The heat-pipes heat-exchanger was a row of 3 by 3 tubes that were composed of 9 mm ID straight copper tube with an inner grooved structure of the length of 500 mm that was fitted with square type aluminium fins. Each of the copper tubes was filled with liquid R134a as the refrigerant medium. An acrylic box in the size of 1000 mm x 820 mm x 620 mm which was modelled as a room was used to collect air diffusions and the temperature distributions. The desired temperature tested is in the range of 303K to 318K and the inlet airflow is in the range of 0.5 to 5 m/s. Table 4.3 shows the working parameters,

4.3 TOOLS AND MEASURING EQUIPMENT

4.3.1 Heat-pipes Heat-exchanger and the Acrylic Box

The experimental work, simulated and investigated the air temperature reduction ability of an R134a heat-pipe heat-exchanger. The effort originated from the capability of gravity-assisted heat-pipes heat-exchanger as a pre-cooled component that does not require electricity or other energy sources to work. The heat-pipes heat-exchanger was a row of 3 by 3 tubes that were composed of 9 mm ID straight copper tube with an inner grooved structure of the length of 500 mm that was fitted with square type aluminium fins. Each of the copper tubes was filled with liquid R134a as the refrigerant medium. An acrylic box in the size of 1000 mm x 820 mm x 620 mm which was modelled as a room was used to collect air diffusions and the temperature distributions. The heat-pipes heat-exchanger was placed at the top and the sidewall of the acrylic box to measure the most suitable flow of air intake.

Box Material	Transparent acrylic board : Method 1 - opening on the sidewall of the box : Method 2 and 3 - openings on the top of the box
Dimension	L 1000 mm x W 820 mm x H 620 mm



Figure 4.25: An acrylic box showing the top opening for Method 2 and 3.

Heat-pipes Heat-exchanger Material	Copper pipe OD 10 mm, ID 9 mm
Quantity	9 x 500 mm each with fin operating area
Fin Type	Aluminium fins of 1 mm gap
Refrigerant	Vacuum and filled with R134a



Figure 4.26: An acrylic box with the heat-pipes heat-exchanger attached to the sidewall. The opening is created to let the air pass through the inlet and outlet.

4.3.2 Heater and Blower

To create warm ambient conditions, a room blower fan and a heater element were used. The blower power was set at 800 W while the range of the flow was 0.5 m/s to 2 m/s, and the heat generated was adjustable up to 80°C.

Variable-speed fan heater	800 W
Speed	0.5 m/s – 2 m/s
Heat	Up to 80°C
Amps	4 A

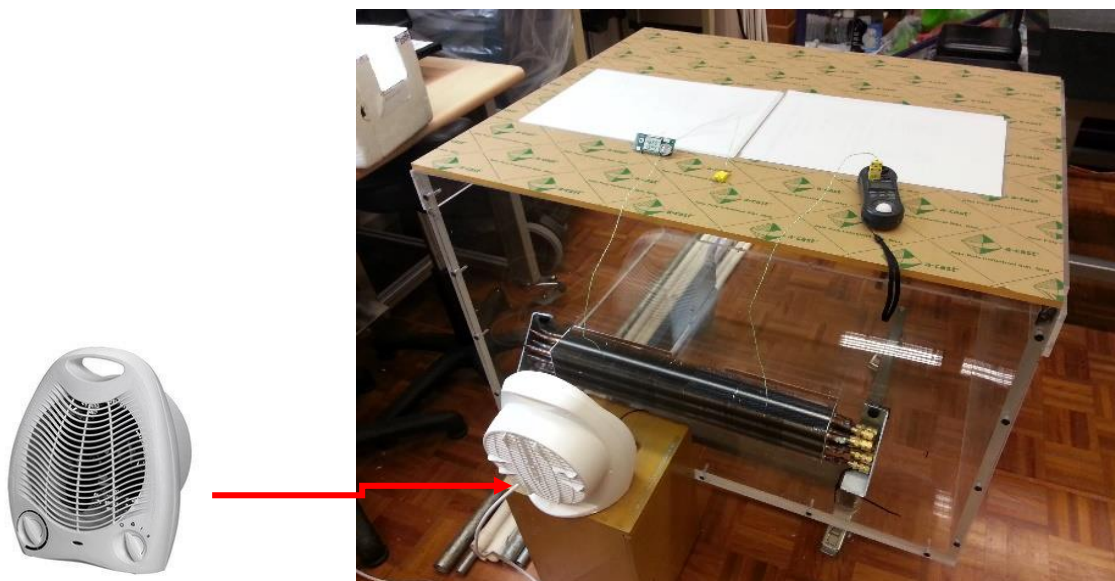


Figure 4.27: A heater blower and the location of its installation. The blower is attached to the inlet of the opening to create a warm air supply to the heat-pipes heat-exchanger.

4.3.3 Digital Equipment

Several digital items were used for the data collection.

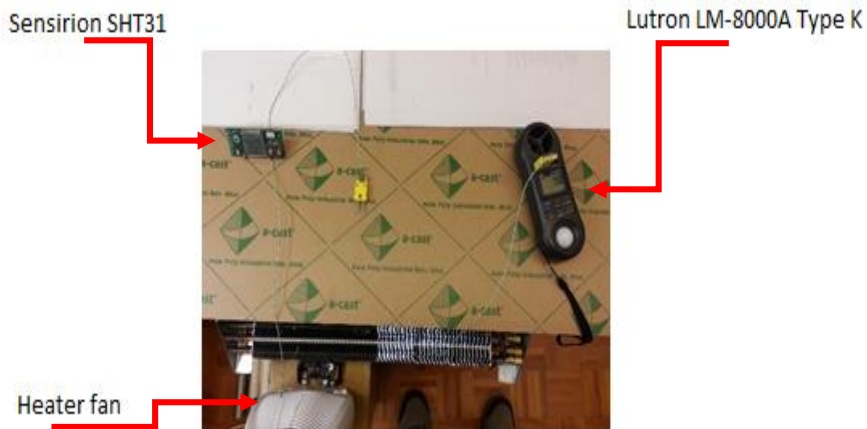


Figure 4.28: The basic method of data collection. The outside ambient air properties are compared to the processed data recorded in the acrylic box.



Figure 4.29: The 10 terminal point data logger for data collections. The main purpose is to measure the outside ambient air temperature and compared it to the processed data recorded in the acrylic box.

4.3.4 Hygrometer

A Sensirion SHT31 hygrometer was used to record the digital temperature and humidity of the outside ambient air.

Voltage range	2.15 V to 5.5 V
Operating temperature	-40 to +125°C
Relative humidity	0-100% RH. The response time is 8 second



Figure 4.30: A Sensirion SHT31 hygrometer records the digital temperature and humidity of the outside ambient air.

4.3.5 Anemometer

A Lutron LM-8000A Type K anemometer was used to record the velocity and the temperature.

Air velocity range	0.4 to 30 m/s.
Humidity	10 to 95%
Temperature range	0 to 50°C



Figure 4.31: A Lutron LM-8000A Type K anemometer collects the velocity and the temperature.

4.3.6 Hot-wire Anemometer

A Testo hot-wire anemometer was used to record the velocity and the temperature.

Air velocity range	0 to +20 m/s
Comfort level	0 to +5 m/s
Humidity	0 to 100%
Temperature range	-100 0 to +400°C



Figure 4.32: A Testo Hot-wire Anemometer record the velocity and the temperature inside the acrylic box.

4.3.7 Thermal Imaging Equipment

Thermal images were recorded using a Testo Thermal Image 875.

Field of vision/min. Focusing distance	Standard lens: 32° x 23°/0.1 m (0.33 ft) Testo 875-2 only (optional): Telephoto lens: 9° x 7°/0.5 m (1.64 ft)
Thermal sensitivity (NETD)	< 100 mK typically, < 110 mK at 30 °C (86 °F)
Geometric resolution	Standard lens: 3.3 mrad , Telephoto lens: 1 mrad
Refresh rate	9 Hz
Focus	Manual
Detector type	FPA 160 x 120 pixels, a.Si
Spectral range	8 - 14 μm
Characteristics: Output	Values
Field of vision/min. Focusing distance	33° x 25°/0.4 m (1.31 ft)
Image size	640 x 480 pixels
Refresh rate	8 to 15 Hz



Figure 4.33: A Testo Thermal-Image 875 for digital imaging of temperature distribution.

4.3.8 Data Logger

A Monogram Omega data logger with a 10-point terminal was used to capture the temperature at strategic points.

Front Panel	Programmable for 9 Thermocouple calibration
Resolution	0.01°
Temperature range	0.2° accuracy
Thermocouple	10 channels
Option	RS232 communications



Figure 4.34: A Monogram Omega data logger with a 10-point terminal to record the temperature.

4.3.9 Thermocouple

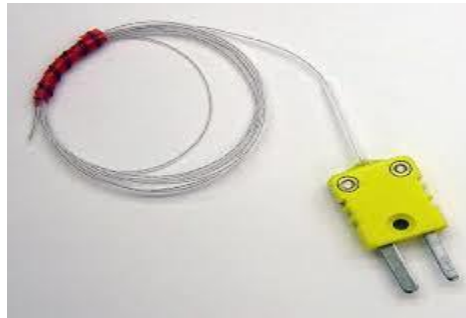


Figure 4.35: A Type k thermocouple.

4.4 DATA COLLECTION

4.4.1 Monitoring Parameters

The experiment included recording certain parameters for analysis. The most important parameter is the temperature difference from the outlet ambient temperature compared to the final result of the process, which the heat-pipes could reduce. Monitoring the temperature gradient from the inlet of the box to the outlet allows the data to be analysed and calculated, including the effectiveness of the system, the energy reduction and the performance of the system with and without passive equipment. Airflows and their properties are calculated from the monitoring parameter equipment. The temperature and humidity sensor recorded the different supply inlet to the outlet of the ambience and the box condition; the flow meter recorded the velocities, and the imaging equipment captured the gradient of the temperature processes.

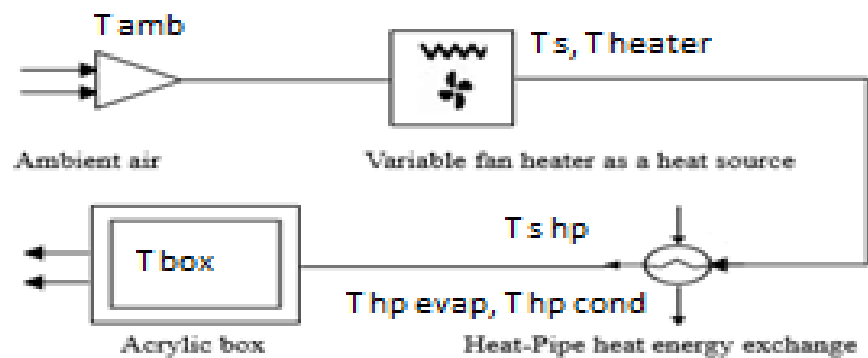
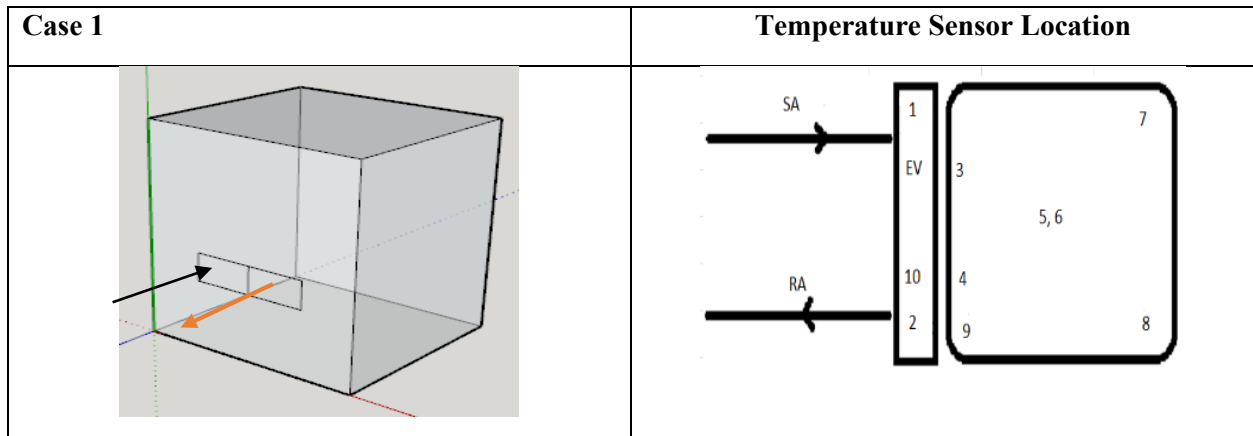


Figure 4.36: The basic concept of the data collections. The outside ambient air properties are compared to the processed data recorded in the acrylic box. *Abdullah (2018)*.

Table 4.4: Temperature monitoring locations of the acrylic box with the heat-pipes attached.

Legends	
SA	Supply Air Temperature
RA	Return Air Temperature
EV	Heat-pipes Evaporator Tube Temperature
1	Evaporator Tube Ends Temperature
2	Condenser Tube Ends Temperature
3	Air Inlet Temperature
4	Air Outlet Temperature
5	Bottom, Box Air Temperature
6	Middle Box Air Temperature
7	Left Side Air Temperature
8	Right Side Air Temperature
9	Return Air Temperature
10	Heat-pipes Condenser Tube Temperature



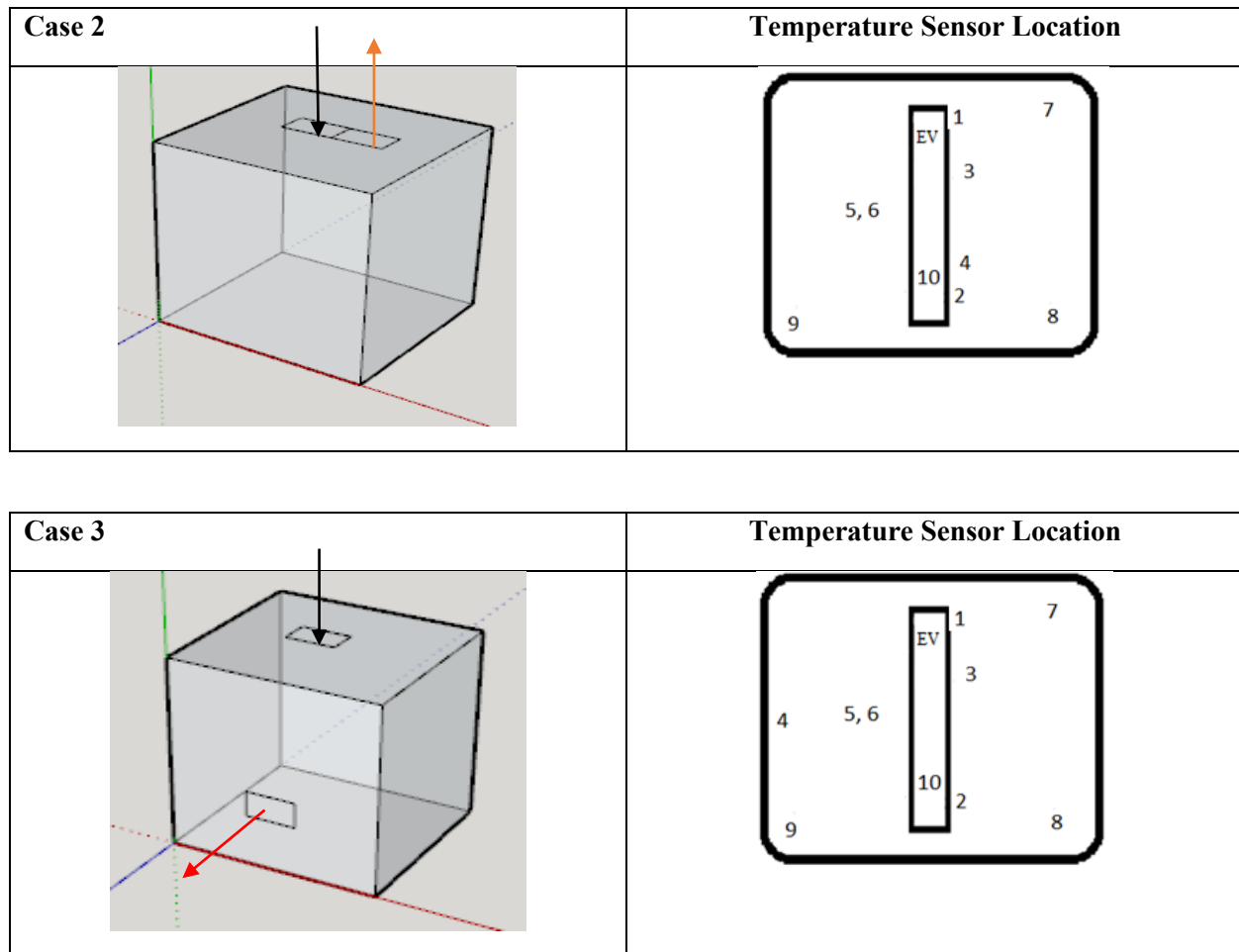


Figure 4.37: Models of acrylic box specification with fresh air intake locations and openings that best suit the domain. *Abdullah (2018)*.

4.5 SIMULATION USING COMPUTATIONAL FLUID DYNAMICS

Before the experimental work begins, a CFD simulation was conducted in the application process. This was done to verify the significance, effectiveness and the expected outcome of the work. Simulation work on the components of the system such as the evaporator, condenser and the application in outdoor room conditions were also performed. The incoming supplied air and the return air were predominantly being simulated with the passive cooling components, that is the heat-pipes heat-exchanger to establish the temperature ranges.

Computational Fluid Dynamics uses numerical methods and algorithms to solve the problem involving fluid flow and predicts the flow behaviours based on mathematical modelling. The model is based on fundamental governing equations of fluid dynamics, namely the

conservation of mass, momentum, and energy. The fundamental basis of any CFD problem is the Navier-Stoke equations (conservation law). The four terms in the general differential equation are the unsteady term (transient), the convection term, the diffusion term, and the source term. The author's works on natural ventilation were used to study the flow structure of fluid-driven ventilation and wind-driven natural ventilation system in buildings with CFD. CFD-ACE from ESI software was used to obtain the result of the satisfactory convergence or when the steady-state is reached. The numerical solution of CFD-ACE's process continuity and the equations work in three steps, namely pre-processing, solving and post-processing.

The general setup for the computational fluid dynamics assumptions of the airflow, heat transfer, domains, meshing and boundary condition had been established. Numbers of simulation works were tested by the following conditions below. The results of the convergence were explained in the sections. Tables 4.5 and 4.6 presented the setup model.

- Case 1: The incoming air was blown from the sidewall with side exit;
- Case 2: The incoming air was blown from the top with the top exit;
- Case 3: The incoming air was blown from the top and the exit air through the sidewall.

Table 4.5: The specification of models for all domains.

Domain	Specification
Case 1	Air at 300 K was blown on the surface of an evaporator side of a heat-pipes heat-exchanger from the sidewall of the test box. The air moves to the inlet of the test box mix with the box air temperature. The air is then, forced to the outlet and the condenser side of the heat-pipes, and then exits to the ambient outlet through the sidewall of the test box. The average temperature difference between the inlet and the outlet air temperatures are recorded.
Case 2	Air at 300 K was blown on the surface of an evaporator side of a heat-pipes heat-exchanger from the top wall of the test box. The air moves to the inlet of the test box mix with the box air temperature. The air is then, forced to the outlet and the condenser side of the heat-pipes, and then exits to the ambient outlet through the top of the test box. The average temperature difference between the inlet and the outlet air temperatures are recorded.
Case 3	Air at 300 K was blown on the surface of an evaporator side of a heat-pipes heat-exchanger from the top wall of the test box. The air moves to the inlet of the test box mix with the box air temperature. The air is then, forced to the outlet and the condenser side of the heat-pipes, and then exits to the ambient outlet through the sidewall of the test box. The average temperature difference between the inlet and the outlet air temperatures are recorded.

Table 4.6: The specification of models and boundaries for computational fluid dynamics domains.

Parameters	Domains	Configurations
Heat-pipe Heat-exchanger.	Heat exchanger.	Straight 3 by 3 rows copper pipes. 500 mm of trans ability of working pipes.
Heat-pipes heat-exchanger cooling refrigerant.	R134a as the refrigerant medium.	Assumption of temperature drop from the evaporator to condenser side at 3K to 9K.
Acrylic Test-box	1000 mm x 820 mm x 620 mm.	Transparent acrylic box with thermocouple at points of measurement.
Computational Fluid Dynamics	ANSYS Fluent.	<p>Dimension: 3D Serial options.</p> <p>General Setup: Pressure based, absolute velocity, transient time, gravity Y direction -9.81 m/s^2.</p> <p>Model: Energy on, viscous turbulent flow.</p> <p>Material: Fluid air, Solid copper.</p> <p>Boundary conditions: Velocity magnitude 1-5 m/s, thermal condition 300K, pressure outlet back pressure at 300K, condenser pipes at 315K to 318K, evaporator pipes at 295K.</p> <p>Wall: Surface body, stationary wall, no-slip.</p> <p>Solution method: Scheme simple/hybrid, gradient least-square cell-based, standard pressure momentum and power-law, energy power-law.</p>

4.5.1 Simulation Study on Heat-pipes Heat-exchanger

The use of a heat-pipes heat-exchanger in the application of air conditioning for comfort cooling in a room is motivated by its properties for the energy-saving device. There is no external power required and it does not need maintenance. Figures 4.35 and 4.36 show the operation and the model of the heat-pipes heat-exchanger. A passive, simple construction and cost-effective heat-exchanger are used as a tool to demonstrate the room airflow pattern which affects temperature differences between the indoor and outdoor air. Figures 4.41, 4.42 and 4.43 show the simulations

series of a three-pipe heat-pipes heat-exchanger run on ANSYS-Fluent using different refrigerants as a working medium. The comparisons were to show the different temperatures between the inlet and the outlet of the heat-pipes. The simulations show that the delta temperature difference which is between 2K to 3K can be easily achieved with a row of three pipes of the heat-pipes heat-exchanger.

Heat-pipes are designed to have high thermal conductance in steady-state operation, and with only a small temperature difference, they can transfer a high amount of heat. Moreover, the simplicity of design and manufacturing, small temperature drop, wide temperature application range and the ability to control and transport high rates of heat at various temperature levels are the unique characteristics of heat-pipes. The heat-pipes heat-exchanger used in this modelling was measured at an area of 1 m² at both the inlet and outlet.

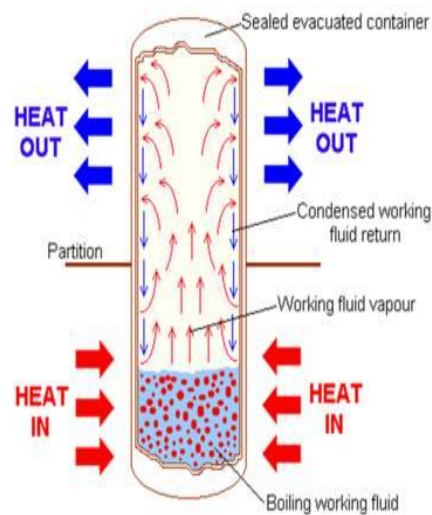


Figure 4.38: Heat-pipes heat-exchanger technology. *Zohuri (2011).*

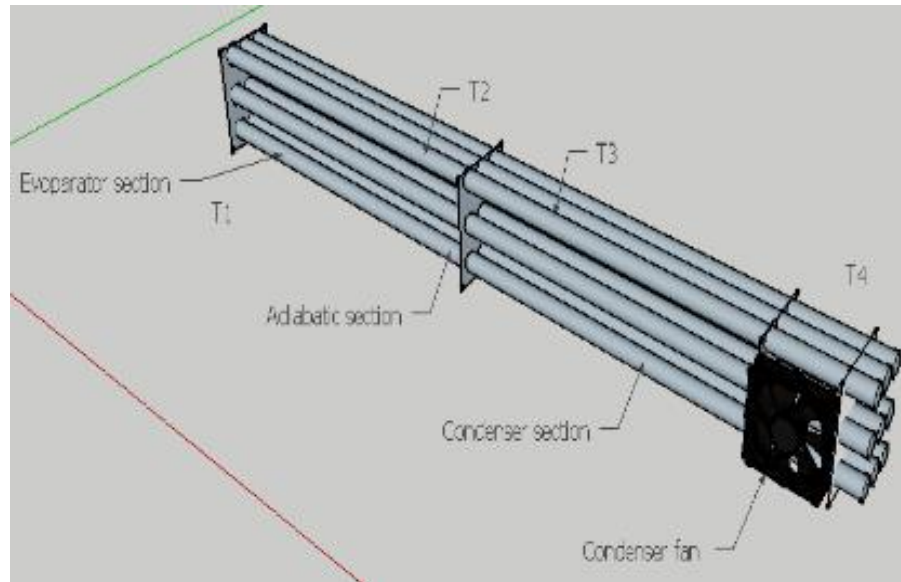


Figure 4.39: Straight heat-pipes model using R134a as a refrigerant medium. An optional ventilation fan is shown to discharge warm air from the condenser side of the heat-pipes to the outdoor. *Abdullah (2015)*.

4.5.2 Mesh, Solver and Post Processing of Heat-pipes heat-exchanger

Several attempts were made when testing the mesh distributions. The mesh below shows the distribution that best suits the domain. Fluid properties were applied in the copper heat-pipes to show different temperature results. Water, acetone, and R134a used the same domains when simulated with ANSYS Fluent to compare the temperature transport capability of the heat-pipes.

Two solvers were used in this study, namely ANSYS Fluent for the heat transfer simulation in the heat-pipes heat-exchanger and the surrounding space, and the CFD-ACE+GEOM, GUI and BG solver to solve the governing equations that are related to the flow physic problem based on the given material properties, flow physic model and the boundary conditions. To satisfactorily converge all properties and conditions, the Finite Volume Method was employed to solve velocity components, pressure, and $k - \epsilon$ (epsilon) scheme. Several attempts at meshing tests were made to satisfy the results. 2nd order spatial differential scheme was used.

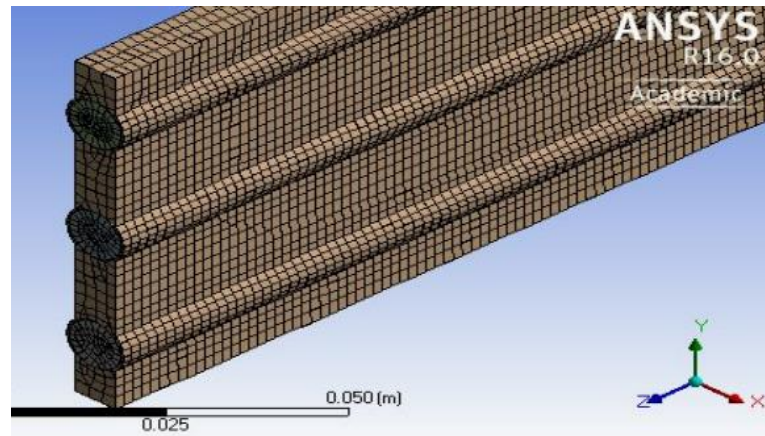


Figure 4.40: Meshes used to run the simulation of the heat-pipes heat-exchanger by ANSYS Fluent. *Abdullah (2015).*

ANSYS Fluent in the CFD-View analysed the convergence results which are presentable in graphical presentation with different plots, streamlines data and curves. Figures 4.41 to 4.43 show the temperature profiles of the heat-pipes heat-exchanger that was filled with water, acetone, and R134a. The highest temperature difference was recorded by the heat-pipes that were filled with R134a at about 5 K of differences from the inlet evaporator end to the outlet condenser end. Table 4.5 shows the properties of the cooling medium used with ANSYS Fluent. The temperature differential between the inlet and the outlet of the heat-pipes show that up to 5 K can be best achieved if R134a is applied as the refrigerant medium and heat transporter.

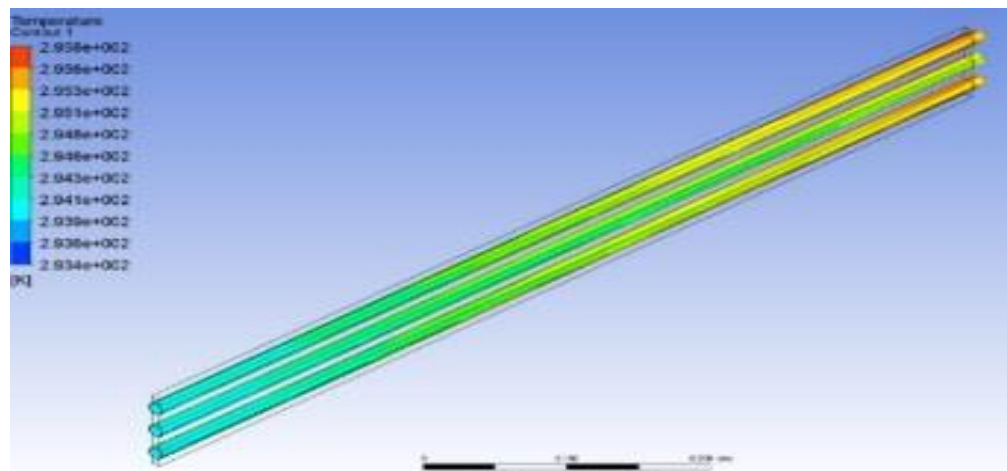


Figure 4.41: Simulation of a heat-pipes heat-exchanger by ANSYS Fluent using water as a cooling medium. The temperature difference is about 2 K. *Abdullah (2015).*

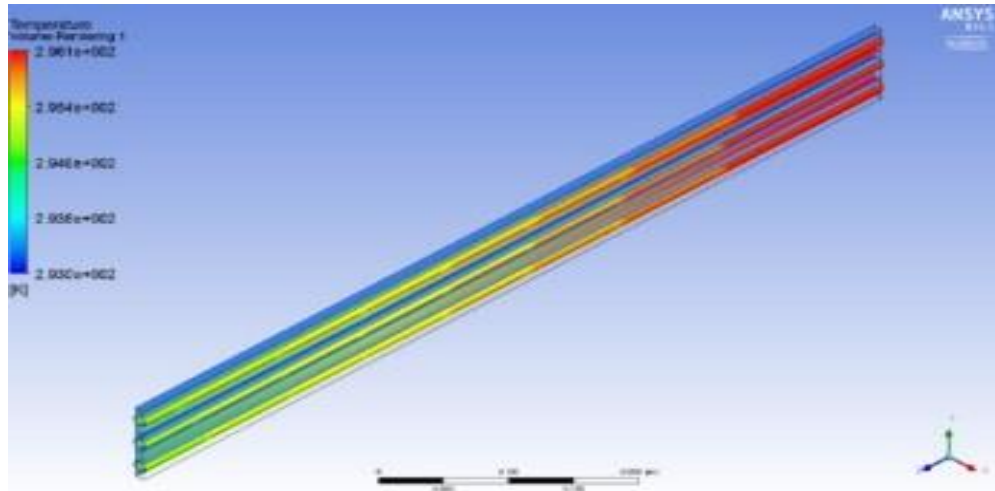


Figure 4.42: Simulation of a heat-pipes heat-exchanger by ANSYS Fluent using acetone as a cooling medium. The temperature difference is about 3 K. *Abdullah (2015)*.

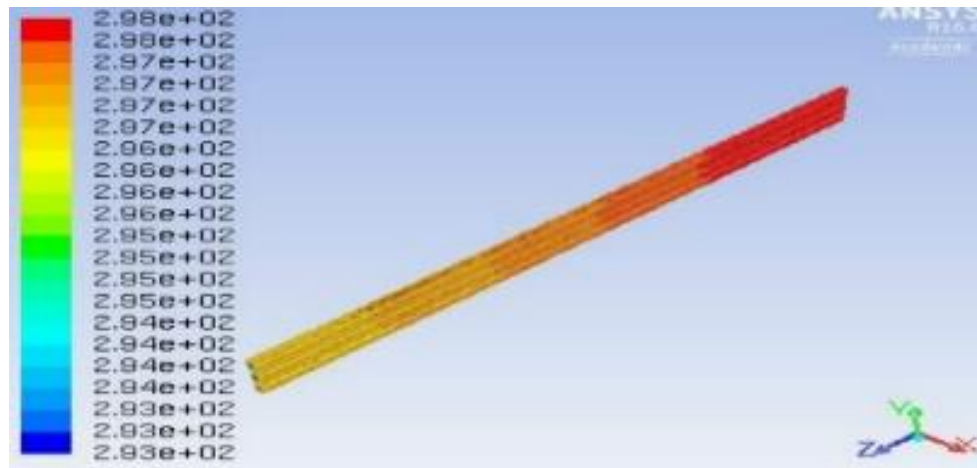


Figure 4.43: Simulation of a heat-pipes heat-exchanger by ANSYS Fluent using R134a as a cooling medium. The temperature difference is about 5 K. *Abdullah (2015)*.

Table 4.7: The properties of the heat-pipes, cooling medium and the temperature of the outlet achieved when running with ANSYS Fluent computational fluid dynamics simulations. *Abdullah (2015)*.

Physical Parameters	Water H ₂ O	Acetone C ₃ H ₆ O	R134a CH ₂ FCF ₃
Density kg/m ³	998.2	791	1207.3
Spec. Heat J/kg.K	4182	2160	1424.41
Thermal Cond. W/m. K	0.6	0.18	0.08119
Viscos kg/m-s	1.003 x 10 ⁻³	3.31 x 10 ⁻⁴	1.9525 x 10 ⁻⁴
Inlet temperature, K	293	293	293
Outlet temperature, K	295	296	298
Differential temperature, K	2	3	5

Fluid properties used for the ANSYS Fluent simulation process correspond to constant air at 293 K and the surrounding temperature was set to the required ambient temperature. Fluid properties used in the CFD-ACE simulation process correspond to constant air at 300 K and standard pressure at sea level of 101.3 kPa as the natural ventilation flow was assumed to be in the +Z direction. Boussinesq approximation, which is the fluid density concerning the buoyancy force, was assumed to be affected by temperature change, with reference temperature T_{ref} at 300 K and Vol. Coef. Th. Exp. at 0.003333 1/K. Other molecular properties included $\rho = 1.1614 \text{ kg/m}^3$, $\mu = 1.846 \times 10^{-5} \text{ N-s/m}^2$, $\nu = 1.589 \times 10^{-5} \text{ m}^2/\text{s}$.

4.5.3 Simulation of a Heat-pipes Heat-exchanger as Passive Cooling Equipment for Pre-Cooling of Air Intake

Since electricity was invented in the mid-1700s, it has played an important role in every aspect of human life. The work performed with electrical appliances moves people and technology faster. The demand for usage goes hand in hand with the increase in the cost as well as environmental issues associated with energy use. Cooling has become essential in designing domestic and commercial buildings. Conventional refrigeration and air-conditioning equipment using the vapour compression cycle consume electrical power in creating pressure and temperature differences during its cycle. In a low-energy and clean building environment, air change needs to be acceptable for thermal comfort.

ASHRAE standard 55 stated that a heat balance model of a human body is exclusively influenced by environmental factors such as temperature, thermal radiation, humidity, airspeed, human activity and clothing (Jones, 2001; Grondzik, 2007; Priyadumkol, 2014). The commission of the European Communities conducted measurements of air change in dwellings. The average air change for a sealed dwelling where the air escapes valves, doors, windows, and ventilation system closed is at 0.68 times per hour and is 3 to 4 times higher for an occupied dwelling. Some 20 % (0.2 times per hour) of occupied dwellings have an extremely low rate of air change. The calculations performed on natural ventilation systems show that air-escape valves with apertures of 30 cm^2 per room are not adequate to create the requisite air change for sealed dwellings (Yau, 2010). It is therefore important to improve the control of the total air changes as this would meet both energy savings and allow for a better indoor climate for the home.

Figures 4.44 to 4.46 show the distributions of temperature simulated through a row of heat-pipes with different temperatures. The flow of the inlet temperature selected refers to tropical ambient temperature at 293 K (20°C), 303 K (30°C) and 318 K (45°C). The simulation shows an airflow through the evaporator section of the heat-pipes heat-exchanger where the inlet opening of the acrylic box is located. The average temperature of 295 K was marked as the evaporator section of the heat-pipes heat-exchanger. The end temperature results of the air that flowed through the heat-pipes heat-exchanger showed a 3K to 7K difference from the supplied air.

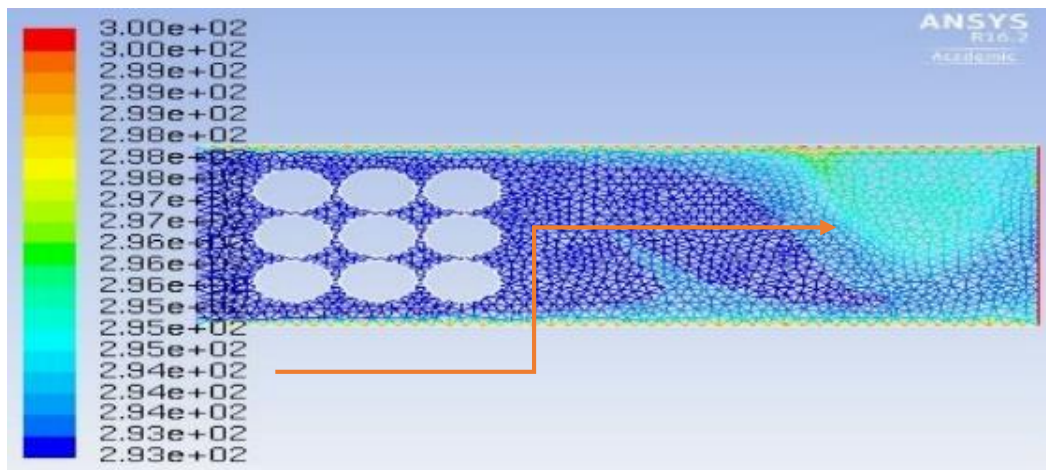


Figure 4.44: Simulation of ANSYS Fluent on a row of heat-pipes heat-exchanger with airflow at a temperature of 293 K passing through the evaporator section of the heat-pipes. The average leaving temperature is about 294 K. *Abdullah (2015).*

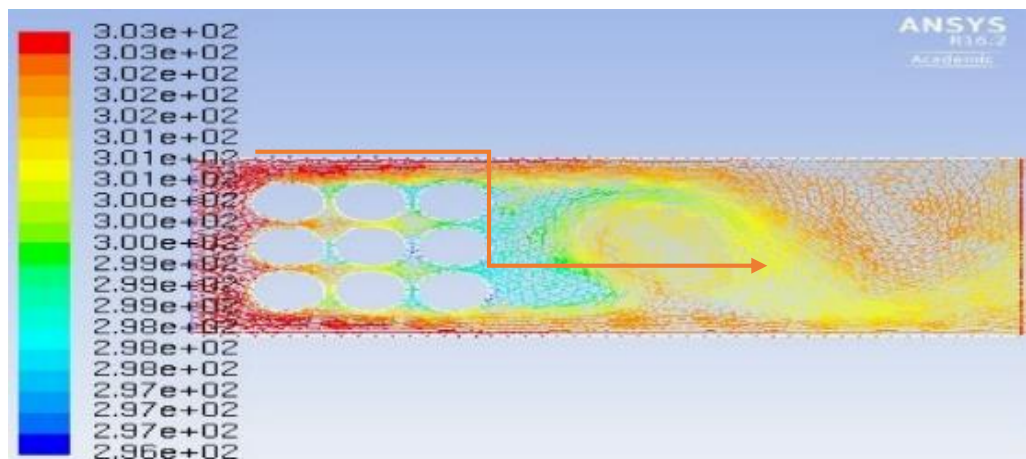


Figure 4.45 Simulation of ANSYS Fluent on a row of heat-pipes heat-exchanger with airflow at a temperature of 303 K passing through the evaporator section of the heat-pipes. The average leaving temperature is about 301 K. *Abdullah (2015).*

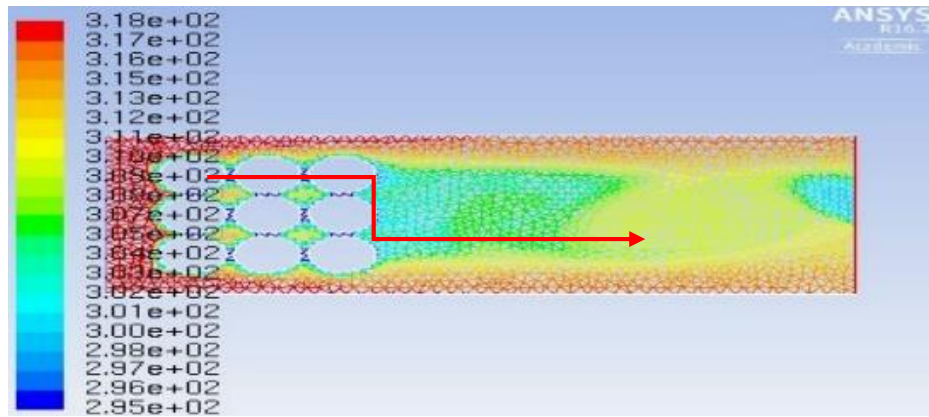


Figure 4.46: Simulation of ANSYS Fluent on a row of heat-pipes heat-exchanger with airflow at a temperature of 318 K. The lowest leaving temperature is 310 K. *Abdullah (2015).*

4.5.4 Simulation of a Heat-pipes Heat-exchanger with Driven Ventilation

The study focused on the heat-pipes heat-exchanger's heat transfer effects on the ventilation and the opening of a room. The study aimed to verify the heat-pipes heat-exchanger's applications on different openings of a building. The work involved two different natural ventilation patterns, namely cross and single-sided ventilation. The computational study focused on natural ventilation entering a room with the dimensions of 8 m x 5 m x 5 m, a comparison to the room size suggested by Idris (2013). As mentioned by Hunt and Linden (1999), the airspeeds induced by a temperature difference of 10°C in a building of 5 m high are on the order of 1.3 m/s, while the average UK wind speeds are around 4 m/s.

The single-sided opening had both an inlet and outlet at the same façade for a room with fewer options for ventilation. The edges of the opening of the single-sided were shaped with sharp edges for Case 1 and with round edges for Case 2. Both were located on the top of the room, as shown in Figures 4.47 to 4.49.

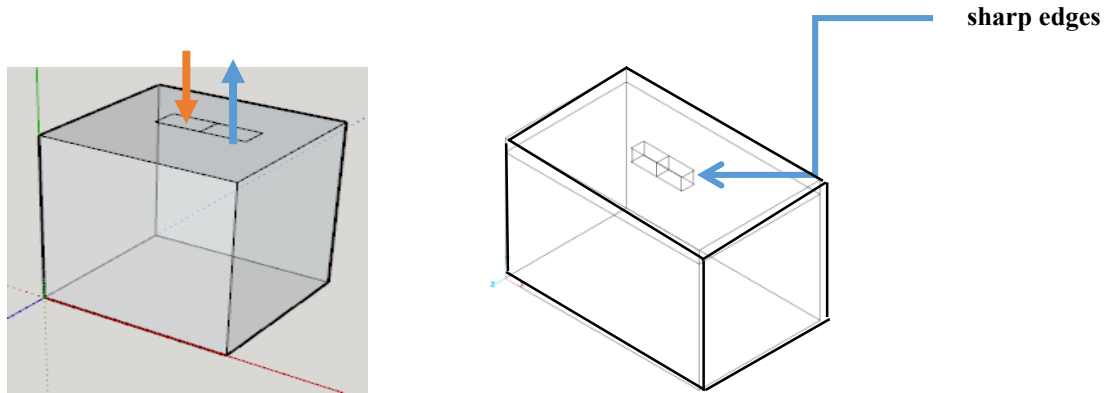


Figure 4.47: Case 1 which is single-sided ventilation with sharp edges at the inlet and the outlet opening. *Abdullah (2014).*

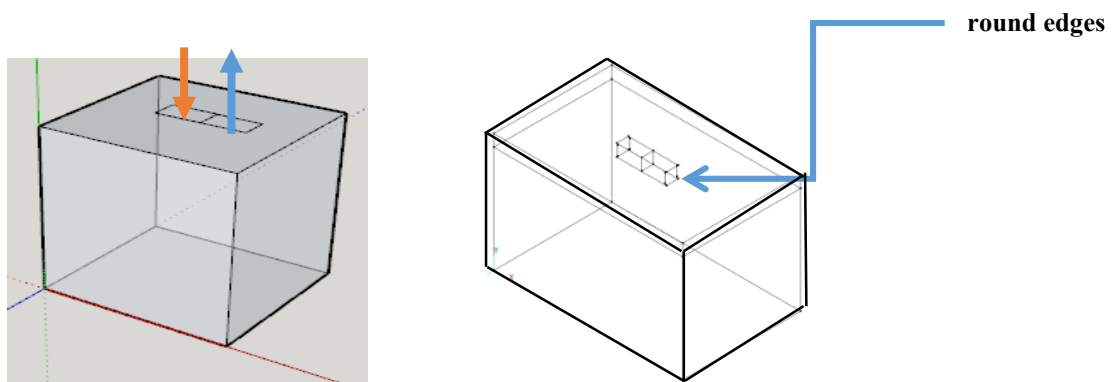


Figure 4.48: Case 2 is single-sided ventilation with round edges at the inlet and the outlet opening. *Abdullah (2014).*

The cross ventilation had two sharp edges for the inlet and outlet opening, each located on the top and the side of the room, respectively. It is to demonstrate the effect of induced air on the roof. This will tend to provide larger flow rates.

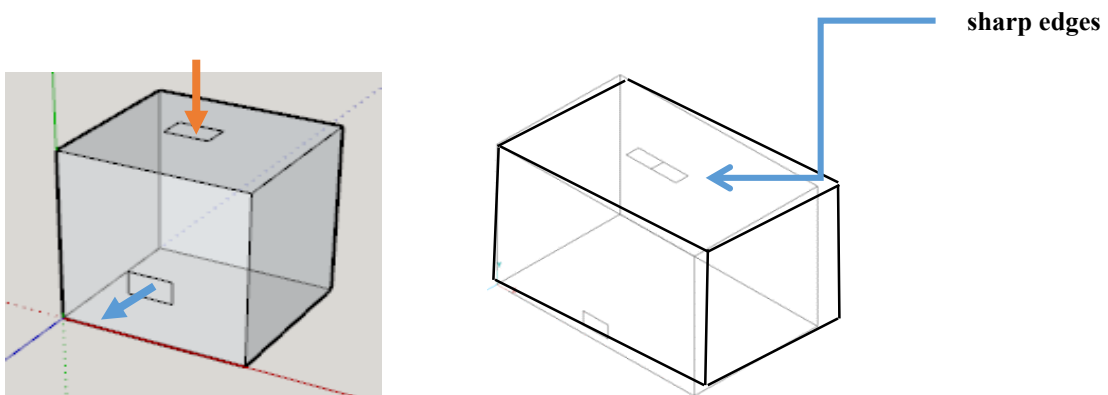


Figure 4.49: Case 3 with an outlet located on the sidewall of the building. *Abdullah (2014).*

Table 4.8: Cases and configurations for the study of the effects of the heat-pipes heat-exchanger to a room with natural ventilation. *Abdullah (2014)*.

Configurations	
Case 1	Top ventilation through a heat-pipes heat-exchanger with both inlet and outlet located on top of the building, sharp edges at the opening of the inlet and outlet.
Case 2	Top ventilation through a heat-pipes heat-exchanger with both inlet and outlet located on top of the building, with round edges at the inlet and the outlet opening.
Case 3	Cross ventilation through the inlet of the HPHE at the top and the air travels to the outlet located on the sidewall of the building. The inlet is located at the centre of the roof and the top outlet opening at the HPHE is closed.

Table 4.9: Total cells and nodes used for modelling from CFD ACE-GEOM and GUI. The grids used are structured grids and the number of cells and nodes are different for all cases as there are only slight differences in air flow rate result at about 1 % when using bigger cells and nodes range. *Abdullah (2014)*.

	Total cells	Total Nodes
Case 1	324000	292668
Case 2	655360	595820
Case 3	216000	185193

The CFD-View analysed the convergence results and the results were then presented in the form of a graphical presentation with different plots, streamlines and curves. The 3-dimensional graphical airflow traces for all cases are presented in Figures 4.50 to 4.52.

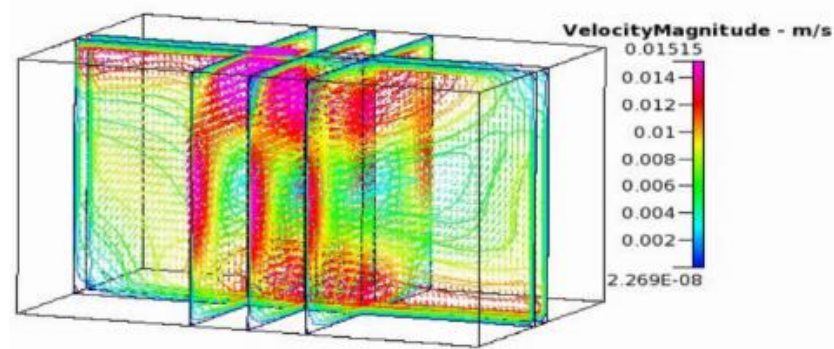


Figure 4.50 a.

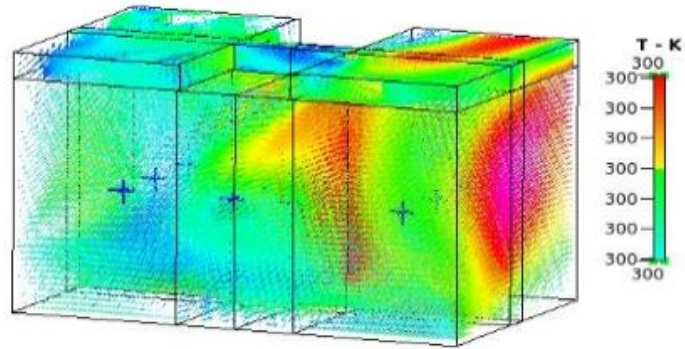


Figure 4.50 b.

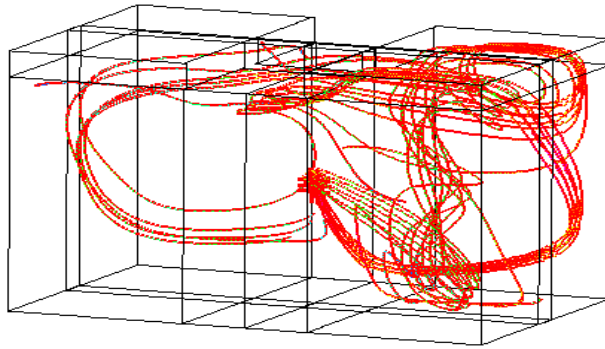


Figure 4.50 c

Figure 4.50: Case 1 showing the graphic distributions of a. Velocity magnitude, b. Temperature, and c. Flow path.
Abdullah (2014).

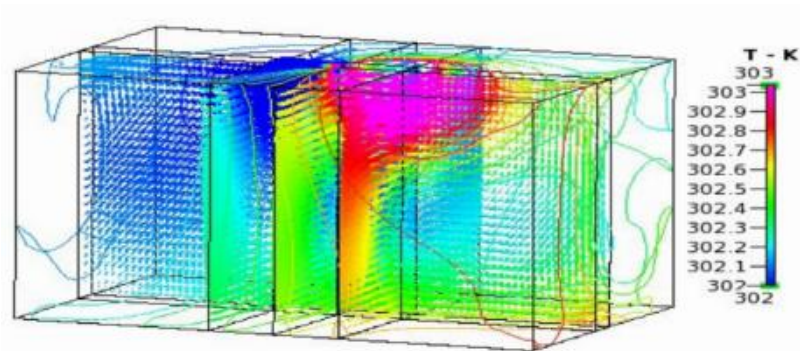


Figure 4.51 a.

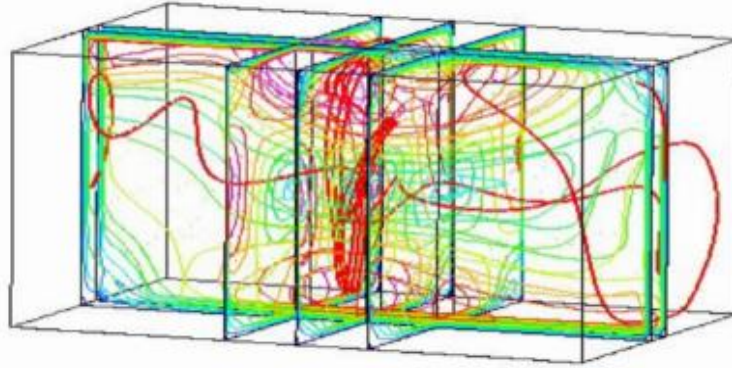


Figure 4.51 b.

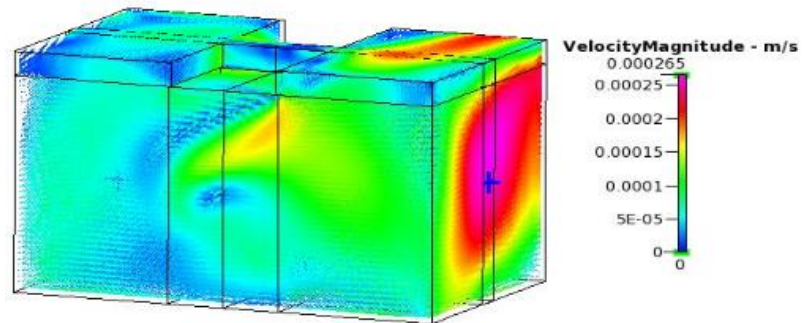


Figure 4.52 c.

Figure 4.51: Case 2 showing the graphic distributions of a. Velocity magnitude, b. Temperature, and c. Flow path.
Abdullah (2014).

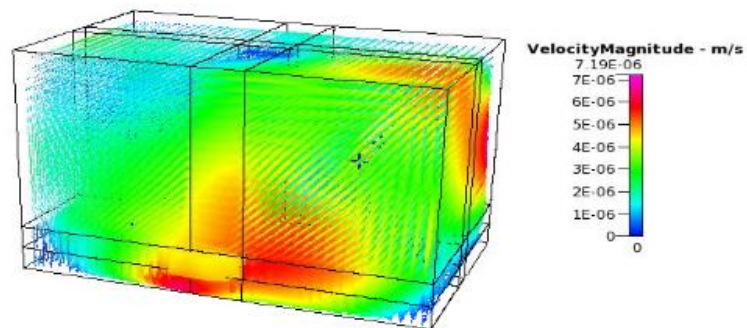


Figure 4.52 a.

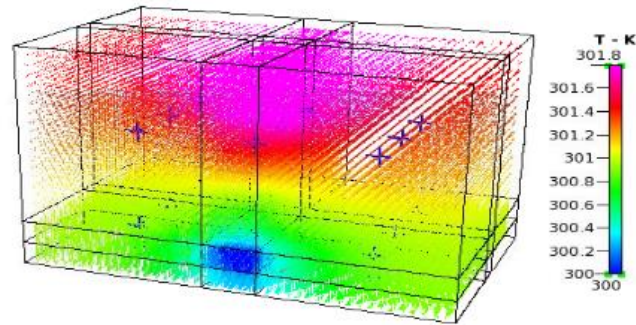


Figure 4.52 b.

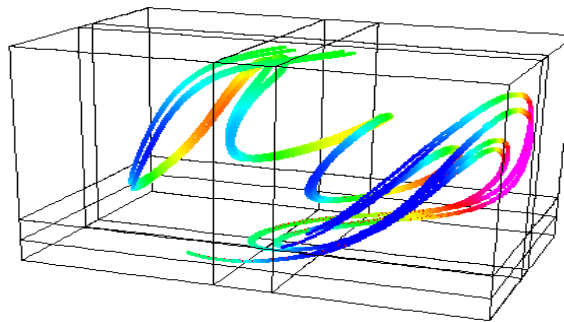


Figure 4.52 c

Figure 4.52: Case 3, show graphic distributions of a. Velocity magnitude, b. Temperature, and c. Flow path. *Abdullah (2014).*

The purpose of the study was to investigate the airflow pattern and flow rate with different openings and the distribution of temperature. The model used the Reynold Average Navier-Stokes (RANS) scheme to show the air distribution in a room with natural ventilation. The inlet opening was equipped with heat-pipes heat-exchanger to increase the temperature from 300 K to 305 K (27°C to 32°C). Cases were evaluated in terms of velocity and velocity magnitude across the room. It was found that case three had the most air velocity flow compared to the other two cases. The position is such that it allowed the greater air velocity rate to enter the room and pushed the air to the sidewall. Figures 4.53 to 4.55 show the velocity profiles of all cases.

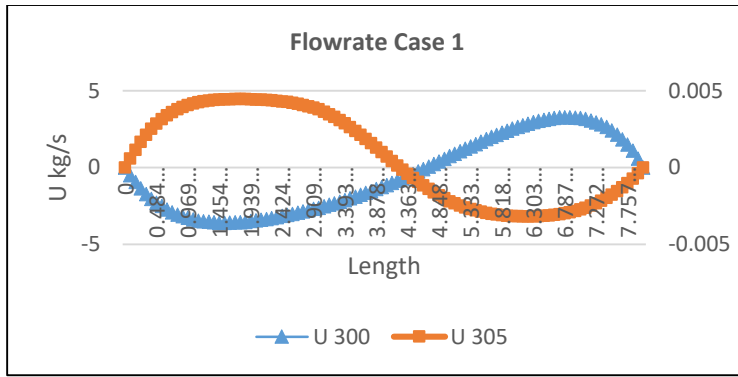


Figure 4.53 a.

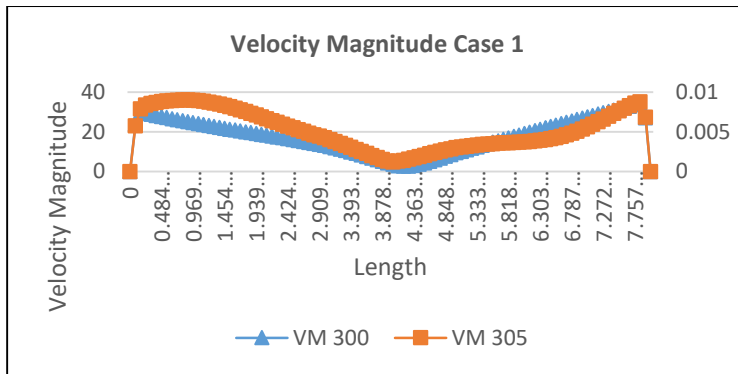


Figure 4.53 b.

Figure 4.53: Case 1 a. Velocity and b. Magnitude. Abdullah (2014).

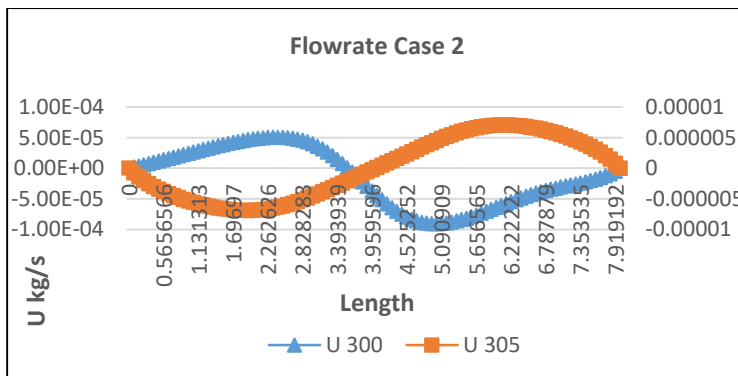


Figure 4.54 a.

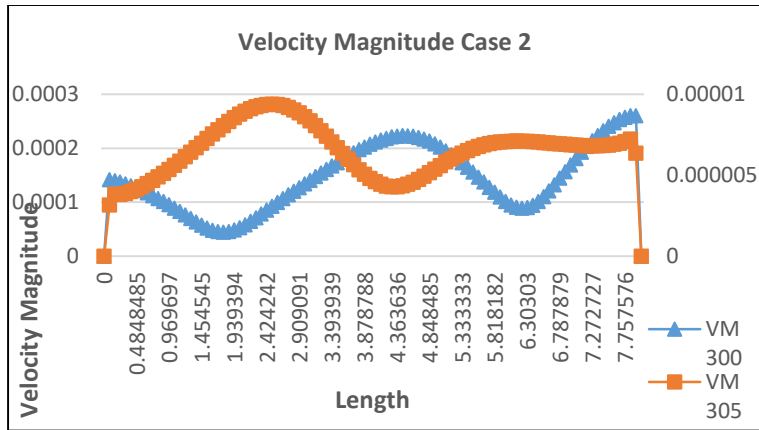


Figure 4.54 b.

Figure 4.54: Case 2 a. Velocity and b. Magnitude. Abdullah (2014).

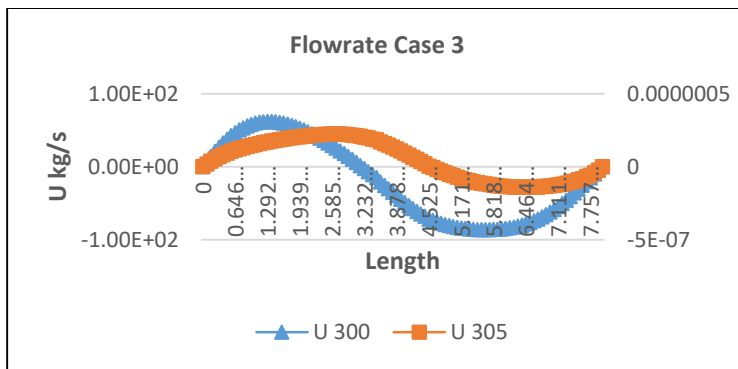


Figure 4.55 a.

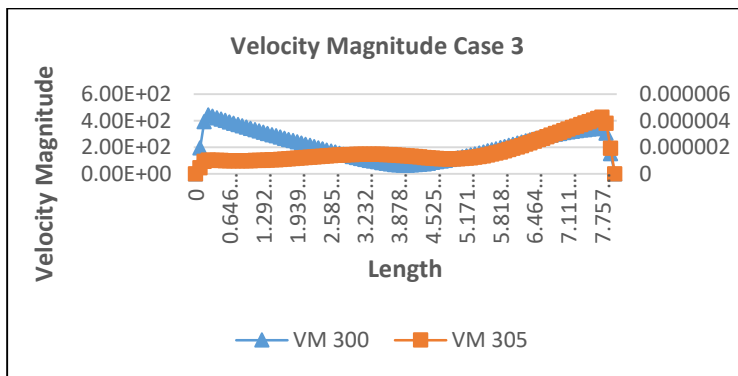


Figure 4.55 b.

Figure 4.55: Case 3 a. Velocity and b. Magnitude. Abdullah (2014).

CHAPTER V

RESULT AND DISCUSSIONS

CHAPTER OVERVIEW

This key chapter discusses the research results of the simulations and the experimental work. The rigorous simulation processes and experiments using heat-pipes heat-exchanger were performed at the Mechanical Laboratory, Faculty of Engineering and Information Technology, University of Technology Sydney while the work on the solar panel and wind turbines were conducted at the Universiti Kuala Lumpur, Malaysia France Institute, Malaysia. A total of eight conference and journal papers were produced related to these topics. Five Excellence in Research Australia (ERA) list ranked-A including one Scopus h-index international conference papers have been published relating to the proposed design. Additionally, two journal papers that had been reviewed earlier were later presented at the Journal of Advanced Manufacturing Technology, International Conference on Advanced Processes and System in Manufacturing (APSIM 2019), Malaysia. Details of the experimental work performed concerning the topic are included in this chapter.

1. The results of using the heat-pipes heat-exchanger showed that once the heat-pipes heat-exchanger was used, a 9 K difference of temperature between the outside ambient air and the room air could be achieved. The energy-saving calculations were made using the sensible cooling load temperature difference method and the psychrometric chart calculations. The energy-saving from the reduced air temperature was found to save 90 W/m³ to 140 W/m³ of cooling energy. Depending on the configuration of the heat-pipes and the air inlet opening, the energy-saving was between 25% to 33% of the room volume.

2. The experimental work with photovoltaic solar panels was found to have saved 31% of the energy required by the refrigerator.

3. Simulations and experimental work on wind energy were found to be capable of running a refrigerator for 7 hours.

5.1 INTRODUCTION

In this chapter, the actual system performances are presented. The various circumstances of the experimental study were compared to the simulation data. In the heat-pipes heat-exchanger study, the performance of the system was designed for Sydney's weather conditions even though the required ambient condition was adjusted to specific input needs as measured at the workshop of the Faculty of Engineering and Information Technology, University of Technology Sydney.

The study included calculations of the power consumption, coefficients of performance (COP) and the energy that the system could save as well as the effectiveness of the heat-pipes heat-exchanger. The input used in the system was the calculated dry bulb temperature of incoming supply air and the standard room air temperature. It should be noted that the heat-pipes heat-exchanger was capable of transferring heat and reducing the temperature and was manipulated based on several conditions in the study.

The refrigeration cycle as the cooling equipment and the air side of the system was studied to relate the heat-pipes heat-exchanger's assistance to the topic. R134a refrigerant which is a safe, zero global warming potential (GWP) heat transfer medium was used in the tubes to absorb and desorb heat. To increase the heat transfer capacity of the system, a copper tube with a grooved internal structure was used, replacing the standard smooth internal surface of the tube. The process of heat transfer from the evaporator to the condenser section of the heat-pipes heat-exchanger was successfully shown through the simulations and the experimental study.

The psychrometric state of the system has been calculated in Chapter III. Computational fluid dynamics simulations have been established to verify the proposed system's accuracy. The measured result is divided into three processes with a lower and higher supplied air temperature applied in each process, as listed below:

- Case 1: The incoming air was blown from the sidewall with side exit;
- Case 2: The incoming air was blown from the top with the top exit;
- Case 3: The incoming air was blown from the top and the exit air through the sidewall.

A total of eight conference and journal papers have been produced and published related to this topic. Five of the papers are of the Scopus-Elsevier ERA Ranked-A category, including one paper of Scopus h-index international conference. The outcome and the results that have been produced in the papers are presented in this section. This section will be divided into two topics; the flow field and the temperature distribution in the room, and heat transfer of heat-pipes heat-exchanger.

5.2 FLOW FIELD AND THE TEMPERATURE DISTRIBUTION IN THE ROOM

Before the experimental work begins, a CFD simulation was conducted in the application process. This was done to verify the significance, effectiveness and the expected outcome of the work. Simulation work on the components of the system such as the evaporator, condenser and the application in outdoor room conditions were also performed. The incoming supplied air and the return air were predominantly being simulated with the passive cooling components, that is the heat-pipes heat-exchanger to establish the temperature ranges.

Computational Fluid Dynamics uses numerical methods and algorithms to solve the problem involving fluid flow and predicts the flow behaviours based on mathematical modelling. The model is based on fundamental governing equations of fluid dynamics, namely the conservation of mass, momentum, and energy. The fundamental basis of any CFD problem is the Navier-Stoke equations (conservation law). The four terms in the general differential equation are the unsteady term (transient), the convection term, the diffusion term, and the source term. The author's works on natural ventilation were used to study the flow structure of fluid-driven ventilation and wind-driven natural ventilation system in buildings with CFD. CFD-ACE from ESI software was used to obtain the result of the satisfactory convergence or when the steady-state is reached. The numerical solution of CFD-ACE's process continuity and the equations work in three steps, namely pre-processing, solving and post-processing.

5.2.1 Simulation of a Heat-pipes Heat-exchanger with High Ambient Outdoor Temperature Condition

Paper presented at The American Society of Mechanical Engineering - International Mechanical Engineering Congress and Exposition 2015, Houston, Texas.

Title: Numerical Simulations of the Flow and Heat Behaviour for a Heat-pipes heat-exchanger in an Outdoor Power Supply Cabinet.

The aim of the research was to study the heat-pipes heat-exchanger's heat transfer effects on the outdoor cabinet where the inner temperature is high. The main issue to be addressed in the simulation was to demonstrate the effectiveness of the heat-pipes heat-exchanger and the temperature drop that the heat-pipes could achieve. Figure 5.1 shows the modelling of a straight heat-pipes heat-exchanger that is attached to the front face of an outdoor power supply cabinet. The incoming air inlet is passed through the heat-pipes before entering and leaving the cabinet. A different method of cooling the outdoor power supply cabinet using a heat-pipes heat-exchanger was proposed to replace the thermosiphon system which normally uses the gravity method of evaporation. CFD simulation using CFD ACE and ANSYS Fluent was used to solve the issues of effectiveness of the heat-pipes to show the air profile in the cabinet. The heat-pipes heat-exchanger was placed vertically in the evaporator section at the bottom. The distribution of air when entering and leaving were set with the air entering the bottom face of the heat-pipes and leaving from the upper face of the cabinet. The ambient temperature was 293 K (20°C), while the inner temperature of the cabinet was set to 328 K (55°C).

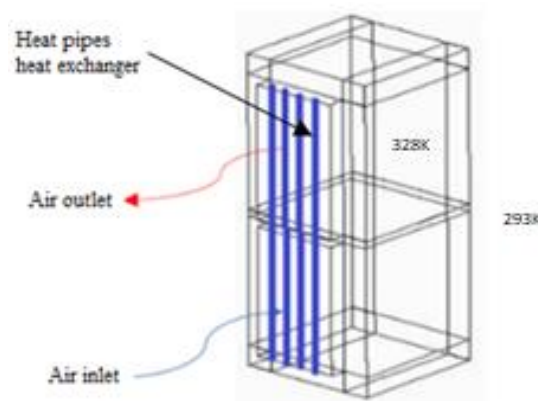


Figure 5.1. Schematic of an outdoor cabinet with the application of straight heat-pipes showing the inlet and outlet air paths. The source of heat is from the operation of the electro-mechanical equipment inside the cabinet and the solar heat. *Abdullah (2015)*.

Table 5.1: The nodes and elements of the fluid-solid meshes when running with ANSYS Fluent.

Domain	Nodes	Elements
Fluid	111276	94326
Solid	99724	66495
All Domains	211000	160821

Figure 5.3 shows the air distributions on the inside of the power supply cabinet, while Figures 5.2 and 5.4 show the distribution of temperature and airflow inside the cabinet. The heat-pipes heat-exchanger was installed at the front of the cabinet air intake. The air enters the inlet opening of the cabinet located at the bottom front of the wall. The ambient air was passed through the cooled heat-pipes heat-exchanger and was mixed with the warm air inside the cabinet as generated by the working equipment.

The liquid-state R134a refrigerant in the heat-pipes was boiled by the heat from the ambient and the inner heat of the cabinet. The cabinet's inside space heat was set to 328 K (55°C), transferring its heat to the cold side of the evaporator and thus reducing the inside temperature to about 315 K (42°C). Heat-pipes effectiveness is determined by assessing its required performance at the local design condition (Jouhara, 2010), and in this case, the cabinet's inside temperature of 328 K (55°C). As both the evaporators and condenser's flow rates were assumed identical, the heat capacity was cancelled out. The off-coil temperature of the evaporator was about 286 K (13°C) and the inlet supplied air temperature was 300 K (27°C).

The effectiveness of the heat-pipes in function to the flow rate across the heat-pipes were found to be

$$\frac{T_4 - T_3}{T_1 - T_3} = \frac{27 - 13}{55 - 13} = 0.33 = 33\%$$

where,

$$\begin{aligned} T_{mix} &= T_1 - \left(\frac{T_4}{2}\right) \\ &= 55 - \left(\frac{27}{2}\right) \\ &= 41.5^\circ\text{C} \end{aligned}$$

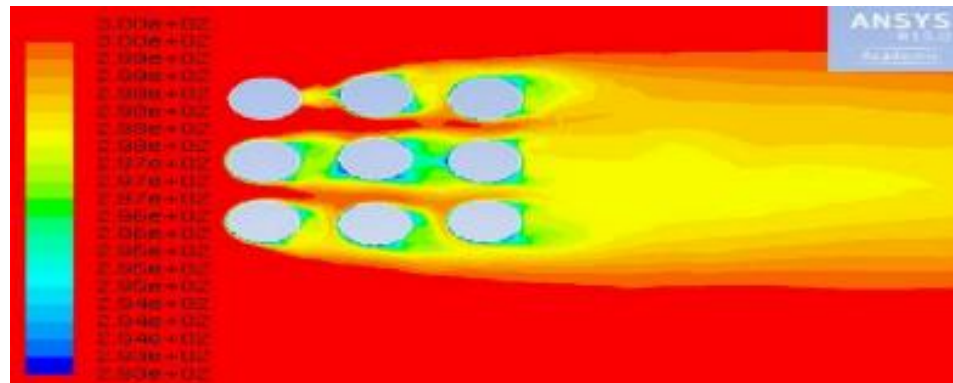


Figure 5.2 a.

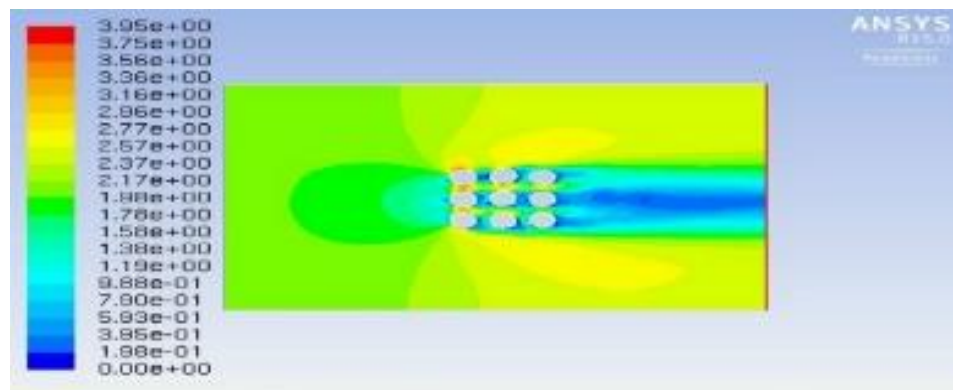


Figure 5.2 b.

Figure 5.2: The contour of a. Air temperature and b. The airflow is simulated to a heat-pipes heat-exchanger by ANSYS Fluent. *Abdullah (2015)*.

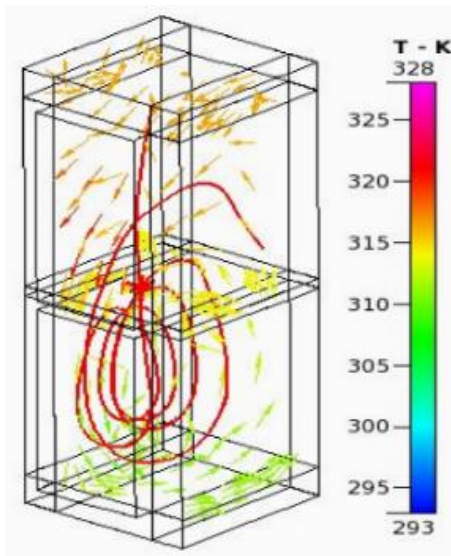


Figure 5.3 a.

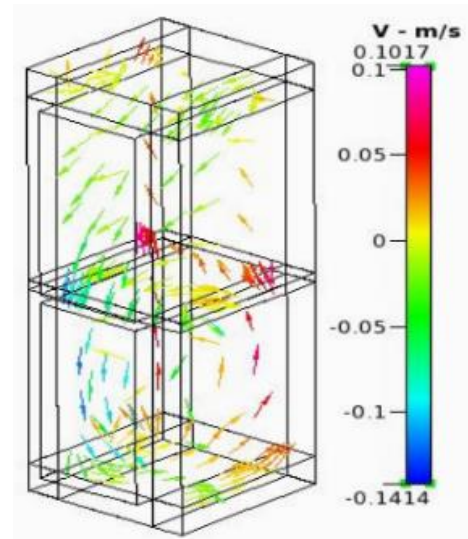


Figure 5.3 b.

Figure 5.3: Airflow traces inside the outdoor cabinet after passing through the heat-pipes heat-exchanger inlet based on the simulation model run on CFD-ACE. The air velocity shows that the warmer air moves to the upper side of the cabinet before exiting to the outlet. a. Temperature. b. Velocity. *Abdullah (2015)*.

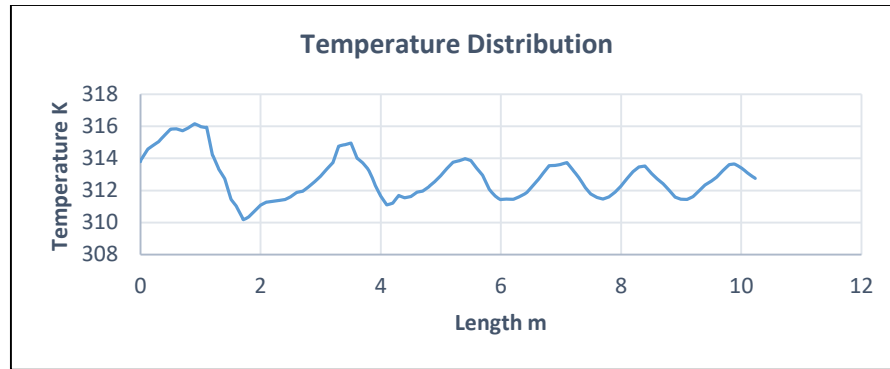


Figure 5.4a.

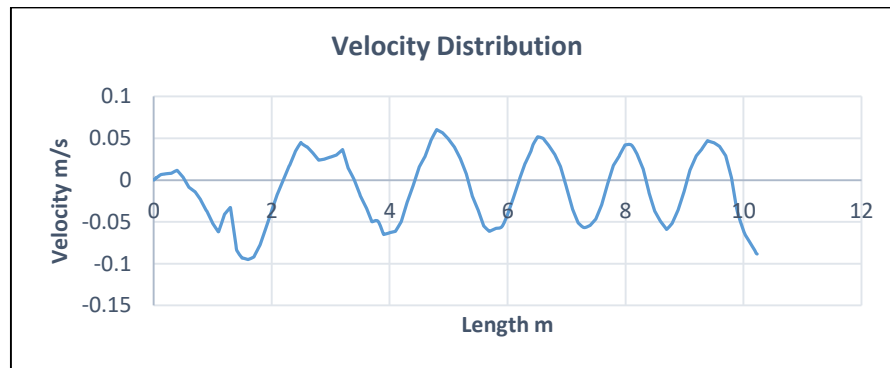


Figure 5.4 b.

Figure 5.4: a. Temperature b. Velocity distribution along the inside length of the outdoor cabinet. *Abdullah (2015)*.

When the air temperature process was plotted on a psychrometric chart, it was found that T_{mix} of 314.5 K (41.5°C), 22% RH was equal to and corresponded with the average temperature recorded by the simulation model of 314 K (40.85°C). The details of the Psychrometric Chart can be referred to in Appendix 1. Table 5.2 shows the air properties in the process.

Table 5.2: Temperature, relative humidity, and enthalpy when the air circulated in the outdoor cabinet. *Abdullah (2015)*.

Temperature K	RH %	Enthalpy h, kJ/kg	Flowrate \dot{m} m ³ /s
300	50	56	0.017
314.5	22	71	0.016
328	9	84	0.016

The rate of energy transfer to the air can be calculated by

$$W = \dot{m} \Delta h$$

$$\begin{aligned}
 &= 0.05 * 0.3 * \left(\frac{1}{0.865}\right) * (84 - 56) \\
 &= 0.5 \text{ kW}
 \end{aligned}$$

where the velocity was at 0.05 m/s, cabinet inlet opening was 0.3 m² and the specific volume of inlet air was 0.0865 m³/kg.

5.2.2 Simulation of a Heat-pipes Heat-exchanger Effect on an Air-Cooled Condenser

Paper presented at The American Society of Mechanical Engineering - International Mechanical Engineering Congress and Exposition 2016, Phoenix, Arizona.

Title: CFD-Simulation of a Heat-pipes Heat-Exchanger Effect on a Tubular Air-Cooled Condenser. The aim of the research was to study the heat-pipes heat-exchanger's heat transfer effects on the condenser side of an air-conditioner.

The main issue to be addressed in the simulation process was the effectiveness of the heat-pipes heat-exchanger and the temperature drop that the heat-pipes achieved at the end of the process when attached to a condenser of an air-cooled air conditioner. This is a unique method of pre-cooling the air intake to the condenser coil using a heat-pipes heat-exchanger in an air-cooled refrigeration system.

The heat-pipes heat-exchanger evaporator section was attached to an air inlet façade of an air-cooled refrigeration condenser where the ambient air-cooled the refrigerant in the condenser tube. Attaching the heat-pipes to the front air intake of the condenser should lower the ambient air temperature before touching the surface of the condenser tube. The advantage of heat-pipes is that they can be positioned in any configurations, whereas the cooling loops and the thermos-siphons are operated vertically, gravitational mass can be used to return the refrigerant to the evaporator.

CFD simulation using ANSYS Fluent was used to solve the issues of the effectiveness of the heat-pipes heat-exchanger and to show the air profiles. The distributions of air were set off with the air flowing through the heat-pipes to the condenser coil, leaving to the other side of the condenser. The incoming ambient air temperature was set to 300 K, while the heat-pipes were set to 295 K. The refrigerant R134a inside the condenser coil left the compressor at a temperature of

319 K at the upper side of the coil and gradually dropped at about 1K to finally reach 315 K at the bottom of the coil.

The CFD simulations used a standard 3D Reynold Averaged Navier-Stokes equation, continuity, and energy equation simulation. The results of ANSYS Fluent with R134a and the distribution of air were presented in 2D figures to show the interactions between the air and the heat-pipes heat-exchanger in relation to the air-cooled condenser.

In a standard refrigeration cycle, R134a in a vapour compression system leaves the compressor with a temperature of 319 K (46°C) and pressure of 109200 Pa (1 bar) and enters the condenser coil. Jones (2001) and Grondzik (2007) suggested a range of 313 K (40°C); however, in this simulation, the maximum temperature of 319 K (46°C) was used for the condensing temperature. The condenser rejected heat to the airflow across the condenser coil surfaces and cooled the refrigerant inside its tube to a temperature of 315 K, at the same pressure. In the process, the refrigerant medium changed its phase from vapour to a liquid state. A heat-pipes heat-exchanger was installed at a distance of 100 mm before the condenser to pre-cool the extracting air to the condenser. The heat-pipes heat-exchanger was used as a heat sink to reduce the air temperature before it flowed towards the condenser.

This 2D computational study focused on the air flows crossing the condenser where the temperature dropped from 319 K to 315 K. Only the evaporator side of the heat-pipes heat-exchanger was shown in the simulation. Three models were simulated, namely simulation of a condenser for reference, simulation of heat-pipes attached close to the condenser, and simulation of heat-pipes separated 100 mm away from the heat-pipes heat-exchanger. By monitoring the air outlet that crosses the heat-pipes and crossing off the condenser coils, it was possible to compare which method reduced heat the most. Figures 5.5 and 5.6 show the proposed idea of a closed tube heat-pipes heat-exchanger, with R134a as the refrigerant medium.

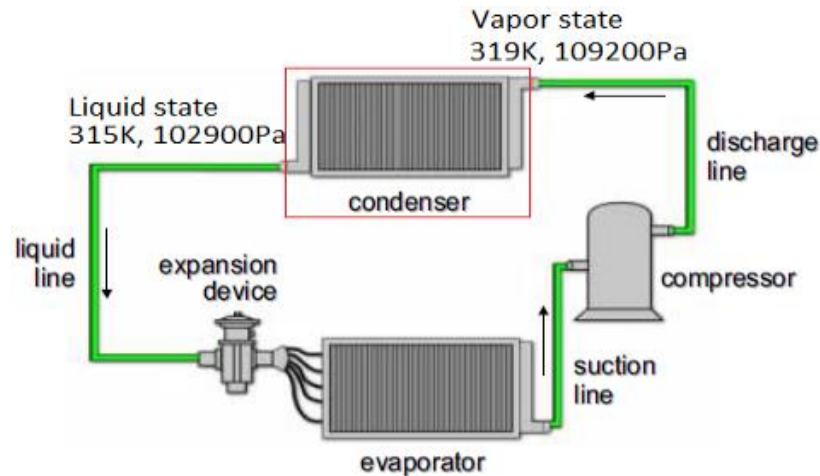


Figure 5.5: The condenser is a heat exchanger used to reject the heat of the refrigerant to another medium. The high-pressure refrigerant vapour flows in the tube of the condenser and rejects heat, condensing from vapour to a liquid state in the process. *Abdullah (2016)*.

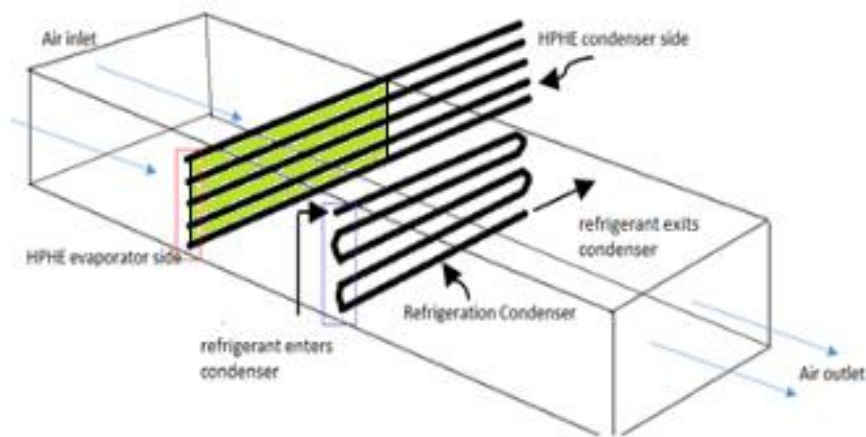


Figure 5.6: Schematic of a condenser with the application of straight horizontal heat-pipes showing the inlet and outlet of air paths. The source of heat is from the condenser refrigerant inlet with a temperature of 319 K and it then exits through the liquid line with a reduced temperature of 315 K. *Abdullah (2016)*.

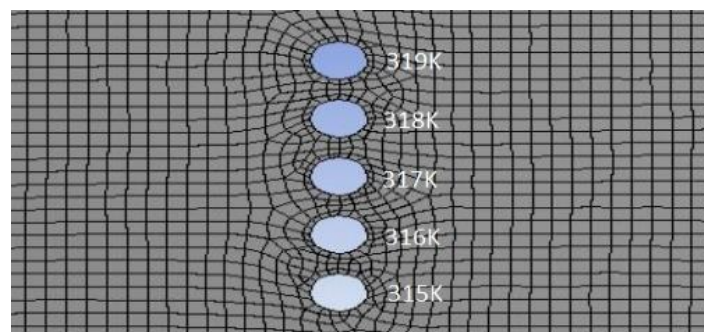
Table 5.3: The specification of models for all domains.

Domain	Specification
Case 1	Air at 300 K flows on the surface of an air-cooled condenser. The condensing temperature of the condenser inlet is 319K and the exit temperature is 315 K.
Case 2	Air at 300 K flows on the surface of a heat-pipes and a condenser that is attached closely together. The temperature of the heat-pipes heat-exchanger is 295 K while the condensing temperature of the condenser is from 319 K to 315 K.
Case 3	Air at 300 K flows on the surface of a heat-pipes and a condenser that are separated 100 mm apart. The temperature of the heat-pipes heat-exchanger is 295 K while the condensing temperature of the condenser is from 319 K to 315 K.

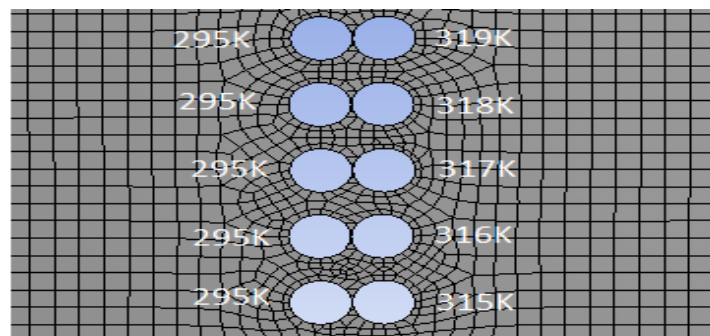
Table 5.4: The specification of nodes and elements for all domains

Domain	Nodes	Elements
Condenser	2209	2074
HP + Condenser	1817	1643
HP + 100 mm gap + Condenser	1623	1455

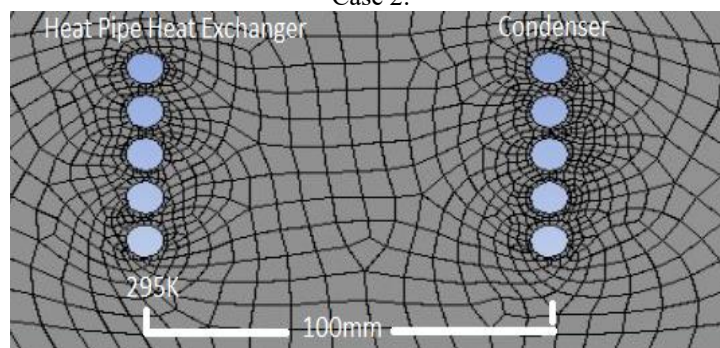
The mesh for the cases was shown in Figure 5.7. Several attempts were taken when testing the mesh distribution.



Case 1.



Case 2.



Case 3.

Figure 5.7: The model and meshes used to run the simulations on an air-cooled condenser by ANSYS Fluent.
Abdullah (2016).

Figures 5.8 to 5.11 show the distributions of temperature simulated through an air-cooled condenser. The end temperature of the air that flows through the condenser was about 304 K to 307 K, an increase of 4K to 7K from the supplied air of 300 K.

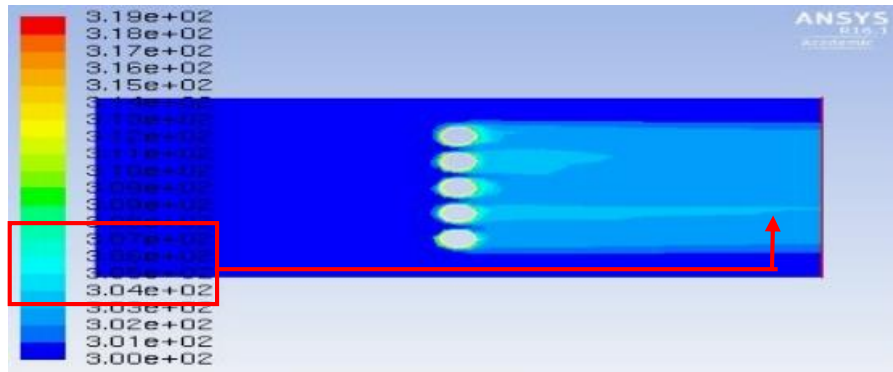


Figure 5.8: Simulation of ANSYS Fluent on an air-cooled condenser. The lowest temperature recorded for the condenser is about 304 K to 307 K of heat rejection to the ambient. *Abdullah (2016)*.

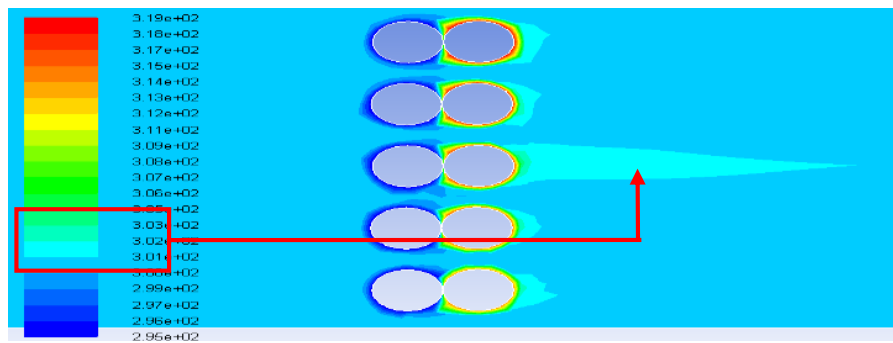


Figure 5.9: Case 2 with a heat-pipes heat-exchanger attached closely together. The lowest temperature recorded is about 303 K to 304 K. *Abdullah (2016)*.

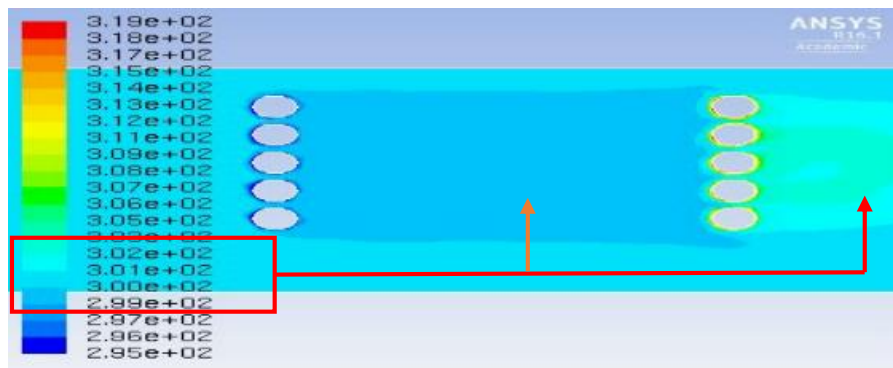


Figure 5.10: Simulation of ANSYS Fluent on an air-cooled condenser with a heat-pipes heat-exchanger attached separately 100 mm from the condenser air inlet. The lowest temperature recorded is 302 K. *Abdullah (2016)*.

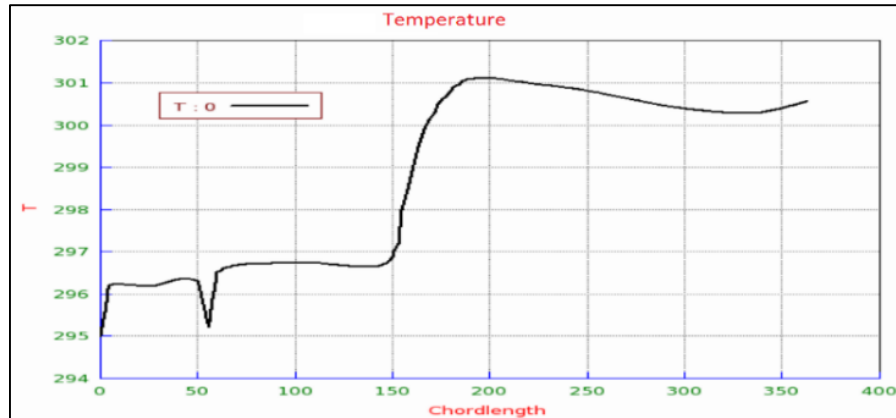


Figure 5.11: Graph from CFD-ACE for Case 3. The air flowing over the condenser coil is recorded to be at about 301 K. *Abdullah (2016)*.

From the simulation of a condenser and an attachment of a heat-pipes heat-exchanger to the air-cooled condenser, it was found that the efficiency was increased. The air-cooled condenser was recorded to reject heat at between 12K to 15K temperature difference, while with the attachment of the heat-pipes, it was found that the temperature difference could be increased to about 14K to 18K, which is a condenser operating temperature difference of 319 K (46 °C) to 305 K (32 °C). Table 5.8 shows the inlet and outlet temperature profiles of the three cases to demonstrate the capability of heat-pipes in transferring heat. Table 5.5 shows the work performed by the refrigeration system corresponding to the condenser T_c achieved. The COP of the system can be increased from 6.5 to 10.5 by reducing the supplied air temperature of the condenser. The results of the calculation from the pressure-enthalpy diagrams of the air-cooled refrigeration system corresponded to an evaporating temperature of $T_e=278$ K (5°C), condensing temperature $T_c=319$ K (46°C), with 10K superheat and 20K sub-cooling when compared to a condensing temperature of $T_c'=305$ K (32°C) while using the heat-pipes heat-exchanger.

Table 5.5: Comparison of the temperature difference between cases. Case 3 shows the highest temperature difference compared to other cases.

Parameters	Case 1	Case 2	Case 3
Air Inlet Temp, K	300	300	300
Heat-pipes Evaporator Temp T_e K	295	295	295
Condensing Temp T_c K	315-319	315-319	315-319
Air Outlet Temp, K	304-307	303-304	301-305
Differential Temp, K	12-15	15-16	14-18

Table 5.6: Comparison of the refrigeration cycle parameters when the condensing temperature changed from 319 K (46°C) to 305 K (32°C).

Parameters	Condenser	Heat-pipes + Condenser
Evaporating T_e , K	278	278
Condensing T_c , K	319	305
Condenser Surface Temp (°C)	331	318
Superheat (different K)	10	10
Subcooled (different K)	20	20
Evaporator Work Done Q_e (kJ/kg)	173.8	193.3
Condenser Work Done Q_c (kJ/kg)	200.5	211.7
Compressor Work Done W (kJ/kg)	26.73	18.42
COP	6.5	10.5

5.3 SOLAR RADIATION

The radiation intensity of the 6000°C solar surface corresponds to 70000 to 80000 kW/m²; however, the earth receives only a very small portion of this energy. Despite this, the incoming solar energy from radiation in a year is some 200,000,000 billion kWh (200 x 10¹⁴); this is more than 10000 times the yearly energy requirements of the whole world. The solar radiation intensity outside the atmosphere is on the average of 1360 W/m² with constant solar but when the solar radiation penetrates through the atmosphere, some of the radiation is lost. On a clear sky on a sunny day in summer, only between 600 to 1000W/m² can be obtained on the ground.

The operating costs of air conditioning mainly come from the rotational components such as the compressors, heaters, and ventilators. Solar radiation applies to air conditioning systems because of its cost-saving in terms of a free energy source. Depending on the gradation and location of radiation received, solar radiation is about 0.600 kW/m² to 1 kW/m². Appendix 3 shows that Australia receives from 2000 to 2500 kW/m².an of solar irradiance per year. A converter is required to convert thermal energy into electrical energy.

Data taken from the calculations of Photovoltaic is

$$\text{Power of the System/Energy} = A.r.H.PR$$

where A is the area of the panel, m^2 ; r is solar panel yield; H is the annual average irradiation of the tilted panel which is taken as $2000K \text{ Wh/m}^2.\text{an}$ for Australia; and PR is the performance ratio, the coefficient for losses (default value 0.75).

With 20 m^2 of PV installed and 15% of solar panel yield, the total power of a standard solar power for an air conditioner is about 3 kW.

5.3.1 Experimental Study on Solar Energy Air-Conditioning Booster

Paper presented at:

1. Australasian Fluid Mechanics Conference (2016), Perth, Australia.

Title: CFD-Simulation of the Effect of Heat-pipes Attached to an Evaporator and Condenser of an Air-Cooled-Air-Conditioner.

2. Journal of Advanced Manufacturing Technology, International Conference on Advanced Processes and System in Manufacturing (APSIM 2019).

Title: Simulation Study of Cooling a Small Domestic Refrigeration System Using Solar-Assisted Energy in Bangi, Malaysia.

The aim of the research was separated into two experimental works. The first was to study the heat-pipes heat-exchanger's heat transfer effects on the evaporator and condenser air intake of an air-conditioner. The second was to study the solar-assisted energy capability on a domestic refrigerator at a high ambient temperature. Experiments were set up to boost the air-conditioning capacity and to reduce the energy consumption of the cooling system. The heat-pipes heat-exchanger was used to assist the solar cooling system by reducing the operating temperatures. Figure 5.12 shows the solar air conditioning and booster installation.

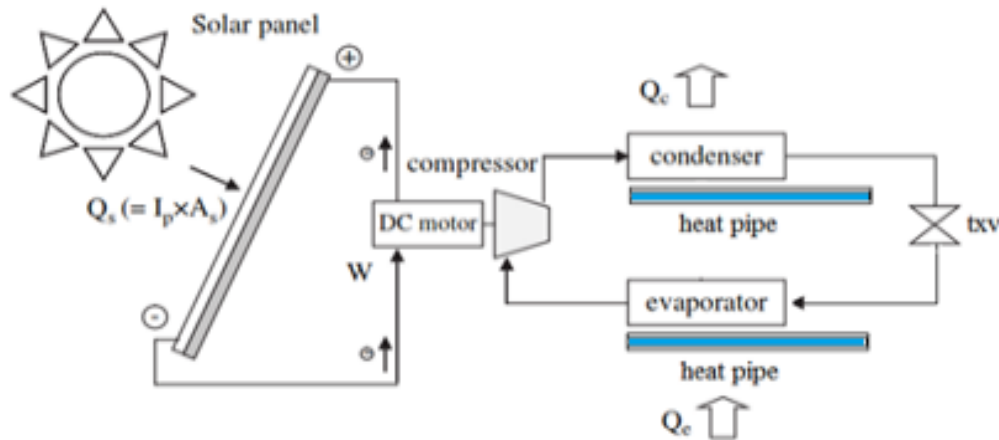


Figure 5.12: Solar air conditioning booster. *Meunir (2015)*.

In this experiment, an air-cooled refrigeration cycle condenser coil of 319K and an evaporator of 278K were being simulated. In the condenser coils, the condensing temperature dropped from 319K to 315K while the evaporating temperature increased from 278 to 282K. As suggested by Jones (2001) and Grondzik (2007), the author used the maximum temperature of 319K for the condensing temperature and 278K for the evaporating temperature. A heat-pipes heat-exchanger was installed 100mm before the coils and acted as a heat sink to reduce the air temperature and pre-cooled the flowing air. Attaching the heat-pipe to the front air intake of the refrigeration coils would have lowered the ambient air temperature before touching the surface of the coils. Passive cooling technologies have been studied by Riehl (2006), Joung et al. (2008), Charoensawan and Terdtoon (2008) and Meng et al. (2007) proposed a passive cooling system technology using methanol as the cooling medium. This 2D computational study focused on air flows crossing a condenser and an evaporator. Only the evaporator side of the heat-pipe heat-exchanger which absorbed the surrounding heat was shown in the simulation. Three models of each coil were simulated, namely simulation of a coil for reference, simulation of a heat-pipe attached close to the coil, and simulation of a heat-pipe separated 100mm away from the coil by monitoring the air outlet that crosses the heat-pipe and crossing off the coils. Figures 5.13 and 5.14 show the proposed idea of a closed tube heat-pipe heat-exchanger with R134a as the refrigerant medium which was used to transfer heat from one end to the other and attached to the coil side of the refrigeration system. Figures 5.15 to 5.16 show the meshes and the results of the simulations.

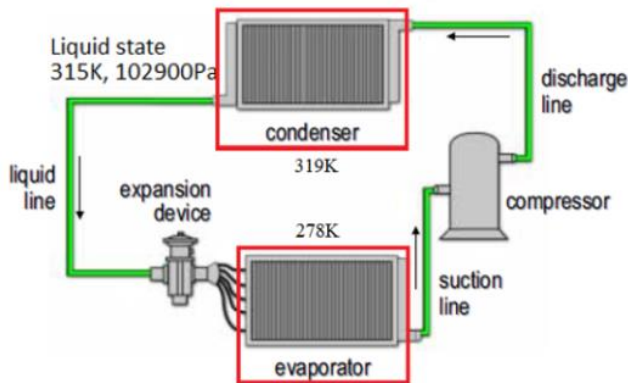


Figure 5.13: The Refrigeration Cycle. The condenser coil is a heat exchanger used to reject the heat of the refrigerant to the surrounding. The evaporator coil absorbs room heat and lowers the room temperature. *Abdullah (2016).*

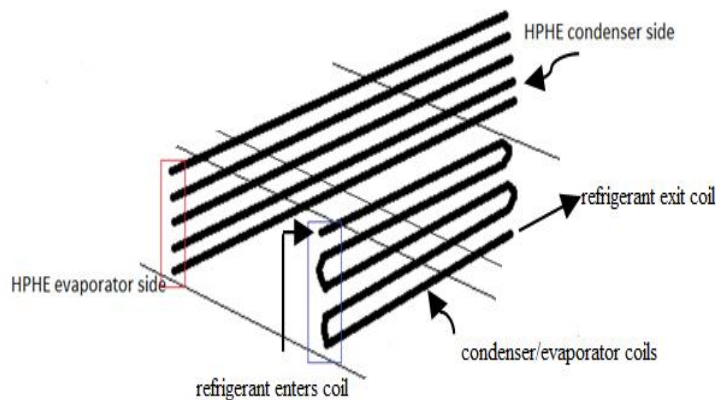


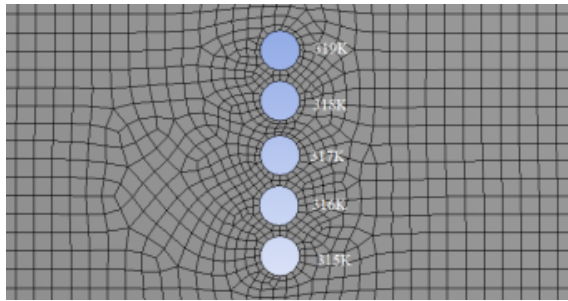
Figure 5.314 Schematic of the refrigeration coil with the application of straight horizontal heat-pipe showing the inlet and outlet of air paths. An evaporation temperature of 295K is used for the simulation of the heat-pipes heat-exchanger. *Abdullah (2016).*

Table 5.7: Problem description in all cases.

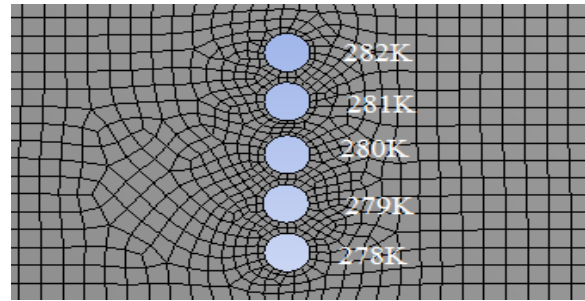
Domain	Specification
Case 1	Air at 300K flows on the surface of an air-cooled condenser/evaporator.
Case 2	Air at 300K flows on the surface of heat-pipes and a condenser/evaporator that are attached closely together.
Case 3	Air at 300K flows on the surface of heat-pipes and a condenser/evaporator that are separated 100mm apart.

Table 5.8: The specification of nodes and elements for the condenser.

Domain	Nodes	Elements
Case 1a, b	1572	1447
Case 2	1817	1643
Case 3	1623	1455



Case 1a



Case 1b

Figure 5.15: Case 1a for the condenser and 1b for the evaporator. *Abdullah (2016).*

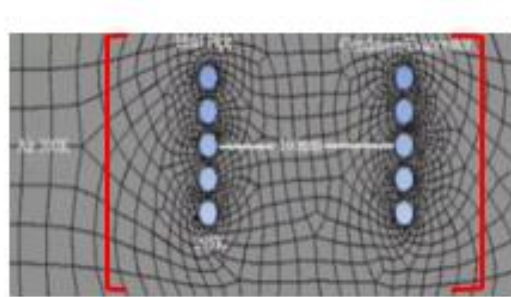
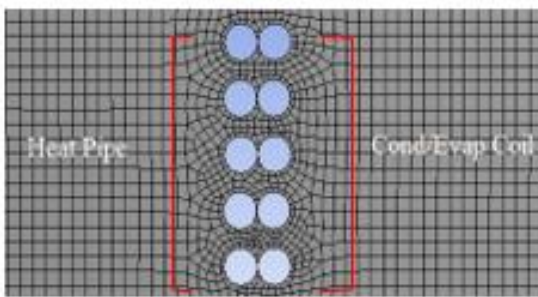


Figure 5.16: Case 2 and 3. *Abdullah (2016).*

<p>Case 1a: Condenser. Lowest temperature 305K</p>	
<p>Case 1b: Evaporator. Lowest temperature 293K</p>	
<p>Case 2: Condenser Lowest temperature 303K</p>	
<p>Case 2: Evaporator Lowest temperature 294K</p>	

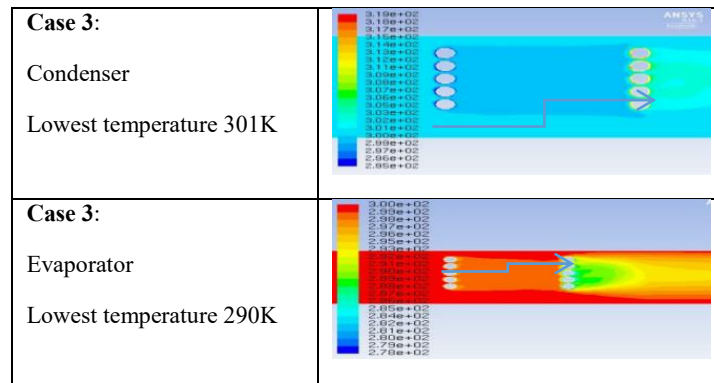


Figure 5.17: The simulation for all cases. *Abdullah (2016).*

The purpose of this study was to study the temperature decreasing effect of a heat-pipes heat-exchanger by simulating the airflow to air-cooled air-conditioner coils. The heat-pipes were used to reduce the temperature of the supplied air to the coils. The flow pattern was recorded by the simulation software ANSYS Fluent. The previous simulation showed that a difference of 5K was obtained when R134a was used as the refrigerant medium in the heat-pipes. From the simulation of the heat-pipes to the coils of an air-cooled system, it was found that efficiency can be increased with the attachments of the heat-pipes to the coils inlet airflow. When simulated, the air-cooled condenser was recorded to reject heat at about 12K to 15K, and the evaporator coils were lowered to 8K. Tables 5.9 to 5.11 show the inlet and outlet temperature profile of the three cases to highlight the capability of the heat-pipes in transferring heat.

Table 5.9: Comparison of the temperature difference K at the condenser coil for all the cases. Case 3 shows the best result.

Condenser	Case 1	Case 2	Case 3
Inlet, K	300	300	300
HP, K		295	295
Cond. T_c K	315-319	315-319	315-319
Outlet, K	305-307	303-304	301-303
Different, K	10	12	14

Table 5.10: Comparison of temperature difference K at the evaporator coils for all the cases. Case 3 shows the best result.

Evaporator	Case 1	Case 2	Case 3
Inlet, K	300	300	300
HP, K		295	295
Evap. T_e K	278-282	278-282	278-282
Outlet, K	293-294	294-295	290-292
Different, K	11	12	8

Table 5.11: Comparison of the normal refrigeration cycle compared to coils with a heat pipe.

Parameters	Coils	HP + Coils
Evaporating T_e (°C)	5	5
Condensing T_c (°C)	46	32
Condenser Surface Temp (°C)	58	45
Superheat (different K)	10	10
Subcooled (different K)	20	20
Evaporator Work Done Q_e (kJ/kg)	173.8	193.3
Condenser Work Done Q_c (kJ/kg)	200.5	211.7
COP	6.5	10.5
Compressor Work Done W (kJ/kg)	26.73	18.42

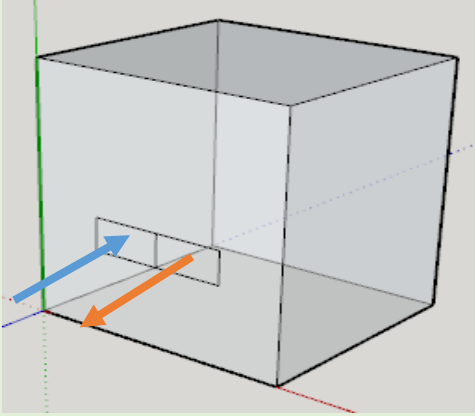
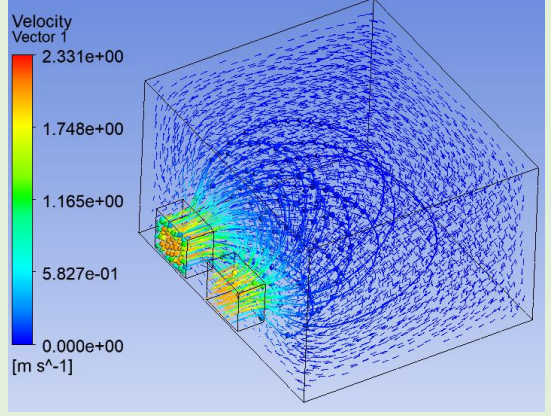
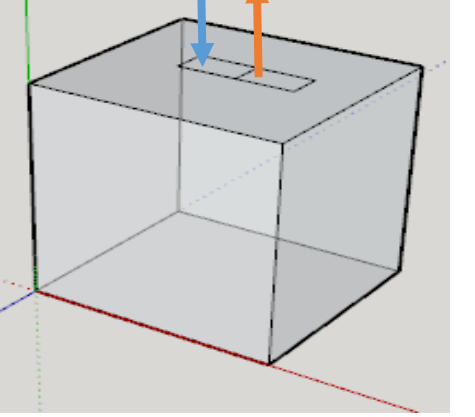
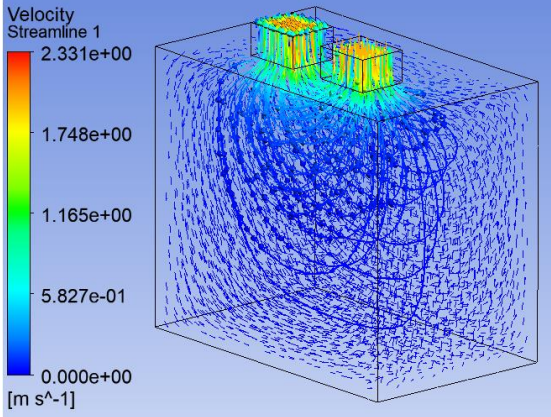
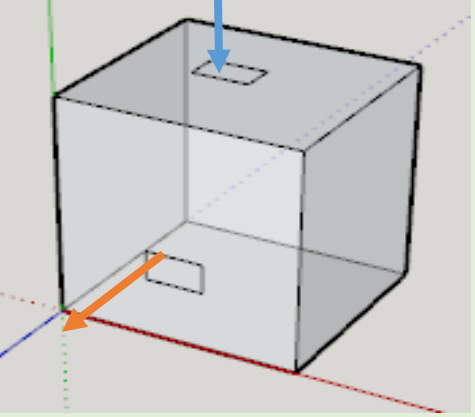
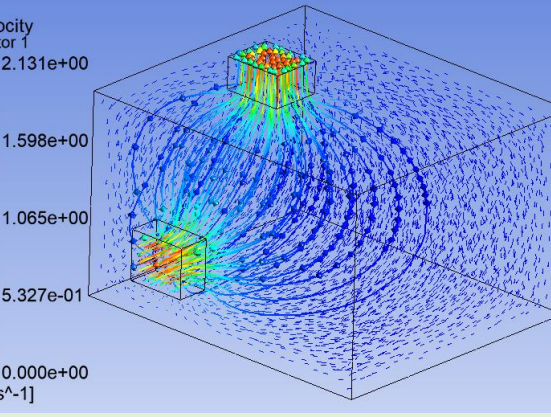
Based on the refrigeration cycle plotted, it was found that the evaporating capacity and the condensing capacity can be increased, with the fall of condensing temperature. The heat-pipes heat-exchanger may be used as one of the solutions to decrease the condensing temperature to the ambient temperature. Other simulations using a different refrigerant medium in the heat-pipe heat-exchanger should be tested.

5.4 HEAT TRANSFER OF THE HEAT-PIPES HEAT-EXCHANGER

The aim of the research was to evaluate the heat-pipes heat-exchanger's capability in transferring heat. The experimental work was carried out at the University of Technology Sydney, Australia. The study focused on the evaporator section of the heat-pipes heat-exchanger which works by absorbing heat from the incoming ambient air and transferring it to the condenser section. The heat is then released back to the ambient surroundings. The transferring processes of heat are determined by the R134a refrigerant inside the tubes in contact with the ambient surrounding air, and in the process, cooling the supplied air that passes through the heat exchanger into the room. As suggested by Jung (2008), two ranges of hot ambient temperature were taken as a guide as the inlet temperature, namely 303 K (30°C) and 318 K (45°C). A heat-pipe heat-exchanger was installed on the façade of the box before the supplied air enters the acrylic box. The heat-pipes heat-exchanger was used as a heat sink to reduce the air temperature before it flowed into the box. In this experimental study, the focus was on air flows crossing the room in which the temperature dropped from 303 K to 298 K.

The locations of the heat-pipes were at the top and the side of an acrylic box. Three models were tested, the first was an airflow passing a heat-pipes heat-exchanger from the side of the box, releasing the heat off on the same side. For the second model, the airflow was from the topside and the heat was released off at the top. Finally, in the third model, the airflow was from the top, but the hot air was released off to the side of a wall opening. Figures 5.18 and 5.19 show the proposed idea of the heat-pipes heat-exchanger which was used to transfer heat from one end to the other, attached to an acrylic box with high tropical ambient temperature. Thermocouples were placed in several locations within the box and these were read by a data logger to show the air temperature profile.

Table 5.12: Model specifications with fresh air intake locations that best suit the domain.

Case	Flow	Specification
Case 1		
Case 2		
Case 3		

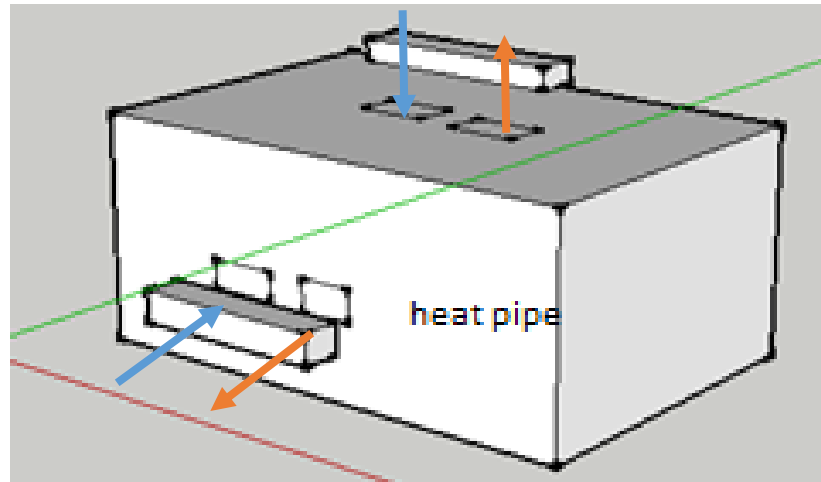


Figure 5.18: The layout of the fresh air intake locations with the heat-pipes heat-exchanger installed at the side and the top of the box.

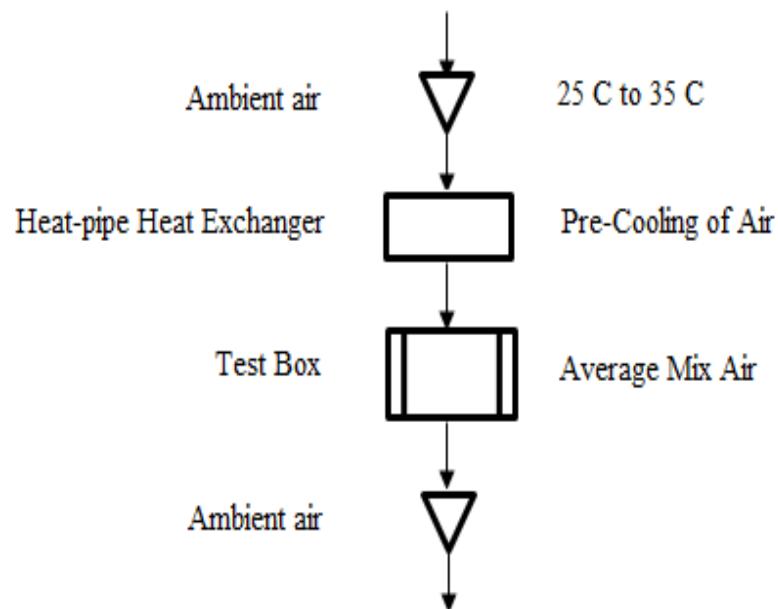


Figure 5.19: The workflow of the experimental project. The ambient airflow and the temperature are regulated by a variable fan and heater before passing a finned type heat-pipes heat-exchanger. The acrylic box then collects the result of the inside temperature distributions. Thermocouples are used in several locations for temperature data collection.

The results from the experimental study of the heat-pipes heat-exchanger show that it is an important component to reduce the sensible heat in a room. Figures 5.38 to 5.43 show the heat-pipes heat-exchanger used for the experiment and the thermal imaging recorded. A cross-flow heat-exchanger with a row of in-line 3 by 3 straight copper tubes that had fins filled with 11ml of liquid R134a was used. The overall length of the heat-pipes was 650 mm, with 500 mm of the working length finned. The liquid volume was about one-third of the straight copper tube, allowing

the optimum process of evaporation and condensation within the tube. The motivation came from a groove structured copper tube in which the surface area is bigger than the standard smooth structured copper tube. Table 5.13 shows the specification of the heat-pipes heat-exchanger used in the experiment.



Figure 5.20: Finned type cross-flow in-line heat-pipes -heat-exchanger with R134a as the cooling medium.

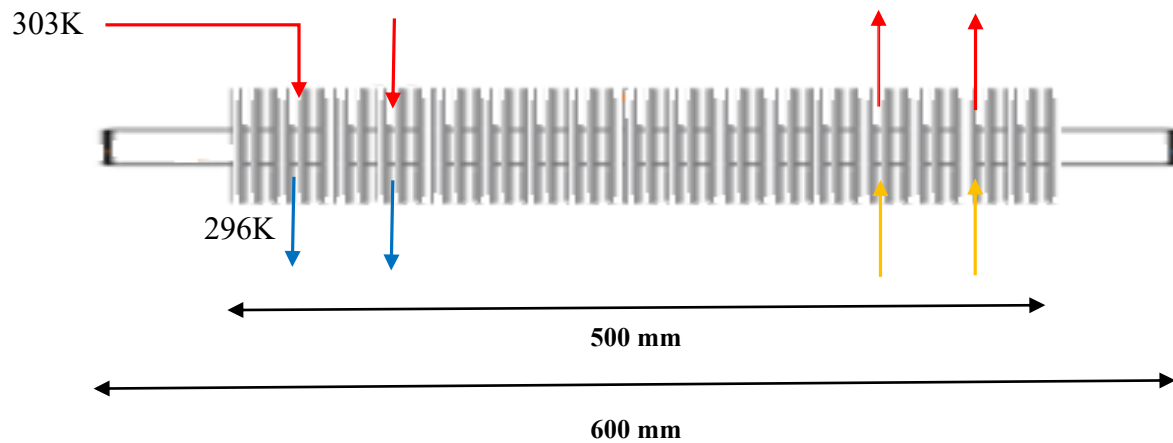


Figure 5.34 a.



Figure 5.34 b.

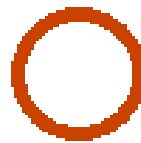


Figure 5.34 c.

Figure 5.21: Finned type cross-flow in-line heat-pipes heat-exchanger with R134a as the cooling medium. a. Temperature profile of the experimental test. b. Heat-pipes heat-exchanger of grooves structured copper tube was used for the experiment compared to c. Smooth structured copper tube.

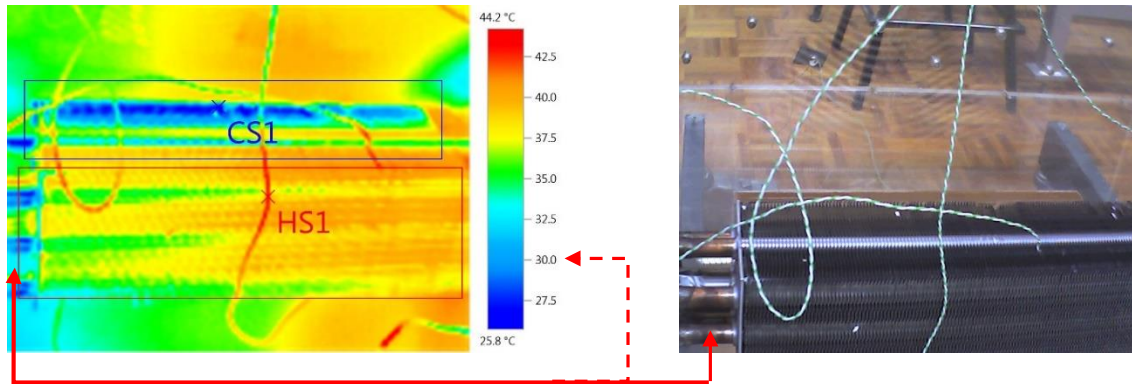


Figure 5.22: The temperature distributions recorded by Testo Imaging on the evaporator side of the heat-pipes heat-exchanger set-up.

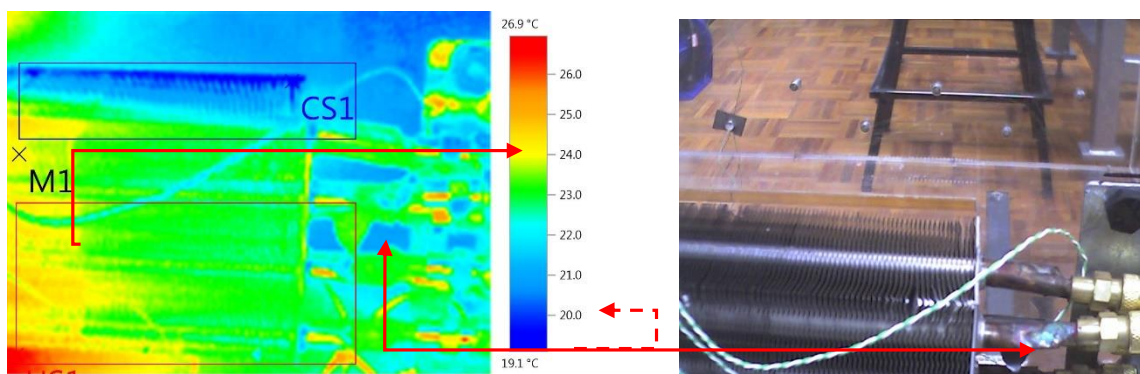


Figure 5.23: The temperature distributions recorded by Testo Imaging on the condenser side of the heat-pipes heat-exchanger set-up.

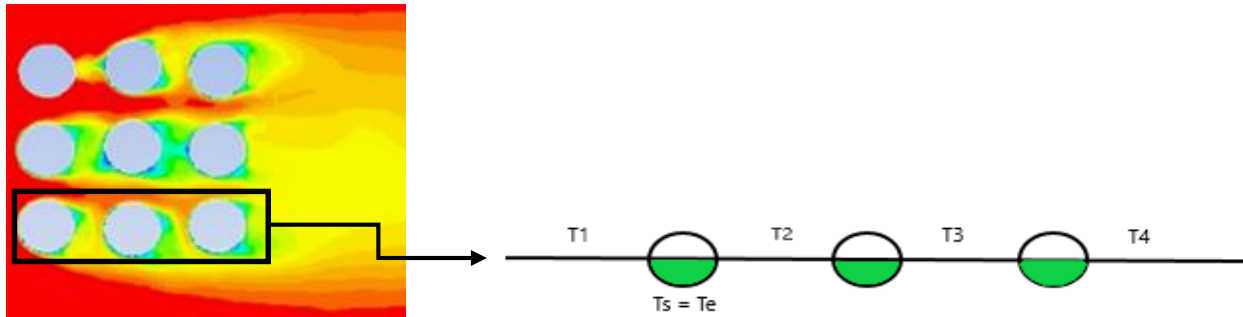
The amount of air passing through the heat-pipes heat-exchanger fins and tube at different temperatures ΔT can be calculated from the up and downstream air passing through the exchanger. The inlet air was recorded at 303 K (30°C), the outlet air at 293 K (20°C), and the temperatures of the copper tube where the refrigerant R134a flowed at the inlet and outlet were 297 K (24°C) and 293 K (20°C), respectively.

The energy calculated from the tube is based on the formula

$$\dot{Q} = \dot{m}C_p\Delta T$$

where,

$$\Delta T = \left(\left(\frac{T_1 + T_2}{2} \right) - T_e \right) - \left(\left(\frac{T_2 + T_3}{2} \right) - T_e \right) - \left(\left(\frac{T_3 + T_4}{2} \right) - T_e \right)$$



In the calculations, \dot{m} was taken as 1.18 kg/s (velocity of 1 m/s, the specific volume used was 0.845 m³/kg, the face area of heat-pipes was 0.0325 m², Cp was 1.213 J/kg.K for standard air, and the temperature difference was 4.18K. Figure 5.42 and Table 5.16 show the temperature profiles.

The heat transfer coefficient is written as

$$U_1 = \frac{\dot{Q}}{A \cdot \Delta T}$$

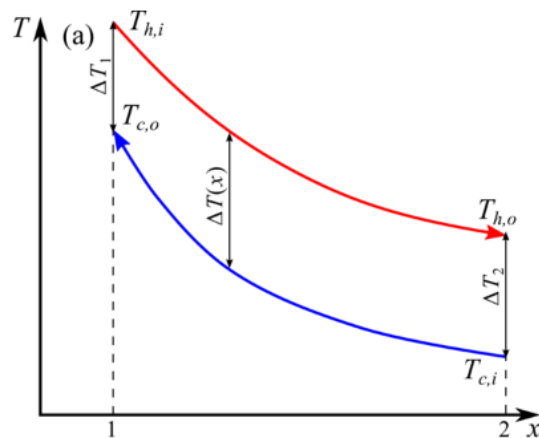


Figure 5.24: The temperature profile of the air-to-heat-pipes heat-exchanger.

Table 5.13: The specifications of the heat-pipes-heat-exchanger used.

Domains	Specifications
Cp air, kJ/kg.K	1.213
Diameter, ID mm	9
Length, mm finned	500
Heat transfer coef U ₁ , kW/m ² .K	0.171
Energy balance \dot{Q} , kW	0.195
ΔT , °C/K	4.18/277.18

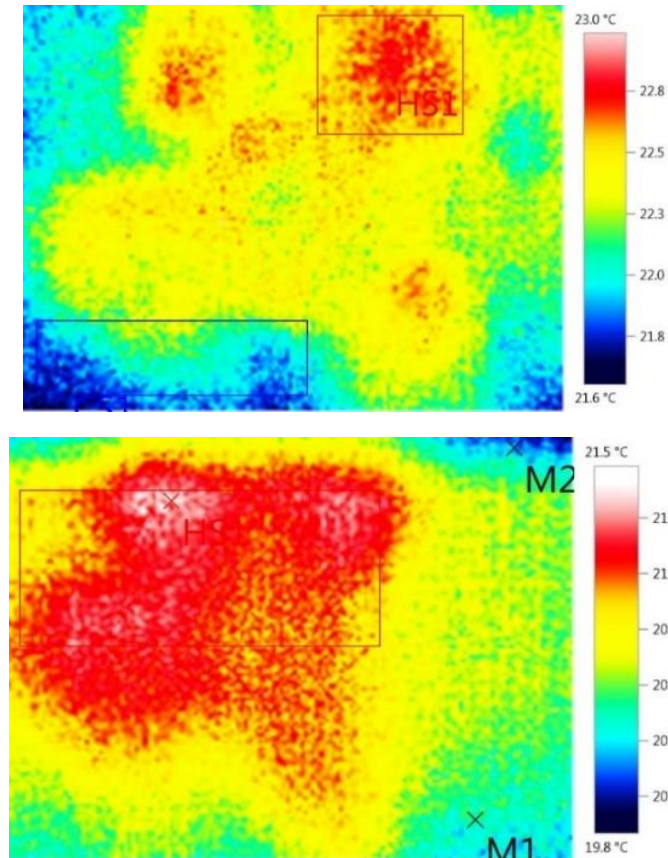


Figure 5.25: The temperature distribution inside the box captured by Testo Imaging.

5.4.1 Case 1: Supply and Exhaust Openings on the Sidewall

Figure 5.26 shows the path of the air blown from the supplied air (SA) to the heat-pipes evaporator side (1); the air then moved to the inlet of the test-box (3), was mixed with the box air temperature (5-9) and forced to the outlet (2) by the fan's pressure to the condenser side of the heat-pipes (10) and exited to the ambient outlet (4). The average temperature difference recorded was 8K to 10K. Figure 5.45 shows the average temperature inside the acrylic box when the supplied air of 303 K flowed past the heat-pipes heat-exchanger before entering the experimental box. The thermocouple inside the box recorded that the average temperature was about 293 K. This is a 10K difference that the heat-pipes could convert. Figure 5.46 shows the average temperature with the supplied air of 318 K. The average temperature inside the box was about 303 K. As the surface temperature of the condenser side of the heat-pipes heat-exchanger T_{cs} is considered as the conversion temperature between the average temperature of the box and the heat-pipes, the temperature difference shows the actual value that the heat-pipes can convert.

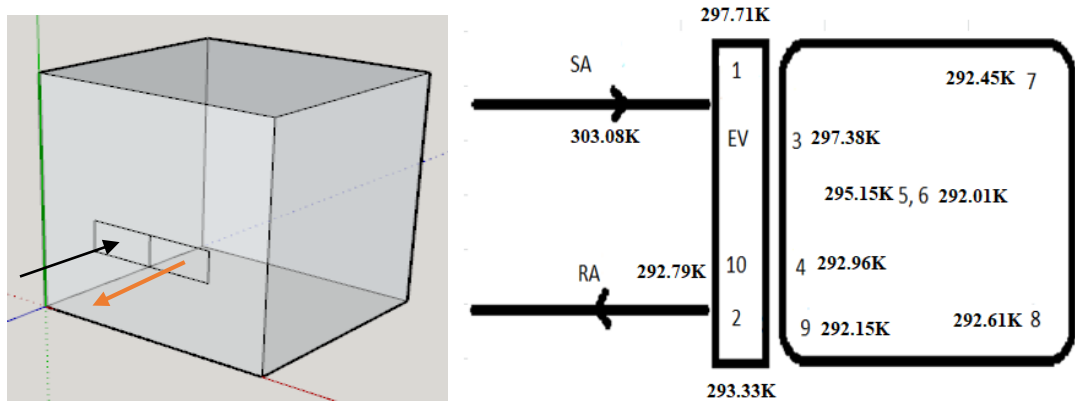


Figure 5.26 a.

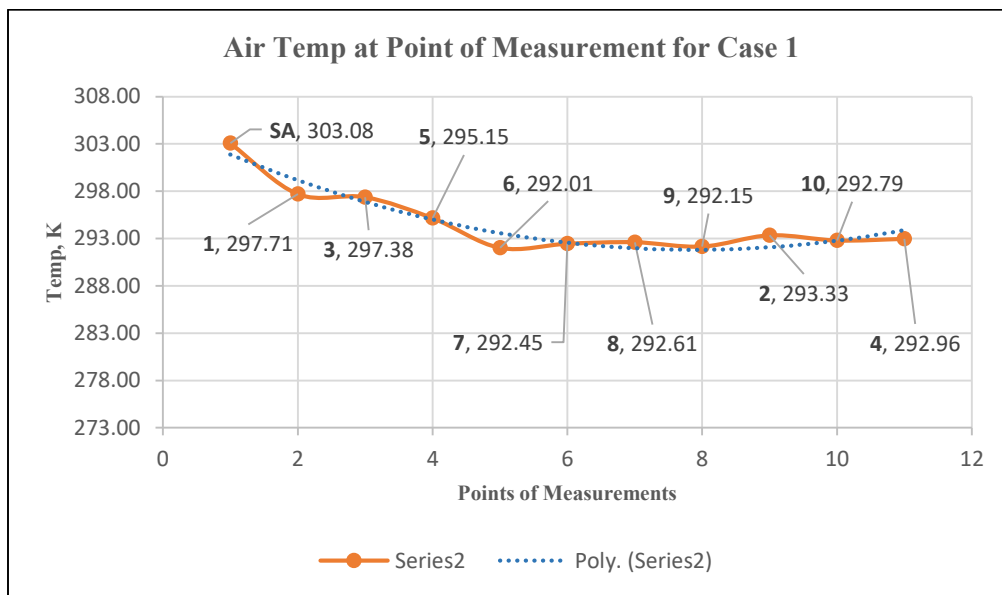


Figure 5.26 b.

Figure 5.26: Case 1a and b: The path of air temperature blown from the supplied air (SA) to the heat-pipes evaporator side (1) moves to the inlet of the test-box (3), mixes with the box air temperature (5-9), is forced to the outlet (2) and the condenser side of the heat-pipes (10), and then exits to the ambient outlet (4). The average temperature difference is 8K to 10K.

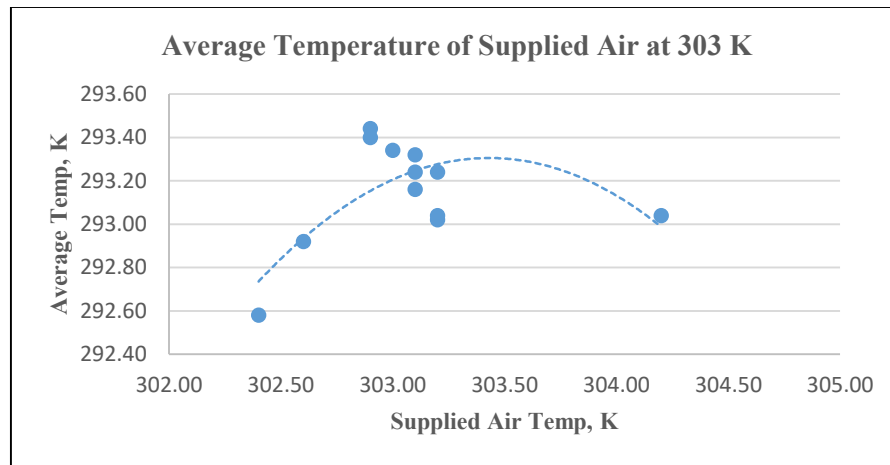


Figure 5.27: Case 1. The average temperature inside the box with supplied air of 303 K (30°C) is about 293 K (20°C).

In Figure 5.27 for Case 1-303 K which was at a lower supplied air temperature of < 303 K, the heat-pipes heat-exchanger could gradually convert the outside heat until the temperature reached its maximum point at about 293 K. A further increase of temperature to the outside supplied air will tend to decrease the heat-pipes' capability to convert heat.

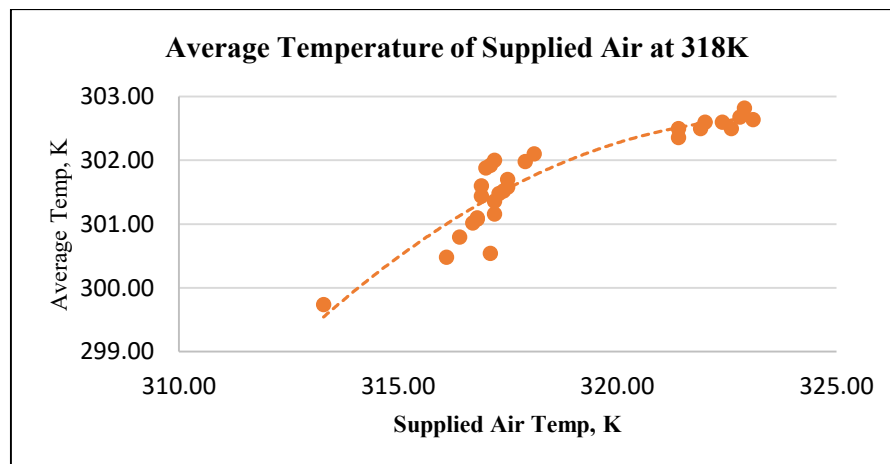


Figure 5.28: Case 1. The average temperature inside the box with supplied air of 318 K (45°C) is about 302 K (29°C).

For Case 1-318 K, the average temperature in the box was recorded at about 302 K. As can be observed in Figure 5.28 the polynomial prediction curve shows that if a higher supplied air temperature is applied to the heat-pipes, it will tend to maintain the average temperature of the box at 302-303 K.

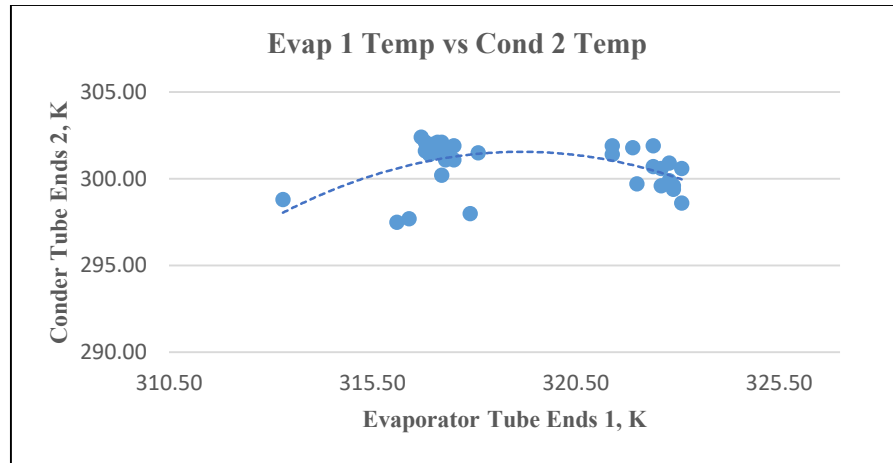


Figure 5.29: Case 1. The maximum temperature of the heat-pipes heat-exchanger at evaporator end 1 compared to the condenser end 2.

Figure 5.29 shows the comparison of temperature between the evaporator and condenser end for Case 1. With the geometry and the volume of the refrigerant cooling medium in the heat-pipes, the temperature difference was between 15K to 25K.

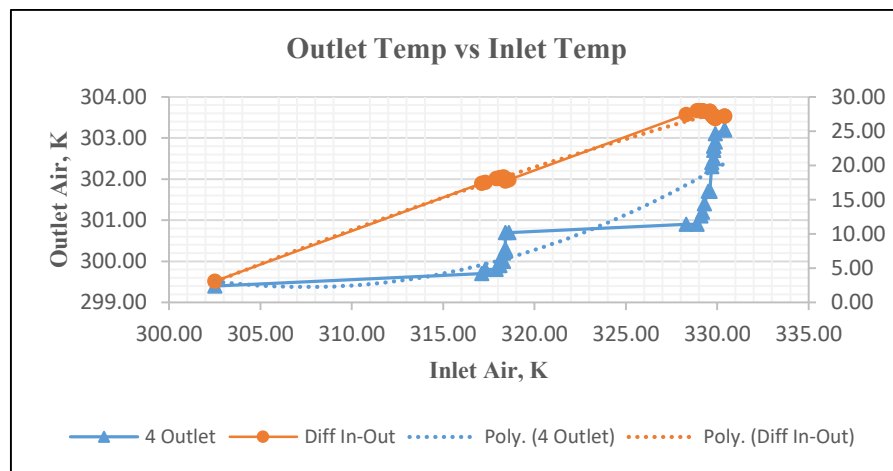


Figure 5.30: Case 1. The inlet air temperature at the box opening is compared to the outlet air. The comparison of the temperature at the evaporator and the condenser side of the heat-pipes. The high heat from the temperature of 303 K to 333 K (30°C to 60°C) is being transferred by the heat-pipes from the evaporator to the condenser. The air passing through the evaporator will be cooled down before entering the box and will travel within the box before being blown out to the outlet. The temperature difference between the evaporator and the condenser is about 27K.

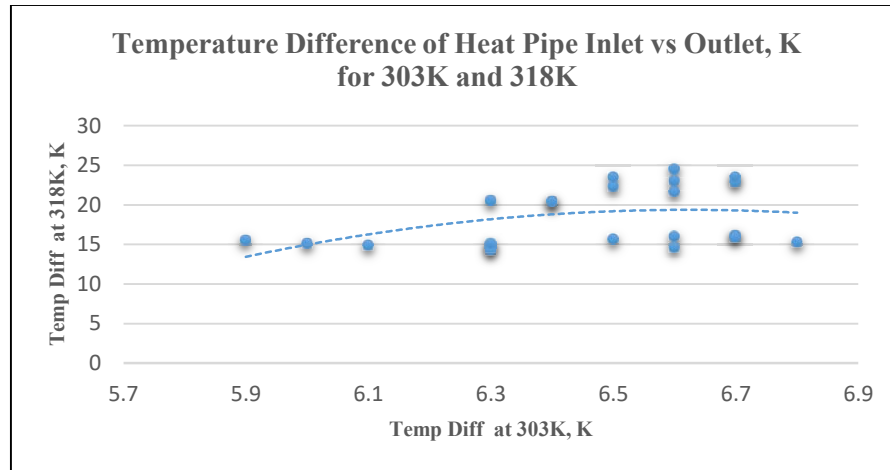


Figure 5.31: Case 1. Comparison of the temperature difference between the heat-pipes inlet and the pipe outlet for both 303 K and 318 K.

Figures 5.30 to 5.41 show that the heat-pipes heat-exchanger is capable of converting heat at a difference of about 6K to 27K. The cooling capacity of the solar air-conditioning system for the room which needs to be cooled will increase as the outside supplied air temperature is treated with the heat-pipes before entering the evaporator coils. Tables 5.17 and 5.18 show the temperature differences and the energy-saving for Case 1.

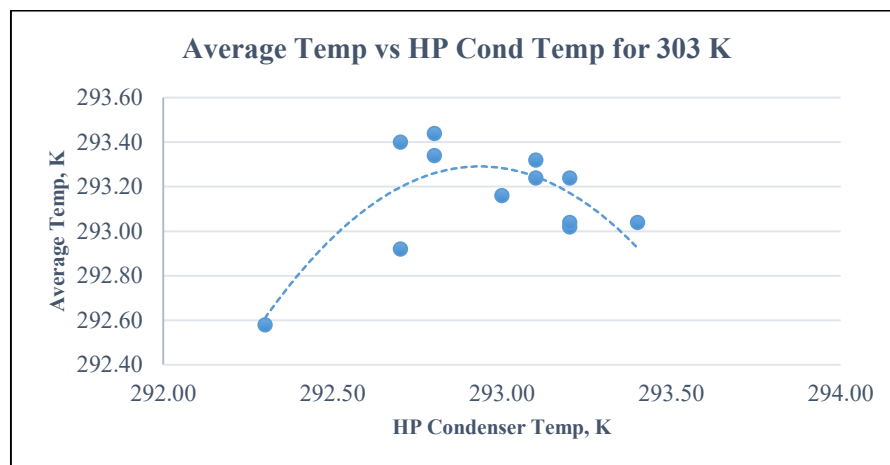


Figure 5.32: Case 1. The average temperature inside the box compared to the heat-pipes heat-exchanger's condenser section where the outlet air flows. The supplied air is 303 K.

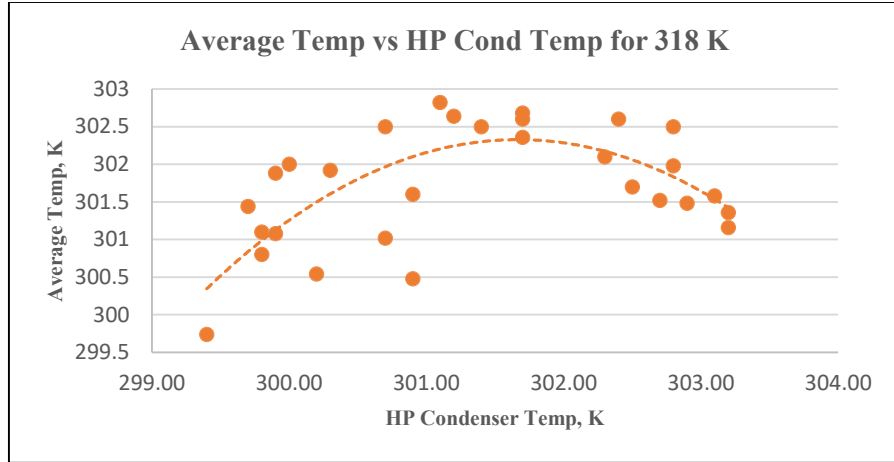


Figure 5.33: Case 1. The average temperature inside the box compared to the heat-pipes heat-exchanger's condenser section where the outlet air flows. The supplied air is 318 K.

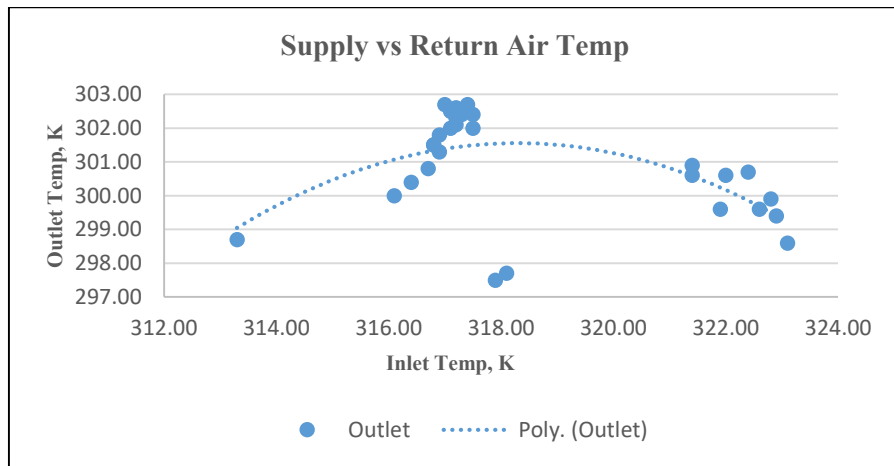


Figure 5.34: Comparison of the supply air inlet and the return air outlet of the acrylic box. The high heat from the temperature of 303K to 333K (30°C to 50°C) is being cooled by the heat-pipes heat-exchanger at the inlet's supplied-air opening of the acrylic box. The cooled air travels within the box and is blown out to the outlet. The temperature difference between the inlet and the outlet is about 27 K. Any increase or additional heat to the heat-pipes will not increase the reduction capability of the installation.

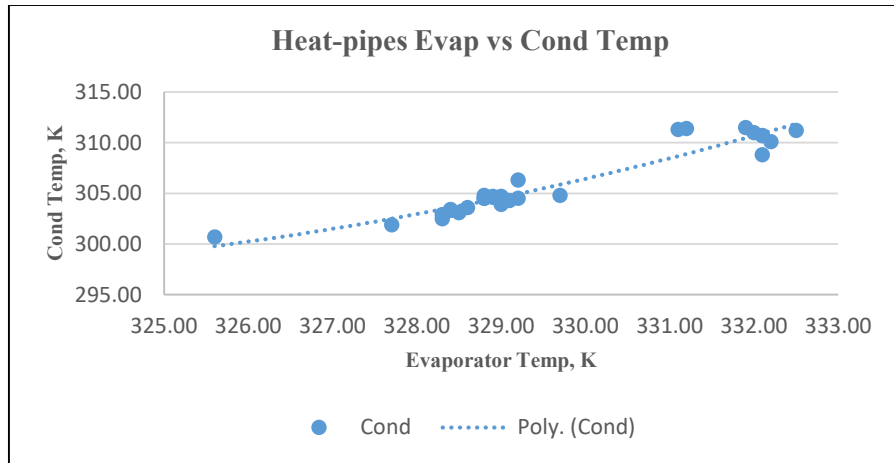


Figure 5.35: Comparison of the temperature at the evaporator and the condenser side of the heat-pipes. The high heat from the temperature of 303K to 333K (30°C to 60°C) is being transferred by the heat-pipes from the evaporator to the condenser. The air passing through the evaporator will be cooled down before entering the box and will travel within the box before being blown out to the outlet. The temperature difference from the evaporator to the condenser is about 27 K.

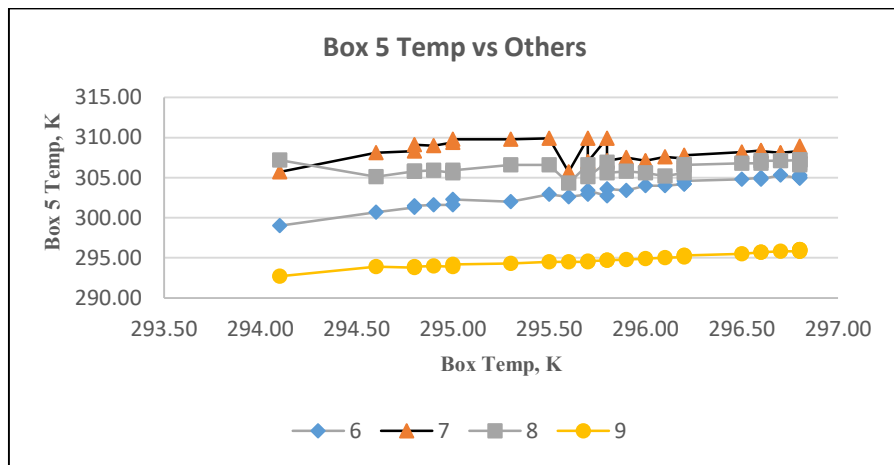


Figure 5.36: The graph shows the temperature recorded inside the acrylic test box 5 & 6 where the thermocouple is placed in the middle-lower and upper level, 7 on the left, 8 on the right side, and 9 at the air return side near the exit of the box. Thermocouple 9 shows the lowest temperature (294K) before the air is being blown away to the exit opening.

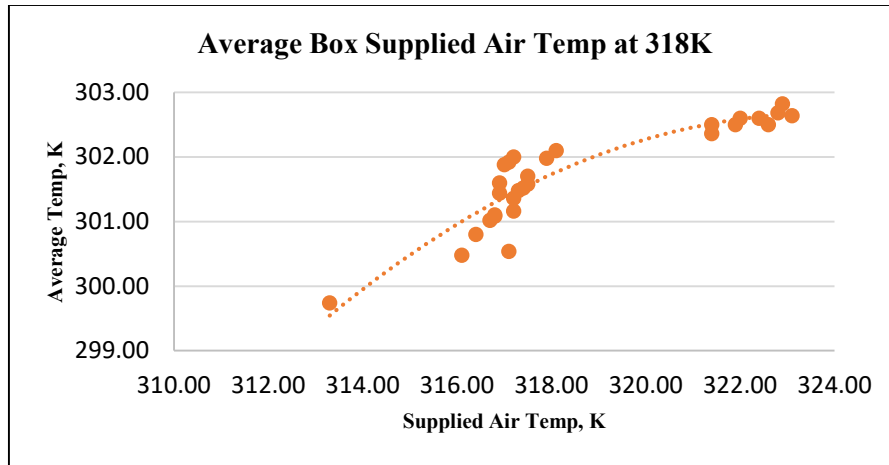


Figure 5.39: The average temperature when the air temperature of 318K is supplied to the heat-pipes and the acrylic box. At 318K, the average temperature reduced is about 302K, a differential of 16 K. This is compared to the difference between the average temperature and the temperature of the condenser section of the heat pipe at 311K, which is 7 K. The rate of energy-saving is calculated to be at 14% of the installation.

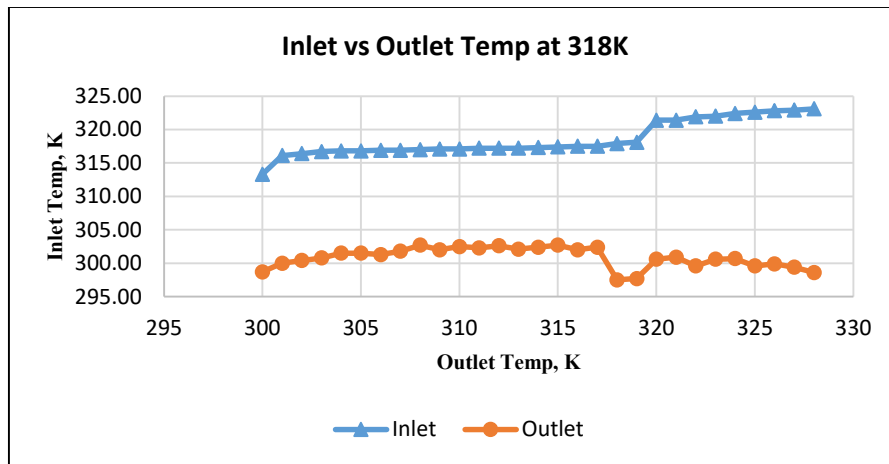


Fig 5.40: Case 1: Comparison of air temperature at supply and exit.

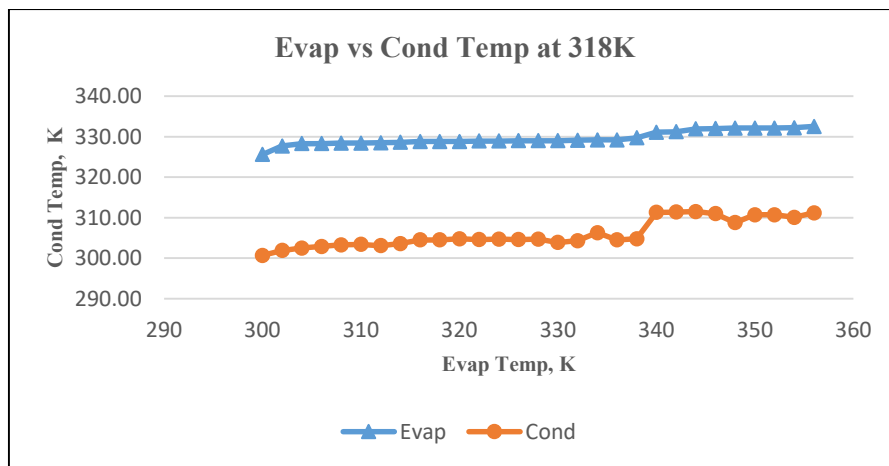


Fig 5.41: Case 1: Comparison of air temperature at the evaporator and condenser side.

Table 5.14: Comparison of temperature difference K in Case 1.

Parameters	Case 1	
	303K	318K
Supplied Air Temp, K	303	318
Heat-pipes Evaporator Section Temp K	301	332
Heat-pipes Condenser Section Temp K	295	311
Average Box Temp K	293	302
Differential Temp of Heat-pipes Evaporator and Condenser Section, K	6	21
The differential of Supplied Air Temp and Heat-pipes Condenser Section Temp, K	8	7

Table 5.15: Rate of energy-saving for Case 1.

Parameters	Case 1		Case 2		Case 3	
	303K	318K	303K	318K	303K	318K
Differential Temp of Supplied Air and HP Condenser Section, K (S_A-HP_C)	8	7	7	8	9	7
Q_o, Estimated sensible cooling load, kW	0.373	0.327	0.327	0.373	0.420	0.327
Energy-saving $Q_o'-Q_o$, kW	0.93	0.47	0.47	0.93	0.140	0.47
The rate of energy-saving $(Q_o'-Q_o/Q_o') \propto, \% \times 100$	0.25	0.14	0.17	0.33	0.33	0.14

5.4.2 Case 2: Supply and Exhaust Opening at the Top

Figure 5.42 shows the path of the air blown from the topside supplied air (SA) to the heat-pipes evaporator side (1). The air moved to the inlet of the test-box (3), was mixed with the box air temperature (5-9) and forced to the outlet (2) by the fan's pressure and the less dense air to the condenser side of the heat-pipes (10) and then exited to the ambient outlet (4). The average temperature difference recorded was 8K. Figures 5.60 and 5.61 show the average temperature inside the box when the air supplied at 303 K passed through the heat-pipes heat-exchanger before entering the experimental box. The locations of the entering and exiting air were from the top of the box. The thermocouple inside the box recorded that the average temperature was about 294 K (21°C). This indicates an 8K difference that the heat-pipes could convert. Figures 5.62 to 5.73 show the average temperature with supplied air of 318 K, while the average temperature was about 303 K. Tables 5.19 and 5.20 present the temperature comparisons and the energy-saving for Case 2.

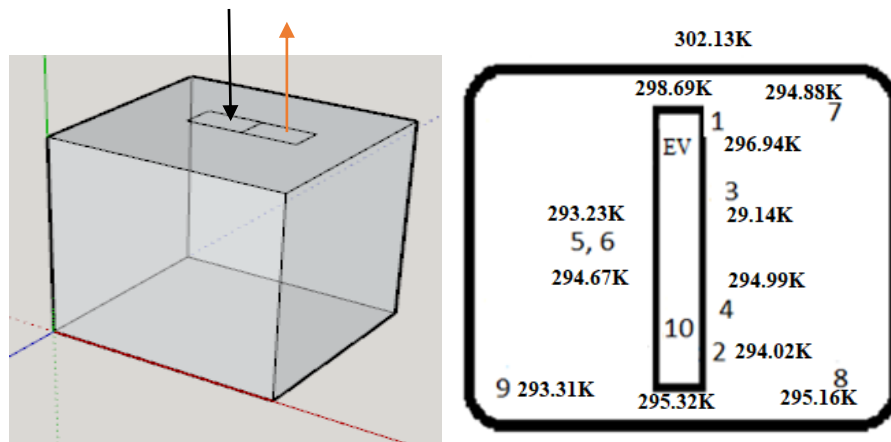


Figure 5.42 a

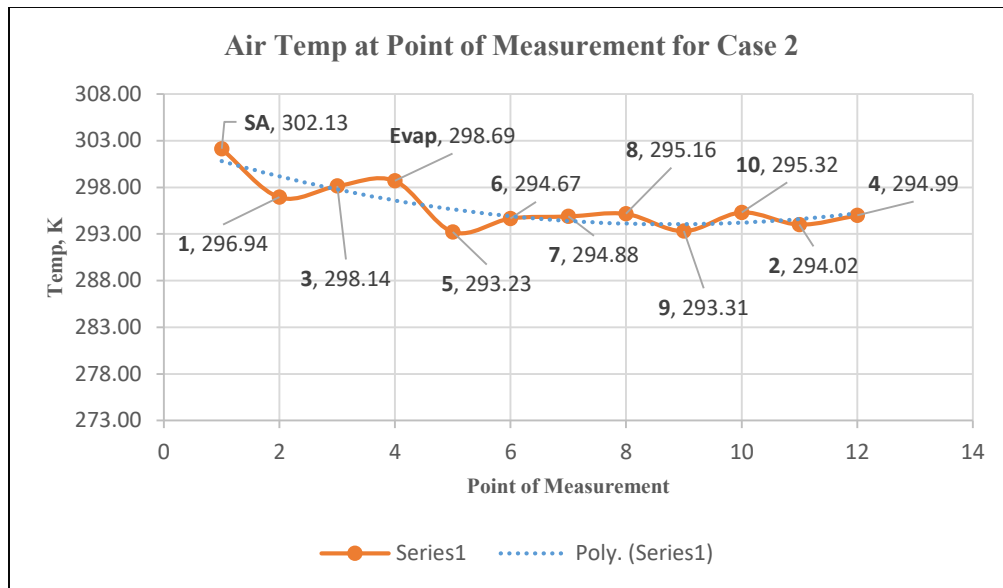


Figure 5.42 b.

Figure 5.42: Case 2a and b: The path of air temperature that is blown from the supplied air (SA) to the heat-pipes evaporator side (1) moves to the inlet of the test-box (3), mixes with the box air temperature (5-9), is forced to the outlet (2) and the condenser side of the heat-pipes (10), and then exits to the ambient outlet (4). The average temperature difference is 8K.

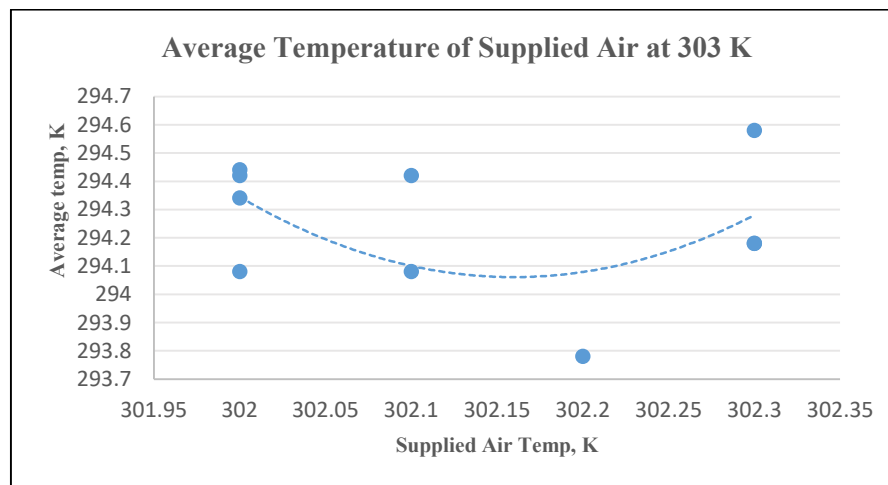


Figure 5.43: Case 2. The average temperature inside the box with supplied air of 303 K (30°C) is about 294 K (21°C).

Figure 5.43 shows that the average temperature in the box was about 294 K. The opening of the supplied and return air was side-by-side at the top of the box. As the low-density air would try to exit at the opening at the top of the box, the low-temperature air was 'short circuited' to the return air opening. Thus, the higher the supplied air intake into the room, the less heat the heat-pipes could convert as some of the lower temperature air exited as soon as it entered the box.

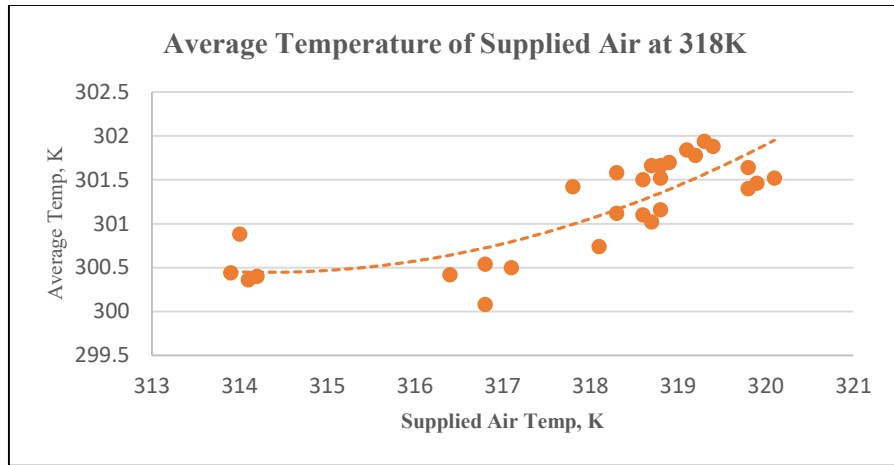


Figure 5.44: Case 2. The average temperature inside the box with supplied air of 318 K (45°C) is about 301 K (28°C).

For Case 2-318 K, the average temperature in the box was recorded at about 301 K. The polynomial prediction curve in Figure 5.44 shows that a higher supplied air temperature was applied to the heat-pipes, with an average box temperature of 302 K.

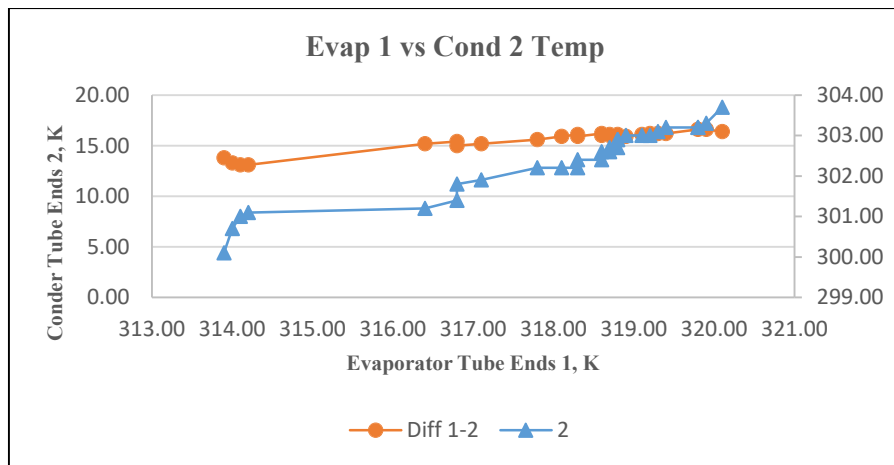


Figure 5.45: Case 2. The temperature of the heat-pipes heat-exchanger at the evaporator ends 1 compared to the condenser ends 2.

Figures 5.45 to 5.55 show the comparison of temperature between the evaporator and condenser end for Case 2. With the geometry and the volume of the refrigerant cooling medium in the heat-pipes, the temperature difference was between 13K to 16K.

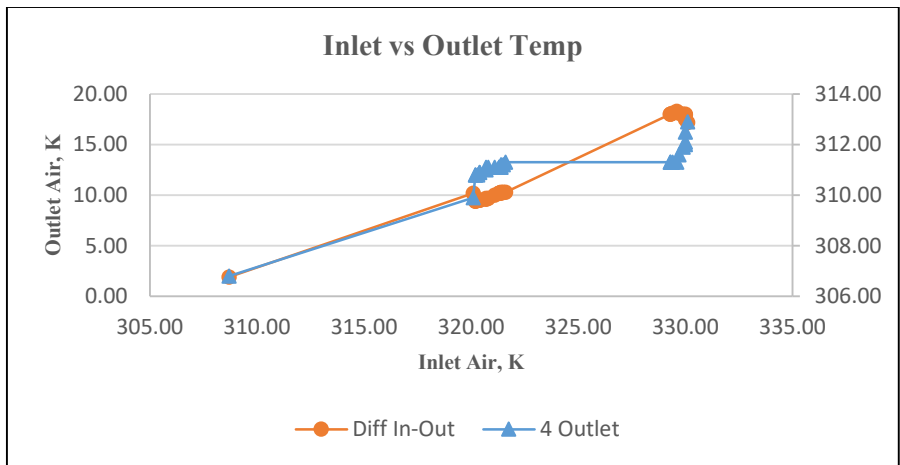


Figure 5.46: Case 2. The inlet air temperature at the box opening is compared to the outlet air.

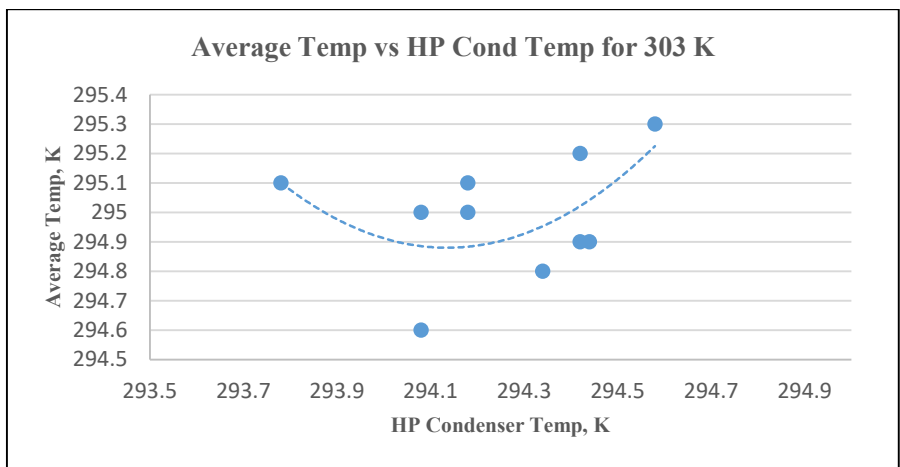


Figure 5.47: Case 2. The average temperature inside the box compared to the heat-pipes heat-exchanger’s condenser section where the outlet air flows. The supplied air is 303 K.

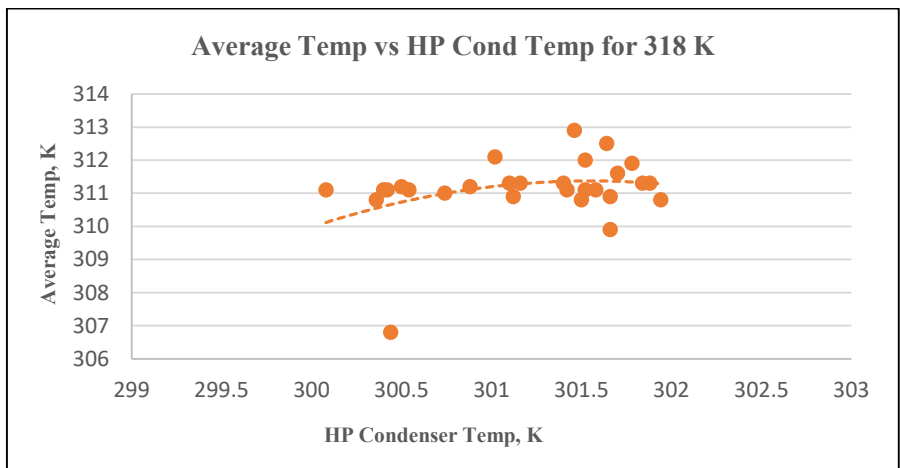


Figure 5.48: Case 2. The average temperature inside the box compared to the heat-pipes heat-exchanger’s condenser section where the outlet air flows. The supplied air is 318 K.

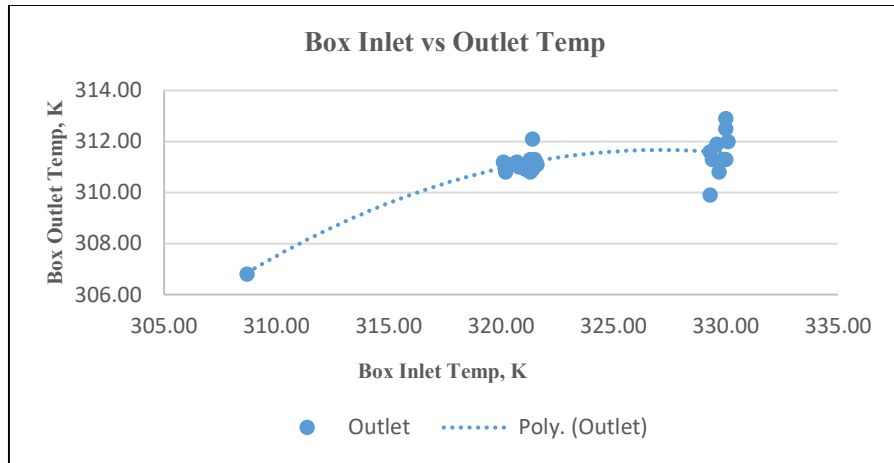


Figure 5.51: Comparison of the temperature at the acrylic box inlet 3 and the box outlet 4. The inlet temperature is 325K (52°C) compared to 301K (28°C) at the outlet. In lowering the box temperature, about 13 K of heat is reduced by the heat-pipes transfer process. The hypothesis is that the bigger the heat-pipes or the more refrigerant inside the heat-pipes, the bigger the temperature difference that could be achieved.

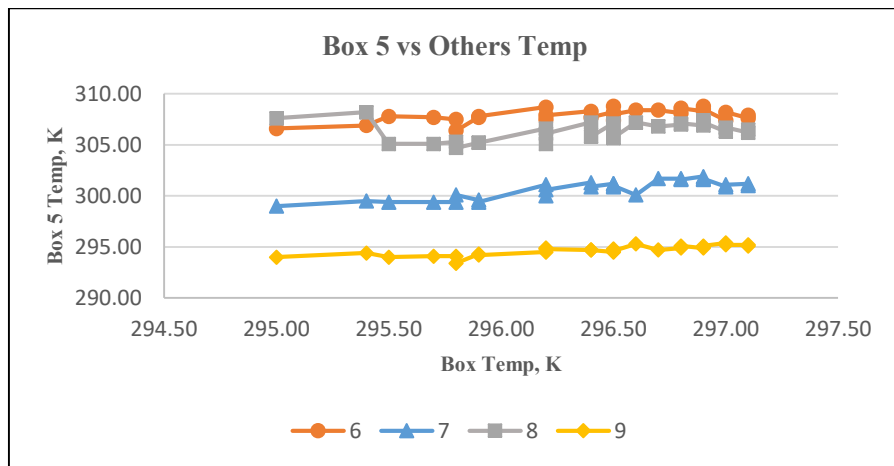


Figure 5.52: The graph shows the temperature recorded inside the acrylic test box 5 & 6 where the thermocouple is placed in the middle-lower and upper level, 7 on the left, 8 on the right side, and 9 at the air return side near the exit of the box. Thermocouple 9 shows the lowest temperature (294K) before the air is being blown away to the exit opening.

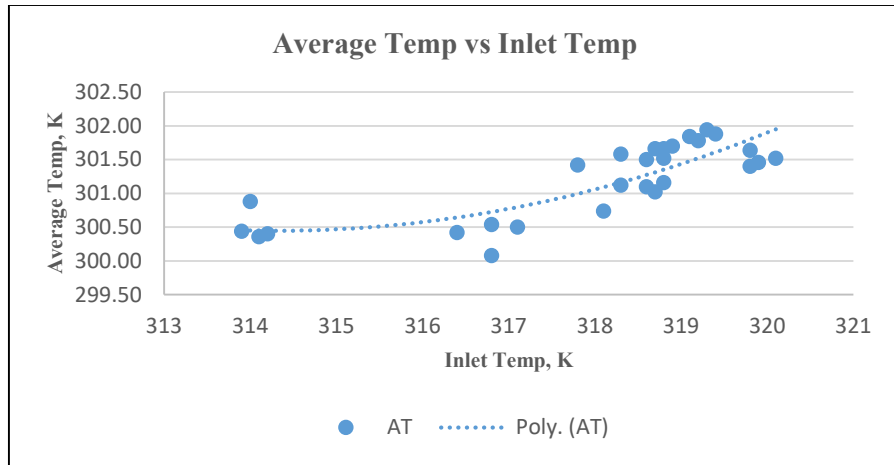


Figure 5.53: The graph shows the average temperature recorded inside the acrylic test box. The average box temperature is about 301K (28°C), agreeing with the return air temperature.

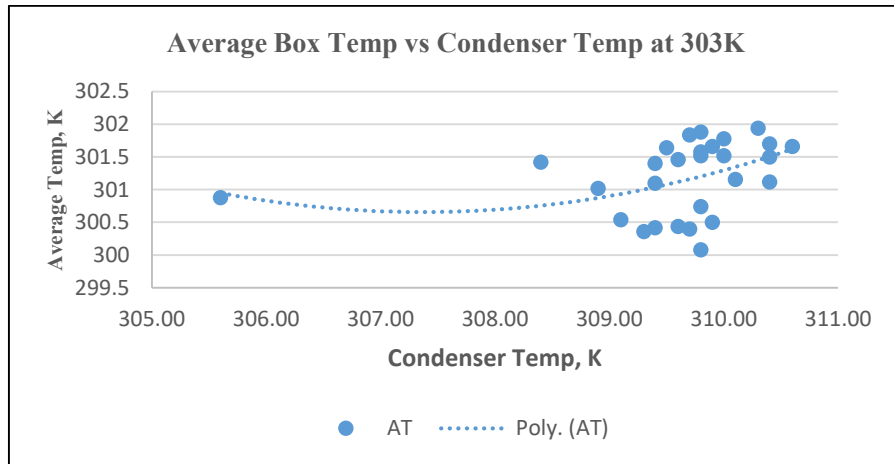


Figure 5.54: When the average temperature of 303K is supplied to the heat-pipes and the acrylic box, the average temperature is reduced to about 296K, a differential of 7 K. This is compared to the difference between the average temperature and the temperature of the condenser section of the heat pipes at 310K, which is 8 K. For the energy-saving calculation, the differential temperature of the average box temperature and the condenser section of the heat pipe (7 K) is used as the minimum value. The rate of energy-saving is calculated to be at 17% of the installation.

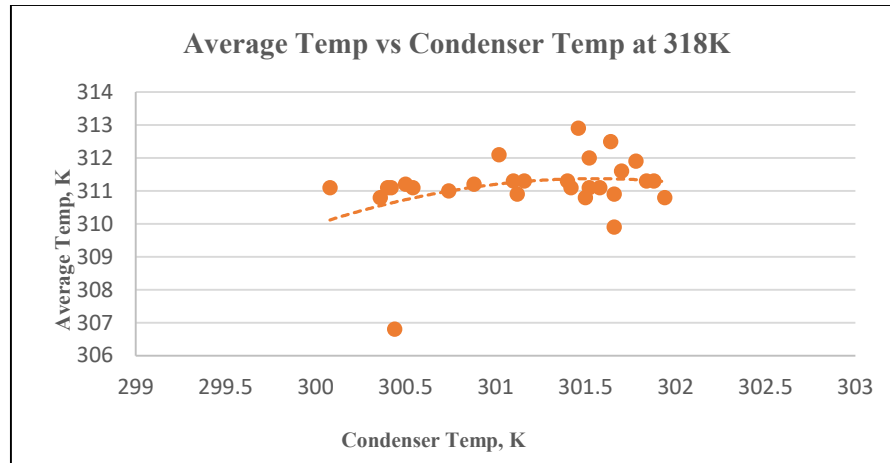


Figure 5.55: The average temperature when the air temperature of 318K is supplied to the heat-pipes and the acrylic box. At 318K, the average temperature reduced is about 310K, a differential of 8 K. This is compared to the difference between the average temperature and the temperature of the condenser section of the heat pipe at 310K, which is 8 K. The rate of energy-saving is calculated to be at 33% of the installation. Even though the energy-saving is higher than Case 1, the temperature of the supplied air at 318K at the time will be reduced and the savings returned to 17%.

Table 5.16: Comparison of the temperature difference, K in Case 2. The supplied air is from the top of the box.

Parameters	Case 2	
Supplied Air Temp, K	303	318
Heat-pipes Evaporator Section Temp, K	299	331
Heat-pipes Condenser Section Temp, K	296	310
Average Box Temp, K	294	301
Differential Temp of Heat-pipes Evaporator and Condenser Section, K	3	21
A differential of Supplied Air Temp and Heat-pipes Condenser Section Temp, K	7	8

Table 5.17: Rate of energy-saving for Case 2

Parameters	Case 1		Case 2		Case 3	
	303K	318K	303K	318K	303K	318K
Differential Temp of Supplied Air and HP Condenser Section, K (SA-HPc)	8	7	7	8	9	7
Q_o , Estimated sensible cooling load, kW	0.373	0.327	0.327	0.373	0.420	0.327
Energy-saving $Q_o' - Q_o$, kW	0.93	0.47	0.47	0.93	0.140	0.47
The rate of energy-saving $(Q_o' - Q_o / Q_o') \propto, \% \times 100$	0.25	0.14	0.17	0.33	0.33	0.14

5.4.3 Case 3: Supply Opening at the Top and Exhaust on the Sidewall

Figure 5.56 shows the path of air temperature that was blown from the top of the supplied air (SA) to the heat-pipes evaporator side (1) which then moved to the inlet of the test-box (3), was mixed with the box air temperature (5-9) and forced to the outlet (2) and the condenser side of the heat-pipes (10), and then exited to the ambient outlet (4). The average temperature difference was 7K. Figure 5.75 shows the average temperature inside the box when the air supplied at 303K flowed through the heat-pipes heat-exchanger before entering the experimental box. The location of the entering air opening was at the top of the box; however, the exiting air opening was on the sidewall of the box. The condenser section of the heat-pipes was left to be cooled by the ambient temperature. The thermocouple inside the box recorded that the average temperature was about 295 K (22°C). This is an 8 K difference in terms of the heat that the heat-pipes could convert. Figure 5.76 shows the average temperature with supplied air of 318 K. The average temperature was about 303 K. Table 5.16 shows that the temperature of the evaporator section was at 333 K (60°C), which is somewhat higher than Case 2. This is because the condenser section of the heat-pipes could not convert the heat fast enough to the surrounding ambient as it is left to be cooled only by the ambient temperature without any velocity flow passing through the fins.

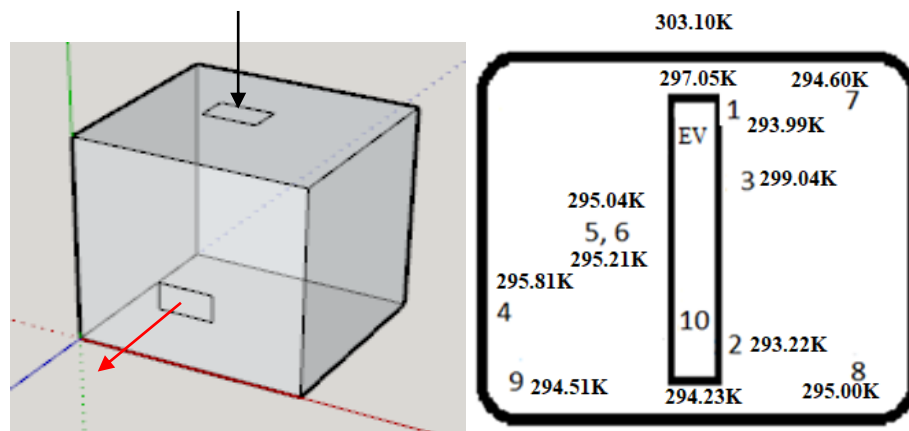


Figure 5.56 a

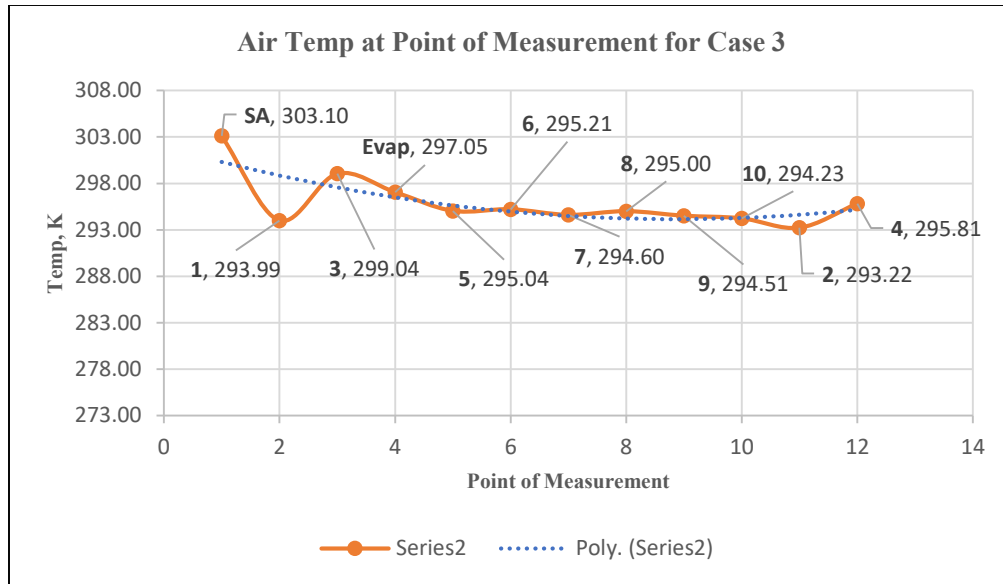


Figure 5.56 b.

Figure 5.56 Case 3. a and b: The path of air temperature blown from the top of the supplied air (SA) to the heat-pipes evaporator side (1) moves to the inlet of the test-box (3), mixes with the box air temperature (5-9), is forced to the outlet (2) and the condenser side of the heat-pipes (10), and exits to the ambient outlet (4). The average temperature difference is 7K.

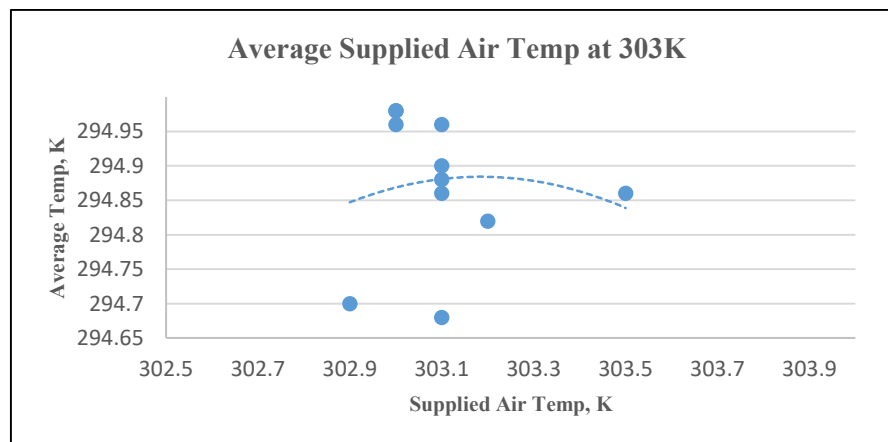


Figure 5.57: Case 3. The average temperature inside the box with supplied air of 303 K (30°C) is about 294 K (21°C).

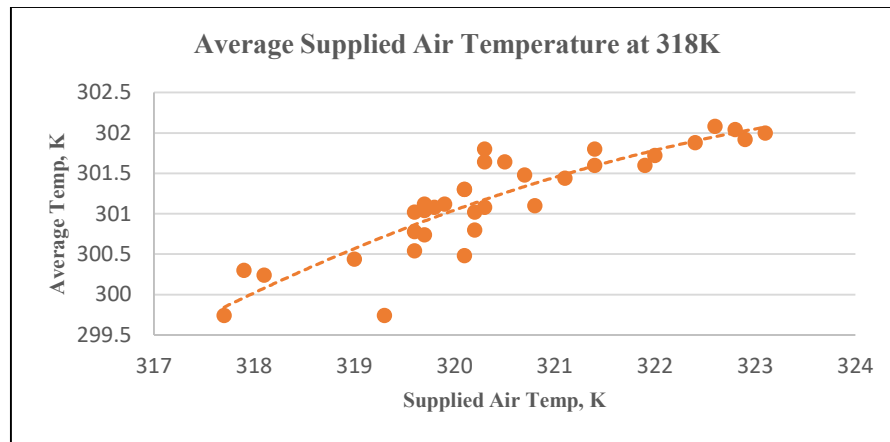


Figure 5.58: Case 3. The average temperature inside the box with supplied air of 318 K (45°C) is about 301 K (28°C).

Figures 5.57 and 5.58 show that the average temperature in the box is about 294 K and 301 K respectively. The opening of the supply air is at the top and returns at the side of the box. A further increase of temperature to the outside supply air will tend to decrease the heat-pipes' capability to convert heat.

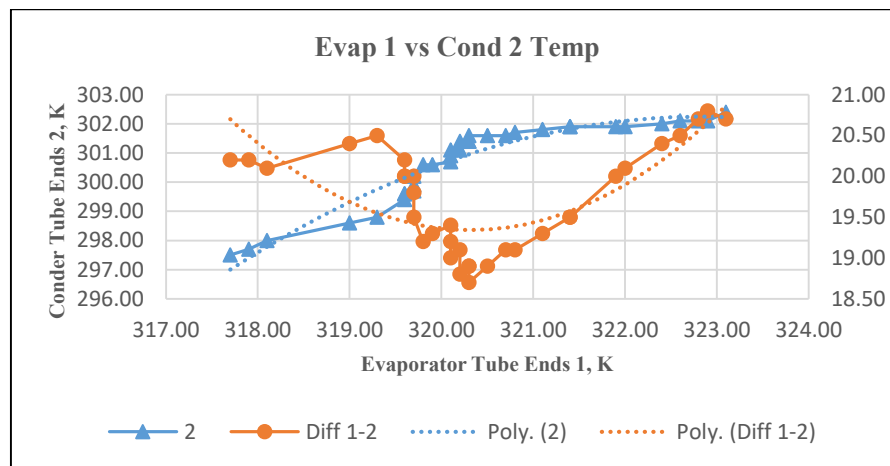


Figure 5.59: Case 3. The temperature of the heat-pipes heat-exchanger at the evaporator ends 1 compared to the condenser ends 2.

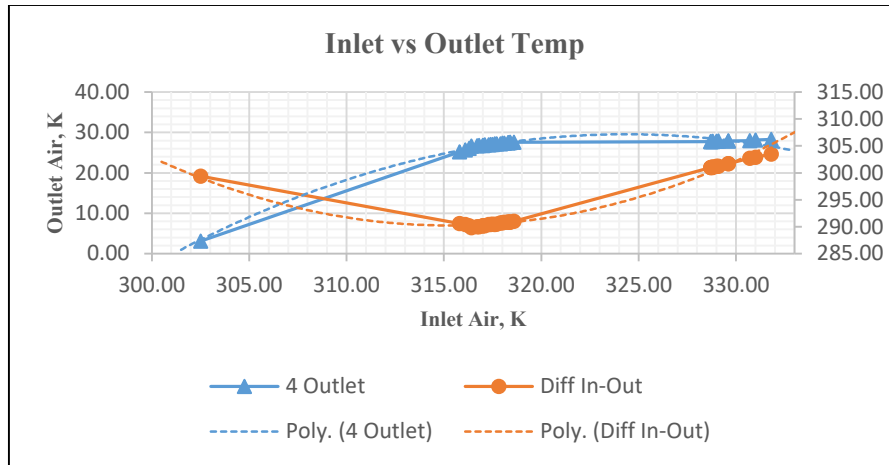


Figure 5.60: Case 3. The inlet air temperature at the box opening is compared to the outlet air.

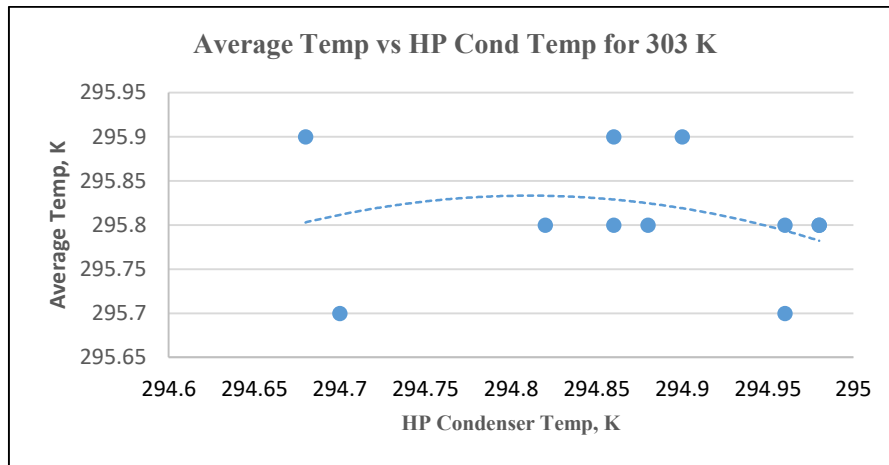


Figure 5.61: Case 3. The average temperature inside the box compared to the heat-pipes heat-exchanger's condenser section where the outlet air flows. The supplied air is 303 K.

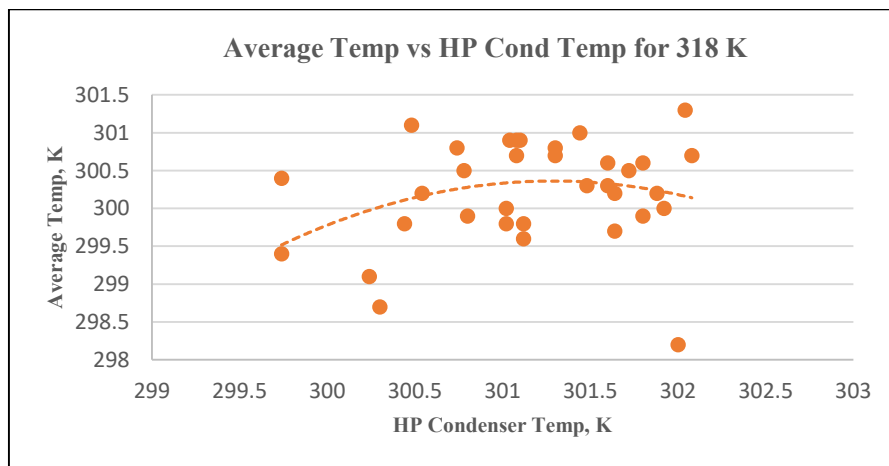


Figure 5.62: Case 3. The average temperature inside the box compared to the heat-pipes heat-exchanger's condenser section where the outlet air flows. The supplied air is 318 K.

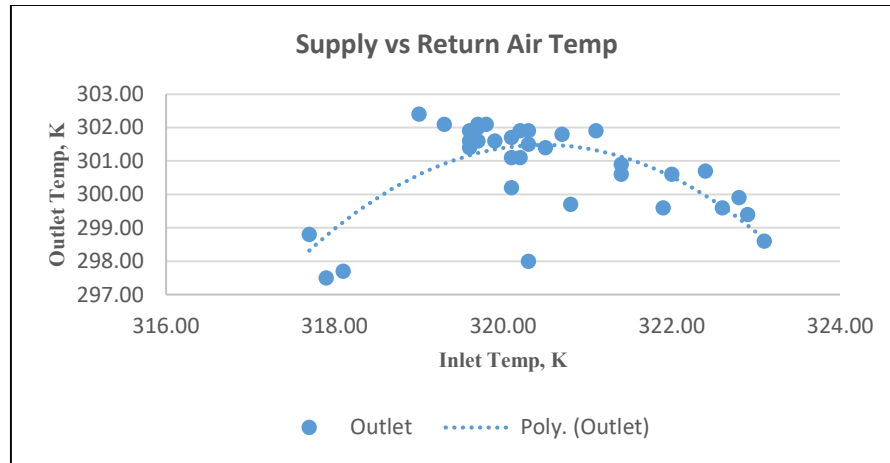


Figure 5.63: Comparison of the temperature of the supplied air inlet and the return air outlet of the acrylic box. The high heat from the temperature of 303K to 333K (30°C to 50°C) is being cooled by the heat-pipes at the inlet supplied-air opening of the acrylic box. The cooled air travels within the box and is blown out to the outlet. The temperature difference between the inlet and the outlet is about 20 K. Any increase or additional heat to the heat-pipes will not increase the temperature reduction capability of the installation.

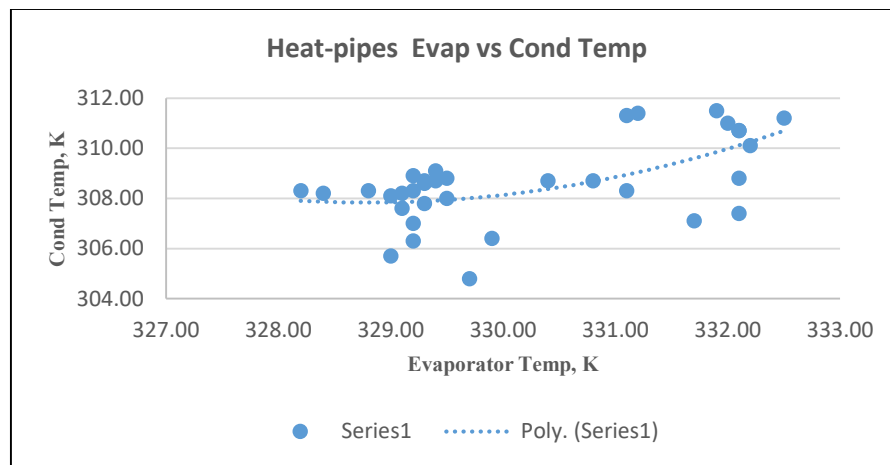


Figure 5.64: Comparison of the temperature at the evaporator and the condenser section of the heat-pipes. The high heat from the temperature of 303K to 333K (30°C to 60°C) is being transferred by the heat-pipes from the evaporator to the condenser. The air passing through the evaporator will be cooled down before entering the box and will travel within the box before being blown out to the outlet. The temperature difference from the evaporator to the condenser is about 22 K.

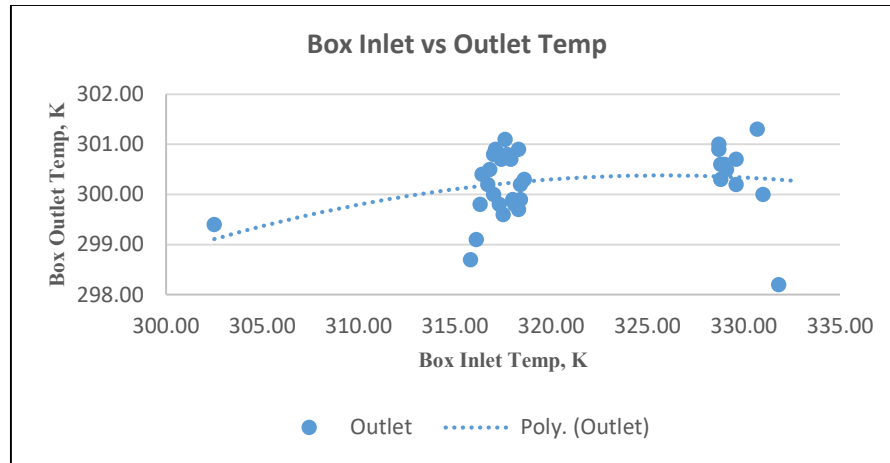


Figure 5.65: Comparison of the temperature at the acrylic box inlet and outlet. The average inlet temperature is about 321K compared to 300K (48°C to 27°C) at the outlet. About 21 K of heat is reduced by the heat-pipes transfer process in lowering the temperature of the box. The hypothesis is that the bigger the heat-pipes or the more refrigerant inside the heat-pipes, the bigger the temperature difference that could be achieved.

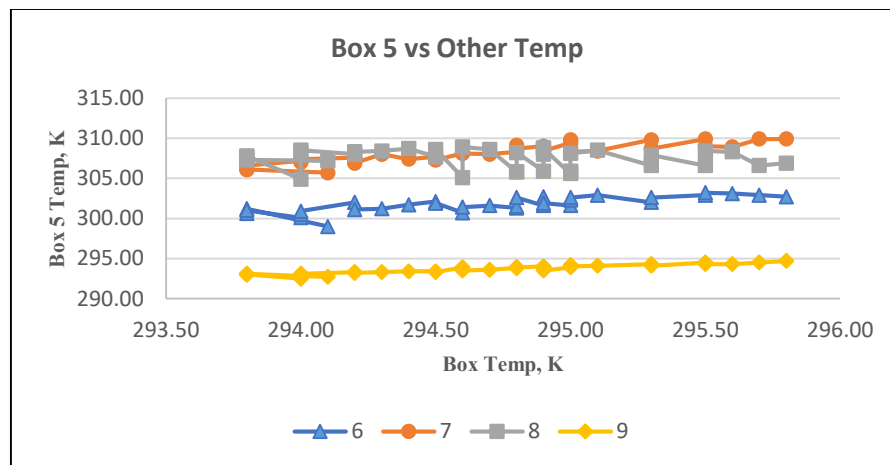


Figure 5.66: The graph shows the temperature recorded inside the acrylic test boxes 5 & 6 where the thermocouple is placed in the middle-lower and upper level, 7 on the left, 8 on the right side, and 9 at the air return side near the exit of the box. Thermocouple 9 shows the lowest temperature (294K) before the air is being blown away to the exit opening.

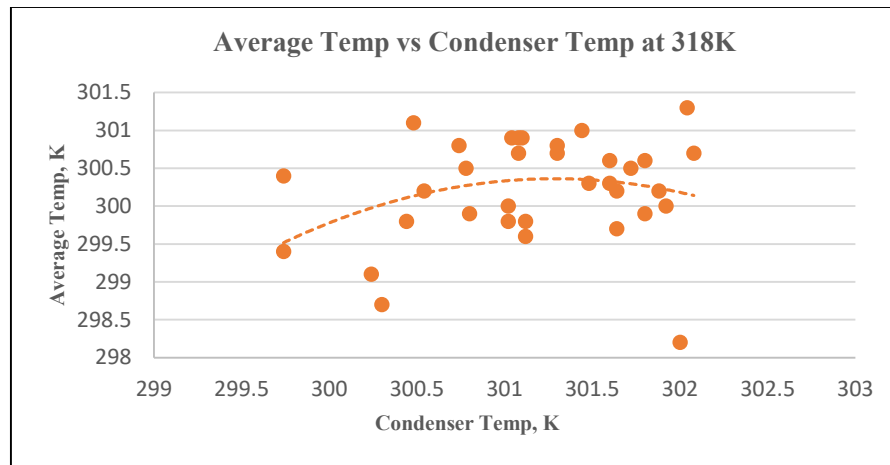


Figure 5.69: The average temperature when the air temperature of 318K is supplied to the heat-pipes and the acrylic box. At 318K, the average temperature reduced is about 302K, a differential of 16 K. This is compared to the difference between the average temperature and the temperature of the condenser section of the heat pipe at 311K, which is 7 K. The rate of energy-saving is calculated to be at 14% of the installation.

Table 5.18: The table shows the comparison of temperature difference K in Case 3. The supplied air is from the top of the box and the exit opening is on the sidewall of the box.

Parameters	Case 3	
Supplied Air Temp, K	303	318
Heat-pipes Evaporator Section Temp, K	297	333
Heat-pipes Condenser Section Temp, K	294	311
Average Box Temp, K	294	301
Differential Temp of Heat-pipes Evaporator and Condenser Section, K	3	22
A differential of Supplied Air Temp and Heat-pipes Condenser Section Temp, K	9	7

Table 5.19: Rate of energy-saving for Case 3

Parameters	Case 1		Case 2		Case 3	
	303K	318K	303K	318K	303K	318K
Differential Temp of Supplied Air and HP Condenser Section, K (S_A-HP_C)	8	7	7	8	9	7
Q_o , Estimated sensible cooling load, kW	0.373	0.327	0.327	0.373	0.420	0.327
Energy-saving $Q_o'-Q_o$, kW	0.93	0.47	0.47	0.93	0.140	0.47
The rate of energy-saving $(Q_o'-Q_o/Q_o') \times 100$	0.25	0.14	0.17	0.33	0.33	0.14

Figures 5.70 and 71 show the comparisons of differential temperature between the inlet and the box temperature. The heat-pipes were found to be capable of converting between 6K to 9K of temperature difference, and at an air temperature of 318 K, the heat-pipes could convert between 15K to 17K. Table 5.20 shows the temperature differences for all cases. It shows that the heat-pipes worked better with higher ambient supplied air temperature compared to when the air temperature was lower. The evaporation and condensation of the refrigerant medium by the heat-pipes worked well at higher temperatures.

Table 5.20: Comparison of the temperature difference across the heat-pipes inlet and outlet for supplied air of between 303 K and 318 K. The higher temperature of the supplied air shows a bigger differential temperature of the heat-pipes in relation to its capability to transfer heat from the evaporator section to the condenser section.

Parameters	Temperature Difference of Supplied Air and Heat-pipes Condenser Section, K	
	303	318
Supplied Air Temp, K		
Case 1	8	7
Case 2	7	8
Case 3	9	7

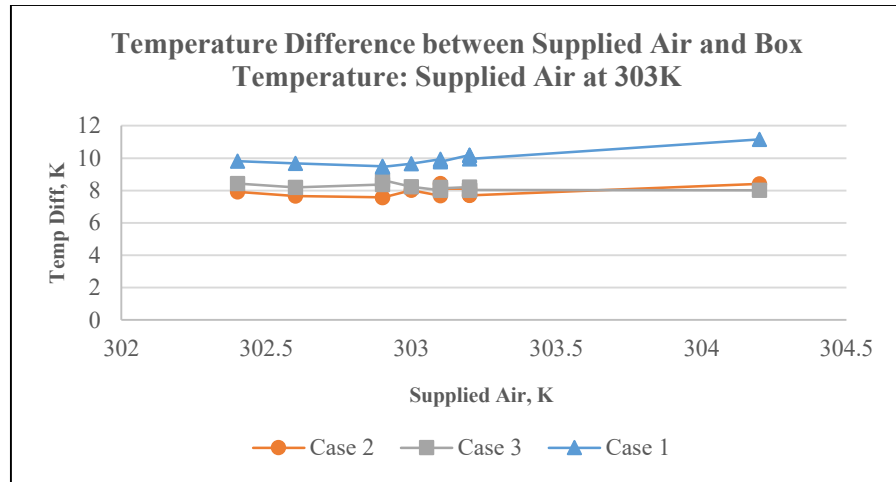


Figure 5.70: Comparison of the temperature difference between supplied-air inlet temperature at 303K (30°C) and the average temperature of the box for all the cases.

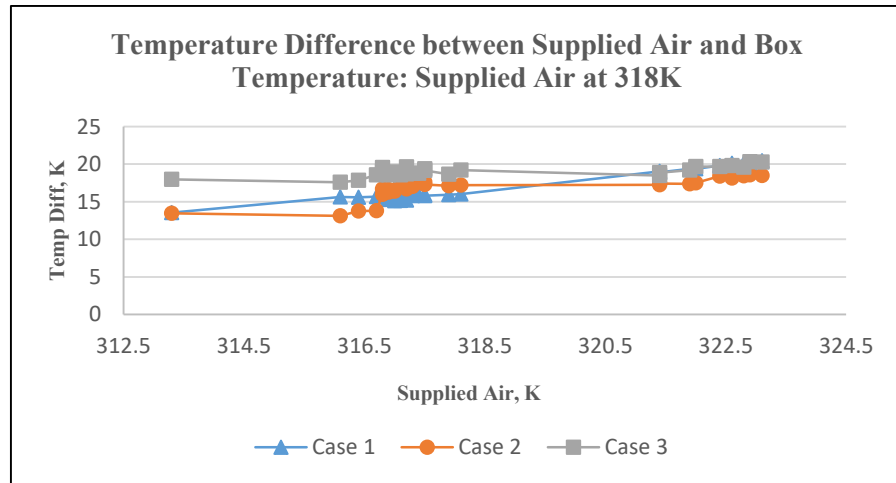


Figure 5.71: Comparison of the temperature difference between supplied-air inlet temperature at 318 K (45°C) and the average temperature of the box for all the cases.

5.4.4 Development on the Work: Case 4

This chapter discusses the latest work progress and development being carried out related to solar energy comfort cooling and energy-saving using the passive cooling method. The heat-pipes heat-exchanger experimental test, solar-energy cooling and wind-assisted cooling were performed at the workshop and field area of Universiti Kuala Lumpur, Malaysia France Institute, Malaysia. The outdoor ambient temperature was about 308 K (35°C) with 65% relative humidity.

A continuation of the research work in comfort cooling has been carried out. To date, several papers relating to comfort cooling have been published. The author is either directly or indirectly involved in the research work concerning energy-saving in heating, ventilating, and air-conditioning. The topics of the published papers are listed below, with the full papers attached in the appendixes:

- Passive cooling using a heat-pipes heat-exchanger in a tropical climate condition.
- A solar-assisted cooling system using PV panels.
- A wind-assisted cooling system using wind turbines.

5.4.4.1 Experimental Study of a Heat-Pipes Heat-Exchanger as Passive Cooling Equipment for A Tropical Climate Condition

The experimental work was carried out at Universiti Kuala Lumpur, Malaysia France Institute, Malaysia. The aim of the research was to validate the heat-pipes heat-exchanger's abilities in a high ambient temperature. The author thoroughly worked with simulations and experimental studies in high ambient conditions by collecting temperature data in Malaysia (Bangi 2.9° N, 101.7° E) where the climate is about 303 K to 308 K (30°C to 35°C). In a tropical climate condition where the outside ambient temperature can reach up to 308 K, a slight decrease in temperature will contribute to electricity consumption. As the evaporator tries to obligate to the setting temperature, the compressor will work harder and in due, increase the energy consumption of the air-conditioner. A heat-pipe heat-exchanger is a form of passive cooling equipment with a refrigerant-filled tube, proposed to improve room temperature by pre-cooling the outside air without consuming any sources of energy. The heat-pipe heat-exchanger lowered the air temperature that passed through its tubes before entering the room and then released the room's

warm air back to the outside ambient. The result showed that the heat-pipes were capable of transferring up to 3.3K heat from the test box. The energy savings were found to be at about 21% to 26% of the installation.

The realisation of using heat-pipes heat-exchanger was carefully studied through the experimental work to show the exchange and distribution of heat. The heat pipe used was a row of 3 x 3 fin-type straight copper tube heat-exchanger, of 12 mm internal diameter with a length of 1 m, and utilized R134a as the refrigerant medium. A wooden box with a size of 1200 x 600 x 1140 mm was used for the air collector insulator to analyse the air-temperature process. Two cases of positions as regards to where the heat-pipes are attached were experimented to show the distribution of air inside the box. Continuing from the previous experiments, Case 4 had a heat-pipes heat-exchanger inclining at 10° horizontal and Case 5 with a 90° vertical position. It was found that the R134a heat-pipes heat-exchanger was capable of transferring an average of 3.3 K temperature difference compared to the outside ambient air.

The main issue to be addressed in the experiment was reducing the heat load of a room. The technique to decrease the power consumption was by manipulating the heat transferability of a heat-pipes heat-exchanger in assisting the cooling process. The author proposed a passive cooling method of transferring heat of the supplied air by pre-cooling the air intake using the R134a heat-pipes heat-exchanger. A heat-pipes heat-exchanger is a device that quickly transfers heat from one end to the other without needing any energy sources. It differs from a thermosiphon by its ability to transport heat against gravity by an evaporation-condensation cycle with almost no heat loss. The advantage of the low boiling condition in atmospheric pressure in an R134a heat-pipe heat-exchanger is that it works passively with natural or driven air circulation without the need for any energy input. Beckert and Herwig (1996) suggested that the heat-pipes' inclination position should be at least 6° for the reason of gravity-return of the fluid refrigerant from the condenser section, back to the evaporator section of the pipe. This experiment utilised a horizontal position of a 10° inclination. The straight sealed tube heat-pipes were divided into three sections, namely the evaporator, adiabatic and condenser section. Figures 5.72 and 5.73 show the maximum temperatures and humidity levels recorded at the Kuala Lumpur International Airport, the nearest weather station from Bangi (weatheronline.co.uk).

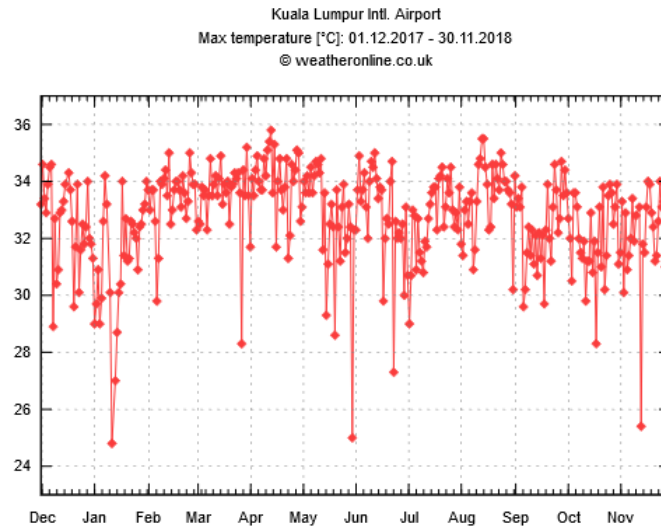


Figure 5.72: The maximum temperature recorded in Kuala Lumpur for the year 2018. The average maximum condition is about 305 K (32°C). *weatheronline.co.uk*

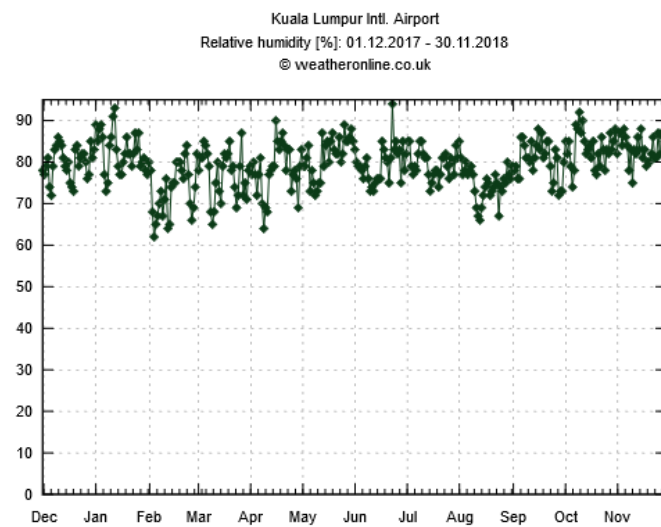


Figure 5.73: The relative humidity recorded in Kuala Lumpur for the year 2018. The average maximum condition is about 80%. *weatheronline.co.uk*

5.4.4.2 Problem Description: Thermal Modelling

Pre-cooling the outside ambient air will reduce energy consumption and increase sensible cooling to a room. The passive cooling method using a heat-pipe heat-exchanger does not require any energy input to decrease the temperature. Heat is absorbed and desorbed by the refrigeration medium and forced to move from the tube, end to end. The evaporation makes use of the vapour's lower density and the void action in the adiabatic section to move upward, and the condensation

uses gravity to return to the evaporator section. This method of cooling allows the evaporation to carry the heat to the condenser where the condensation releases the heat away.

The total heat flow is proportional to the temperature difference between the evaporator and the condenser. An electrical Ohms Law resistance analogue has to be applied to generate a thermal model for a heat-pipe

$$Q = \frac{T_e - T_c}{R_{THR,eq}} \quad I = \frac{\Delta V}{R_{eq}}$$

where Q is the heat transfer rate, T_e is the surface temperature of the evaporator, T_c is the surface temperature of the condenser and $R_{THR,eq}$ is the thermal resistance. In the calculation, it was found that the Q was about 82 W for each tube.

As the equivalent thermal resistance R is comprised of all those regions that provide a blockage to the flow of heat, the overall thermal resistance can be calculated based on the resistances shown in Figure 5.74 using the formula:

$$R = \frac{1}{\frac{1}{R_2 + R_3 + R_4 + R_6 + R_7} + \frac{1}{R_5}}$$

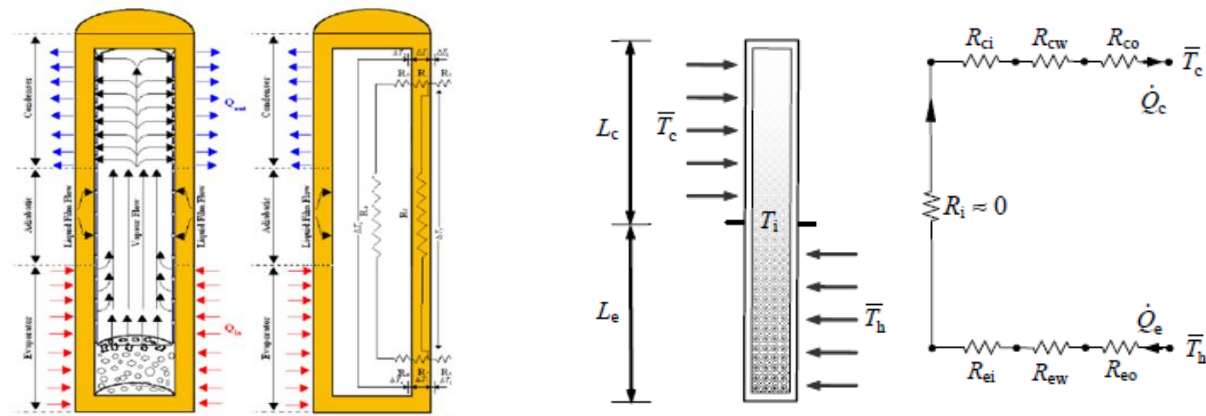


Figure 5.74: Thermosiphon operation of a heat-pipe heat-exchanger and the associated thermal resistance network. *Abdullah (2018).*

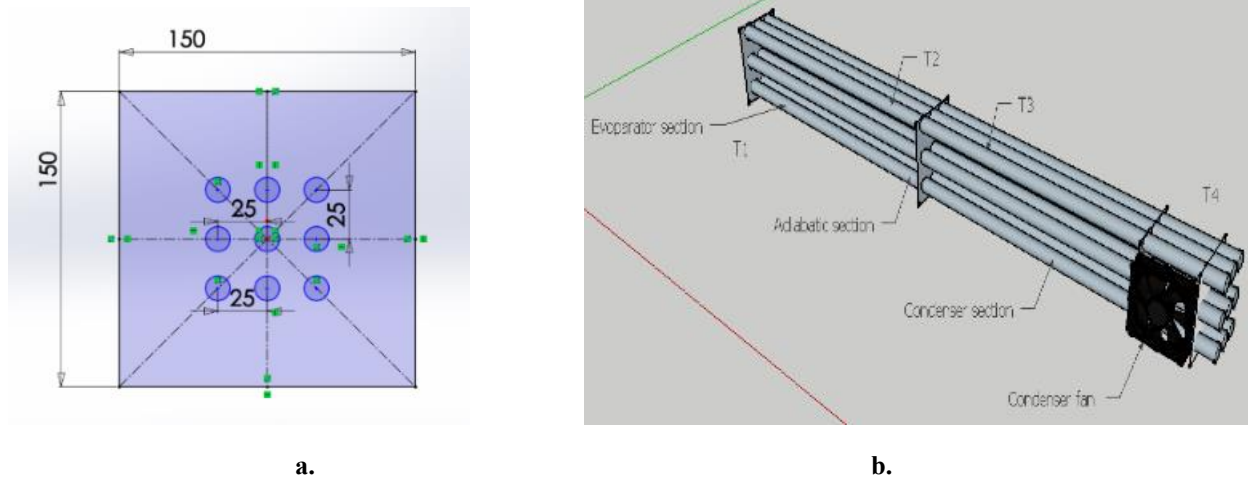


Figure 5.75: The experimental unit of a. Aluminium fins. b. Staged type 3x3 heat-pipes heat-exchanger excluding the fins. *Abdullah (2018)*.

Figure 5.75 shows the heat-pipes experimental unit. Table 5.21 shows the thermal resistance calculation of heat-pipes. It was found that the thermal resistance R for the heat-pipes was 0.0428 K/W.

Table 5.21: The thermal resistance calculations. *Abdullah et al. (2018)*.

Description	Formula	K / W
The thermal resistance between the heat sink and the condenser external surface	$R_1 = \frac{1}{h_{co}A_{co}}$	1.808318
The thermal resistance across the thickness of the condenser wall	$R_2 = \frac{\ln(D_o/D_i)}{2\pi L k_s}$	17.42089
The internal thermal resistance of the condensing fluid in the thermosyphon. h_{ci} refer to ESDU (1981).	$R_3 = \frac{1}{h_{ci}A_{ci}}$	1.956947
The resistance is due to the pressure drop of the vapour as it flows from the evaporator to the condenser. According to ESDU (1981) and ESDU (1979), this resistance is the ratio between the drop in saturation temperature between the evaporator and the condenser over the rate of heat transfer	$R_4 = \frac{\Delta T_{sat-e-c}}{Q}$	1.956947
The axial resistance across the length of the thermosyphon	$R_5 = \frac{(0.5Le + La + 0.5Lc)}{Acs Ks}$	25379.75
The internal thermal resistance of the boiling fluid in the thermosyphon h_{ei} was obtained from ESDU (1981).	$R_6 = \frac{1}{h_{ei}A_{ei}}$	1.956947
The thermal resistance across the thickness of the evaporator wall	$R_7 = \frac{\ln(D_o/D_i)}{2\pi Le Ks}$	17.42089
The thermal resistance between the heat source and the evaporator external surface	$R_8 = \frac{1}{h_{eo}A_{eo}}$	1.808318
Total R		0.042828061

5.4.4.3 Summary of the Temperature Pathway Graph by Points of Measurement

Thermocouples were located at important points on the heat-pipes heat-exchanger and inside the test box. The data logger recorded the temperature readings. Decision on the inlet and the outlet of air intake and exit was performed through simulations to show the best configurations. The points are as follows:

Table 5.22: Point of measurements where the thermocouples were located.

Points	Measurement Remarks
1	Evaporator Tube Temperature
2	Condenser Tube Temperature
3	Air Inlet Temperature
4	Air Outlet Temperature
5	Test-box Bottom Air Temperature
6	Test-box Middle Air Temperature
7	Test-box Left Side Air Temperature
8	Test-box Right Side Air Temperature
9	Test-box Bottom Return Air Temperature
10	Heat Pipe Condenser Tube Temperature
SA	Supply Air Temperature
RA	Return Air Temperature

Case 1: Air Flowing from the Sidewall

The inlet and outlet were located on the sidewall of the test box. Figures 5.76 and 5.77 show the paths of the air and the temperature measurement points.

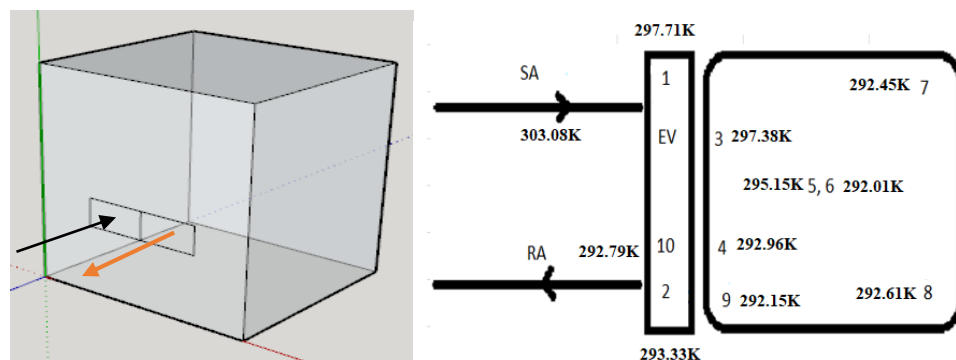


Fig 5.76: Case 1: The air path and temperature points.

Points of Measurement: °C

The data logger recorded the measurements in °Celsius. Table 5.23 shows the average temperature measured at 302 K (29°C) to 304 K (3°C) while Table 5.24 shows the average temperature in Kelvin.

Table 5.23: Measured average temperature at every point in Case 1, in °C.

SA	1 Evap	3 Inlet	5	6	7	8	9	4 Outlet	10 Cond	2
29.40	26.00	27.70	18.90	19.50	20.50	20.20	18.80	19.30	20.60	19.40
29.60	26.70	29.00	19.30	19.90	21.00	20.60	18.80	19.80	20.70	20.00
31.20	26.70	29.20	19.30	20.00	21.20	20.80	18.90	19.70	21.00	20.10
30.20	26.90	29.10	19.40	20.00	21.20	20.60	18.90	19.70	21.10	20.20
30.20	27.00	29.20	19.40	20.10	21.10	20.70	18.90	19.80	21.20	20.20
30.10	26.90	29.40	19.50	20.30	21.30	20.80	18.90	20.00	21.20	20.40
30.10	26.80	29.20	19.50	20.30	21.40	21.00	19.00	20.10	21.30	20.50
30.10	26.80	29.20	19.50	20.40	21.50	21.20	19.00	20.10	21.30	20.50
30.20	26.90	29.40	19.50	20.40	21.50	20.80	19.00	20.20	21.30	20.60
30.00	26.70	29.10	19.50	20.50	21.60	21.10	19.00	20.20	21.40	20.60
29.90	26.60	28.90	19.60	20.50	21.70	21.20	19.00	20.20	21.40	20.70
29.90	26.80	28.80	19.70	20.50	21.80	21.10	19.10	20.40	21.50	20.80
30.08	26.73	29.02	19.43	20.20	21.32	20.84	18.94	19.96	21.17	20.33

Table 5.24: Measured average temperature at every point in Case 1, in K.

SA	1	3	5	6	7	8	9	2	10	4
303.08	297.71	297.38	295.15	292.01	292.45	292.61	292.15	293.33	292.79	292.96

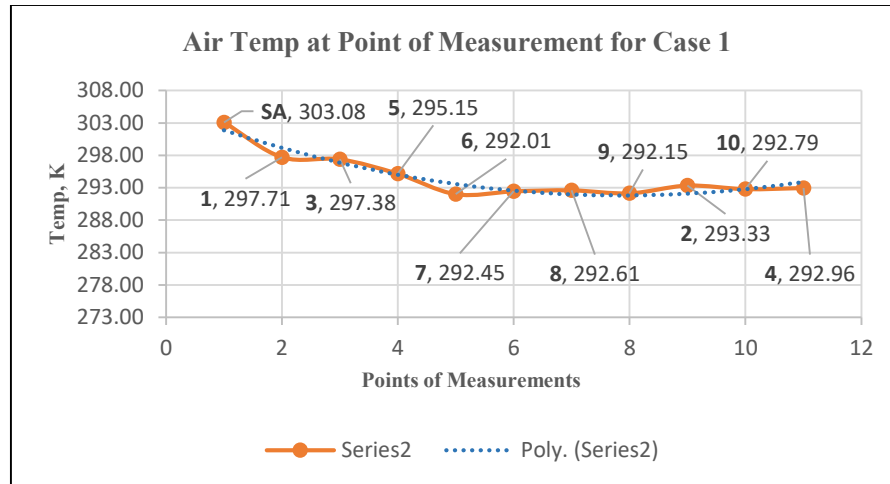


Figure 5.77: Case 1: The path of air temperature blown from the supplied air (SA) to the heat-pipes evaporator side (1) moves to the inlet of the test-box (3), is mixed with the box air temperature (5-9) and is forced to the outlet (2) and the condenser side of the heat-pipes (10), and then exits to the ambient outlet (4). The average temperature difference is between 8K to 10K.

The supplied air's (SA) heat at 303.08K was absorbed by the refrigerant inside the heat-pipes to the lowest temperature of 292.01K (6) and was mixed with the box's inside air (5-9). Depending on the location of the thermocouples inside the test box, the temperature of the mixed air increased and flowed to the condenser (2) at 292.33K and the airflow then exited to the outlet (4). The surface temperature on the condenser's side was 292.79K (10).

Case 2: Air Flowing from the Top

The inlet and outlet were located on the top side of the test box. The data logger recorded the measurements in °Celsius. Table 5.25 shows the temperature measured at 302 K (29°C) to 303 K (30°C) while Table 5.26 shows the average temperature in Kelvin. Figures 5.78 and 5.79 show the paths of the air and the temperature measurement points.

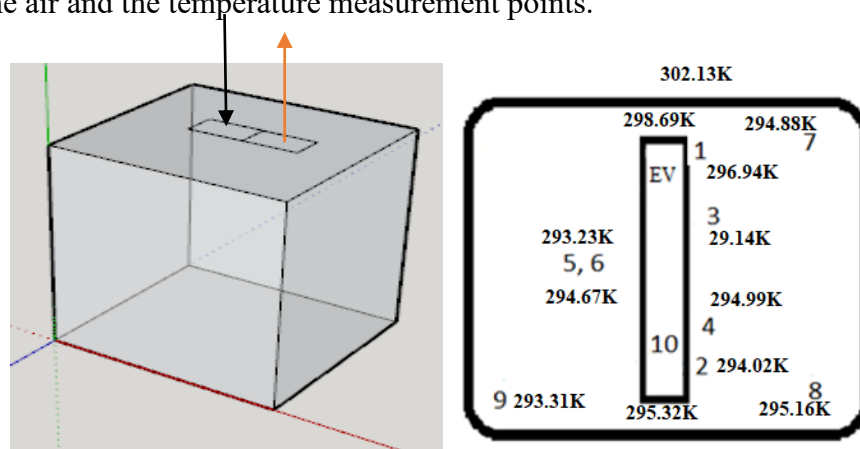


Fig 5.78: Case 2: The air path and temperature points.

Points of Measurement, °C

Table 5.25: Measured average temperature at every point in Case 2, in °C.

SA	1	3	Evap	5	6	7	8	9	10	2	4
	Inlet								Cond		Outlet
29.20	23.30	24.80	25.20	20.00	21.20	21.40	21.50	19.80	21.70	20.20	21.60
29.00	23.70	25.30	25.80	20.10	21.40	21.70	22.10	20.10	22.20	20.70	21.80
29.10	24.00	25.10	25.60	20.20	21.50	21.60	21.90	20.20	22.20	21.00	21.90
29.30	24.10	25.00	25.80	20.20	21.50	21.70	22.10	20.40	22.30	21.00	21.90
29.30	23.90	25.40	25.90	20.20	21.60	21.70	22.20	20.20	22.40	21.10	22.00
29.00	24.10	25.30	25.80	20.30	21.80	22.00	22.40	20.20	22.40	21.10	22.20
29.00	24.10	25.10	25.70	20.30	21.90	22.10	22.30	20.50	22.50	21.20	22.10
29.10	24.10	25.20	25.80	20.40	21.80	22.00	22.40	20.50	22.50	21.30	22.10
29.30	24.00	25.20	25.60	20.30	22.10	22.60	22.30	20.60	22.50	21.30	22.00
29.00	24.10	25.00	25.70	20.30	21.90	22.00	22.40	20.60	22.50	21.30	22.30

Table 5.26: Measured average temperature at every point in Case 2, in K.

SA	1	3	Evap	5	6	7	8	9	10	2	4
									Cond		Outlet
302.13	296.94	298.14	298.69	293.23	294.67	294.88	295.16	293.31	295.32	294.02	294.99

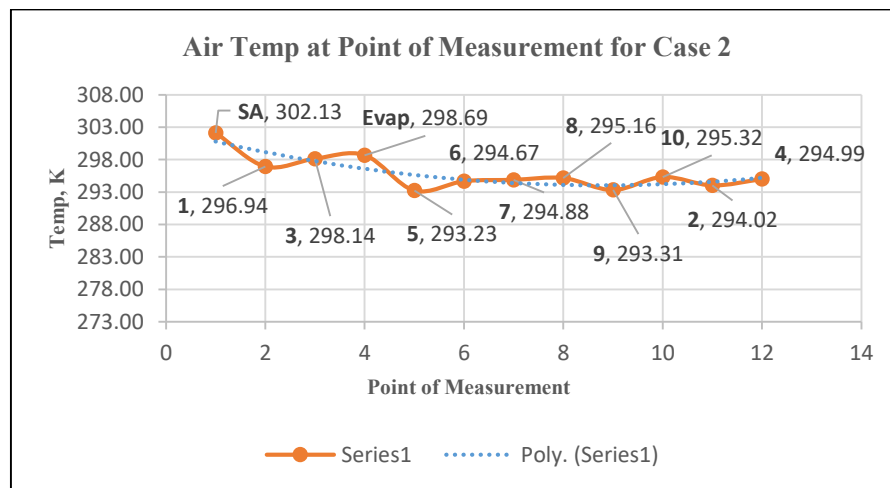


Fig 5.79: Case 2: The path of air temperature blown from the supplied air (SA) to the heat-pipes evaporator side (1) moves to the inlet of the test-box (3), is mixed with the box air temperature (5-9), forced to the outlet (2) and the condenser side of the heat-pipes (10), and then exits to the ambient outlet (4). The average differential temperature is 8K.

The supplied air's (SA) heat which was blown from the top at 302.13K was absorbed by the refrigerant inside the heat-pipes to the lowest temperature of 293.23K (5) and was mixed with the box's inside air (5-9). Depending on the location of the thermocouples inside the test box, the

temperature of the mixed air increased. As the less dense air moved to the upper side of the test-box, the temperature at (8) showed an increase at 295.16K. The airflow to the condenser (2) was at 294.02K and the airflow then exited to the outlet (4). The surface temperature on the condenser's side was 295.32K (10).

Case 3: Air Flowing from the Top

The inlet was located on the top side of the test box, and the outlet was on the sidewall. The data logger recorded the measurements in °C. Table 5.27 shows the temperature measured at 302 K (29°C) to 304 K (31°C) while Table 5.28 shows the average temperature in Kelvin. Figures 5.94 and 5.95 show the paths of the air and the temperature measurement points.

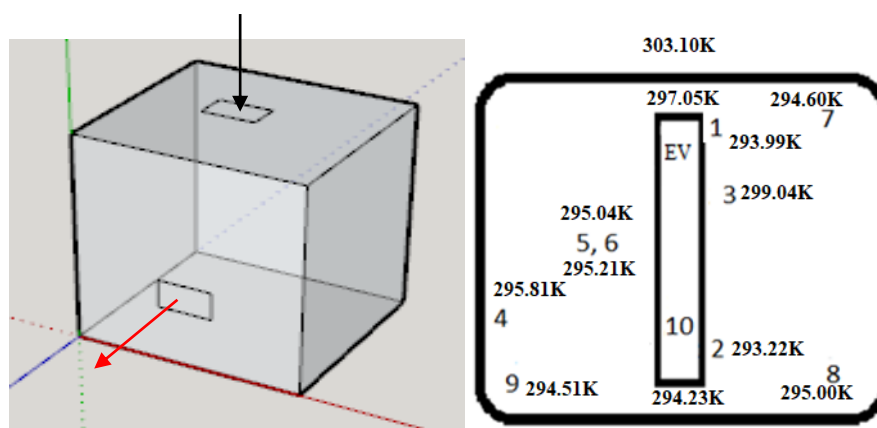


Fig 5.80: Case 3: The air path and temperature points.

Point of Measurements, °C

Table 5.27: Measured average temperature at every point in Case 3, in °C.

SA	1	3	Evap	5	6	7	8	9	10	2	4	
	inlets											outlets
30.10	21.00	26.10	23.70	21.80	22.00	21.40	21.70	21.50	21.20	20.30	22.70	
29.90	20.90	25.80	24.00	21.90	22.00	21.40	21.80	21.40	21.20	20.20	22.80	
30.20	21.00	26.00	24.20	21.90	22.30	21.50	22.00	21.40	21.40	20.20	22.80	
30.50	21.00	26.00	24.10	22.00	22.20	21.50	22.00	21.60	21.10	20.20	22.70	
30.10	21.00	26.00	24.00	22.10	22.20	21.50	21.90	21.60	21.20	20.20	22.90	
30.00	21.00	26.00	24.00	22.10	22.30	21.60	22.20	21.70	21.20	20.20	22.80	
30.10	20.90	26.20	24.10	22.10	22.30	21.60	22.00	21.50	21.20	20.20	22.90	
30.10	21.10	26.10	24.10	22.10	22.30	21.70	22.20	21.50	21.10	20.10	22.80	
30.10	21.00	26.00	24.10	22.10	22.20	21.80	21.90	21.40	21.40	20.20	22.80	
30.00	21.00	26.10	24.10	22.10	22.20	21.90	22.20	21.50	21.20	20.30	22.80	
30.00	21.00	26.10	24.20	22.20	22.30	21.70	22.10	21.50	21.30	20.30	22.90	

Table 5.28: Measured average temperature at every point in Case 3, in K.

SA	1	3	Evap	5	6	7	8	9	10	2	4
303.10	293.99	299.04	297.05	295.04	295.21	294.60	295.00	294.51	294.23	293.22	295.81

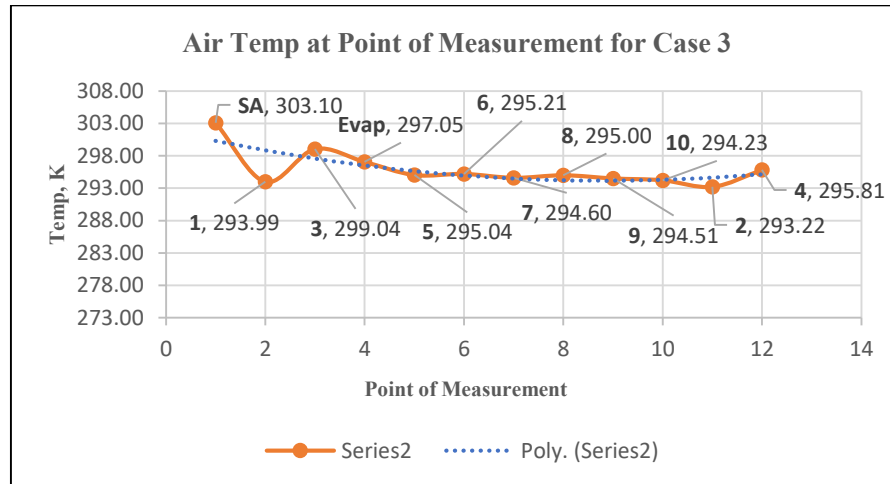


Fig 5.81: Case 3: The path of air temperature blown from the top of the supplied air (SA) to the heat-pipes evaporator side (1) moves to the inlet of the test-box (3), is mixed with the box air temperature (5-9), forced to the outlet (2) and the condenser side of the heat-pipes (10), and then exits to the ambient outlet (4). The average differential temperature is 7K.

The supplied air's (SA) heat which was blown from the top at 303.10K was absorbed by the refrigerant inside the heat-pipes to the lowest temperature of 294.51K (9) and was mixed with the box's inside air (5-9). Depending on the location of the thermocouples inside the test box, the temperature of the mixed air increased. As the air was blown to the sidewall of the test-box, the condenser side of the heat-pipes heat-exchanger showed a temperature of 293.22K (2). The air flowed to the condenser and the airflow then exited to the outlet (4). The surface temperature on the condenser's side was 294.23K (10).

Case 4: Heat-pipes 10° Horizontal

As tested in the previous simulations and experimental work, the heat-pipes used R134a as the refrigerant medium. The heat-pipes filled with R134a offer different temperatures and it, therefore, presents a better option than other refrigerants. Table 5.29, and Figures 5.82 and 5.83 show the simulation parameters.

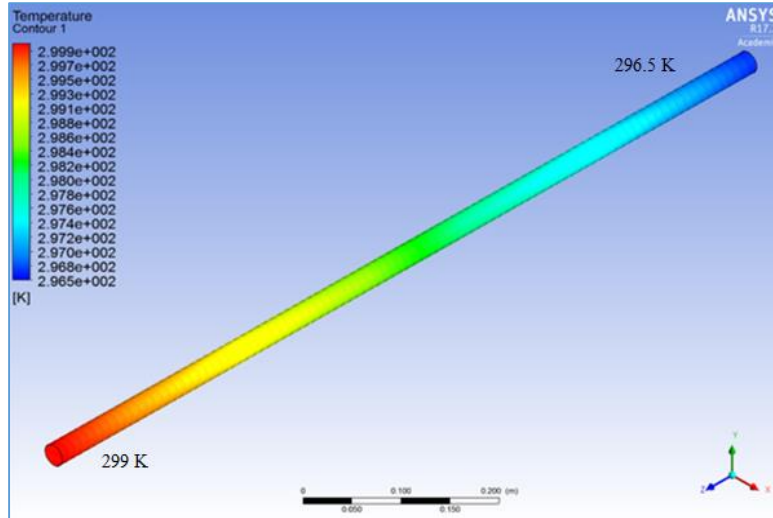


Figure 5.82: The heat-pipes with R134a as refrigerant show that the lowest temperature is 296.5 K. The inlet and outlet difference is 3.5K

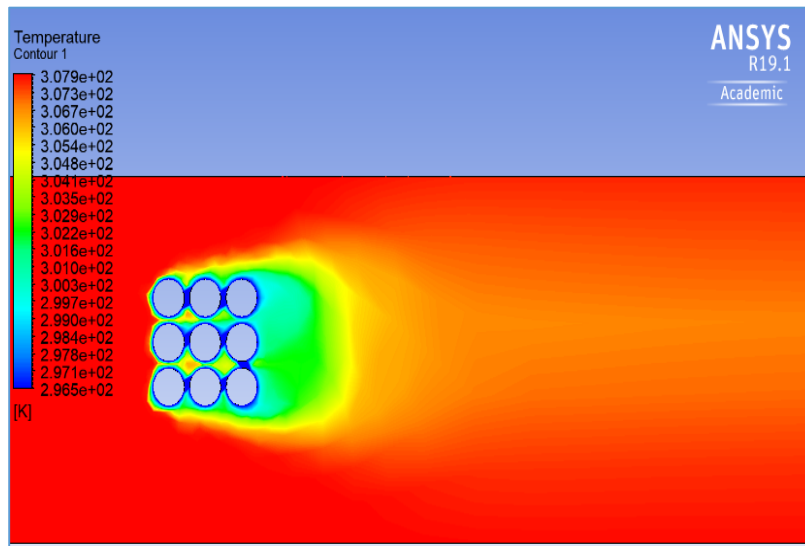
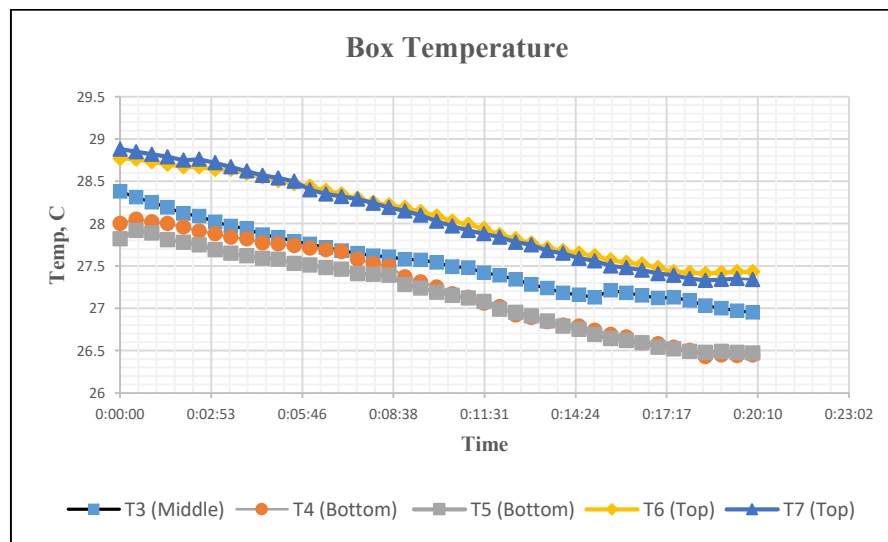


Figure 5.83: The heat transfers from the R134a heat-pipes heat-exchanger could achieve a temperature difference of 7 K (300K – 307K) as shown by ANSYS Fluent simulation.

Table 5.29: The parameters of R134a when simulated using ANSYS Fluent.

Parameters	R134a
Density kg/m ³	1206
Spec. Heat J/kg. K	1425
Viscos kg/m-s	1.9525x10 ⁻⁴
Inlet Temp, K	300
Outlet Temp, K	296.5
Differential In and Out Temp, K	3.5

Figures 5.135 and 5.136 show the thermocouple positions of the test box and the result of the experiment. In Case 4 where the heat-pipes heat-exchanger was placed in a horizontal 10° inclinations, the temperature could be lowered to 298.7 K for the evaporator section and 299.2 K for the condenser section.

**Figure 5.84:** The temperature recorded by the thermocouple inside the test box has a difference of about 3K.

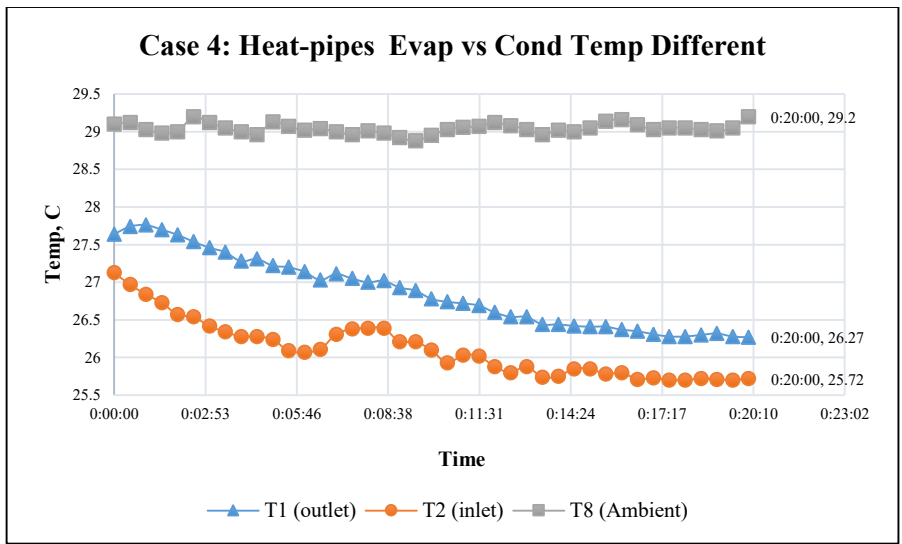


Figure 5.85: The heat-pipes heat-exchanger is capable of transferring heat of about 2.3K to 3.3K from the evaporator end towards the condenser end.

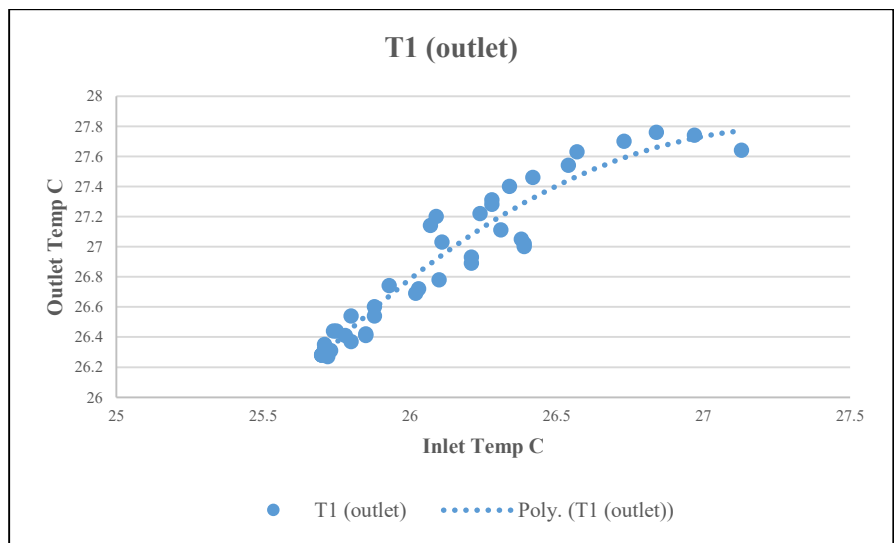


Figure 5.86: In Case 4, the polynomial curve predicts that the outlet temperature stays at about 300.7 K (27.7°C).

Case 5: Heat-pipes 90° Vertical

Figures 5.87 to 5.89 show the results of the experiment in Case 5 where the heat-pipes heat-exchanger was placed in a vertical 90° position. The temperature could be lowered to 299.94 K for the evaporator section and 300.64 K for the condenser section.

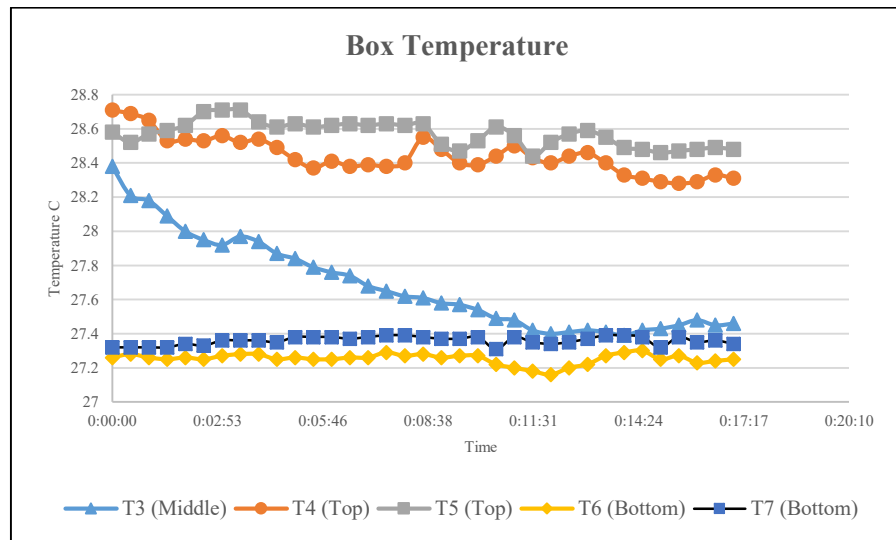


Figure 5.87: The temperature recorded by the thermocouple inside the test box has a difference of about 2K.

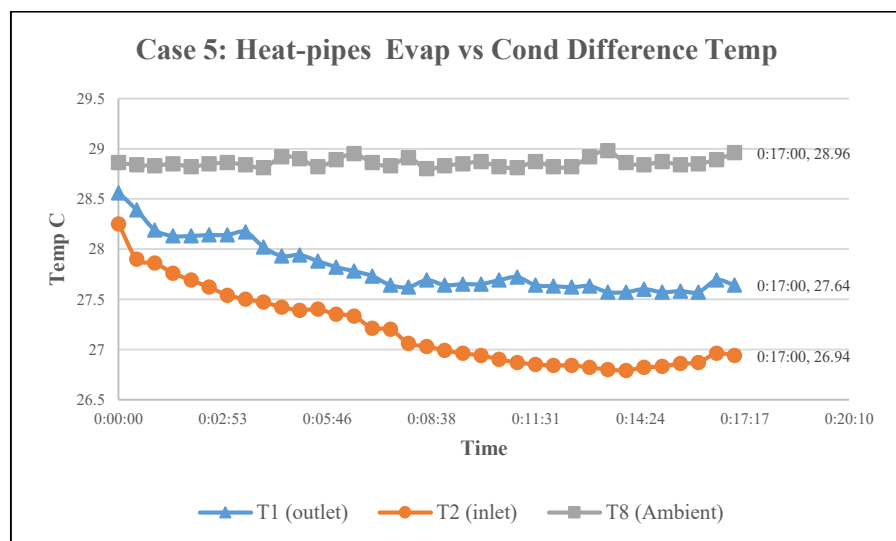


Figure 5.88: The heat-pipes heat-exchanger is capable of transferring heat of about 1.3K to 1.6K from the evaporator end towards the condenser end.

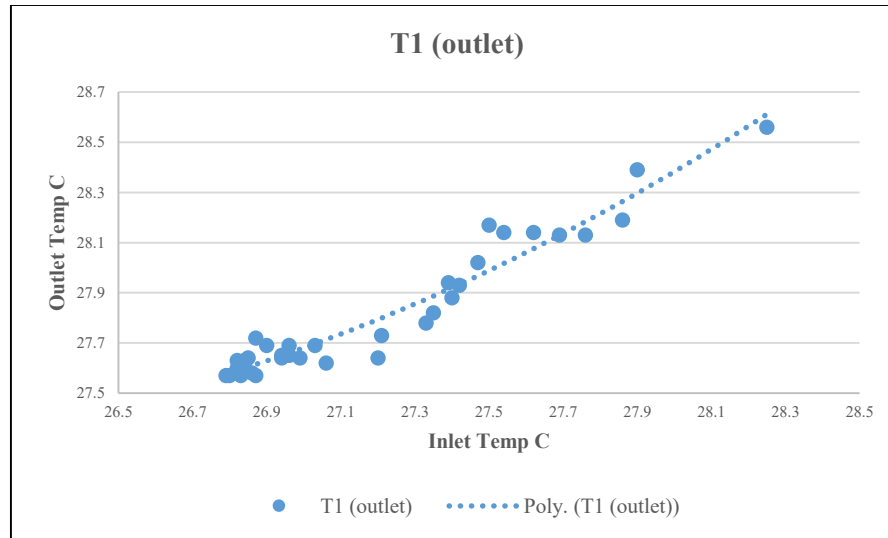


Figure 5.89: In Case 5 the polynomial curve predicts that the outlet temperature stays at about 301.5 K (28.5°C). With added heat to the heat-pipes, the heat-pipes will not be capable of converting any more heat and the temperature will be linear for both the inlet and outlet.

5.4.4.4 Estimated Energy-Saving by the Heat-Pipes Heat-Exchanger

ASHRAE 55 (2004) and the ASHRAE Fundamental Handbook (1989) specify a design temperature range of 295.8 K (22.8°C) to 298 K (25°C) as the comfortable indoor temperature for domestic air conditioning systems. Taking the average temperature of 297 K (24°C) as the design indoor temperature and 308 K (35°C) as the outdoor temperature for domestic air conditioning systems, the sensible cooling load calculated by Wan (2007) found that the cooling load for the box Q_o is 9.607 kW of sensible load. The parameters taken for all cases are shown in Table 5.43, and the rate of energy-saving can be calculated as

$$\alpha = \frac{Q_o - Q_o' \text{ at standard sensible condition}}{Q_o - Q_o' \text{ at tested condition}}$$

where α is the rate of energy-saving by the heat-pipes %, $Q_o - Q_o'$ the difference between the sensible load at constant indoor Q_o (9.6 kW) and the calculated sensible load and heat-pipes heat-exchanger Q_o' . Figure 5.90 compared the sensible load of both cases.

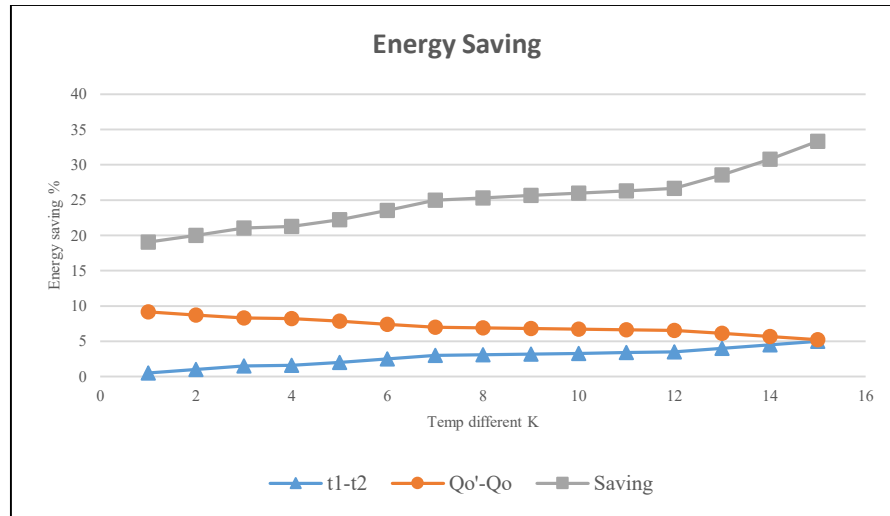


Figure 5.90: The energy-saving recorded in the experiment compared to the temperature difference of the heat-pipes heat-exchanger Q_o and Q_o' . The graph shows that the heat-pipes heat-exchanger could save an average of 20% of the installation.

5.4.4.5 Conclusion

The novelty of the energy-saving development using heat-pipes heat-exchanger as passive cooling tools is accomplished with this study. Simulation and experimental studies of the heat-pipes heat-exchanger application as passive cooling equipment were performed in the tropical climate where the ambient temperature can reach up to 308 K (35°C). Two cases were tested with the heat-pipes configuration set on a horizontal position with a 10° incline and on a vertical position at 90°.

The results indicate that the heat-pipes heat-exchanger is capable of transferring 1.6 K to 3.3 K differential temperature of the inlet air to the outlet. The results show that the designed fin-type heat-pipes heat-exchanger is capable of saving up energy. Table 5.30 shows that Case 4 is capable of saving 2.88 kW and Case 5 is capable of saving 1.4 kW of sensible heat gain. Energy savings of 26% (Case 1) and 21% (Case 2) have therefore been determined.

Table 5.30: The energy-saving with the application of heat-pipes heat-exchanger.

Parameters	Case 4	Case 5
Outside temp K	305	305
Box – Outside temp K	3.3	1.6
Q_0 sensible kW	9.607	9.607
$Q_0 - Q_o'$ Sensible kW	1.747	1.747
$Q_0 - Q_o'$ At 3.3°C kW	6.725	1.397
Energy-saving α , % x 100	0.259	0.213

The results indicate that Case 4 has a better configuration than Case 5 in terms of energy saving. For equipment that does not require any energy sources, heat-pipes heat-exchanger performed well as a promising tool for an energy-saving application.

5.5 Estimated Energy-saving by the Heat-pipes Heat-exchanger Using Energy Calculation Method

ASHRAE 55 specifies that a design temperature of 295.8 K (22.8°C) to 298 K (25°C) is a comfortable indoor temperature for domestic air conditioning systems. Taking the average temperature of 297 K (24°C) as the design indoor temperature and 303 K (30°C) as the outdoor temperature for domestic air conditioning systems, the sensible cooling load for the box can be calculated (Wan 2007) using the formula

$$Q = 1.213 \times qv \times (t_r - t_o)$$

where

- Q = estimated sensible cooling load, kW,
- 1.213 = specific heat of moist air (1.025 kJ/kg. K) / The specific volume of moist air (0.845 m³/kg), at standard sea level
- qv = airflow rate, m³/s
- t_r = acrylic box dry bulb temperature, K.
- t_o = outlet or supply air dry bulb temperature, K
- A = face area at 0.0325 m²

Given the face area of 0.0325 m², velocity of 1 m/s, and the temperature difference of 6 K, the calculated capacity of the box was found to be 0.280 kW. The rate of energy-saving by the heat-pipes heat-exchanger can thus be calculated based on Ehsan (2008) using the formula

$$\alpha = \frac{Q_o' - Q_o}{Q_o'}$$

where α = rate of energy-saving, %
 Q_o = sensible cooling load at constant indoor design temperature, kW
 Q_o' = sensible cooling load at constant indoor design temperature with heat-pipes heat-exchanger, kW.

Table 5.31 shows the estimated sensible cooling load for the box at 303 K and 318 K and the energy-saving percentage rate of the heat-pipes heat-exchanger. Figures 5.91 to 5.104 compared the energy-saving percentage rate of the heat-pipes heat-exchanger between all cases at the temperature of 303 K and 318 K.

Table 5.31: The estimated sensible cooling load for all cases with the air supply temperature of 303 K and 318 K. The rate of the energy-saving capability of the heat-pipes heat-exchanger in the table is compared to standard air of 297 K.

Parameters	Case 1		Case 2		Case 3	
	303K	318K	303K	318K	303K	318K
Differential Temp of Supplied Air and HP Condenser Section, K (S_A-HP_C)	8	7	7	8	9	7
Q_o , Estimated sensible cooling load, kW	0.373	0.327	0.327	0.373	0.420	0.327
Energy-saving $Q_o'-Q_o$, kW	0.93	0.47	0.47	0.93	0.140	0.47
The rate of energy-saving ($Q_o'-Q_o/Q_o'$) α , % x 100	0.25	0.14	0.17	0.33	0.33	0.14

Case 1

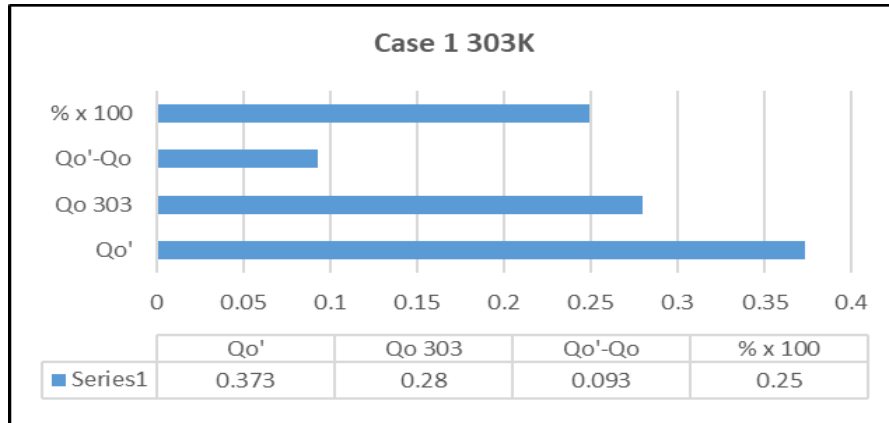


Figure 5.91: The graph shows the energy-saving using a heat-pipes heat-exchanger for Case 1 (303 K).

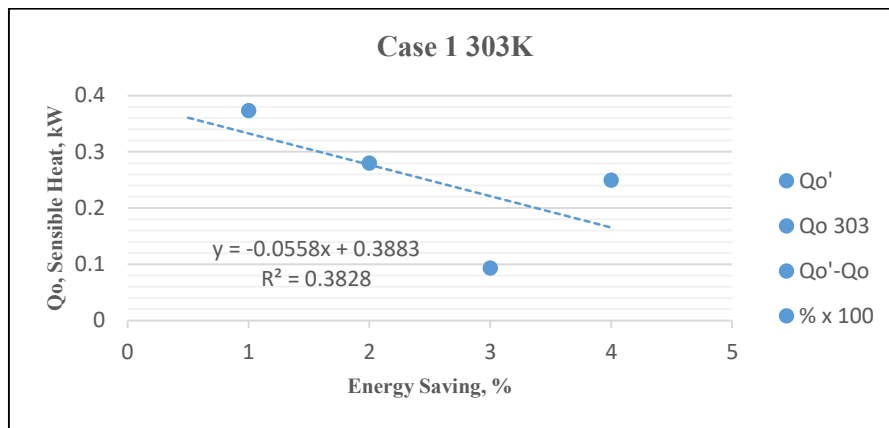


Figure 5.92: The graph shows the sensible cooling load of Case 1 with a supplied inlet temperature of 303 K.

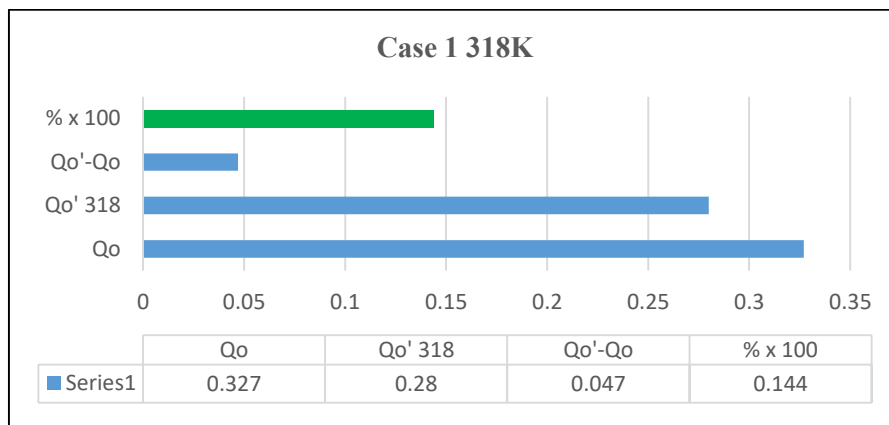


Figure 5.93: The graph shows the energy-saving using a heat-pipes heat-exchanger for Case 1 (318).

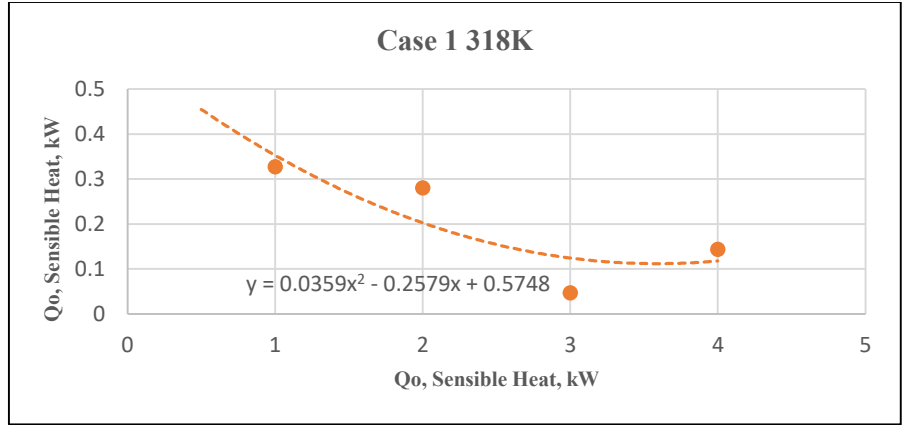


Figure 5.94: The graph shows the sensible cooling load of Case 1 with a supplied inlet temperature of 318 K.

Case 2

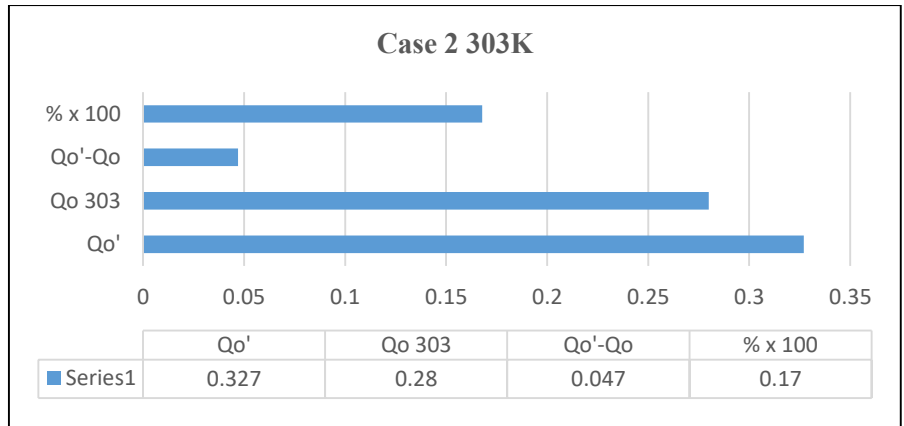


Figure 5.95: The graph shows the energy-saving using a heat-pipes heat-exchanger for Case 2 (303K).

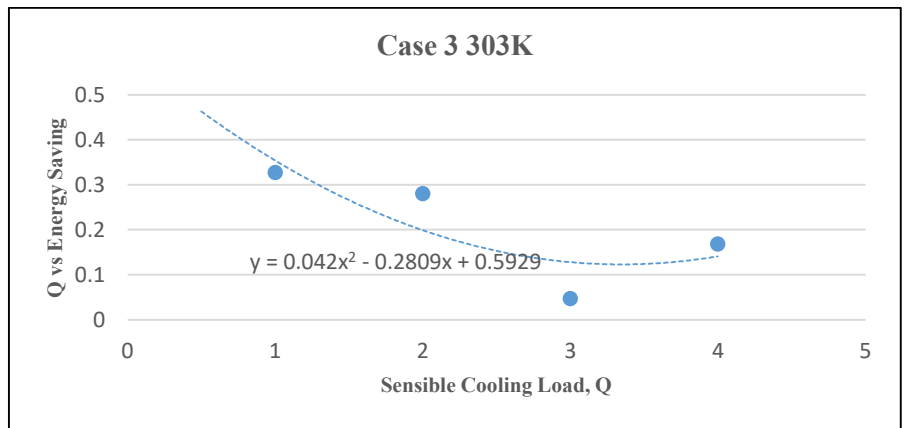


Figure 5.96: The graph shows the sensible cooling load of Case 2 with a supplied inlet temperature of 303 K.



Figure 5.97: The graph shows the energy-saving using a heat-pipes heat-exchanger for Case 2 (318).

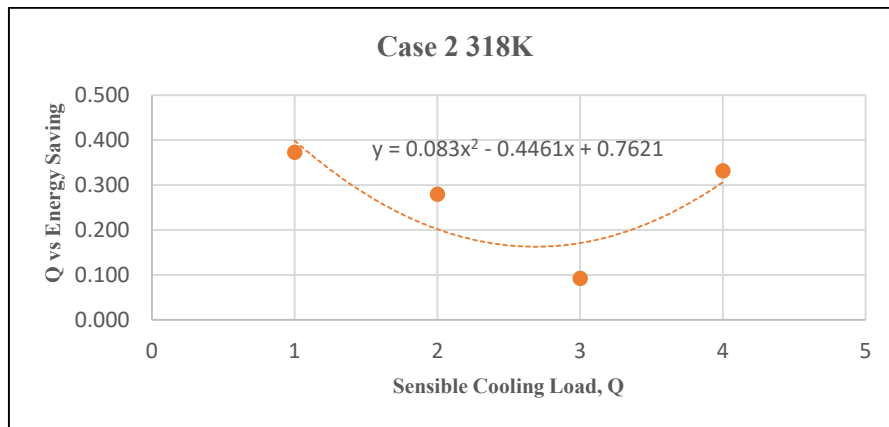


Figure 5.98: The graph shows the sensible cooling load of Case 2 with the supplied inlet temperature of 318 K.

Case 3

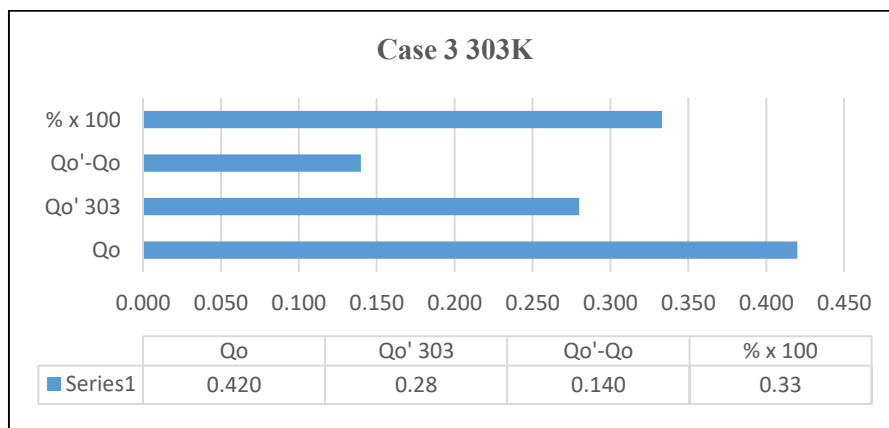


Figure 5.99: The graph shows the energy-saving using a heat-pipes heat-exchanger for Case 3 (303K).

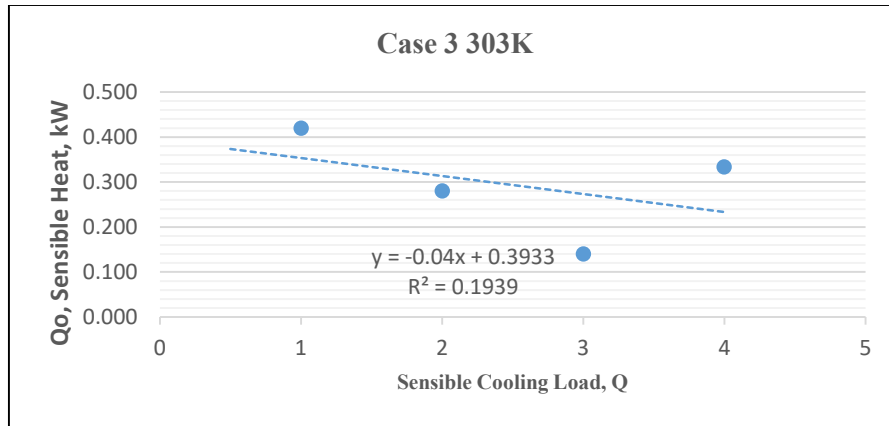


Figure 5.100: The graph shows the sensible cooling load of Case 3 with the supplied inlet temperature of 303 K.

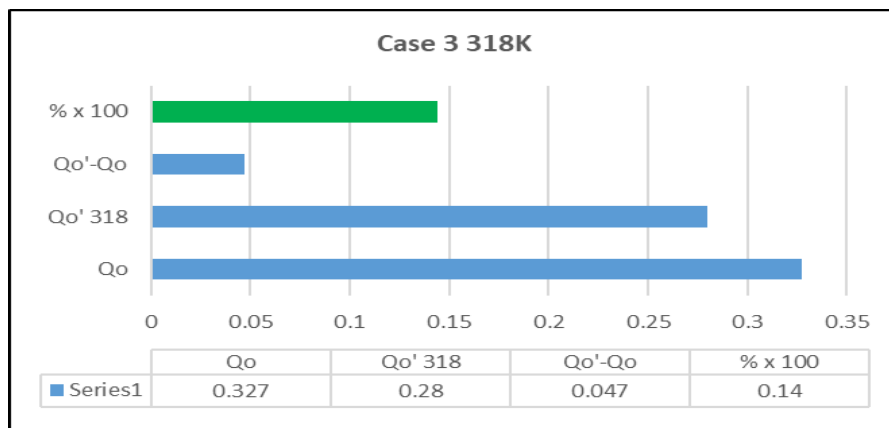


Figure 5.101: The graph shows the energy-saving using a heat-pipes heat-exchanger for Case 3 (318).

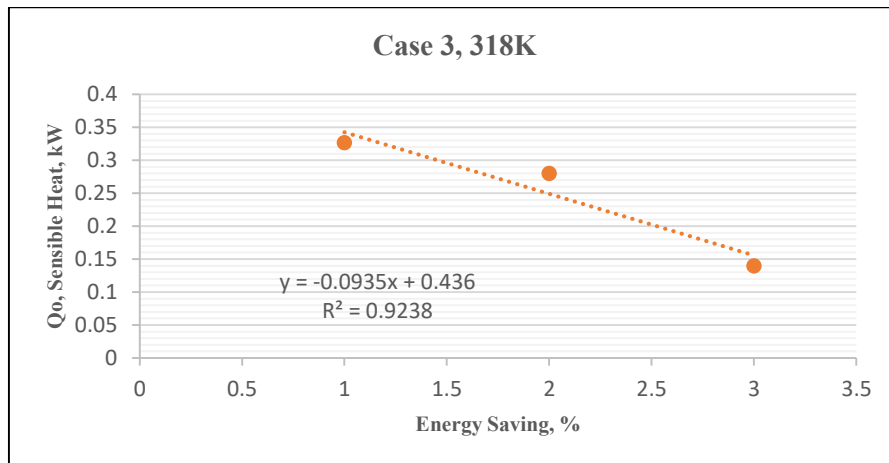


Figure 5.102: The graph shows the sensible cooling load of Case 3 with the supplied inlet temperature of 318K.

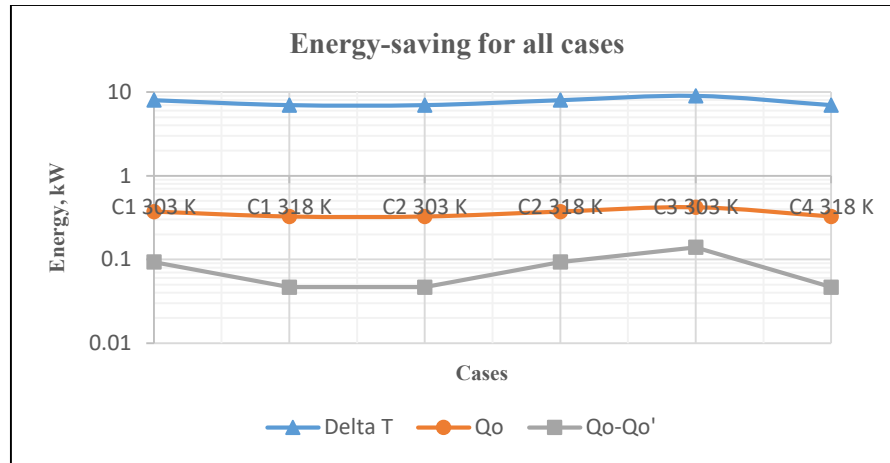


Figure 5.103: Comparison of the energy-saving using a heat-pipes heat-exchanger for all cases.

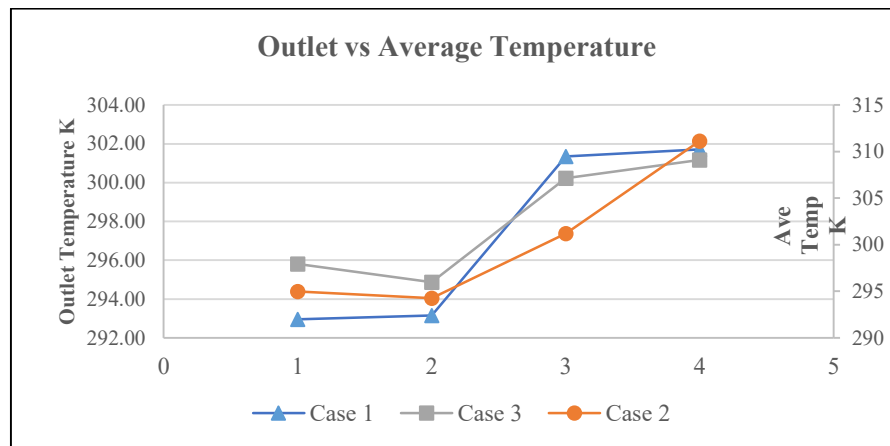


Figure 5.104: The outlet air temperature and the average temperature of the acrylic box for all cases.

5.6 THE TEMPERATURE COMPARISONS BETWEEN THE SIMULATION AND EXPERIMENTAL WORKS

The results from the simulation and the experimental work have been produced and reviewed in several journal and conference papers related to the heat-pipes heat-exchanger. Using engineering drawings to sketch the models, computational fluid dynamics software CFD- ACE and ANSYS Fluent were used to verify the outcome. Several cases had been simulated to find the best optimum configurations in terms of room air intake opening, air velocity and the suitable operating temperature. Experimental works for selected cases based on the result of the simulation

are performed. The simulation results and lastly the comparison to the experimental outcomes are shown in Table 5.32 to Table 5.36.

The edges of the opening configurations were selected to perform the airflow with natural and driven ventilation. Air velocity and pressure, as well as gravity, are taken as important values in the simulation to influence the temperature across the room. The model used the Reynold Average Navier-Stokes (RANS) scheme to show air distribution in a room with natural ventilation. The inlet opening was equipped with heat-pipes heat-exchanger to increase the temperature from 300 K to 305 K (27°C to 32°C). Cases were evaluated in terms of velocity, velocity magnitude and temperature across the room. It was found that case three had the most air velocity flow compared to the other two cases. The position is such that it allowed a greater air velocity rate to enter the room and pushed the air to the sidewall. The temperature distributions are almost the same for all cases.

Table 5.32: The result of the simulation for the heat-pipes heat-exchanger in assisting the pre-cooling of intake air to a room with driven ventilation. *Abdullah (2012)*.

Simulation using CFD		
Supplied air temperature, K	300K	305K
Temperature difference at Heat-pipes R134a, K	3	5
Case 1 sharp edges, K	1	1
Case 2 round edges, K	1	1.9
Case 3 sharp edges, K	1	1.6

The temperature inside of an outdoor power supply cabinet attached with a heat-pipes heat-exchanger was simulated. The main issue to be addressed in the simulation was to demonstrate the effectiveness of the heat-pipes heat-exchanger and the temperature drop that the heat-pipes could achieve. The rate of the energy transfer to the air is calculated.

Table 5.33: The comparisons of the result between the simulation and the experimental work for the heat-pipes heat-exchanger in assisting the pre-cooling of intake air to an outdoor power cabinet. The high temperature of 328K in the cabinet is reduced to 14K different. *Abdullah (2015)*.

	Simulation using CFD	Experimental work
Outdoor cabinet temperature	328K	328K
Temperature differences, K	13.5	14.15
Energy transfer, kW	-	0.5

The main issue to be addressed in the next simulation process was the effectiveness of the heat-pipes heat-exchanger and the temperature drop that the heat-pipes achieved at the end of the process when attached to a condenser of an air-cooled air conditioner. This is a unique method of pre-cooling the air intake to the condenser coil using a heat-pipes heat-exchanger in an air-cooled refrigeration system. From the simulation of a condenser and an evaporator with an attachment of a heat-pipes heat-exchanger to the air-cooled condenser, it was found that the efficiency was increased. The air-cooled condenser was recorded to reject heat at between 12K to 15K temperature difference, while with the attachment of the heat-pipes, it was found that the temperature difference could be increased to about 14K to 18K, which is a condenser operating temperature difference of 319 K (46 °C) to 305 K (32 °C). While with the evaporator, the temperature difference is in the range of 8K to 11K.

Table 5.34: The results of the simulation work for the heat-pipes heat-exchanger in assisting the pre-cooling of supplied air that passed through an air conditioning condenser. *Abdullah (2016)*.

Parameters	Case 1	Case 2	Case 3
Air Inlet Temp, K	300	300	300
Heat-pipes Evaporator Temp T_e K	295	295	295
Condensing Temp T_c K	315-319	315-319	315-319
Air Outlet Temp, K	304-307	303-304	301-305
Differential Temp, K	12-15	15-16	14-18

Table 5.35: The results of the simulation work for the heat-pipes heat-exchanger in assisting the pre-cooling of supplied air that passed through an air conditioning evaporator. *Abdullah (2016)*.

Evaporator	Case 1	Case 2	Case 3
Inlet, K	300	300	300
HP, K		295	295
Evap. T_e K	278-282	278-282	278-282
Outlet, K	293-294	294-295	290-292
Different, K	11	12	8

Three cases where heat-pipes heat-exchanger assist in lowering the temperature in the room was simulated and tested experimentally. The result of the experiment models shows an agreement to the simulations convergence result with 2 to 3 degrees' differences in temperature drop. This would be considered acceptable as the temperature of the acrylic test box was exposed to the ambient temperature. Table 5.36 shows the comparison of temperature extracted from the simulation and the results from the experimental test.

Table 5.36: The comparison of temperature difference showing the results recorded by simulations and by the experimental studies. The temperature across the heat-pipes inlet and outlet for the supplied air of between 303 K and 318 K. The higher temperature of the supplied air shows a bigger differential temperature of the heat-pipes in relation to its capability to transfer heat from the evaporator section to the condenser section.

Parameters		Temperature Difference of Supplied Air and Heat-pipes Condenser Section, K By Simulation	Temperature Difference of Supplied Air and Heat-pipes Condenser Section, K By Experiments	
Supplied Temp, K	Air	303	303	318
Case 1		10	8	7
Case 2		8	7	8
Case 3		10	9	7

5.7 ESTIMATED ENERGY SAVINGS OF THE SOLAR AIR-CONDITIONING WITH HEAT-PIPES HEAT-EXCHANGER BASED ON PSYCHROMETRIC CHART CALCULATIONS

The average temperature for all cases can be seen in Table 5.37. As most Psychrometric charts work in degrees Celsius or Fahrenheit, a table in Kelvin temperature and degrees Celsius is presented. A comparison of energy from the air temperature inlet and outlet is also included.

Table 5.37: The outlet air temperature and the average temperature of the acrylic box presented in a. K and b. °C for all cases. The temperature of 273K is taken as equal to 0°C.

	303K		318K	
	Outlet K	Ave Temp K	Outlet K	Ave Temp K
Case 1	292.96	293.15	301.34	301.71
Case 2	294.99	294.25	301.19	311.13
Case 3	295.81	294.87	300.22	301.17

a.

	30°C		45°C	
	Outlet °C	Ave Temp	Outlet	Ave Temp
Case 1	19.96	20.15	28.34	28.71
Case 2	21.99	21.25	28.19	38.13
Case 3	22.81	21.85	27.22	28.17

b.

The calculations for the energy consumption and the air properties using the application of the Psychrometric charts were performed based on the temperature result of the experimental studies. The schematic diagram of comfort cooling using a solar air conditioning system is shown in Figures 5.105 and 106. In a general solar air conditioning system, the heat from the sun radiation is converted to become electrical energy by the converter. The electricity is used to turn the compressor and fans to operate the refrigeration cycle. Temperature point 3 was the supplied air inlet to the room that the cycle had to cool down to 297 K (24°C). In this method, the supplied air at entry points 1 and 2 was assisted by the heat-pipes heat-exchanger to reduce the temperature of

the supplied air before entering point 3. Table 5.38 shows the temperature points taken to plot the charts.

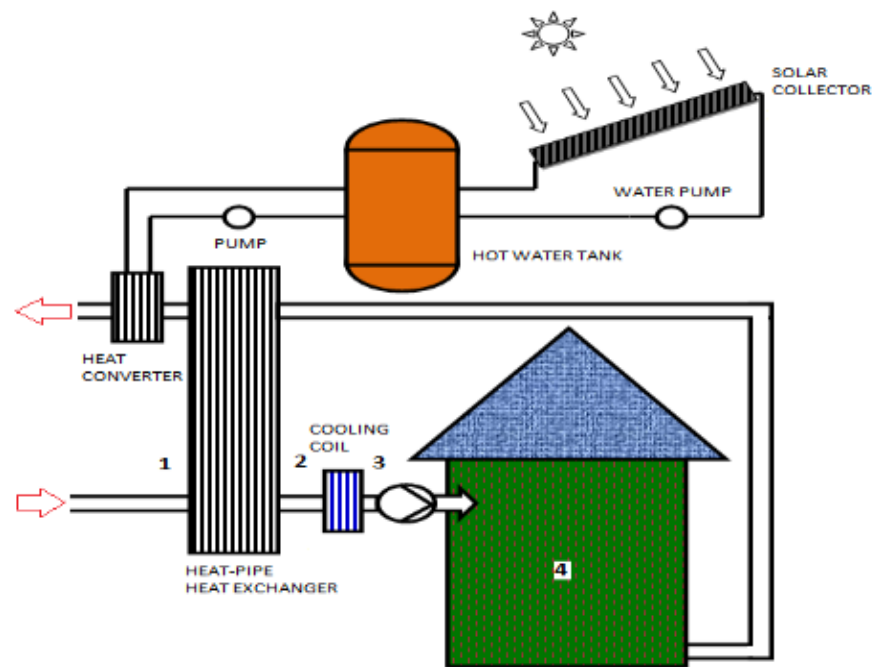


Figure 5.105: Schematic drawing of a building that uses a solar air conditioning system. A heat-pipes heat-exchanger is used as passive equipment to reduce the supplied air that enters the building.

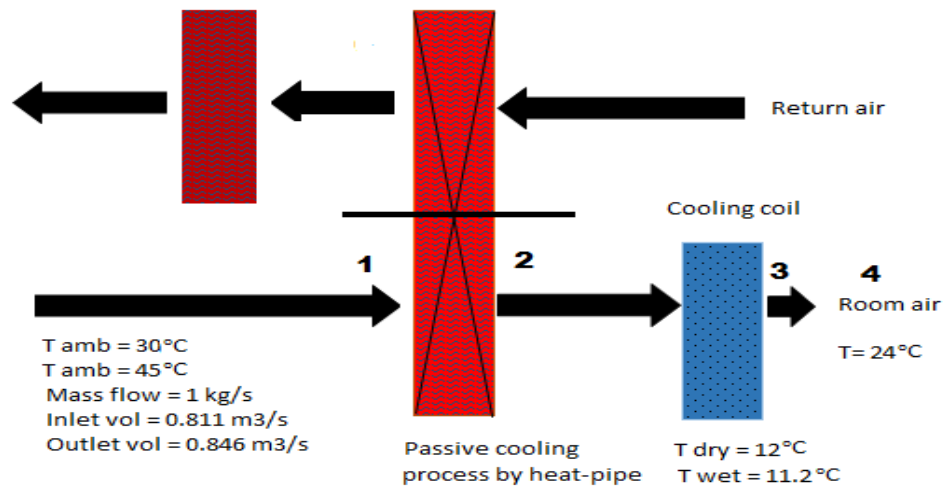


Figure 5.106: The proposed schematic process of air distribution from the ambient to the room. The heat-pipes feed the cooling coil with a lower temperature of supplied air from the outdoor ambient temperature.

Table 5.38: The air temperature properties taken for plotting the psychrometric charts. The wet-bulb result will correspond to the dry-bulb result of the room air temperature at 297 (24°C).

Parameters	Points	
	Dry bulb K/C	Wet-bulb K/C
Inlet supplied-air 303K, K/°C. Process 1	303/30	300.1/27.1
Inlet supplied-air 318K, K/°C. Process 1	318/45	303/30
Apparatus dew point temperature, K/°C. Process 2.	285/12	284.2/11.2
Comfortable room temperature, K/°C. Process 3.	297/24	289/16
Mass flow, kg/s	1.00	
Inlet volume, m ³ /s	0.811	
Outlet volume, m ³ /s	0.846	

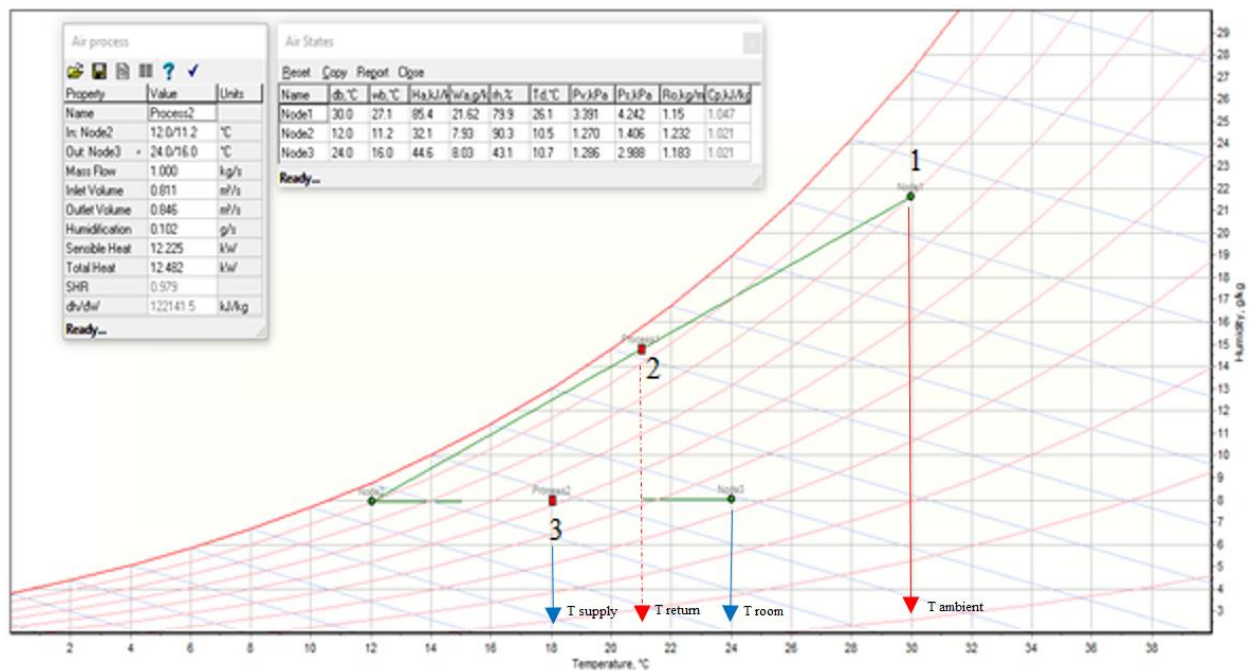


Figure 5.107: Normal solar air conditioning operating condition for a supplied-air temperature of 303 K (30°C).

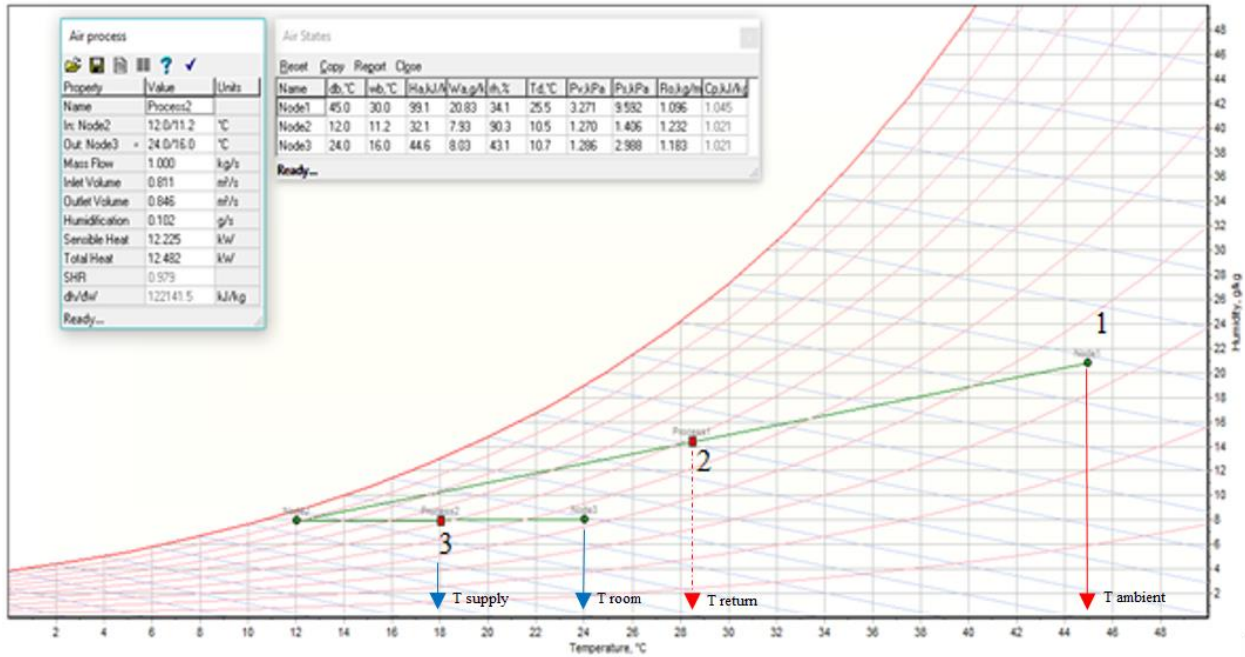


Figure 5.108: Normal air conditioning operating condition for a supplied-air temperature of 318K (45°C).

Plotted on a Psychrometric chart and using the formula below, Table 5.28 shows the air energy consumed by the air conditioning,

$$Q = \dot{m} \Delta h$$

$$\frac{\text{kJ}}{\text{s}} = \text{kW} = \frac{\text{kg}}{\text{s}} \cdot \frac{\text{kJ}}{\text{kg}}$$

where Q is the power consumed, \dot{m} are the mass flow rate (the flow rate m^3/s divided by the specific volume m^3/kg) and Δh is the enthalpy for the inlet and out air.

Table 5.39: The air temperature properties taken for plotting the psychrometric charts. The wet-bulb result will correspond to the dry-bulb result of the room air temperature.

Parameters	Power, kW
Q at 303K (30°C), kW	40.8
Q at 318K, (45°C), kW	54.5
Different, kW	13.7
Percentage, %	25

5.7.1 303K vs New Supplied Air Temperature

Figures 5.109 to 5.112 show the process of air temperature properties from the ambient to the acrylic box. A comparison between the supplied air of 303 K and the new air temperature, manipulated by the heat-pipes heat-exchanger is shown.

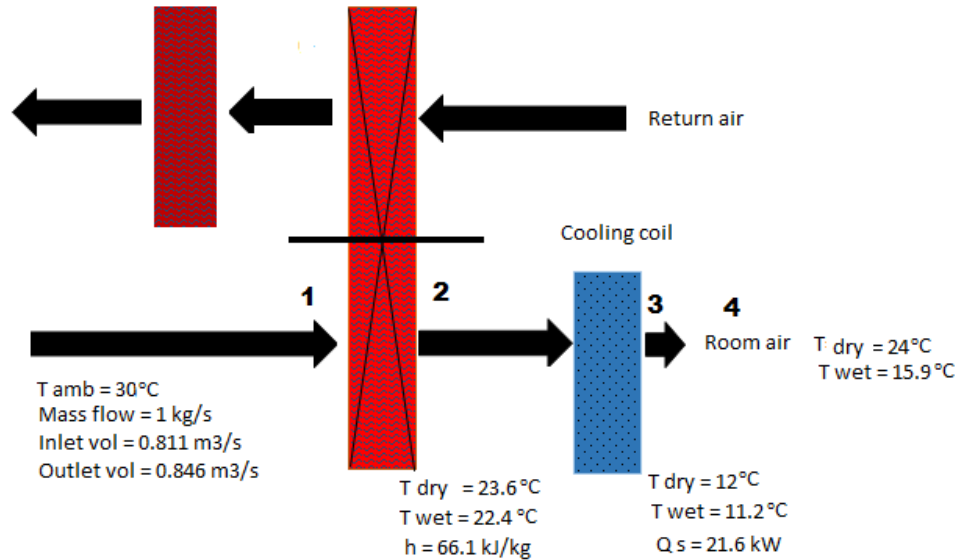


Figure 5.109: The schematic process of air distribution.

In the experiment, point 1 (supplied ambient air) and point 2 (return outlet air) was recorded. The differential temperature of the experiment revealed that the heat pipe is capable of reducing the supplied air intake into the acrylic box. The psychrometric works in degrees Celsius; thus, the results are shown in both °C and K as presented in Table 5.40.

Table 5.40: The air temperature difference recorded between the inlet and out air.

Parameters	Case 1		Case 2		Case 3	
	303K	318K	303K	318K	303K	318K
Differential Temp of Supplied and Return Air	6.4	15.44	2.92	14.12	3.85	19.23
New Supplied Air, K	296.6	302.56	300.08	303.88	299.15	298.77
New Supplied Air, °C	23.6	29.56	27.08	30.88	26.15	25.77

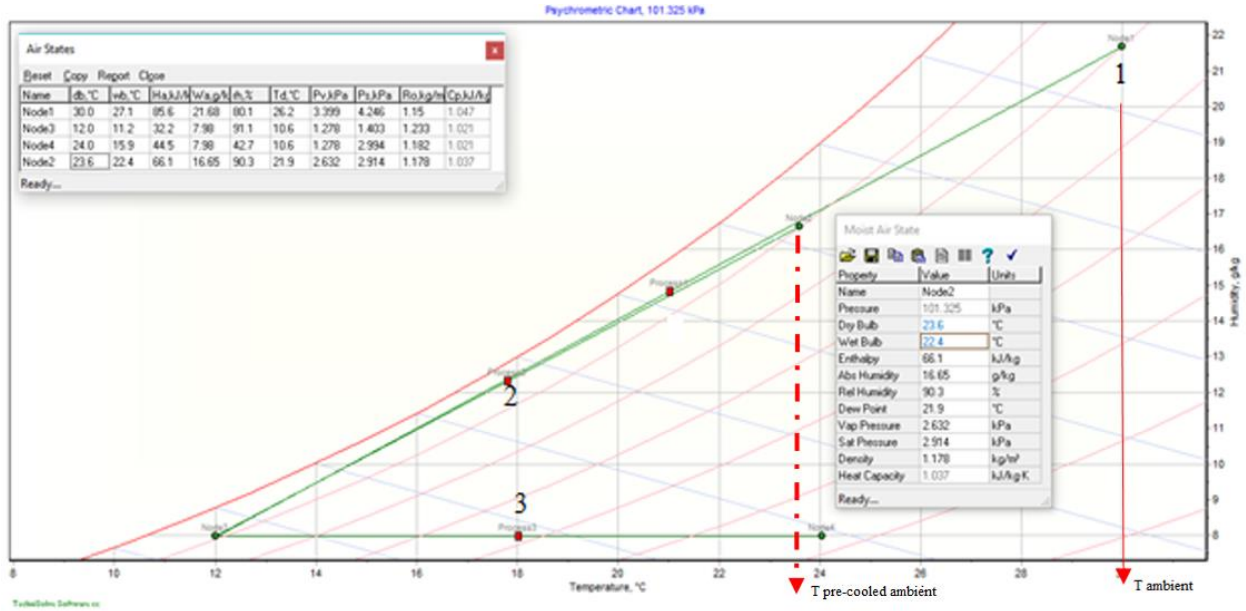


Figure 5.110: The air states comparison between 303 K and the new supplied temperature of 296.6 K (23.6°C) for Case 1. The temperature difference that the heat-pipes reduced is 6.4K.

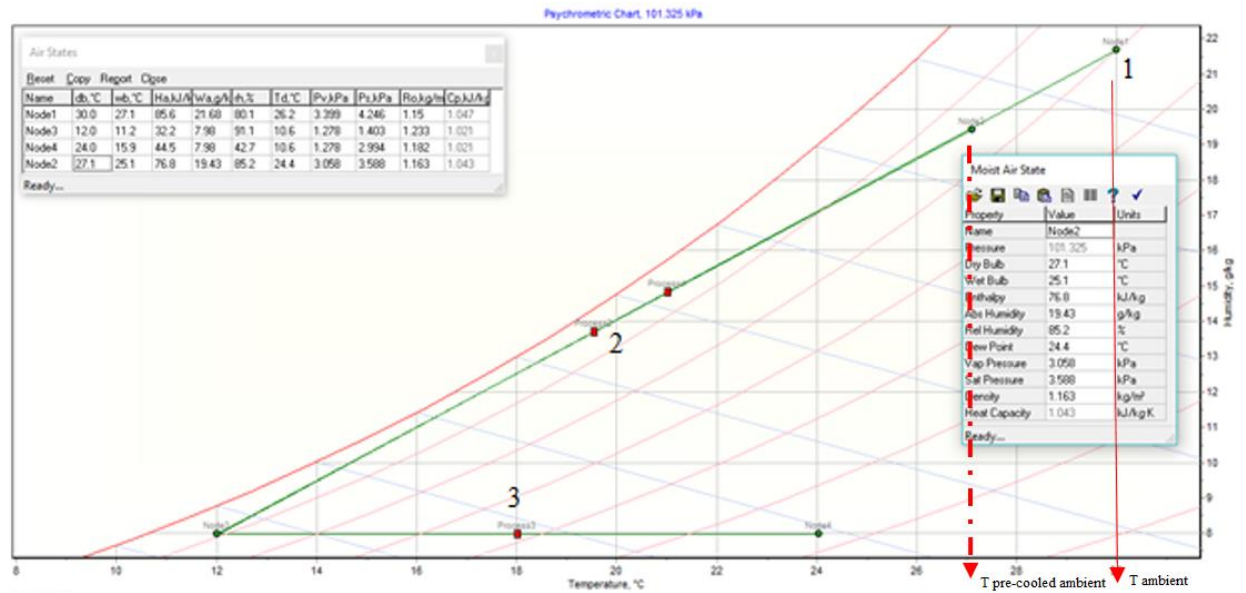


Figure 5.111: The air states comparison between 303 K and the new supplied temperature of 300.08 K (27.08°C) for Case 2. The temperature difference that the heat-pipes reduced is 2.92K.

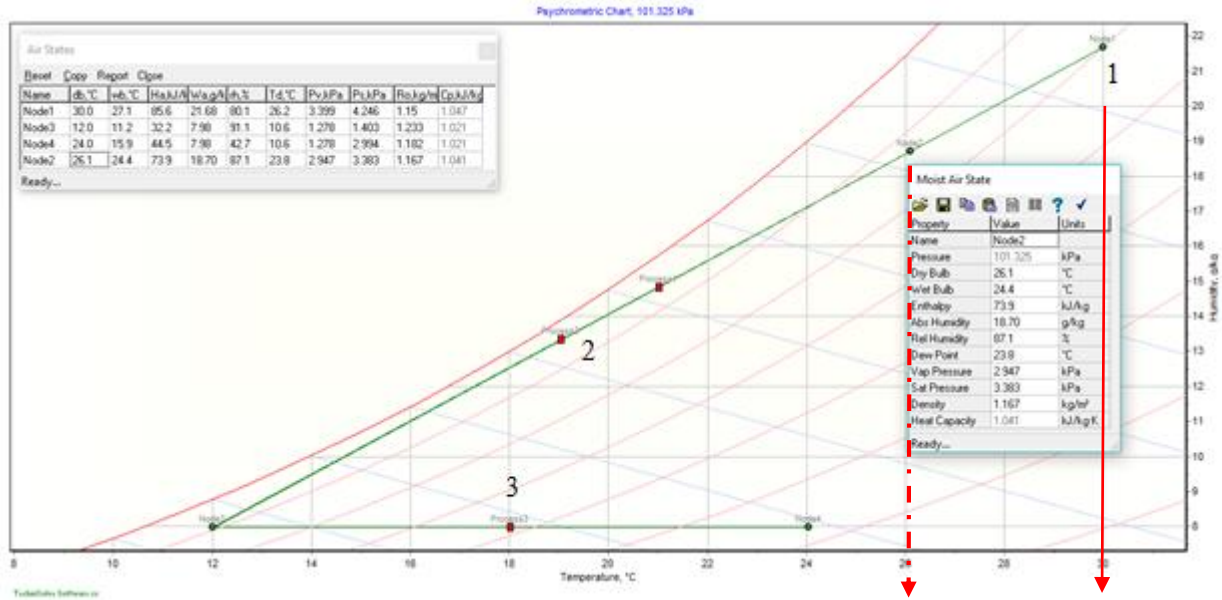


Figure 5.112: The air states comparison between 303 K and the new supplied temperature of 299.15 K (26.15°C) for Case 3. The difference temperature that the heat-pipes reduced is 3.85K.

5.7.2 318K vs New Supplied Air Temperature

Figures 5.113 to 5.115 show the process of air temperature properties from the ambient to the acrylic box. A comparison between the supplied air of 318 K and the new air temperature, manipulated by the heat-pipes heat-exchanger is shown.

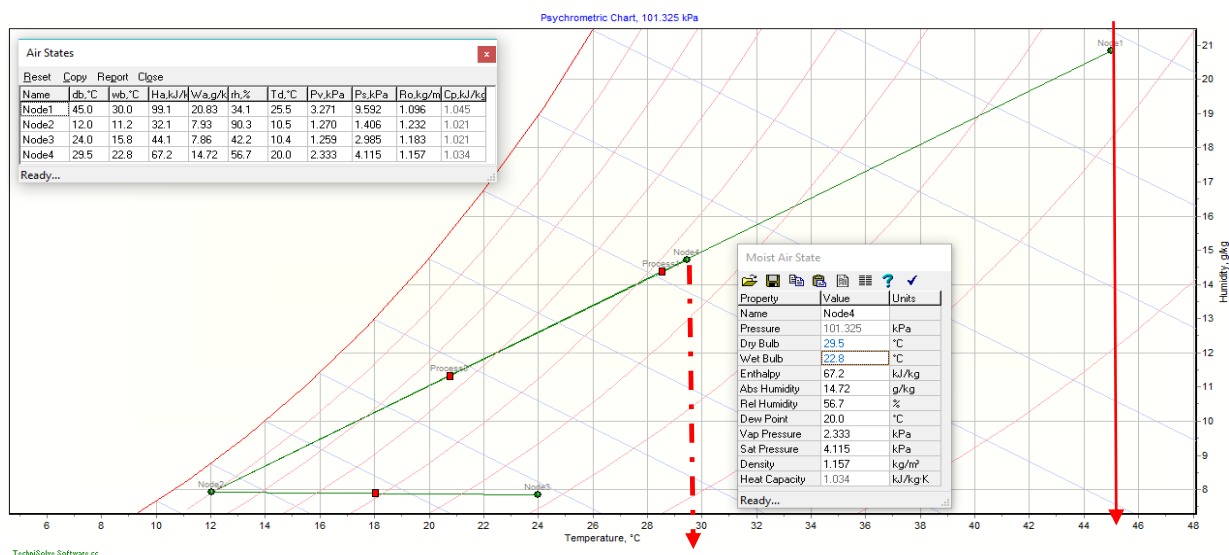


Figure 5.113: The air states comparison between 318 K and the new supplied temperature of 302.56 K (29.56°C) for Case 1. The temperature difference that the heat-pipes reduced is 15.44K.

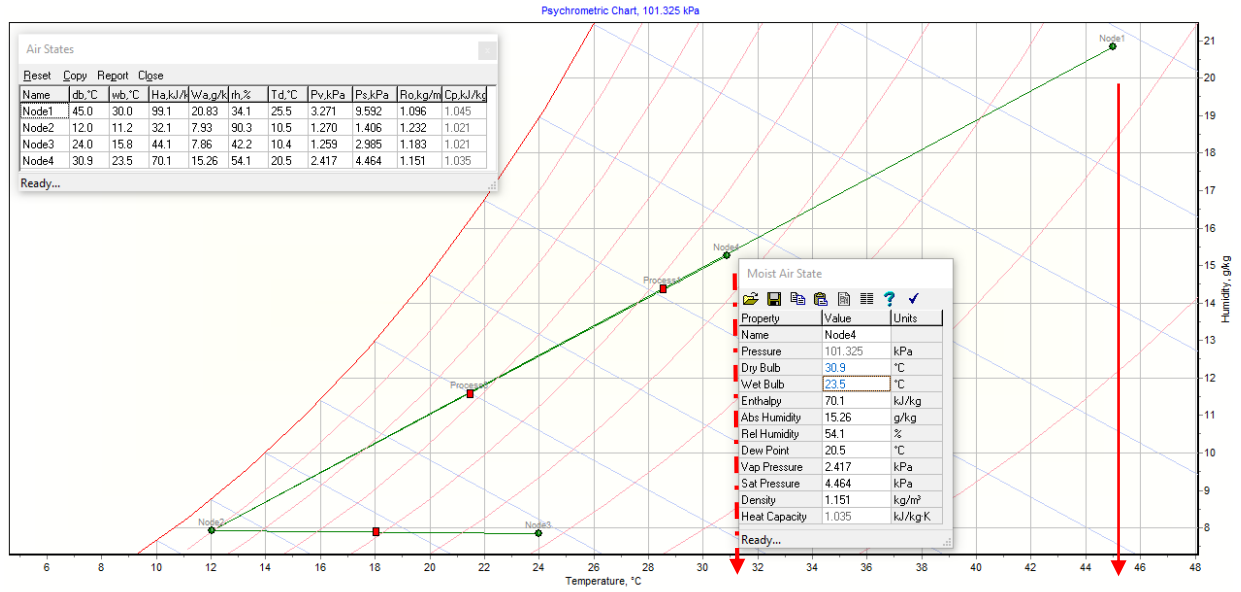


Figure 5.114: The air states comparison between 318 K and the new supplied temperature of 303.88 K (30.88°C) for Case 2. The temperature difference that the heat-pipes reduced is 14.12K.

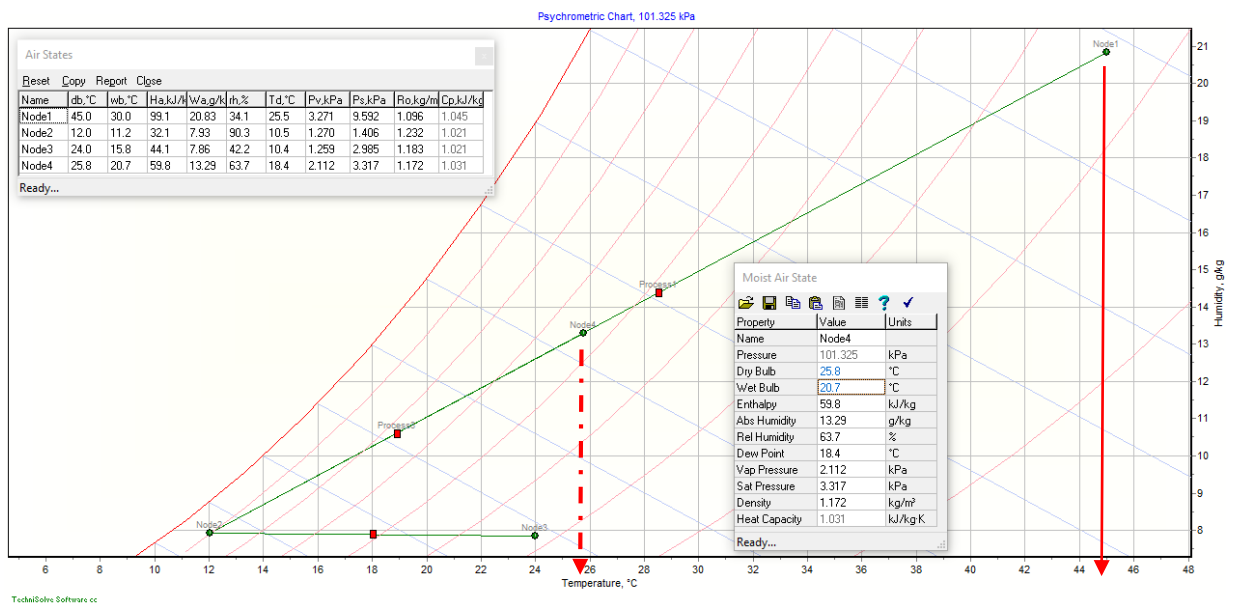


Figure 5.115: The air states comparison between 318 K and the new supplied temperature of 298.77 K (25.77°C) for Case 3. The temperature difference that the heat-pipes reduced is 19.23K.

5.7.3 Summary of the Comparison of New Supplied Air Temperature

From the processes shown in the Psychrometric chart, enthalpy can be determined, and the sensible heat can be calculated. Table 5.41 shows the air properties and the sensible heat processes

for all cases. Figure 5.116 shows the comparison of sensible heat between 303K and 318K for all cases.

Table 5.41: The air temperature properties taken for plotting the psychrometric charts for **a.** 303 K and **b.** 318 K.

Parameters		Points			
Supplied air 303K	h_i , kJ/kg	h_o , kJ/kg	Q, kW	Diff from 303K	% saving
Case 1	66.1	44.5	21.6	19.2	47
Case 2	76.8	44.5	32.3	8.5	21
Case 3	73.9	44.5	29.4	11.4	28

a.

Parameters		Points			
Supplied air 318K	h_i , kJ/kg	h_o , kJ/kg	Q, kW	Diff from 318K	% saving
Case 1	67.2	44.5	23	1.4	3
Case 2	70.1	44.5	25.9	6.4	12
Case 3	59.8	44.5	15.6	13.8	25

b.

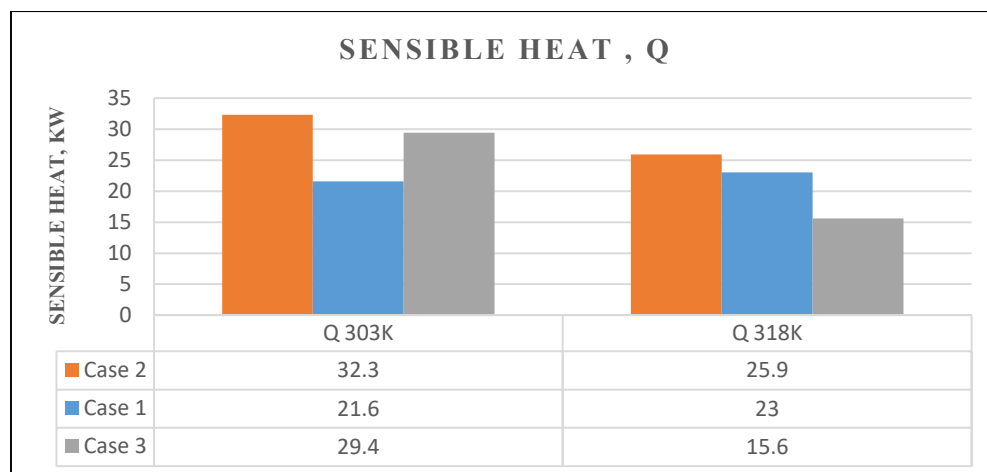


Figure 5.116: Comparison of the sensible heat between 303 K and 318 K for all cases.

5.8 SUMMARY OF THE TEMPERATURE PROFILE AND ESTIMATED ENERGY SAVINGS FOR ALL CASES

The thesis included a series of data taken from the heat-pipes heat-exchanger temperature changes in the heat transfer capability test. Three test configurations of computational fluid dynamic simulations and manual practical tests were carried out. Figure 5.117 shows the test model. Case 1 began by blowing artificial hot supplied air into an acrylic test box from the side and blowing the air to the exit on the side. Case 2 involved blowing artificial hot supplied air into an acrylic test box from the top and blowing the air exiting to the top. Meanwhile, Case 3 involved blowing artificial hot supplied air into an acrylic test box from the top and blowing the air exiting on the side.

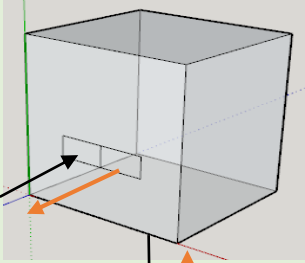
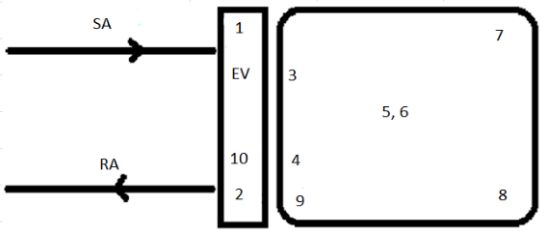
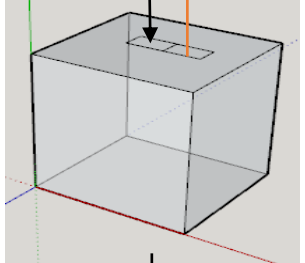
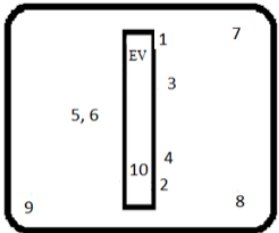
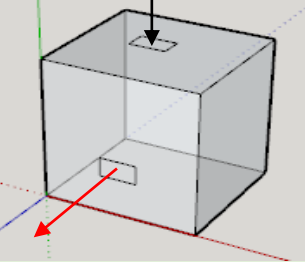
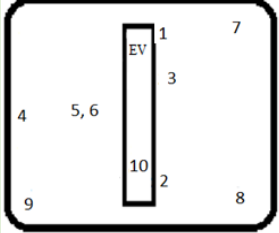
Case	Model	Parameter
Case 1		
Case 2		
Case 3		

Figure 5.117: The different air supply inlet and outlet for all cases. The parameter shows the location of thermocouples for temperature reading. *Abdullah (2018)*.

Figures 5.118 and 5.119 show the temperature graph comparison of all cases, while Tables 5.42 to 5.44 show the temperatures between the air supply, the evaporator and the condenser side of the heat-pipes, and the average box temperature that the heat-pipes can reduce from one end to the other. Table 5.45 shows the rated energy-saving as calculated from the temperature reduction achieved by the heat-pipes.

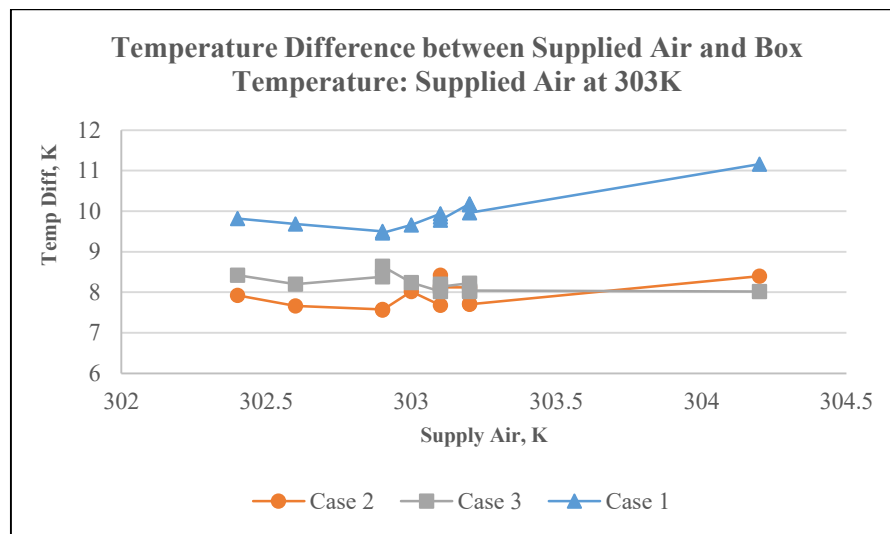


Figure 5.118: The different temperature comparison of cases, between supplied-air inlet at 303K (30°C) and the box average temperature.

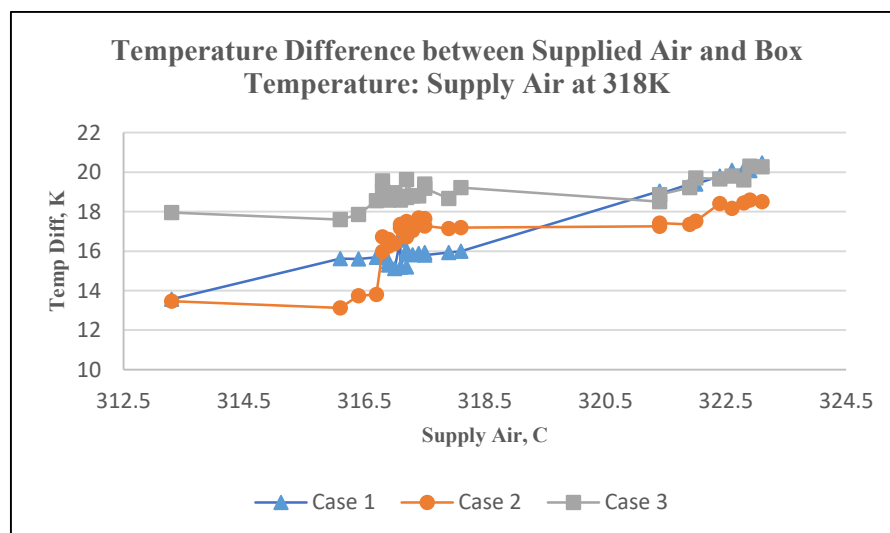


Figure 5.119: Comparison of temperature difference for all the cases between the supplied air inlet at 318 K (45°C) and the box average temperature.

Table 5.42: Case 1

Parameters	Case 1	
Supplied Air Temp, K	303	318
Heat-pipes Evaporator Section Temp K	301	332
Heat-pipes Condenser Section Temp K	295	311
Average Box Temp K	293	302
Differential Temp of Heat-pipes Evaporator and Condenser Section, K	6	21
A differential of Supplied Air Temp and Heat-pipes Condenser Section Temp, K	8	7

Table 5.43: Case 2

Parameters	Case 2	
Supplied Air Temp, K	303	318
Heat-pipes Evaporator Section Temp K	299	331
Heat-pipes Condenser Section Temp K	296	310
Average Box Temp K	294	301
Differential Temp of Heat-pipes Evaporator and Condenser Section, K	3	21
A differential of Supplied Air Temp and Heat-pipes Condenser Section Temp, K	7	8

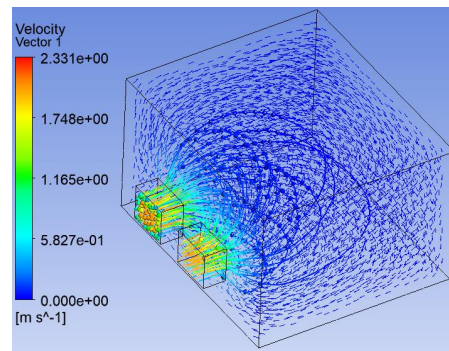
Table 5.44: Case 3

Parameters	Case 3	
Supplied Air Temp, K	303	318
Heat-pipes Evaporator Section Temp K	297	333
Heat-pipes Condenser Section Temp K	294	311
Average Box Temp K	294	301
Differential Temp of Heat-pipes Evaporator and Condenser Section, K	3	22
A differential of Supplied Air Temp and Heat-pipes Condenser Section Temp, K	9	7

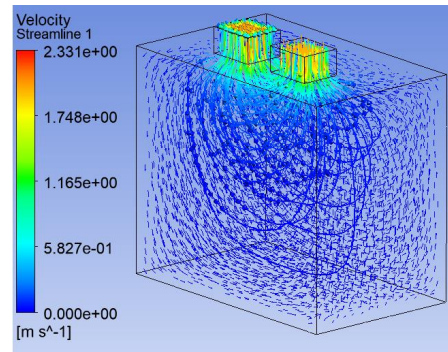
Table 5.45: Energy-saving rate for all cases

Parameters	Case 1		Case 2		Case 3	
	303K	318K	303K	318K	303K	318K
Differential Temp of Supplied Air and HP Condenser Section, K (S_A-HP_C)	8	7	7	8	9	7
Q_o , Estimated sensible cooling load, kW	0.373	0.327	0.327	0.373	0.420	0.327
Energy-saving $Q_o'-Q_o$, kW	0.93	0.47	0.47	0.93	0.140	0.47
The rate of energy-saving $(Q_o'-Q_o/Q_o') \propto, \% \times 100$	0.25	0.14	0.17	0.33	0.33	0.14

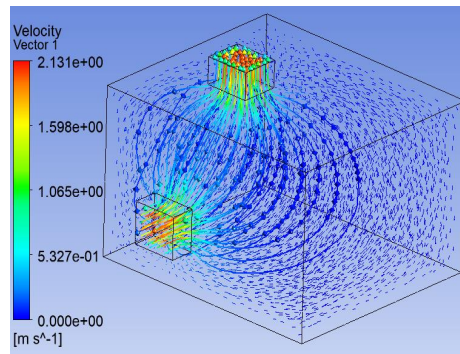
Using the Psychrometric charts, Tables 5.45 shows the energy-saving calculations based on enthalpy and the work done from the difference of temperature. Case 2 and 3 recorded the highest percentage with 33% energy-saving; however, Case 3 showed the best configuration. The air distributions for Case 1 and 2 were not scattered in the box as the opening for the supplied and exit air were adjacent to each other. The supplied air is 'short-circuited' to the exit. Figure 5.120 shows the distribution of air for all cases. The simulation process is provided in Appendix 4.



Case 1



Case 2



Case 3

Figure 5.120: Air distributions for all cases. The simulations were run by ANSYS Fluent software.

CHAPTER VI

CONCLUSION

CHAPTER OVERVIEW

This chapter concludes the discussion regarding the combination of solar energy and passive cooling equipment for comfort cooling. The primary heat-pipes heat-exchanger test was realized at the UTS workshop, while the secondary heat-pipes heat-exchanger, solar cooling and wind-assisted cooling were performed at the workshop and field area at UniKL MFI. The condition of about 308 K (35°C) with 65% relative humidity and wind speed of 5 m/s in the area was deemed suitable for the experiments. Simulation studies using CFD-ACE and ANSYS Fluent were run on laminar and RANS methods. The outdoor temperature simulated ranged from 20°C to 50°C. Based on the ASHRAE comfort cooling standards, the practical test was found to agree with the simulations. The energy savings for the overall test were found to be about 25% to 33% of the installation.

6.1 ACHIEVEMENT OF THIS RESEARCH

New and significant knowledge has been obtained to address the knowledge gap discussed in Section 2.17. In this research, simulation and experimental studies were performed. All the simulations used computational fluid dynamics CFD-ACE+ or ANSYS-Fluent and were run on laminar and Reynolds Average Navier-Stokes (RANS) conditions. In particular, the following achievements have been obtained, as presented and published in conferences and journals:

- i. The study of the natural airflow and forced ventilation, as well as wind energy from a wind turbine to a room, has been conducted. The best air inlet opening and the outlet configuration have been verified. The air distribution in the room has been studied. Papers have been presented in ERA Rank-A conferences as highlighted below:
 - American Society of Mechanical Engineers IMECE2014 Montreal, Canada. This paper discussed the natural airflow of a room through the designated opening with different

configurations and edges. The heat-pipes heat-exchanger created air density differences which increased the airflow. The case in which the inlet opening and the heat-pipes were located in the centre of the room showed the best options.

Heat pipe heat-exchanger was the main equipment used to create differences in the air density, hence increase the room inlet air temperature. Different temperatures between the inlet and the room created a flow of natural ventilation. Simulations were performed using a standard $k-\epsilon$ model from Reynolds Average Navier-Stokes (RANS) turbulence equation. The result of the velocity and flow rate distribution was determined according to the cases of opening configurations. Case 3 where the inlet opening of the heat-pipes heat-exchanger is located at the centre of the roof, shows a good option for a better flow rate if using natural ventilation. Compared to the other configurations, the opening in the centre of a roof shows better results for natural ventilation with different air densities. With natural ventilation entering from the top of a roof, Case 2 with round edges shows a greater mass flow rate than Case 1 with sharp edges opening.

- Australasian Fluid Mechanics Conference 19th AFMC2014 Melbourne, Australia. This paper discussed the driven ventilation airflow to a room through the designated opening with different configurations and edges. A cross-flow configuration where the inlet air flowed from the top edge of the room was found to be the best option.

The result of the velocity and flow rate distribution was determined according to cases of opening configurations. Case 3, with a cross-ventilation configuration where the inlet opening of the heat-pipes heat-exchanger is located at the edge of the roof, shows a good option for a better flow rate using driven ventilation. Agreement with other studies shows that cross-ventilation flow is still favourable when choosing flow ventilation.

- Journal of Advanced Manufacturing Technology, International Conference on Advanced Processes and System in Manufacturing (APSIM 2019), Malaysia. The work presented a study on a small horizontal-axis wind turbine in cooling a refrigerator as a test unit, where the available wind speed was less than 5 m/s. The wind speed data was collected in Bandar Baru Bangi, Malaysia. The wind energy from the conversion of wind turbines showed that the refrigeration cycle could be energised for up to 7 hours. From the study, despite the small amount of wind speed, it was found that the wind turbine conversion energy

was capable of running a small refrigerator chiller unit to 278 K (5 °C) with available power of 151.33 W.

- ii. The simulation and experimental studies on the heat-pipes heat exchanger have been performed in several configurations and extreme conditions. The results indicate that the heat-pipes are capable of transferring heat with only a small ambient temperature difference. In the experiments, about 3.3K to 9K of temperature difference was transferred by the heat-pipes. Straight pipe, finned heat-exchanger were used for the experiments. A refrigerant, R134a was filled in the tube and the result showed that its heat absorbing and de-sorbing capability is as expected. 4 ERA Rank-A conference papers have been published regarding the topics. The list of conferences throughout the years are as follows:

- American Society of Mechanical Engineers IMECE2015 Houston, Texas, USA. In the study, the author proposed a numerical simulation for the usage of a copper tube heat-pipes heat-exchanger in a power supply cabinet, particularly for an outdoor cabinet where the temperature inside the space of the cabinet is high. The result shows that the straight heat-pipes heat-exchanger is capable of transferring high heat from the inside of the cabinet to the outside ambient. A temperature difference of 5 K was achieved with the R134a filled heat-pipes.

The heat-pipes was proposed to be installed in an outdoor power supply cabinet as a main heat sink equipment to decrease the high temperature inside the cabinet. The different temperature and the air density between the inlet and the outlet created a flow of natural ventilation. Simulations using CFD-ACE were performed using the standard k- ϵ model from Reynolds Average Navier Stokes (RANS) turbulence equation. A small amount of air circulation can be traced inside the cabinet when the heat interacted with the evaporator side of the heat-pipes heat-exchanger. The presence of the heat pipes heat-exchanger created natural ventilation and flow inside the cabinet.

- American Society of Mechanical Engineers IMECE2016 Phoenix, Arizona, USA. The study investigated and simulated forced ventilation of air around a circular air-cooled-condenser tube for an air conditioning system. The temperature of the refrigerant in the tube was reduced at a constant pressure of 5K by the heat-pipes heat-exchanger, heat transfer exchange of ambient air and the condenser tubes.

There are possibilities of using a heat pipe heat-exchanger to lower down the ambient supply air to the condenser. From the refrigeration cycle plotted, it is found that, with the fall of condensing temperature T_c from 319K (46°C) to 305K (32°C), the evaporating capacity and the condensing capacity increased. Evaporator capacity increased to 11.2% and the condenser capacity increased to 5.6%. The power consumption of the compressor work decreased at -31% from 26.73 kJ/kg to 18.42kJ/kg. The surface temperature of the condenser is found to be lowered from 331K (58°C) to 318K (45°C) and the flash gas of the refrigerant where the liquid turns to vapour in the evaporator decreased from 15% to about 5%.

- Australasian Fluid Mechanics Conference 20th AFMC2016, Perth, Australia. The study investigated and simulated forced ventilation of air around a circular air-cooled evaporator and condenser tubes for an air conditioning system. The air gap between the heat-pipes and the air-conditioner coils was studied. The application of the heat-pipes heat-exchanger to the coils was found to increase the coils' COP to 10.5.

From the refrigeration cycle plotted, the evaporating and the condensing capacity were increased with the fall of condensing temperature T_c . The heat-pipes heat-exchanger may be used as one of the solutions to decrease the condensing temperature to the ambient.

- Australasian Fluid Mechanics Conference 21st AFMC2018, Adelaide, Australia. The experiment worked on the pre-cooling of air intake into a room to reduce the warm outside air temperature. By decreasing the air inlet temperature of the room, the work done on the evaporator cooling capacity increases. The calculation of the cooling energy consumption was found to have saved between 90 W/m³ to 273 W/m³ or about 25% to 33% of the box volume.

Simulation and experimental study on energy savings of a heat-pipes heat-exchanger ability are presented in this paper. The temperature condition is set to 303k and 318K. Simulations using CFD-ACE and ANSYS-Fluent show that the heat-pipes heat-exchanger develops a heat transfer capability of 3 to 5 K differential temperature from one end to the other end and achieved a 9K differences of the air inlet to outlet airflow. The results found that the designed fins-type heat-pipes heat-exchanger is capable to lower the heat to 293K and with an optimum application could save 33% of energy consumption. Between 327W and 420W of sensible heat gain had been determined and

an energy-saving between 93W to 140W had been achieved from the studies. Passively cooling, for equipment that did not require any energy sources, the heat-pipes heat-exchanger could perform an influential role for energy-saving applications. Outdoor high ambient temperature appliances where cooling maintenance is limited are the best suit for this application.

iii. Solar energy is capable of maintaining comfort cooling. In a hot ambient temperature where the solar radiation is high, solar energy works well in operating a refrigeration cycle. Simulation and experimental studies were performed in Malaysia where the ambient is hot and humid all year long, including simulations using SOLARGIS. The experimental test showed that about 31% of electrical energy could be saved by applying solar PV panels to the cooling cycle. A peer-reviewed journal paper regarding solar cooling was presented at:

- Journal of Advanced Manufacturing Technology, International Conference on Advanced Processes and System in Manufacturing (APSIM 2019), Malaysia. The study on solar radiation and energy-saving found that the energy supplied by solar radiation from a photovoltaic panel successfully operated a small refrigerator to the desired cooling of 278K (5 °C). The calculations showed that the solar power from the plate collectors could produce 470.3 kWh annually, assisting the 0.9 kW/day power consumption of a small domestic refrigerator. As the refrigerator required 324 kWh annually, energy savings could be achieved through the use of solar power.

6.2 SUGGESTIONS

In general, the hybrid solar air conditioning-heat-pipes heat-exchanger experiment is intended both to upgrade and challenge the cooling industry by offering energy-saving equipment while still meeting comfort cooling standards. The use of solar cooling helps reduce electrical consumption and assists in electrical grid supply as the heat-pipes heat-exchanger reduces the ambient air temperature without any energy sources.

The study used R134a as the refrigerant medium; however, with its small heat transfer coefficient, a big volume of refrigerant is required to transfer heat from the evaporator section to the condenser section. The tubes of the heat-pipes, then, ought to be bigger to accommodate the

refrigerant. Other simulations and experiments using a different refrigerant medium in the heat-pipes heat-exchanger and an actual room with a hot ambient temperature should be tested. A comparison with the normal hollowed-section copper tube for heat-pipes showed that the groove-structured tube for heat-pipes heat-exchanger performed better at 33 % energy-saving. As the heat-pipes have the capability of '*extreme fast heat transfer*' between the tube section ends, the heat-pipes application is best for pre-cooling of spaces when coupled with cooling coils such as data centre, dehumidification and energy recovery area as the experimental study results suggested.

An experiment with an actual situation such as a designed room placed in an artificially high ambient temperature condition ranging from 40°C to 50°C can be conducted, as the capability of the solar heat-pipes heat-exchanger and other hybrid systems can be tested. Some future work on a hybrid system to increase energy reduction as listed below can be considered:

- Solar collection for electrical energy conversion using various collectors such as vacuum tubes increases the COP of the system while keeping the environment clean.
- Upgrading of the heat-pipes heat-exchanger design to increase the component performance and the system performance as a whole.
- Waste energy usage of a vapour compression system that reduces electrical consumption.
- A room in an actual high ambient temperature environment such as an artificial desert condition should be built to test the hybrid solar cooling heat-pipes heat-exchanger and other humidification/dehumidification components to show its effectiveness.

6.2.1 Drawbacks

The drawbacks of the applications of a heat-pipes heat-exchanger include its bulky dimension and the refrigerant medium to allow for optimum heat transfer processes from the evaporator to the condenser side. A low-temperature refrigerant has not been fully tested in the

context of a heat-pipes heat-exchanger, and the heat transfer surface area of the tube must be considered when dimensioning the coils.

6.2.2 Application to the UTS HVAC System

A continuous study of the UTS HVAC system is proposed in Figure 6.1. The heat-pipes heat-exchanger can be embedded to assist in the cooling and heating of the supply/return air into the building. The treated air will supply the displacement ventilation and the Central Thermal Plant as well as make use of the PV panels. As the building accommodates research staff and students and runs 24/7 for nearly the entire year, even a slightly reduced power consumption of the space condition will make a great impact. Figures 6.2 to 6.4 show the installations of solar panels and wind turbines at the University of Technology Sydney.

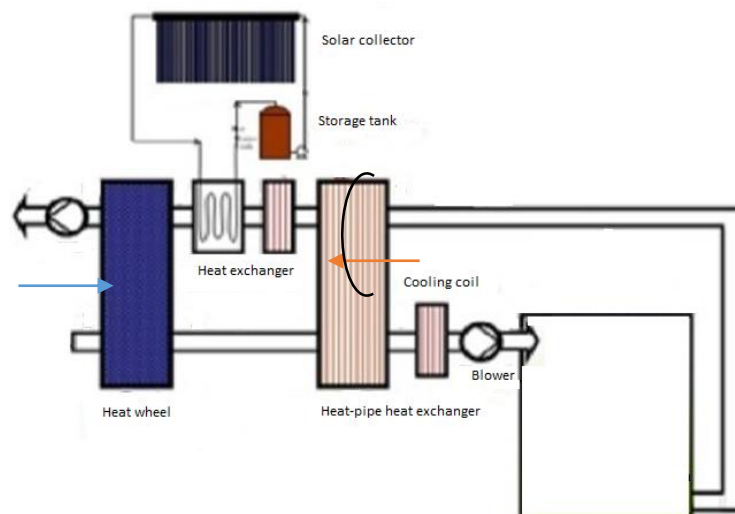


Figure 6.1: A proposed schematic drawing to upgrade the HVAC system embedded with a hybrid system to Building 11 at the University of Technology, Sydney. *UTS Building 11.*



Figure 6.2: The plant room with the Organic Rankine Cycle (ORC) in Building 11 University of Technology Sydney. *UTS Building 11.*



Figure 6.3: The fluid thermal expansion system in Building 11 University of Technology Sydney. *UTS Building 11.*



Figure 6.4: The PV panels and the wind turbine on the rooftop of Building 11, University of Technology Sydney. *UTS Building 11.*

REFERENCES

- Abou-Ziyan, H.Z., Helali, A., Fatouh, M., Abo El-Nasr, M.M. (2001). Performance of a Stationary and Vibrated Thermosyphon Working with Water and R-134a. *Applied Thermal Energy*, 21, 813–830.
- Akbari, H., Kurn, D., Bretz, S., Hanford, J. (1997). Peak Power and Cooling Energy-savings of Shade Trees. *Energy and Buildings* 25, 139–148.
- Akbari, H., Taha, H. (1992). The Impact of Trees and White Surfaces on Residential Heating and Cooling Energy Use in Four Canadian Cities. *Energy* 17: 141–150.
- Alario, J., Haslett, R., and Kosson, R., (1982). The Monogroove High-Performance Heat Pipe. *Progress in Astronautics and Aeronautics*, 83, 305-324.
- Anderson, W. G., and Tarau, C., (2008). Variable Conductance Heat-pipes for Radioisotope Stirling Systems. *Proceedings of STAIF*, 969, 679-688.
- A. Khalid., (2007). *Hybrid Desiccant Cooling System for Hot Regions, Alternative Space Cooling System*, LAP Lambert Academic Publishing.
- Argiriou A.A., Balaras C.A., Kontoyiannidis S., Michel E. (2005). Numerical Simulation and Performance Assessment of a Low Capacity Solar Assisted Absorption Heat Pump Coupled with A Sub-Floor System. *Solar Energy*, 79, 290–301.
- ASHRAE Fundamentals Handbook. (1989). *Ventilation for Acceptable Indoor Air Quality*. American Society of Heating, Refrigeration and Air Conditioning Engineers. GA, USA.
- ASHRAE Standard. (2001). *Ventilation for Acceptable Indoor Air Quality*. American Society of Heating, Refrigerating and Air-Conditioning Engineers. GA, USA.
- ASHRAE, ANSI/ASHRAE Standard 55. (2004). *Thermal Environment Conditions for Human Occupancy*. American Society of Heating, Ventilating and Air-Conditioning Engineers, GA, USA.

- Assilzadeh F., Kalogirou S.A., Alia Y., Sopian K. (2005). Simulation and Optimization of a Libr Solar Absorption Cooling System with Evacuated Tube Collectors. *Renewable Energy*, 30, 1143–59.
- Atkins C., (2007). *All in the Mind*. Essential Matters.
- Avara, A. & E. Daneshgar. (2008). Optimum Placement of Condensing Units of Split-Type Air Conditioning by Numerical Simulation, *Energy and Building*, 40, 1268-1272
- B. P. Huynh. (2012). Natural-Ventilation Flow in A 3-D Room Fitted with Solar Chimney. *International Mechanical Engineering Congress & Exposition, Texas, USA*.
- B. Zohuri. (2011). *Heat Pipe Design and Technology, A Practical Approach*, CRC Press.
- Ballaney, P. L. (2005). *Refrigeration and Air Conditioning: In S.I. Units*. Air Conditioning Refrigeration and Refrigerating Machinery.
- Bangalee, M.Z.I., Miao, J.J., Lin, S.Y., and Yang, J.H. (2013). Flow Visualization, PIV Measurement and CFD Calculation for Fluid-Driven Natural Cross-Ventilation in a Scale Model, *Energy and Buildings*, 66, 306-314.
- Beckert, K Herwig, H. (1996). Inclined Air to Air Heat-exchanger s with Heat-pipes: Comparing Experimental Data with Theoretical Results, *Intersociety Energy Conversion Engineering Conference 2 1441-1446*
- Bencheikh, H., Daoudji, Y. (2018). Numerical Investigation of a Coupled Passive Cooling System Earth to Air Heat Exchange and Solar Chimney in Hot Arid Zone. *Innov Ener Res 7: 188*. doi: 10.4172/2576-1463.1000188
- Best, R., Ortega, N. (1998). Solar Refrigeration and Cooling. *Renewable Energy Congress V*, 685-690.
- Betz, A. (1994). Wind energy and its extraction through windmills. The fundamental formula for estimating the maximum power and efficiency of wind machines. *Wind-energie und ihre ausnutzung durch windmühlen, bandenhoek & ruprect, Göttingen, 1926. Facsimile edition by Ökobuch Verlag, Staufen, 1994. ISBN 3-922964-11-7*.
- Brooke, T. (2007). *Optimizing Wrap-Around Heat-pipes*. Heat Pipe Technology.

- Cengel, Y.A. (1998). *Heat Transfer: A Practical Approach*. New York: The McGraw-Hill Companies, Inc.
- Charoensawan P., Terdtoon P. (2008). Thermal Performance of Horizontal Closed-Loop Oscillating Heat Pipe. *Applied Thermal Engineering* 28 460-466
- Chi, S. W. (1976). *Heat Pipe Theory and Practice*. Hemisphere Publishing Corporation, Washington, DC.
- Cotter, T. P. (1965). *Theory of Heat-pipes*. Los Alamos Scientific Laboratory Report No. LA-3246-MS.
- Critoph, R.E. (2002). Carbon–Ammonia Systems – Previous Experience, Current Projects and Challenges for the Future. *Proceedings of International Sorption Heat Pump Conference, Shanghai, China*.
- de Dear, R.J., & Brager, G.S. (2002). Thermal Comfort in Naturally Ventilated Buildings: Revisions to ASHRAE Standard 55. *Energy and Buildings*, 34, (6), 549-561.
- Demira, H., Mobedi, M. Ulku, S. (2007). A Review on Adsorption Heat Pump: Problems and Solutions. *Renewable and Sustainable Energy Reviews*, 12, 2381–2403.
- Dossat, R. J. & Horan, T. J. (2001). *Principles of Refrigeration, Fourth Edition*. Prentice-Hall Publication.
- Douglas Kosar. (2006). Dehumidification System Enhancements. *ASHRAE Journal* 48.
- Duff, W.S., Winston, R., O’Gallagher, J.J., Bergquam, J., Henkel, T. (2004). Performance of The Sacramento Demonstration ICPC Collector and Double Effect Chiller. *Solar Energy* 76, 175–180.
- Duffie, J.A. & Beckman, W.A. (1991). *Solar Engineering of Thermal Processes. 2nd Edition*. John Wiley & Sons, Inc.
- Ehsan Firouzfard, & Maryam Attaran. (2008). A Review of Heat Pipe Heat-exchanger s Activity in Asia. *World Academy of Science, Engineering and Technology International Journal of Chemical, Nuclear, Materials and Metallurgical Engineering*, 2:11.

- El-Genk, M. S., and Huang, L. (1993). An Experimental Investigation of the Transient Response of a Water Heat Pipe. *International Journal of Heat and Mass Transfer*, 36(15), 3823-3830.
- ESDU, (1979). *Heat-pipes Performance of Capillary Driven Designs. Data Item No 79013*. ESDU International Plc, London.
- Evola, G., and Popov, V. (2006). Computational Analysis of Wind-Driven Natural Ventilation in Building. *Energy and Buildings*, 38, (5), 491-501
- Faghri, A. (1995). *Heat Pipe Science and Technology, 1st Ed.* Taylor & Francis, Washington, D.C.
- Faghri, A., and Thomas, S. (1989). Performance Characteristics of a Concentric Annular Heat Pipe: Part I-Experimental Prediction and Analysis of the Capillary Limit. *Journal of Heat Transfer*, 111 (1-4). 844-850.
- Faghri, A. (2014). Heat-pipes: Review, Opportunities and Challenges. *Frontiers in Heat-pipes (FHP)*, 5, 1
- Farber E.A., Flanigan F.M., Lopez L., Polifka R.W. (1996). Operation and Performance of the University of Florida Solar Air-Conditioning System. *Solar Energy*, 10, 91–5.
- Garg, H. P. & Datta, G. (1984). The Top Loss Calculation of Flat Plate Solar Collectors. *Solar Energy* 32, 141-143.
- Gaugler, R. (1944). *Heat Transfer Device*. U.S. Patent No. 2350348
- Grenier, Ph., Guilleminot, J.J., Meunier, F., Pons, M. (1988) Solar Powered Solid Adsorption Cold Store. *Journal of Solar Energy Engineering*, 110, 192–197.
- H. Xue, B. Xu, J. Wu, Y. Wei. (2007). Prediction of Temperature Rise Near Condensing Units in the Confined Space of a High-Rise Building, *Building and Environment*, 42, 2480–2487.
- Hewett, R. (1995). Solar Absorption Cooling: An Innovative Use of Solar Energy. *AIChE Symposium Series 91*, 306, 291–299.
- Hildbrand, C., Dind, Ph., Pons, M., Buchter, F. (2004). A New Solar-Powered Adsorption Refrigerator with High Performance. *Solar Energy*, 77, 311–318.

- Henning, H. M. (2007). Solar Assisted Air Conditioning of Buildings-An Overview. *Applied Thermal Engineering*, 27, 1734-1749.
- Hoefker, G. (2001). *Desiccant Cooling with Solar Energy*. Thesis Dr Fal, University of De Montforte, UK.
- Hunt, G.R., and Linden, P.P. (1999). The Fluid Mechanics of Natural Ventilation Displacement Ventilation by Buoyancy-Driven Flows Assisted by Wind. *Building and Environment*, 34, (6), 707-720.
- Huynh, B.P. (2012). Natural-Ventilation Flow in a 3-D Room Fitted with Solar Chimney. *International Mechanical Engineering Congress & Exposition, Houston, Texas, USA*
- Idris, A. (2013). Computational Study of Single-Sided Ventilation Through A 3-Dimensional Room with Rounded Edges, *International Mechanical Engineering Congress & Exposition, San Diego, USA*
- Jamaluddin, A.A., Hussein, H., Mohd Ariffin, A.R., and Keumala, N. (2014). A Study On Different Natural Ventilation Approaches at A Residential College Building with The Internal Courtyard Arrangement. *Energy and Buildings*, 72, 340-352
- Jouhara, H., and Robinson, A. J. (2009). An Experimental Study of Small-Diameter Wickless Heat-pipes Operating in the Temperature Range 200°C to 450°C. *Heat Transfer Engineering*, 30(13), 1041-1048.
- Jouhara, H., Meskimmon, R. (2010). Experimental Investigation of Wraparound Loop Heat Pipe Heat-exchanger Used in Energy Efficient Air Handling Units. *Energy*, 35, 4592-4599.
- Jurinak & Mitchell, J. W. (1984). Open Cycle Desiccant Cooling Air Conditioning as an Alternative to Vapour Compression Cooling in Residential. *Solar Engineering 106*: 252–260
- Kalogirou, S.A. (1996). Economic Analysis of Solar Energy System Using Spreadsheets. *Proceeding of The Fourth World Renewable Energy Congress. Denver, Colorado 2*: 1303-1307.

- Kapur J.C. A (1960). Report on the Utilization of Solar Energy for Refrigeration and Air Conditioning Application. *Solar Energy*, 4, 39–47.
- Kefti O., Merzouk M., Merzouk N. K., El Metenan S. (2015). Performance of a Single Effect Solar Absorption Cooling System (Libr-H₂O). *International Conference on Technologies and Materials for Renewable Energy, Environment and Sustainability, TMREES15*.
- Khalkhali, H., Faghri, A., and Zuo, Z. J. (1999). Entropy Generation in a Heat Pipe System. *Applied Thermal Engineering*, 19(10), 1027-1043.
- Kempers, R., Robinson, A. J., Ewing, D., and Ching, C. Y. (2008), Characterization of Evaporator and Condenser Thermal Resistances of a Screen Mesh Wicked Heat Pipe. *International Journal of Heat and Mass Transfer*, 51 (25-26), 6039-6046.
- Kulkarni, P.P. (1994). Solar Absorption Cooling for Demand-Side Management. *Energy Engineering* 91 (5), 29–39.
- Lee, Y., Mital, U. (1972). A Two-Phase Closed Thermosyphon. *International Journal of Heat Mass Transfer*, 1972, 15, 1695 –1770.
- Marongiu, M.J. et al. (1998). Design and Development of a Passively Cooled Remote Outdoor Cabinet. *Twentieth International Telecommunications Energy Conference*, 568-575.
- Maydanik, Y. F., Ferchtater, Y. G., and Goncharov, K. A. (1991). Capillary Pump Loop for the systems of Thermal Regulation of Spacecraft. *4th European Symposium on Space Environment and Control Systems, ESA SP-324. Florence, Italy*.
- Mazzei, P., Minichiello, F. & Palma. (2002). Desiccant HVAC System for Commercial Buildings. *Applied Thermal Engineering* 22, 545-560.
- Meunir F., Mugnier D., (2013). *La Climatisation Solaire, Thermique ou Photovoltaïque*, Dunod, Paris.
- Ming Qu, Hongxi Yin, David H. Archer. (2010). A Solar Thermal Cooling and Heating System for A Building: Experimental and Model-Based Performance Analysis and Design, *Solar Energy*, 84, 166–182.
- M. Y. Othman. (2002). *Teknologi Tenaga Suria*. Universiti Kebangsaan Malaysia (UKM).

- Nicol, J.F., and Humphreys, M.A. (2002). Adaptive Thermal Comfort and Sustainable Thermal Standards for Buildings. *Energy and Buildings*, 34, (6), 563-572.
- Niu, J. L., Zhang, L. Z., & Zuo, H. G. (2002). Energy-saving Potential of Chilled-Ceiling Combined with Desiccant Cooling in Not and Humid Climates. *Energy Building 14*: 487-495.
- Ong, K.S., and Haider-E-Alahi, M. (2003). Performance of a R-134a-Filled Thermosyphon. *Applied Thermal Engineering*, 23, (18), 2373-2381.
- P. F. Linden. (1999). The Fluid Mechanics of Natural Ventilation. *Annual Rev. Fluid Mechanic*, 31, 201-238.
- Plesch, D., Bier, W., Seidel, D., and Schubert, K., (1991). Miniature Heat-pipes for Heat Removal from Microelectronic Circuits. *Proceedings of the ASME Winter Annual Meeting, Atlanta, GA*.
- Pons, M., Guilleminot, J.J. (1986). Design of Experimental Solar-Powered, Solid-Adsorption Ice Maker. *Journal of Solar Energy Engineering*, 108, 332–337.
- Priyadumkol, J., and Kittichaikarn, C. (2014). Application of the Combined Air-Conditioning Systems for Energy Conservation in Data Center. *Energy and Buildings*, 68, Part A, 580-586.
- Qu, M., Yin, H., Archer, D.H. (2010). A Solar Thermal Cooling and Heating System for a Building: Experimental and Model-Based Performance Analysis and Design. *Solar Energy*, 84, 166–182.
- Reader, G.T., Hooper, C., (1983). *Stirling Engines*. Cambridge University Press, London.
- R. Opoku, K. Mensah-Darkwa, A. Samed Muntaka., (2018). Techno-Economic Analysis of a Hybrid Solar PV-Grid Powered Air-Conditioner for Daytime Office Use in Hot-Humid Climates – A Case Study in Kumasi City, Ghana. *Solar Energy*, Vol.165, 65-174.
- Rosler, S., Groll, M., Supper, W., and Konev, S., (1987). Analysis and Experimental Investigation of a Cryogenic Methane Heat Pipe, *Proceedings of the 6th International Heat Pipe Conference, Grenoble, France*, 219-222.

- Roucoult, J.M., Douzane. & O. Langlet, T. (1999). Incorporation of Thermal Inertia in The Aim of Installing a Natural Night Time Ventilation System in Buildings. *Energy & Buildings* 29(2), 129-133.
- Saba, A.S., Sohif, M. Sopian, K., Saleh, E., Alkhair, M. (2014). “Simulation analysis of Venturi-Vertical Axis Wind Turbine (V-VAWT)”, *8th International Conference on Renewable Energy Sources*, 25.
- Sauciuc, I., Akbarzadeh, A., Johnson, P. (1995). Characteristics of A Two-Phase Closed Thermosyphon for Medium Temperature Heat Recovery Applications. *Heat Recovery Systems & CHP*, 14 (7), 631–640.
- Savino, R., Piccolo, C., Fortezza, R., Abe, Y. (2007). Heat-pipes with Self-Rewetting Fluids under Low-Gravity Conditions. *International Conference on Two-Phase System for Ground and Space Applications, Kyoto, Japan*.
- Sayegh, M. A. (2007). The Solar Contribution to Air Conditioning Systems for Residential Buildings. *Desalination*, 209, 171–176
- Seppanen, O., Fisk, W. J., Mendell, M. J. (2002). Ventilation Rates and Health.
- Serageldin, A.A., Abdelrahman, A. K., Shinichi, O. (2018). Parametric Study and Optimization of a Solar Chimney Passive Ventilation System Coupled with an Earth-to-Air Heat Exchanger. *Sustainable Energy Technologies and Assessments* 30 (2018), 263-278.
- Shamsuddin, A. H. (2012). Development of renewable energy in Malaysia strategic initiatives for carbon reduction in the power generation sector. *Procedia Engineering*, 384 – 391.
- Shaw, M, R., Treadaway, K. W. & Willis, S. T. P. (1994). Effective Use of Building Mass. *Renewable Energy* 5(8), 1028-1038.
- Shiraishi, M., Kikuchi, K., Yamanishi, T. (1981). Investigation of Heat Transfer Characteristics of a Two-Phase Closed Thermosyphon. *Heat Recovery Systems & CHP*, 1, 287–297.
- Solar Thermal Systems and Components, Southern African Solar Thermal Training and Demonstration Initiative, Project 2608-00/2009, *AEE-Institute for Sustainable Technologies*.

- Stoecker, W. F. & Jones, J. W. (1982). Refrigeration and Air Conditioning, Second Edition, *McGraw-Hill, New York, NY*.
- Su, X., Zhang, X., and Gao, J. (2009). Evaluation Method of Natural Ventilation System Based On Thermal Comfort in China. *Energy and Buildings, 41, (1), 67-70*
- Sukhamte, S.P. (2002). Solar Energy Principles of Thermal Collector and Storage 2nd Edition *New Delhi, Tata McGraw-Hill*.
- Sumathy K., Li, Z. F. (1999). A Solar-Powered Ice Maker with the Solid Adsorption Pair of Activated Carbon and Methanol. *International Journal of Energy Research, 23, 517-27*.
- Syeda A., Izquierdod M., Rodriguez P., Maidment G., Missenden J., Lecuona A. et al. (2005). A Novel Experimental Investigation of a Solar Cooling System in Madrid. *International Journal of Refrigeration, 28, 859–71*.
- T. Kivva, B.P. Huynh, M. Gaston, D. Munn. (2009). A Numerical Study of Ventilation Flow Through A 3-Dimensional Room with a Fan. *Turbulence, Heat and Mass Transfer 6*.
- T.T. Chow, Z. Lin, J.P. Liu. (2002). Effect of Condensing Unit Layout at Building Re-Entrant on Split-Type Air-Conditioner Performance. *Energy and Buildings, 34, 237–244*.
- T.T. Chow, Z. Lin, X.Y. Yang. (2002). Placement of Condensing Units of Split-Type Air-Conditioners at Low-Rise Residences. *Applied Thermal Engineering, 22, 1431–1444*.
- T.T. Chow, Z. Lin. (1999). Prediction of On-Coil Temperature of Condensers Installed at Tall Building Re-Entrant. *Applied Thermal Engineering, 19, 117–132*.
- Tournier, J. M., and El-Genk, M. S. (2003). Start-up of a Horizontal Lithium Molybdenum Heat Pipe from a Frozen State. *International Journal of Heat and Mass Transfer, 46(4), 671-685*.
- Trefethen, L. (1962). On The Surface Tension Pumping of Liquids or A Possible Role of the Candlewick in Space Exploration. *G.E. Tech. Info., Serial No. 615 D114*.
- van Hooff, T., and Blocken, B. (2013). CFD Evaluation of Natural Ventilation of Indoor Environments by the Concentration Decay Method: CO₂ Gas Dispersion from a Semi-Enclosed Stadium. *Building and Environment, 61, (0), 1-17*

- Vieira da Cunha, A. F., and Mantelli, M. H. (2009), Analytical and Experimental Analysis of a High-Temperature Mercury Thermosiphon. *Journal of Heat Transfer*, 131(9), 1-7.
- Voss, K. Lohnert, G., Herkel, S., Wagner, A., Wambsganß, M. (Eds.). (2005). Bürogebäude mit Zukunft, 2nd edition. *Solarpraxis, Berlin, Germany, ISBN 3-93 45 95-59-6 www.bine.info*
- W. Joung, T. Yu, J. Lee. (2008). Experimental Study on the Loop Heat Pipe with a Planar Bifacial Wick Structure, *International Journal of Heat and Mass Transfer*, 51, 1573-1581.
- W. P. Jones, (2001). *Air Conditioning Engineering (Fifth Edition)*. Butterworth-Heinemann.
- W. T. Grondzik, (2007). *Air-Conditioning System Design Manual (Editor, Second Edition)*, American Society of Heating Refrigerating and Air-Conditioning Engineer Special Publication.
- Wadowski, T., Akbarzadeh, A., Johnson, P. (1992). Hysteresis in Thermosiphon Based Heat-exchangers and Introduction of a Novel Triggering System for Low-Temperature Difference Heat-Recovery Applications. *Heat Recovery Systems & CHP*, 11(6), 523–531.
- Wan J.W., Zhang J.L., Zhang W.M., (2007). The Effect of Heat Pipe Air Handling Coil On Energy Consumption in Central Air-Conditioning System, *Energy Build*, 39, 1035-1040.
- Wang, R.Z., Jia, J.P., Zhu, Y.H., Teng, Y., Wu, J.Y., Cheng, J. (1997). Study on a New Solid Adsorption Refrigeration Pair: Active Carbon Fibre-Methanol. *Journal of Solar Energy Engineering*, 119, 214–219.
- Wang, R.Z., Oliveira, R.G., (2005). Adsorption Refrigeration – An Efficient Way to Make Good Use of Waste Heat and Solar Energy. *Proceedings of International Sorption Heat Pump Conference, Denver, USA*.
- Weber, L. (2002). Energie in Bürogebäuden-Verbrauch Und Energiier-Elevant Entscheidungen, vdf Hochschulverlag an der ETH Zurich, Swiss.
- Westphalen, D. & Koszalinski, S. (2001). Energy Consumption Characteristics of Commercial Building HVAC Systems.
- Wimolsiri P. Solar Cooling and Sustainable Refrigeration, (2005). <http://www.egi.kth.se/proj/courses/4A1623/files/>

- Wong, N.H., Feriadi, H., Lim, P.Y., Tham, K.W., Sekhar, C., and Cheong, K.W. (2002). Thermal Comfort Evaluation of Naturally Ventilated Public Housing in Singapore, *Building and Environment*, 37, (12), 1267-1277
- Yau, Y.H., and Ahmadzadehtalatapah, M. (2010). A Review on the Application of Horizontal Heat Pipe Heat-exchangers in Air Conditioning Systems in The Tropics. *Applied Thermal Engineering*, 30, (2-3), 2010, 77-84.
- Yeung M.R., Yuen P.K., Dunn A., Cornish L.S. (1992). Performance of a Solar-Powered Air Conditioning System in Hong Kong. *Solar Energy*, 48, 309-19.
- Yuping, H., (2008). Cooling System of Outdoor Cabinet using Underground Heat Pipe, *Telecommunications Energy Conference, IEEE 30*, 1-5.
- Z. Abdullah, B.P. Huynh, A. Idris. (2014). CFD Numerical Study of Heat-pipes Effects to a 3-Dimensional Room with Natural Driven Ventilation. *19th Australasian Fluid Mechanics Conference, Perth, Australia*
- Z. Abdullah, B.P. Huynh, A. Idris. (2015). Numerical Simulations of the Flow and Heat Behaviour for a Heat Pipe Heat-exchanger in an Outdoor Power Supply Cabinet. International Mechanical Engineering Congress & Exposition, Houston, Texas, USA
- Z. Abdullah, B.P. Huynh, A. Idris. (2016). CFD-Simulation of A Heat-pipes -Heat-exchanger Effect On a Tubular Air-Cooled Condenser. *International Mechanical Engineering Congress & Exposition, Phoenix, Arizona*
- Z. Engsa, (2016). Performance Analysis of Solar Assisted Hybrid Desiccant Air Conditioning System with Heat Pipe Heat-exchanger. *Institute of Solar Energy Research, Universiti Kebangsaan Malaysia*.
- Zimmermann, M. (Ed.). (2003). Handbuch der Passiven Khlung. *Fraunhofer IRB Verlag, Stuttgart, ISBN 3-8167-6267-0*
- Zöld, A. (2004). Ecobuild: Online Electronic Teaching Package.
<http://www egt.bme.hu/ecobuild/pcool/>

APPENDIXES

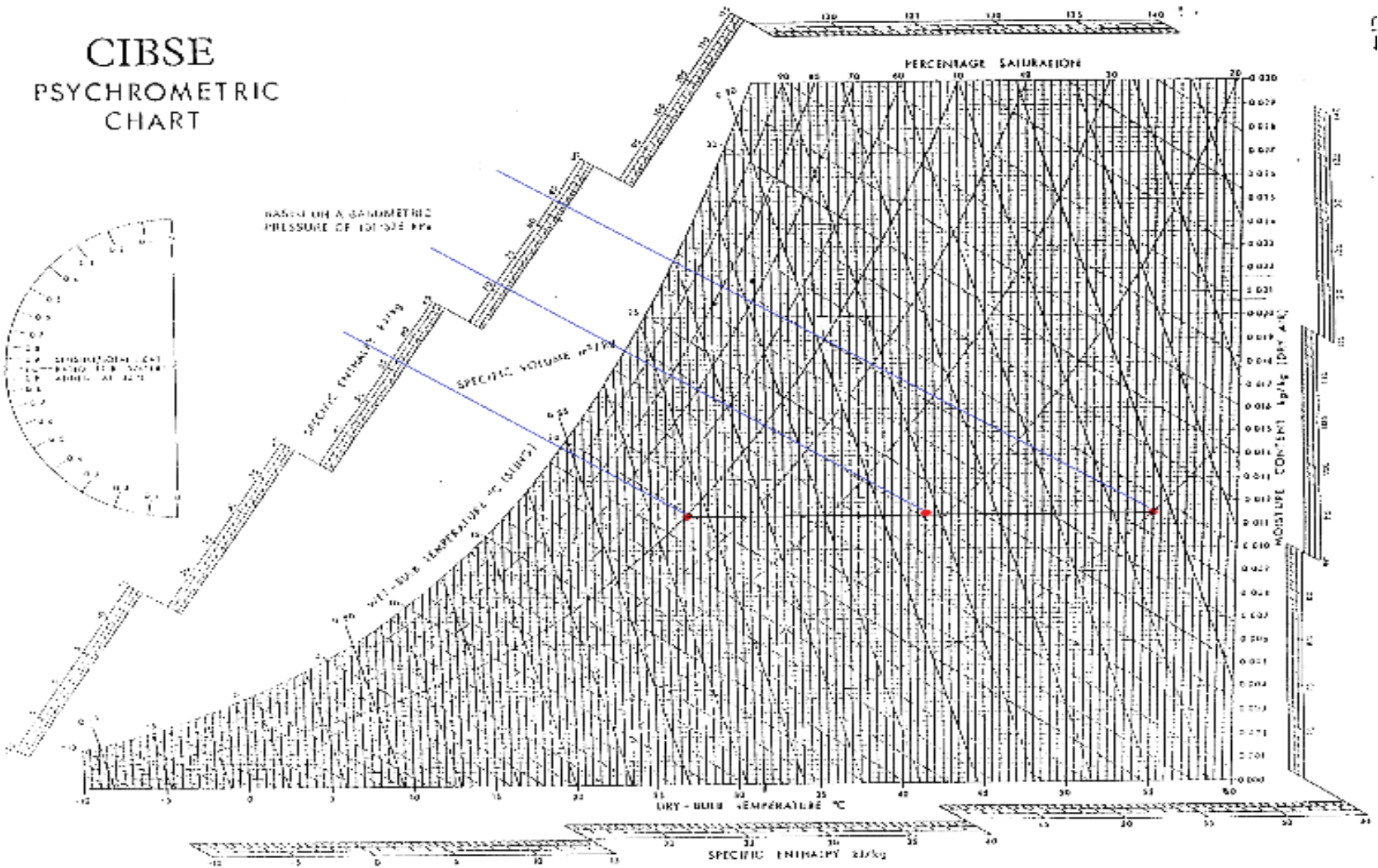
Appendix 1

CIBSE PSYCHROMETRIC CHART

BASED ON A BAROMETRIC
PRESSURE OF 101325 Pa



Fig. C1.2 CIBSE Psychrometric Chart (1) to (10) to BS 5413
Copyright © 2001 CIBSE. All rights reserved. This chart is based on a barometric pressure of 101325 Pa.



Appendix 2

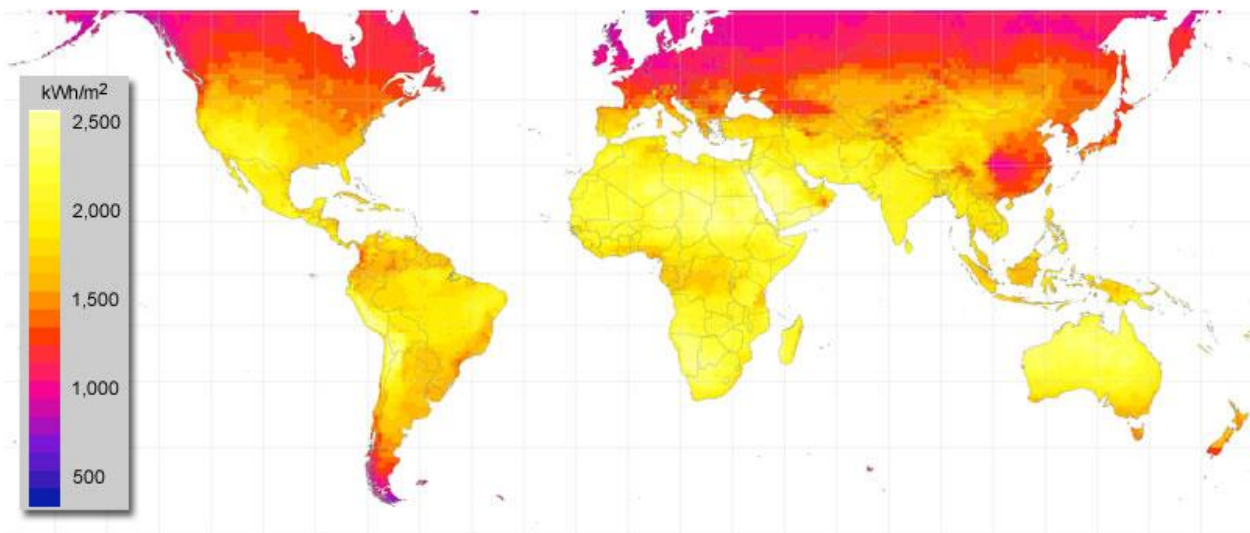
Heat-pipes Heat-exchanger Calculation

Description	Formula
The thermal resistances between the heat sink and condenser external surface	$R_1 = \frac{1}{h_{co}A_{co}}$
The thermal resistance across the thickness of the condenser wall	$R_2 = \frac{\ln(D_o / D_i)}{2\pi L_c k_s}$
The internal thermal resistance of the condensing fluid in the thermosyphon. h_{ci} was obtained from ESDU (1981).	$R_3 = \frac{1}{h_{ci}A_{ci}}$
The resistance due to the pressure drop of the vapour as it flows from evaporator to condenser. According to ESDU (1981) and ESDU (1979), this resistance is the ratio between the drop in saturation temperature between the evaporator and the condenser over the rate of heat transfer	$R_4 = \frac{\Delta T_{sat-e-c}}{Q}$
The axial resistance across the length of the thermosyphon	$R_5 = \frac{(0.5L_e + La + 0.5L_c)}{A_{cs}k_s}$
The internal thermal resistance of the boiling fluid in the thermosyphon. h_{ei} was obtained from ESDU (1981).	$R_6 = \frac{1}{h_{ei}A_{ei}}$
The thermal resistance across the thickness of the evaporator wall	$R_7 = \frac{\ln(D_o / D_i)}{2\pi L_e k_s}$
The thermal resistance between the heat source and the evaporator external surface	$R_8 = \frac{1}{h_{eo}A_{eo}}$

R1	R2	R3	R4	R5	R6	R7	Do	Di
4.000	16.598	4.444	4.444	40100.000	4.444	16.598	0.010	0.009
Pipe length	Lc	250	mm	Surface	Ao	0.0025	m ²	
	Le	250	mm		Ai	0.00225	m ²	
	La	150	mm					
	ks	401	W/m.K	Temp		4.18	K	
heat transfer coefficient			hco	100	W/(m2K).			
			hci	100	W/(m2K).			
			heo	100	W/(m2K).			
			hei	100	W/(m2K).			
			hair	100	W/(m2K).			
Rtotal	0.033343							
Q	125.3651	W						

Appendix 3

Yearly sum of global irradiance



Calculation of the solar PV energy output of a photovoltaic system

Global formula : $E = A * r * H * PR$

E = Energy (kWh)	4497 kWh/an
A = Total solar panel Area (m ²)	20 m ²
r = solar panel yield (%)	15%
H = Annual average irradiation on tilted panels (shadings not included)*	2000 kWh/m ² .an
PR = Performance ratio, coefficient for losses (range between 0.9 and 0.5, default value = 0.75)	0.75

Total power of the system kWp

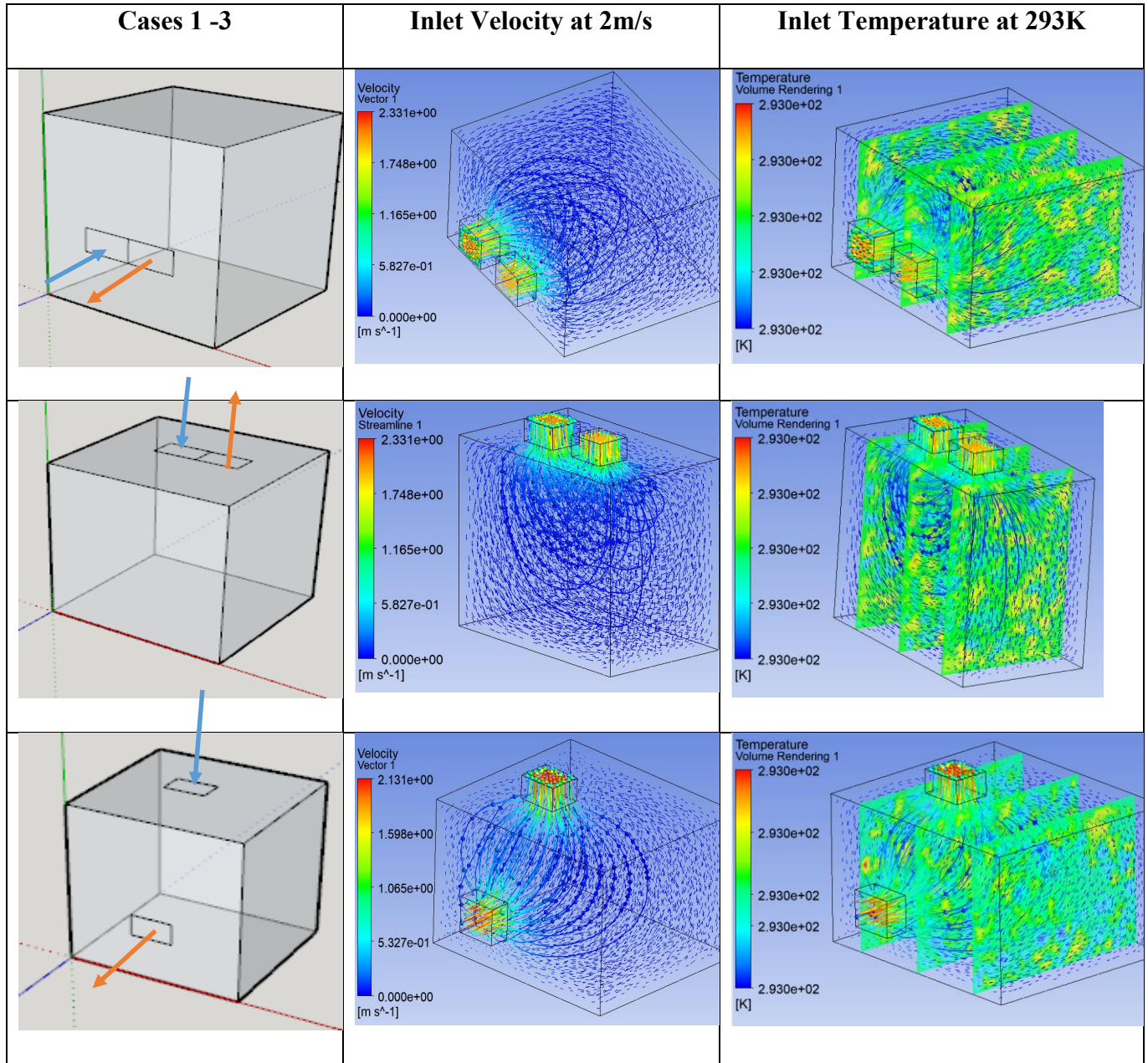
Losses details (depend of site, technology, and sizing of the system)

- Inverter losses (6% to 15%)
- Temperature losses (5% to 15%)
- DC cables losses (1 to 3%)
- AC cables losses (1 to 3%)
- Shadings 0% to 40% (depends of site)
- Losses weak irradiation 3% yo 7%
- Losses due to dust, snow... (2%)
- Other Losses

8%
8%
2%
2%
3%
3%
2%
0%

Appendix 4

Simulations of heat-pipes heat-exchanger with different configurations.



Appendix 5

Works that have been done related to refrigeration and cooling.

5. STUDY OF WIND-ASSISTED ENERGY FOR COOLING SYSTEM IN BANGI, MALAYSIA

The author's work with simulation and experimental studies using wind-assisted energy in cooling energy consumptions. Wind data collection was taken in Malaysia (Bangi 2.9° N, 101.7° E) where the average 'high' velocity recorded is 5 m/s. A small wind turbine designed to collect electricity from the rotation of a blade was installed for the study. A journal paper describing the work outcome has been presented. The ever-increasing rate of demand for electrical energy has spurred researchers to explore alternative energy sources. The annual report from The Energy Commission of Malaysia revealed that from 2015 to 2016, there was an 8.9% to 10.5% increase in electrical consumption. The principal operation of a wind turbine in assisting energy consumption is by converting the kinetic energy of the blowing wind through a fan blade rotation into electrical energy. The kinetic energy available depends mainly on the wind speed and the blade swept area of the turbine. The work presented was a study of a small horizontal-axis wind turbine in cooling a refrigerator as a test unit, where the available wind speed was less than 10 m/s. The wind speed data was collected in Bandar Baru Bangi, and the aims were to operate a refrigeration cycle that chilled a refrigerator to about 278K (5 °C). The realism of using a wind turbine was carefully studied through a computational fluid dynamics ANSYS-Fluent modelling, where a series of wind speed data was taken on-site and a mathematical model of wind turbine power calculation was performed. The structure of the wind turbine included a 6 m high tower with a 2.6 m diameter blade while the available high wind speed taken on-site was 5 m/s. From the studies, albeit with a small amount of wind speed, it was found that the wind turbine conversion energy was capable of running a small refrigerator's chiller unit to 278 K (5 °C), with an available power of 151.33 W.

Renewable energy sources such as sunlight, wind, tidal, wave and geothermal energy could be used to operate electromechanical equipment. The wind flows are created by the uneven warming of the environment and the inconsistencies of the earth's surface which could be turned into electrical energy by assuming only the cost of installation and maintenance.

The author proposed a method of cooling a small refrigerator that operates on a minimum electricity source from the outcome of wind energy. A manual data collection of wind speed at Bandar Baru Bangi was conducted. The 'high' average speed was found to be at 5 m/s on-site, which is higher than the finding of Saba et al. (2014) at 2m/s for Malaysia's average condition. The speed and the gust were averaged to supply an electrical source for a small refrigerator's chiller unit.

The energy-saving calculation is shown to compare the rate of saving with the normal electricity tariffs. The simulation of the wind turbine focused on the energy outcome. As predicted by Betz (1994) using a one-dimensional model, the largest power that can be extracted from the wind is less than 16/27 or 59.3% of the kinetic energy in the wind. Figure 5.143 shows the rotor as an ‘actuator disk’ that creates a pressure discontinuity of area A and local velocity V (Jonkman 2003; White 1988).

The paper analysed the energy that the wind could offer by cooling a refrigerator to a required temperature level. In a location where wind speed averages less than 10 m/s, the possibility of applying wind turbines as an alternative source was tested. A small wind turbine was applied to grid-connected home applications (Elliot 2002). Table 5.44 shows the power available, calculated from the wind in Bandar Baru Bangi. The power available from the wind turbine can be calculated by the following equation:

$$P_{available} = \frac{1}{2} \rho A v^3 C_p$$

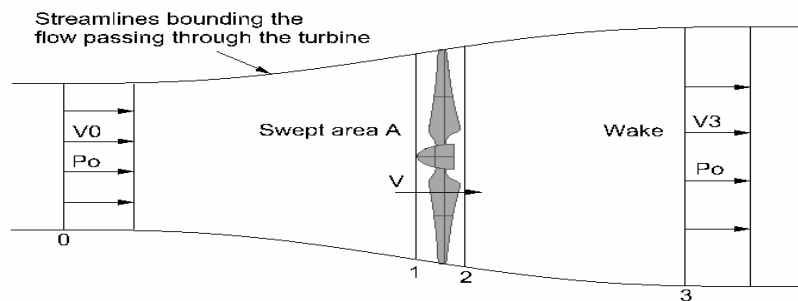


Figure 5.142: Control volume for the idealised actuator-disk analysis. *David and Andrej. (2008).*

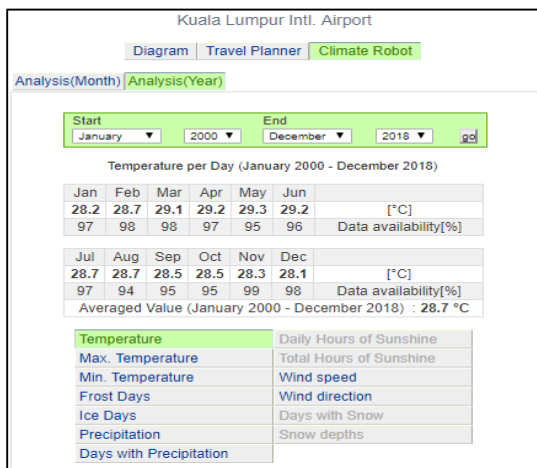
Table 5.44: Wind turbine power calculation of average high wind speed in Bandar Baru Bangi. At 5 m/s, the power that the wind turbine can generate is about 151.33 W.

Parameter	Measurement
Blade length, m	1.3
Wind Speed, m/s, rpm	5 m/s, 36.73 rpm
Air density, kg/m ³	1.14
Power coefficient	0.4
Power available, W	151.33

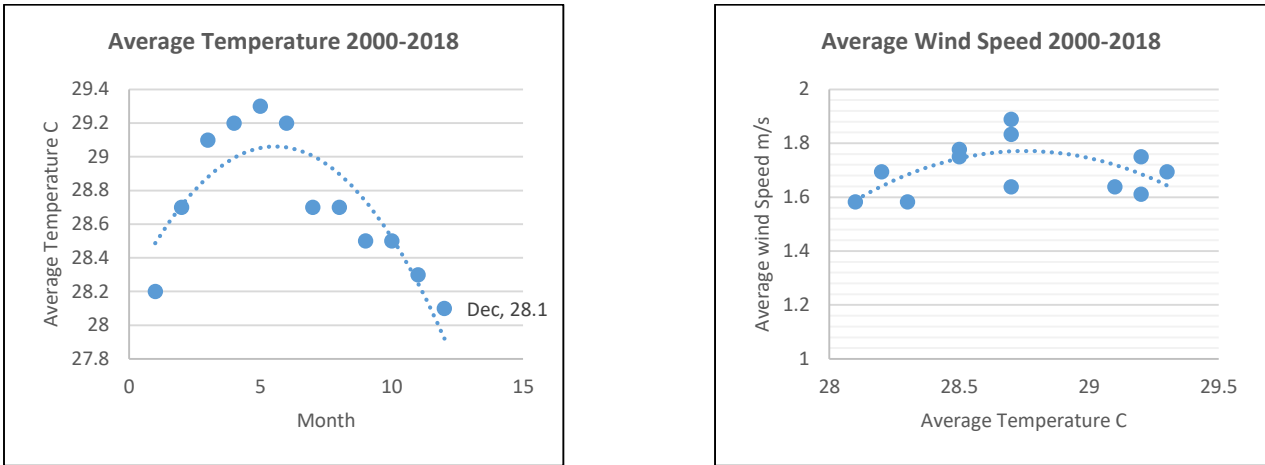
Subject to the blowing wind, a room in Bandar Baru Bangi can be very warm and humid as the high temperature could reach up to 308 K (35°C) outdoors. Figure 5.143 shows the wind recorded in Kuala Lumpur in the last eighteen years since 2000 (weatheronline.co.uk). An average wind speed of 1.7 m/s (6.1 km/h) was recorded; however, the required speed of the wind turbine to rotate is in the range of 3.5 m/s to 10 m/s. A small wind turbine was therefore proposed to be tested at a strategic location where the highest average wind speed is about 5 m/s. The wind turbine had a 2600 mm blade diameter, a rotation rate of 400 rpm, and a rate of power at 300 W. The refrigeration system test unit was a 50 W refrigerator with 48 W energy consumption.

5.1 Problem Description: Wind-Assisted Energy

Mechanical cooling needs electrical power to run the refrigeration cycle. Wind turbine acts as a substitution of electrical grid power to benefit electricity by generating mechanical power through rotating propellers. This study worked on wind power generated in an open space next to a traffic highway where the flow and the gusting air were recorded to be higher, to cool a refrigerator at about 5°C. As the average wind flow in Kuala Lumpur is 1.7 m/s, locating the wind turbine at the predicted high wind flow area is expected to show promising results. Simulation using ANSYS Fluent was used to observe the rotating fan-blade air velocity, as predicted by the k- ϵ method of calculation.



a.



b.

Figure 5.143a and b: The average wind speed recorded in Kuala Lumpur for the year 2000 to 2018 is at about 6.1 km/h (1.7 m/s) with a temperature of 28. 8°C. *weatheronline.co.uk*

5.2 Methodology

The method of study was by collecting a series of wind speed data and processing it to find the average wind speed in Bandar Baru Bangi. Figure 5.144 shows the average wind speed data collected in Bandar Baru Bangi for the experiment.

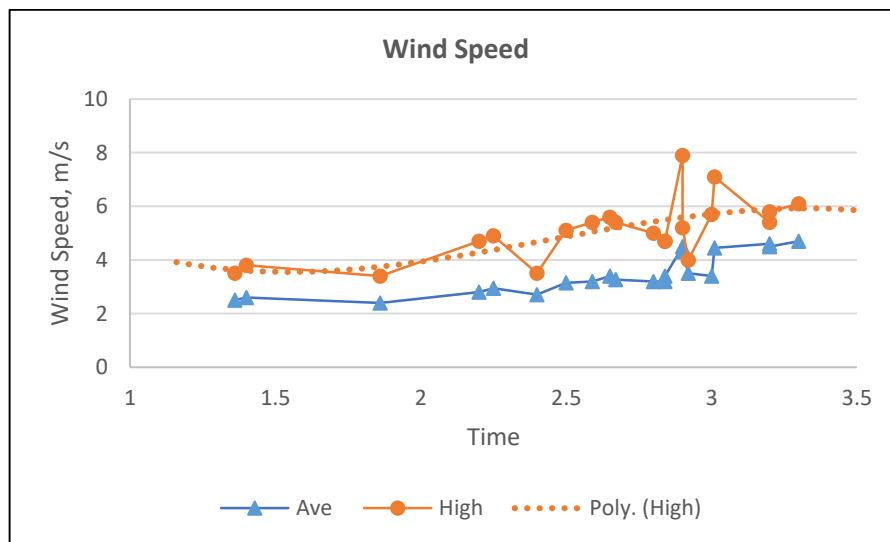


Figure 5.144: The wind turbine model and the average of high wind speed taken at Bandar Baru Bangi. The highest average is about 5 m/s.

The flow chart in Figure 5.145 shows the work process. The work began with the processing of the input data, manual collection of field data, construction of a factual decision and processing of the output data.

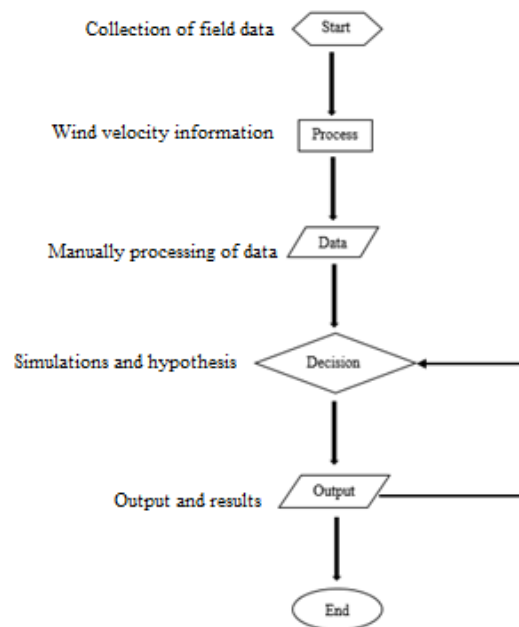


Figure 5.145: Flow chart of the wind turbine study.

5.3 Results and Discussion: The Wind Energy

Wind speed from 3 to 5 m/s was simulated using ANSYS Fluent to predict the velocity output range. Three components, namely enclosure, rotating parts, and fan-blade mesh were formed in the workbench. The meshed and boundary conditions are listed in Table 5.45. Basic nodes and element mesh were applied to the components as shown in Figure 5.146. Tables 5.46 and 5.47 show the simulation process and the range of velocity that the software predicted, respectively.

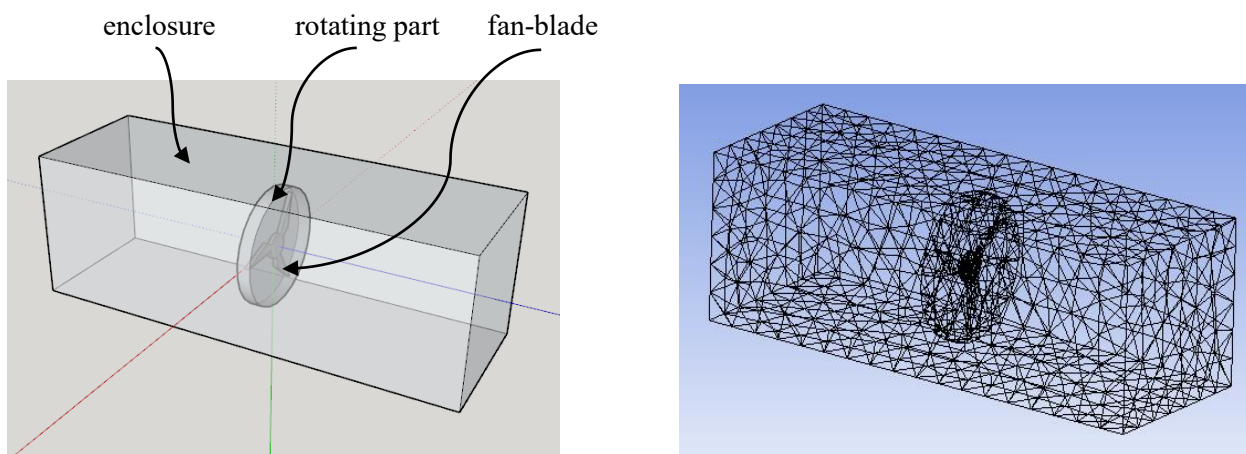
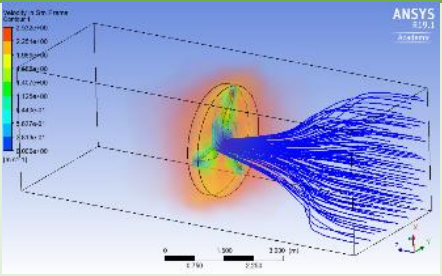
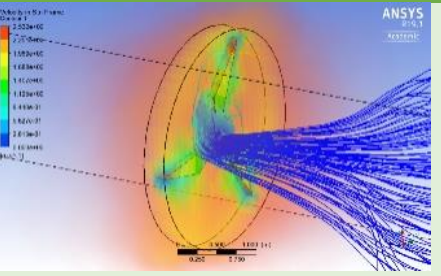
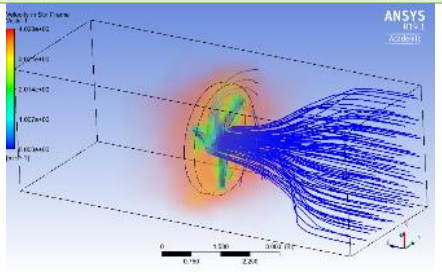
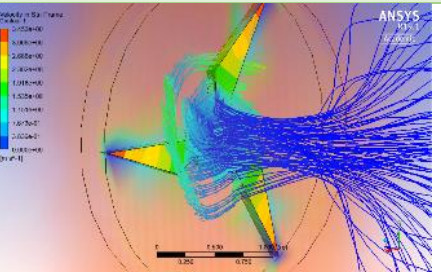


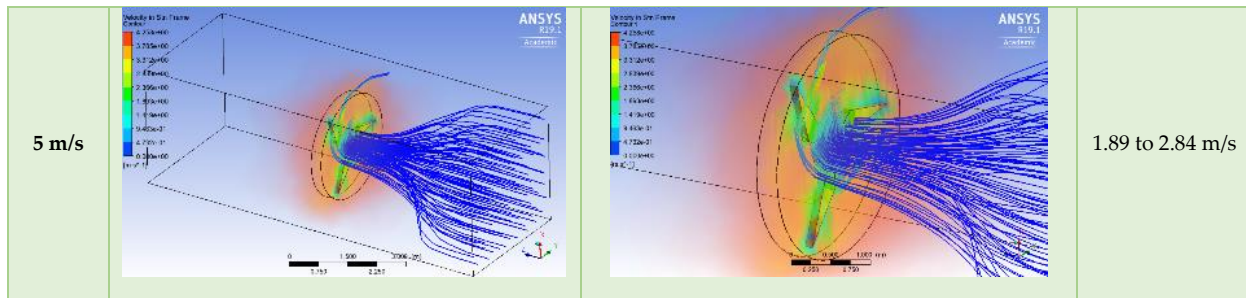
Figure 5.146: The boundary and mesh for the enclosure, rotating part and the fan-blade.

Table 5.45: Meshing elements and boundary conditions run on ANSYS Fluent.

Domains	Nodes: Enclosure 1276, Rotating part 173, Total 1449 Elements: Enclosure 5652, Rotating part 611, Total 6263
General	Pressure based, Absolute velocity formulation, Transient
Model	Energy equations, k-epsilon, realizable model, scalable wall functions
Material	Air, Aluminium
Cell Zone Conditions	Enclosure rotation-axis Z direction, Rotating mesh motion, rpm
Boundary Conditions	Inlet pressure-based, Outlet pressure based
Solution	Simple, Least-square cell-based, Second-order pressure, Second-order upwind momentum, First order upwind turbulent kinetic energy, First order upwind turbulent dissipation rate, First order upwind transient formulation
Initialisation	Hybrid

Table 5.46: Simulation using the air velocity range from 3 m/s to 5 m/s. The simulations predicted that with 5 m/s wind velocity, about 1.89 m/s to 2.84 m/s will be utilised for energy generation.

Input	Enclosure	Rotating Parts	Output Range
3 m/s			1.12 to 1.97 m/s
4 m/s			1.9 to 2.3 m/s



From the simulation and the data collected, a new calculation for the wind turbine was established. Table 5.46 shows the predicted results.

Table 5.47: New wind turbine power calculation based on simulation results.

Parameter	Measurement
Blade length	1.3 m
Air density	1.14 kg/m ³
Power coefficient	0.4
Input Wind Speed	5 m/s, 36.74 rpm
Output Wind Speed	2.84 m/s, 20.87 rpm
Power Max	151.33 W
Power Min	27.73 W

5.4 Results and Discussion: Refrigeration Process

Hypotheses for the refrigeration cycle are as shown in Figures 5.147 and 5.148 (Coolpack). The system is a direct expansion of R134a with evaporating temperature $T_e=5^\circ\text{C}$, condensing temperature $T_c=40^\circ\text{C}$, 10 K sub-cooling, and 5 K superheat. Tables 5.48 and 5.49 show the properties of the complete cycle.

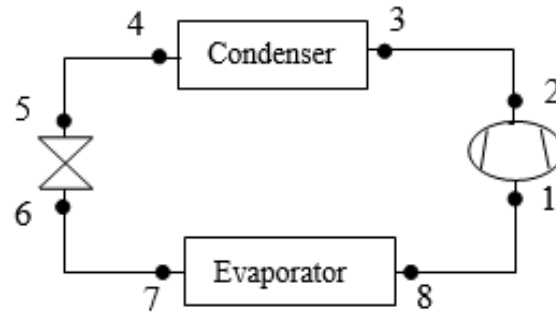


Figure 5.147: The schematic drawing of the refrigeration installation. *CoolPack*.

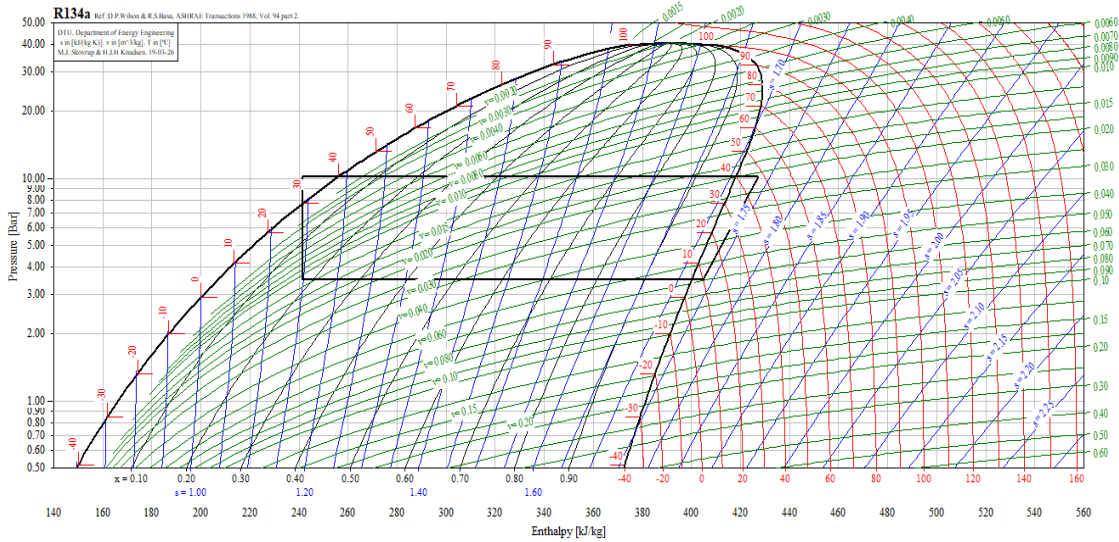


Figure 5.148: The pressure-enthalpy curve of the refrigeration cycle. *CoolPack*.

Table 5.48: The thermodynamic cycle of the R134a refrigerator. *CoolPack*.

Point	T	P	v	h	s
	°C	bar	m ³ /kg	kJ/kg	kJ/kg.K
1	9.999	3.496	0.059596	404.785	1.7361
2	47.921	10.164	0.020989	427.428	1.7361
3	47.921	10.164	0.020989	427.428	1.7361
5	30.000	10.164		241.463	
7		3.496		241.463	
8	10.000	3.496	0.059592	404.785	1.7361

Table 5.49: The output results of the refrigeration cycle.

Parameter	Measurement
Te, °C	5
Tc, °C	40
Superheat, K	5
Subcool, K	10
Evaporator work Qe, kJ/kg	163.322
Condenser work Qc, kJ/kg	185.965
COP	7.21
Compressor work, kJ/kg	22.642
Pressure ratio	2.907
Refrigerant flow rate, kg/s	0.927 × 10 ⁻³
Compressor power, W	21

5.5 Conclusion

The ambient in Bandar Baru Bangi was 30°C dry bulbs, 75% relative humidity, with 5 m/s of wind speed. The power obtained from the wind turbine was found to be capable of operating a small refrigerator chiller unit. The wind turbine location was on higher ground, near a busy traffic highway. The turbine, therefore, derived benefit from the high gusting wind created by the traffic. To assist the calculations, ANSYS Fluent was simulated from the wind speed ranging from 3 m/s to 5 m/s. It was found that when 5 m/s of the wind blew on the wind turbine, only a part of the velocity at 2.84 m/s was generated to rotate the propellers. The power from the wind turbine was estimated to be between 27.73 W to 151.33 W.

A refrigerator operating conditions of Te 5°C and Tc 40°C, and its working compressor require 21 W for a cycle as shown in Table 5.49. The calculations show that wind power could generate enough energy to assist the refrigerator's requirement. This could last for about 7 hours of cooling operation. The wind turbine is viable for the operation of a small energy consumption unit such as the chiller refrigerator without the need for any grid electrical source.

Appendix 6

6. SIMULATION STUDY ON COOLING A SMALL DOMESTIC REFRIGERATION SYSTEM USING SOLAR-ASSISTED ENERGY IN BANGI, MALAYSIA

The research aimed to verify solar-assisted energy in the cooling process. The experimental work was carried out at Universiti Kuala Lumpur, Malaysia France Institute, Malaysia. The author worked collaboratively with Universiti Kuala Lumpur researchers on solar energy as an alternative source to electrical grid energy. Solar data collection was carried out in Malaysia (Bangi 2.9° N, 101.7° E) where the outdoor ambient temperature can reach up to 308 K (35°C). Solar energy was found to save 31% of the energy required by the refrigerator. A journal paper from the work outcome has been presented.

A simulation study on cooling a small domestic refrigeration system using solar-assisted energy was carried out in Bangi, Malaysia. In a tropical climate condition, where the outdoor ambient temperature can reach up to 308 K (35 °C), even a slight reduction of energy consumption would contribute to the heat load of a refrigeration system. Photovoltaic (PV) panels convert solar energy into electrical energy to run a small domestic refrigeration system. A simulation study using SOLARGIS software calculated the power that the PV can convert. A flat plate PV that converts 360 W was used for this simulation study. The objectives of the study included making use of solar radiation and energy-saving. It was found that the energy supplied by the solar radiation from the PV panels successfully operated a small refrigerator to the desired cooling of 5 °C.

Solar energy is one of the sources of renewable energy which is increasingly gaining the attention of the community. Awareness of the need to preserve the environment and the lack of energy has given rise to the effort to find alternative energy sources. However, solar energy has for centuries only been used for drying clothes and agricultural products such as coffee beans, paddy, cocoa, black pepper, tobacco, tea leaves, anchovies, and others (Othman, 2002; Shamsuddin, 2012). Nevertheless, the use of solar energy is susceptible to environmental pollution. There are four solar energy technologies, namely air heating for the drying process, water heating, light through radiation and conversion of solar energy to the electricity-photovoltaic system (Othman, 2002). The layout of the solar array is shown in Figure 5.149. However, solar energy's use for the production of electrical power using solar Photovoltaic only began in the 1990s (Shamsuddin, 2012). Solar energy is essentially divided into two types: solar thermal and solar photovoltaic technology. Solar thermal technology shifts solar energy into thermal energy via solar thermal collectors. Meanwhile, solar photovoltaic technology converts solar energy into electricity.

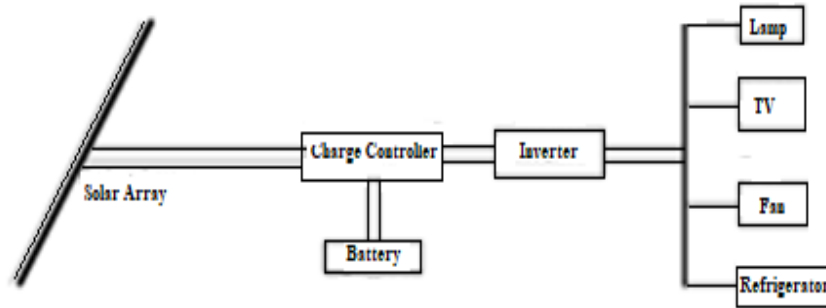


Figure 5.149: Photovoltaic system for residential use. *Othman 2002*

Figure 5.150 shows the forecast of Malaysia's energy source, where Pusat Tenaga Malaysia (Malaysia Energy Centre) predicted that Malaysia would turn into a net importer of energy between 2010 and 2015. The graph indicates that Malaysia must find better ways to utilise renewable energy. Once again, overcoming these matters can be accomplished by applying solar energy as a renewable energy source.

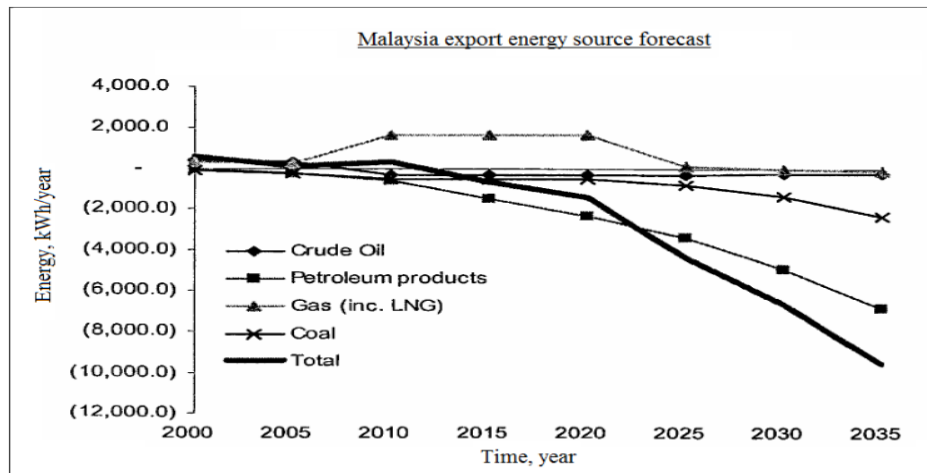


Figure 5.150: Forecast of Malaysia's export energy source for the year 2000-2035. *Pusat Tenaga Malaysia.*

Table 5.50 shows that home energy consumption relies on the appliances installed, the hours of use and the efficiency of the equipment. Generally, in a typical Malaysian terraced house of the size of about 180 m², the refrigerator is the appliance with the highest electricity consumption. However, the air-conditioning system will progressively become more essential as living standards improve (CETDEM Survey, 2004). Although the water heater coil consumes more energy, usage in high ambient temperatures is lower. A rotating machine has a higher percentage of utilisation.

Table 5.50: Electricity power consumption in Malaysia. *Malaysia CETDEM 2004.*

Item	kW	hrs/yr.	kWh	kWh/m ² /yr.	%
Air Conditioner	1	1440	1440	8	21
Fan	0.05	3600	162	0.9	2
Fluorescent Lamps 18W	0.22	576	64.51	0.36	1
Iron	1	180	180	1	3
Radio	0.25	72	18	0.1	0
Refrigerator	0.3	8760	2628	14.6	38
Rice cooker	0.65	360	234	1.3	3
Television	0.06	1080	64.8	0.36	1
Water heater	2.7	360	972	5.4	14
Washing machine	2.2	540	1188	6.6	17
Vacuum cleaner	0.3	96	28.8	0.16	0
Total	8.73	17064	6980.11	38.78	100

6.1 Methodology

Solar radiation data was collected in Bandar Baru Bangi to find the average solar radiation and to calculate the electrical energy that the radiation could convert. Based on the location, it was found that the highest solar radiation was 1220 W/m², and it is capable of operating an electric refrigeration system as a test unit. Figure 5.151 shows the solar collector plates and the data collection used. The work started with the processing of the input data, manual collection of field data, construction of the factual decision and processing of the output data. Figure 5.152 shows the process and Figure 5.153 shows the average solar radiation data collected in Bandar Baru Bangi from SOLARGIS.

Refrigerator

The load was a small refrigerator model XC-40 that requires 65W of power to produce an operating condition of 0°C to 8°C for a 40-litre capacity. The cooling used the absorption method so that the compressor which consumed high power was replaced by a heater element to create differential

pressure in the refrigeration cycle. For a 24-hour cooling application, the refrigerator needs to consume about 0.9 kW/day of power. The specification is presented in Table 5.51.

Table 5.51: Refrigerator specification

No	Parameter	Specification
1	Model	XC-40
2	Capacity	40L
3	Temperature	0°C to 8°C
4	Cooling model	Absorption
5	Body Material	Iron Coated
6	Product Size	440 mm x 400mm 550mm
7	Net Weight	16.5Kg
8	Power	65 Watt
9	Power Consumption	0.9 Kw.h/24h
10	Voltage/Frequency	220v-240v/50Hz

Solar Panel

The solar panel (PV) was a poly plate panel of 156 x 156 cells. The 4 panels carried 90W on each plate, producing 360W (90W x 4 panels). Based on the angle of the latitude which was about 3°, the solar panel could harvest full radiation for about 4 hours in Malaysia's condition and this should produce 360W x 4 = 1440 Whrs from the solar panels. Table 5.52 shows the specifications.

Table 5.52: Solar panel specification

No	Parameter	Specification
1	Model	BSM90P-36
2	Solar cell Type	Poly 156 x 156 Cell
3	Pm	90 Watt
4	Vmp	17.5 Volt
5	1 mp	5.15 Amp
6	Voc	21.6 Volt
7	1sc	5.18 Amp
8	Maximum Sytem Voltage	1000 Volt
9	Size	1000 mm x 670 mm x 30 mm
10	Weight	75 Kg
11	Operating Testing	-40 to +85°C

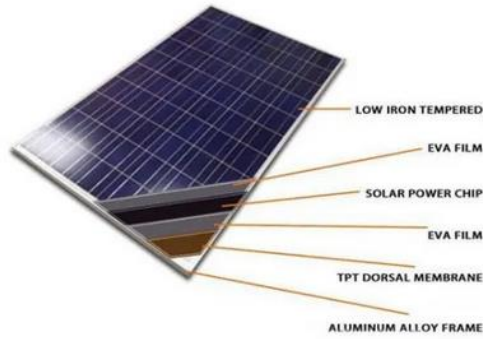


Figure 5.151: Poly-Crystalline Silicon Solar Panel

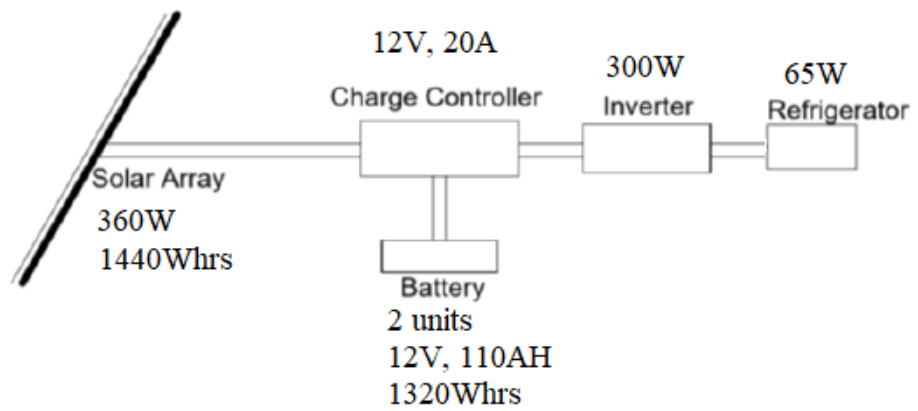


Figure 5.152: Photovoltaic system for chiller refrigerator.



Figure 5.153: Plate-PV for solar energy collector. UniKL MFI field research area.

Month	Es_m	Es_d	Et_m	E_{SHARE}	PR
Jan	103	3.33	37.1	7.9	76.9
Feb	106	3.79	38.2	8.1	76.5
Mar	125	4.02	44.9	9.5	76.6
Apr	114	3.81	41.1	8.7	76.8
May	115	3.70	41.3	8.8	76.7
Jun	105	3.48	37.6	8.0	76.7
Jul	107	3.46	38.6	8.2	76.8
Aug	111	3.57	39.8	8.5	76.7
Sep	113	3.76	40.6	8.6	76.8
Oct	111	3.58	40.0	8.5	76.8
Nov	101	3.36	36.3	7.7	77.1
Dec	97	3.11	34.7	7.4	77.2
Year	1306	3.58	470.3	100.0	76.8

Long-term monthly averages:

Es_m	Monthly sum of specific electricity prod. [kWh/kWp]
Es_d	Daily sum of specific electricity prod. [kWh/kWp]
Et_m	Monthly sum of total electricity prod. [kWh]

Figure 5.154: Monthly sum of specific electricity production in Bandar Baru Bangi's electricity production. *SOLARGIS*.

The formula used to calculate the power is given as

$$P = IV$$

where, P = power in kW, I = current in amps, V = voltage in Volt.

6.2 Result and Discussion

A series of solar radiation data collection was performed between Block D and E of UniKL MFI to compare the average solar energy gained. Figure 5.155 shows that the average solar energy collected was 1220 W/m².

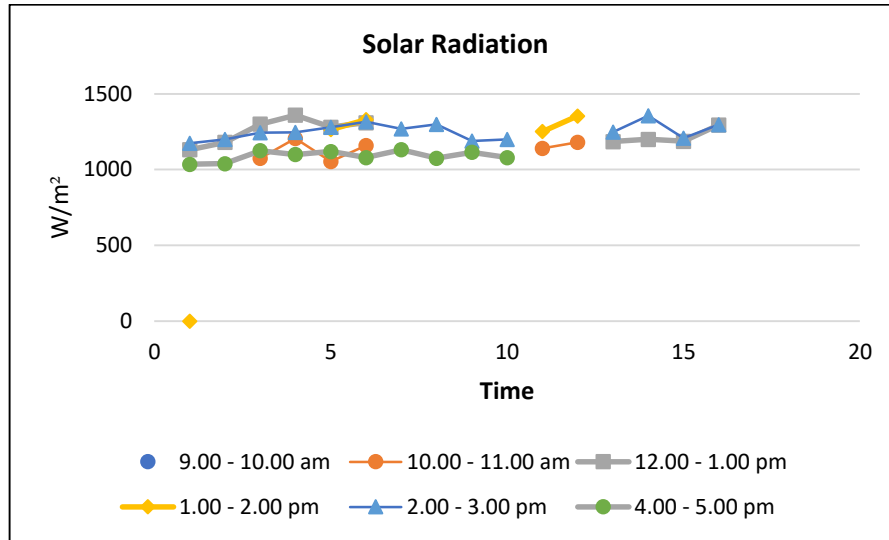


Figure 5.155: The average solar radiation at UniKL MFI is $1220W/ m^2$.

The hypotheses for the refrigeration cycle are presented in Figures 5.156 and 5.157 (Coolpack). The system was a direct expansion of R134a with evaporating temperature $T_e= 5^{\circ}C$, condensing temperature $T_c=40^{\circ}C$, 10 K sub-cooling and 5 K superheat. Table 5.53 shows the properties of the complete cycle.

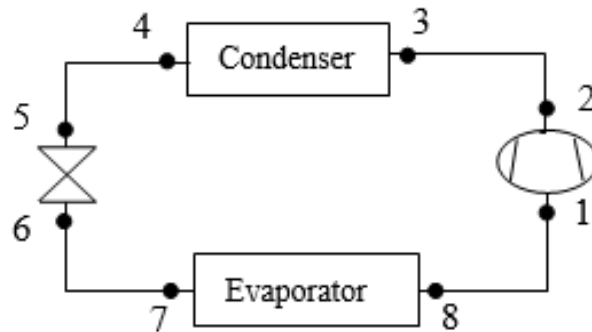


Figure 5.156: The schematic drawing of the refrigeration installation. *CoolPack*.

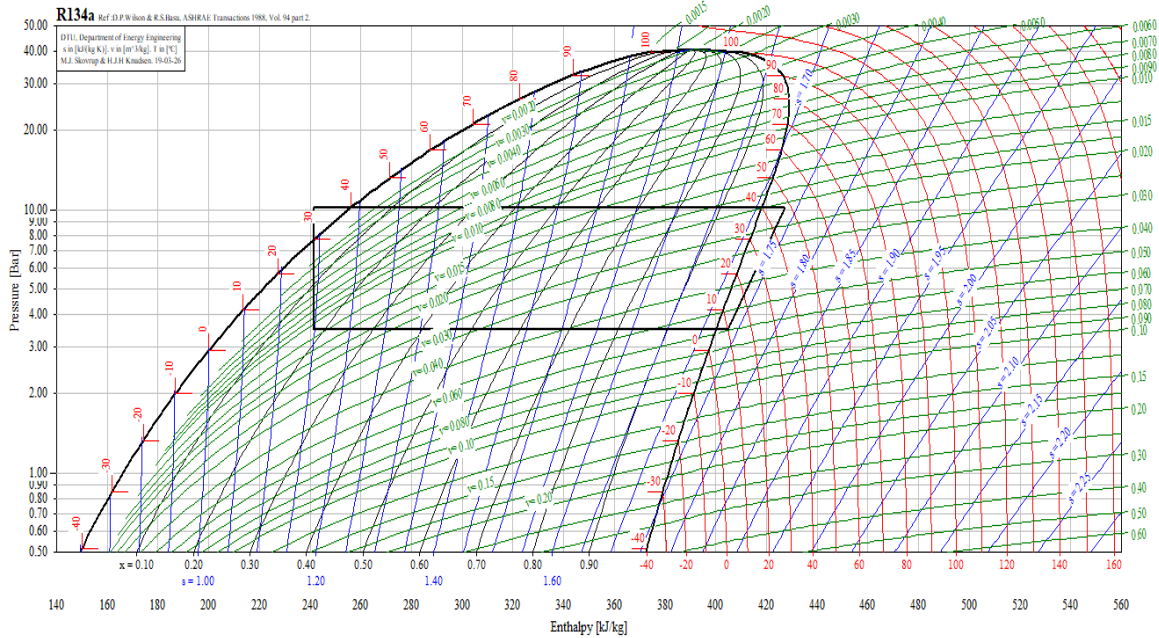


Figure 5.157: The pressure-enthalpy curve of the refrigeration cycle. *CoolPack*.

Table 5.53: The thermodynamic cycle of the R134a refrigerator. *CoolPack*.

Point	T	P	v	h	s
	°C	bar	m ³ /kg	kJ/kg	kJ/kg.K
1	9.999	3.496	0.059596	404.785	1.7361
2	47.921	10.164	0.020989	427.428	1.7361
3	47.921	10.164	0.020989	427.428	1.7361
5	30.000	10.164		241.463	
7		3.496		241.463	
8	10.000	3.496	0.059592	404.785	1.7361

6.3 Conclusion

The calculations in Table 5.54 show that the solar power from the plate collectors could produce 470.3 kWh annually, assisting the 0.9 kW/day power consumption of the small domestic refrigerator. The refrigerator requires 324 kWh annually.

Table 5.54. Solar energy power calculation. *SOLARGIS*.

PV system	Specification
Installed power	0.36 kW
Type of modules	crystalline silicon (c-Si)
Mounting system	fixed mounting, free-standing
Azimuth/inclination	180° south / 2°
Inverter Euro eff.	97.5%
DC / AC losses	5.5% / 1.5%
Availability	99.0%
Annual average electricity production	470.3 kWh
Average performance ratio	76.8%

With the power of 0.36kW installed in the PV system in Bandar Baru Bangi, it was found through the simulation taken from SOLARGIS that the annual average electricity production from the solar collectors was 470.3 kWh/year. A mini-refrigerator that requires 0.9kWh/day was tested to run on solar energy. The annual power consumption for the refrigerator was calculated to be 324 kWh/year. Thus, a 31% energy saving could be achieved from the solar PV system.

List of Reviewed Paper Attached

Author

1. Numerical Study of Heat-pipes heat-exchanger to a 3-Dimensional Room with Natural Driven Ventilation. Abdullah Z., Huynh B.P., Idris A. ASME IMECE2014 Montreal, Canada.
2. Numerical Study of Heat-pipes Effects to a 3-Dimensional Room with Driven Ventilation. Abdullah Z., Huynh B.P., Idris A. 19th AFMC Melbourne, Australia.
3. CFD-Simulation of the Effect of Heat-pipes Attached to an Evaporator and Condenser of an Air-Cooled-Air-Conditioner. Z. Abdullah, B.P. Huynh, and A. Idris. 20th Australasian Fluid Mechanics Conference, Perth, Australia.
4. Numerical Simulation of the Flow and Heat Behaviour for a Heat Pipe Heat-exchanger in an Outdoor Power Supply Cabinet. Abdullah Z., Huynh B.P., Idris A. ASME IMECE2015 Houston, Texas, USA.
5. CFD-Simulation of a Heat-pipes -Heat-Exchanger Effect on a Tubular Air-Cooled Condenser. Abdullah Z., Huynh B.P., Idris A. ASME IMECE2016 Phoenix, Arizona, USA.
6. Passive Cooling Method of Energy Reduction Using Fins-Type Heat-pipes heat-exchanger. Abdullah Z., Huynh B.P. 21th Australasian Fluid Mechanics Conference, Adelaide, Australia.
7. Z. Abdullah, M. S. Shaadan, Z. Jusoh, Z. Engsa. (2019). Study of Wind-Assisted Energy for Cooling System in Bangi, Malaysia. Journal of Advanced Manufacturing Technology, International Conference on Advanced Processes and System in Manufacturing (APSIM 2019), Malaysia.

Co-author

8. Possibility of Using Silica Gel-Water Adsorption Chiller in the Cold Chain. M. A. Ahamat, M. J. Tierney, Zulkarnaini Abdullah, Zakaria Jusoh, 2nd IIR International Conference on Sustainability and Cold Chain, Paris.
9. Theoretical and Experimental Analysis of Desiccant Wheel Performance of Solar Hybrid Desiccant Air-Conditioning System. Zuraini Hashim, Tri Suyono, Arifidian Rachman, Zulkarnaini, Sohif Mat. Solar Energy Research Institute UKM, Malaysia, National University of Malaysia

10. Simulation Study of Cooling a Small Domestic Refrigeration System Using Solar-Assisted Energy in Bangi, Malaysia. Z. Jusoh, N. Ibrahim, Z. Abdullah and Z. M. Engsa. APSIM2019, UKM, Malaysia.

IMECE2014-37705

NUMERICAL STUDY OF HEAT-PIPES EFFECTS TO A 3-DIMENSIONAL ROOM WITH NATURAL DRIVEN VENTILATION

Z. Abdullah¹

Faculty of Mechanical Engineering & IT
 University of Technology, Sydney
 Sydney, NSW, Australia

B. P. Huynh

Faculty of Mechanical Engineering & IT
 University of Technology, Sydney
 Sydney, NSW, Australia

A. Idris

Department of Mechanical Engineering,
 Universiti Kuala Lumpur,
 Malaysia, Spanish Institute
 Kulim Hi-Tech Park, 09000 Kulim, Kedah
 Malaysia

ABSTRACT

A Computational Fluid Dynamics (CFD) software package is used to investigate numerically a 3-dimensional rectangular-box room installed with a heat-pipes heat-exchanger (HPHE). Heat pipe heat-exchanger utilizing refrigerant using working fluid is installed on top of a room. The air-side heat transfers and the flow pattern of thermo-siphon heat-pipes are studied with natural driven ventilation of a building. Different openings of the inlet and outlet air where the heat pipe was installed are tested with round edges opening as well as sharp edges. The standard RANS k - ϵ turbulence model is used. Results with different settings of the heat pipe and opening characteristic, airflow rate, and flow pattern as well as its temperature effects are examined.

Keywords: *Computational Fluid Dynamics, heat-pipes heat-exchanger, heat transfer, rectangular-box, airflow rate, the temperature flow pattern*

NOMENCLATURE

$U_j (j = 1 - 3)$ - Component of average velocity vector, m/s
 g - Gravity acceleration, m/s²
 μ_t - Turbulent viscosity, Pa/s

C_μ - Empirical constant, 0.09
 k - Turbulent kinetic energy, m²/s²
 ϵ - Dissipation rate, m²/s³
 κ - Von Karman's constant, 0.41
 U_{ave} - The average flow velocity, m/s
 T_i - Turbulence intensity
 L - Length scale, m

1. INTRODUCTION

1.1 Heat-pipes heat-exchanger (HPHE)

This paper proposed the use of a heat pipe heat-exchanger (HPHE) in a room, hence analyses the airflow pattern of 100% outside air. HPHE is becoming popular as an energy-saving device as there is no external power required and it has no need for maintenance. Linden [1] noted that 30% of the total energy consumption in the US is used by non-domestic buildings and 30% of that fraction is in heating and cooling. HPHE might be one of the responses for building thermal comfort.

Figures 1a and 1b show a model of HPHE used. HPHE a passive, simple construction and cost-effective heat-exchanger

are used as a tool to demonstrate the room airflow pattern which effects by its temperature difference between indoor and outdoor air. Figure 1c and 1d show the simulations series of a three pipe heat-pipes exchanger run on ANSYS-Fluent using water and acetone respectively, as the working medium. The comparisons were to show a different temperature between the inlet and the outlet of the heat-pipes, although the study of the HPHE efficiency itself is not discussed in detail in this paper. The simulations show that the delta temperature difference between 2 to 3°C can be easily achieved with a row of three pipes, a heat-pipes heat-exchanger. The HPHE used in this modelling was measured in an area of 1 m² (2 m x 0.5m) at both inlet and outlet.

HPHE is designed to have high thermal conductance in steady-state operation, and with only a small temperature difference, it can transfer a high amount of heat. Moreover, the simplicity of design and manufacturing, small temperature drops, wide temperature application range and the ability to control and transport high heat rates at various temperature levels are the unique characteristics of heat-pipes [2].

According to Ong et al. [3] in his experiment of air heat-exchangers with long heat-pipes, temperature differences from 1 to 5°C were experienced when experimental with temperature differences between bath and evaporator temperatures.

Analysis from Tom Brooke from Heat Pipe Technology [4] with a wrap-around heat pipe installed in an air conditioning system, found that the air is pre-cooled from 95°F(35°C) /78% to 78.5°F(25.8°C)/73.7% relative humidity, and re-heat from 55°F(12.8°C)/95% to 73.0°F(22.8°C)/61.8% relative humidity. This is a differential of 10°C change of sensible heat that the heat-pipes were capable to convert.

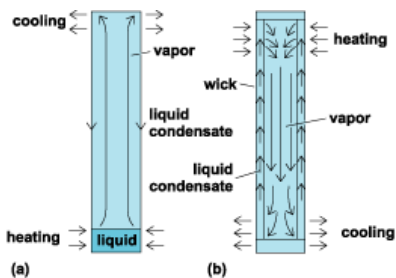


Figure 1a: Heat Pipe Heat-exchanger (HPHE) as a heat transfer tool for cooling and heating.

¹ Zulkarnaini Abdullah is currently pursuing a PhD in UTS, sponsored by MARA and Universiti Kuala Lumpur, Malaysia.

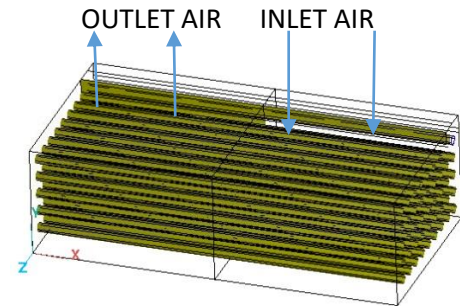


Figure 1b: Heat Pipe Heat-exchanger (HPHE) model.

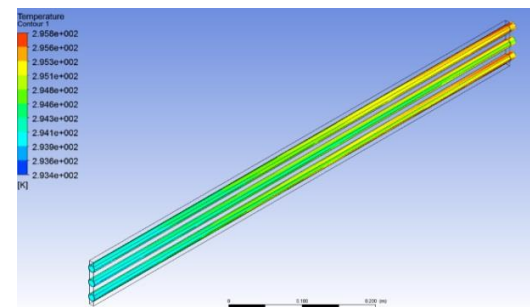


Figure 1c: Heat Pipe Heat-exchanger (HPHE) simulation model runs on ANSYS-Fluent using water as a working medium.

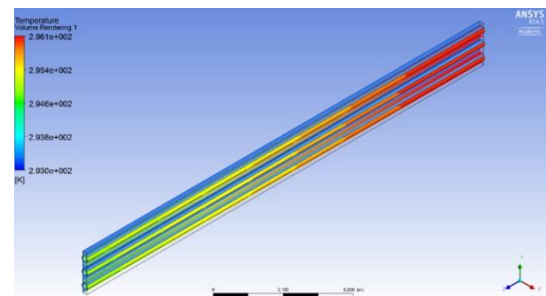


Figure 1d: Heat Pipe Heat-exchanger (HPHE) simulation model runs on ANSYS-Fluent using acetone as a working medium.

1.2 Natural Ventilation

The differences in air density between the inside and outside of the building created natural ventilation. To achieve low-energy building and a clean environment, air change is needed to be acceptable for human thermal comfort. Regarding ASHRAE standard 55, a heat balance model of a human body is exclusively influenced by environmental factors such as temperature, thermal radiation, humidity, airspeed, human activity and clothing [5]. Great attention to the design of natural ventilation to replace indoor air with fresh outdoor air without any energy consumption is being focused on as it also helps to overcome health problems related to insufficient maintenance of

the HVAC system [6]. As suggested by [7], [8], [9] and [10], compared to heating, ventilation and air conditioning (HVAC) systems, natural ventilation is the best approach in providing comfort.

Introduced by [11], the ‘natural ventilation triangle’ as in Figure 1e below, shows buoyancy-driven displacement flows assisted by the wind. He indicated that there is a non-linear relationship between the natural forces of wind and buoyancy.

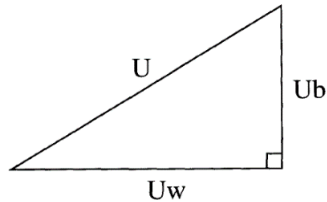


Figure 1e: The natural ventilation triangle for buoyancy-driven displacement flow assisted by the wind. The base and vertical sides of the triangle are set by the magnitudes of the wind and buoyancy produced velocities, U_w and U_b respectively. The length of the hypotenuse determines the total fluid velocity U produced by buoyancy forces reinforced by the wind.

1.3 Computational Fluid Dynamics (CFD)

Computational Fluid Dynamics uses numerical methods and algorithms to solve the problem involves fluid flow and predict flow behaviour based on mathematical modelling. The model is based on fundamental governing equations of fluid dynamics, namely the conservation of mass, momentum, and energy. The fundamental basis of any CFD problem is the Navier-Stoke equations (conservation law). The four terms in the general differential equation are the unsteady term (transient), the convection term, the diffusion term and the source term [12]. There are many research works on natural ventilation such as Bangalee et al. [13] who studied the flow structure of fluid-driven natural ventilation systems using Particle Image Velocimetry (PIV) measurement and Computational Fluid Dynamics (CFD), van Hooff [14] simulated natural ventilation of a large semi-enclosed stadium in an urban area using CO₂ concentration decay method with CFD and Evola [6] study on wind-driven natural ventilation in the building.

2. METHODOLOGY

2.1 Problem Description

The work involved studies of two different natural ventilation patterns, namely cross and single-sided ventilation.

The single-sided opening has both an inlet and outlet at the same façade for a room with fewer options for ventilation. The edges of the opening of the single-sided are shaped with sharp edges for Case 1 and round edges for Case 2. Both are located on top of the room. It is shown in Figures 2a and 2b.

The cross ventilation has two openings for the inlet and outlet, each located on the top and the side of the room respectively. The location of the inlet for Case 3 is in the centre of the roof while in Case 4 the inlet is placed near to an edge of a wall. It is to show the effect of induced air on the roof. It will

tend to provide larger flow rates. It is shown in Figures 2c and 2d.

This computational study focused on natural ventilation, entering a room of dimensions 8m x 5m x 5m, a comparison to room size suggested by Idris [15]. As mentioned by Hunt and Linden [11] the airspeeds induced by a temperature difference of 10°C in a building of 5 m high are of the order of 1.3 m/s and the average of the UK average wind speeds are in the order of 4 m/s.

3. COMPUTATIONAL METHOD

CFD-ACE is used to obtain the result of the satisfactory convergence or when the steady-state is reached. The numerical solution of CFD-ACE processes, continuity and Navier-Stokes equations work in three steps; pre-processing, solving and post-processing.

3.1 Pre-Processing

Pre-processing helps in geometry, the domain of interest and meshing. The modelling in this paper works with CFD-GEOM as the first process. Four building models are used as below;

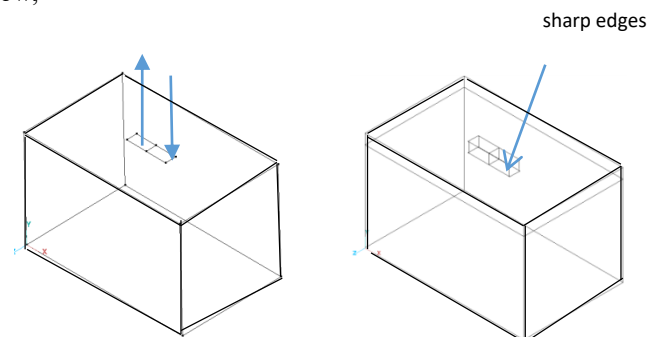


Figure 2a. Case 1 with sharp edges at the inlet and outlet opening

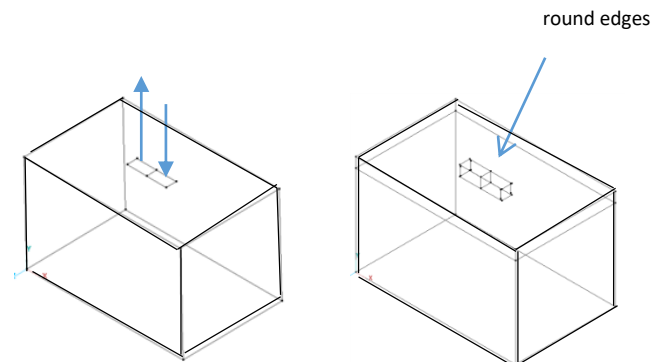


Figure 2b. Case 2 with round edges at the inlet and outlet opening

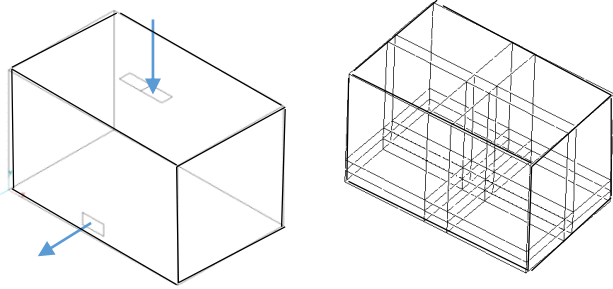


Figure 2c. Case 3 with an outlet located on the sidewall of the building.

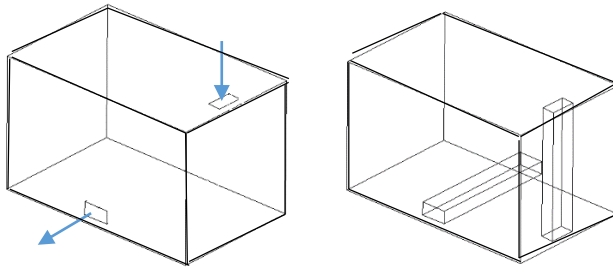


Figure 2d. Case 4 with inlet located at the edge of the roof and outlet located on the sidewall of the building.

Figure 2: Opening for inlet and outlet configurations for all cases. Arrows show the airflow directions inlet and outlet of the room.

Configurations	
Case 1	Top ventilation through an HPHE with both inlet and outlet located on top of the building, sharp edges at the inlet and out the opening.
Case 2	Top ventilation through an HPHE with both inlet and outlet located on top of the building, with round edges at the inlet and the outlet opening.
Case 3	Cross ventilation through the inlet of the HPHE at the top and the air travel to the outlet located on the sidewall of the building. The inlet was located at the centre of the roof, floor and the top outlet opening at the HPHE is closed.
Case 4	Cross ventilation through the inlet of the HPHE at the top and the air travel to the outlet located on the sidewall of the building. The inlet was located at the edge of the roof floor and the top outlet opening at the HPHE is closed.

Table 1: Cases and configurations for the study of the effects of HPHE on a 3-dimensional room with natural ventilation.

The mathematical model for the computational solution used the turbulent flow, 3D Navier-Stokes continuity, and energy equation. The governing equations are [13], [14];

$$\frac{\partial U_j}{\partial x_j} = 0 \quad (1)$$

$$\frac{\partial U_i}{\partial t} + U_j \frac{\partial U_i}{\partial x_j} = -\frac{1}{\rho} \frac{\partial p}{\partial x_i} + \frac{\partial}{\partial x_j} \left[v \left(\frac{\partial U_i}{\partial x_j} + \frac{\partial U_j}{\partial x_i} \right) - \overline{u_i u_j} \right] - \beta(T - T_{ref}) \quad (2)$$

$$\overline{u_i u_j} = v_t \left(\frac{\partial U_i}{\partial x_j} + \frac{\partial U_j}{\partial x_i} \right) - \frac{2}{3} K \delta_{ij}$$

$$\rho c \left(\frac{\partial T}{\partial t} + U_j \frac{\partial T}{\partial x_j} \right) = k \frac{\partial^2 T}{\partial x_j \partial x_j} - \rho c \frac{\partial}{\partial x_j} (\overline{u_j T'}) + \Phi + \Phi \quad (3)$$

$$\overline{u_j T'} = \frac{v_t}{\sigma_t} \left(\frac{\partial T}{\partial x_j} \right)$$

$$\Phi = \mu \left(\frac{\partial U_i}{\partial x_j} + \frac{\partial U_j}{\partial x_i} \right) \frac{\partial U_i}{\partial x_j}$$

$$\frac{\partial K}{\partial t} + U_j \frac{\partial K}{\partial x_j} = \frac{\partial}{\partial x_j} \left[\left(v + \frac{v_t}{\sigma_K} \right) \frac{\partial K}{\partial x_j} \right] + v_t \left(\frac{\partial U_i}{\partial x_j} + \frac{\partial U_j}{\partial x_i} \right) \frac{\partial U_i}{\partial x_j} - \varepsilon \quad (4)$$

$$K = \frac{1}{2} \overline{U_i U_j}$$

$$\varepsilon = v \left(\frac{\partial u_i}{\partial x_j} \right) \left(\frac{\partial u_i}{\partial x_j} \right)$$

$$\frac{\partial \varepsilon}{\partial t} + U_j \frac{\partial \varepsilon}{\partial x_j} = \frac{\partial}{\partial x_j} \left[\left(v + \frac{v_t}{\delta \varepsilon} \right) \frac{\partial \varepsilon}{\partial x_j} \right] + C_{1r} \frac{\varepsilon^2}{K} v_t \left[\left(\frac{\partial U_i}{\partial x_j} + \frac{\partial U_j}{\partial x_i} \right) \frac{\partial U_i}{\partial x_j} \right] - C_{1l} \frac{\varepsilon^2}{K} \quad (5)$$

Where subscript t refers to turbulence

$$\mu_t = \rho C_\mu K^2 / \varepsilon; v_t = \mu_t / \rho;$$

$C_\mu=0.09$; $C1=1.44$; $C2=1.92$; $\sigma K=1.0$; $\sigma\varepsilon=1.0$; reference temperature = 300K. For the simulation, the pressure assumed to be constant, the K and ε value at inlet used;

$$k = \frac{3}{2} (U_{ave} T_i)^2 \tag{6}$$

$$\varepsilon = \frac{C_\mu^{3/4} K^{3/2}}{KL} \tag{7}$$

Where U_{ave} is inlet velocity, T_i is turbulence intensity, $L = 1$ and $K = 0.41$ is the Von Karman constant.

3.2 Solver

A CFD-ACE+GEOM, GUI and BG solver is used in this paper to solve the governing equations that are related to the flow physic problem, based on the given material properties, flow physic model and the boundary conditions. To satisfactorily converge all properties and conditions, the Finite Volume Method is employed to solve velocity components, pressure, and k - ε (epsilon) scheme. Several attempts of meshing tests were taken to satisfy the results. 2nd order spatial differential scheme is used.

Fluid properties used for the simulation processes are corresponding to constant air at 300 K and standard pressure at sea level of 101.3 kPa, where the temperature inlet through the HPHE is assumed to be 305 K; Boussinesq approximation where the fluid density concerning the buoyancy force is affected by temperature change is assumed. Other molecular properties include $\rho = 1.1614 \text{ kg/m}^3$, $\mu = 1.846 \times 10^{-5} \text{ N-s/m}^2$, $\nu = 1.589 \times 10^{-5} \text{ m}^2/\text{s}$. Total nodes and cells that satisfied the convergence were given below for all cases;

	Total cells	Total Nodes
Case 1	324000	292668
Case 2	655360	595820
Case 3	216000	185193
Case 4	81000	73167

Table 2: Total cells, and nodes used for modelling using CFD ACE-GEOM and GUI.

3.3 Post Processing

CFD-View analysed the convergence results and are presentable in a graphical presentation with different plots, streamlines, and data curves. Below are the 3-dimensional graphical airflow traces for all cases;

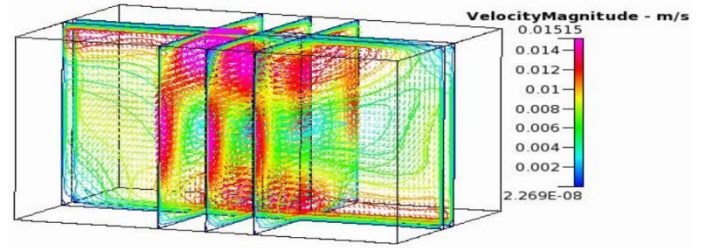


Figure 3a.

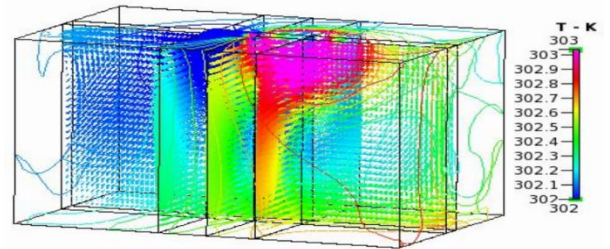


Figure 3b.

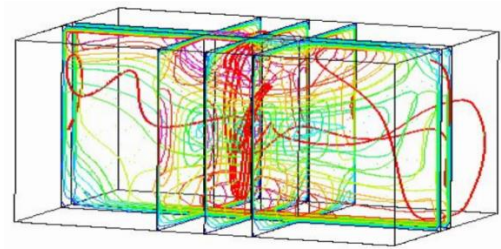


Figure 3c.

Figure 3a, 3b, 3c: **Case 1**, show graphically distributions of velocity magnitude, temperature, and flow path.

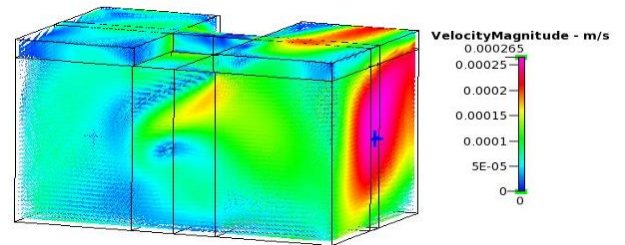


Figure 3d.

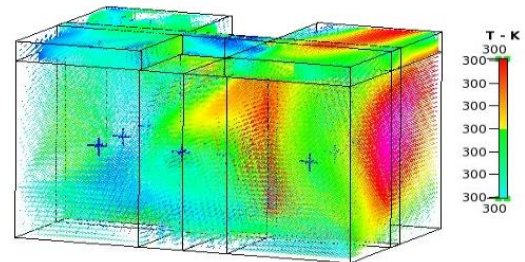


Figure 3e.

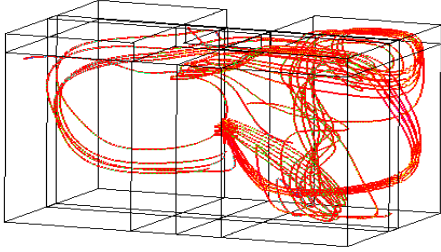


Figure 3f.

Figure 3d, 3e, 3f: **Case 2**, show graphically distributions of velocity magnitude, temperature, and flow path.

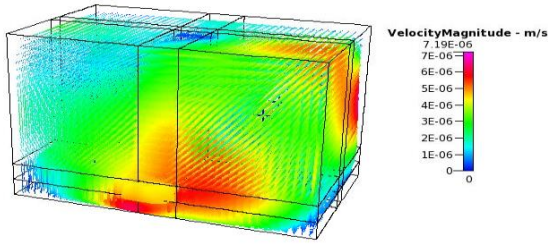


Figure 3g.

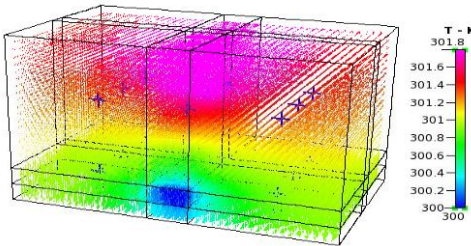


Figure 3h.

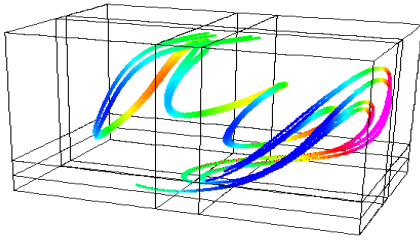


Figure 3i.

Figure 3g, 3h, 3i: **Case 3**, show graphically distributions of velocity magnitude, temperature, and flow path.

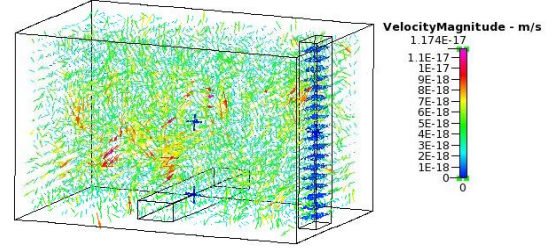


Figure 3j.

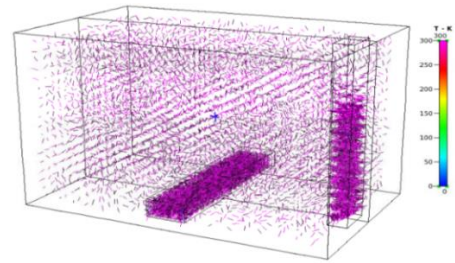


Figure 3k.

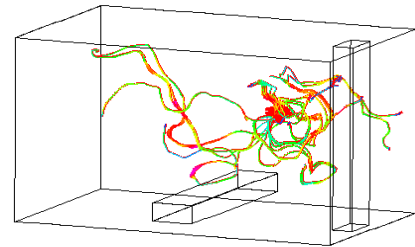


Figure 3l.

Figure 3j, 3k, 3l: **Case 4**, show graphically distributions of velocity magnitude, temperature, and flow path.

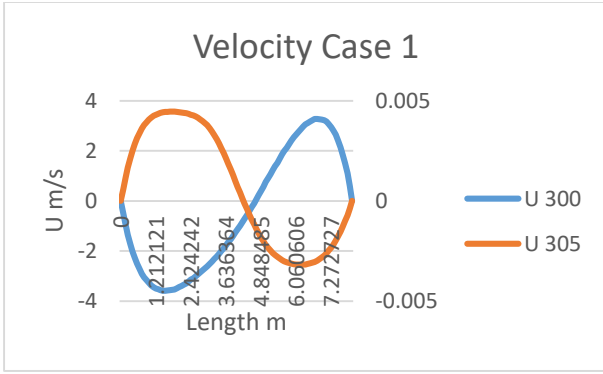
4. RESULT AND DISCUSSION

The purpose of the study is to investigate the airflow pattern and flow rate with different openings and the distribution of temperature. The model used the RANS scheme to show air distribution in a room with natural ventilation. The inlet opening is equipped with Heat Pipe Heat-exchanger (HPHE) to increase the temperature from 300K (27°C) to 305K (32°C). Cases were evaluated by (a) velocity (b) velocity magnitude and (c) flow rate across the room.

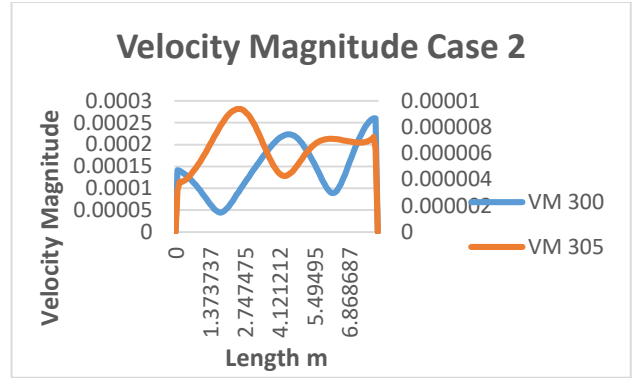
A. Case 1

Case 1a graph shows the distribution of air velocity across the room with the normal sharp opening. It shows that at 305K the velocity of air take-off is greater than the air velocity at temperature 300K, but at the end of the 8 m room, the flow rate of 300K is greater than the flow rate at 305K.

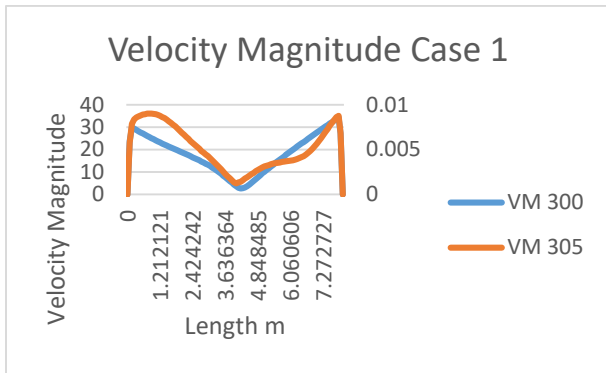
Case 1b shows that the velocity magnitude is higher at a distance of 1 m when the air is warmer by +5°C.



Case 1a: Normal opening with a flow rate at 300K and 305K. The velocity is shown as a positive and negative value when reading from the head and tail from the CFD-ACE software.



Case 2b: Round edge opening with velocity magnitude at 300K and 305K.

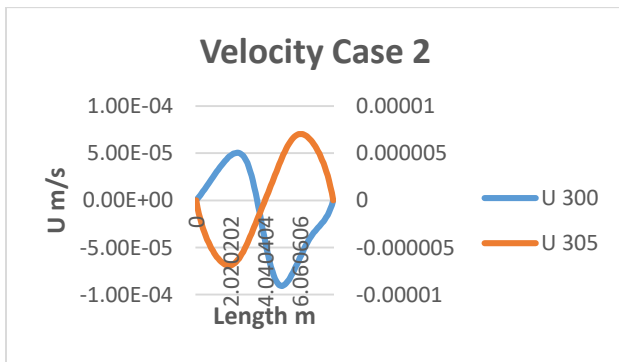


Case 1b: Normal opening with velocity magnitude at 300K and 305K.

B. Case 2

Case 2a shows the distribution of air velocity across the room with round edges opening. As the temperature of 300K, the flow increase in the middle of the room and slowly decreases, while at 305K the velocity increase towards the end of the outlet.

Case 2b shows that the velocity magnitude has a greater effect in the room than at 300K.

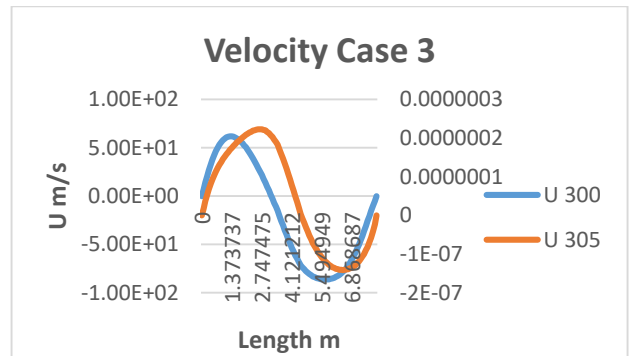


Case 2a: Round edge opening with a flow rate at 300K and 305K

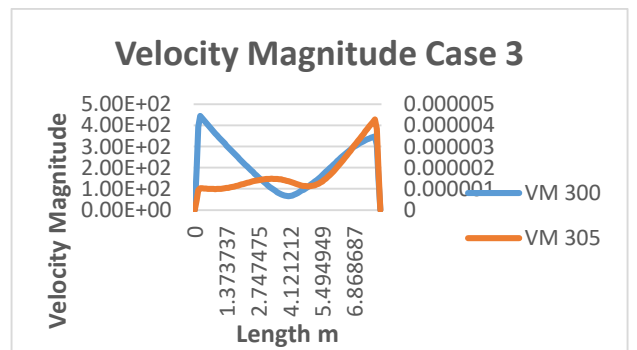
C. Case 3

Case 3a shows the distribution of air velocity around the room with the HPHE is in the centre position on the rooftop. At 300K, the air velocity is less than airflow at 305K when moving in a 4 m distance.

Case 3b shows that the velocity magnitude is higher for air velocity at temperature 300K when it enters the room. At 305K the velocity magnitude is lower at entering the room but gradually higher at the end of 8 m length.



Case 3a: Center inlet opening with a flow rate at 300K and 305K

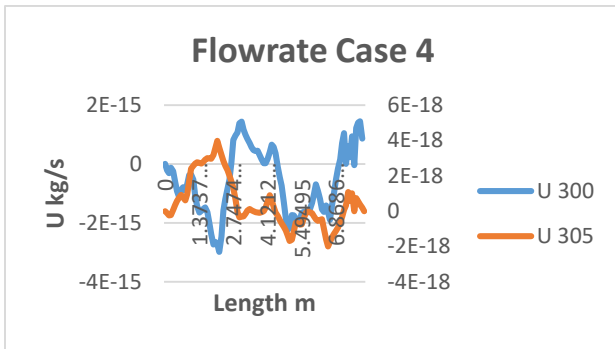


Case 3b: Center inlet opening with a flow rate at 300K and 305K

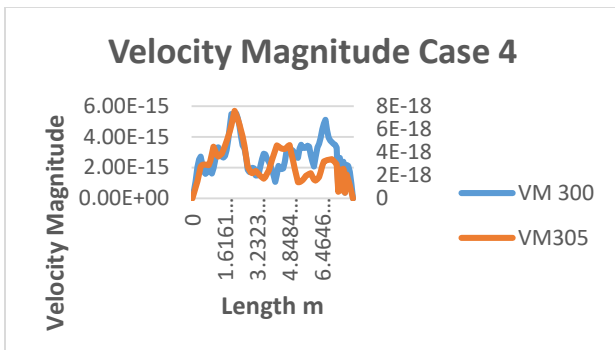
D. Case 4

Case 4a shows the distribution of air velocity around the room when the outlet opening is located on the sidewall of the room. When the air entering the inlet of the opening, it increases to a distance of 2 m and slowly loses its flow afterwards before increasing toward the outlet.

Case 4b shows that the velocity is almost at the same magnitude, but higher at the end for a temperature of 300K.



Case 4a: Edge of rooftop inlet opening with a flow rate at 300K and 305K



Case 4b: Edge of rooftop inlet opening with velocity magnitude at 300K and 305K.

Tables 2 and 3 show the numerical values of the airflow rate to each opening configuration. Table 2 shows the flow rate values for 300K while Table 3 for 305K.

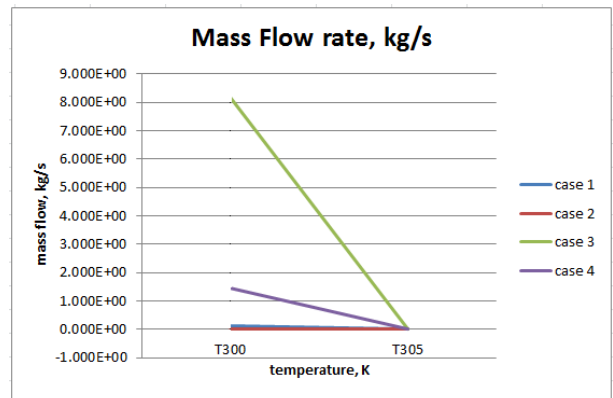
It is found that the highest flow rate was recorded by Case 3a which is cross-ventilation with the inlet opening located at the centre of the rooftop and the outlet located at the sidewall of the room. The position is such that it allows a greater flow rate to enter the room and push the air to the sidewall. Case 4a has an advantage of the top inlet, located on top-edges of the roof. Graph 1 below shows the mass flow rate recorded in all cases. The other configuration seems to record lower values of flow rate.

Opening configuration	A flow inlet at 300K, kg/s	Flow outlet at 300K, kg/s
Case 1a	1.110E-01	-1.207E-01
Case 2a	2.435E-07	-5.819E-07
Case 3a	8.191E+00	-8.599E+00
Case 4a	1.452E+00	-1.452E+00

Table 3: Numerical values of mass flow rate in all cases at inlet 300K.

Opening configuration	A flow inlet at 305K, kg/s	Flow outlet at 305K, kg/s
Case 1b	1.141E-04	-1.141E-04
Case 2b	5.086E-07	-5.941E-07
Case 3b	1.037E-07	-1.049E-07
Case 4b	1.429E-11	-4.801E-12

Table 4: Numerical values of mass flow rate in all cases at inlet 305K.



Graph 1: Mass flow rate for all cases, show that Case 3 and 4 with a centre inlet opening and sidewall outlet recorded the largest flow rate.

5. CONCLUSION

Heat pipe heat-exchanger was the main equipment used to create differences in air density, hence increase the room inlet temperature. Different temperature between the inlet and the room created a flow of natural ventilation. Simulations were performed using a standard k-ε model from Reynolds Average Navier-Stokes (RANS) turbulence equation. The result of the velocity and flow rate distribution was determined according to cases of opening configurations. Case 3 where the inlet opening of an HPHE is located at the centre of the roof, shows a good option for a better flow rate using natural ventilation.

Compare to other configurations, the opening in the centre of a roof shows better results for natural ventilation with different air densities. With natural ventilation entering from the top of a roof, Case 2a with round edges shows a greater mass flow rate

than Case 1a with sharp edges opening and for cross ventilation, Case 3a where the opening is at the top-centre shows the best result of mass flow rate than Case 4a. Of all the cases with top and cross ventilation, Case 3 is the most suitable configuration for natural ventilation.

An experimental investigation is needed to validate the opening configuration for natural ventilation numerical results. Further investigation involving experimental studies of HPHE to increase and decrease the inlet temperature for thermal comfort is needed to validate the numerical results.

References

- 1 P. F. Linden: 'The fluid mechanics of natural ventilation', *Annual Review of Fluid Mechanics*, vol. 31, pp. 201-238, 1999
- 2 Yau, Y.H., and Ahmadzadehtalatapeh, M.: 'A review on the application of horizontal heat pipe heat-exchangers in air conditioning systems in the tropics', *Applied Thermal Engineering*, 2010, 30, (2–3), pp. 77-84
- 3 Ong, K.S., and Haider-E-Alahi, M.: 'Performance of an R-134a-filled thermosyphon', *Applied Thermal Engineering*, 2003, 23, (18), pp. 2373-2381
- 4 Brooke, T.: 'Optimizing Wrap-Around Heat-pipes', *Heat Pipe Technology*, 2007
- 5 de Dear, R.J., and Brager, G.S.: 'Thermal comfort in naturally ventilated buildings: revisions to ASHRAE Standard 55', *Energy and Buildings*, 2002, 34, (6), pp. 549-561
- 6 Evola, G., and Popov, V.: 'Computational analysis of wind-driven natural ventilation in buildings', *Energy and Buildings*, 2006, 38, (5), pp. 491-501
- 7 Jamaluddin, A.A., Hussein, H., Mohd Ariffin, A.R., and Keumala, N.: 'A study on different natural ventilation approaches at a residential college building with the internal courtyard arrangement', *Energy and Buildings*, 2014, 72, (0), pp. 340-352
- 8 Nicol, J.F., and Humphreys, M.A.: 'Adaptive thermal comfort and sustainable thermal standards for buildings', *Energy and Buildings*, 2002, 34, (6), pp. 563-572
- 9 Su, X., Zhang, X., and Gao, J.: 'Evaluation method of a natural ventilation system based on thermal comfort in China', *Energy and Buildings*, 2009, 41, (1), pp. 67-70
- 10 Wong, N.H., Feriadi, H., Lim, P.Y., Tham, K.W., Sekhar, C., and Cheong, K.W.: 'Thermal comfort evaluation of naturally ventilated public housing in Singapore', *Building and Environment*, 2002, 37, (12), pp. 1267-1277
- 11 Hunt, G.R., and Linden, P.P.: 'The fluid mechanics of natural ventilation—displacement ventilation by buoyancy-driven flows assisted by the wind', *Building and Environment*, 1999, 34, (6), pp. 707-720
- 12 Priyadumkol, J., and Kittichaikarn, C.: 'Application of the combined air-conditioning systems for energy conservation in data centre', *Energy and Buildings*, 2014, 68, Part A, (0), pp. 580-586
- 13 Bangalee, M.Z.I., Miao, J.J., Lin, S.Y., and Yang, J.H.: 'Flow visualization, PIV measurement and CFD calculation for fluid-driven natural cross-ventilation in a scale model', *Energy and Buildings*, 2013, 66, (0), pp. 306-314
- 14 van Hooff, T., and Blocken, B.: 'CFD evaluation of natural ventilation of indoor environments by the concentration decay method: CO2 gas dispersion from a semi-enclosed stadium', *Building and Environment*, 2013, 61, (0), pp. 1-17
- 14 Kivva T., Huynh, B. P., Gaston, M. and Munn, D.: 'A Numerical Study of Ventilation Flow Through a 3 Dimensional Room with a Fan', *Turbulence, Heat, and Mass Transfer 6*, Hanjalić, K., Nagano, Y. and Jakirlić, S., (Editors), Begell House, Inc., 2009
- 15 Idris, A.: 'Computational Study of Single-Sided Ventilation Through a 3-Dimensional Room with Rounded Edges', in Editor (Ed.) (Eds.): 'Book Computational Study of Single-Sided Ventilation Through a 3-Dimensional Room with Rounded Edges' (American Society of Mechanical Engineer, 2013, ed.), pp. 9

Numerical Study of Heat-pipes Effects on a 3-Dimensional Room with Driven Ventilation

Z. Abdullah¹, B.P. Huynh¹, and A. Idris²

¹ Faculty of Mechanical Engineering & IT

University of Technology Sydney, Sydney NSW 2006, Australia

² Department of Mechanical Engineering,

Universiti Kuala Lumpur, Malaysia Spanish Institute
Kulim Hi-Tech Park, 09000 Kulim, Kedah, Malaysia

Abstract

The purpose of the study is to investigate the airflow pattern and flow rate with different openings and distribution of temperature in a 3-dimension room. A Computational Fluid Dynamics (CFD) software package is used to investigate numerically a 3-dimensional rectangular-box room installed with a heat-pipes heat-exchanger (HPHE). Heat pipe heat-exchanger utilizing refrigerant using working fluid is installed on top of a room. The air-side heat transfer and the flow pattern of thermo-siphon heat-pipes are studied with natural driven ventilation of a building. Different opening of the inlet and outlet air where the heat pipe installed are tested with round edges opening as well as sharp edges. The standard RANS $k-\epsilon$ turbulence model is used. Results with different settings of the heat pipe and opening characteristic, airflow rate, and flow pattern as well as its temperature effects are examined.

Keywords: Computational Fluid Dynamics, heat-pipes heat-exchanger, natural ventilation, fluid flow, flow pattern.

Nomenclature

$U_j (j = 1 - 3)$	- Component of the average velocity vector
g	- Gravity acceleration
μ_t	- Turbulent viscosity
C_μ	- Empirical constant
K	- Turbulent kinetic energy
ϵ	- Dissipation rate
κ	- Von Karman's constant
U_{ave}	- The average flow velocity
T_i	- Turbulence intensity
L	- Length scale

Introduction

Heat-pipes heat-exchanger (HPHE)

This paper proposed the use of a Heat Pipe Heat-exchanger (HPHE) in a room, hence analyses the airflow pattern of 100% outside air. HPHE is becoming popular as an energy-saving device as there is no external power required and it has no need for maintenance. Noted by [1], 30% of the total energy consumption in the US is used by non-domestic buildings and 30% of that fraction is in

heating and cooling. HPHE might be one of the responses for building thermal comfort. Figure 1 shows the operation and model of HPHE used. HPHE a passive, simple construction and cost-effective heat-exchanger are used as a tool to demonstrate the room airflow pattern which effects by its temperature difference between indoor and outdoor air. Figures 2 and 3 show the simulations series of a three pipe heat-pipes heat-exchanger run on ANSYS-Fluent using acetone as a working medium. The comparisons were to show different temperatures between the inlet and the outlet of the heat-pipes, although the study of the HPHE efficiency itself is not discussed in detail in this paper. The simulations show that the delta temperature difference between 2 to 3°C can be easily achieved with a row of three pipes, a heat-pipes heat-exchanger.

HPHE is designed to have high thermal conductance in steady-state operation, and with only a small temperature difference, it can transfer a high amount of heat. Moreover, the simplicity of design and manufacturing, small temperature drops, wide temperature application range and the ability to control and transport high-heat rates at various temperature levels are the unique characteristics of heat-pipes [2]. The HPHE used in this modelling is measured in an area of 1 m² (2 m x 0.5m) at both inlet and outlet. According to [3] in his experiment of air heat-exchangers with long heat-pipes, temperature differences from 1 to 5°C were experienced when experimental with temperature differences between bath and evaporator temperatures. Analysis from Tom Brooke from Heat Pipe Technology [4] with a wrap-around heat pipe installed in an air conditioning system, found that the pre-cooled air was capable to convert a differential of 10°C sensible heat.

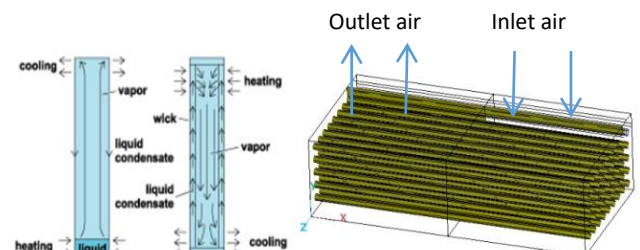


Figure 1: Heat Pipe Heat-exchanger (HPHE) model, as a heat transfer tool for cooling and heating.

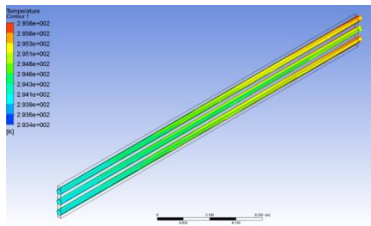


Figure 2: Heat Pipe Heat-exchanger (HPHE) simulation model runs on ANSYS-Fluent using water as a working medium.

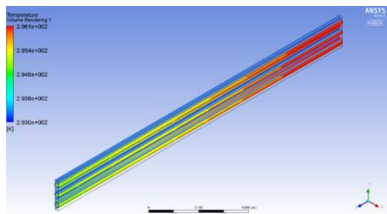


Figure 3: Heat Pipe Heat-exchanger (HPHE) simulation model runs on ANSYS-Fluent using acetone as a working medium.

Ventilation

The differences in air density between the inside and outside of the building created natural ventilation. To achieve low-energy building and a clean environment, air change is needed to be acceptable for human thermal comfort. According to ASHRAE standard 55, a heat balance model of a human body is exclusively influenced by environmental factors such as temperature, thermal radiation, humidity, airspeed, human activity and clothing [5]. Great attention to the design of natural ventilation to replace indoor air with fresh outdoor air without any energy consumption is being focused on as it also helps to overcome health problems related to insufficient maintenance of the HVAC system [6]. As suggested by [7], [8], [9] and [10], compared to heating, ventilation and air conditioning (HVAC) systems, natural ventilation is the best approach in providing comfort.

This computational study focused on driven ventilation, assumed at 3m/s, entering room dimensions of 8m x 5m x 5m, a comparison to room size suggested by [14] and [15]. As mentioned by [16], the airspeeds induced by a temperature difference of 10°C in a building of 5 m high are of the order of 1.3 m/s and the average of the UK average wind speeds are in the order of 4 m/s.

Computational Fluid Dynamics (CFD)

Computational Fluid Dynamics uses numerical methods and algorithms to solve the problem involves fluid flow and predict flow behaviour based on mathematical modelling. The model is based on fundamental governing equations of fluid dynamics, namely the conservation of mass, momentum, and energy. The fundamental basis of any CFD problem is the Navier-Stoke equations (conservation law). The four terms in the general differential equation are the unsteady term (transient), the convection term, the diffusion term and the source term [11]. There are many research work on natural ventilation such as [12], which studied the flow structure of fluid-driven natural ventilation

systems using Particle Image Velocimetry (PIV) measurement and Computational Fluid Dynamics (CFD), [13] simulated natural ventilation of a large semi-enclosed stadium in an urban area using CO2 concentration decay method with CFD and [6] study on wind-driven natural ventilation in buildings.

CFD-ACE from ESI software is used to obtain the result of the satisfactory convergence or when the steady-state is reached. The numerical solution of CFD-ACE processes, continuity and Navier-Stokes equations work in three steps; pre-processing, solving and post-processing.

Methodology

Problem Description

The work involved studies of two different driven ventilation patterns, namely cross and single-sided ventilation. A wind velocity of 3m/s is assumed to enter the inlet of an opening, guided by a guide vane.

The single-sided opening has both an inlet and outlet at the same façade for a room with fewer options for ventilation. The edges of the opening of the single-sided are shaped with sharp edges for Case 1. The cross ventilation has two openings for the inlet and outlet, each located on the top and the side of the room respectively. The location of the inlet for Case 2 is in the centre of the roof while in Case 3 the inlet is placed near to an edge of a wall. It is to show the effect of an induced air on the roof. It will tend to provide larger flow rates. It is shown in Figures 5 to 7.

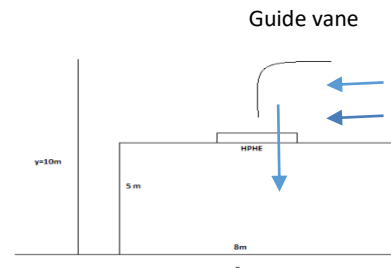


Figure 4. Wind velocity of 3 m/s is assumed to enter the room through the inlet opening on top by the guide vane.

Pre-Processing

Pre-processing helps in geometry, the domain of interest and meshing. The modelling in this paper works with CFD-GEOM as the first process. Four building models were used as below;

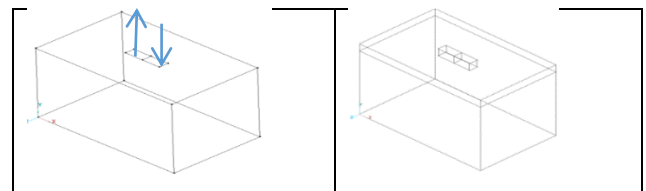


Figure 5. Case 1.

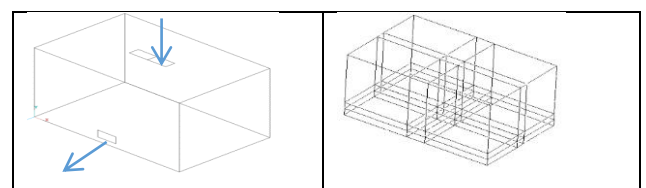


Figure 6. Case 2

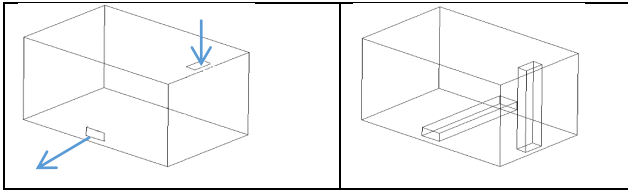


Figure 7. Case 3

Figure 4-7: Opening for inlet and outlet configurations for all cases. Arrows show the air down-flow directions at the inlet and outlet of the room.

The mathematical model for the computational solution used turbulent flow, 3D Navier-Stokes continuity, and energy equation. The governing equations are [13], [14];

$$\frac{\partial U_j}{\partial x_j} = 0 \quad (1)$$

$$\frac{\partial U_i}{\partial t} + U_j \frac{\partial U_i}{\partial x_j} = -\frac{1}{\rho} \frac{\partial p}{\partial x_i} + \frac{\partial}{\partial x_j} \left[v \left(\frac{\partial U_i}{\partial x_j} + \frac{\partial U_j}{\partial x_i} \right) - \overline{u_i u_j} \right] - \beta(T - T_{ref}) \quad (2)$$

$$\overline{u_i u_j} = v_t \left(\frac{\partial U_i}{\partial x_j} + \frac{\partial U_j}{\partial x_i} \right) - \frac{2}{3} K \delta_{ij}$$

$$\rho c \left(\frac{\partial T}{\partial t} + U_j \frac{\partial T}{\partial x_j} \right) = k \frac{\partial^2 T}{\partial x_j \partial x_j} - \rho c \frac{\partial}{\partial x_j} (u_j T) + \Phi + \phi \quad (3)$$

$$\overline{u_j T} = \frac{v_t}{\sigma_t} \left(\frac{\partial T}{\partial x_j} \right)$$

$$\Phi = \mu \left(\frac{\partial U_i}{\partial x_j} + \frac{\partial U_j}{\partial x_i} \right) \frac{\partial U_i}{\partial x_j}$$

$$\frac{\partial K}{\partial t} + U_j \frac{\partial K}{\partial x_j} = \frac{\partial}{\partial x_j} \left[\left(v + \frac{v_t}{\sigma_K} \right) \frac{\partial K}{\partial x_j} \right] + v_t \left(\frac{\partial U_i}{\partial x_j} + \frac{\partial U_j}{\partial x_i} \right) \frac{\partial U_i}{\partial x_j} - \varepsilon$$

(4)

$$K = \frac{1}{2} \overline{U_i U_j}$$

$$\varepsilon = v \left(\frac{\partial u_i}{\partial x_j} \right) \left(\frac{\partial u_i}{\partial x_j} \right)$$

$$\frac{\partial \varepsilon}{\partial t} + U_j \frac{\partial \varepsilon}{\partial x_j} = \frac{\partial}{\partial x_j} \left[\left(v + \frac{v_t}{\sigma_\varepsilon} \right) \frac{\partial \varepsilon}{\partial x_j} \right] + C_1 r \frac{\varepsilon^2}{K} v_t \left[\left(\frac{\partial U_i}{\partial x_j} + \frac{\partial U_j}{\partial x_i} \right) \frac{\partial U_i}{\partial x_j} \right] - C_2 \frac{\varepsilon^2}{K}$$

(5)

Where subscript t refers to turbulence

$$\mu_t = \rho C_\mu K^2 / \varepsilon; v_t = \mu_t / \rho;$$

$C_\mu=0.09$; $C_1=1.44$; $C_2=1.92$; $\sigma_K=1.0$; $\sigma_\varepsilon=1.0$; reference temperature = 300K

For the simulation, the pressure assumed to be constant, the K and ε value at inlet used;

$$K = \frac{3}{2} (U_{ave} T_i)^2$$

(6)

$$\varepsilon = \frac{C_\mu^{3/4} K^{3/2}}{KL}$$

(7)

Where U_{ave} is inlet velocity, T_i is turbulence intensity (here taken to be about 2%), L is here taken to be a "reasonable length" of 1m and $K = 0.41$ is the Von Karman constant. Experience has shown, however, that the values of k and ε imposed at the inlet to the computational domain play only an insignificant role, as long as they are both small.

Solver

A CFD-ACE+GUI and CFD-ACE + BG solver is used to solve the governing equations that are related to the flow physic problems, based on the given material properties, flow physic model and boundary conditions. To satisfactorily converge all properties and conditions, the Finite Volume Method is employed to solve velocity components, pressure, and K - ε (epsilon) scheme. Several attempts of meshing tests were taken to satisfy the results. 2nd order spatial differential scheme is used. Fluid properties used for the simulation processes are corresponding to constant air at 300 K and standard pressure at sea level of 101.3 kPa, where the temperature inlet through the HPHE is assumed to be 305 K. Other molecular properties include $\rho = 1.1614 \text{ kg/m}^3$, $\mu = 1.846 \times 10^{-5} \text{ N-s/m}^2$, $\nu = 1.589 \times 10^{-5} \text{ m}^2/\text{s}$.

Total nodes and cells that satisfied the convergence were given below for all cases;

	Total cells	Total Nodes
Case 1	324000	292668
Case 2	216000	185193
Case 3	81000	73167

Table 1: Show the total cells and nodes used for solving processes.

Post Processing

CFD-View analysed the convergence results and are presentable in a graphical presentation with different plots, streamlines data and curves. Below are the 3-dimensional graphical velocity magnitudes for airflow traces for all cases.

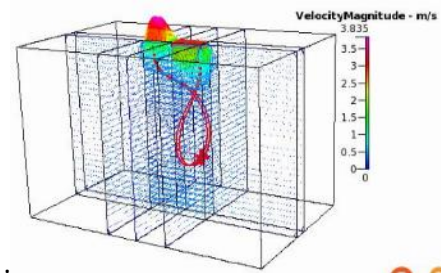


Figure 8. Case 1

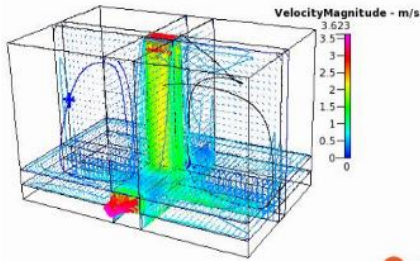


Figure 9. Case 2

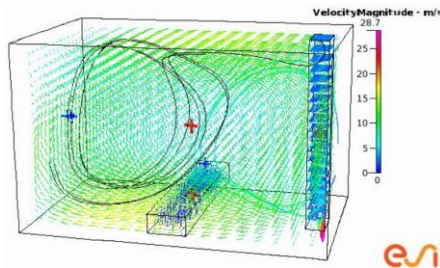


Figure 10. Case 3.

Figure 8-10: Show the graphical velocity magnitude in all cases

Result and Discussion

Cases were evaluated by velocity and mass flow rate across the room. Figure 11 shows the distribution of air velocity across the room with all cases at 300K. It shows that the velocity take-off is lower in all cases when entering the inlet. Halfway through the room shows that Case 2 and Case 3 have larger velocities than the other cases. Case 3 which is cross-ventilation shows the highest velocity at 1.47 m/s.

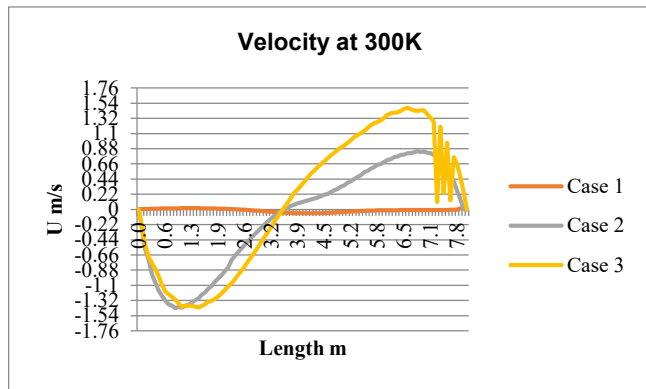


Figure 11: Velocity profile for all cases at 300K.

Figure 12 shows the distribution of air velocity across the room when the temperature is increased to 305K when the air passes through heat-pipes. Case 3 shows the highest velocity at 1.47 m/s

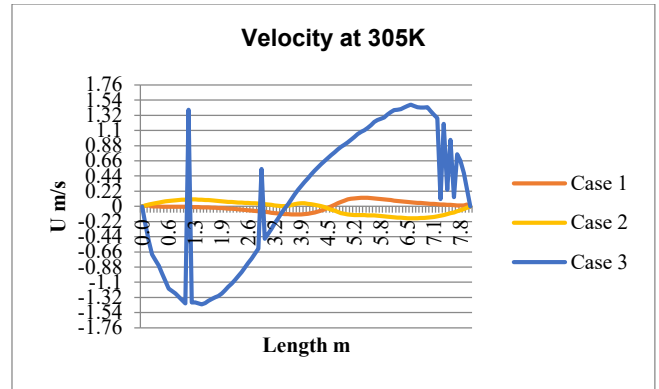


Figure 12: Velocity profile for all cases at 305K.

It is found that both flow rate records the same value at 1.81 kg/s with either 300K or 305K. The highest flow rate was recorded in Case 3 which is cross-ventilation with the inlet opening located at the edge of the rooftop. The position is such that it allows a greater flow rate to enter the room. The other configurations seem to record lower values of flow rate.

	Flow at 300K, kg/s	Flow at 305K, kg/s
Case 1	1.74210	1.74210
Case 2	1.74210	1.74210
Case 3	1.81096	1.81096

Table 2: Numerical values of flow rate in all cases at inlet 300K.

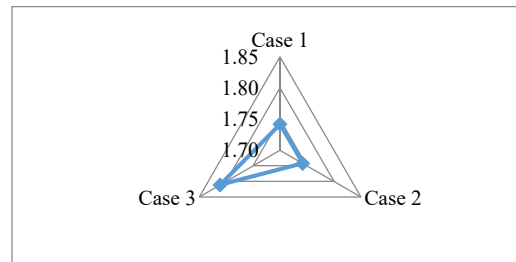


Figure 13: Comparison of the mass flow rate for all cases.

Conclusion

Heat pipe heat-exchanger was the main equipment used to increase the inlet temperature. Different temperatures and air density between the inlet and the room created a flow of natural driven ventilation. A wind velocity of 3 m/s guided by a guide vane is assumed to enter the inlet of an opening and passed through heat-pipes. Simulations were performed using a standard k-ε model from Reynolds Average Navier-Stokes (RANS) turbulence equation. The result of the velocity and flow rate distribution was determined according to cases of opening configurations. Case 3, a cross-ventilation where the inlet opening of an HPHE is located at the edge of the roof, shows a good option for a better flow rate using driven ventilation. Agreement with other studies shows that cross-ventilation flow is still favourable when choosing flow ventilation. Further investigation involving experimental studies of HPHE to influence the air density to the room for thermal comfort is needed to validate the numerical result. Applications such as ventilation fans may be used to create turbulences for room or cabin applications. Other configurations of opening for

inlet and outlet, the direction of driven ventilation and temperature difference should be performed.

References

- [1] P. F. Linden, The Fluid Mechanics of Natural Ventilation, *Annual Review of Fluid Mechanics*, 1999, **31**, 201-238.
- [2] Yau, Y.H. & Ahmadzadehtalatapeh, M., A Review on the Application of Horizontal Heat Pipe Heat-exchangers in Air Conditioning Systems in the Tropics, *Applied Thermal Engineering*, 2010, **30**, 77-84.
- [3] Ong, K.S. & Haider-E-Alahi, M., Performance of an R-134a-Filled Thermosyphon, *Applied Thermal Engineering*, 2003, **23**, 2373-2381.
- [4] Brooke, T. *Optimizing Wrap around Heat-pipes*, Heat Pipe Technology, 2007
- [5] de Dear, R.J. & Brager, G.S., Thermal Comfort in Naturally Ventilated Buildings: Revisions to ASHRAE Standard 55', *Energy and Buildings*, 2002, **34**, 549-561.
- [6] Evola, G. & Popov, V., Computational Analysis of Wind-Driven Natural Ventilation in Buildings, *Energy and Buildings*, 2006, **38**, 491-501.
- [7] Jamaluddin, A.A., Hussein, H., Mohd Ariffin, A.R., & Keumala, N., A Study on Different Natural Ventilation Approaches at a Residential College Building with the Internal Courtyard Arrangement, *Energy and Buildings*, 2014, **72**, 340-352.
- [8] Nicol, J.F., & Humphreys, M.A., Adaptive Thermal Comfort and Sustainable Thermal Standards for Buildings, *Energy and Buildings*, 2002, **34**, 563-572.
- [9] Su, X., Zhang, X., & Gao, J., Evaluation Method of Natural Ventilation System Based on Thermal Comfort in China, *Energy, and Buildings*, 2009, **41**, 67-70.
- [10] Wong, N.H., Feriadi, H., Lim, P.Y., Tham, K.W., Sekhar, C., & Cheong, K.W., Thermal Comfort Evaluation of Naturally Ventilated Public Housing in Singapore, *Building and Environment*, 2002, **37**, 1267-1277.
- [11] Priyadumkol, J., & Kittichaikarn, C., Application of the Combined Air-Conditioning Systems for Energy Conservation in Data Centre, *Energy and Buildings*, 2014, **68**, Part A, 580-586.
- [12] Bangalee, M.Z.I., Miao, J.J., Lin, S.Y., & Yang, J.H., Flow Visualization, PIV Measurement and CFD Calculation for Fluid-Driven Natural Cross-Ventilation in a Scale Model, *Energy and Buildings*, 2013, **66**, 306-314.
- [13] van Hooff, T., & Blocken, B., CFD Evaluation of Natural Ventilation of Indoor Environments by the Concentration Decay Method: CO₂ Gas Dispersion from a Semi-Enclosed Stadium, *Building and Environment*, 2013, **61**, 1-17.
- [14] Kivva T., Huynh, B. P., Gaston, M. & Munn, D., A Numerical Study of Ventilation Flow Through a 3 Dimensional Room with a Fan, *Turbulence, Heat, and Mass Transfer 6*, Hanjalić, K., Nagano, Y. & Jakirlić, S., (editors), Begell House, Inc., 2009
- [15] Idris, A., Computational Study of Single-Sided Ventilation through a 3-Dimensional Room with Rounded Edges, *American Society of Mechanical Engineer*, 2013, **9**.
- [16] Hunt, G.R., & Linden, P.P., The Fluid Mechanics of Natural Ventilation, Displacement Ventilation by Buoyancy-Driven Flows Assisted by Wind, *Building and Environment*, 1999, **34**, 707-720.

CFD-Simulation of the Effect of Heat-pipes Attached to an Evaporator and Condenser of an Air-Cooled-Air-Conditioner.

Z. Abdullah^{1,2}, B. Phuoc Huynh¹ and A. Idris³

¹Faculty of Engineering & IT,

University of Technology Sydney, NSW 2007, Australia

²HVAC&R Department, Universiti Kuala Lumpur,

Malaysia France Institute, Bandar Baru Bangi, Selangor, Malaysia

³Department of Mechanical Engineering,

Universiti Kuala Lumpur, Malaysia Spanish Institute Kulim, Kedah, Malaysia

Abstract

Cooling technology with a normal vapour compression cycle relies on electricity to increase and decrease the pressure, hence the temperature, within its cycle. Passive cooling using heat pipe heat-exchangers is being applied to the refrigeration cycle components to assist with temperature reduction of the cooling process. The return and supply air temperatures of an evaporator and condenser are being pre-cooled by passive cooling equipment to assist in reducing the compressor work done. Computational fluid dynamics software is used to run simulations and results are presented in terms of temperature, contour, velocity vectors, and flow patterns. The objective of this study is to investigate and simulate air around a circular air-cooled evaporator and condenser tube for an air conditioning system. The tube from the evaporator is a row of five copper tubes (10mm OD) exposed to a room temperature of 297K and the tube for the condenser is exposed to ambient air of 300K. The system is set to an evaporating temperature of $T_e=278\text{K}$ and the condensing temperature of $T_c=319\text{K}$. An air gap between the heat pipe heat-exchanger and the tube where the simulation of heat transfer is assumed to be the key process is discussed. The results of the air outlet of the evaporator and condenser with the effect of the heat pipe heat-exchanger attached to it are discussed. It is found that the operating temperature is reduced when a heat pipe heat-exchanger is attached to the components. Increasing the heat transfer rate between the heat pipe and the component's tube will increase the system capacity.

Introduction

Heat-exchanger plays an important role in the refrigeration cycle to absorb and remove the heat of indoor to the outdoor, or vice versa. A refrigerant is compressed by a compressor to increase its pressure and temperature compared to the ambient condition. Heat transfer between the ambient air occurs on the condenser surfaces when removing heat and turns the refrigerant inside the condenser tube to the liquid phase of reduced temperature. Adversely, the expansion valve drops the refrigerant temperature in the evaporator to absorb the room heat, and in the process turns the liquid to the vapour phase.

The heat-pipes heat-exchanger is a device that transfers the surrounding heat by absorbing and desorbing heat through its tube. Tubes are filled with refrigerant, to be evaporated and condenses from liquid to vapour state from one end of the tube to the other. In the evaporator section of the tube, the cool refrigerant liquid absorbs the surrounding heat and evaporates the liquid into vapour. The evaporated vapour moved to the condenser section of the tube and releases the heat to the surrounding, which in turn condenses the refrigerant vapour back to a liquid phase. With gravitational force and the capillary action of a wick inside the tube, the liquid moves back to the evaporator section and repeat the cycle. In steady-state operation, a heat pipe with a metalworking fluid will have a high thermal conductance compared to a solid metal conductor. Among the unique characteristics of heat, the pipe is a small temperature drop, a wide temperature application range and the ability to control and transport high-heat rates at various temperature levels [1]. Although the heat pipe heat-exchanger had been applied in a variety of heating, ventilation and air conditioning systems and energy recovery processes, only the application to the refrigeration cycle will be discussed in this paper. A numerical study using ANSYS Fluent and CFD-ACE + is used to view the behaviours of refrigerant R134a, the heat transfer medium in the tubes, the temperature profile of the air passing through the heat-pipes and then through the refrigeration condenser and evaporator.

1. Application of Heat Pipe Heat-exchanger Attached to a Condenser and Evaporator Coils in a Refrigeration System

Heat-pipes were capable of converting a differential change of heat by transferring heat from one end to the other. Ong et al. [2] made an experiment with long heat-pipes, air heat-exchangers, and compared the bath temperature to the evaporator temperature and recorded a differential of 1K to 5K. Tom Brooke [3] experimented with an air conditioning system with a wraparound heat pipe installed and found that the air can be pre-cooled from 35°C (308K) to 25.8°C (298.8K) and can be re-heat from 12.8°C (285.8K) to 22.8°C (295.08K). Figure 1 shows the heat pipe technology and the model of heat-pipes used.

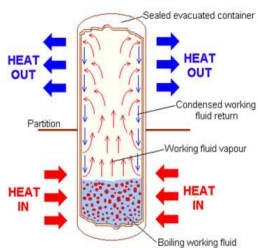


Figure 1: The Heat Pipe Heat-exchanger. The refrigerant liquid in the heat pipe heat-exchanger at the bottom of the tube absorbed heat at the evaporator section and release it at the condenser at the upper section. The liquid evaporates into a vapour phase in the evaporator and moves towards the condenser section, which in turn changes back to the liquid phase by releasing the heat to the surrounding.

2. Problem Description

An air-cooled refrigeration cycle condenser coil of 319K and an evaporator of 278K are being simulated. In the condenser coils, the condensing temperature drops from 319K to 315K while the evaporating temperature increase from 278 to 282K. As suggested by [4], [5], the author used the maximum temperature of 319K for the condensing temperature and 278K for the evaporating temperature. A heat pipe heat-exchanger is installed 100mm before the coils and acts as a heat sink to reduce the air temperature and pre-cooled the flowing air. Attaching the heat pipe to the front air intake of the refrigeration coils will have lowered the ambient air temperature before touching the surface of the coils. Passive cooling technologies had been studied by [6], [7], [8], and [9] has proposed a passive cooling system technology using methanol as the cooling medium. This 2D computational study focused on air flows, crossing a condenser and an evaporator. Only the evaporator side of the heat pipe heat-exchanger which absorbs the surrounding heat is shown in the simulation. Three models of each coil are simulated; a simulation of a coil for reference, a heat pipe attached close to the coil and a heat pipe separated 100mm away from the coil by monitoring the air outlet that crosses the heat pipe and crossing off the coils. Figure 3 shows the proposed idea of a closed tube heat pipe heat-exchanger with R134a as a refrigerant medium, used to transfer heat from one end to the other, attached to a coil side of a refrigeration system.

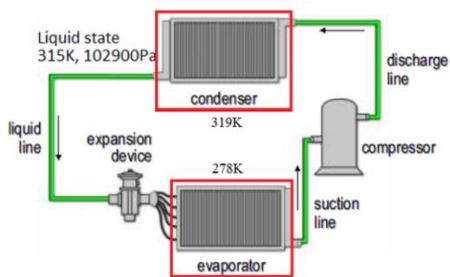


Figure 2: The Refrigeration Cycle. The condenser coil is a heat exchanger used to reject the heat of the refrigerant to the surrounding. The evaporator coil absorbs room heat and lowers the room temperature.

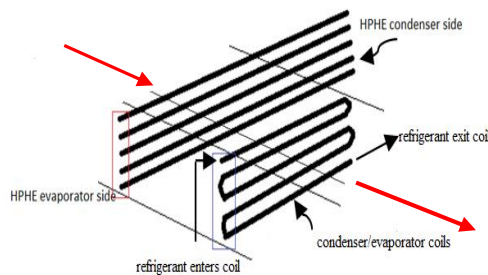


Figure 3: Schematic of a refrigeration coil with the application of straight horizontal heat pipe showing the inlet and outlet of air paths. An evaporation temperature of 295K is used for the simulation of the heat pipe heat exchanger.

3. Simulation Models/Mesh

Several attempts are taken when testing with the mesh distribution as in Table 2 and Figures 4 to 6.

Domain	Specification
Case 1	Air at 300K flows on the surface of an air-cooled condenser/evaporator.
Case 2	Air at 300K flows on the surface of a heat pipe and a condenser/evaporator that is attached closely together.
Case 3	Air at 300K flows on the surface of a heat pipe and a condenser/evaporator that is separated 100mm apart.

Table 1: Problem description in all cases

Domain	Nodes	Elements
Case 1a, b	1572	1447
Case 2	1817	1643
Case 3	1623	1455

Table 2: The specification of nodes and elements for condenser

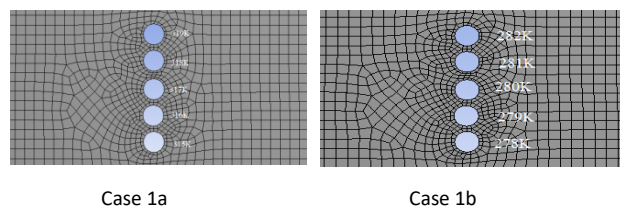


Figure 4: Case 1a for the condenser and 1b for the evaporator.

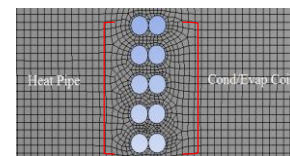


Figure 5: Case 2.

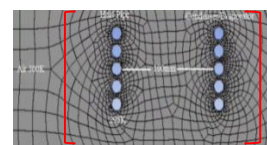


Figure 6: Case 3.

4. Boundary Conditions

Domain	Heat Pipe + Condenser/Evaporator
Dimension 2D	Serial Options
General	Pressure based, Absolute velocity, Time: steady, 2D planar, Gravity: Y direction -9.81 m/s ²
Model	Energy: on, Viscous: standard k-ε
Material	Fluid: air, Solid: copper
Boundary conditions	Velocity magnitude: 1m/s, Thermal: 300K. Pressure outlet, Backpressure: 300K. Condenser tube temp 315K to 319K. Heat pipe tube temp 295K
Wall	Surface body: stationary wall, No-slip
Solution Methods	Scheme: simple, Gradient: Least square cell-based, Pressure: Standard, Momentum: Power-law, Energy: Power law

Table 3: Boundary condition runs on ANSYS Fluent.

The 3D Navier-Stokes continuity and energy equation are used as the mathematical model for the computational solution for turbulent flow as suggested by [10], [11] and [12];

$$\frac{\partial u_j}{\partial x_j} = 0 \quad (1)$$

$$\frac{\partial u_i}{\partial t} + U_j \frac{\partial u_i}{\partial x_j} = -\frac{1}{\rho} \frac{\partial p}{\partial x_i} + \frac{\partial}{\partial x_j} \left[v \left(\frac{\partial u_i}{\partial x_j} + \frac{\partial u_j}{\partial x_i} \right) - \overline{u_i u_j} \right] - \beta(T - T_{ref})g_i \quad (2)$$

$$\overline{u_i u_j} = v_t \left(\frac{\partial u_i}{\partial x_j} + \frac{\partial u_j}{\partial x_i} \right) - \frac{2}{3} \kappa \delta_{ij}$$

$$\rho c \left(\frac{\partial T}{\partial t} + U_j \frac{\partial T}{\partial x_j} \right) = k \frac{\partial^2 T}{\partial x_j \partial x_j} - \rho c \frac{\partial}{\partial x_j} (\overline{u_j T'}) + \Phi + \emptyset \quad (3)$$

$$\overline{u_j T'} = \frac{v_t}{\sigma_t} \left(\frac{\partial T}{\partial x_j} \right)$$

$$\Phi = \mu \left(\frac{\partial u_i}{\partial x_j} + \frac{\partial u_j}{\partial x_i} \right) \frac{\partial u_i}{\partial x_j}$$

$$\emptyset = \mu \left[\left(\frac{\partial u_i}{\partial x_j} \right) \left(\frac{\partial u_i}{\partial x_j} \right) + \left(\frac{\partial u_i}{\partial x_j} \right) \left(\frac{\partial u_i}{\partial x_j} \right) \right]$$

$$\frac{\partial K}{\partial t} + U_j \frac{\partial K}{\partial x_j} = \frac{\partial}{\partial x_j} \left[\left(v + \frac{v_t}{\sigma_K} \right) \frac{\partial K}{\partial x_j} \right] + v_t \left[\left(\frac{\partial u_i}{\partial x_j} + \frac{\partial u_j}{\partial x_i} \right) \frac{\partial u_i}{\partial x_j} + \frac{\beta}{\sigma_t} g_j \frac{\partial T}{\partial x_j} \right] - \varepsilon \quad (4)$$

$$K = \frac{1}{2} \overline{U_i U_j}$$

$$\varepsilon = v \left(\frac{\partial u_i}{\partial x_j} \right) \left(\frac{\partial u_i}{\partial x_j} \right)$$

$$\frac{\partial \varepsilon}{\partial t} + U_j \frac{\partial \varepsilon}{\partial x_j} = \frac{\partial}{\partial x_j} \left[\left(v + \frac{v_t}{\sigma_\varepsilon} \right) \frac{\partial \varepsilon}{\partial x_j} \right] + C_1 \frac{\varepsilon}{K} v_t \left[\left(\frac{\partial u_i}{\partial x_j} + \frac{\partial u_j}{\partial x_i} \right) \frac{\partial u_i}{\partial x_j} + \frac{\beta}{\sigma_t} g_j \frac{\partial T}{\partial x_j} \right] - C_2 \frac{\varepsilon^2}{K} \quad (5)$$

Where subscript t refers to turbulence

$$\mu_t = \rho C_\mu K^2 / \varepsilon; v_t = \mu_t / \rho;$$

$C_\mu=0.09$; $C_1=1.44$; $C_2 =1.92$; $\sigma_K =1.0$; $\sigma_\varepsilon=1.3$; reference temperature = 300K. For the simulation, the pressure assumed to be constant, the K and ε value at inlet used;

$$K = \frac{3}{2} (U_{ave} T_i)^2 \quad (6)$$

$$\varepsilon = \frac{C_\mu^{3/4} K^{3/2}}{KL} \quad (7)$$

Where U_{ave} is inlet velocity, T_i is turbulence intensity (here taken to be about 2%), L is here taken to be a "reasonable length" of 1m and $\kappa = 0.41$ is the Von Karman constant.

5. Solver

ANSYS Fluent solver is used in this case, to solve the governing equations that are related to the flow physic problem, based on the given material properties, flow physic model and the boundary conditions. All properties and conditions are satisfactorily converging using the Finite Volume Method to solve velocity components, pressure, and k - ε (epsilon) scheme.

Fluid properties used for the simulation process with heat pipe heat-exchanger are corresponding to constant air at 293K. Several attempts using water, acetone, and R134a were simulated. To show the flow of the air when moving to pass the tube, a 0.2 m/s of flow rate is applied. Fluid properties used in the

heat pipe-condenser simulation processes are corresponding to constant air at 300 K and standard pressure at sea level of 101.3 kPa, where the temperature inlet through the heat pipe heat-exchanger is assumed to be 300 K and the ventilation flow is assumed to be in +X direction. Boussinesq approximation where the fluid density concerning the buoyancy force is affected by temperature change is assumed, with reference temperature T_{ref} is 300K and Vol. Coef. Th. Exp. is 0.003333 1/K. Other molecular properties include $\rho = 1.1614 \text{ kg/m}^3$, $\mu = 1.846 \times 10^{-5} \text{ N-s/m}^2$, $\nu = 1.589 \times 10^{-5} \text{ m}^2/\text{s}$.

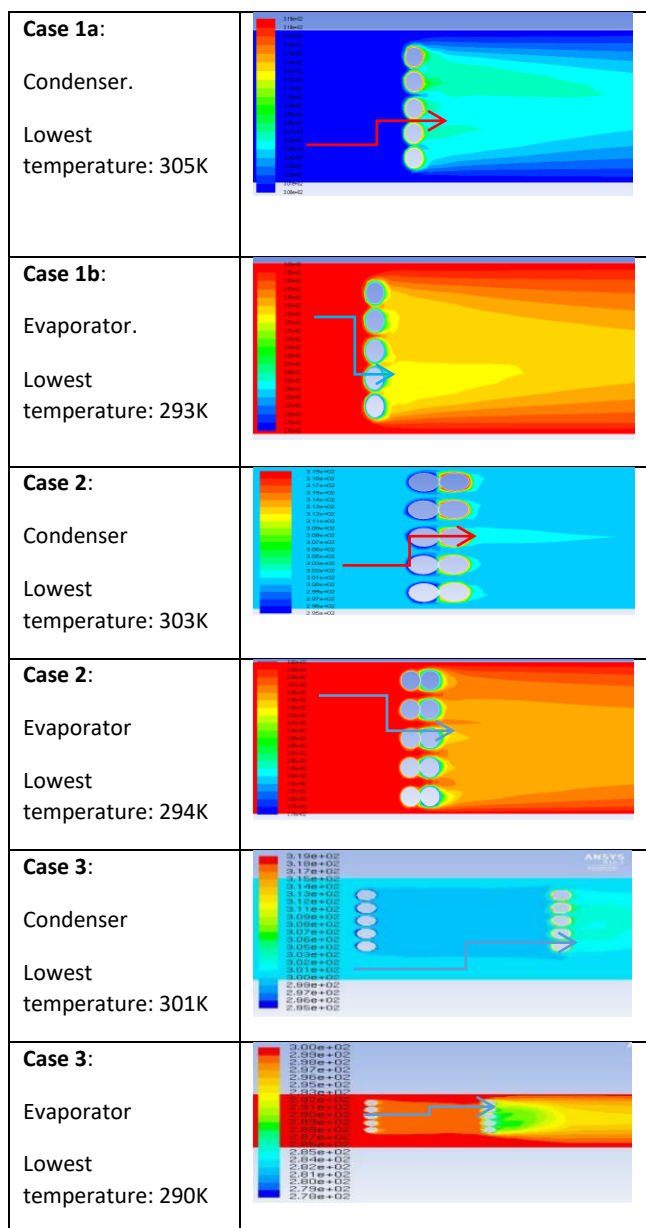


Figure 7: Simulation for all cases.

6. Result and Discussion

The purpose of this study is to study the temperature decreasing effect of a heat pipe heat-exchanger by simulating an airflow to air-cooled air-conditioner coils. The heat pipe is used to investigate the possibilities of reducing supply air temperature to the coils. The flow pattern is recorded by simulation software ANSYS Fluent. The previous simulation shows a difference of 5K is

obtained when R134a is used as a refrigerant medium in the heat pipe. From the simulation of the heat pipe to the coils of an air-cooled system, it is found that efficiency can be increased with the attachments of the heat pipe to the inlet of airflow of coils. When simulated, an air-cooled condenser is recorded to reject heat at about 12K to 15K, and the evaporator coils are lowered to 8K. Table 5 shows the inlet and outlet temperature profile of three cases to point out the capability of the heat pipe in transferring heat.

Condenser	Case 1	Case 2	Case 3
Inlet, K	300	300	300
HP, K		295	295
Cond. T_c K	315-319	315-319	315-319
Outlet, K	305-307	303-304	301-303
Different, K	10	12	14

Table 4: The table shows the comparison of the temperature difference between cases at a condenser coil. Case 3 shows the best result.

Evaporator	Case 1	Case 2	Case 3
Inlet, K	300	300	300
HP, K		295	295
Evap. T_e K	278-282	278-282	278-282
Outlet, K	293-294	294-295	290-292
Different, K	11	12	8

Table 5: The table shows the comparison of temperature different K between cases at evaporator coils. Case 3 shows the best result.

Base on the pressure-enthalpy diagrams of an air-cooled refrigeration system corresponding to an evaporating temperature of $T_e = 5^\circ\text{C}$ (278K), condensing temperature $T_c = 46^\circ\text{C}$ (319K) [14], with 10K superheat and 20K sub-cooling; compared to a condensing temperature of $T_c' = 32^\circ\text{C}$ (305K) using heat pipe, the work-done can be calculated as;

$$\text{Evaporator work done } Q_e = h_4 - h_1 \quad (8)$$

$$\text{Condenser work done, } Q_c = h_3 - h_2 \quad (9)$$

$$\text{Compressor Work Done, } W = h_2 - h_1 \quad (10)$$

$$\text{Coefficient of performance, COP} = h_4 - h_1 / h_2 - h_1 \quad (11)$$

Parameters	Coils	HP + Coils
Evaporating T_e ($^\circ\text{C}$)	5	5
Condensing T_c ($^\circ\text{C}$)	46	32
Condenser Surface Temp ($^\circ\text{C}$)	58	45

Superheat (different K)	10	10
Subcooled (different K)	20	20
Evaporator Work Done Q_e (kJ/kg)	173.8	193.3
Condenser Work Done Q_c (kJ/kg)	200.5	211.7
COP	6.5	10.5
Compressor Work Done W (kJ/kg)	26.73	18.42

Table 6: The table shows the comparison of the normal refrigeration cycle compared to coils with a heat pipe.

with a Fan, Turbulence, Heat and Mass Transfer 6, K. Hanjalić, Y. Nagano and S. Jakirlić (Editors), Begell House Inc., 2009.

- [11] Bangalee, M.Z.I., Miao, J.J., Lin, S.Y., and Yang, J.H., Flow Visualization, PIV Measurement and CFD Calculation for Fluid-Driven Natural Cross-Ventilation in a Scale Model, *Energy and Buildings*, 66, 2013, 306-314.
- [12] van Hooff, T., and Blocken, B., CFD Evaluation of Natural Ventilation of Indoor Environments by the Concentration Decay Method: CO₂ Gas Dispersion from a Semi-Enclosed Stadium, *Building and Environment*, 61, 2013, 1-1

7. Conclusion

From the refrigeration cycle plotted, it is found that the evaporating capacity and the condensing capacity can be increased, with the fall of condensing temperature T_c . The heat pipe heat-exchanger may be used as one of the solutions to decrease the condensing temperature to the ambient. Other simulations using the different refrigerant mediums in the heat pipe heat-exchanger should be tested.

References

- [1] Yau, Y.H., and Ahmadzadehtalatapeh, M., A Review on the Application of Horizontal Heat Pipe Heat-exchangers in Air Conditioning Systems in The Tropics, *Applied Thermal Engineering*, **30**, (2-3), 2010, 77-84.
- [2] Ong, K.S., and Haider-E-Alahi, M., Performance of an R-134a-Filled Thermosyphon, *Applied Thermal Engineering*, **23**, (18), 2003, 2373-2381.
- [3] Brooke, T., Optimizing Wrap around Heat-pipes, *Heat Pipe Technology*, 2007.
- [4] W. P. Jones, *Air Conditioning Engineering* (Fifth Edition), Butterworth-Heinemann, 2001.
- [5] W. T. Grondzik, *Air-Conditioning System Design Manual* (Editor, Second Edition), American Society of Heating Refrigerating and Air-Conditioning Engineer Special Publication, 2007.
- [6] R.R. Riehl, T.C.P.A. Siqueira., Heat Transport Capability and Compensation Chamber in Fluence in Loop Heat-pipes Performance, *Applied Thermal Engineering* 26, 2006, 1158 - 1168.
- [7] W. Joung, T. Yu, J. Lee., Experimental Study on the Loop Heat Pipe with a Planar Bifacial Wick Structure, *International Journal of Heat and Mass Transfer*, 51, 2008, 1573-1581.
- [8] P. Charoensawan, P. Terdtoon., Thermal Performance of Horizontal Closed-Loop Oscillating Heat Pipe, *Applied Thermal Engineering*, 28, 2008, 460-466.
- [9] C. T. Meng, S.H. Chih, W.K. Shung., Experimental Study of a Loop Thermosyphon Using Methanol as Working Fluid, 14th IHPC, 2007.
- [10] T. Kivva, B.P. Huynh, M. Gaston and D. Munn, A Numerical Study of Ventilation flow through a 3-Dimensional Room

IMECE2015-50489

NUMERICAL SIMULATIONS OF THE FLOW AND HEAT BEHAVIOUR FOR A HEAT PIPE HEAT-EXCHANGER IN AN OUTDOOR POWER SUPPLY CABINET

Z. Abdullah^{1,2}

¹Faculty of Mechanical Engineering & IT
University of Technology, Sydney
Sydney, NSW, Australia

²HVAC&R Department

Universiti Kuala Lumpur, Malaysia France Institute
Bandar Baru Bangi, Selangor, Malaysia

A. Idris

Department of Mechanical Engineering,
Universiti Kuala Lumpur, Malaysia Spanish Institute
Kulim Hi-Tech Park, 09000 Kulim, Kedah
Malaysia

B.P. Huynh

Faculty of Mechanical Engineering & IT
University of Technology, Sydney
Sydney, NSW, Australia

ABSTRACT

This paper proposed a numerical simulation for the usage of a copper tube heat pipe heat-exchanger (HPHE) in a power supply cabinet, particularly for an outdoor cabinet where the inside space of the cabinet temperature is high. A cabinet containing electro-mechanical parts is situated outdoors, where the temperature of the ambient combining with the heat generated by the operational parts of the power supply can reach + 55°C. A fin type copper tube heat pipe heat-exchanger is proposed to cool the inside space of the cabinet with natural driven ventilation by circulating and replacing the outside air to the inside. The operating system of the electrical and the mechanical parts inside the cabinet generated a high temperature, and with the sun heating from outside of the cabinet, cooling and fresh air are needed. The fresh ambient air is cooled by the evaporator side of the heat-pipes before circulating within the inner cabinet. The outlet opening is equipped with an exhaust fan to reject hot air. The cooling and the distributions of air are

essential for protecting the electro-mechanical parts from overheated, hence tripping the system. The feasibility of using heat-pipes heat-exchanger for an outdoor cabinet was carefully studied through modelling using ANSYS Workbench. A fin-type heat-exchanger with a straight copper tube heat pipe heat-exchanger using R134a as a heat transfer medium was proposed instead of a thermos-siphon or loop heat-pipes with normal applications. A Computational Fluid Dynamics (CFD) software packages are used to investigate numerically the temperature changes by the heat-pipes refrigerant medium to the air in the cabinet. The temperature behaviour of the refrigerant inside the heat pipe heat-exchanger is studied. A heat transfer simulation between the copper pipes and the refrigerant is shown using ANSYS-Fluent software. The heat transfer pattern at the heat pipe heat-exchanger as well as the flow pattern of the air through the heat-pipes was shown with a given constant flow rate. CFD-ACE software package for cabinet space simulation is used to show the distributions of the inside air. Several angle positions and locations of the heat-pipes, air inlet and outlet are tested to

show the distribution inside the cabinet, hence an optimum heat transfer condition and distribution of air inlet and outlet of the cabinet are proposed. The standard K- ϵ turbulence model is used. A Boussinesq approximation where the fluid density concerning the buoyancy force is affected by temperature change is assumed. Air's flow rate and flow pattern, as well as its temperature effects, are compared and examined when using a heat pipe heat-exchanger with other environmentally-friendly refrigerants medium. The heat pipe heat-exchanger efficiency is predicted. The result shows that the straight heat pipe heat-exchanger is capable of transferring high heat from the inside of the cabinet to the ambient. A temperature difference of 5 K is achieved with R134a filled heat-pipes.

Keywords: *computational fluid dynamics, heat pipe heat-exchanger, fin tubes, outdoor cabinet, power supply box, heat transfer, airflow rate, the temperature flow pattern*

NOMENCLATURE

$U_j (j = 1 - 3)$	- Component of average velocity vector, m/s
g	- Gravity acceleration, m/s ²
μ_t	- Turbulent viscosity, Pa/s
C_μ	- Empirical constant, 0.09
k	- Turbulent kinetic energy, m ² /s ²
ϵ	- Dissipation rate, m ² /s ³
κ	- Von Karman's constant, 0.41
U_{ave}	- The average flow velocity, m/s
T_i	- Turbulence intensity
L	- Length scale, m
T_1	- Cabinet temperature °C
T_3	- Evaporator off coil temperature °C
T_4	- Inlet air temperature °C

INTRODUCTION

The heat pipe heat-exchanger is a heat transfer device by transferring the latent heat of vaporization from one end to the other. An individual closed tube filled with refrigerant fluid evaporates and condenses, from a liquid state to vapour, and then returns to the evaporator section by gravitational force and the capillary action of a wick inside the tube. In steady-state operation, a heat pipe with

a metalworking fluid will have a high thermal conductance compared to a solid metal conductor. Among the unique characteristics of heat-pipes are a small temperature drop, wide temperature application range and the ability to control and transport high-heat rates at various temperature levels [1]. The heat pipe heat-exchanger had been used in a variety of heating, ventilation and air conditioning systems and energy recovery processes, but only the application in a power supply cabinet with high temperature will be discussed in this paper. The study separated the applications of heat-pipes in the numerical study using ANSYS Fluent and CFD ACE + to view the behaviours of refrigerant R134a as the heat transfer medium in the tubes, the temperature profile of the air passing through the heat-pipes and the air distribution in the power supply cabinet.

1. Application of Heat Pipe Heat-exchanger in a Power Supply Cabinet

According to Ong et al. [2] in his experiment of air heat-exchangers with long heat-pipes, temperature differences from 1°C to 5°C were experienced when experimental with temperature differences between bath and evaporator temperatures. Analysis from Tom Brooke from Heat Pipe Technology [3] with a wraparound heat pipe installed in an air conditioning system, found that the air is pre-cooled from 35°C, 78% to 25.8°C, 73.7% relative humidity, and re-heat to 12.8°C, 95% to 22.8°C, 61.8% relative humidity. This is a differential of 10K change of sensible heat that the heat-pipes were capable to convert. Figure 1 shows the heat pipe technology and the model of heat-pipes used. A closed tube with a refrigerant medium is used to transfer heat from one end to the other.

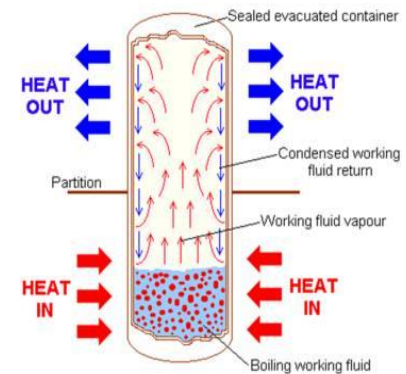


Figure 1. Heat pipe technology.

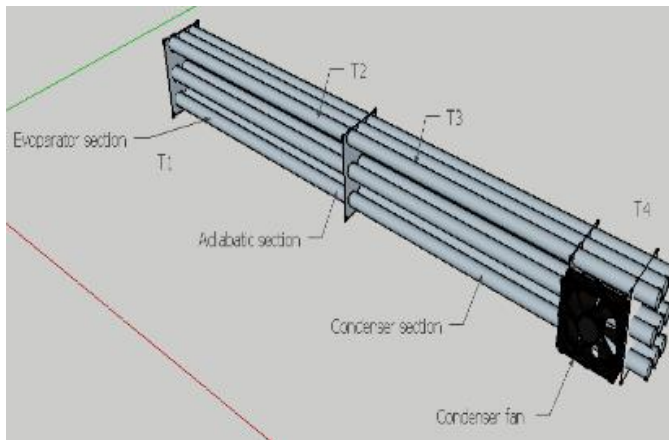
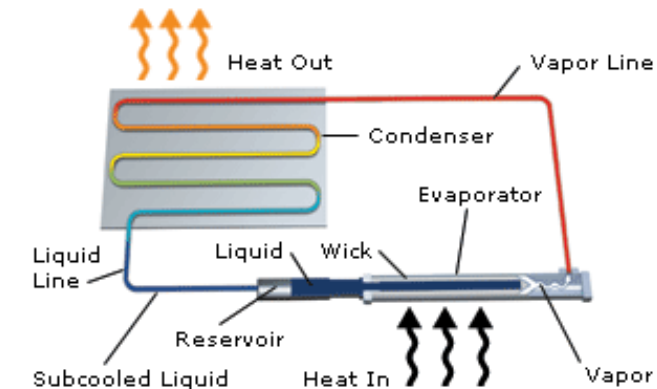
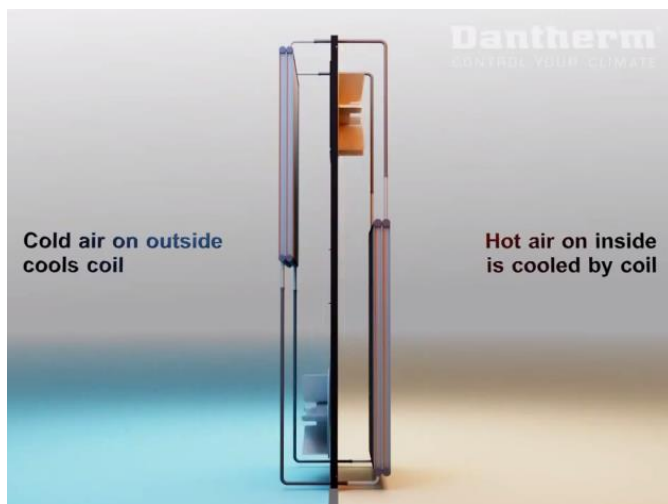


Figure 2. Straight heat-pipes model using R134a as a refrigerant medium. An optional ventilation fan is shown to discharge warm air from the condenser side of the outdoors.



a.



b.

Figure 3. Thermo-siphon or loop heat pipe a. The system, and b. An application that is commonly used by a power supply cabinet for transferring heat to the

outdoors. It has no wick structure and has to be gravity-aided for the liquid vapour to move from one section to the other. Source: Dantherm [15].

The operating process of a heat pipe begins at the evaporator section filled with a working fluid as a saturated liquid. The evaporator section heated by the ambient space at one end changes the liquid to vapour and moves to the condenser section. The vapour at the condenser section then transfers the heat to the ambient space of the other end, which turns the fluid into liquid again. Figure 2 shows the model of heat-pipes for the simulation with an exhaust fan installed at the condenser side to create a circulating air in the cabinet. Figure 3 compares the heat pipe system to the commonly used loop heat pipe system in power supply cabinets. The disadvantage of the loop system is, it has to be gravity-aided and has no wick structure.

1.1 Outdoor Cabinets

An outdoor cabinet for power supply requires fresh air ventilation to cool down the heat generated by the electro-mechanical parts inside and the heat subjected by solar from the outside. The equipment is designed to withstand a temperature up to 55°C, but the normal safety cut-out setting is lower at about 45°C. In general, a closed cooling loop or thermos-siphons are used to operate the cooling of an outdoor cabinet. Passive cooling technologies had been studied by [4], [5], [6] and [7] has proposed a passive cooling system technology using methanol as the cooling medium. A heat-pipes that contains R134a operate passively with natural circulation without any additional energy input needed. The advantage of heat-pipes is that it can be positioned in any configurations, where else the cooling loops and the thermos-siphons are operated vertically, using the gravitational mass concept for the refrigerant to return to the evaporator.

The process begins with the fresh air at a temperature of 20°C enter the inlet opening of the outdoor cabinet. The air is cooled by the heat pipe and mixed with internal air in the cabinet. The internal cabinet room air, which had been heated by the operational equipment and from solar radiation can reach up to 55°C, mixed with the cool temperature inlet air. Cooled mix air will then be exhausted out through the outlet. The process continues to maintain the temperature inside the cabinet to be lower than the cut-out setting temperature.

1.2 Computational Fluid Dynamics (CFD)

To solve problems that involve fluid flow and to predict flow behaviour, Computational Fluid Dynamics

with numerical methods and algorithms are used. A model that is based on fundamental governing equations of fluid dynamics, namely the conservation of mass, momentum, and energy is used to build simulation modelling. The fundamental basis of any CFD problem is the Navier-Stokes equations (conservation law). The four terms in the general differential equation are the unsteady term (transient), the convection term, the diffusion term and the source term [8]. There is much research work on outdoor cabinets such as Samba et al. [9] who studied two-phase thermosiphon loop for outdoor telecommunication equipment cooling, Yuping et al. [9] study the cooling system of the outdoor cabinet using underground heat pipe by simulation and experimentally and Marongiu et al. [10] proposed a design and development of passive cooling for an outdoor cabinet.

1.3 Introduction to Paper

The main issue to be addressed in the paper is to show the effectiveness of a heat pipe heat-exchanger and the temperature drop that the heat pipe could be achieved. A straight heat pipe heat-exchanger is used instead of a thermosiphon and loop heat-pipes. The heat pipe is attached to a front face of an outdoor power supply cabinet where the air inlet and outlet are situated. The author proposed a different method of cooling an outdoor power supply cabinet which normally using a gravity method thermosiphon heat pipe.

CFD simulation using ANSYS Fluent is used to solve the issues of effectiveness of the heat pipe and CFD ACE to show the air profile in the cabinet. The distribution of air when entering and leaving is set with the air enter the bottom face of the heat pipe and leave on the upper face of the cabinet. The ambient temperature is 293K while the inner temperature of the cabinet is set to 328K.

The results are presented according to the previous method of calculation of heat pipe effectiveness. The CFD used standard 3D Navier-Stokes continuity and energy equation using the RANS method of simulation. The result of ANSYS Fluent with R134a and the distribution of air inside the cabinet is presented in 3-D while 2-D figures are presented to show the contact between the air and heat pipe heat-exchanger.

2. Methodology

2.1 Problem Description

The work involved an outdoor cabinet with a single-sided opening having both inlet and outlet at the same

façade. It is located at the side of the outdoor cabinet as in Figure 4. The heat generated by the operational equipment inside the outdoor cabinet and the solar heat from outside can reach a temperature of 55°C inside the cabinet. Marongiu et al. [10] proposed an operation temperature of 65°C for the inside cabinet temperature in summer. A vertical heat pipe heat-exchanger is used as a heat sink to reduce the temperature. This computational study focused on natural ventilation, entering an outdoor cabinet of dimensions 2.3m x 0.8m x 0.8m. The inlet air is cooled by the R134a heat pipe evaporator section, where heat from the incoming outside air and the generated heat are absorbed. In a process of vaporization, the liquid in the evaporator pipe section turns to vapour and move up to the condenser pipe section. The cool air that passed the evaporator pipes, then circulate inside the cabinet to cool down the space condition and intersect with the warm equipment. The mixed air between the incoming air and the equipment air reduces the outdoor cabinet temperature. The warm air is rejected through the outlet.

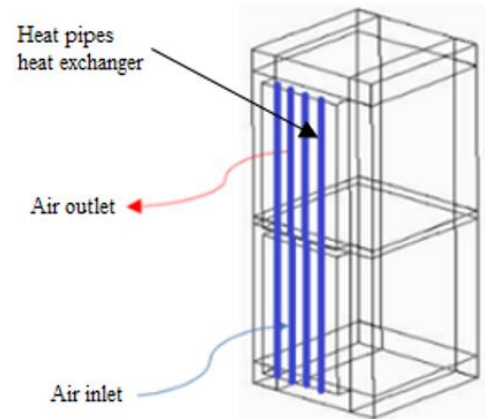


Figure 4. Schematic of an outdoor cabinet with the application of straight heat pipe showing the inlet and outlet air paths. The source of heat is from the operation of the electro-mechanical equipment inside the cabinet and the solar heat.

The mathematical model for the computational solution used the turbulent flow, 3D Navier-Stokes continuity, and energy equation. The governing equations are [11], [12];

$$\frac{\partial u_j}{\partial x_j} = 0 \quad (1)$$

$$\frac{\partial U_i}{\partial t} + U_j \frac{\partial U_i}{\partial x_j} = -\frac{1}{\rho} \frac{\partial p}{\partial x_i} + \frac{\partial}{\partial x_j} \left[\nu \left(\frac{\partial U_i}{\partial x_j} + \frac{\partial U_j}{\partial x_i} \right) - \overline{u_i u_j} \right] - \beta(T - T_{ref}) \quad (2)$$

$$\overline{u_i u_j} = \nu_t \left(\frac{\partial U_i}{\partial x_j} + \frac{\partial U_j}{\partial x_i} \right) - \frac{2}{3} K \delta_{ij}$$

$$\rho c \left(\frac{\partial T}{\partial t} + U_j \frac{\partial T}{\partial x_j} \right) = k \frac{\partial^2 T}{\partial x_j \partial x_j} - \rho c \frac{\partial}{\partial x_j} (\overline{u_j T'}) + \Phi + \phi \quad (3)$$

$$\overline{u_j T'} = \frac{\nu_t}{\sigma_t} \left(\frac{\partial T}{\partial x_j} \right)$$

$$\Phi = \mu \left(\frac{\partial U_i}{\partial x_j} + \frac{\partial U_j}{\partial x_i} \right) \frac{\partial U_i}{\partial x_j}$$

$$\frac{\partial K}{\partial t} + U_j \frac{\partial K}{\partial x_j} = \frac{\partial}{\partial x_j} \left[\left(\nu + \frac{\nu_t}{\sigma_K} \right) \frac{\partial K}{\partial x_j} \right] + \nu_t \left(\frac{\partial U_i}{\partial x_j} + \frac{\partial U_j}{\partial x_i} \right) \frac{\partial U_i}{\partial x_j} - \varepsilon \quad (4)$$

$$K = \frac{1}{2} \overline{U_i U_j}$$

$$\varepsilon = \nu \left(\frac{\partial u_i}{\partial x_j} \right) \left(\frac{\partial u_i}{\partial x_j} \right)$$

$$\frac{\partial \varepsilon}{\partial t} + U_j \frac{\partial \varepsilon}{\partial x_j} = \frac{\partial}{\partial x_j} \left[\left(\nu + \frac{\nu_t}{\sigma_\varepsilon} \right) \frac{\partial \varepsilon}{\partial x_j} \right] + C_1 r \frac{\varepsilon^2}{K} \nu_t \left[\left(\frac{\partial U_i}{\partial x_j} + \frac{\partial U_j}{\partial x_i} \right) \frac{\partial U_i}{\partial x_j} \right] - C_2 \frac{\varepsilon^2}{K} \quad (5)$$

Where subscript t refers to turbulence

$$\mu_t = \rho C_\mu K^2 / \varepsilon; \nu_t = \mu_t / \rho;$$

$C_\mu=0.09$; $C_1=1.44$; $C_2 =1.92$; $\sigma_K =1.0$; $\sigma_\varepsilon =1.0$; reference temperature = 300K. For the simulation, the pressure assumed to be constant, the K and ε value at inlet used;

$$k = \frac{3}{2} (U_{ave} T_i)^2 \quad (6)$$

$$\varepsilon = \frac{C_\mu^{3/4} K^{3/2}}{KL} \quad (7)$$

Where U_{ave} is inlet velocity, T_i is turbulence intensity (here taken to be about 2%), L is here taken to be a “reasonable length” of 1m and $K = 0.41$ is the Von Karman constant. Experience has shown, however, that the values of k and ε imposed at the inlet to the computational domain play only an insignificant role, as long as they are both small.

2.2 Solver

There are two solvers used in this case, ANSYS Fluent for the heat transfer simulation of R134a in the heat pipe and the surrounding space, i.e. The outdoor cabinet, and CFD-ACE+GEOM, GUI and BG solver to solve the governing equations that are related to the flow physic problem, based on the given material properties, flow physic model and the boundary conditions. To satisfactorily converge all properties and conditions, the Finite Volume Method is employed to solve velocity components, pressure, and k - ε (epsilon) scheme. Several attempts of meshing tests were taken to satisfy the results. 2nd order spatial differential scheme is used.

Fluid properties used for ANSYS Fluent simulation process are corresponding to constant air at 293 K and the surrounding temperature is set at 328 K. To show the flow of the air when moving to pass the tube, a 1 m/s of flow rate is applied. Fluid properties used in the CFD-ACE simulation processes are corresponding to constant air at 300 K and standard pressure at sea level of 101.3 kPa, where the temperature inlet through the HPHE is assumed to be 300 K; as the natural ventilation flow is assumed to be in +Z direction. Boussinesq approximation where the fluid density concerning the buoyancy force is affected by temperature change is assumed, with reference temperature T_{ref} is 300K and Vol. Coef. Th. Exp. is 0.003333 1/K. Other molecular properties include $\rho = 1.1614 \text{ kg/m}^3$, $\mu = 1.846 \times 10^{-5} \text{ N-s/m}^2$, $\nu = 1.589 \times 10^{-5} \text{ m}^2/\text{s}$. Total nodes and cells that satisfied the convergence were given in Table 1 below for all cases;

Solver	Cells	Faces	Nodes	Partitions
ANSYS Fluent	1000	2205	1206	1
CFD-ACE+	1088		2125	

Table 1: Total cells and nodes used for modelling are ANSYS Fluent and CFD ACE. The grids used are structured grids and the number of cells, and nodes are different from the solver.

2.3 Mesh

The mesh for the fluid-solid domains is given in Table 2 below for all cases. Several attempts have been taken when testing the mesh distribution. Table 2 below shows the mesh distribution that best suits the domain. Fluid properties are applied in the copper heat pipe to show the difference in temperature results. Water, acetone, and R134a used the same domains when ANSYS Fluent run the simulations.

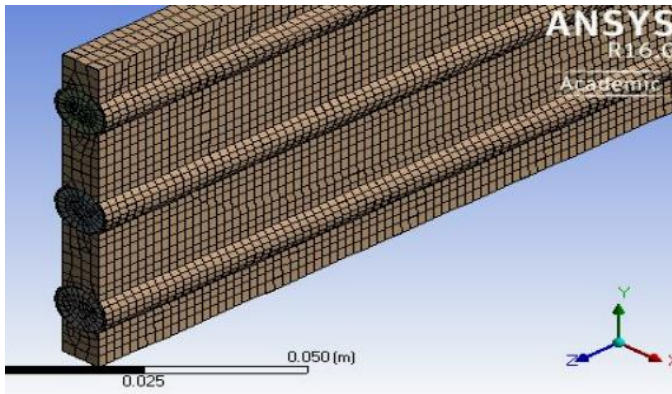


Figure 5: Meshes used to run the Simulation of heat pipe heat-exchanger by ANSYS Fluent.

Domain	Nodes	Elements
Fluid	111276	94326
Solid	99724	66495
All Domains	211000	160821

Table 2: Shows the nodes and elements of the fluid-solid meshes when running with ANSYS Fluent.

2.4 Post Processing

ANSYS Fluent in the CFD-View analysed the convergence results and are presentable in a graphical presentation with different plots, streamlines data and curves. Figure 6 to 8 shows the temperature profile of the heat pipe heat-exchanger that filled with water, acetone, and R134a. The highest different temperature is recorded

by the heat-pipes that filled with R134a at about 5k different.

Table 3 below shows the properties of the cooling medium used when running with ANSYS Fluent. The temperature differential between the inlet and the outlet of the heat-pipes show that up to 5 K can be achieved if R134a is applied as a refrigerant medium.

Physical Parameters	Water H ₂ O	Acetone C ₃ H ₆ O	R134a CH ₂ FCF ₃
Density kg/m ³	998.2	791	1207.3
Spec. Heat J/kg.K	4182	2160	1424.41
Thermal Cond. W/m.K	0.6	0.18	0.08119
Viscos kg/m-s	0.001003	0.000331	0.00019525
Inlet temperature, K	293	293	293
Outlet temperature, K	295	296	298
Different temperature, K	2	3	5

Table 3: Shows the properties of the heat pipe cooling medium and the temperature outlet achieved, when running with ANSYS Fluent simulations.

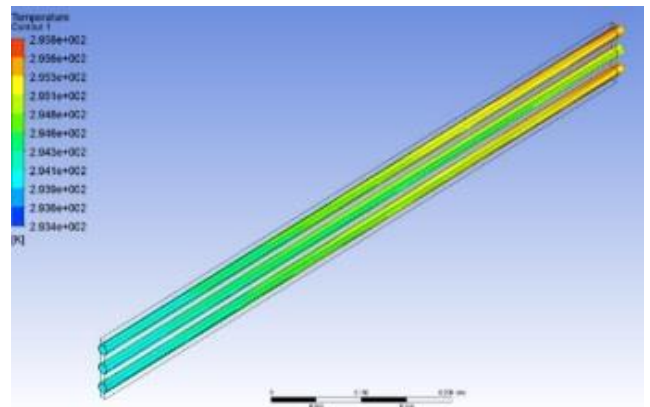


Figure 6: Simulation of heat pipe heat-exchanger by ANSYS Fluent using water as a cooling medium. The temperature difference is about 2 K.

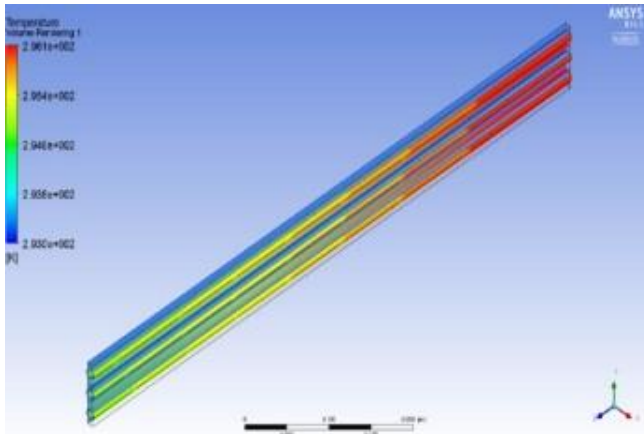


Figure 7: Simulation of heat pipe heat-exchanger by ANSYS Fluent using acetone as a cooling medium. The temperature difference is about 3 K.

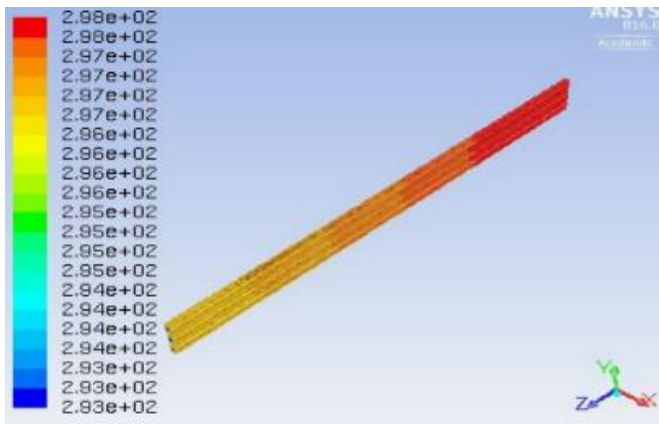


Figure 8: Simulation of heat pipe heat-exchanger by ANSYS Fluent using R134a as a cooling medium. The temperature difference is about 5 K.

Figure 9 and 10 shows a two-dimensional graphical traces of temperature and airflow through the heat pipe heat exchanger. Heat-pipes are configured in a row to show the distribution and the results of the temperature. A base temperature of 293 K is used inside the heat-pipes and a temperature of 328 K to represent the inner temperature of the cabinet. Different contours can be seen to differentiate the temperature and flow.

2.4.1 Inlet

Figures 11 and 12 show the air distributions of an inside power supply cabinet, simulated using CFD-ACE software. The heat pipe heat-exchanger is being installed at the front air intake and air exit.

The air enters the inlet opening of a cabinet located at the bottom front of the wall. The ambient air passed a cooled heat pipe heat-exchanger and mixed with the warm air inside the cabinet generated by the working equipment. The liquid-state R134a refrigerant in the heat-pipes boils

by the heat from the ambient and the inner heat of the cabinet.

2.4.2 Outlet

The warmer mixed air then moved upward and rejected to the outside ambient air through an outlet opening located on the upper front side of the cabinet wall. The vapour-state of the R134a refrigerant on the upper condenser side of the heat-pipes rejected heat to the ambient and turn to liquid-state. The liquid-state refrigerant then returns to the evaporator side at the bottom via a wick or by gravity method.

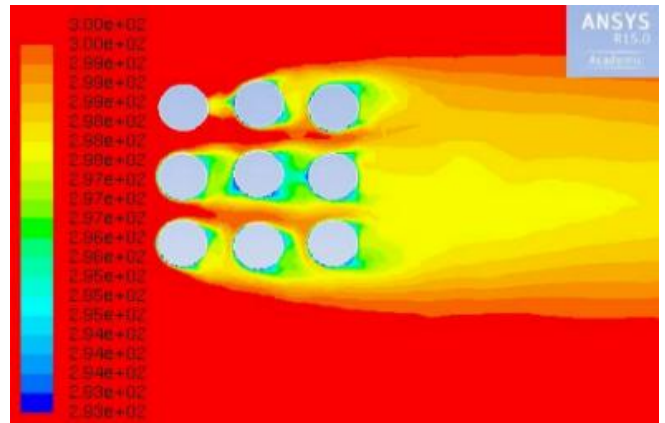


Figure 9: The contour of air temperature, simulated to a heat pipe heat-exchanger by ANSYS Fluent.

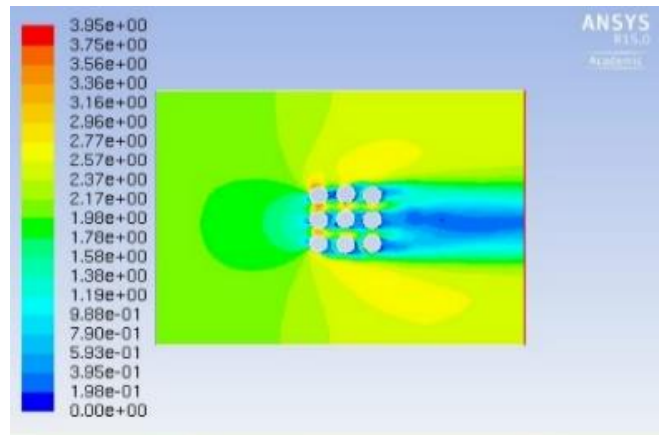


Figure 10: The contour of airflow, simulated to a heat pipe heat-exchanger by ANSYS Fluent.

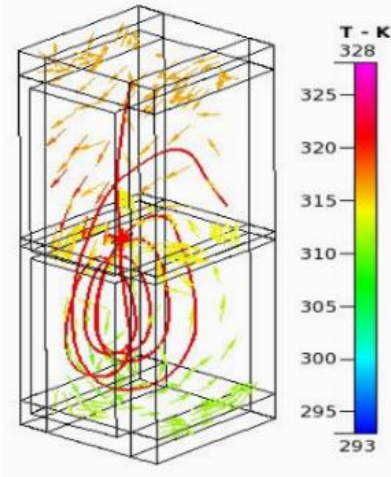


Figure 11: Traces of air temperature distributions in a heat pipe heat-exchanger application to an outdoor power supply cabinet run with CFD-ACE. The air inlet temperature of 293 K was mixed with the inner temperature before leaving to outdoor.

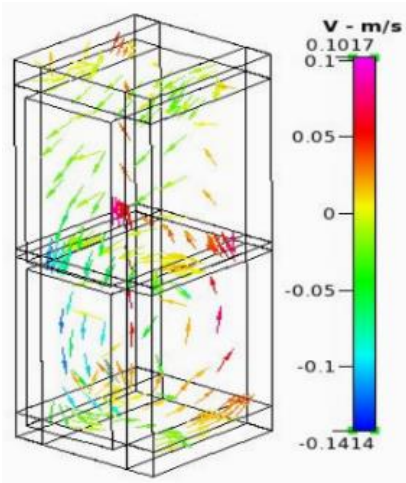


Figure 12: Airflow traces inside the outdoor cabinet after passing a heat pipe heat-exchanger (HPHE) inlet, simulation model run on CFD-ACE. The air velocity shows that the warmer air moves to the upper side of the cabinet before the exit to the outlet.

3. Result and Discussion

The purpose of this study is to investigate the possibilities of using a straight heat pipe heat-exchanger in an outdoor power supply cabinet. The heat transfer, airflow pattern and flow rates of heat-pipes, are recorded by simulation software. The model uses ANSYS Fluent to show the heat transfer inside the heat-pipes which filled with R134a. Both inlet and outlet temperatures are recorded when applying to set temperature.

The different temperature of the air when passing through a heat pipe is recorded with CFD-ACE to show air's temperature and flow pattern inside the cabinet. The model uses the RANS scheme to show the air distribution

where inlet opening is installed with a straight heat pipe heat-exchanger instead of a commonly used thermosiphon or loop heat-pipes.

The cabinet inside space heat is set to 328 K, transfer its heat to the cold side of the evaporator, hence reduced the inside temperature to about 315 K. Heat-pipes effectiveness is determined by assessing its required performance at the local design condition [13], in this case, the cabinet's inside temperature, at 55°C. As both evaporators and condenser's flow rates are assumed identical, the heat capacity is cancelled out. The off-coil temperature of the evaporator is about 13°C and the inlet supply air temperature is 27°C. The effectiveness of the heat-pipes in function to the flow rate across the heat pipe can be calculated as,

$$\frac{T_4 - T_3}{T_1 - T_3} = \frac{27 - 13}{55 - 13} = 0.33 = 33\%$$

Physical Parameters	Water H ₂ O	Acetone C ₃ H ₆ O	R134a CH ₂ FCF ₃
Different temperature, K	2	3	5
Efficiency, %	26	30	33

Table 3: Shows the comparison of temperature drop and efficiency between water, acetone, and R134a heat pipe heat-exchangers.

With the effect increases as the velocity reduced [13], and at a given flow rate and temperature, the air in contact with the heat pipe recorded a 33% effectiveness. The result shows a better efficiency than 20%, concerning the investigation made by [13] with a loop heat pipe heat-exchanger in an air handling unit.

3.1 Temperature

The temperature distribution can be seen in Figure 13. The air with a maximum temperature of 328 K inside the cabinet mixed with the air from the incoming inlet and pass through a heat pipe where the temperature is 314 K. The off-coil temperature recorded was at 316 K and the average temperature inside the cabinet is 314 K before its exit out through the outlet.

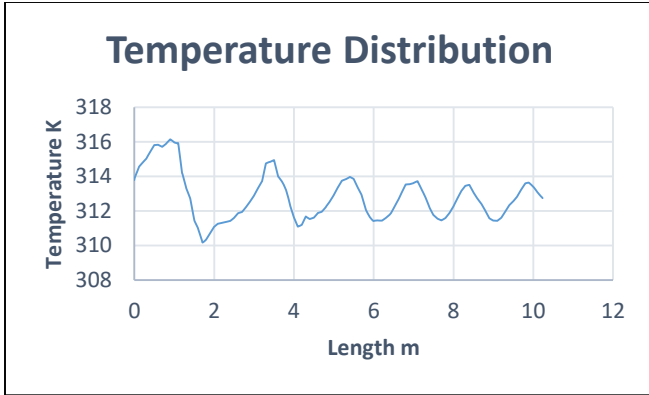


Figure 13: Temperature distribution of the inside length of the outdoor cabinet.

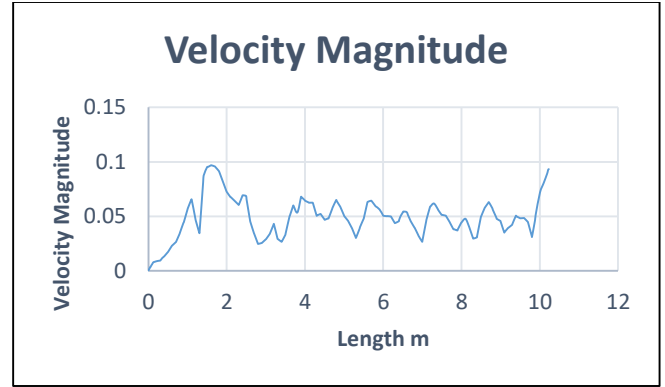


Figure 15: Velocity magnitude distributions to the inside length of the outdoor cabinet.

3.2 Velocity

Simulations for the models are run in 328K to compare the velocity between cases. Figure 14 shows the distribution of air velocity across the outdoor power supply cabinet inside space with the air inlet and outlet at the front. It shows that the air velocity is less at the inlet but increases in the middle of the cabinet. This was due to the warm temperature of the equipment that created a different density of air, hence created natural ventilation. Towards the end of the room length, the velocity is constant until it's faded away through the outlet. The maximum velocity recorded is 0.05 m/s. Figure 15 shows the distribution of air velocity to the velocity magnitude across the cabinet.

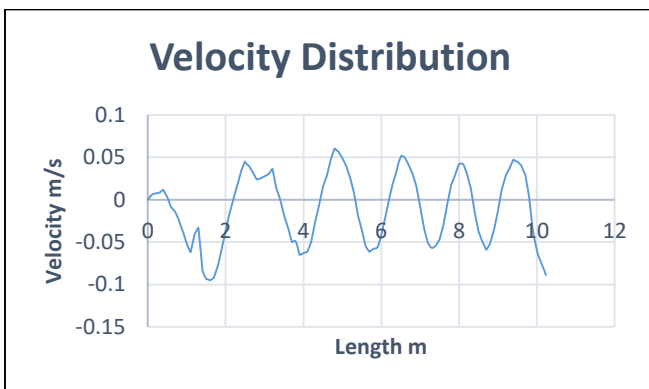


Figure 14: Velocity distributions to the inside length of the outdoor cabinet.

3.3 Air properties using Psychrometric Chart

A psychrometric chart is used to show the properties of air inside the cabinet and to calculate the energy transfer from the heat-pipes to the air. Assumed that the airflow rate is the same for inlet and outlet, the mixed temperature can be calculated as;

$$\begin{aligned}
 T_{mix} &= T_1 - \left(\frac{T_4}{2}\right) \\
 &= 55 - \left(\frac{27}{2}\right) \\
 &= 41.5^\circ\text{C}
 \end{aligned}$$

When the air temperature process is plotted on the psychrometric chart, it is found that T_{mix} of 41.5°C , 22% RH is equal and agreed to the average temperature recorded by the simulation model of 314K (40.85°C). See Appendix 1 for Psychrometric Chart details. Table 3 shows the air properties from the process.

Temperature K	RH %	Enthalpy h, kJ/kg	Flowrate \dot{m} m ³ /s
300	50	56	0.017
314.5	22	71	0.016
328	9	84	0.016

Table 4: Shows the temperature, relative humidity, and enthalpy when the air circulated in the outdoor cabinet.

The rate of energy transfer to the air can be calculated by;

$$W = \dot{m} \Delta h$$

$$= 0.05 * 0.3 * \left(\frac{1}{0.865}\right) * (84 - 56)$$

$$= 0.5kW$$

Where, \dot{m} is the velocity at 0.05 m/s, cabinet inlet opening 0.3 m² and specific volume of inlet air is 0.0865m³/kg.

4. Conclusion

The ANSYS Fluent solver is used to simulate the heat transfer of a heat pipe heat-exchanger with R134a as a refrigerant medium at an outdoor power supply cabinet. From the model of the simulation, it is found that the heat pipe heat-exchanger with R134a can transfer heat, up to 5 K temperature differentials.

The heat pipe is proposed to be installed in an outdoor power supply cabinet as a main heat sink equipment to decrease inside cabinet temperature. Different temperatures and air densities between the inlet and the outlet created a flow of natural ventilation. Simulations using CFD-ACE were performed using the standard k- ϵ model from Reynolds Average Navier Stokes (RANS) turbulence equation. A small amount of air circulation can be traced inside the cabinet when the heat interacted with the evaporator side of the heat pipe. The presence of the heat pipe is creating natural ventilation and flow inside the cabinet. The results of the temperature, velocity and velocity magnitude are validated.

An experimental investigation is needed to validate configuration for natural ventilation numerical results. Further investigation involving experimental studies of heat pipe heat-exchanger to increase or decrease the inlet temperature and the velocity for outdoor power supply cabinet is needed to validate the numerical results.

References

- [1] Yau, Y.H., and Ahmadzadehtalatapeh, M., A Review on the Application of Horizontal Heat Pipe Heat-exchanger s in Air Conditioning Systems in The Tropics, *Applied Thermal Engineering*, **30**, (2–3), 2010, 77-84.
- [2] Ong, K.S., and Haider-E-Alahi, M., Performance of an R-134a-Filled Thermosyphon, *Applied Thermal Engineering*, **23**, (18), 2003, 2373-2381.
- [3] Brooke, T., Optimizing Wrap-Around Heat-pipes', *Heat Pipe Technology*, 2007.
- [4] R.R. Riehl, T.C.P.A. Siqueira., Heat Transport Capability and Compensation Chamber in Fluence in Loop Heat-pipes Performance, *Applied Thermal Engineering* **26**, 2006, 1158 - 1168.
- [5] W. Joung, T. Yu, J. Lee., Experimental Study on the Loop Heat Pipe with a Planar Bifacial Wick Structure, *International Journal of Heat and Mass Transfer*, **51**, 2008, 1573-1581.
- [6] P. Charoensawan, P. Terdtoon., Thermal Performance of Horizontal Closed-Loop Oscillating Heat Pipe, *Applied Thermal Engineering*, **28**, 2008, 460-466.
- [7] C. T. Meng, S.H. Chih, W.K. Shung., Experimental Study of a Loop Thermosyphon Using Methanol as Working Fluid, *14th IHPC*, 2007.
- [8] Priyadumkol, J., and Kittichaikarn, C., Application of the Combined Air-Conditioning Systems for Energy Conservation in Data Center, *Energy and Buildings*, **68**, Part A, (0), 2014, 580-586.
- [9] Yuping, H., Cooling System of Outdoor Cabinet using Underground Heat Pipe, *Telecommunications Energy Conference*, **IEEE 30**, 2008, 1-5.
- [10] Marongiu, M.J. et al., Design and Development of Passively Cooled Remote Outdoor Cabinet, *Twentieth International Telecommunications Energy Conference*, 1998, 568-575.
- [11] Bangalee, M.Z.I., Miao, J.J., Lin, S.Y., and Yang, J.H., Flow Visualization, PIV Measurement and CFD Calculation for Fluid-Driven Natural Cross-Ventilation in a Scale Model, *Energy and Buildings*, **66**, 2013, 306-314.
- [12] van Hooff, T., and Blocken, B., CFD Evaluation of Natural Ventilation of Indoor Environments by the Concentration Decay Method: CO₂ Gas Dispersion from a Semi-Enclosed Stadium, *Building, and Environment*, **61**, 2013, 1-17.
- [13] Jouhara, H., Meskimmon, R., Experimental Investigation of Wraparound Loop Heat Pipe Heat-exchanger Used in Energy Efficient Air Handling Units, *Energy*, **35**, 2010, 4592-4599.
- [14] Psychrometric Chart., Chartered Institution of Building Services Engineers.
- [15] <https://www.dantherm.com/us/electronics-cooling/products/thermosiphon-heat-exchange/>

IMECE2016-65968

CFD-SIMULATION OF A HEAT-PIPES -HEAT-EXCHANGER EFFECT ON A TUBULAR AIR-COOLED CONDENSER

Z. Abdullah^{1,2}

¹ HVAC&R Department
Universiti Kuala Lumpur, Malaysia France Institute
Bandar Baru Bangi, Selangor, Malaysia

² Faculty of Engineering & IT
University of Technology, Sydney
Sydney, NSW, Australia

B. Phuoc Huynh

Faculty of Engineering & IT
University of Technology, Sydney
Sydney, NSW, Australia

A. Idris

Department of Mechanical Engineering,
Universiti Kuala Lumpur, Malaysia Spanish
Institute
Kulim, Kedah, Malaysia

ABSTRACT

A continuous increase in electricity tariff and its power consumption has brought an alteration towards the development of cooling technologies. Cooling technology with a normal vapour compression cycle relies on electricity to increase and decrease the pressure, hence the temperature, within its cycle. Alternative technology such as passive cooling, using heat pipe heat-exchanger s is being applied to the refrigeration cycle components to assist in a temperature reduction of the cooling process. The supply and return air temperatures of an evaporator and condenser are being pre-cooled by passive cooling equipment to assist in reducing the compressor work done. The objective of this study is to investigate and simulate a force-ventilation of air around a circular air-cooled-condenser tube for an air conditioning system. The incoming air supplied to the condenser is assisted by air that had been pre-cooled by a heat pipe heat-exchanger attached 100mm from the condenser. This study investigates the effect of the heat pipe heat-exchanger in removing the energy and its temperature, in assisting the condenser heat removal process. In a normal refrigeration cycle, the heat of a condenser at a constant pressure at 109200Pa and a temperature of 319K is reduced by the forced convection ventilation to 315K. The temperature of the refrigerant in the tube is being reduced at a constant pressure of 5K by a heat transfer exchange of ambient air and the

condenser tube. This simulation showed the effect of a heat pipe heat-exchanger attached before the condenser by using the computational fluid dynamic software. A condenser from a refrigeration cycle with refrigerant R134a is being simulated using CFD software. The condenser tube is a row of 5 copper tubes (9.5mm OD) in a vertical straight line exposed to ambient air of 300K. A hot vapour refrigerant temperature leaving a compressor enters a condenser inlet at 319K and exit the outlet tube at a liquid temperature of 315K. The inlet and outlet pressures of the condenser tube are assumed constant throughout the process at 109200Pa. Using a computational fluid dynamics simulation, a normal condenser inlet and outlet air are being studied. The simulation results are then compared to a simulation of a condenser tube that had been attached to a heat pipe heat-exchanger at the air inlet section. A 100mm air gap between the heat pipe heat-exchanger and the condenser where the simulation of heat transfers is assumed to be the key process is discussed. The result of the air outlet of the condenser and the effect of the heat pipe heat-exchanger attached to it is discussed. ANSYS Fluent and CFD ACE+ software are being used to run the simulation and the results are presented in terms of the temperature contour, velocity vectors and flow patterns. It is found that the outlet temperature of the condenser is reduced when a heat pipe heat-exchanger is attached before the condenser. It is an advantage to use a heat pipe heat-exchanger to increase the temperature difference between a refrigerant fluid at the inlet and outlet of the condenser. By increasing the heat transfer rate of the heat pipe and the condenser tube, hence lowering the condenser temperature output, the system capacity will increase.

Keywords: *computational fluid dynamics, heat pipe heat-exchanger, air-cooled condenser, heat transfer, and flow pattern.*

INTRODUCTION

Condensers play an important role in the refrigeration system to remove the heat indoor to the outdoor or vice versa. The high pressure, the high-temperature refrigerant compressed from the compressor enters the condenser in the vapour phase. The heat transfer between the ambient airs on the condenser surfaces turns the refrigerant inside the condenser tube to the liquid phase of reduced temperature.

The heat pipe heat-exchanger is a heat transfer tube device by transferring refrigerant fluid latent heat of vaporization, from one end to the other. Tubes are filled with cooling refrigerants such as R134a, to evaporate and condenses, from liquid to vapour state from one end of the tube to the other. The refrigerant liquid evaporates into vapour in the evaporator section of the tube, by absorbing the surrounding heat. The evaporated vapour moved to the condenser section of the tube and releases the heat to the surrounding, which turns the vapour back to the liquid phase. With gravitational force and the capillary action of a wick inside the tube, the liquid moves back to the evaporator section and repeat the cycle. In

steady-state operation, a heat pipe with a metalworking fluid will have a high thermal conductance compared to a solid metal conductor. Among the unique characteristics of heat-pipes are a small temperature drop, wide temperature application range and the ability to control and transport high-heat rates at various temperature levels [1]. The heat pipe heat-exchanger had been used in a variety of heating, ventilation and air conditioning systems and energy recovery processes, but only the application to the condensing side of the refrigeration cycle will be discussed in this paper. The study separated the applications of heat-pipes in the numerical study using ANSYS Fluent and CFD ACE + to view the behaviours of refrigerant R134a, the heat transfer medium in the tubes, the temperature profile of the air passing through the heat-pipes and the air distribution at the condenser.

NOMENCLATURE

$U_j(j = 1 - 3)$ - Component of average velocity vector, m/s

g	- Gravity acceleration, m/s^2
μ_t	- Turbulent viscosity, Pa/s
C_μ	- Empirical constant, 0.09
K	- Turbulent kinetic energy, m^2/s^2
ε	- Dissipation rate, m^2/s^3
κ	- Von Karman's constant, 0.41
U_{ave}	- The average flow velocity, m/s
T_i	- Turbulence intensity
L	- Length scale, m
T_e	- Evaporating temperature $^\circ C$
T_c	- Condensing temperature $^\circ C$
Q_e	- Evaporator work-done kJ/kg
Q_c	- Condenser work-done kJ/kg
W	- Compressor work-done kJ/kg
COP	- Coefficient of performance
x	- Flash gas %

1. APPLICATION OF HEAT PIPE HEAT-EXCHANGER ATTACHED TO AN AIR-COOLED CONDENSER IN A REFRIGERATION SYSTEM

Ong et al. [2] made an experiment with long heat-pipes air heat-exchangers, and compared the bath temperature to the evaporator temperature and recorded a differential of 1K to 5K. Tom Brooke [3] experimented with an air conditioning system with a wraparound heat pipe installed and found that the air can be pre-cooled from 35°C (308K) to 25.8°C (298.8K) and can be re-heat from 12.8°C (285.8K) to 22.8°C (29508K). It shows that the heat-pipes were capable of converting a differential change of heat of about 10K. Figure 1 shows the heat pipe technology and the model of heat-pipes used.

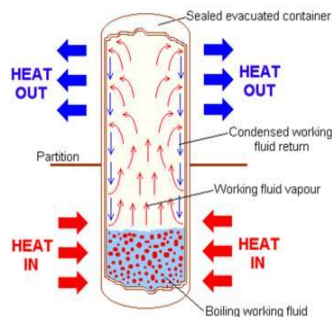


Figure 1: The Heat Pipe Heat-exchanger. The refrigerant liquid in the heat pipe heat-exchanger at the bottom of the tube absorbed heat at the evaporator section and release it at the condenser at the upper section. The liquid evaporates into a vapour phase in the evaporator and moves towards the condenser section, which in turn

changes back to the liquid phase by releasing the heat to the surrounding.

In a modern vapour compression cycle, the condenser task is to reject the heat from the refrigerant compressed by the compressor to the ambient air.

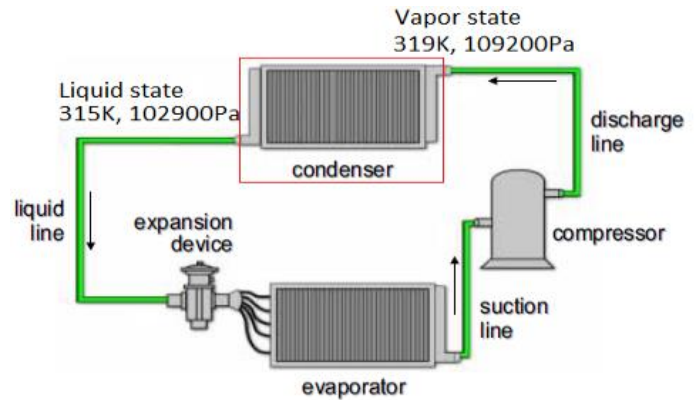


Figure 2: The condenser is a heat exchanger used to reject the heat of the refrigerant to another medium. The high-pressure refrigerant vapour flows in the tube of the condenser and rejects heat, condenses from vapour to liquid state in the process.

1.1 COMPUTATIONAL FLUID DYNAMICS (CFD)

Computational Fluid Dynamics with numerical methods and algorithms are used to solve problems that involve fluid flow and to predict flow behaviour. The fundamental governing equations of fluid dynamics, namely the conservation of mass, momentum, and energy are used to build simulations modelling. The equation of conservation law is used as the basic fundamental in solving CFD problems. The four terms in the general differential equation are the unsteady term (transient), the convection term, the diffusion term and the source term [4].

There are many research studies on condenser efficiency and on-coil temperature of condensers. The cooling air temperature at the outdoor unit has a significant effect on the air-conditioner performance. If the on-coil temperature of an outdoor unit is raised by 1°C, the coefficient of performance (COP) of the air-conditioner drops by around 3% [5]. The optimal placement of condensers is an important factor that can lead to a lower on-coil temperature and consequently lower energy consumption [6]. Chow et al. [7],

[8] used EXACT3 CFD code to simulate a location and the arrangements of condenser unit and analysed the effect of different condenser arrangements in the building re-entrant case on the on-coil temperature and efficiency of the condensing unit. Xue et al. [9] Studied the effect of re-entrant dimensions, air velocity across the condenser and heat rejection of each condenser on the velocity and temperature distribution of the air at re-entrant. In this study, CFD modelling is used to determine the optimum distance of installation, of the heat pipe heat-exchanger from the condenser to enhance the heat rejection process of the condenser.

2. INTRODUCTION TO THE PAPER

The main issue to be addressed in the paper are to show the simulation process of the effectiveness of a heat pipe heat-exchanger and the temperature drop that the heat pipe could have achieved at the end of the process when attached to the condenser of an air-cooled air conditioner. The author proposed different methods of pre-cooling of the condenser coil. A straight heat pipe heat-exchanger is used to the pre-cooled air intake to an air-cooled condenser in a refrigeration system. The heat pipe is attached to an air inlet facade of an air-cooled refrigeration condenser where the ambient air, cooled the refrigerant in the condenser tube. Attaching the heat pipe to the front air intake of the condenser will have lowered the ambient air temperature before touching the surface of the condenser tube. Passive cooling technologies had been studied by [10], [11], [12] and [13] have proposed a passive cooling system technology using methanol as the cooling medium. A heat-pipes that contains R134a operate passively with natural circulation without any additional energy input needed. The advantage of heat-pipes is that it can be positioned in any configurations; where else the cooling loops and the thermos-siphons are operated vertically, using the gravitational mass concept for the refrigerant to return to the evaporator. CFD simulation using ANSYS Fluent and CFD ACE is used to solve the issues of effectiveness of the heat pipe and to show the air profile. The distribution of air when entering and

leaving are set with the air flows through the heat pipe, to the condenser coil and leave to the other side of the condenser. The incoming ambient temperature is set to 300K while the heat pipe is set to 295K. The refrigerant R134a inside the condenser coil temperature leaves the compressor at 319K at the upper side of the coil and gradually drops at 1K to 315K at the bottom of the coil. The CFD used standard 3D Navier-Stokes equation, continuity, and energy equations using the RANS method of simulation. Three models of heat pipe using water, acetone, and R134a as a medium had been simulated, but only the average temperature of R134a at 295K had been used for the simulation with the condenser. The result of ANSYS Fluent with R134a and the distribution of air is presented in 3D to show the contact between the air and heat pipe heat-exchanger, where else 2D simulation is presented concerning the air-cooled condenser.

3. METHODOLOGY

3.1 PROBLEM DESCRIPTION

The work involved an air-cooled condenser from a refrigeration system, rejecting heat to the ambient air. R134a in a vapour compression system left the compressor with a temperature of 319K and a pressure of 109200Pa enters a condenser coil. Suggested by [14], [15] at 313K, the author used the maximum temperature of 319K for the condensing temperature. The condenser rejected heat to the air flowing across the condenser coil surfaces and cooled the refrigerant inside its tube to a temperature of 315K, but with the same pressure. In the process, the refrigerant medium changes phase from vapour to a liquid state. A heat pipe heat-exchanger is installed 100mm before the condenser to pre-cooled the flowing air to the condenser. The heat pipe heat-exchanger is used as a heat sink to reduce the air temperature before it flows through the condenser. This 2D computational study focused on air flows, crossing a condenser, which temperature drop from 319K to 315K. Only the evaporator side of the heat pipe heat-exchanger is shown in the simulation. Three models are simulated, a

Domain	Specification
Case 1	Air at 300K flows on the surface of an air-cooled condenser. The condensing temperature of the condenser inlet is 319K and the exit temperature is 315K.
Case 2	Air at 300K flows on the surface of a heat pipe and a condenser that is attached closely together. The temperature of the heat pipe heat-exchanger is 295K while the condensing temperature of the condenser is from 319K to 315K.
Case 3	Air at 300K flows on the surface of a heat pipe and a condenser that is separated 100mm apart. The temperature of the heat pipe heat-exchanger is 295K while the condensing temperature of the condenser is from 319K to 315K.

Table 1: The specification of models for all domains

simulation of a condenser for reference, a heat pipe attached close to the condenser and a heat pipe separated 100mm away from the heat pipe as to compare which method reduced the most heat, by monitoring the air outlet that crosses the heat pipe and crossing off the condenser coils. Figure 3 shows the proposed idea of a closed tube heat pipe heat-exchanger with R134a as a refrigerant medium, used to transfer heat from one end to the other, attached to a condenser side of a refrigeration system.

3.1 SIMULATION MODELS

Table 1 shows the model specification that best suits the domain.

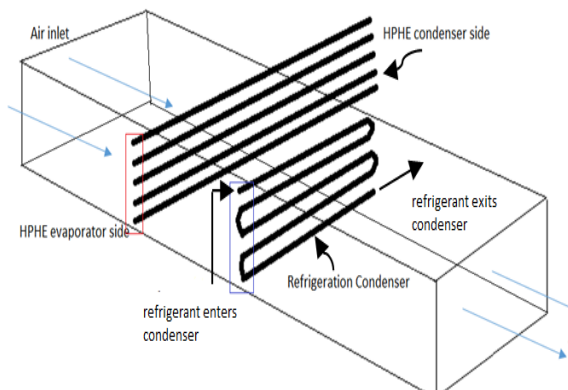


Figure 3: Schematic of a refrigeration condenser with the application of straight horizontal heat pipe showing the inlet and outlet of air paths. The source of heat is from the condenser refrigerant inlet with a temperature of 319K and exit to the liquid line with a reduced temperature of 315K.

3.3 MESH

The mesh for the cases is given below. Several attempts are taken when testing the mesh distribution. Table 2 below shows the nodes and elements and Figure 4 to 6 shows the mesh distribution that best suit the domain. When running the simulation, fluid pressure and temperature are applied in the copper heat pipe and the condenser to show the difference in temperature results.

Domain	Nodes	Elements
Condenser	2209	2074
HP + Condenser	1817	1643
HP + 100mm gap + Condenser	1623	1455

Table 2: The specification of nodes and elements for all domains

Case 1

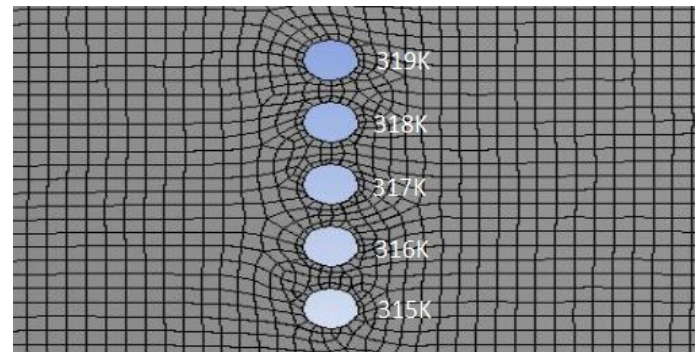


Figure 4: Case 1. The model and meshes used to run the Simulation of the air-cooled condenser by ANSYS Fluent. From the upper tube, the refrigerant inlet temperature gradually drops from 319K to 315K to the bottom of the condenser.

Case 2

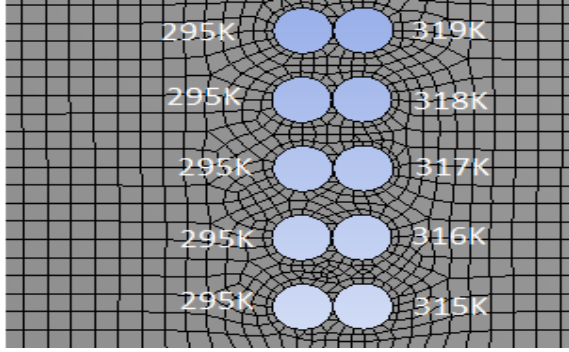


Figure 5: Case 2. The model and meshes used to run the Simulation of the air-cooled condenser by ANSYS Fluent. Heat pipe heat-exchanger at a temperature of **295K** is attached closely together to a condenser.

Case 3

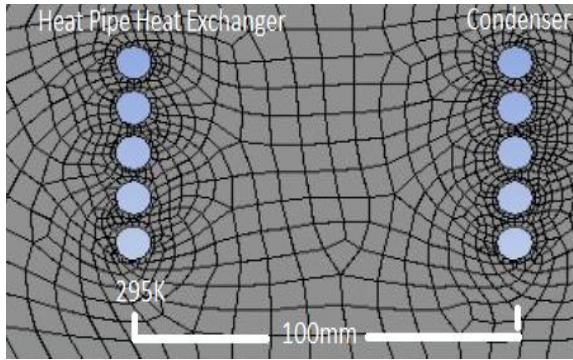


Figure 6: Case 3. The model and meshes used to run the Simulation of the air-cooled condenser by ANSYS Fluent. Heat pipe heat-exchanger at a temperature of **295K** is separated **100mm** from a condenser.

1.1 BOUNDARY CONDITIONS

Table 3 below shows the boundary conditions used to run the models.

Domain	Heat Pipe + Condenser
Dimension 2D	Serial Options
General	Pressure based, Absolute velocity, Time: steady, 2D planar, Gravity: Y direction -9.81 m/s ²
Model	Energy: on, Viscous: laminar
Material	Fluid: air, Solid: copper
Boundary conditions	Velocity magnitude: 1m/s, Thermal: 300K Pressure outlet, Backpressure: 300K Condenser tube temp 315K to 319K

	Heat pipe tube temp 295K
Wall	Surface body: stationary wall, No-slip
Solution Methods	Scheme: simple, Gradient: Least square cell-based, Pressure: Standard, Momentum: Power-law, Energy: Power law

Table 3: Boundary condition runs on ANSYS Fluent.

The mathematical model for the computational solution used the continuity and energy equations, 3D Navier-Stokes equation and turbulent flow. As suggested by [16] the governing equations are [17], [18];

$$\frac{\partial U_j}{\partial x_j} = 0 \quad (1)$$

$$\frac{\partial U_i}{\partial t} + U_j \frac{\partial U_i}{\partial x_j} = -\frac{1}{\rho} \frac{\partial p}{\partial x_i} + \frac{\partial}{\partial x_j} \left[v \left(\frac{\partial U_i}{\partial x_j} + \frac{\partial U_j}{\partial x_i} \right) - \overline{u_i u_j} \right] - \beta (T - T_{ref}) g_i \quad (2)$$

$$\overline{u_i u_j} = v_t \left(\frac{\partial U_i}{\partial x_j} + \frac{\partial U_j}{\partial x_i} \right) - \frac{2}{3} K \delta_{ij}$$

$$\rho c \left(\frac{\partial T}{\partial t} + U_j \frac{\partial T}{\partial x_j} \right) = k \frac{\partial^2 T}{\partial x_j \partial x_j} - \rho c \frac{\partial}{\partial x_j} (\overline{u_j T'}) + \Phi + \phi \quad (3)$$

$$\overline{u_j T'} = \frac{v_t}{\sigma_t} \left(\frac{\partial T}{\partial x_j} \right)$$

$$\Phi = \mu \left(\frac{\partial U_i}{\partial x_j} + \frac{\partial U_j}{\partial x_i} \right) \frac{\partial U_i}{\partial x_j}$$

$$\phi = \mu \left[\left(\frac{\partial u_i}{\partial x_j} \right) \left(\frac{\partial u_i}{\partial x_j} \right) + \left(\frac{\partial u_i}{\partial x_j} \right) \left(\frac{\partial u_i}{\partial x_j} \right) \right]$$

$$\frac{\partial K}{\partial t} + U_j \frac{\partial K}{\partial x_j} = \frac{\partial}{\partial x_j} \left[\left(v + \frac{v_t}{\sigma_K} \right) \frac{\partial K}{\partial x_j} \right] + v_t \left[\left(\frac{\partial U_i}{\partial x_j} + \frac{\partial U_j}{\partial x_i} \right) \frac{\partial U_i}{\partial x_j} + \frac{\beta}{\sigma_\epsilon} g_j \frac{\partial T}{\partial x_j} \right] - \epsilon \quad (4)$$

$$K = \frac{1}{2} \overline{U_i U_j}$$

$$\epsilon = v \left(\frac{\partial u_i}{\partial x_j} \right) \left(\frac{\partial u_i}{\partial x_j} \right)$$

$$\frac{\partial \epsilon}{\partial t} + U_j \frac{\partial \epsilon}{\partial x_j} = \frac{\partial}{\partial x_j} \left[\left(v + \frac{v_t}{\sigma_\epsilon} \right) \frac{\partial \epsilon}{\partial x_j} \right] + C_{1\frac{\epsilon}{K}} v_t \left[\left(\frac{\partial U_i}{\partial x_j} + \frac{\partial U_j}{\partial x_i} \right) \frac{\partial U_i}{\partial x_j} + \frac{\beta}{\sigma_\epsilon} g_j \frac{\partial T}{\partial x_j} \right] - C_{2\frac{\epsilon^2}{K}} \quad (5)$$

Where subscript t refers to turbulence

$$\mu_t = \rho C_\mu K^2 / \epsilon; v_t = \mu_t / \rho;$$

$C_\mu=0.09$; $C_1=1.44$; $C_2 = 1.92$; $\sigma_K = 1.0$; $\sigma_\epsilon=1.3$; reference temperature = 300K. For the simulation, the pressure assumed to be constant, the K and ϵ value at inlet used;

$$K = \frac{3}{2} (U_{ave} T_i)^2 \quad (6)$$

$$\epsilon = \frac{C_\mu^{3/4} K^{3/2}}{KL} \quad (7)$$

Where U_{ave} is inlet velocity, T_i is turbulence intensity (here taken to be about 2%), L is here taken to be a “reasonable length” of 1m and $\kappa = 0.41$ is the Von Karman constant. Experience has shown, however, that the values of K and ϵ impose at the inlet to the computational domain play only an insignificant role, as long as they are both small.

2. SOLVER

There are two solvers used in this case, ANSYS Fluent and CFD-ACE solver to solve the governing equations that are related to the flow physic problem, based on the given material properties, flow physic model and the boundary

conditions. All properties and conditions are satisfactorily converging using the Finite Volume Method to solve velocity components, pressure, and k - ϵ (epsilon) scheme.

Fluid properties used for the simulation process with heat pipe heat-exchanger are corresponding to constant air at 293K. Several attempts using water, acetone, and R134a were simulated. To show the flow of the air when moving to pass the tube, 0.5 to 1 m/s of flow rate are applied. Fluid properties used in the heat pipe-condenser simulation processes are corresponding to constant air at 300 K and standard pressure at sea level of 101.3 kPa, where the temperature inlet through the heat pipe heat-exchanger is assumed to be 300 K and the ventilation flow is assumed to be in +X direction. Boussinesq approximation where the fluid density concerning the buoyancy force is affected by temperature change is assumed, with reference temperature T_{ref} is 300K and Vol. Coef. Th. Exp. is 0.003333 1/K. Other molecular properties include $\rho = 1.1614 \text{ kg/m}^3$, $\mu = 1.846 \times 10^{-5} \text{ N-s/m}^2$, $\nu = 1.589 \times 10^{-5} \text{ m}^2/\text{s}$.

3. POST-PROCESSING: HEAT PIPE HEAT-EXCHANGER

ANSYS Fluent in the CFD-View analysed the convergence results and is presentable in a graphical presentation with different plots, streamlines and data curves. Three cases are simulated using ANSYS Fluent to show the heat transfer pattern of the refrigerant medium inside the heat pipe heat-exchanger, but only the Simulation of refrigerant R134a is shown. Figure 7 shows a temperature profile of three heat pipe heat-exchangers in a row filled with R134a. Table 4 below shows the properties of the cooling medium used when running with ANSYS Fluent. The temperature difference between the inlet and the outlet of the heat-pipes show that up to 5 K can be achieved when R134a is applied as a refrigerant medium.

Physical Parameters	Water H ₂ O	Acetone C ₃ H ₆ O	R134a CH ₂ FCF ₃
Density kg/m ³	998.2	791	1207.3

Spec. Heat J/kg.K	418 2	216 0	1424.4 1
Thermal Cond. W/m.K	0.6	0.18	0.0811 9
Viscos kg/m-s	0.00 100 3	0.00 033 1	0.0001 9525
Inlet temperature, K	293	293	293
Outlet temperature, K	295	296	298
Different temperature, K	2	3	5

Table 4: The table shows the comparison of temperature different K between refrigerant medium, used in a heat pipe heat-exchanger

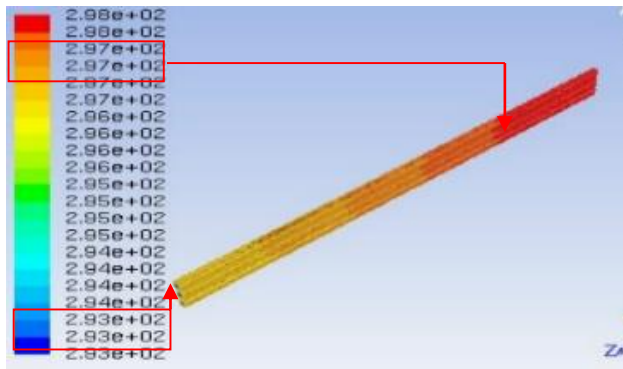


Figure 7: Simulation of heat pipe heat-exchanger by ANSYS Fluent using R134a as a cooling medium. The temperature difference from the evaporator side inlet to the condenser side is about 5 K.

4. POST-PROCESSING FOR HEAT PIPE HEAT-EXCHANGER AND AIR-COOLED CONDENSER

Figure 8a to 8c shows the distributions of temperature and velocity profile simulated through an air-cooled condenser. The end temperature of the air that flows through the condenser is about 304K to 307K, an increase of 4K to 7K from the supply air of 300K.

6.1 CASE 1

CASE 1: Temperature

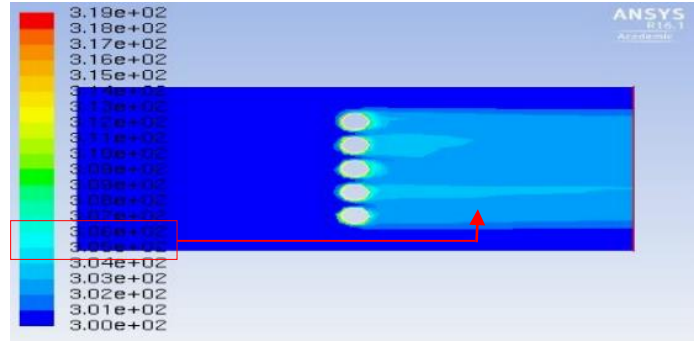


Figure 8a: Simulation of ANSYS Fluent on an air-cooled condenser. The lowest temperature recorded for a condenser is about 304K to 307K heat rejection to the ambient.

CASE 1: Temperature

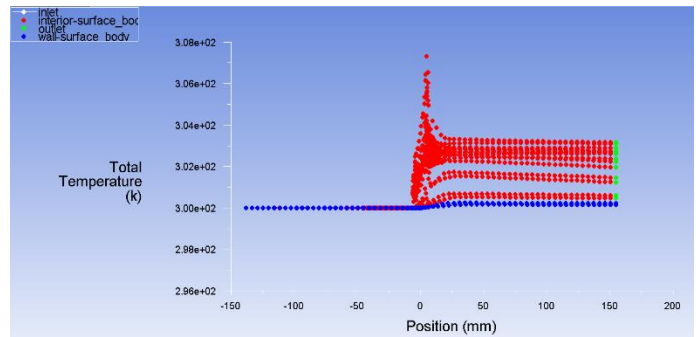


Figure 8b: Graph from ANSYS Fluent for Case 1 with a condenser. The lowest average temperature recorded is 304K.

CASE 1: Velocity

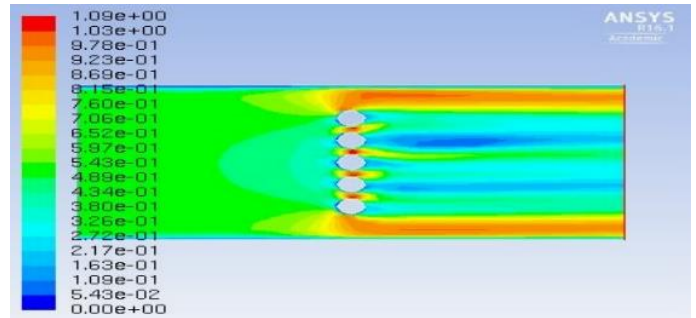


Figure 8c: Velocity profile of air through an air-cooled condenser runs on ANSYS Fluent.

6.2 CASE 2

Figure 9a to 9c shows the distributions of temperature and velocity profile simulated through a condenser with a heat pipe heat-exchanger attached to it. The end temperature of the air that flows through the condenser is about

302K to 304K, an increase of 2K to 4K from the supply air of 300K.

CASE 2: Temperature

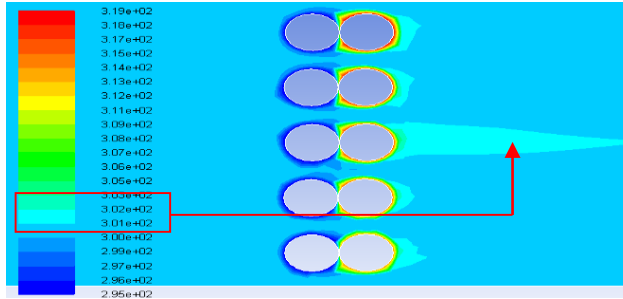


Figure 9a: Simulation of ANSYS Fluent on an air-cooled condenser of Case 2 with a heat pipe heat-exchanger attached closely together. The lowest temperature recorded is about **303K to 304K**

CASE 2: Temperature

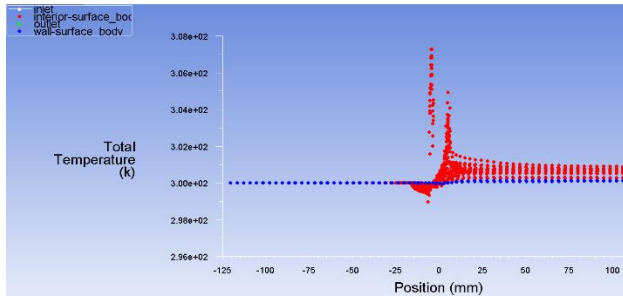


Figure 9b: Graph from ANSYS Fluent for Case 2 with a heat pipe heat-exchanger attached closely together. The lowest average temperature recorded is **302K**.

CASE 2: Velocity

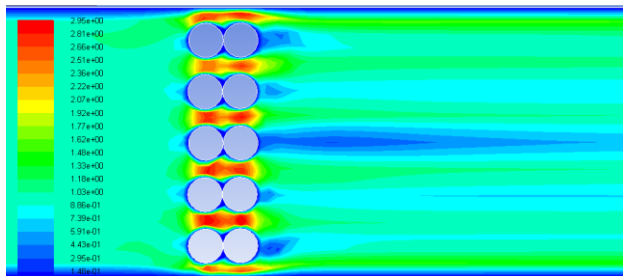


Figure 9c: Velocity profile of air through an air-cooled condenser with heat pipe closely attached.

6.3 CASE 3

Figure 10a to 10e shows the distributions of temperature and velocity profile simulated through a condenser with a heat pipe heat-exchanger attached 100mm in front of it. Figure

10c shows the temperature graph of air passing through case 3 plotted by CFD-ACE. The end temperature of the air that flows through the condenser is about 301K to 305K, an increase of 1K to 5K from the supply air of 300K. A simulation of Case 3 is done with both ANSYS Fluent and CFD ACE to show the lowest temperature that the heat pipe has achieved.

CASE 3: Temperature

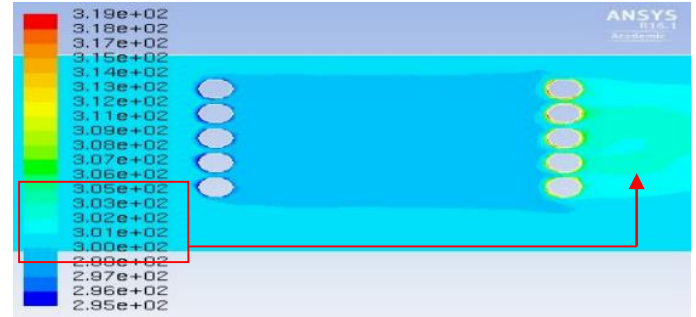


Figure 10a: Simulation of ANSYS Fluent on an air-cooled condenser with a heat pipe heat-exchanger separately attached 100mm at the air inlet. The lowest temperature recorded is **302K**.

CASE 3: Temperature

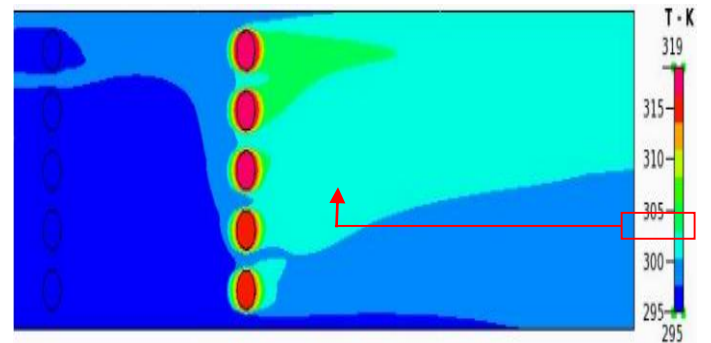


Figure 10b: Simulation of CFD-ACE on an air-cooled condenser with a heat pipe heat-exchanger separately attached 100mm at the air inlet. The lowest temperature recorded is **301K to 305K**.

CASE 3: Temperature

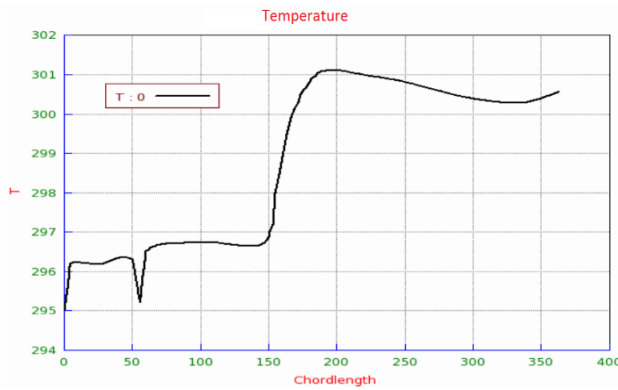


Figure 10c: Graph from CFD-ACE for Case 3. The airflows over the condenser coil were recorded at about 301K.

CASE 3: Velocity

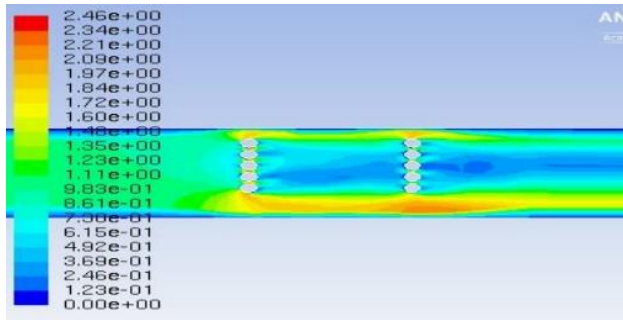


Figure 10d: Velocity profile of air through an air-cooled condenser with a heat pipe heat-exchanger separately attached 100mm at the air inlet runs on ANSYS Fluent.

CASE 3: Velocity

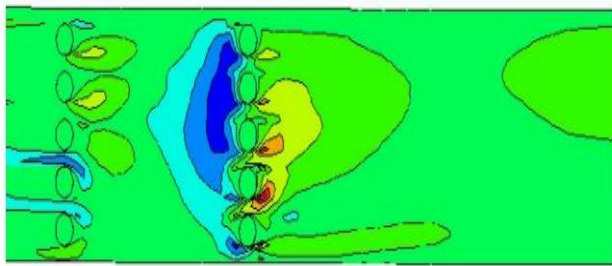


Figure 10e: Velocity profile of air through an air-cooled condenser with a heat pipe heat-exchanger separately attached 100mm at the air inlet runs on CFD-ACE.

5. RESULT AND DISCUSSION

The purpose of this study is to simulate an airflow passing through a heat pipe heat-exchanger and an air-cooled condenser, to investigate possibilities of reducing temperature supply to the condenser. The flow pattern of a

heat pipe temperature and the condenser is recorded by simulation software. A model of a straight heat pipe uses ANSYS Fluent to show heat transfer inside the heat pipe which is filled with R134a. Both inlet and outlet temperatures are recorded when applying to an ambient temperature of 293K. A difference of 5K is obtained when R134a is used as a refrigerant medium in the heat pipe. The lower temperature of the air when passing through a heat pipe and the condenser is recorded with ANSYS Fluent and CFD-ACE software.

From the simulation of a condenser and an attachment of the heat pipe to the air-cooled condensing system, it is found that efficiency can be increased with the attachments of the heat pipe to the inlet airflow of the condenser. An air-cooled condenser is recorded to reject heat at about 12K to 15K when simulated. With an attachment of a heat pipe heat exchanger, it is found that the temperature difference can be increased to about 14K to 18K. Table 5 shows the inlet and outlet temperature profile of three cases to point out the capability of the heat pipe in transferring heat.

Parameters	Case 1	Case 2	Case 3
Air Inlet Temp, K	300	300	300
Heat Pipe Evaporator Temp T_e K	295	295	295
Condensing Temp T_c K	315-319	315-319	315-319
Air Outlet Temp, K	304-307	303-304	301-305
Different Temp, K	12-15	15-16	14-18

Table 5: The table shows the comparison of the temperature of different K between cases. Case 3 shows the highest different temperatures compare to other cases.

Table 6 shows the work done by the refrigeration system corresponding to the condenser T_c achieved.

Parameters	Cond	HP + Cond
Evaporating T_e ($^{\circ}$ C)	5	5

Condensing T_c ($^{\circ}\text{C}$)	46	32
Condenser Surface Temp ($^{\circ}\text{C}$)	58	45
Superheat (different K)	10	10
Subcooled (different K)	20	20
Evaporator Work Done Q_e (kJ/kg)	173.8	193.3
Condenser Work Done Q_c (kJ/kg)	200.5	211.7
COP	6.5	10.5
Compressor Work Done W (kJ/kg)	26.73	18.42

Table 6: The table shows the comparison of refrigeration cycle parameters when the condensing temperature changed from 46°C to 32°C .

Figure 12 shows the pressure-enthalpy diagrams of an air-cooled refrigeration system corresponding to an evaporating temperature $T_e=5^{\circ}\text{C}$ (278K), condensing temperature $T_c=46^{\circ}\text{C}$ (319K) [14], with 10K superheat and 20K subcooling; compared to a condensing temperature of $T_c=32^{\circ}\text{C}$ (305K) using heat pipe heat-exchanger. The calculation for the parameters is;

$$\text{Evaporator work done } Q_e = h_4 - h_1 \quad (8)$$

$$\text{Condenser work done, } Q_c = h_3 - h_2 \quad (9)$$

$$\text{Compressor Work Done, } W = h_2 - h_1 \quad (10)$$

$$\text{Coefficient of performance, COP} = \frac{h_4 - h_1}{h_2 - h_1} \quad (11)$$

6. CONCLUSION

There are possibilities of using a heat pipe heat-exchanger to lower down the ambient air supply to the condenser. From the refrigeration cycle plotted, it is found that, with the fall of condensing temperature T_c from 46°C (319K) to 32°C (305K), the evaporating capacity and the condensing capacity increased. Evaporator capacity increased to 11.2% and the condenser capacity increased to 5.6%. The power consumption of the compressor work decreased at -31% from 26.73 kJ/kg to 18.42kJ/kg. The surface temperature of the condenser is found to be lowered from 58°C

(331K) to 45°C (318K) and the flash gas of the refrigerant where the liquid turns to vapour in the evaporator decreased from 15% to about 5%.

Other simulations using the different refrigerant mediums in the heat pipe heat-exchanger should be tested.

REFERENCES

- [1] Yau, Y.H., and Ahmadzadehtalatapeh, M., A Review on the Application of Horizontal Heat Pipe Heat-exchanger s in Air Conditioning Systems in The Tropics, *Applied Thermal Engineering*, **30**, (2-3), 2010, 77-84.
- [2] Ong, K.S., and Haider-E-Alahi, M., Performance of an R-134a-Filled Thermosyphon, *Applied Thermal Engineering*, **23**, (18), 2003, 2373-2381.
- [3] Brooke, T., Optimizing Wrap-Around Heat-pipes, *Heat Pipe Technology*, 2007.
- [4] Priyadumkol, J., and Kittichaikarn, C., Application of the Combined Air-Conditioning Systems for Energy Conservation in Data Center, *Energy and Buildings*, **68** (Part A, 0), 2014, 580-586.
- [5] T.T. Chow, Z. Lin, X.Y. Yang, Placement of Condensing Units of Split-Type Air-Conditioners at Low-Rise Residences, *Applied Thermal Engineering*, **22**, 2002, 1431-1444.
- [6] A. Avara & E. Daneshgar, Optimum Placement of Condensing Units of Split-Type Air Conditioning by Numerical Simulation, *Energy and Building*, **40**, 2008, 1268-1272
- [7] T.T. Chow, Z. Lin, Prediction of On-Coil Temperature of Condensers Installed at Tall Building Re-Entrant, *Applied Thermal Engineering*, **19**, 1999, 117-132.
- [8] T.T. Chow, Z. Lin, J.P. Liu, Effect of Condensing Unit Layout at Building Re-entrant on Split-Type Air-Conditioner Performance, *Energy and Buildings*, **34**, 2002, 237-244.
- [9] H. Xue, B. Xu, J. Wu, Y. Wei, Prediction of Temperature Rise Near Condensing Units in the Confined Space of a High-Rise Building, *Building and Environment*, **42**, 2007, 2480-2487.
- [10] R.R. Riehl, T.C.P.A. Siqueira., Heat Transport Capability and Compensation Chamber in Fluence in Loop Heat-pipes Performance, *Applied Thermal Engineering* **26**, 2006, 1158 -1168.

- [11] W. Joung, T. Yu, J. Lee., Experimental Study on the Loop Heat Pipe with a Planar Bifacial Wick Structure, *International Journal of Heat and Mass Transfer*, **51**, 2008, 1573-1581.
- [12] P. Charoensawan, P. Terdtoon., Thermal Performance of Horizontal Closed-Loop Oscillating Heat Pipe, *Applied Thermal Engineering*, **28**, 2008, 460-466.
- [13] C. T. Meng, S.H. Chih, W.K. Shung., Experimental Study of a Loop Thermosyphon Using Methanol as Working Fluid, *14th IHPC*, 2007.
- [14] W. P. Jones, *Air Conditioning Engineering (Fifth Edition)*, Butterworth-Heinemann, 2001.
- [15] W. T. Grondzik, *Air-Conditioning System Design Manual (Editor, Second Edition)*, American Society of Heating Refrigerating and Air-Conditioning Engineer Special Publication.
- [16] T. Kivva, B.P. Huynh, M. Gaston, and D. Munn, A Numerical Study of Ventilation flow through a 3-Dimensional Room with a Fan, *Turbulence, Heat, and Mass Transfer 6*, K. Hanjalić, Y. Nagano and S. Jakirlić (Editors), Begell House Inc., 2009.
- [17] Bangalee, M.Z.I., Miao, J.J., Lin, S.Y., and Yang, J.H., Flow Visualization, PIV Measurement and CFD Calculation for Fluid-Driven Natural Cross-Ventilation in a Scale Model, *Energy and Buildings*, **66**, 2013, 306-314.
- [18] van Hooff, T., and Blocken, B., CFD Evaluation of Natural Ventilation of Indoor Environments by the Concentration Decay Method: CO₂ Gas Dispersion from a Semi-Enclosed Stadium, Building, and Environment, **61**, 2013, 1-1

STUDY OF WIND-ASSISTED ENERGY FOR COOLING SYSTEM IN BANGI, MALAYSIA

Z. Abdullah, M. S. Shaadan, Z. Jusoh, Z. Engsa

HVAC&R Section,

Universiti Kuala Lumpur Malaysia France Institute,

43650 Bandar Baru Bangi, Selangor, Malaysia

Corresponding Author's Email: zulkarnaini@unikl.edu.my

Article History: Received xxxxx; Revised xxx; Accepted xxxx

ABSTRACT: The ever-increasing rate of demand for electrical energy, urge researchers to explore an alternative energy source. The annual report from The Energy Commission of Malaysia shows that from the year 2015 to 2016, there are 8.9% and 10.5% increments of electrical consumption. The principal operations of a wind turbine in assisting energy consumption are by converting the kinetic energy of the blowing wind through a fan blade rotation, into electrical energy. The kinetic energy available depends mainly on the wind speed and the blade swept area of the turbine. The work presented is a study of a small horizontal-axis wind turbine in cooling a refrigerator as a test unit, where the available wind speed is less than 10 m/s. The wind speed data is collected in Bandar Baru Bangi and the aims are to operate a refrigeration cycle that chilled a refrigerator to about 278K (5 °C). The realism of using the wind turbine is carefully studied through a computational fluid dynamics ANSYS-Fluent modelling, a series of wind speed data taken on-site and a mathematical model of wind turbine power calculation. The structure of the wind turbine is a 6 m height tower with 2.6 m diameter blades and the available high wind speed taken on site is 5 m/s. From the studies, albeit with a small amount of wind speed, it is found that the wind turbine conversion energy is capable to run a small refrigerator chiller unit to 278 K (5 °C) with an available power of 151.33 W.

KEYWORDS: *Computational fluid dynamics; wind turbine; refrigeration cycle; renewable energy*

1.0 INTRODUCTION

Renewable energy sources such as sunlight, wind, tidal, waves and geothermal energy could be used to operate electromechanical equipment. The wind flows are created by the uneven warming of the environment and the inconsistencies of the earth's surface could be turned into electrical energy by assuming only the cost of installation and maintenance. The author proposed a method of cooling a small refrigerator that operates on a minimum electrical source, from an outcome of wind energy. A manual data collection of wind speed

at Bandar Baru Bangi had been collected and the ‘high’ average speed was found to be at 5 m/s on-site, which is higher than the finding of (Saba et al. 2014) at 2m/s for Malaysia average condition. The speed and the gust had been averaged, to supply an electrical source for a small refrigerator chiller unit. The energy-saving calculation is shown to compare the rate of saving to the normal electrical tariffs. The simulation of the wind turbine focus on the energy outcome. As predicted by Betz (Betz A. 1926) using a one-dimensional model, the largest power that can be extracted from the wind is less than 16/27 or 59.3% of the kinetic energy in the wind. Figure 1 shows the rotor as an ‘actuator disk’ that creates a pressure discontinuity of area A and local velocity V (Jonkman 2003, White 1988). This paper analyses the energy that the wind could offer by cooling a refrigerator to a required temperature level. In a location where wind speed averages less than 10 m/s, the possibility of applying wind turbines as an alternative source is tested. A small wind turbine applies to grid-connected home applications (Elliot 2002). Figure 1 shows the control volume for the idealized actuator disk analysis and the calculation of available power for a site at Bandar Baru Bangi. Table 1 shows the power available calculated from the wind in Bandar Baru Bangi. The power available of the wind turbine can be calculated as,

$$P_{available} = \frac{1}{2} \rho A v^3 C_p \quad (1)$$

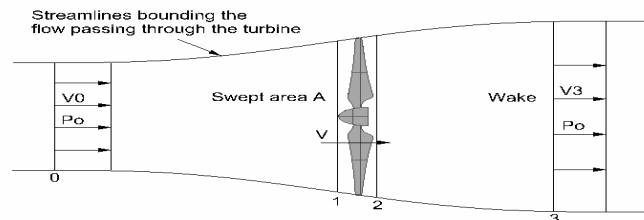


Figure 1: Control volume for the idealized actuator-disk analysis. (David H. and Andrej H. 2008).

Table 1: Wind turbine power calculation at average high wind speed in Bandar Baru Bangi.

At 5 m/s, the power that the wind turbine can generate is about 151.33 W.

Parameter	Measurement
Blade length	1.3 m
Wind Speed	5 m/s, 36.73 rpm
Air density	1.14 kg/m ³
Power coefficient	0.4
Power available	151.33 W

2.0 THE APPLICATION OF WIND TURBINES

Subject to the blowing wind, a room in a Bandar Baru Bangi can be very warm and humid as the high temperature could reach up to 308 K (35°C) outdoor temperature. Figure 2 shows the wind recorded in Kuala Lumpur for the last eighteen years since 2000 (weatheronline.co.uk). An average wind speed of 1.7 m/s (6.1 km/h) was recorded but, the required speed for the wind turbine to rotate is in the range of 3.5 m/s to 10 m/s. A small wind turbine is proposed to be tested at a strategic location where the high average wind speed is about 5 m/s. The wind turbine is a 2600 mm blade diameter, 400 rated rpm, rated power at 300 W. The refrigeration system test unit is a 50 W refrigerator with 48 W energy consumption.

3.0 PROBLEM DESCRIPTION

Mechanical cooling needs electrical power to run the refrigeration cycle. Wind turbine acts as a substitution of electrical grid power to benefit electricity by generating mechanical power through rotating propellers. This study works on a wind power generated at an open space next to a highway where the flow and the gusting air are recorded higher, to cool a refrigerator at about 5°C. As the average wind flow in Kuala Lumpur is 1.7 m/s, locating the wind turbine at the predicted high wind flow area will show promising results. Simulation using ANSYS Fluent is tested to see the rotating fan-blade air velocity, predicted by the k- ϵ method of calculation.

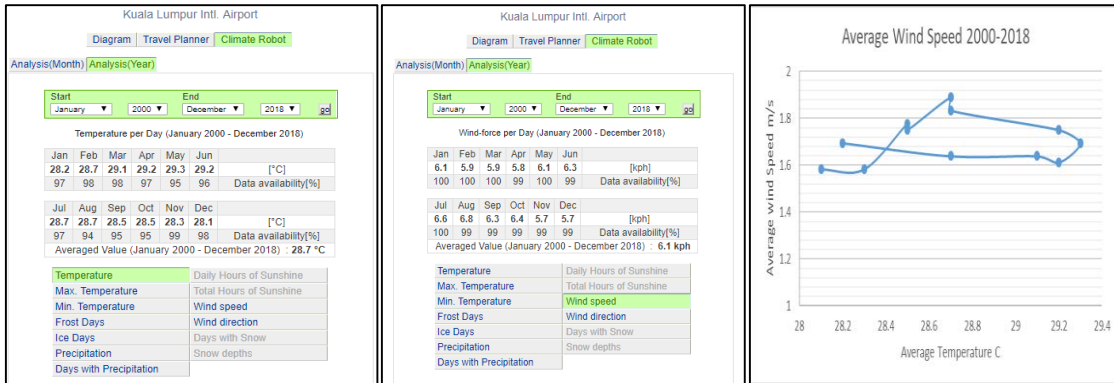


Figure 2: The average wind speed for Kuala Lumpur from the year 2000 to 2018 is recorded at about 6.1 km/h (1.7 m/s) with a temperature of 28.8°C. Source weatheronline.co.uk

4.0 METHODOLOGY

This paper study the result of a wind turbine electrical power in Bandar Baru Bangi by collecting a series of wind speed data to find the average wind speed. Refer to the location proposed, it is found that the average high wind speed is at 5 m/s and is capable of operating an electric refrigeration system as a test unit. The flow chart in Figure 3 shows the work process. The work started with processing input data, manual collection of field data, construct a factual decision and processing the output data. Figure 4 shows the average wind speed data collected in Bandar Baru Bangi for the experiment.

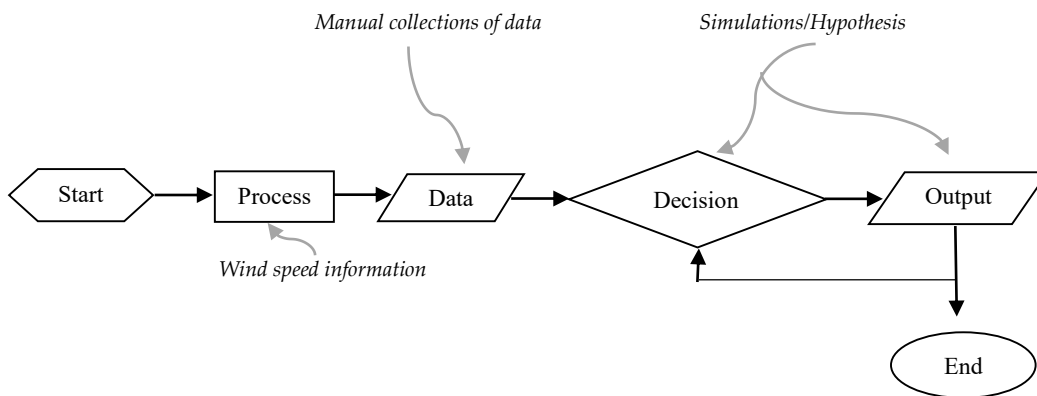


Figure 3: Flow chart of the wind turbine study.

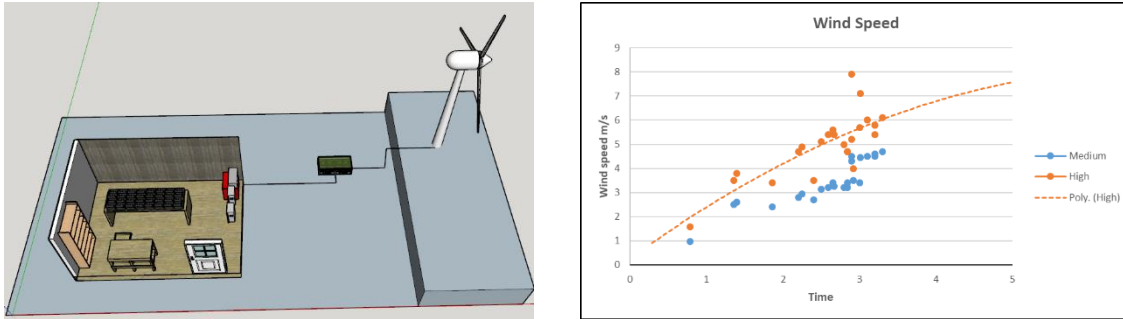


Figure 4: The wind turbine model and the average of high wind speed taken at Bandar Baru Bangi. The high average is about 5 m/s.

5.0 RESULT AND DISCUSSION

5.1 Simulation Process

The wind speed from 3 to 5 m/s are simulated using ANSYS Fluent to predict the velocity output range. Three components namely enclosure, rotating part and fan-blade mesh. The meshed and boundary conditions are listed in Table 2. Basic nodes and elements mesh is applied to the components as Figure 4. Tables 3 and 4 show the simulation processes and the range of velocity that the software predicted.

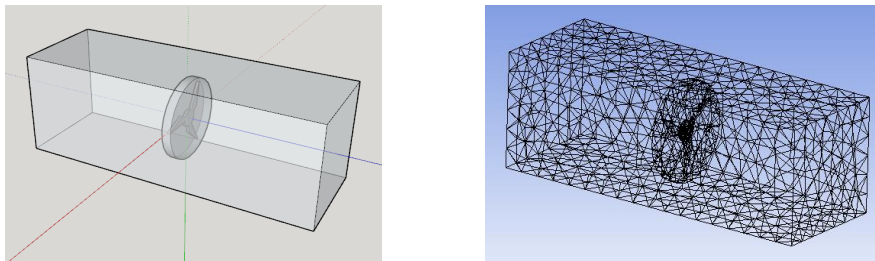


Figure 4 The boundary and mesh for an enclosure, rotating part and the fan-blade.

Table 2: Meshing elements and boundary conditions run on ANSYS Fluent.

Domains	Nodes: Enclosure 1276, Rotating part 173, Total 1449 Elements: Enclosure 5652, Rotating part 611, Total 6263
General	Pressure based, Absolute velocity formulation, Transient
Model	Energy equations, k-epsilon, realizable model, scalable wall functions
Material	Air, Aluminium
Cell Zone Conditions	Enclosure rotation-axis Z direction, Rotating mesh motion, rpm

Boundary Conditions	Inlet pressure-based, Outlet pressure based
Solution	Simple, Least-squares cell-based, Second-order pressure, Second-order upwind momentum, First order upwind turbulent kinetic energy, First order upwind turbulent dissipation rate, First order upwind transient formulation
Initialization	Hybrid

Table 3: Simulation using the air velocity range from 3 m/s to 5 m/s. The simulations predicted that with 5 m/s wind velocity, about 1.89 m/s to 2.84 m/s will be utilized for energy generations.

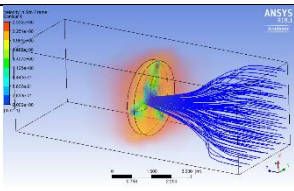
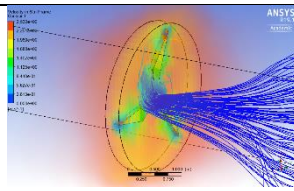
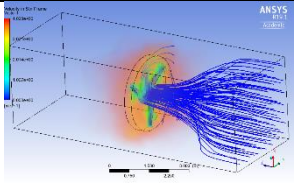
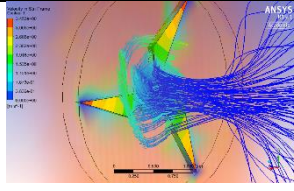
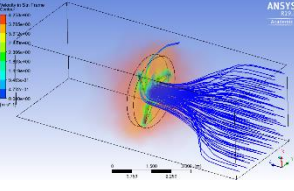
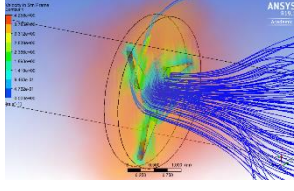
Input	Enclosure	Rotating Part	Output Range
3 m/s			1.12 to 1.97 m/s
4 m/s			1.9 to 2.3 m/s
5 m/s			1.89 to 2.84 m/s

Table 4: New wind turbine power calculation based on simulation results.

Parameter	Measurement
Blade length	1.3 m
Air density	1.14 kg/m ³
Power coefficient	0.4
Input Wind Speed	5 m/s, 36.74 rpm
Output Wind Speed	2.84 m/s, 20.87 rpm
Power Max	151.33 W
Power Min	27.73 W

5.2 Refrigeration Process

Hypotheses of the refrigeration cycle are, as for Figures 5 and 6 (Coolpack). The system is a direct expansion R134a with evaporating temperature $T_e = 5^\circ\text{C}$, condensing temperature $T_c = 40^\circ\text{C}$, 10 K subcooling and 5 K superheat.

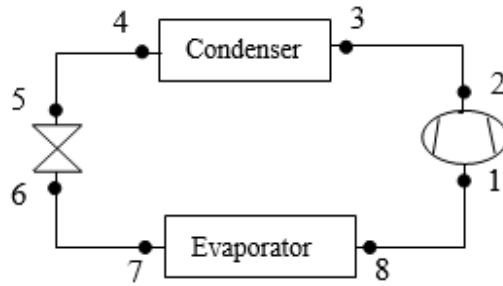


Figure 5: The schematic drawing of the refrigeration installation

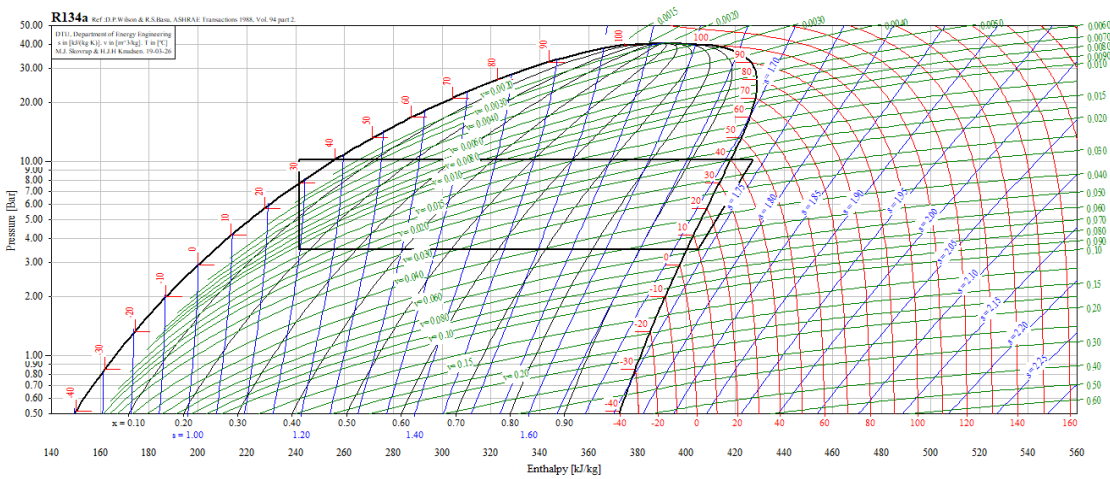


Figure 6: The pressure-enthalpy curve of the refrigeration cycle. (CoolPack)

Table 5: The thermodynamic cycle of the R134a refrigerator

Point	T	P	v	h	s
	$^\circ\text{C}$	bar	m^3/kg	kJ/kg	$\text{kJ}/\text{kg}\cdot\text{K}$
1	9.999	3.496	0.059596	404.785	1.7361
2	47.921	10.164	0.020989	427.428	1.7361
3	47.921	10.164	0.020989	427.428	1.7361
5	30.000	10.164		241.463	
7		3.496		241.463	
8	10.000	3.496	0.059592	404.785	1.7361

Table 6: The output results of the refrigeration cycle

Parameter	Measurement
T_e	5 °C
T_c	40 °C
Superheat	5 K
Subcool	10 K
Evaporator work Q_e	163.322 kJ/kg
Condenser work Q_c	185.965 kJ/kg
COP	7.21
Compressor work	22.642 kJ/kg
Pressure ratio	2.907
Refrigerant flowrate	0.927×10^{-3} kg/s
Compressor power	21 W

6.0 CONCLUSION

Based on the data taken in Bandar Baru Bangi where the average ambient temperature is 30°C, 75% relative humidity and 5 m/s of high average wind speed, the power obtained from the wind turbine is capable of operating a small refrigerator chiller unit. The wind turbine location is on higher ground, near a busy traffic highway. This makes benefit from the high gusting wind created by the traffic. To assist with the calculations, ANSYS Fluent has been simulated to runs from the range of 3 m/s to 5 m/s wind speed. It is found that when 5 m/s of wind blowing to the wind turbine, only a part of 2.84 m/s is generated to rotate the propellers. The power from the wind turbine will be estimated between 27.73 W to 151.33 W. With the operating conditions of T_e 5 °C and T_c 40 °C, the compressor work of the refrigerator only requires about 21 W for a cycle. The calculations show that wind power could generate enough energy in assisting the refrigerator requirement. This could last for about 7 hours of cooling operation. The wind turbine is viable for the operation of a small energy consumption unit such as the refrigerator chiller without the need for any electrical source.

REFERENCES

- [1] A. S. Saba, M. Sohif, K. Sopian, E. Saleh, M. Alkhair, "Simulation analysis of Venturi-Vertical Axis Wind Turbine (V-VAWT)", *8th International Conference on Renewable Energy Sources*, 25, 2014.
- [2] A. Betz, *Wind energy and its extraction through windmills. The fundamental formula for estimating the maximum power and efficiency of wind machines. Wind-energie und ihre ausnutzung durch windmühlen*, bandenhoeck & ruprect, Göttingen, 1926. Facsimile edition by Ökobuch Verlag, Staufen, 1994. ISBN 3-922964-11-7
- [3] J.M. Jonkman, "Modelling of the UEA wind turbine for refinement of FAST_AD", *National Renewable Energy Laboratory*, TP-500-34755, 2003
- [4] F. M. White, *Fluid Mechanics 2nd Edition*, McGraw-Hill, Singapore, 1988
- [5] D. Elliot, "Assessing the world's wind resources", *IEEE Power Engineering Review*, 22 (9), 4-9, 2002
- [6] H. David, H. Andrej, "3D Modelling of a wind turbine using CFD". *NAFEMS UK Conference Engineering Simulation: Effective use and Best Practice*, 2008
- [7] Weather Online, <https://www.weatheronline.co.uk/weather>
- [8] ANSYS Software, <https://www.ansys.com/academic>
- [9] CoolPack Software, <https://www.ipu.dk/products/coolpack>

POSSIBILITY OF USING SILICA GEL-WATER ADSORPTION CHILLER IN THE COLD CHAIN

M. A. AHAMAT^{(a)*}, M. J. TIERNEY^(b), ZULKARNAINI ABDULLAH^(a), ZAKARIA JUSOH^(a)

^(a)Universiti Kuala Lumpur, Malaysia France Institute,
Section 14, Jalan Teras Jernang, 43650 Bandar Baru Bangi, Selangor, Malaysia.

E-mail: ^{(a)*}asmidzam@mfi.unikl.edu.my

^(b)Mechanical Engineering Department, University Walk, Bristol, BS8 1TH, United Kingdom

ABSTRACT

This paper proposed the usage of the adsorption cooling system in a cold chain transportation system, particularly for vehicles that are using diesel engines. The feasibility of using a silica gel-water adsorption chiller in the cold chain was carefully studied through mathematical modelling. An adsorption chiller that uses a compact heat-exchanger as its adsorber was proposed. The potential amount of waste heat recovery through adsorption chiller was predicted using an energy balance method. The overall efficiency of the diesel engines and chiller combinations could be improved compared to the efficiency of the diesel engines alone. Adsorption dynamic and equilibrium data of silica gel-water pair were obtained from the recently developed adsorption calorimeter. This data was used to model the performance of the adsorption chiller at the lowest possible evaporator temperature, which is at 1 °C. It is concluded that a 1 mm diameter silica gel is a better option for cold chain applications.

1. INTRODUCTION

Carbon dioxide is one of the gases that contribute to global warming. Food chain contributions to the total carbon emission are estimated to be 1 % (James (2010)). By using an adsorption chiller as the cooling system in the vehicles, the emission of carbon by the food chain industry could be reduced.

Adsorption chiller is a heat-driven cooling cycle that can utilize heat sources at the temperature as low as 55°C (Saha et. al (2003)). The heat source could be waste heat from the internal combustion engines or solar radiation. Adsorption chillers do not have any moving parts such as in vapour compression cooling system which makes it require a minimum level of maintenance.

In transportations, the application of adsorption chiller is still limited. An adsorption chiller has been used in cooling the locomotive driver cabin (Wang et. al (2002)). A Four-degree Celsius reduction in the cabin temperature compared to outside temperature was obtained. Alternatively, car air-conditioning also could employ an adsorption chiller (Tamainot-Telto et. al (2009)). In the fishing industry, waste heat from diesel engines could be used to drive adsorption chiller for fish conservation in the boat (Wang et. al (2004)). All of these adsorption chillers use ammonia or methanol as a refrigerant. This could create a potential hazard in cold chain applications. Therefore, we are proposing the adsorption chiller that is using water as a refrigerant. Water does not have any potential hazards in the case of leakage.

This paper proposed the application of silica gel-water adsorption chiller in cold chain transportation with a minimum temperature of 1 °C. Adsorption data obtained from our novel calorimeter were used to develop an adsorption chiller model. Then, the discussion on the usefulness of the model is presented.

2. BASIC OPERATION OF AN ADSORPTION CHILLER

An adsorption chiller requires an active material (hereafter termed “adsorbent”) that can attract refrigerant molecules onto its surface by either physical or chemical force when it is cooled. When the adsorbent is heated, some of the refrigerant molecules have sufficient energy to overcome these bonds and desorb. In commercial adsorption chillers, silica gel or zeolite has been used as adsorbents and water as the refrigerant (Jakob (2010)). Adsorbent could be packed around or adhered to the surface of a cooling/heating coil, the adsorbent and coil being contained in a vessel (hereafter termed “adsorber”). The adsorber acts as a thermal compressor that drives the refrigeration cycle, and it is equivalent to the mechanical compressor in a vapour compression refrigeration system.

A basic adsorption chiller consists of an adsorber, an evaporator, a condenser and valves between each of these components as in Figure 1. The cycle is operated in four stages: adsorption-evaporation, pre-heating and pressurization, desorption-condensation, and pre-cooling and depressurization.

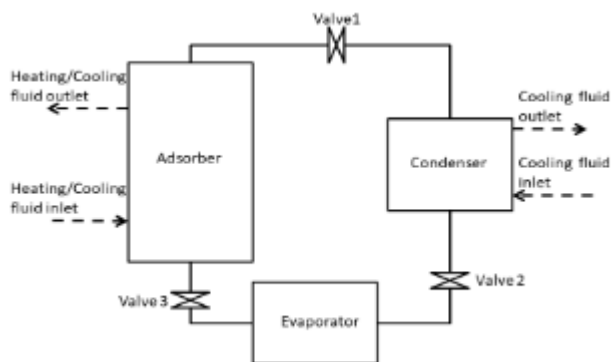


Figure 1. Schematic of a basic configuration of an adsorption chiller

The cycle begins with the adsorption-evaporation stage. The adsorbent has a low concentration of refrigerant on its surface. With the adsorber connected to the evaporator (Valve 3 opened), the refrigerant evaporates and is adsorbed. As the adsorption process occurs, the heat of adsorption is liberated. Cooling fluid is circulated to extract the heat of adsorption and maintain the adsorber at a relatively cold temperature (say $\sim 30^{\circ}\text{C}$), ensuring continuous adsorption. Once the adsorbent is almost saturated with adsorbate, Valve 3 is closed to isolate the adsorber.

Then, the cycle continues with the pre-heating and pressurization stages. Heating fluid is circulated through the adsorber. When the pressure inside the adsorber reaches condenser pressure, Valve V1 is opened. No net changes in refrigerant concentration occur on the adsorbent surface during this stage. The adsorbent is regenerated during the desorption-condensation stage. Refrigerant desorbs from the adsorbent surface and condenses. Heating fluid is continuously circulated through the adsorber to increase the adsorbent temperature and compensate for the heat loss through a phase change. The condenser is cooled to extract the heat liberated by the refrigerant during the condensation process. Valve 1 is closed at the end of this stage to isolate the adsorber.

The cycle is completed by the pre-cooling and depressurization stage. Cooling fluid is circulated through the adsorber. When the pressure inside the adsorber reaches evaporator pressure, Valve V3 is opened. Similar to the pre-heating phase, no net changes in refrigerant concentration occur on the adsorbent surface.

3. EXPERIMENTAL METHODS TO OBTAIN ADSORPTION DATA

A novel colourimetric method (Ahamat & Tierney (2012)) was developed to enable the assessment of adsorption equilibrium and dynamic data of silica gel bonded to the heat exchange surface. The schematic of this novel adsorption calorimeter is presented in Figure 2. The calorimeter comprised a glass evaporator section and a glass adsorbing section, each bounded by a thermoelectric module system (Ahamat & Tierney (2012)), and the two sections connected via a diaphragm valve (Edwards Speedivalve SP16, rated at 1.7 litres/second maximum volumetric flow). The glass sections were custom made at the University of Bristol and measured 60 mm outer diameter x 60 mm height. Pressures were monitored by active strain gauges (Edwards model D35726000 (Serial no. 105000034) and Baraton Type 222BHS-A-B-100-gauge head (Serial no. 25544-1A)). The output voltage of the pressure gauges was recorded using a Labjack U12 (analog to digital converter). The internal volume of the adsorber section was determined from the measured change in mass before and after the section was filled with water.

This calorimetric method was designed for the experiment that mimicked the adsorption-evaporation stage within an adsorption chiller. The temperature of the heat exchange surface (aluminium endplate in Figure 2(b)) was controlled, and a step-change in vapour pressure was imposed. Heat rejected through the heat exchange surface was recorded.

The adsorber and evaporator sections were initially isolated. The silica gel was initially dry (uptake(X) ~ 0), and the adsorber section was maintained under vacuum (<100 Pa as the limit of the pressure gauge measurement range). The water temperature in the evaporator was maintained at a specified value which creates a constant vapour pressure inside the evaporator section. When the adsorber and evaporator sections were connected, water vapour entered the adsorber section. Silica gel then started to adsorb water vapour, liberating the heat of adsorption. The equal and opposite cooling power from the thermoelectric module (maintaining a constant adsorber temperature) indicated the instantaneous heat flow.

The cumulative heat rejection (Figure 3(a)) achieved at equilibrium was used to infer either the adsorptive capacity or the specific heat of adsorption. The time taken to reach 63.2% of the total cumulative heat rejection was taken as a characteristic time (This, in turn, was the reciprocal of the Linear Driving Force constant (K_{ldf}), as shown in Figure 3(b)).

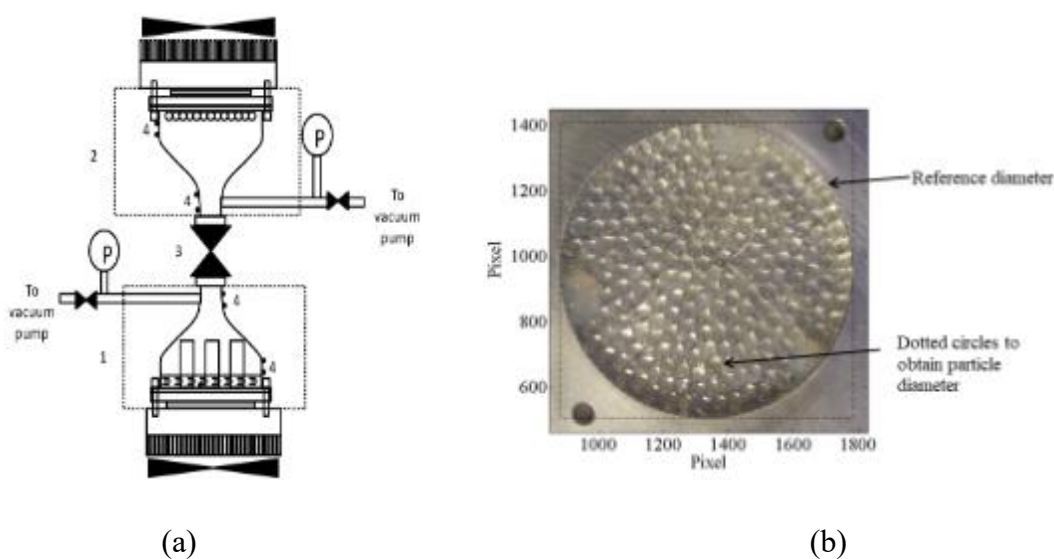


Figure 2. (a) The schematic of calorimetric apparatus with (1) evaporator section (2) adsorber section (3) connecting valve and (4) thermocouple locations (black dots). The total height of the assembly is about 350 mm. (b) The photograph of 3 mm diameter silica gel bonded to aluminium

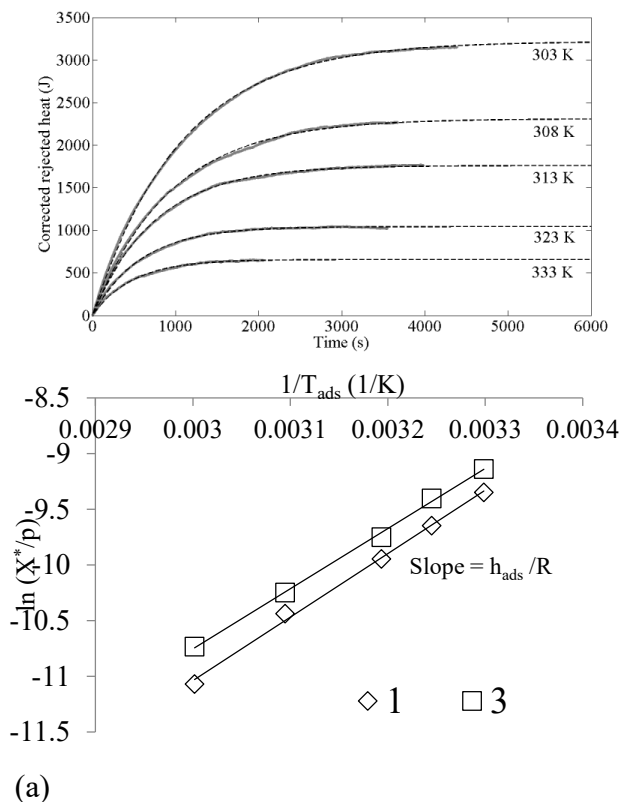


Figure 3. (a) Statistical fitting to net heat rejection versus time 3 mm diameter gel beads. Nominal sorbent temperatures are written on the graph. The water vapour is 3000 Pa. (Dashed line – curve fitting; solid line – experimental). (b) Arrhenius plot of adsorption rate for 1 and 3 mm diameter silica gel

4. MODEL OF ADSORPTION CHILLER FOR COLD CHAIN APPLICATION

The proposed adsorber of adsorption chiller is as shown in Figures 4(a) and 4(b), which is adopting a compact heat-exchanger design. Silica gel is bonded to the heat-exchanger surfaces. The hot and cold fluid is flowing through the heat exchange in the horizontal direction while the refrigerant (water) is flowing in the vertical direction. The separation between two plates (made of aluminium with a thickness of 1 mm) of the fluid channel is 2 mm. The separation on the adsorbent channel is 3 mm for 1 mm diameter silica gel and 7 mm for 3 mm diameter silica gel. It is estimated that 1 mm diameter silica gel has a surface density (mass of silica gel per unit area of heat transfer surface) of 0.62 kg/m^2 while the 3 mm diameter silica gel has a surface density of 1.84 kg/m^2 . Dimensions of the generator are determined by the cooling capacity of the adsorption chiller. It is worth to note the vertical and horizontal dimensions are much larger than the separation between plates in fluid channels.

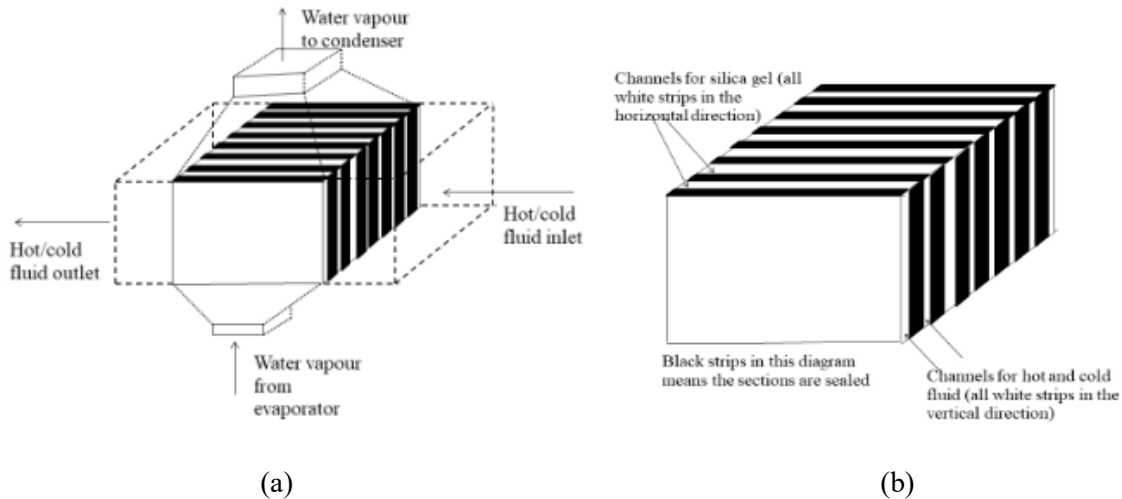


Figure 4. (a) The schematic of a proposed adsorber and (b) detail on the location of silica gel and fluid channels

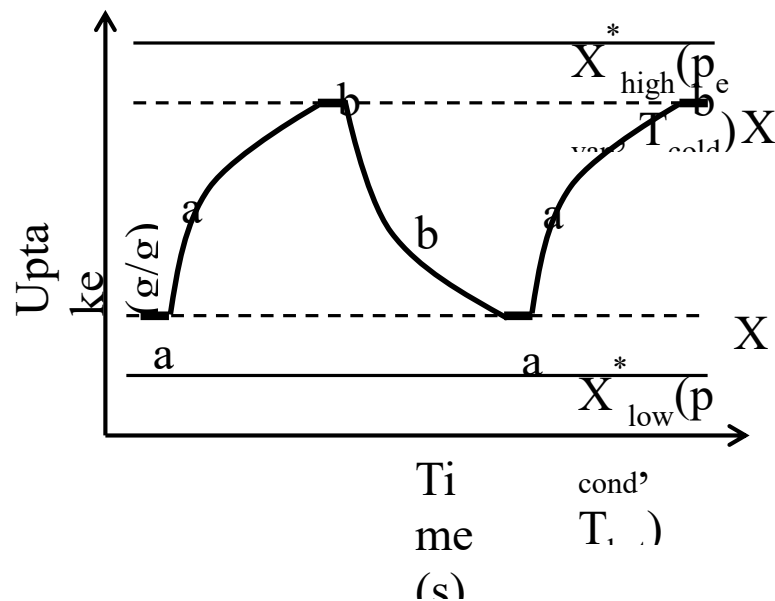


Figure 5: Idealized variation in uptake at cyclic steady-state

The physics of adsorption is complicated, but our calorimetric tests often reveal that the progress of adsorption against time can be fitted to a simple mathematical function. In each test, the adsorbent is exposed to a step-change in refrigerant concentration (or near to a step change). The plot of adsorptive capacity (uptake) versus time follows an exponential recovery

$$X(t) = X^*(p, T_{ads})(1 - \exp(-K_{ldf}t)) \quad 1$$

where $X(t)$ is the instantaneous adsorptive capacity (uptake), X^* is adsorptive capacity at equilibrium, t is the time since the adsorption started, K_{ldf} is the apparent Linear Driving Force constant, p is water vapour pressure and T_{ads} is adsorbent temperature.

The Coefficient of Performance (CoP) and Specific Cooling Power (SCP) could be estimated from the heat of adsorption. For the basic adsorption cycle presented in Figure 1, the average changes in water uptake of silica gel after many cycles and thus cyclic steady-state can be idealized as in Figure 5. The equilibrium adsorptive capacity is presented as the solid line (X_{high}^* and X_{low}^*), calculated from Henry's Law with the parameters obtained from the calorimeter in Section 3. In an adsorption chiller cycle, there is insufficient time for the adsorbent to reach this equilibrium capacity without a very low cooling power production. Thus the swing in water uptake is reduced to lines X_2 and X_1 in Figure 5.

The basic adsorption chiller modelled in this chapter can be briefly explained as follows:

- Stage a_1 (pre-cooling and depressurization) – The adsorber is cooled to an assumed mid-point temperature $\sim ((T_{hot} + T_{cold})/2)$ to reduce its pressure from the condenser to evaporator pressure. The assumption that this stage ends at the temperature $\sim ((T_{hot} + T_{cold})/2)$ is an approximation. This stage is isosteric, there is no net change in average loading (X).
- Stage a_2 (adsorption-evaporation) – Adsorbent adsorbs refrigerant from the evaporator and the adsorptive capacity increases to X_2 . The apparent K_{ldf} for the adsorbent is evaluated at the mid-point temperature $\sim ((T_{hot} + T_{cold})/2)$.
- Stage b_1 (pre-heating and pressurization) – The adsorber is heated to mid-point temperature to increase its pressure from the evaporator to condenser pressure. Again, this stage is isosteric.
- Stage b_2 (desorption-condensation) – Adsorbent desorbs refrigerant into the condenser and the water uptake is reduced to X_1 . The apparent K_{ldf} for the adsorbent is evaluated at the mid-point temperature.

Cycle time (t_{cycle}) is the summation of the times taken to complete these four stages.

The time to de-pressurize and pressurize the adsorber is assumed to be governed by heat transfer.

Thus, if the temperature is shifted from T_{hot} or T_{cold} to mid-point temperature using a heating fluid at temperature T_{hot} or coolant at temperature T_{cold}

$$t_{a1} \approx t_{b1} \approx \ln(2) \frac{m_{al}c_{p,al} + m_{sg}c_{p,sg}}{h_{film}A} \quad 2$$

where A is the area of heat transfer surface where silica gel is bonded, h_{film} is film heat transfer coefficient at the fluid-metal interface, m_{al} is the mass of aluminium, $c_{p,al}$ is the specific heat capacity of aluminium, m_{sg} is the mass of silica gel and $c_{p,sg}$ is the specific heat capacity of silica gel.

The heat rejection/addition during the isosteric stages (stage a_1 and b_1), follows from:

$$Q_{a1} = Q_{b1} = \frac{1}{2}(T_{hot} - T_{cold})(m_{al}c_{p,al} + m_{sg}c_{p,sg}) \quad 3$$

The time for stage a_2 (and b_2) is specified. The line X_1 and X_2 in Figure 5 can be found by solving two simultaneous equations (Equation 4 and 5)

$$X_2 = X_1 + (1 - \exp(-K_{ldf}t_{a2}))(X_{high}^* - X_1) \quad 4$$

$$X_1 = X_{low}^* + \exp(-K_{ldf}t_{b2})(X_2 - X_{low}^*) \quad 5$$

The water uptake at X_1 follows from

$$X_1 = \frac{X_{low}^* + \exp(-K_{ldf}\tau_{cycle})X_{high}^* + [\exp(-K_{ldf}\tau_{cycle})]^2 X_{high}^* - \exp(-K_{ldf}\tau_{cycle})X_{low}^*}{1 - [\exp(-K_{ldf}\tau_{cycle})]^2} \quad 6$$

where X_2 can be found by substituting the value of X_1 into equation 4 and the time (t_{a2} , t_{b2} , and τ_{cycle} which are equal) is the time allowed for processes a_2 and b_2 .

The heat input during desorption is in stages b_1 and b_2 . The total heat input during these processes is

$$Q_b = 2Q_{b1} + m_{sg}h_{ads}(X_2 - X_1) \quad 7$$

The heat transfer into the evaporator (Q_{ref}) can be approximated as

$$Q_{ref} = \left[m_{sg} \left(h_{fg}(\text{at } T = T_{evap}) + c_{p,water}(T_{evap} - T_{cond}) \right) \right] (X_2 - X_1) \quad 8$$

where h_{fg} is the latent heat of vaporization of water, $c_{p,water}$ is the specific heat of water, T_{evap} is evaporator temperature and T_{cond} is condenser temperature.

The Coefficient of Performance (CoP) and Specific Cooling Power (SCP) follow from

$$CoP = \frac{Q_{ref}}{Q_b} \quad 9$$

$$SCP = \frac{Q_{ref}}{m_{sg}t_{cycle}} \quad 10$$

The average film heat transfer coefficient at the waterside was taken as 2700 W/m²K., by assuming the hydraulic diameter is twice the plate separation, Nusselt number is equal to 8.23 (Incropera et. al (2007)) and the properties of air were taken at the average hot and cold air temperature.

In this model, the evaporator, condenser and cold fluid (T_{cold}) temperatures are 1 °C, 35°C and 35°C respectively. The heat source temperature (T_{hot}) was taken as 70 and 90 °C.

5. RESULTS AND DISCUSSIONS

Figures 6 and 7 presented the SCP and CoP of the proposed adsorption chiller at two different heat source temperatures for various cycle times. The highest SCP of 1 mm diameter silica gel is more than 2 times higher than the SCP for the 3 mm diameter silica gel. As expected, the highest CoP for the 3 mm diameter silica gel is almost 2 times higher than the CoP for the 1 mm diameter silica gel. For both silica gels, the maximum SCP occurs at a relatively short cycle time, while the maximum CoP occurs at a longer cycle time. Since this adsorption chiller is driven by the waste heat from the diesel engine, CoP is relatively less important than the SCP. It can be concluded that a 1 mm diameter silica gel is the most appropriate adsorbent in the cold chain application.

Another usefulness of Figures 6 and 7 is in the sizing of the adsorber. For instance, 1 kg of 1 mm diameter silica gel is required to produce 250 W cooling power if the heat source temperature is 90 °C. Alternatively, these graphs indicate the minimum mass of silica gel required to achieve the specified cooling power if all the operational temperatures are known. For example, maximum cooling power produced by the adsorption chiller drops drastically from 250 W/kg to 75 W/kg if the heat source temperature is reduced from 90 °C to 70 °C. Furthermore, the optimum cycle time also could be obtained from these graphs.

It is estimated that 0.245 kW of heat from diesel engines could be recovered by an adsorption chiller (that has 1 kg of 1 mm diameter silica gel if the conditions in Figure 6 are considered. Assuming the combustion inside the diesel engine produces 10 kW, 4 kW will be converted to useful mechanical work (assuming the efficiency of the engine is 40%). If 1 kW (this value was calculated using equation 9 and data were taken from Figure 6) of the heat rejected to the environment is recovered by the adsorption chiller, the overall efficiency of the heat engine and adsorption chiller is 50%. This can be considered as a reasonable improvement.

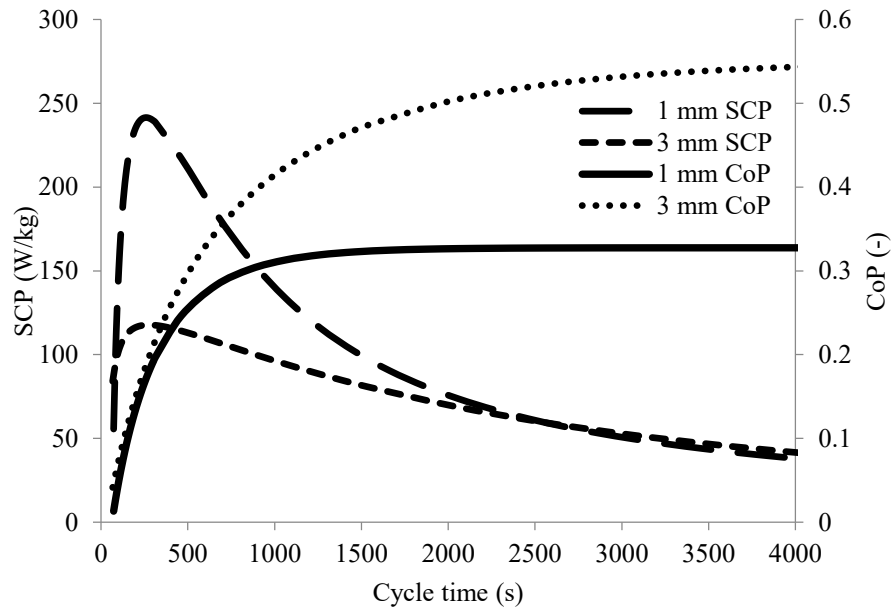


Figure 6. SCP and CoP at various cycle times for the heat source temperature at 90 °C

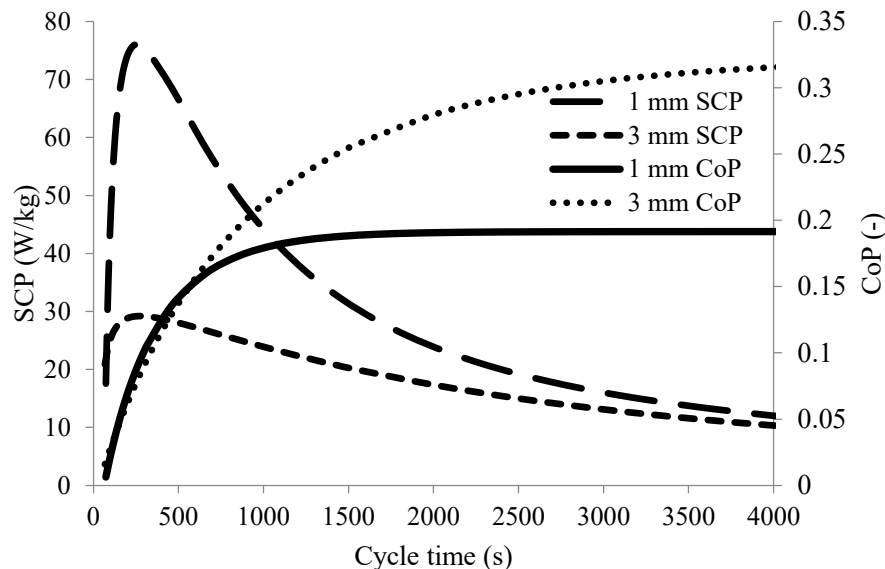


Figure 7. SCP and CoP at various cycle times for the heat source temperature at 70 °C

Several issues should be solved before the adsorption chiller can be employed in the cold chain transportation system. Thermal storage is required to ensure the chiller could be operated when the diesel engine is not running. Alternatively, a small vapour compression cooling system could be used

as a backup in the cooling system. To enhance the cooling power produced by this chiller, at least two adsorbers are required to avoid the intermittent operation of the adsorption chiller. These two issues could be resolved by developing a transient model of adsorption chiller and simulate the likely conditions of the cold chain operation. Another issue is the low heat transfer coefficient if the air is used as the hot and cold fluid. It is estimated that for the current heat-exchanger, the heat transfer coefficient for the airside is about $120 \text{ W/m}^2\text{K}$, which is about 22 times smaller compared to the heat transfer coefficient if the water is used as the heat transfer fluid. The addition of fins at the airside could increase the heat transfer coefficient; this could be investigated in the future. A study on the effect of fluctuations in the hot and cold fluid temperatures on the cooling power is also a possible future work.

6. CONCLUSIONS

It is possible to employ a silica gel-water adsorption chiller in cold chain applications. Based on our work, 1 mm diameter silica gel are suitable for this application since it has a higher Specific Cooling Power compared to the 3 mm diameter silica gel. The graphs presented in this paper provide essential information on the sizing of the heat-exchanger, the effect of heat source temperature on the performance of the adsorption chiller and the optimum cycle time for the chiller operation. Future works including the transient modelling of adsorption chiller performance under various conditions in cold chain applications. The simulation may include the variation in cooling load due to different operational conditions. Detailed design of adsorber is required before the development of the adsorption chiller prototype. It is worth building a prototype of an adsorption chiller and carry out field tests to ensure the adsorption chiller could fulfil the requirement in cold chain application.

REFERENCE

1. Ahamat, M. A. and M. J. Tierney (2011). "Time-wise temperature control with heat metering using a thermoelectric module." *Applied Thermal Engineering* 31: 1421-1426.
2. Ahamat, M. A. and M. J. Tierney (2012). "Calorimetric assessment of adsorbents bond to metal surfaces: Application to silica gel bonded to aluminium." *Applied Thermal Engineering* 40: 258-266.
3. Incropera et al. (2007). *Fundamentals of Heat and Mass Transfer*. The United States of America, John Wiley & Sons.
4. Jakob, U. (2010). *Performance analysis of small-scale sorption chillers*. Innovative Materials for Processes in Energy Systems 2010. Singapore: 238 -244.
5. James, S. J. & C. James (2010). "The food cold chain and climate change." *Food Research International* 43: 1944-1956.
6. Wang et al. (2002). "Experimental investigations on adsorption air-conditioner used in internal-combustion locomotive driver-cabin." *Applied Thermal Engineering* 22: 1153-1162.
7. Saha et al. (2003). "Performance evaluation of a low-temperature waste heat driven multi-bed adsorption chiller." *International Journal of Multiphase Flow* 29: 1249-1263.
8. Tamainot-Telto et al. (2009). "Novel compact sorption generators for car air conditioning." *International Journal of Refrigeration* 32: 727-733.
9. Wang, et al. (2004). "Compound adsorbent for the adsorption ice maker on fishing boats." *International Journal of Refrigeration* 27: 401-408.

SIMULATION AND EXPERIMENTAL STUDY OF COOLING A SMALL DOMESTIC REFRIGERATOR USING SOLAR-ASSISTED ENERGY IN BANGI, MALAYSIA

Z. Jusoh, N. Ibrahim, Z. Abdullah and Z. M. Enggsa

HVAC&R Section,

Universiti Kuala Lumpur Malaysia France Institute, Section 14, Jalan Teras Jernang,

43650 Bandar Baru Bangi, Selangor Darul Ehsan, Malaysia.

Corresponding Author's Email: zakariajusoh@unikl.edu.my

Article History: Received xxxxx; Revised xxxx; Accepted xxxx

ABSTRACT: A simulation study was carried out in Bangi, Malaysia for cooling a small domestic refrigeration system using solar-assisted energy. In a tropical climate condition, the outdoor ambient temperature can reach up to 308 K (35 °C), a reduction of energy consumption will contribute to the heat load of a refrigeration system. Photovoltaic (PV) panels convert solar energy into electrical energy to run a small domestic refrigeration system. A simulation study using SOLARGIS software calculated the power that the PV can convert. The simulation result in annual average electricity production is 407.3 kWh. A flat plate PV that converts 360 W (from specification) are being used for this simulation study. The objectives of the study are to make use of solar radiation and energy saving. It is found that the energy supply by the solar radiation from the PV successfully operates the small refrigerator to the desired cooling of 5 °C.

KEYWORDS: *Solar energy, Flat plate PV, small domestic refrigeration system, solar radiation, energy saving*

1.0 INTRODUCTION

Solar energy is one of the renewable energy sources and it is one of the sources that start get the community's attention. Awareness to preserve the environment and lack of energy concerns cause an effort to find alternative energy. However, for centuries solar energy is used only to dry clothes and agricultural products such as coffee beans, paddy, cocoa, black pepper, tobacco, tea leaves, anchovies, and others (Othman, 2002, Shamsuddin, 2012). Nevertheless, the use of it is susceptible to environmental pollution. There are now four technologies of solar energy, that is, air heating for the drying process, water heating, light through radiation and conversion of solar energy to electricity -photovoltaic system (Othman, 2002). However, solar energy had been used for the production of electrical power using solar Photovoltaic started in the 1990s (Shamsuddin, A. H. 2012). Solar energy is especially divided into two technologies which are solar thermal technology and solar photovoltaic technology. Solar thermal technology is to shift solar energy into thermal energy per solar thermal collector. Meanwhile, solar photovoltaic technology assumes a form of solar energy into electricity.

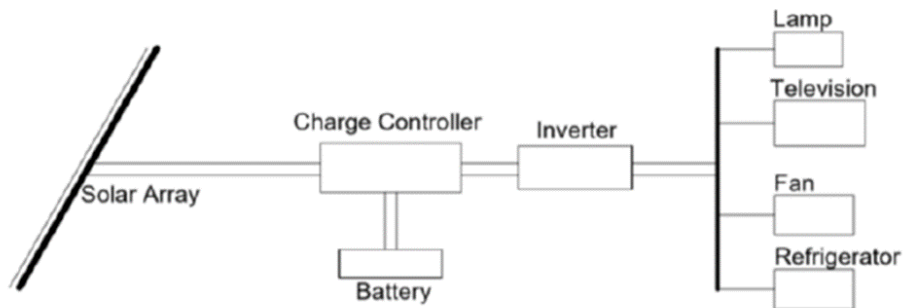


Figure 1: Photovoltaic system for residential use. (Othman, 2002)

According to Figure 2 below, which shows the forecast of Malaysia's energy source, Pusat Tenaga Malaysia has predicted that Malaysia would turn into a net importer of energy within the year 2010 and 2015. From the above graph details, need to find ways to better utilize renewable energy in Malaysia. Once again, overcoming these matters can be done by applying solar energy as a renewable energy source.

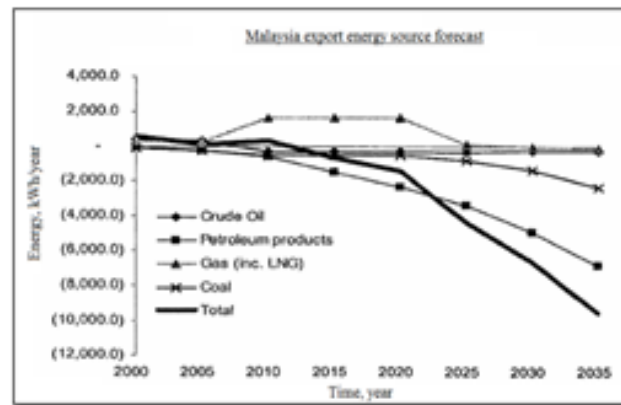


Figure 2: Malaysia export energy source forecast in the year 2000-2035 (Wahab, 2011)

The benefit of renewable energy sources such as solar is the sustainable energy that is pure, smooth and silent. The general awareness of the benefits that will be gained from the application of renewable energy is increasing. In 2016, the demand for energy increase by around 5.2 % in Malaysia (Energy Commission Malaysia 2016). Solar energy is one of the energy resources that are not harmful to the environment. Since the beginning of time, Humanity has tried to find ways to exploit solar energy as the sun can radiate extra energy in one second.

In general, solar energy is labelled as alternative energy to fossil fuel energy sources such as coal and oil (Wahab, A. K. 2011). At the present, solar energy is a good resource for renewable energy solutions. The straightforward employment of solar radiation gives high advantages to many parties in creating a relevant application.

The analysis and simulation result shows that the COP of the refrigeration cycle for the selected days is around 2.25 when the compressor runs at low speed, and the COP drops to its lowest value of 1.85 when the compressor operates at the highest speed. Furthermore, the simulation results indicated that an estimated radiation intensity of 315W/m² is

required to be received on the tilted panel to run the considered compressor at its minimum rotational speed of 1800rpm. To drive the compressor at its maximum rotational speed (4200rpm), an estimated radiation intensity of 700W/m² is required to fall on the PV panel. Finally, the proposed method can be used to estimate the performance of a directly coupled solar PV refrigeration system with a variable speed compressor under specific weather conditions (Elias M. Salilih, et al, 2019).

Zhang X, et al, 2013 studied a new system of solar air conditioning that when the solar radiation intensity is high (0.8kW/m²), the cooling capacity of the new system is 1.7 times the original system under the given conditions. When the solar radiation intensity is low (0.2kW/m²), the cooling capacity of the new system is decreased by 70% compared to high radiation intensity conditions, and the original system could not provide refrigeration. Zhang studied the solar air conditioning system with a heat pump.

A prototype refrigeration system that uses solar energy as a heat source to drive an adsorption refrigeration cycle, intended for food preservation in rural, off-grid locales, was discussed. This system is designed to be relatively compact and use low cost, easily available materials and construction methods while allowing solar-powered adsorption refrigeration cycles to be studied. On completion of a final design, considerable cost savings could be made by replacing these fittings with cheaper alternatives and making direct tube-tube connections where possible (Ahamat, M.A., et. Al, 2012).

2.0 METHODOLOGY

This paper study the result of a solar radiated electrical power in Bandar Baru Bangi by collecting a series of solar radiation data to find the average solar radiation. Refer to the proposed location, it is found that the average solar radiation is at about 1400 W/m² and is capable to operate an electric refrigeration system as a test unit. Figure 8 shows photographs of the example of solar collectors that can be used. The flow chart in Figure 9 shows the work process. The work started with processing input data, manual collection of field data, construct a factual decision and processing the output data. Figure 5 shows the average solar radiation data collected in Bandar Baru Bangi from SOLARGIS.

In the experiment, the weather data were taken out of the site for a few days. For simulation, SOLARGIS was used to get annual power production as shown in Figure 5. Mathematical modelling was used for the basic refrigeration cycle as discussed in the result and discussion.

For the application of our project, a load is an absorption unit, a refrigerator that consumed 65 Whrs. The aims are to run the refrigerator using the solar photovoltaic (PV) which harvest the solar radiation for an estimation of 4 hours' full solar radiation. Below are the equipment specifications to run the system.

2.1 Refrigerator

The load is a small refrigerator model XC-40 that requires 65W of power to produce an operating condition of 0°C to 8°C for a 40-litre capacity. The cooling uses the absorption method so that the compressor which consumed high power is replaced by a heater element to create differential pressure in the refrigeration cycle. For an eight hours cooling application, the refrigerator needs to consume about 520W of power. The specification is as below,

Table 1: Refrigerator specification

No	Parameter	Specification
1	Model	XC-40
2	Capacity	40L
3	Temperature	0°C to 8°C
4	Cooling model	Absorption
5	Body Material	Iron Coated
6	Product Size	440 mm x 400mm 550mm
7	Net Weight	16.5Kg
8	Power	65 Watt
9	Power Consumption	0.9 Kw.h/24h
10	Voltage/Frequency	220v-240v/50Hz

2.2 Solar Panel

The solar panel (PV) is a poly plate panel 156 x 156 cells. 4 panels carry 90W of each plate, which produce 360W (90W x 4 panels). With regards to the angle of latitude which is about 3°, the solar panel can harvest full radiation for about 4 hours in Malaysia condition and should produce 360W x 4 = 1440 Whrs from the solar panels.

Table 2: Solar panel specification

No	Parameter	Specification
1	Model	BSM90P-36
2	Solar cell Type	Poly 156 x 156 Cell
3	Pm	90 Watt
4	Vmp	17.5 Volt
5	1 mp	5.15 Amp
6	Voc	21.6 Volt
7	1sc	5.18 Amp
8	Maximum Sytem Voltage	1000 Volt
9	Size	1000 mm x 670 mm x 30 mm
10	Weight	75 Kg
11	Operating Testing	-40 to +85°C

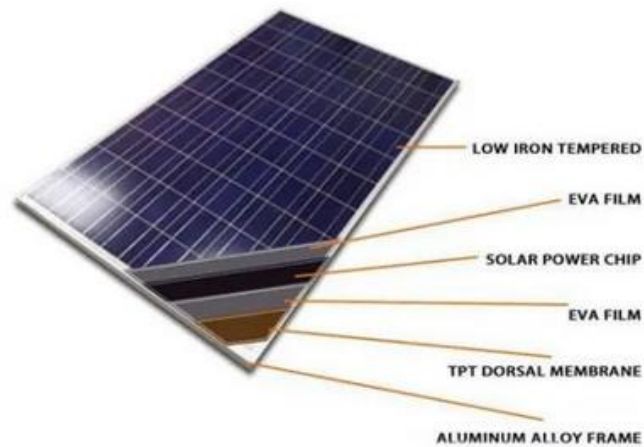


Figure 3: Poly-Crystalline Silicon Solar Panel

2.3 Current Inverter

The power needed for the refrigerator load is 65W, a 300W inverter will be sufficient.



Figure 4: Pure Sine Wave Inverter, Off Grid Inverter 300W DC24 to AC220V Converter Surge Power 600W Solar Power Inverter

2.4 Power Storage Battery

A Sealed Lead Acid type battery is selected for current storage. A 12V 110AH Solar Deep Cycle Rechargeable battery is capable to store 1320 Whrs power (12V x 110A). As the solar panel generates 1440 Whrs power, two 12V batteries connected in series are required to store the available current.



Figure 5: Battery Box Battery up to 110 Ah, Charge Controller

2.5 Solar Charge Controller

The solar charge controller selection depends on the battery and the capacity of the solar panels. The solar panels will absorb about 360 W of solar power, but approximately 80% of that will be captured by the solar charge controller. So only about 288W (360 x 0.8) will be charged to the controller. A single battery carries a 12V voltage, so we need 2 batteries that produce 24V (288W/12V).



Figure 6: High-Quality MPPT solar charge controller 12V/24V/48V automatic recognition 10A 20A 30A 40A

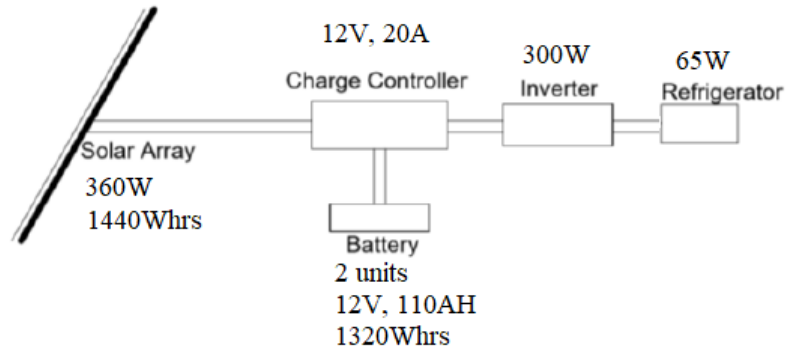


Figure 7: Photovoltaic system for chiller refrigerator runs from 0°C to 8°C.



Figure 8: Photographs of the solar-assisted cooling study

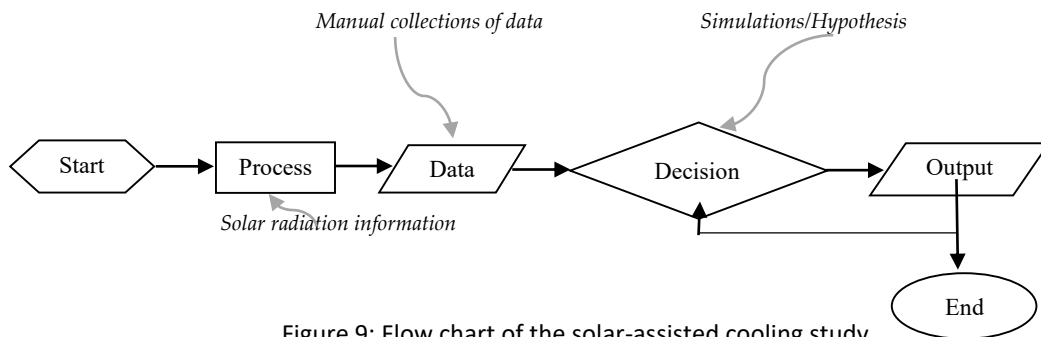


Figure 9: Flow chart of the solar-assisted cooling study

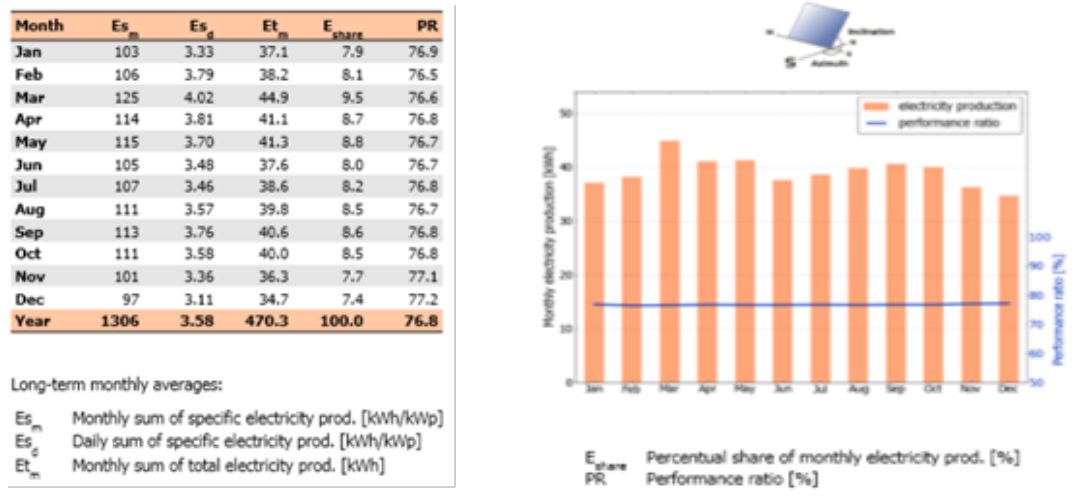


Figure 10: Monthly sum of specific production in Bandar Baru Bangi and the percentage share of monthly electricity production

The formula used to calculate the power is

$$P = IV \quad (1)$$

Where, P = power in kW, I = current in amps, V = voltage in Volt.

3.0 RESULT AND DISCUSSION

With the PV system installed power of 0.36 kW at Bandar Baru Bangi, it is found by the simulation taken from SOLARGIS, the annual average electricity production is 470.3 kWh.

Table 3. Solar energy power calculation

PV system	Specification
Installed power	0.36 kWp
Type of modules	Crystalline silicon (c-Si)
Mounting system	Fixed mounting, free-standing
Azimuth/inclination	180° south / 2°
Inverter Euro eff.	97.5%
DC / AC losses	5.5% / 1.5%
Availability	99.0%
Annual average electricity production	470.3 kWh
Average performance ratio	76.8%

In Table 3, the annual average electricity production was obtained from SOLARGIS software. This figure is sufficient to power the refrigerator, which requires only 0.36 kW or 360 W.

3.1 Refrigeration Process

Hypotheses of the vapour refrigeration cycle are carried out using Coolpack software as shown in Figures 6 and 7. The system is a direct expansion using refrigerant R134a with evaporating temperature $T_e = 5^\circ\text{C}$, condensing temperature $T_c = 40^\circ\text{C}$, 10 K subcooling and 5 K superheat.

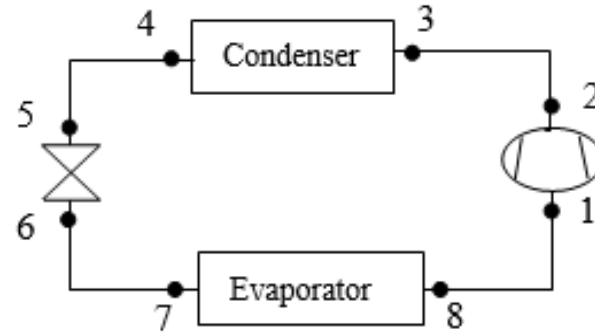


Figure 11: The schematic drawing of the refrigeration installation

Figure 11 shown the refrigeration cycle process where refrigerant R134a is used. Point 1 is suction before the refrigerant enters the compressor. It is in the form of gas. Point 2 is a gas compression process, leaving the compressor. Points 4 and 5 are in liquid form at high pressure and high temperature. After passing through the expansion valve from point 5 to point 6, the pressure was reduced and the gas was in a liquid and vapour state. Lastly, point 7 is the liquid and vapour state at low pressure and low temperature. Figure 12 is the Mollier chart showing the process at subcool and superheat processes.

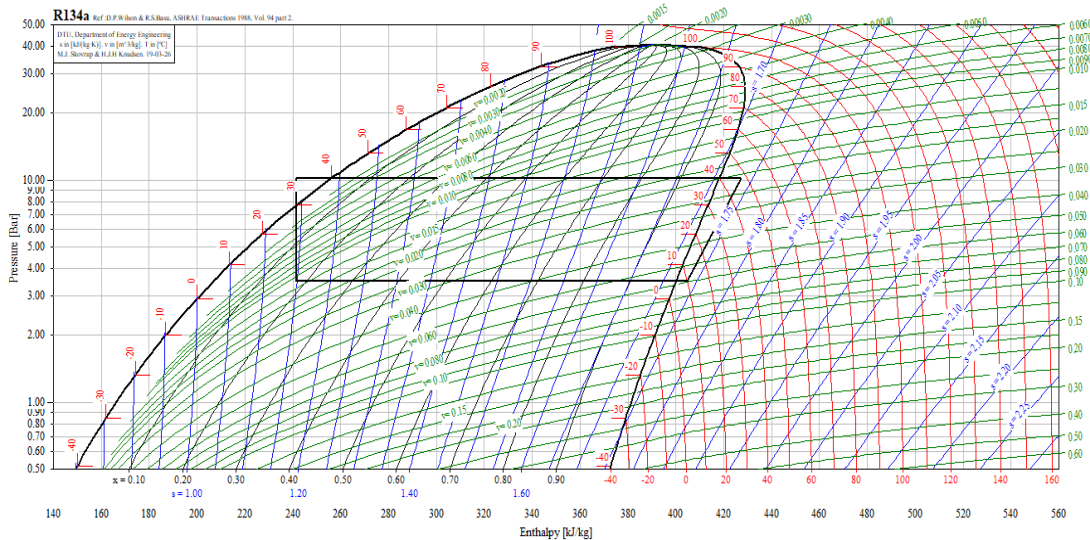


Figure 12: The thermodynamic curve of the refrigeration cycle. (CoolPack)

Table 2: The thermodynamic cycle of the R134a refrigerator

Point	T	P	v	h	s
	°C	bar	m ³ /kg	kJ/kg	kJ/kg.K
1	9.999	3.496	0.059596	404.785	1.7361
2	47.921	10.164	0.020989	427.428	1.7361
3	47.921	10.164	0.020989	427.428	1.7361
5	30.000	10.164		241.463	
7		3.496		241.463	
8	10.000	3.496	0.059592	404.785	1.7361

3.2 Mathematical modelling

The cooling capacity is defined as,

$$Q = \dot{m} \Delta h$$

Where,

Q is cooling capacity measured in kW or kJ/s

\dot{m} is the mass flow rate measured in kg/s

Δh is the enthalpy difference between point 1 and point 2

Therefore,

$$\dot{m} = Q/\Delta h$$

$$\dot{m} = 0.050 \text{ kJ/s} / (427.428 - 404.785) \text{ kJ/kg [compression process]}$$

$$= 0.050 \text{ kJ/s} / 22.643 \text{ kJ/kg}$$

$$= 0.002208 \text{ kg/s}$$

For real capacity, $Q = \dot{m} \Delta h$ [Evaporator capacity]

$$= 0.002208 \text{ kg/s} (404.785 - 241.463) \text{ kJ/kg}$$

$$= 0.36061498 \text{ kJ/s (kW)}$$

$$= 360.61 \text{ W.}$$

4.0 CONCLUSION

The calculations show that the solar power from the plate collectors could produce 470.3 kWh annually, assisting the 0.9 kW/day power consumption of a small domestic refrigerator. The refrigerator requires 324 kWh annually.

ACKNOWLEDGEMENT

I would like to thank all the management of Universiti Kuala Lumpur, Malaysia France Institute for their facilities and equipment contributions.

REFERENCES

- [1] Energy Commission of Malaysia. (2016).
- [2] M. Y. Othman, *Teknologi Tenaga Suria*. Universiti Kebangsaan Malaysia (UKM). Bangi, 2002
- [3] Shamsuddin, A. H, “Development of renewable energy in Malaysia strategic initiatives for carbon reduction in the power generation sector” *Procedia Engineering*, 384 – 391, 2012
- [4] A. K. Wahab, *Application of Solar Energy.*, Universiti of Malaya, Kuala Lumpur 2011
- [5] Elias M. Salilih, Yilma T. Birhane, “Modelling and performance analysis of directly coupled vapour compression solar refrigeration system” *Solar Energy*, 228 – 238, 2019
- [6] Zhang Xingjuan, SongBojie, Bai Qingyuan, Yang Chunxin, “Performance analysis on a new type of solar air conditioning system” *Energy and Buildings*, 280 – 285, 2013
- [7] Laurence Ketteringham, Michael Tierney, Asmidzam Ahamat, Hind Saidani-Scott, Rebecca Selwyn, “Design and construction of a low-cost solar chiller, with a calorimetric assessment of the adsorbent bed” *World Renewable Energy Forum & Exhibition, WREF 2012, Denver, USA*

Passive Cooling Method of Energy Reduction Using Fins-Type Heat-pipes Heat-exchanger

Z. Abdullah^{1,2}, B. Phuoc Huynh¹

¹Faculty of Engineering & IT
University of Technology Sydney, NSW 2007, Australia

²HVAC&R Department
Universiti Kuala Lumpur, Malaysia France Institute, 43650 Selangor, Malaysia

Abstract

The increase in the operating cost and the risk of environmental pollution has turned the technology of heating and cooling, from an active to a passive approach to energy consumption. Current refrigeration technology with vapour compression cycles, rely on electricity to build up pressure and refrigerant phase-change within its cycles to create temperature differences in the heat-exchanger coil. A passive cooling method using a heat-pipes heat-exchanger is being tested by attaching it to a fresh air inlet, in assisting with a cooling process mechanism. The supply air is being pre-cooled to help to reduce the incoming air temperature, therefore, lower the room's evaporator operating condition. The study aims are to simulate and investigate experimentally, air temperature reduction ability of an R134a heat-pipes heat-exchanger. The effort comes from a gravity-assisted heat-pipes heat-exchanger ability as a pre-cooled component that does not need electricity or other energy sources to work. The heat-pipes heat-exchanger is a row of 3 by 3 tubes, 9 mm ID straight copper tube with inner grooves structured, length of 500 mm fitted with square type aluminium fins. Each of the copper tubes is quarterly filled with liquid R134a as a refrigerant medium. An acrylic box in the size of 1000 mm x 820 mm x 620 mm, modelled as a room has been used to collect air diffusion and temperature distributions. The location of the heat-pipes heat-exchanger had been set at the top and the sidewall of the acrylic box to measure the most suitable air intake flow. A computational fluid dynamic software CFD-ACE and ANSYS-Fluent are being used to run simulations of the experiment. In the experiments, it is found that the heat-pipes heat-exchanger has the capability of pre-cooling a room fresh air up to 9 K different. The cooling energy consumption had been calculated to save up between 90 W/m³ to 273 W/m³ or about 25% to 33% to the box volume. It is an advantage to use a heat-pipes heat-exchanger to decrease energy consumption by reducing the temperature between the warm ambient intake air and the supply air to a room.

Keywords: *computational fluid dynamics, heat-pipes heat-exchanger, passive cooling*

Introduction

This experiment works on a pre-cooling of air intake to a room, to reduce the warm outside air temperature. By decreasing the air inlet temperature to the room, the work done on the evaporator cooling capacity will increase. The simulation process of the effectiveness of the heat-pipes heat-exchanger and the temperature drops that the heat-pipes could have achieved at the end of the processes is experimentally tested. The author proposed a method of pre-cooling of air intake of a room using a straight heat-pipes heat-exchanger to reduce the heat entering a room. Researchers [1], [2], [3] and [4] have proposed a passive cooling system technology using methanol as a cooling medium and mostly proposed in a heat recovery system application [5], [6], [7]. An R134a heat-pipes heat-exchanger works passively with natural or driven air circulation without any other energy input needed. As suggested by [8], the heat-pipes inclination position should be at least 6° concerning the horizontal; this experiment set-up had taken a position of 10° inclination for the refrigerant gravitational-return purpose.

Problem Description: R134a Heat-pipes Heat-Exchanger

The R134a refrigerant as a safe, zero global warming potential (GWP) index is used in the tubes to absorb and desorb heat. To increase the heat transfer capacity of the system, a grooves internal structure of the copper tube is being used, replacing the standards smooth internal surface of the tube. Table 1 shows the computational fluid dynamics simulations result, that had been established rigorously to verify the proposed refrigerant for the system.

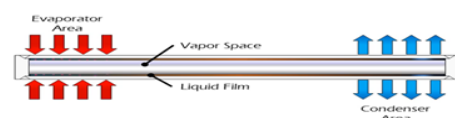


Figure 1. The working principle of heat-pipes heat-exchanger.

Methodology

The experiments study on the heat sink of a heat-pipes heat-exchanger evaporator section ability that absorbed heat from the surrounding air. As the liquid evaporates, and by the tube void factor, the vapour pressurizes and transfers the heat to the condenser section.

Parameters	Water	Acetone	R134a
Density kg/m ³	998.2	791	1207.3
Spec. Heat J/kg.K	4182	2160	1424.41
Thermal Cond. W/m. K	0.6	0.18	0.08119
Viscos kg/m-s	1.003x10 ⁻³	3.31x10 ⁻⁴	1.9525x10 ⁻⁴
Inlet Temp, K	293	293	293
Outlet Temp, K	295	296	298
Diff In-Out Temp, K	2	3	5

Table 1. The properties of the heat-pipes cooling medium and the temperature outlet achieved when running with ANSYS Fluent computational fluid dynamics simulations.

Figure 1 shows the working principle of a heat-pipes, Figures 2 and 3 show the simulation works. The set-up of the experiment is shown in Figure 4 and Figure 5 shows the experimental acrylic model arrangement for the air inlet and outlet openings. Thermocouples are placed in several locations within the box and read by a data logger to show the distribution of air temperature. As suggested by [4], the author used the hot ambient temperature in the range of 303K to 318K for the inlet temperature. A heat-pipes heat-exchanger is installed on the façade of the box before the supply air enters the acrylic box. The measured result is divided into three processes with each process to apply a lower and high supply temperature:

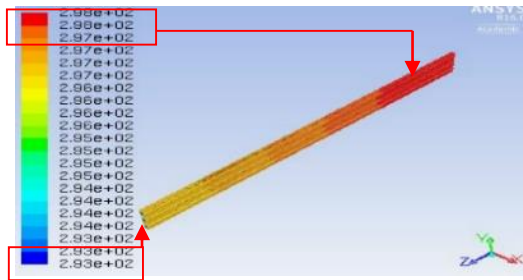


Figure 2: Simulation of heat pipe heat-exchanger for R134a by ANSYS-Fluent.

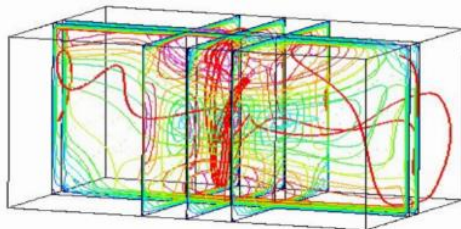


Figure 3: Simulation of air distribution by CFD-ACE.

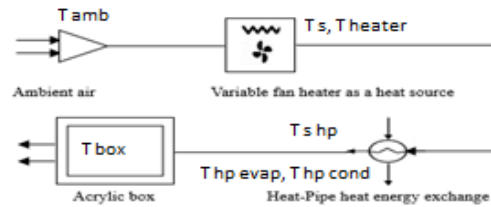


Figure 4: The workflow of the experimental project.

Case	Flow	Specification
Case 1		Incoming air at 303K and 318K flows on the surface of a heat-pipes heat-exchanger from the side and exits on the sidewall.
Case 2		Air at 303K and 318K flows on the surface of a heat-pipes heat-exchanger from the top and exits on the top side.
Case 3		Air at 303K and 318K flows on the surface of a heat-pipes heat-exchanger from the top and exits at the side of the box.

Figure 5: Models of acrylic boxes specification where fresh air intake locations and openings that best suits the domain.

Result and Discussion

The purpose of this study is to simulate and experimentally discuss a flow of ambient air through a heat-pipes heat-exchanger, for the reason of investigating the possibilities of reducing the high air temperature supply from outside, to a room using heat-pipes heat-exchanger as passive cooling equipment. Copper tubes with grooves inner structure were being used instead of a smooth structure heat-pipes heat-exchanger from earlier work, to show the enhanced capabilities of grooves heat-pipes in reducing the air temperature to a room. Different temperature between the inlet ambient supply air and the condenser section temperature of the heat-pipes is taken as the capability of the heat-pipes to transfer heat. The supply inlet air from the ambient is heated to a required temperature and in the process, the condenser section released the heat back to the ambient. Tables 2,3 and 4 show the results.

Case 1

Parameters	Case 1	
Supply Air Temp, K	303	318
Heat-pipes Evaporator Section Temp K	301	332
Heat-pipes Condenser Section Temp K	295	311
Average Box Temp K	293	302
Different Temp of Heat-pipes Evaporator and Condenser Section, K	6	21

Different Supply Air Temp and Heat-pipes Condenser Section Temp K	8	7
---	---	---

Table 2. The parameters for Case 1.

Case 2

Parameters	Case 2	
	303	318
Supply Air Temp, K	303	318
Heat-pipes Evaporator Section Temp K	299	331
Heat-pipes Condenser Section Temp K	296	310
Average Box Temp K	294	301
Different Temp of Heat-pipes Evaporator and Condenser Section, K	3	21
Different Supply Air Temp and Heat-pipes Condenser Section Temp K	7	8

Table 3. The parameters for Case 2.

Case 3

Parameters	Case 3	
	303	318
Supply Air Temp, K	303	318
Heat-pipes Evaporator Section Temp K	297	333
Heat-pipes Condenser Section Temp K	294	311
Average Box Temp K	294	301
Different Temp of Heat-pipes Evaporator and Condenser Section, K	3	22
Different Supply Air Temp and Heat-pipes Condenser Section Temp K	9	7

Table 4. The parameters for Case 3.

Estimated Energy Saving by the Heat-pipes Heat-exchanger

ASHRAE 55 specifies that a design temperature of 295.8 K (22.8°C) to 298 K (25°C) is a comfortable indoor temperature for domestic air conditioning systems. Taken average temperature of 297 K (24°C) as a design indoor temperature and 30°C outdoor temperature for domestic air conditioning systems, the sensible cooling load for the box can be calculated as Wan [9],

$$Q = 1.213 \times qv \times (t_r - t_o) \tag{1}$$

where Q is the estimated sensible cooling load at standard sea level kW, 1.213 kJ/m³. K (1.025 kJ/kg. K / 0.845 m³/kg), qv is the airflow rate m³/s and (t_r - t_o) is the delta temperature of the box and the supply air. The face area is taken as 0.0325 m².

The rate of energy saving can be calculated by,

$$\alpha = \frac{Q_o' - Q_o}{Q_o'} \tag{2}$$

Where α is the rate of energy saving by the heat-pipes %, Q_o is the sensible load at constant indoor, (that is 0.280kW) and

Q_o' is the calculated sensible load with heat-pipes heat-exchanger.

Parameters	Case 1		Case 2		Case 3	
	303	318	303	318	303	318
SA-HP _{cond} , K	8	7	7	8	9	7
Q _o ', kW	0.373	0.327	0.327	0.373	0.420	0.327
Energy saving Q _o '-Q _o , kW	0.93	0.47	0.47	0.93	0.140	0.47
α, % x 100	0.25	0.14	0.17	0.33	0.33	0.14

Table 5. The energy-saving comparison for all cases.

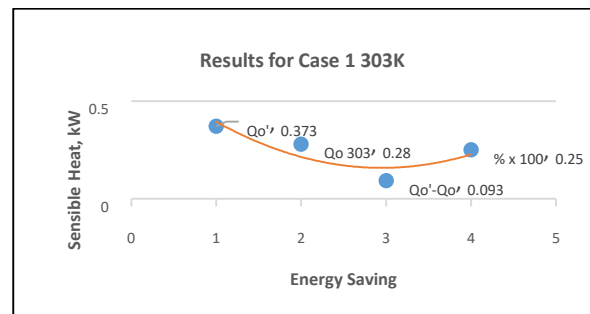
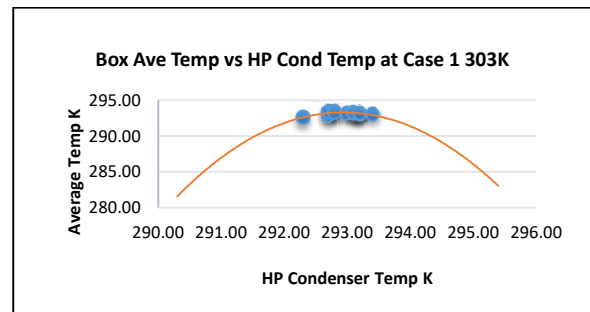
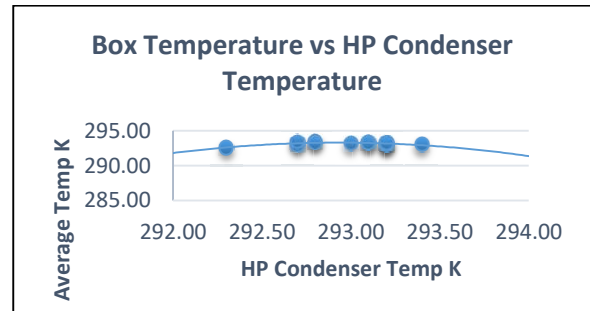
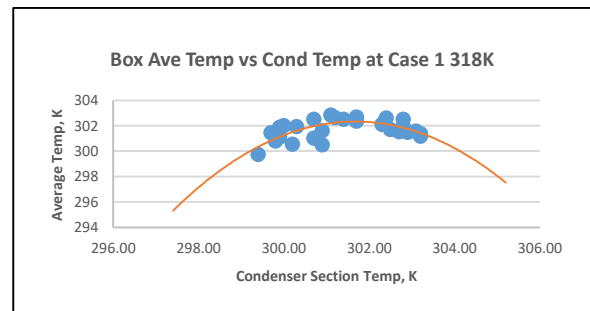


Figure 4: Energy saving at 303K for Case 1.



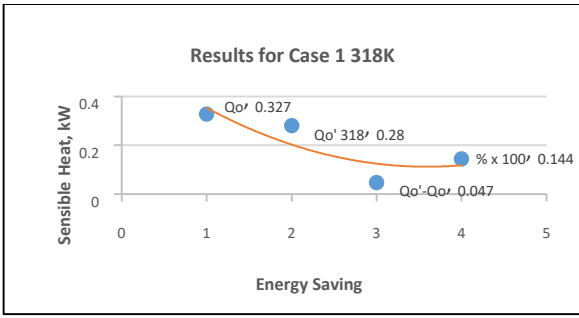


Figure 5: Energy saving at 318K for Case 1.

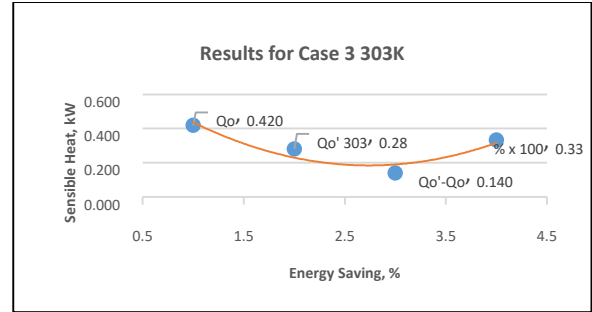
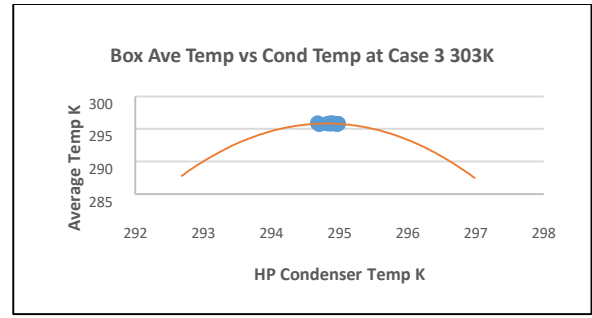


Figure 8: Energy saving at 303K for Case 3.

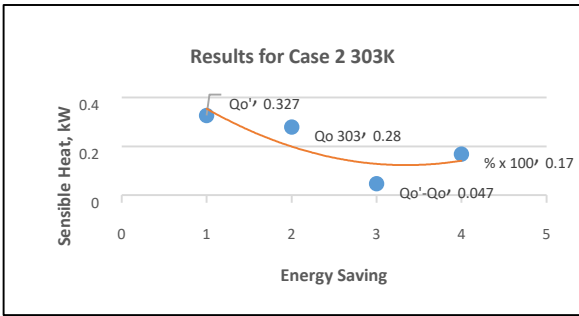


Figure 6: Energy saving at 303K for Case 2.

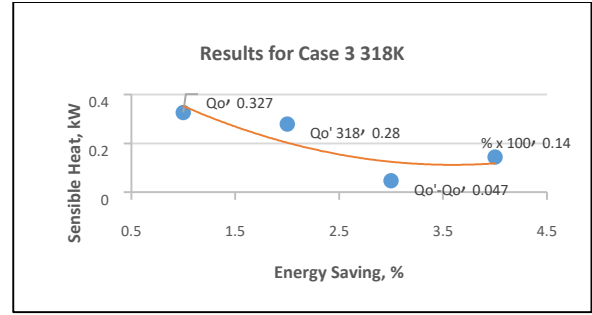
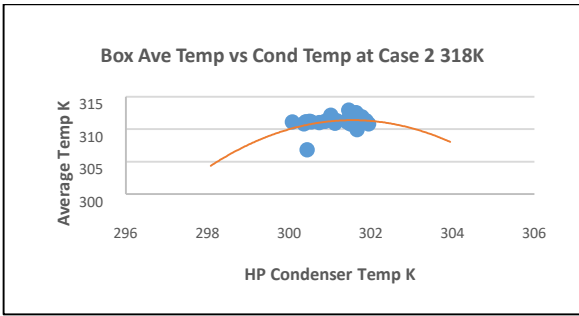
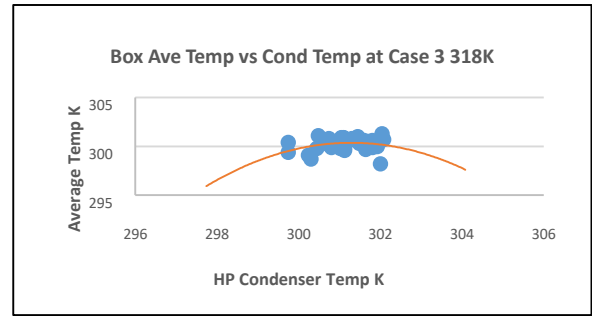


Figure 9: Energy saving at 318K for Case 3.

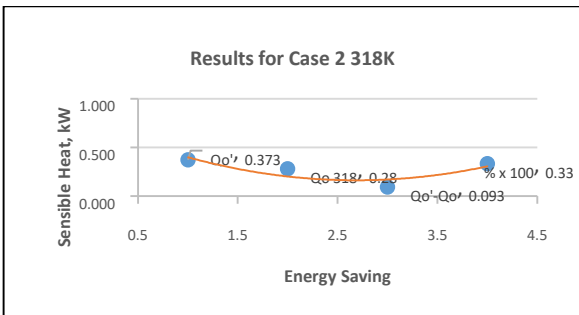


Figure 7: Energy saving at 318K for Case 2.

Conclusions

Simulations and experimental studies on energy savings of a heat-pipes heat-exchanger ability are presented in this paper. The temperature condition is set to 303K and 318K. Simulations using CFD-ACE and ANSYS-Fluent show that the heat-pipes heat-exchanger develops a heat transfer capability of 3 to 5 K differential temperature from end-to-end and achieved a 9K difference of air inlet-outlet. The results found that the designed fins-type heat-pipes heat-exchanger is capable to lower the heat to 293K and with an optimum application could save up to 33% energy consumption. Figure 10 shows that between 327W and 420W of sensible heat gain had been determined and an energy-saving between 93W to 140W was achieved from the studies. Passively cooling, for equipment that did not require any energy sources, the heat-

pipes heat-exchanger could perform an influential role for energy-saving applications. Outdoor high ambient temperature appliances where cooling maintenance is limited are the best suit for this application.

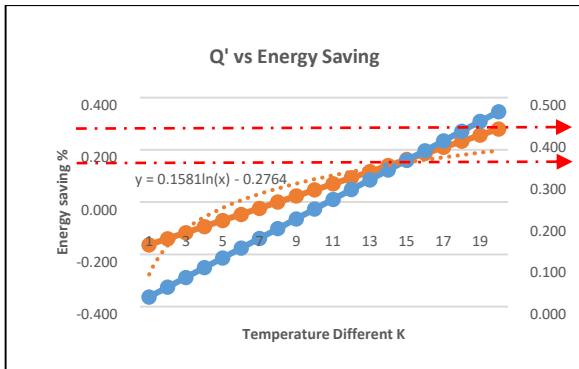


Figure 10: The sensible gain is between 327W to 420W and the energy saving is about 33%.

References

- [1] B. Kvisgaard, P.F. Collet, J. Kure. Research On Fresh-Air Change Rate: 1 Occupants' Influence On Air-Change. *Commission Of The European Communities*, 1985.
- [2] R.R. Riehl, T.C.P.A. Siqueira., Heat Transport Capability and Compensation Chamber in Fluence in Loop Heat-pipes Performance, *Applied Thermal Engineering* **26**, 2006, 1158 -1168.
- [3] W. Joung, T. Yu, J. Lee., Experimental Study on the Loop Heat-pipes with a Planar Bifacial Wick Structure, *International Journal of Heat and Mass Transfer*, **51**, 2008, 1573-1581.
- [4] P. Charoensawan, P. Terdtoon., Thermal Performance of Horizontal Closed-Loop Oscillating Heat-pipes, *Applied Thermal Engineering*, **28**, 2008, 460-466.
- [5] C. T. Meng, S.H. Chih, W.K. Shung., Experimental Study of a Loop Thermosyphon Using Methanol as Working Fluid, *14th IHPC*, 2007.
- [6] Mostafa A. Abd El-Baky & Mousa M. Mohamed. (2007). Heat-pipes heat-exchanger for heat recovery in air conditioning. *Applied Thermal Engineering* **27**, 795–801.
- [7] Beckert, K. and Herwig, H. (1996). Inclined air to air heat-exchangers with heat-pipes: comparing experimental data with theoretical results. *Intersociety Energy Conversion Engineering Conference*, **2**, 1441-1446.
- [8] ASHRAE, Standard 55-92/ISO7730-94: Air Diffusion Performance Index, *American Society of Heating, Ventilating and Air-Conditioning Engineers, Inc.*
- [9] Wan J.W., Zhang J.L., Zhang W.M. (2007). The Effect of Heat Pipe Air Handling Coil On Energy Consumption in Central Air-Conditioning System, *Energy Build*, **39**, 1035-10.

Theoretical and Experimental Analysis of Desiccant Wheel Performance for Solar Hybrid Desiccant Air-Conditioning System

Zuraini Hashim^{1,2, a}, Tri Suyono², Arifidian Rachman², Zulkarnaini¹, Sohif Mat²,

¹University Kuala Lumpur Malaysia France Institute

Bandar Baru Bangi, Malaysia 43650

²Solar Energy Research Institute

National University of Malaysia

UKM Bangi 43000

zurainimfi@yahoo.com, sohif@ukm.my

Abstract. Dehumidification is considered a key feature of HVAC systems for thermal comfort. Malaysia is located in the South East Asia region which has a sufficiently high temperature and humidity of approximately 80% RH. This requires a process that can reduce moisture in the air. A desiccant wheel is used to provide dehumidification. Desiccant wheel with model no. 770 WSG produced by NOVELAIRE having operating system 1:1 and a maximum flow rate of 1500 cfm has been theoretically and experimentally analysed for its performance. The results show good matching between theoretical and experimental results in terms of sensible and latent effectiveness of the dehumidification process as well as the regeneration process. This desiccant wheel is capable of condensing water at $0.05\text{kg}_{\text{H}_2\text{O}}/\text{s}$ and providing 3.3639 kW load reduction. With this significant load reduction, the component integrated into the solar hybrid desiccant air-conditioning system can perform comfort cooling to an area with high latent loads such as a hall, hypermarket, and commercial building.

Keywords: performance, a desiccant wheel, air-conditioning system, thermal comfort.

1. Introduction

As there is a decrease in energy resources while energy demands increase, new regulatory policies and more energy-efficient systems are needed to provide comfort cooling. Due to this, the air-conditioning function requires air dehumidification to reduce the latent load of outdoor air and provide energy-efficient, good air quality and comfort solutions for the industry. According to Harriman [14], there are currently more than 500 supermarkets that use desiccant dehumidification packages integrated with the electric-driven refrigeration system. The desiccant wheel acts as a pre-conditioner for outside air to remove its latent load before being supplied to the air-conditioning unit.

2. Desiccant System

Desiccant exhibits an affinity so strong for moisture that they can draw water directly from the surrounding air. This affinity can be regenerated repeatedly by applying heat to the desiccant material to drive off the collected moisture. A desiccant wheel is widely used to lower the humidity of air in the cooling system [2], and it has a good ability to absorb water in the air [3]. In the dehumidification process, the processed airflow

through the desiccant wheel where latent and sensible heat is absorbed. The processed air becomes dry and also experiences an increase in temperature [4-10]. Noting that the use of the desiccant wheel in the process of air-conditioning is considered appropriate. Dry air is good for comfort especially in hot and humid countries such as Malaysia [11]. A system using the desiccant wheel for air-conditioning can reduce cooling load up to 35% [14]. Mazzei et al. [15] have found that the use of hybrid systems with desiccant wheel result in remarkable savings in operating costs and higher plant costs and significant reduction of the power electric demand, better control of ambient humidity [15]. The solar hybrid desiccant air-conditioning system has been designed, fabricated and experimented in Universiti Kebangsaan Malaysia (UKM) to produce an energy-saving system that offers good air quality and comfort air as in Figure 3.

The system is designed for comfort on a commercial scale. The system consists of the solar collector (evacuated tube) with a 13:32 wide m², 0.62 m² area heat-exchanger 0.15m thick and desiccant wheel maximum 1.500 cfm flow rate. To operate the equipment at night or when there is no sun available, an electrical air heater is used for the regeneration process. The desiccant system uses a heat source of the evacuated tube collector in the form of hot water, then poured into a hot water heat-exchanger to heat the air. The flow rate in this experiment was made at 929.6 cfm / 1,579.5 m³/h for both processes (regeneration and dehumidification). This means that the ratio between the regeneration of the desiccant wheel and dehumidification was 1:1.

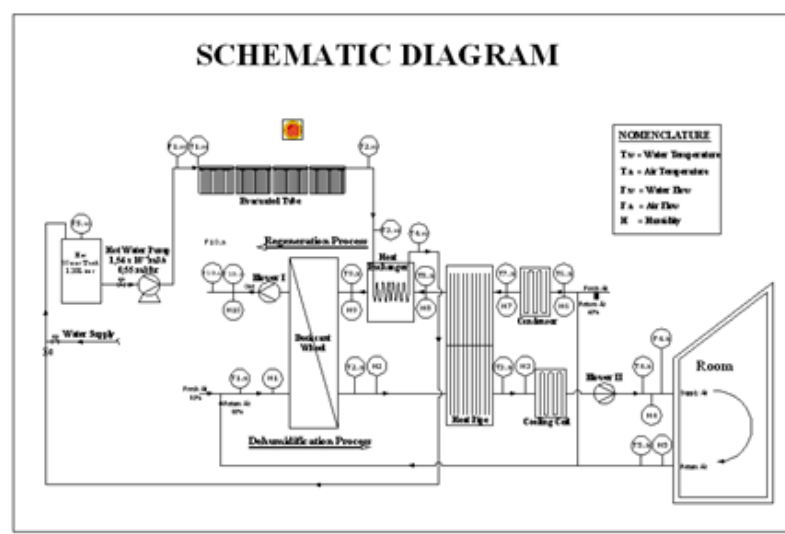


Fig.1 Schematic diagram of solar hybrid desiccant AC system

3. Analytical Method

This system uses solar energy as a heat resource. Heat energy from the sun is transferred to the water through the heat pipe evacuated tube. Hot water flows into the heat-exchanger to heat water that passes through a heat-exchanger. This process takes place continuously throughout the process. Hot air generated by the heat exchanger is used for the regeneration of the desiccant wheel. This paper will only discuss the performance of the desiccant wheel.

There are two processes of desiccant wheel system, namely regeneration and dehumidification process [10]. The regeneration or recovery process is the process of drying in a silica gel of desiccant that has been wet during the dehumidification process. The dehumidification process is the process of water absorption in the air so the air will become drier and the temperature is increased [12]. Desiccant wheel performance will be evaluated using the effectiveness dehumidification and regeneration process (Sensible and latent), and the adiabatic effectiveness [4].

3.1 Dehumidification process

Sensible/thermal Effectiveness

$$\varepsilon_{dh.sbl} = \frac{\dot{m}_{dh}}{\dot{m}_{min}} \frac{T_1 - T_2}{T_1 - T_7} \quad (1)$$

Latent Effectiveness

$$\varepsilon_{dh.ltn} = \frac{\dot{m}_{dh}}{\dot{m}_{min}} \frac{w_1 - w_2}{w_1 - w_7} \quad (2)$$

From the above equation, the temperature and absolute humidity of the air that has passed the dehumidification process can be calculated by the following equation:

$$T_2 = \frac{\dot{m}_{min}}{\dot{m}_{dh}} \varepsilon_{dh.sbl} (T_7 - T_1) + T_1 \quad (3)$$

$$w_2 = \frac{\dot{m}_{min}}{\dot{m}_{dh}} \varepsilon_{dh.ltn} (w_7 - w_1) + w_1 \quad (4)$$

3.2 Regeneration Process

The process of regeneration can be written as follows:

Sensible / thermal Effectiveness

$$\varepsilon_{reg.sbl} = \frac{\dot{m}_{reg}}{\dot{m}_{min}} \frac{T_8 - T_7}{T_1 - T_7} \quad (5)$$

Latent Effectiveness

$$\varepsilon_{reg.ltn} = \frac{\dot{m}_{dh}}{\dot{m}_{min}} \frac{w_8 - w_7}{w_1 - w_7} \quad (6)$$

Thus the temperature and absolute humidity of the air that has passed through the process of regeneration can be written as the following equation:

$$T_{reg.out} = \frac{\dot{m}_{min}}{\dot{m}_{dh}} \varepsilon_{reg.sbl} (T_1 - T_7) + T_7 \quad (7)$$

$$w_{reg.out} = \frac{\dot{m}_{min}}{\dot{m}_{dh}} \varepsilon_{reg.ltn} (w_1 - w_7) + w_7 \quad (8)$$

Adiabatic efficiency can be calculated by the following equation:

$$\varepsilon_{adiabatic} = 1 - \frac{(h_2 - h_1)}{h_1} = \frac{(2h_1 - h_2)}{h_1} \quad (9)$$

3.3 Moisture Removal Rate

The moisture removal of desiccant can be calculated using the following equation:

$$(w_{out} - w_{in}) \times \frac{\dot{V}}{v} = \dot{m}_{removal} \quad (10)$$

While latent and sensible loads are determined using the following equation:

$$Load = \dot{m}\Delta H \quad (11)$$

4. Result and Discussion

The overall performance of the desiccant wheel is strongly influenced by the air used in the process of regeneration and the air that goes into the process of dehumidification. When hotter and drier air is used in the regeneration process, the air generated in the dehumidification process will be hotter and drier because the desiccant wheel operation experiences the sensible and latent process as shown in Figure 2. The Sensible process occurs because the process is a valid isotherm process.

4.1 Dehumidification Process

The dehumidification process in this system produces higher temperatures and lower humidity. An additional component such as heat recovery is needed to reduce its temperature before moving to the cooling coil for the air conditioning process. Theoretically, In the dehumidification process with an average of 33.9°C incoming air, and 67°C incoming air, the regeneration process will result in the temperature of outlet regeneration 58.8°C as in Fig 2. Experiment results show that the dehumidification process in the same conditions produces 58.02°C air temperature. This indicates that the results approach theoretical calculation as shown in Figure 3. The sensible effectiveness of this system is calculated at an average of 0.73 as shown in Figure 4.

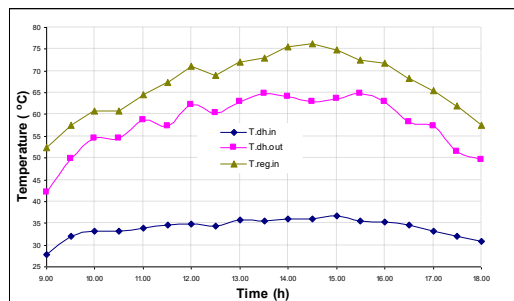


Fig.2 Sensible process of the desiccant wheel

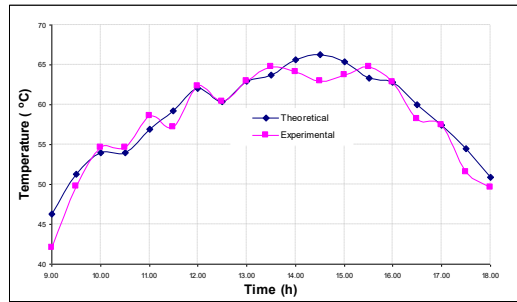


Fig.3 Theoretical and experimental sensible dehumidification

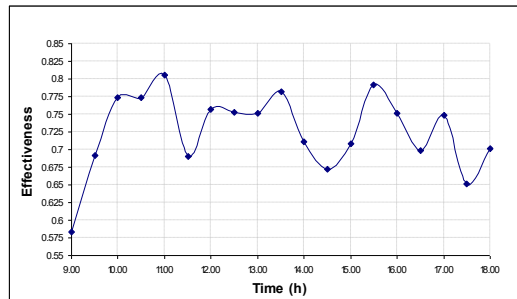


Fig.4 Dehumidification Sensible Effectiveness

Theoretically, the value of absolute humidity $0.024 \text{ kg}_{\text{H}_2\text{O}}/\text{kg}_{\text{dry air}}$ at the dehumidification process results in a reduction to $0.017 \text{ kg}_{\text{H}_2\text{O}}/\text{kg}_{\text{dry air}}$ while the experimental value is $0.0167 \text{ kg}_{\text{H}_2\text{O}}/\text{kg}_{\text{dry air}}$. From the results of these experiments, it is known that the latent effectiveness of this system is at an average of 0.793. This process can be seen in Figures 5 and 6.

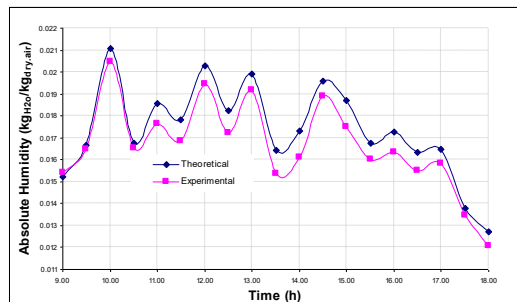


Fig.5 Theoretical and experimental latent dehumidification

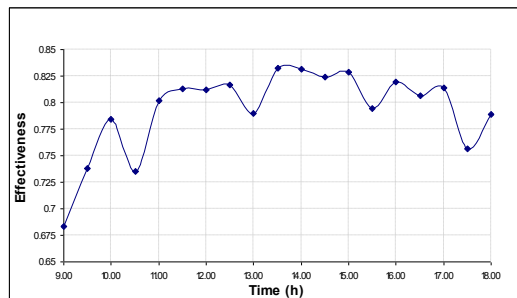


Fig.6 Dehumidification Latent Effectiveness

4.2 Regeneration Process

A regeneration process aims to dry the silica gel desiccant wheel to function again as a dehumidifier. This process results in the outlet air becoming lower in temperature and higher in moisture content. In the system, the theoretical regeneration process occurs at an average temperature of 42°C while experiment results show that an air temperature of 39.8°C. The absolute humidity of air increases at an average of 0.022 kg_{H2O}/kg_{dry air} theoretically, while experiment results are 0.0218 kg_{H2O}/kg_{dry air}, as shown in Figures 7 and 8. Sensible effectiveness of the regeneration process at an average of 0.82, while the regeneration of latent effectiveness is at 0.789 as shown in Figures 9 and 10. Several process conditions of absolute humidity at the dehumidification and regeneration process are shown in Figure 11, while the adiabatic effectiveness of the desiccant wheel can be seen in Figure 12 which is at an average of 0.93.

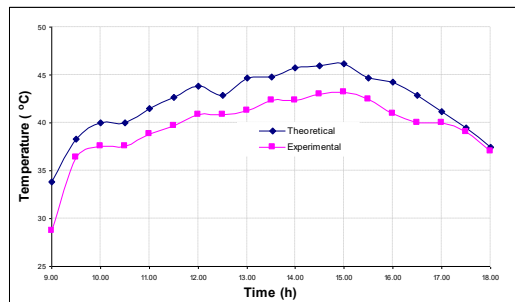


Fig.7 Theoretical and experimental sensible regeneration

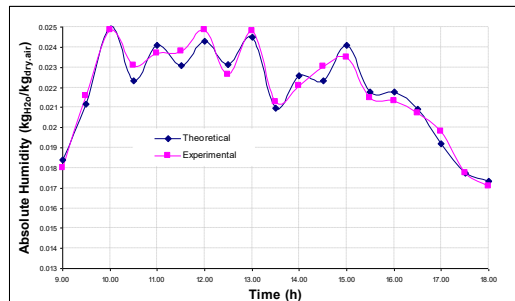


Fig.8 Theoretical and experimental latent regeneration

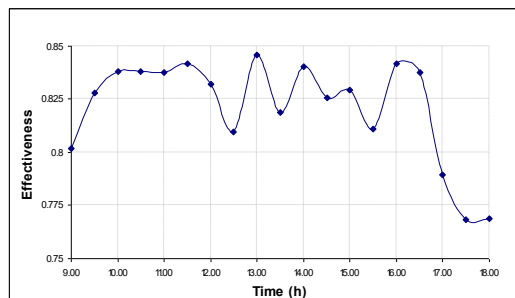


Fig.9 Regeneration sensible effectiveness

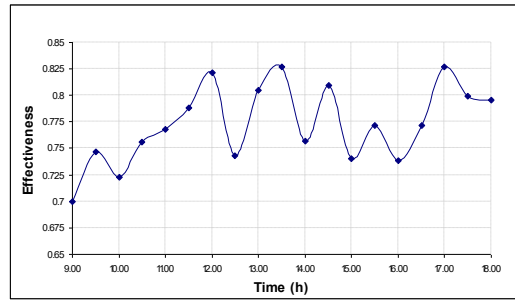


Fig.10 Regeneration Latent Effectiveness

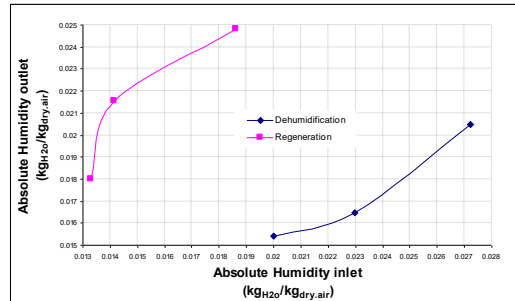


Fig.11 Absolute humidity at dehumidification and regeneration processes.

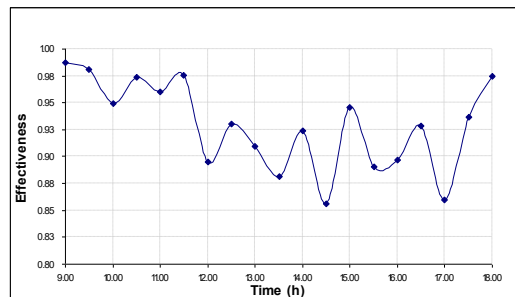


Fig.12 Adiabatic desiccant wheel effectiveness

4.3 Moisture Removal

Based on the analytical calculation, the removal moisture rate is 0.05 kg/s, while the load is removed by the process is 3.3639 KW. This pre-treatment air will lessen the load to the cooling coil and therefore reduce its capacity, power consumption, and electrical demand.

5. Conclusion

The performance of the desiccant wheel for air-conditioning applications has been studied theoretically and experimentally. The results obtained show that the desiccant wheel application is suitable for the air-conditioning system as a significant amount of moisture is removed, thus reducing air-conditioning latent load. Experimental results for the given dehumidification process on this system produces an average air temperature of 58.02°C with absolute humidity of 0.0167 kg_{H2O}/kg_{dry air}. Sensible effectiveness is at 0.73 whereas the average of latent effectiveness is at 0.793. In the regeneration process, theoretically, sensible heat generates temperature at 42°C while experimental results show the value of 39.8°C. Theoretically, the latent process produces 0.022 kg_{H2O}/kg_{dry air}, while the experimental value is at 0.0218 kg_{H2O}/kg_{dry air}. Sensible effectiveness is at 0.82, while regeneration latent effectiveness is at 0.789. The performance of the desiccant wheel in good condition concludes the significant usage of the desiccant wheel in the air-conditioning application.

Acknowledgments

The authors would like to thank the Solar Energy Research Institute, Universiti Kebangsaan Malaysia, and the University Kuala Lumpur – Malaysia France Institute for support.

Nomenclature

$\varepsilon_{dh.sbl}$	Dehumidification sensible effectiveness
\dot{m}_{dh}	Mass airflow rate for dehumidification process (kg _{dry air} /hr)
\dot{m}_{dh}	Mass airflow rate for the regeneration process (kg _{dry air} /hr)
\dot{m}_{min}	The minimum value of either mass flow rate (kg _{dry air} /hr)
T_1	Dry bulb temperature of air into dehumidification process (°C)
T_2	Dry bulb temperature of air out from dehumidification process (°C)
T_7	Dry bulb temperature of air into the regeneration process (°C)
T_8	Dry bulb temperature of air out from the regeneration process (°C)
w_1	The absolute humidity of air into the dehumidification process (°C)
w_2	The absolute humidity of air out from the dehumidification process (°C)
w_7	The absolute humidity of air into the regeneration process (°C)
w_8	The absolute humidity of air out from the regeneration process (°C)
w_{in}	The absolute humidity of the air entering the drying chamber (%)
w_{out}	The absolute humidity of air leaving the drying chamber (%)
w_{as}	The absolute humidity of the air entering the dryer at the point of adiabatic saturation (%)
h_1	Enthalpy of air in the dehumidification process (kJ/kg)
h_2	Enthalpy of air out dehumidification process (kJ/kg)
V	Volumetric airflow rate (m ³ /s)
W	Weight of water evaporated from the product (kg)
WAC	Water absorption capacity

- ρ Density of air (kg/m^3)
- \dot{G}_a Dry air Mass airflow rate ($\text{kg}_{\text{dry air}}/\text{hr}$)

References

- [1] V. Shanmugam, E. Natarajan. *Applied Thermal Engineering* 27 (2007), p. 1543–1551.
- [2] D. La, Y.J. Dai, Y. Li, R.Z. Wang, T.S. Ge. *Renewable and Sustainable Energy Reviews* 14 (2010), p. 130–147.
- [3] A.E. Kabeel. *Energy* 35 (2010), p. 5192-5201.
- [4] M. Ali Mandegari, H. Pahlavanzadeh. *Energy* 34 (2009), p. 797–803.
- [5] Giovanni A. Longo, Andrea Gasparella. *Solar Energy* 83 (2009), p. 511-521.
- [6] M.H. Ahmed, N.M. Kattab, M. Fouad. *Renewable Energy* 30 (2005) 305–325
- [7] Stefano De Antonellis, Cesare Maria Joppolo, Luca Molinaroli. *Energy and Buildings* 42 (2010), p. 1386–1393.
- [8] T.S. Ge, Y.J. Dai, R.Z. Wang. *Energy Conversion and Management* 52 (2011), p. 2329–2338.
- [9] Mihajlo N. Golubovic, H.D.M. Hettiarachchi, William M. Worek. *International Journal of Heat and Mass Transfer* 49 (2006), p. 2802–2809.
- [10] Giovanni Angrisani, Alfonso Capozzoli, Francesco Minichiello, Carlo Roselli, Maurizio Sasso. *Applied Energy* 88 (2011), p. 1354–1365.
- [11] Aydin Kilic. *Journal of Food Engineering* 91 (2009), p. 173–182.
- [12] Kosuke Nagaya, Ying Li, Zhehong Jin, Masahiro Fukumuro, Yoshinori Ando a, Atsutoshi Akaishi. *Journal of Food Engineering* 75 (2006), p. 71–77.
- [13] V. Shanmugama, E. Natarajan. *Renewable Energy* 31 (2006), p. 1239–1251.
- [14] Harriman, L.G.,111, *Engineered Systems* (1994), p. 63-68.
- [15] Pietro Mazzei, Francesco Minichiello, Daniele Palma. *Applied Thermal Engineering* 25 (2005), p. 677-707.